THE JOURNAL OF CHEMICAL PHYSICS

VOLUME 22 NUMBER 1

JANUARY, 1954

UNIVERSITY OF MICHIGAN
FEB 22
PHYSICS LIBRARY

Published by the
AMERICAN INSTITUTE OF PHYSICS
NEW YORK, N. Y.

The American Institute of Physics

INCORPORATED

57 East 55th Street New York 22, N.Y.

MEMBERS:

American Physical Society
Karl K. Darrow, *Secretary*, Columbia University, New York 27, New York.

Optical Society of America
Arthur C. Hardy, *Secretary*, Massachusetts Institute of Technology, Cambridge 39, Massachusetts.

Acoustical Society of America
Wallace Waterfall, *Secretary*, 57 East 55th Street, New York 22, New York.

Society of Rheology
W. R. Willets, *Secretary*, Titanium Pigment Corporation, 99 Hudson Street, New York 13, New York.

American Association of Physics Teachers
R. F. Paton, *Secretary*, University of Illinois, Urbana, Illinois.

AFFILIATED SOCIETIES:

American Crystallographic Association
American Society for Metals
Electron Microscope Society of America
Physical Society of Pittsburgh
Physics Club of Chicago
Physics Club of Philadelphia
Cleveland Physics Society
Physics Club of the Lehigh Valley
Sigma Pi Sigma

ASSOCIATES:

Over seventy-five leading industrial enterprises and other institutions which contribute to the support of the Institute.

JOURNALS:

The Physical Review
S. A. Goudsmit, *Editor*, Brookhaven National Laboratory, Upton, Long Island, New York.

Reviews of Modern Physics
J. W. Buchta, *Editor*, University of Minnesota, Minneapolis, Minnesota.

Journal of the Optical Society of America
Wallace R. Brode, *Editor*, National Bureau of Standards, Washington 25, D. C.

The Journal of the Acoustical Society of America
Floyd A. Firestone, *Editor*, 57 East 55th Street, New York 22, New York.

American Journal of Physics
Thomas H. Osgood, *Editor*, Michigan State College, East Lansing, Michigan.

The Review of Scientific Instruments
Gaylord P. Harnwell, *Editor*, Randal Morgan Laboratory of Physics, University of Pennsylvania, Philadelphia, Pennsylvania.

The Journal of Chemical Physics
Clyde A. Hutchison, Jr., *Editor*, Institute for Nuclear Studies, University of Chicago, Chicago 37, Illinois.

Journal of Applied Physics
Eugene Hutchisson, *Editor*, Case Institute of Technology, Cleveland 6, Ohio.

Physics Today
Robert R. Bacon, *Editor*, American Institute of Physics, 57 East 55 Street, New York 22, New York.

OFFICERS

George R. Harrison, *Chairman*
Massachusetts Institute of Technology

George B. Pegram, *Treasurer*
Columbia University

GOVERNING BOARD

J. W. Buchta
Karl K. Darrow
G. J. Dienes
S. A. Goudsmit
George R. Harrison
Frederick V. Hunt
Deane B. Judd
Hugh S. Knowles
C. C. Lauritsen
William F. Meggers
Philip M. Morse
Brian O'Brien
George B. Pegram
I. I. Rabi
Duane Roller
Frederick Seitz
William Shockley
Richard M. Sutton
J. H. Van Vleck
Mark W. Zemansky

Consultant on Printing
Melvin Loos

ADMINISTRATIVE STAFF

Henry A. Barton, *Director*

Wallace Waterfall,
Executive Secretary

Theodore Vorburger,
Advertising Manager

Ruth F. Bryans,
Publication Manager

Edith I. Neftel,
Circulation Manager

Kathryn Seitz,
Assistant Treasurer

THE American Institute of Physics was founded in 1931 as a federation of leading societies in the field of Physics. It combines into one operating agency those functions on behalf of physics which can best be done by the Societies jointly. Its purpose is the advancement and diffusion of physics and its applications to human welfare. To this end it publishes for itself or the Societies the nine journals listed on this page; promotes unity and effectiveness of effort among all who are interested in physics; renders numerous direct services to physicists and to the public; and cooperates with government agencies, national associations, educational institutions, technical industries, and others in such manner as to realize the opportunities and fulfill the responsibilities of physics as an important and constructive human activity.

Physics
Faxon

THE JOURNAL
OF
CHEMICAL PHYSICS

VOLUME 22, NUMBER 1 JANUARY, 1954

An Experimental Study of the Vibrational Spectra of Hexamethyldisilane and Related Compounds

C. C. CERATO, J. L. LAUER, AND H. C. BEACHELL
Department of Chemistry, University of Delaware, Newark, Delaware

(Received July 20, 1953)

Raman and infrared spectra have been obtained for trimethylphenylsilane, hexamethyldisilylmethylene, hexamethyldisiloxane, hexamethyldisilazine, and hexamethyldisilane. For the last compound the infrared spectral region covered extended from 1–50 microns; for the other compounds the region extended only from 1–15 microns. The intensities and depolarization factors of the Raman bands have been determined photoelectrically. A few tentative frequency assignments have been given.

I. INTRODUCTION

THE vibrational spectra of comparatively few silicon containing hydrocarbons have been studied. A considerable amount of work is still required for the accurate determination of the influence of the substitution of a silicon atom for a carbon atom upon the force constants and frequency shifts. The present work represents an effort in this direction.

One compound, hexamethyldisilane, was studied in the entire spectral region from 1–50 microns in the infrared, and the information so obtained together with that derived from the Raman spectrum permitted at least a tentative frequency assignment of the fundamentals. A number of the more intense lines in the spectra of the other compounds could be assigned to the corresponding vibrational modes by comparison with bands of hexamethyldisilane having similar frequency. The careful study of the infrared spectra in the 1–2 micron (C−H overtone) region proved fruitful in that it showed the existence of a doublet which apparently is characteristic of a silicon-carbon linkage in the molecule.

II. EXPERIMENTAL PROCEDURE

The Raman spectra were obtained with a Hilger four-prism spectrograph ($f/8$) having a reciprocal dispersion of 4.5 A/mm at 4358A. This instrument could be used with either photographic or photoelectric recording. Photographic recording was used to obtain the frequencies of the Raman bands by comparison with an iron arc spectrum taken on the same plate, whereas photoelectric recording was used for the intensity measurements and the determinations of the depolarization factors. The recorder deflections of the spectral bands were referred to the deflection of the 459 cm^{-1} CCl_4 band and corrected for the varying wavelength sensitivity of the spectrometer and detector by comparison with the deflection of a standard NBS-calibrated incandescent lamp by the procedure described previously.[1] The depolarization factors were determined photoelectrically by the method of Edsall and Wilson[2] as modified by Crawford and Hurwitz.[3]

The infrared spectra in the 1–2 micron region were recorded with the Littrow type glass prism spectrophotometer of Lauer and Rosenbaum.[4] This instrument has an actual resolving power of 400 at 1.1 microns and in this region is superior to the conventional rocksalt spectrophotometer.

For the rocksalt region (1–15 microns) a Baird double-beam recording spectrophotometer was employed. A Perkin-Elmer spectrophotometer Model 12 with a KBr prism allowed us to cover the wavelength region from 12 to 24 microns.

III. SOURCE AND PURITY OF COMPOUNDS

The compounds used in this work were furnished by Dr. H. C. Beachell and were prepared from published

[1] Rosenbaum, Cerato, and Lauer, J. Opt. Soc. Am. 42, 670 (1952).
[2] G. Edsall and E. B. Wilson, J. Chem. Phys. 6, 124 (1938).
[3] B. L. Crawford and W. Hurwitz, J. Chem. Phys. 15, 268 (1947).
[4] J. L. Lauer and E. J. Rosenbaum, Appl. Spectroscopy 6, Nov., 1952.

data. The following physical constants check the known literature values:

	B.P. °C	n_D^{20}	d_4^{20}
Hexamethyldisilazine	125.5	1.4062	0.7747
Hexamethyldisiloxane	100.5	1.3774	0.7636
Hexamethyldisilylmethylene	133.3 (at 765 mm)	1.4175	0.7515
Trimethylphenylsilane	171.0	1.4906	0.8682
Hexamethyldisilane	113.0	1.4229	0.7272

IV. RESULTS

The Raman frequencies with the corresponding intensities and depolarization factors in parentheses are given in Table I. In all cases the exciting line was

TABLE I. Raman frequency displacements.

Hexamethyldisilane $(CH_3)_3Si \cdot Si(CH_3)_3$

87 (v.w.); 124 (v.w.); 180[a] (1.14*b*, *dp*); 216 (0.10, *dp*); 251 (0.21, *dp*); 305 (0.01, 0.50); 346 (0.03, 0.60); 373 (v.w.); 404 (0.63*s*, 0.13); 510 (v.w., *d*); 578 (0.03, *dp*); 598 (v.w., *bd*); 638 (0.61*s*, 0.19); 686 (0.29, *dp*); 753 (0.05, *dp*); 830 (0.05, *dp*); 883 (0.07, 0.54); 1130 (0.05, *dp*); 1190 (0.05, *dp*); 1241 (0.06*s*, *dp*); 1256 (0.05*s*, 0.35); 1283 (0.04, 0.60); 1315 (0.10, 0.25); 1372 (0.09, *dp*); 1415 (0.07, *dp*); 1443 (0.03, 0.60); 2898 (0.81*b*, 0.17); 2957 (0.75, *dp*).

Hexamethyldisilazine $(CH_3)_3Si \cdot NH \cdot Si(CH_3)_3$

69 (w.); 146 (0.02); 177[a] (0.21b, 0.74); 197[a] (0.13*b*, 0.70); 217 (0.03, *dp*); 231 (0.09, *dp*); 250 (0.12, *dp*); 350 (0.04, 0.32); 517 (0.02 *bd*, *dp*); 575 (0.40, 0.08); 618 (0.02, 0.33); 670 (0.05, 0.25); 688 (0.10, *dp*); 744 (0.04, *dp*); 833 (0.03, 0.43); 889 (0.02, *dp*); 936 (w.); 1035 (w.); 1072 (w.); 1174 (w.); 1243 (0.04, *dp*); 1264 (0.04, *dp*); 1291 (w.); 1413 (0.07, *dp*); 1488 (0.01); 1507 (0.01); 1545 (0.01); 2581 (0.01); 2669 (0.01, 0.10); 2900 (0.36, 0.10); 2959 (0.33, *dp*); 3089 (0.05, 0.31); 3147 (0.05, *dp*); 3381 (0.03, 0.22).

Hexamethyldisiloxane $(CH_3)_3Si \cdot O \cdot Si(CH_3)_3$

69 (w.); 180 (0.43, *dp*); 190 (0.09, 0.20); 219 (0.20, *dp*); 258 (0.13, *dp*); 333 (0.02, *dp*); 522 (0.25, 0.07); 663 (0.16, 0.13); 687 (0.10, *dp*); 752 (0.03, *dp*); 833 (0.05, 0.75); 848 (0.02, *dp*); 890 (0.02, *dp*); 1033 (0.01, 0.16); 1051 (0.01, 0.47); 1224 (0.02, *dp*); 1243 (0.02, *dp*); 1255 (0.02, 0.70); 1264 (0.03, 0.75); 1313 (0.01, 0.40); 1413 (0.07, *dp*); 2697 (0.01, *dp*); 2899 (0.64*b*, 0.10); 2960 (0.56, *dp*); 3089 (0.14, 0.32); 3147 (0.14, *dp*).

Hexamethyldisilylmethylene $(CH_3)_3Si \cdot CH_2 \cdot Si(CH_3)_3$

69 (w.); 166 (0.32b, *dp*); 190[a] (0.28*b*, 0.71); 230 (0.26*b*, *dp*); 252 (0.11*b*, 0.67); 325 (0.05, 0.04); 495 (0.02); 556 (0.59, 0.01); 658 (0.19, 0.01); 691 (0.18, 0.75); 732 (0.03); 835 (0.04, 0.30); 846 (0.04, 0.22); 873 (0.03, 0.47); 1035 (0.03, 0.68); 1056 (0.03, 0.30); 1247 (0.04, 0.53); 1264 (0.01, 0.31); 1280 (w.); 1356 (0.03, *dp*); 1411 (0.04, *dp*); 1427 (0.04, *dp*); 2860 (0.27, 0.13); 2899 (0.72, 0.13); 2959 (0.65, *dp*); 3087 (0.09, 0.17); 3145 (0.09, *dp*).

Trimethylphenylsilane $(CH_3)_3Si \cdot C_6H_5$

103 (w.); 152 (w.); 169 (w.); 180 (0.01, *dp*); 190[a] (0.01*b*, 0.70); 207 (0.18, 0.70); 220 (0.17, 0.70); 237 (0.02, *dp*); 263 (0.04, 0.75); 291 (w.); 303 (0.04, 0.68); 372 (0.19, 0.18); 508 (w.); 548 (0.01, *dp*); 554 (0.01, *dp*); 568 (0.03, 0.29); 621 (0.65, 0.16); 653 (0.01, *dp*); 695 (0.10, 0.74); 734 (0.02, *dp*); 763 (0.03, 0.52); 803 (w.); 835 (0.03, *dp*); 852 (0.06*b*, *dp*); 904 (0.02, *dp*); 947 (0.04, 0.24); 992 (0.67*s*, 0.10); 1035 (0.19, 0.14); 1049 (w.); 1078 (0.04, *dp*); 1117 (0.11*b*, 0.36); 1159 (0.09, *dp*); 1189 (0.11, 0.10); 1212 (0.06, *dp*); 1240 (0.13*s*, 0.66); 1264 (0.10*s*, 0.51); 1413 (0.05, *dp*); 1469 (0.03, 0.61); 1506 (0.02, *dp*); 1569 (0.06, 0.67); 1594 (0.20, 0.73); 2678 (0.06, 0.33); 2899 (0.28, 0.12); 2959 (0.30, 0.80); 3053 (0.30*b*, 0.44); 3089 (0.06, 0.52); 3147 (0.05, *dp*).

[a] A plot of depolarization factor *vs* frequency over the width of the band shows that the band consists of several narrow bands having different polarization characteristics.

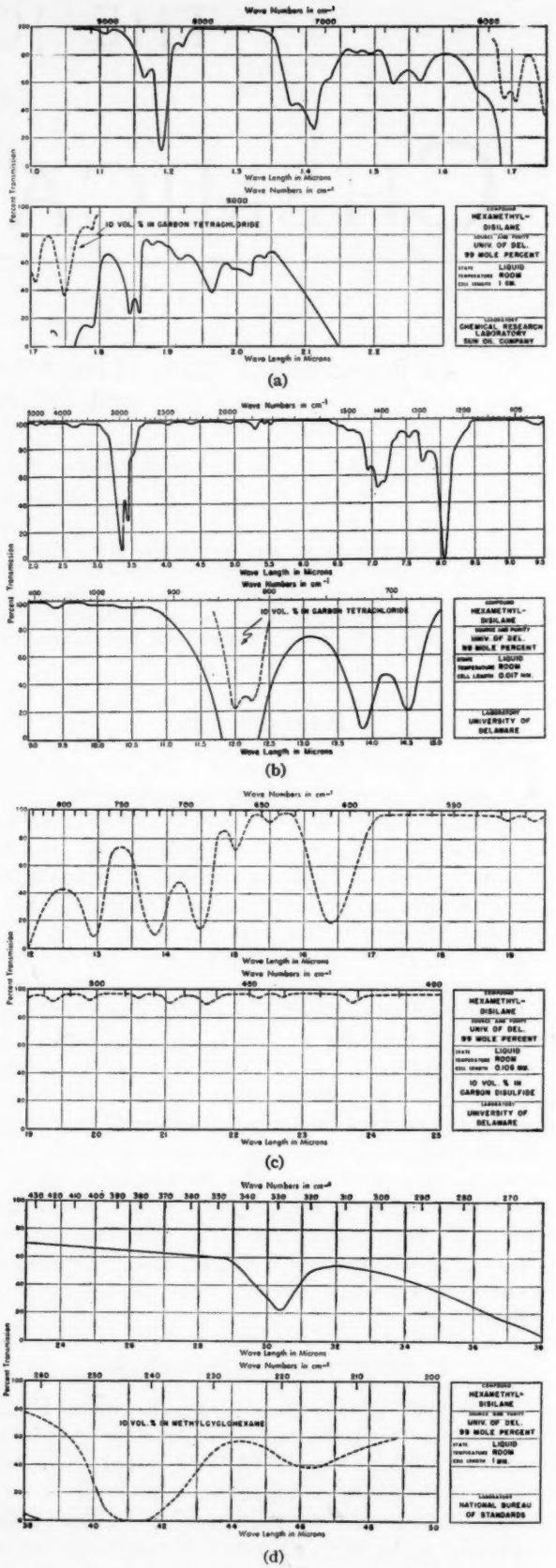

FIG. 1. Infrared spectra of hexamethyldisilane.

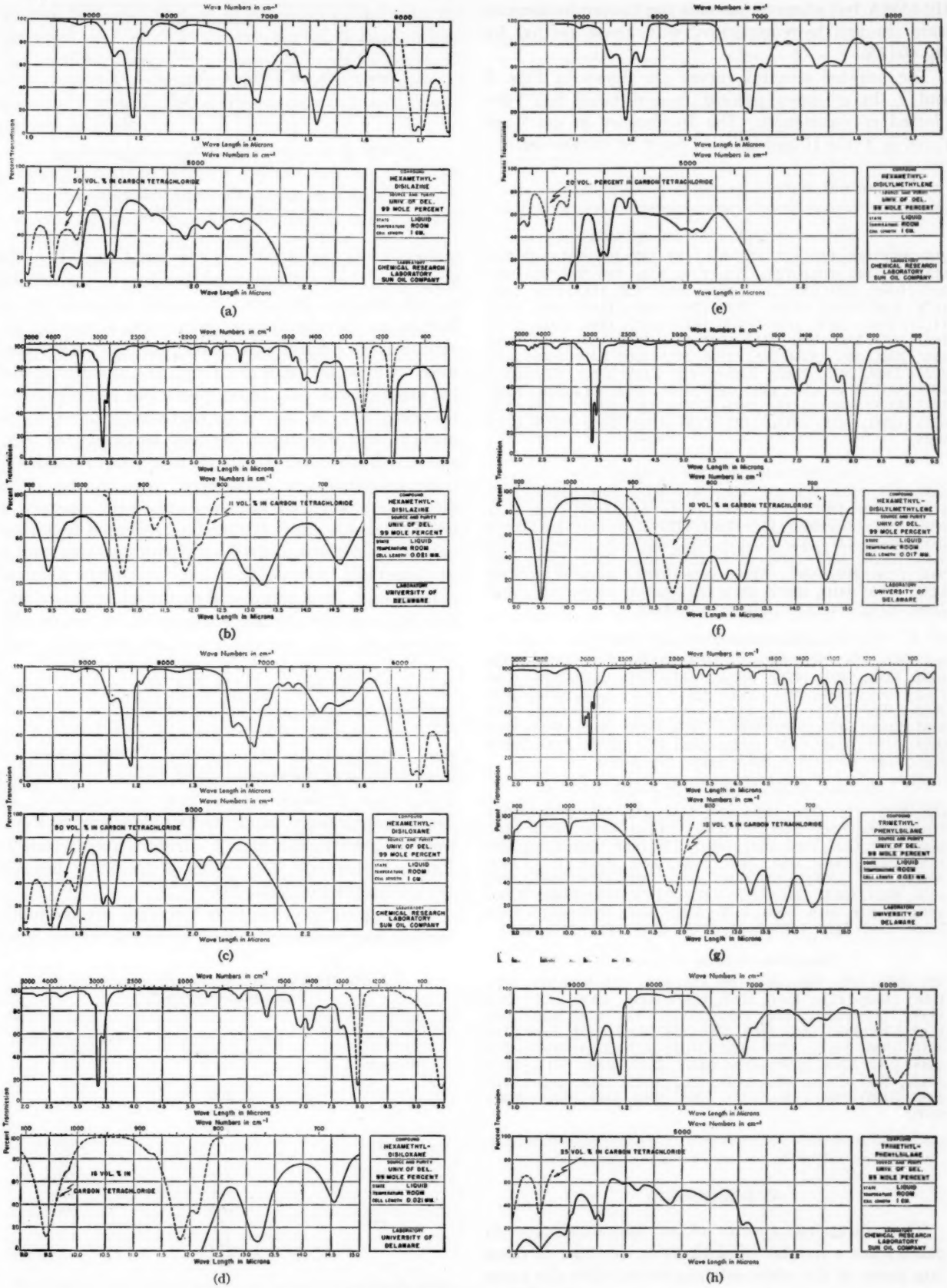

FIG. 2. Infrared spectra of silanes.

Hg 4358A, but wherever possible the Raman frequencies were checked by comparison with those excited by Hg 4047A.

The infrared spectral curves are shown in Figs. 1 and 2. In all cases percent transmittance has been plotted *vs* wavelength. The frequencies in cm^{-1} are listed in Table II and are also given on the curves.

TABLE II. Infrared spectral frequencies (cm^{-1}).[a]

Hexamethyldisilane $(CH_3)_3Si\cdot Si(CH_3)_3$

216; 242*s*, 329; 422; 437; 444; 463; 470; 485; 493; 503; 516; 528; 610*s*; 645; 667; 691*s*; 722*s*; 773*s*; 819*s*; 834*s*; 910; 923; 966; 997; 1013; 1046; 1059; 1068; 1076; 1081; 1093; 1120; 1135; 1161; 1169; 1178; 1187; 1237; 1245*s*; 1268; 1292; 1323; 1343; 1364; 1391; 1412*s*; 1441; 1474; 1503; 1533; 1541; 1551; 1587; 1602; 1610; 1637; 1672; 1685; 1698; 1713; 1797; 1813; 1840; 1886; 1925; 1951; 1988; 2028; 2058; 2084; 2157; 2196; 2283; 2402; 2472; 2594; 2658; 2722; 2849; 2898; 2957*s*; 3067*s*; 3115; 3215; 3368; 3552; 3667; 3741; 3831; 4149; 4308; 4466; 4739; 4895; 4940; 5010; 5080; 5220; 5275; 5325; 5380*s*; 5415*s*; 5585; 5695*s*; 5850*s*; 5890*s*; 6055; 6370; 6535; 6800; 6975; 7095*s*; 7135; 7250; 8200; 8395*s*; 8590; 8755; 9025.

Hexamethyldisilazine $(CH_3)_3Si\cdot NH\cdot Si(CH_3)_3$

663; 685*s*; 757*s*; 773; 826; 876*s*; 885; 931*s*; 1016; 1062*s*; 1131; 1180*s*; 1250*s*; 1301; 1350; 1398*s*; 1414; 1441; 1459; 1486; 1524; 1543; 1562; 1580; 1603; 1630; 1693; 1717; 1792; 1821; 1832; 1890; 1953; 2024; 2272; 2362; 2467; 2652; 2825; 2894; 2959*s*; 3079; 3174; 3380*s*; 3667; 3809; 4144; 4292; 4636; 4810; 4895; 4960; 5045; 5100; 5192; 5385*s*; 5425*s*; 5580*s*; 5718*s*; 5870*s*; 5920*s*; 6050; 6255; 6315; 6410; 6605*s*; 6715; 6815; 6980; 7080*s*; 7135; 7235; 7280; 7612; 7890; 8280; 8410*s*; 8670; 9080.

Hexamethyldisiloxane $(CH_3)_3Si\cdot O\cdot Si(CH_3)_3$

663; 687*s*; 758*s*; 825; 846*s*; 857; 1018; 1056*s*; 1136; 1170; 1255*s*; 1304; 1355; 1401; 1410*s*; 1438*s*; 1449; 1497; 1560; 1575; 1709; 1761; 1835; 1887; 1953; 2020; 2283; 2457; 2639; 2809; 2899; 2960*s*; 3067; 3175; 3731; 4237; 4425; 4740; 4885; 5052; 5208; 5265; 5385*s*; 5422*s*; 5523; 5582*s*; 5715*s*; 5875*s*; 5945*s*; 5955; 5990; 6065; 6108; 6235; 6420; 6560; 6650; 6775; 6840; 7000; 7088*s*; 7135; 7245; 7294; 7810; 8285; 8410*s*; 8745; 9100.

Hexamethyldisilylmethylene $(CH_3)_3Si\cdot CH_2\cdot Si(CH_3)_3$

658; 687*s*; 732; 766*s*; 785*s*; 829; 846*s*; 871; 946; 1054*s*; 1083; 1164; 1251*s*; 1295; 1309; 1315; 1342; 1351; 1400; 1422*s*; 1447; 1462; 1490; 1522; 1560; 1602; 1689; 1776; 1821; 1865; 1890; 1926; 2032; 2304; 2344; 2380; 2470; 2653; 2695; 2832; 2873; 2906; 2967*s*; 3105; 3205; 3649; 3731; 3968; 4202; 4310; 4464; 4890; 4930; 4975; 5015; 5235; 5285; 5385*s*; 5415*s*; 5550; 5600*s*; 5690*s*; 5840*s*; 5880*s*; 6010; 6060; 6180; 6360; 6530; 6695; 6810; 6950; 7120*s*; 7240; 7415; 7855; 8220; 8395*s*; 8595; 8740; 8850; 9020.

Trimethylphenylsilane $(CH_3)_3Si\cdot C_6H_5$

693; 698*s*; 728*s*; 756*s*; 767; 789; 826; 841*s*; 853; 980; 999; 1013; 1066; 1100; 1123*s*; 1161; 1188; 1249*s*; 1258; 1298; 1307; 1314; 1338; 1414; 1432*s*; 1479; 1534; 1575; 1592; 1613; 1640; 1686; 1742; 1795; 1845; 1862; 1908; 1961; 2032; 2267; 2471; 2649; 2786; 2817; 2906; 2967*s*; 3012; 3064; 3169; 3676; 3795; 4085; 4740; 4885; 5052; 5208; 5265; 5385*s*; 5422*s*; 5523; 5582*s*; 5715*s*; 5875; 5945*s*; 5955; 5990; 6065; 6108; 6235; 6420; 6560; 6650; 6775; 6840; 7000; 7088; 7135*s*; 7245; 7295; 7810; 8285; 8410*s*; 8745*s*; 9100.

[a] Frequencies followed by *s* refers to strong absorption maxima.

V. DISCUSSION

The vibrational spectra of all compounds investigated show a number of similarities. In order to correlate some of the observed frequencies with the corresponding vibrational modes, the hexamethyldisilane molecule was examined in some detail since it is the simplest of these molecules and therefore most amenable to calculations. Because of several coincidences of Raman and infrared frequencies the D_{3d} symmetry was excluded for hexamethyldisilane, and the assignments were made on the basis of either a D_{3h} or a $D_{3h'}$ model, the experimental data being insufficient to differentiate between them. A plot of depolarization factor *vs* frequency over the broad Raman band at 180 cm^{-1} showed clearly (Fig. 3) that it was a superposition of both polarized and depolarized components. Other strong and polarized Raman bands were observed at 638 and at 404 cm^{-1}. It therefore appeared reasonable to identify 200, 404, and 638 cm^{-1} with the three type A_1 fundamentals. Approximate force constants were calculated from these values and employed for the calculation by a simple valence force model of the two frequencies of type A_2 which are infrared-active only. The values so obtained were sufficiently close to the observed frequencies of 328 and 610 cm^{-1} to permit their identification. New improved force constants were obtained from the five frequencies now assigned and were employed for the calculation and subsequent identification of the three skeletal Raman and infrared-active type E frequencies at 216, 244 and 690 cm^{-1}. The strong Raman bands at 180, 578, and 883 cm^{-1} were assigned to the type E' fundamentals which are Raman active only. The results of the above reasoning are summarized in Table III.

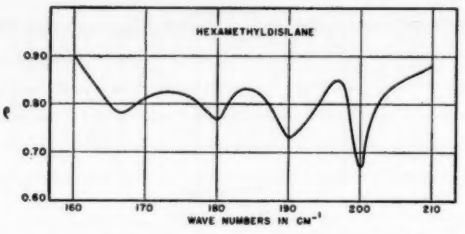

FIG. 3. Resolution of the broad Raman band of hexamethyldisilane at 180 cm^{-1}.

The frequencies of the three low-lying infrared fundamentals had been predicted by us by calculation before

TABLE III. Skeletal fundamental frequencies of hexamethyldisilane.[a]

Species	Observed Raman displacement (cm^{-1})	Observed infrared frequency (cm^{-1})
A_1	200	
	638	
	404	
A_2		328
		610
E	216	216
	251	244
	686	690
E'	180	
	578	
	883	

[a] On the basis of a D_{3h} model.

we had the good fortune of being presented with the spectrum of the 25–50 micron region (Fig. 1) which had been obtained with the new CsI prism by Dr. E. K. Plyler and his co-workers at the National Bureau of Standards. It was very gratifying to us to see our predictions fulfilled.

Figure 4 shows the Raman bands of intensity ratio greater than about 0.05 for convenient comparison between compounds. The most intense (and polarized) bands of all compounds fall into a regular sequence and by analogy with the spectrum of the hexamethyldisilane molecule can be assigned to the symmetrical Si—C stretching vibration. Most of the other bands fall at nearly the same wave numbers for different compounds, and this fact can be interpreted as an indication of similar symmetries. Thus the spectra of hexamethyldisiloxane,[5] hexamethyldisilylmethylene, and hexamethyldisilazine are almost identical and also in most features resemble the spectrum of hexamethyldisilane. Trimethylphenylsilane has a different spectrum because of the widely different symmetry of this molecule; thus it exhibits the characteristic phenyl frequency at 992 cm^{-1}. However, the molecule does retain some of the same frequencies as are present in the others, e.g., the depolarized bands at 200 cm^{-1}, 700 cm^{-1}, and 870 cm^{-1}, which therefore can probably be assigned to Si—C vibrations. It might be interesting to note that all of these compounds except trimethylphenylsilane possess a weak Raman band at 69–87 cm^{-1}. This band could perhaps be due to a torsional mode of vibration about the Si—C bond.

Similar correlations can be made from the infrared spectra (Figs. 1 and 2).

The near-infrared spectra of all these compounds are nearly identical. This is to be expected since most of the bands in this region are known to be due to higher harmonics of the C—H stretching vibrations in methyl groups. The outstanding differences are the 6600 cm^{-1} band in hexamethyldisilazine which is clearly a manifestation of the N—H bond present, the 5950 and 8745 cm^{-1} frequencies in trimethylphenylsilane which undoubtedly are ascribable to the aromatic C—H bond, and the 5600 and 8220 cm^{-1} frequencies in hexamethyldisilylmethylene which are ascribable to CH_2.

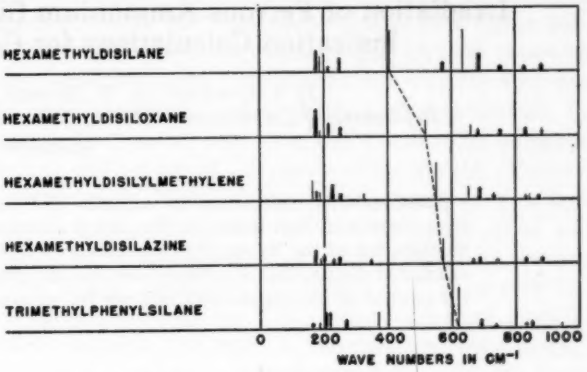

FIG. 4. Characteristic bands in the Raman spectra of related silanes.

An interesting feature which is present in all these near-infrared spectra and which has not been found in hydrocarbons according to our experience, is the doublet consisting of bands at 5380 and 5415 cm^{-1}. It seems most likely that this structure is related to the presence of silicon in these molecules. Because of the constancy of this frequency it might be possible to use it as a criterion for the presence of Si—C bonds.

ACKNOWLEDGMENT

We wish to express our sincere appreciation to Mr. S. S. Kurtz, Jr., of the Sun Oil Company for making available to us the facilities of the spectroscopic laboratory and to Mr. McEvoy for construction of the Raman tubes. We also wish to thank Dr. E. K. Plyler and his co-workers at the National Bureau of Standards for the long-wavelength spectrum.

[5] The infrared spectrum has been reported by N. Wright and M. Hunter, J. Am. Chem. Soc. **69**, 803 (1947).

Irradiation of Ferrous Ammonium Sulfate Solutions: Energy Absorption and Ionization Calculations for Cobalt 60 and Betatron Radiation

D. V. CORMACK,* R. W. HUMMEL,† H. E. JOHNS,* AND J. W. T. SPINKS†
Departments of Chemistry and Physics, University of Saskatchewan, Saskatoon, Saskatchewan, Canada
(Received July 24, 1953)

Solutions of ferrous ammonium sulfate in 0.8N H_2SO_4 have been irradiated with Co^{60} gamma rays and with x-rays from a 25-Mev betatron. The energy absorbed per unit volume of solution has been calculated from a modification of the Bragg-Gray formula, $E_v = J_v W \rho$ in which the factor ρ was determined according to a calculated distribution of primary electron energies. The chemical yield was then calculated in terms of G, the number of ferrous ions oxidized per 100 ev absorbed.

INTRODUCTION

SOLUTIONS of ferrous ammonium sulfate have often been recommended and used as chemical dosimeters for x- and gamma rays. Chemical systems are particularly useful for determinations of integral dose in large or awkward volumes. However, recent determinations of the number of ferrous ions oxidized per 100 ev absorbed in the solution (G) have varied by about 25 percent. Miller[1] and Hardwick[2] have found G values of about 20, while Hochanadel and Ghormley[3] have found G to be about 15.6. It was considered of some interest to calculate G values for our irradiations, based on the distribution of electron energies at a point in the irradiated systems.

EXPERIMENTAL

The ferrous ammonium sulfate solutions were prepared with water distilled once from alkaline permanganate solution and once from alkaline manganous hydroxide suspension, and with c.p. sulfuric acid distilled from a potassium dichromate solution. Freshly prepared solutions were always used. All glassware was Pyrex and cleaned with hot chromic-acid solution followed by multiple rinses with double-distilled water.

TABLE I. Results of irradiations of ferrous ammonium sulfate solutions.

Radiation source	Yield ($\mu M/L/kr$)		Remarks
1.2 curies Co^{60}	16.8		Pyrex tubes
1.2 curies Co^{60}	17.4		Pyrex tubes
1000 curies Co^{60}	17.3	17.1 ± 0.3	Pyrex tubes
1000 curies Co^{60}	16.7		Pyrex tubes
1000 curies Co^{60}	17.3		Pyrex tubes
1000 curies Co^{60}	17.0		Pyrex tubes
1000 curies Co^{60}	17.0		Polystyrene tubes
1000 curies Co^{60}	17.3		Polystyrene tubes
Betatron (18–24.5 Mev)	16.4 ± 0.4		Pyrex tubes Mean of 13 runs
Betatron, 23 Mev	16.1		Polystyrene tubes } done simul-
Betatron, 23 Mev	16.3		Pyrex tubes } taneously

Analyses before and after irradiations were either (1) for ferrous ions by the orthophenanthroline method, using a molar extinction coefficient $\epsilon = 11550$ at 510 mμ on a Beckman DU spectrophotometer, or (2) for ferric ions using their absorption at 304 mμ, where $\epsilon = 2213$. In the latter case the determination of ϵ and subsequent analyses were done with solutions at room temperatures (24 ± 2°C).

The experimental arrangements for irradiations with the betatron and with the Co^{60} source are described elsewhere.[4,5]

The number of ferrous ions oxidized was in all cases found to be directly proportional to the dose received. The slopes of the straight lines thus obtained were calculated by the method of least squares and are given in Table I in terms of the number of micromoles of ferrous ions oxidized per liter of solution per 1000 roentgens as measured with a Victoreen r meter.

In Table I the errors quoted are standard deviations from the mean. Most of the irradiations were made with solutions in Pyrex tubes, but some irradiations in polystyrene tubes were also made and the results of these are included in the table. Their significance will be discussed below.

In carrying out the chemical experiments doses were measured with a 100 r Victoreen chamber in a Pyrex test tube placed in a Lucite block. For the betatron the front wall of this block was about 3 cm thick and for the cobalt, 5 mm thick. This was necessary to build up electronic equilibrium. The walls of the chamber were thus composite, consisting, in the case of the betatron, of 3-cm Lucite, 1 mm of Pyrex, and about 1 mm of red Bakelite with an inner coating of conducting carbon. The collecting electrode in the Victoreen is an aluminum wire, and this must also be considered as part of the wall. It would be very difficult to calculate the ratio of the energy absorbed by the solution to the ionization produced inside the Victoreen chamber if the effects of each of the different layers of wall material were considered. In the theory developed below the ratio of the energy absorbed in the solution to the ionization in a small air cavity in the solution is calculated assuming

* Department of Physics, University of Saskatchewan.
† Department of Chemistry, University of Saskatchewan.
[1] N. Miller, J. Chem. Phys. **18**, 79 (1950).
[2] T. J. Hardwick, Can. J. Chem. **30**, 17 (1952).
[3] C. J. Hochanadel and J. A. Ghormley, J. Chem. Phys. **21**, 880 (1953).
[4] R. W. Hummel and J. W. T. Spinks, Can. J. Chem. **31**, 250 (1953).
[5] Hummel, VanCleave, and Spinks (to be published).

the system to consist only of solution and the cavity within it. Since it is impossible to measure the ionization in such a cavity, a number of experiments have been carried out in an effort to relate the ionization and chemical yield in the actual system with that produced in such an idealized system.

(a) A small ionization chamber, 5-mm outside diameter and 1 cm long, made of "air-wall"[6] material, was connected to an integrating radiation meter. The walls of this chamber were 0.5 mm thick, the minimum thickness which could be achieved. The chamber was placed in a water-filled hole in the Lucite block and and irradiated with betatron radiations to obtain a reading of the ionization current. A close-fitting "air-wall" sleeve 0.5 mm thick was then added and a second reading obtained. A final reading was made with the wall thickness of the chamber equal to 2.0 mm. The thick wall chamber gave a reading about 0.5 percent higher than the reading with the thinnest possible wall. The difference is of the same order of magnitude as the possible experimental error. Since for 25-Mev peak energy betatron radiations the first 0.5 mm of wall contributes only about 20 percent of the total ionization and since the "air-wall" material and water have similar effective atomic numbers and electron densities, it seems reasonable to assume that if the air wall material had been reduced to zero thickness, giving a water wall, the observed ionization current would have been the same to within about 1 percent.

(b) In the following discussion the chemical yield per unit dose of betatron radiation will be compared with that produced by cobalt radiation. Measurements of the ionization were made with a Victoreen 100 r chamber inserted in a Pyrex tube. The ionization current in such a chamber might not show the same dependence on radiation energy as the current produced in an air cavity surrounded by solution. To test this, the thin-walled chamber described above was placed in a water-filled test tube in the Lucite block and irradiated with the two radiation sources. At the same time the dose was measured in the standard way with the Victoreen. For both cobalt and betatron radiation, the ratio of the Victoreen reading to that of the thin-walled chamber was the same to within 0.5 percent, indicating that the Victoreen and "water wall" chambers had the same energy dependence, and hence that the ionization measurements made with the Victoreen could be used to compare the chemical results obtained with the two radiations.

(c) Finally the question arose as to whether the walls of the solution holder could change the chemical yield and yet leave the ionization produced inside the Victoreen essentially unaltered. To test this, solutions of ferrous ammonium sulfate were irradiated in polystyrene tubes with dimensions closely similar (11-mm inner diameter) to those of the Pyrex tubes. When the irradiated solutions were in Pyrex tubes the dose was measured with the Victoreen thimble in a Pyrex tube. For irradiation of solutions in polystyrene tubes the dose determinations were carried out with the Victoreen in an polystyrene tube. With Co^{60} irradiations the measured dose per unit time was found to be independent of the nature of the surrounding sheath (Pyrex or polystyrene). With 23-Mev peak energy x-rays from the betatron the measured dose per unit time with polystyrene was about 2 percent lower than the dose with Pyrex. Similarly, the chemical change with Co^{60} radiations showed no "wall effect" whereas with 23-Mev peak energy x-rays the chemical change was about 1.2 percent lower in polystyrene tubes than in Pyrex tubes. The net effect of these changes in the immediately adjacent wall was about 1 percent, which is considered within the experimental error.

From these experiments we conclude that the chemical yield per measured dose would have been essentially the same had the system been a simple one containing only the solution and air cavity. The error involved in making the assumption is not likely more than 2 to 3 percent, and this is about the size of the unavoidable experimental error.

ENERGY ABSORPTION AND CAVITY IONIZATION

The amount of energy absorbed in a material exposed to radiation may be related to the ionization produced in a small gas-filled cavity in the material. This relation may be expressed by the familiar formula due to Gray;[7] that is, $J=\mathcal{E}/W\rho$ where J is the ionization produced per unit volume of the gas in the cavity, $\mathcal{E}$ is the energy absorbed per unit volume of the material, W is the energy required to form an ion pair in the gas, and ρ is the ratio of the stopping power of the material to that of the gas. In general, the quantity ρ is a function of electron energy, and it is the purpose of the present discussion to show how an average value of ρ may be determined for a given radiation. Values of the ratio $\mathcal{E}/J$ have been calculated for $0.8N$ H_2SO_4 irradiated with Co^{60} and 24 Mev betatron radiations. The method for determining $\mathcal{E}/J$ theoretically and the numerical calculations will be given in detail in the following sections because the method is somewhat new.

Theoretical Expressions for $\mathcal{E}$ and J

When a material of atomic number Z is irradiated, electrons of all energies up to a certain maximum value are set in motion. Let us consider the energy distribution of electrons at some point P in the material. Let $N(E)dE$ represent the number of electrons which pass through one cm^2 at P with energies between E and $E+dE$. The values of $N(E)$ for particular radiations will be calculated later. The energy $d\mathcal{E}$ given up by electrons of energy E to $E+dE$, by collisional processes (ionization and excitation) per unit volume of the

[6] Moulded plastic material developed at the Hammersmith Hospital, London, England.

[7] L. H. Gray, Proc. Roy. Soc. (London) **A156**, 578 (1936).

material at P is given by

$$d\mathcal{E}=\left(\frac{dE}{dx}\right)_z^{\text{coll}}\cdot N(E)dE, \tag{1}$$

where $(dE/dx)_z^{\text{coll}}$ is the linear stopping power, in Mev/cm, for an electron of energy E in material of atomic number Z. Most of the energy lost by electrons by collisional processes is absorbed in the immediate neighborhood of P, whereas the energy lost by electrons by bremsstrahlung may be absorbed at a considerable distance from P. It will be assumed that the energy lost by the electrons by collisional processes, given by Eq. (1), is equal to the energy locally absorbed in the material. It is with this locally absorbed energy that we wish to relate the ionization in a cavity.

For convenience let $S_z^{\text{coll}}(E)$ represent the collisional stopping power $(dE/dx)_z^{\text{coll}}$ of the material of atomic number Z. By integrating equation (1) over all energies which electrons possess as they pass P, the total energy $\mathcal{E}$ absorbed per cm³ at P is obtained, i.e.,

$$\mathcal{E}=\int S_z^{\text{coll}}(E)\cdot N(E)dE. \tag{2}$$

Similarly, the ionization produced per cm³ of air in a small cavity in the material, at P, may be found. Assuming that the cavity is so small that its presence does not disturb the energy distribution of electrons in the material and assuming also that an electron loses a very small fraction of its energy in crossing the cavity, the ionization produced per cm³ of air, J, is given by

$$J=\int\frac{S_a^{\text{coll}}(E)\cdot N(E)dE}{W}, \tag{3}$$

where $S_a^{\text{coll}}(E)$ is the collisional stopping power of air for electrons of energy E and W is the average energy loss by collisional processes in producing one ion pair. The value of W is usually assumed to be independent of energy above about 60 kev, in which case it may be taken outside the integral sign of Eq. (3).

Combining Eqs. (2) and (3) the ratio between energy absorbed per unit volume of material and the ionization produced per unit volume of air in a minute cavity surrounded by the material is obtained. Thus,

$$\frac{\mathcal{E}}{J}=W\frac{\int S_z^{\text{coll}}(E)\cdot N(E)dE}{\int S_a^{\text{coll}}(E)\cdot N(E)dE}. \tag{4}$$

If expression (4) is compared with the formula due to Gray, it is seen that the quantity ρ in Gray's formula has been replaced by an average value $\bar{\rho}$, given by

$$\bar{\rho}=\frac{\int S_z^{\text{coll}}(E)\cdot N(E)dE}{\int S_a^{\text{coll}}(E)\cdot N(E)dE}. \tag{5}$$

If the ratio $S_z^{\text{coll}}(E)/S_a^{\text{coll}}(E)$ is considered constant with energy, expression (5) reduces to

$$\bar{\rho}=S_z^{\text{coll}}(E)/Sa^{\text{coll}}(E)=\rho.$$

This simplified form has generally been used in Gray's formula. For convenience the value of the ratio $S_z^{\text{coll}}(E)/S_a^{\text{coll}}(E)$ for a particular energy E will be denoted by the symbol $\rho(E)$. If one is dealing with a wide distribution of energies, the ratio $\rho(E)$ may vary considerably and $\bar{\rho}$ as given by Eq. (5) should be used as the ρ in Gray's formula.

Determination of the Electron Energy Distribution, $N(E)$

In order to evaluate the quantity $\bar{\rho}$ given in Eq. (5) it is necessary to know the distribution of electron energies at the point in the material under consideration. A method of determining such distributions has been given in a previous paper.[8] A simpler and more accurate method has since been devised and will be explained below.

Consider the distribution of electrons produced in material of atomic number Z irradiated with x or gamma radiation. The electrons will be set in motion with some distribution of initial energies. We shall denote the number of electrons set in motion with initial energies between E_i and E_i+dE_i by the symbol $N(E_i)dE_i$. Such an initial distribution can be obtained from the differential cross sections for the photoelectric, Compton, and pair production effects. Tables of these cross sections have been given by Davisson and Evans[9] for pair production and by Johns *et al.*[10] for Compton electrons. The initial distribution of electron energies $N(E_i)$ should be clearly distinguished from the distribution of energies of electrons crossing one cm² at a point in the material $N(E)$ which is required in the evaluation of Eq. (4). A relation between the distributions $N(E_i)$ and $N(E)$ may be found as follows.

Let us assume that the electrons set in motion by the radiation travel in straight lines in one direction. Consider the distribution of electrons crossing unit area (1 cm²) at the origin P in Fig. 1. Let X be the range of an electron with energy E and $X+dx$ be the range of

[8] D. V. Cormack and H. E. Johns, Brit. J. Radiol. **25**, 369 (1952).
[9] C. M. Davisson and R. D. Evans, Revs. Modern Phys. **24**, 79 (1952).
[10] Johns, Cormack, Denesuk, and Whitmore, Can. J. Phys. **30**, 556 (1952).

electron with energy $E+dE$. Thus electrons which pass P with energies between E and $E+dE$ will come to rest at distances between X and $X+dX$ from P in the element shown. The electrons which pass P and come to rest in this element will be those which initially had ranges greater than X (i.e., energies greater than E). The number of electrons set in motion per cm³ with energies greater than E is given by

$$A=\int_{E}^{E_{i\,\max}} N(E_i)dE_i.$$

Under equilibrium conditions this is also the number of electrons which come to rest in one cm³ having initially had energies greater than E. Hence the number of electrons which come to rest in the element dx having passed through one cm² at P is Adx. This is equal to $N(E)dE$, the number of electrons which pass through one cm² at P with energies between E and $E+dE$. That is

$$N(E)dE=dx\int_{E}^{E_{i\,\max}} N(E_i)dE_i.$$

FIG. 1. Diagram showing the development of the theoretical expression for the electron energy distribution $N(E)$.

The number of electrons crossing one cm² at P per unit energy interval $N(E)$ may then be found by dividing by dE.

$$N(E)=\frac{dx}{dE}\int_{E}^{E_{i\,\max}} N(E_i)dE_i.$$

The expression dx/dE is the differential rate of change of range with energy for electrons of energy E and is the reciprocal of the total stopping power of the material $S_Z{}^{\text{total}}(E)$. That is

$$N(E)=\frac{1}{S_Z{}^{\text{total}}(E)}\int_{E}^{E_{i\,\max}} N(E_i)dE_i. \qquad (6)$$

The total stopping power $S_Z{}^{\text{total}}(E)$ is the sum of the stopping powers for collisional and radiative processes; that is

$$S_Z{}^{\text{total}}(E)=S_Z{}^{\text{coll}}(E)+S_Z{}^{\text{rad}}(E).$$

The argument given above to obtain Eq. (6) may be extended to take into account electrons travelling irregular paths in all directions for a system in which the energy converted into electronic motion per unit volume is equal to the energy lost by electrons per unit volume.

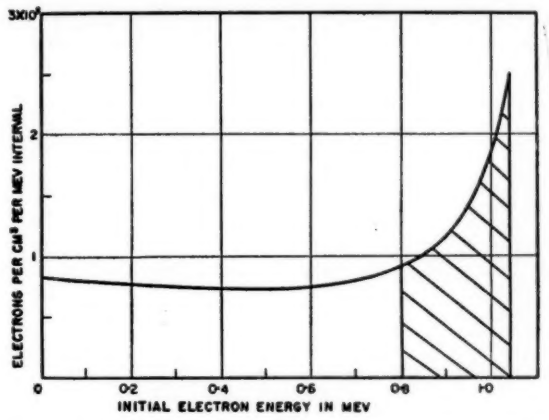

FIG. 2. Initial energy distribution of electrons set in motion in $0.8N$ H_2SO_4 by Co^{60} gamma rays (average energy 1.25 Mev). The ordinates correspond to an incident dose of one roentgen unit.

Numerical Calculations

(a) *Absorption of Co^{60} Radiation in Sulfuric Acid*

In order to compare chemical dosimetry methods of measuring energy absorption with ion chamber techniques, it is necessary to know the value of the ratio $\mathcal{E}/J$ for each of the radiations used. This ratio has been determined for the absorption of Co^{60} gamma rays in $0.8N$ H_2SO_4 since the chemical measurements under consideration here have been carried out under these conditions.

The radiation from Co^{60} consists of two gamma rays of energy 1.172 and 1.332 Mev, emitted in cascade. For these calculations, however, it is sufficiently accurate to consider the radiation to have an average energy of 1.25 Mev. The initial distribution of electron energies produced by Co^{60} radiation has the form given in Fig. 2.[10] Assuming equilibrium conditions in the region surrounding a point in the H_2SO_4 solution, the distribution of electron energies at the point may be determined from Eq. (6).

In the actual physical arrangement, however, we are not dealing with conditions at a point surrounded by an equilibrium thickness of solution. A point in the center of the solution is surrounded by a layer of solution, the wall of the test tube holding the solution, and the Lucite block which holds the test tube. The energy distribution of electrons at this point will not generally be exactly the same as for a point surrounded by an equilibrium thickness of solution. However, since all the materials making up the wall are of approximately the same effective atomic number, the change in electron distribution will be small. In any case, the distribution function $N(E)$ appears in both numerator and denominator of the expression for $\mathcal{E}/J$ and thus the value of $\mathcal{E}/J$ is quite insensitive to changes in $N(E)$. We thus feel justified in using values of $N(E)$ calculated for equilibrium conditions. The experiments previously described indicate that the ionization produced per unit volume of air in a small air cavity in the solution is approximately

TABLE II. Calculation of energy absorption ($\mathcal{E}$) and cavity ionization (J) for 0.8N H_2SO_4 irradiated with Co^{60} radiation.

$$\frac{\mathcal{E}}{J}=W\frac{\int S_z^{\text{coll}}N(E)dE}{\int S_a^{\text{coll}}N(E)dE}$$

E (Mev)	$N(E)$ $\left(\frac{1}{\text{cm}^3\cdot\text{Mev}}\right)$	S_z^{coll} $\left(\frac{\text{Mev}}{\text{cm}}\right)$	$N(E)\cdot S_z^{\text{coll}}$ $\left(\frac{1}{\text{cm}^3}\right)$	$S_z^{\text{coll}}/S_a^{\text{coll}}$ ρ	S_a^{coll} $\left(\frac{\text{Mev}}{\text{cm}}\right)$	$N(E)\cdot S_a^{\text{coll}}$ $\left(\frac{1}{\text{cm}^3}\right)$
0.05	1.26×10^{7}	7.67	9.66×10^{7}	979	7.83×10^{-3}	9.87×10^{3}
0.15	2.38	3.67	8.74	965	3.80	9.06
0.25	2.81	2.85	8.01	960	2.97	8.34
0.35	2.88	2.50	7.20	957	2.61	7.52
0.45	2.76	2.31	6.38	955	2.42	6.68
0.55	2.54	2.21	5.62	953	2.32	5.90
0.65	2.23	2.14	4.77	951	2.25	5.02
0.75	1.88	2.10	3.95	950	2.21	4.16
0.85	1.42	2.07	2.94	949	2.18	3.10
0.95	0.84	2.05	1.72	948	2.16	1.81
1.02	0.25	2.05	0.51	947	2.16	0.22

$$\mathcal{E}=\int S_a^{\text{coll}}N(E)dE=5.92\times10^{7}\ \text{Mev/cm}^3$$

$$\int S_a^{\text{coll}}N(E)dE=6.17\times10^{4}\ \text{Mev/cm}^3$$

$$\bar{\rho}=\frac{\int S_z^{\text{coll}}N(E)dE}{\int S_a^{\text{coll}}N(E)dE}=960$$

$$\frac{\mathcal{E}}{J}=\frac{32.5\times960}{4.80\times10^{-10}}=6.50\times10^{13}\ \frac{\text{ev/cm}^3\text{ of solution}}{\text{esu/cm}^3\text{ of air at 0°C}}$$

equal to the ionization produced per unit volume in a Victoreen chamber placed in the same position as the test tube of solution. The values of $\mathcal{E}/J$ calculated for a small air cavity in 0.8N H_2SO_4 were therefore used to determine the absorbed energy from the Victoreen readings. The errors introduced by this procedure should not be greater than 2 percent.

For Co^{60} radiation, the distribution of electrons, $N(E)$, at a point surrounded by an equilibrium thickness of H_2SO_4, was determined by the evaluation of Eq. (6). That is, the area under the curve shown in Fig. 2, from $E_i=E$ to $E_i=E_i(\text{max})$, was found and the value of this area was divided by $S_z^{\text{total}}(E)$, the total stopping power for electrons of energy E in 0.8N H_2SO_4. Values of the latter were determined using the Bethe-Bloch formula[11] for collisional stopping power, $S_z^{\text{coll}}(E)$, and the Heitler formula for energy loss by bremsstrahlung, $S_z^{\text{rad}}(E)$.

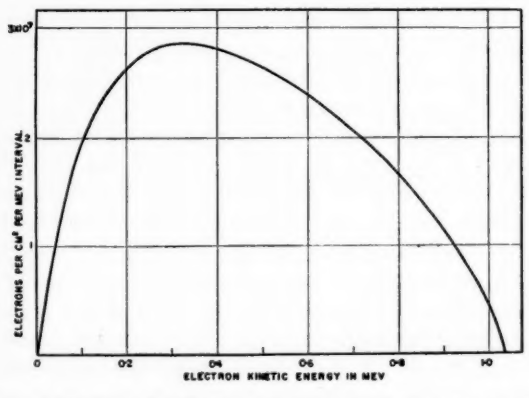

FIG. 3. Energy distribution of electrons at a point in 0.8N H_2SO_4 irradiated with Co^{60} gamma rays. Ordinates normalized to one roentgen.

The value of the average excitation energy used in the Bethe-Bloch formula was determined on the basis of ionization chamber measurements made by Gray.[12] For electrons set in motion by radium gamma rays, Gray gives a value of 1.055 for the ratio between the stopping power of a gelatin solution and the stopping power of graphite. Assuming that the stopping power of the gelatin solution is equal to that of water and taking a value of 75 ev for the average excitation potential of of carbon, based on a summary given by Aron,[13] a value of 43 ev is obtained for the average excitation potential of water. This value is in good agreement with the values given by Platzmann[14] deduced from the stopping power of alpha particles in water. The presence of sulfuric acid increases the value of the average ionization potential to 45 ev for 0.8N H_2SO_4. In calculating the stopping power due to bremsstrahlung, the effective atomic number of 0.8N H_2SO_4 is 6.74. A value of 1.024 was used for the specific gravity of 0.8N H_2SO_4.

The energy distribution of electrons $N(E)$, produced by Co^{60} radiation in the acid was determined from Eq. (6) using the values given above and this distribution is

[11] See W. Heitler, *The Quantum Theory of Radiation* (Oxford University Press, London, 1944.)
[12] L. H. Gray, Brit. J. Radiol. **22**, 677 (1949).
[13] W. A. Aron, University of California Radiation Laboratory Report UCRL 1325 (1951).
[14] In *Symposium on Radiobiology* (John Wiley and Sons, Inc., New York, 1952), p. 108.

shown in Fig. 3. The values of $N(E)$ are normalized for a total radiation flux of one roentgen unit. The roentgen is defined as the radiation flux which when absorbed in air produces by ionization 1 esu of charge per 0.001293 g of air. Knowing the real absorption coefficient of air and the energy required to produce an ion pair (W), the energy or photon flux equivalent to one roentgen may be found. This definition of the roentgen is perfectly satisfactory for theoretical calculations but is difficult to realize experimentally.

Once the energy distribution $N(E)$ has been obtained the value of the ratio $\mathcal{E}/J$ may be determined using Eq. (4). The method of calculation is shown for Co^{60} radiation in Table II. The values of S_z^{coll} for $0.8N$ H_2SO_4 were calculated from the Bethe-Bloch formula, using 45 ev as the average excitation potential. The values of S_a^{coll} were determined in a similar way, using 96 ev as the average exciation potential for air.[15] The areas under the curves of $N(E)\cdot S_z^{\text{coll}}(E)$ and $N(E)\cdot S_a^{\text{coll}}(E)$ plotted *versus* E were determined by numerical methods and are given in the lower part of the table. The quantity $\rho(E)\doteq S_z^{\text{coll}}(E)/S_a^{\text{coll}}(E)$ has the value 960 for electrons of 0.25 Mev. Thus one might regard the electrons produced by Co^{60} in $0.8N$ H_2SO_4 as having an effective energy of 0.25 Mev.

The value of the ratio of energy absorption to ionization was found from Eq. (4) and is shown in the last line of Table II. For Co^{60} radiation the value of $\mathcal{E}/J$ was found to be 6.50×10^{13} ev/cm³ of solution per esu/cm³ of air. W was taken as 32.5 ev per ion pair for air.[12]

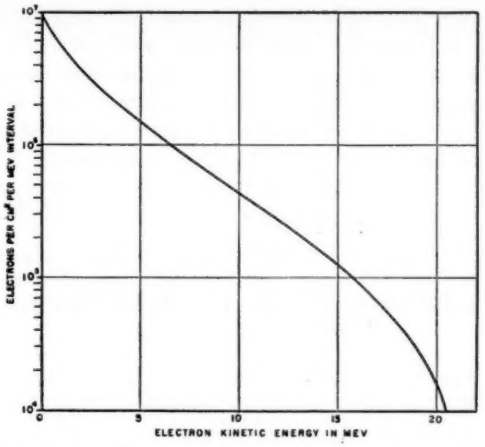

FIG. 4. Energy distribution of electrons at a point in $0.8N$ H_2SO_4 irradiated with 24-Mev bremsstrahlung from betatron. Ordinates normalized to one roentgen.

(b) *Absorption of 24-Mev Betatron Radiation in Sulfuric Acid*

The value of the ratio $\mathcal{E}/J$ of energy absorbed to ionization produced was also determined for betatron bremsstrahlung with a maximum energy of 24 Mev. The calculation of $\mathcal{E}/J$ is shown in Table III. The initial energy distribution of electrons $N(E_i)$ was determined by the method described by Cormack and Johns.[8] From this, the distribution of electrons at a point in $0.8N$ H_2SO_4, $N(E)$, was determined from Eq. (6) and is given in the second column of Table III.

The distribution $N(E)$ is also shown graphically in Fig. 4. It will be noted that this distribution has its

TABLE III. Energy absorption ($\mathcal{E}$) and cavity ionization (J) for $0.8N$ H_2SO_4 irradiated with 24-Mev betatron radiation.

E (Mev)	$N(E)$ $\left(\frac{1}{\text{cm}^2\ \text{Mev}}\right)$	S_z^{coll} $\left(\frac{\text{Mev}}{\text{cm}}\right)$	$N(E)S_z^{\text{coll}}$ $\left(\frac{1}{\text{cm}^3}\right)$	$S_z^{\text{coll}}/S_a^{\text{coll}}$ ρ	S_a^{coll} $\left(\frac{\text{Mev}}{\text{cm}}\right)$	$N(E)S_a^{\text{coll}}$ $\left(\frac{1}{\text{cm}^3}\right)$
0.5	6.92×10^6	2.26	15.64×10^6	953	2.37×10^{-3}	16.41×10^3
1.5	4.42	2.04	9.02	944	2.16	9.56
2.5	2.98	2.07	6.17	941	2.20	6.56
3.5	2.18	2.13	4.64	938	2.27	4.95
4.5	1.65	2.18	3.60	936	2.33	3.85
5.5	1.26	2.23	2.81	935	2.39	3.01
7	0.873	2.28	1.99	934	2.44	2.13
9	0.544	2.34	1.27	932	2.51	1.36
11	0.338	2.39	0.808	931	2.57	0.868
13	0.211	2.425	0.512	930	2.61	0.551
15	0.124	2.46	0.305	929	2.65	0.328
17	0.066	2.49	0.164	929	2.68	0.177
19	0.028	2.52	0.071	928	2.71	0.077

$$\mathcal{E}=\int S_z^{\text{coll}}N(E)dE=5.22\times10^7\ \text{Mev/cm}^3$$

$$\int S_a^{\text{coll}}N(E)dE=5.54\times10^4\ \text{Mev/cm}^3$$

$$\bar{\rho}=\frac{\int S_z^{\text{coll}}N(E)dE}{\int S_a^{\text{coll}}N(E)dE}=942$$

$$\frac{\mathcal{E}}{J}=\frac{32.5\times942}{4.80\times10^{-10}}=6.38\times10^{13}\ \frac{\text{ev/cm}^3\text{ of solution}}{\text{esu/cm}^3\text{ of air at 0°C}}$$

[15] O. Halpern and H. Hall, Phys. Rev. **73**, 477 (1948).

maximum value at zero energy and falls very rapidly. This is because the spectrum of photons from the betatron has a very high maximum at low energies. The average value of the stopping powers of solution and air, $\bar{\rho}$, was determined by a numerical integration and was found to be 942. This corresponds to an electron energy of about 2 Mev. The value of $\mathcal{E}/J$ for 24 Mev betatron radiation was determined to be 6.38×10^{13} ev/cm³ of solution per esu/cm³ or air.

Reduction in Energy Absorption Due to Polarization Effects

The values calculated in the preceding sections for the absorbed energy are based on the assumption that the Bethe-Bloch formula for collisional stopping power of electrons is valid for all the energies considered. The theoretical considerations of Fermi,[16] Halpern and Hall,[15] and Sternheimer[17] predict a reduction in the collisional loss at high energies due to polarization and conduction effects in condensed media. Halpern and Hall give a correction curve for water which may be used to correct the Bethe-Bloch formula to allow for these effects.

The distribution of electrons at a point in H_2SO_4 was redetermined using values of the stopping power applying the Halpern-Hall correction. The ratio of energy absorbed to ionization produced was then redetermined also, the values being as follows: for Co^{60} radiation, 6.45×10^{13} ev/cm³ of solution per esu/cm³ of air and for 24-Mev betatron radiation, 6.01×10^{13} ev/cm³ of solution per esu/cm³ of air. It will be seen that applying the Halpern and Hall corrections decreases the value of $\mathcal{E}/J$ for Co^{60} radiation by only 1 percent, whereas it decreases the value for the betatron radiation by 6 percent.

RESULTS

A summary of the results of the chemical experiments and numerical calculations is given in Table IV, where the numbers in column 2 are taken from Table I. Column 3 shows the calculated ratios of the energy absorbed in the solution to the ionization produced in air, calculated from the Bethe-Bloch formula alone (B.-B.) and from that formula modified by the factors taken from Halpern and Hall (H.-H.). Column 4 shows the resultant G values. It is seen that, using the unmodified Bethe-Bloch formula the G value is 2 percent lower for betatron radiation than for Co^{60}, whereas using the Halpern and Hall values, G is 3 percent higher for the betatron than for Co^{60}. These variations are of the order of magnitude of the experimental errors, and we may conclude that for both types of radiation the chemical yield is 15.9 ± 0.4 ions oxidized per 100 ev absorbed. This is in good agreement with the results of Hochanadel and Ghormley,[3] who found $G = 15.6$ using a calorimetric determination of energy absorption and $G = 16.7$ using a cavity ionization method similar to that used by Miller[1] and later by Hardwick.[2] Our results do not agree with those of Miller, who found $G = 20.3$, of Hardwick, who found $G = 20.4$, or of Rigg *et al.*,[18] who found $G = 20.0$. There is no immediately apparent reason for the discrepancy, although application of the electron distribution principle to Hardwick's tabulated data reduces his G value from 20.4 to 18.3. Hochanadel and Ghormley[3] have suggested that irradiations in polystyrene cells may yield high results because of the presence of organic impurities derived from the wall material. It has been found here that high results are obtained in polystyrene tubes which are new, but after "aging" by continued irradiation (tubes filled with water or solution) the G values gradually decrease until constant values are obtained. The results quoted in Table I for irradiations in polystyrene tubes were obtained in "aged" tubes.

Our calculated G values would be lower if, in the calculations, some allowance was made for ionization due to absorption of scattered radiation, since in that case the electron distributions would become even more peaked at low energies than the distribution calculated here.

It would be useful to have more reliable values for the stopping power for electrons in order to make a more accurate comparison since much of the uncertainty in the values of G arises from uncertainties in the stopping powers.

Two of the authors (D. V. C. and R. W. H.) would like to express their appreciation to the National Research Council of Canada for studentships which helped make this study possible. Financial assistance from the Defence Research Board of Canada and the National Cancer Institute of Canada is gratefully acknowledged.

TABLE IV. Summary of results.

Radiation source	Yield ($\mu M/L/kr$)	$\mathcal{E}/J$ $\left(\frac{\text{ev/cc}}{\text{esu/cc}}\right)$	G (ions oxidized/ 100 ev)
Co^{60}	17.1	6.50×10^{13} (B.-B.)	15.8
		6.45×10^{13} (H.-H.)	16.0
Betatron	16.4	6.38×10^{13} (B.-B.)	15.5
		6.01×10^{13} (H.-H.)	16.4

[16] E. Fermi, Phys. Rev. **57**, 485 (1940).
[17] R. M. Sternheimer, Phys. Rev. **88**, 851 (1952).
[18] Rigg, Stein, and Weiss, Proc. Roy. Soc. (London) **A211**, 375 (1952).

THE JOURNAL OF CHEMICAL PHYSICS VOLUME 22, NUMBER 1 JANUARY, 1954

Kinetics of Isotope-Exchange Reactions of Fluorine with Some Halogen Fluorides*

RICHARD M. ADAMS,† RICHARD B. BERNSTEIN,‡ AND JOSEPH J. KATZ
Chemistry Division, Argonne National Laboratory, Lemont, Illinois

(Received August 19, 1953)

Quantitative kinetic data on the isotope-exchange reaction of fluorine with chlorine trifluoride, bromine pentafluoride, and iodine heptafluoride have been obtained using F^{18} ($t_{\frac{1}{2}}=112$ min) tracer. The materials were handled in a metal vacuum line, and the exchanges were carried out in a 2-liter nickel reaction vessel at three temperatures in the range 181–257°C. While the experimental data do not uniquely determine the mechanism, they strongly suggest that exchange takes place either through a heterogeneous catalysis by the metal fluoride coating on the walls of the reaction vessel, or by a combination of the heterogeneous mechanism plus a homogeneous gas-phase exchange in those cases where a measurable amount of dissociation of the halogen fluoride occurs at the temperature of exchange. It has been shown to be unlikely that the observed exchanges take place through either an atomic mechanism or a purely homogeneous mechanism. It has also been shown that all fluorine atoms in the halogen fluoride molecules are exchangeable.

I. INTRODUCTION

THE radioactive nuclide F^{18} has been used in three previous investigations of the exchangeability of fluorine between various fluorine-containing molecules.

Dodgen and Libby[1] found a measurable amount of exchange at about 200°C between fluorine and hydrogen fluoride; the reaction was postulated to occur primarily through heterogeneous catalysis. Rogers and Katz[2] employed F^{18} to study the exchange between hydrogen fluoride and some halogen fluorides. Exchange was found to be practically instantaneous at room temperature in the gas phase, and it was postulated that reaction took place via a homogeneous mechanism involving the formation of relatively stable molecular complexes.

Recently a qualitative investigation of the gas-phase exchange between some halogen fluorides and elemental fluorine has been carried out by Bernstein and Katz.[3] The results indicated that there was no exchange below about 100°C, but that measurable rates of exchange occurred above 200°C.

The present study was undertaken to obtain quantitative kinetic data leading to the elucidation of the mechanisms of the fluorine-halogen fluoride exchanges.

II. MATERIALS AND APPARATUS

Anhydrous chlorine trifluoride and bromine pentafluoride were obtained from Harshaw Chemical Company. Iodine heptafluoride was prepared by the method of Schumb and Lynch.[4] The compounds were purified before use, and vapor pressures and molecular weight determinations (see Table I) were used to establish their purity. Fluorine (Pennsylvania Salt Company) was used directly from the tank. Analysis showed a fluorine content of 93.5±1.0 percent. Mass spectrometric analysis indicated that the inert residual 6.5-percent impurity was essentially air. Certain check experiments were run with another cylinder of fluorine of 100±1 percent purity in order to determine that the air had no effect on the results.

Lithium fluoride (used in the preparation of samples for irradiation to produce F^{18} activity) was Baker's Analyzed Reagent Grade, with a chloride impurity of 0.002 percent. Aluminum oxide used in the preparation of these samples was Linde, synthetic gem quality, Type A-5175, with a maximum chloride impurity of 0.002 percent. It is important that the chloride impurity in these compounds be as low as possible, because an interfering Cl^{38} activity is produced by neutron irradiation.

The 112-minute nuclide F^{18} was prepared by the nuclear reaction[5] $O^{16}(t,n)F^{18}$ by irradiating a mixture of Al_2O_3 and LiF with thermal neutrons in a nuclear pile.[3] The usual procedure was to irradiate about 1.5 grams of an equimolar mixture for 7 hours and allow 4 hours cooling time before the first count. This ratio of

TABLE I. Physical properties of halogen fluorides.

XF_n	Vapor pressure (mm) Obs	Calc	t°C	Molecular weight Obs	Calc
ClF_3	47	47.5[a]	−40	92.21	92.46
IF_7	600	617[b]	0	260.7	259.9
BrF_5	370	375[c]	23	···	174.9

[a] Grisard, Bernhardt, and Oliver, J. Am. Chem. Soc. 73, 5725 (1951).
[b] O. Ruff and R. Keim, Z. anorg. u. allgem. Chem. 193, 176 (1930).
[c] O. Ruff and W. Menzel, Z. anorg. u. allgem. Chem. 202, 49 (1931).

* Presented in part before the national meeting of the American Chemical Society in Chicago, Illinois, September, 1953. Further details may be found in Argonne National Laboratory Report No. ANL-5046 (April, 1953).

† This paper is abstracted from a Ph.D. thesis submitted to the Graduate School of Illinois Institute of Technology by R.M.A.

‡ Department of Chemistry, Illinois Institute of Technology, Participating Institution Program. Present address: Department of Chemistry, University of Michigan, Ann Arbor, Michigan.

[1] H. W. Dodgen and W. F. Libby, J. Chem. Phys. 17, 951 (1949).

[2] M. T. Rogers and J. J. Katz, J. Am. Chem. Soc. 74, 1375 (1952).

[3] R. B. Bernstein and J. J. Katz, J. Phys. Chem. 56, 885 (1952).

[4] W. C. Schumb and M. A. Lynch, Ind. Eng. Chem. 42, 1383 (1950).

[5] Knight, Novey, Cannon, and Turkevich, *National Nuclear Energy Series* (McGraw-Hill Book Company, Inc., New York, 1951), Div. IV, Vol. 9, Book 3, Paper 326.

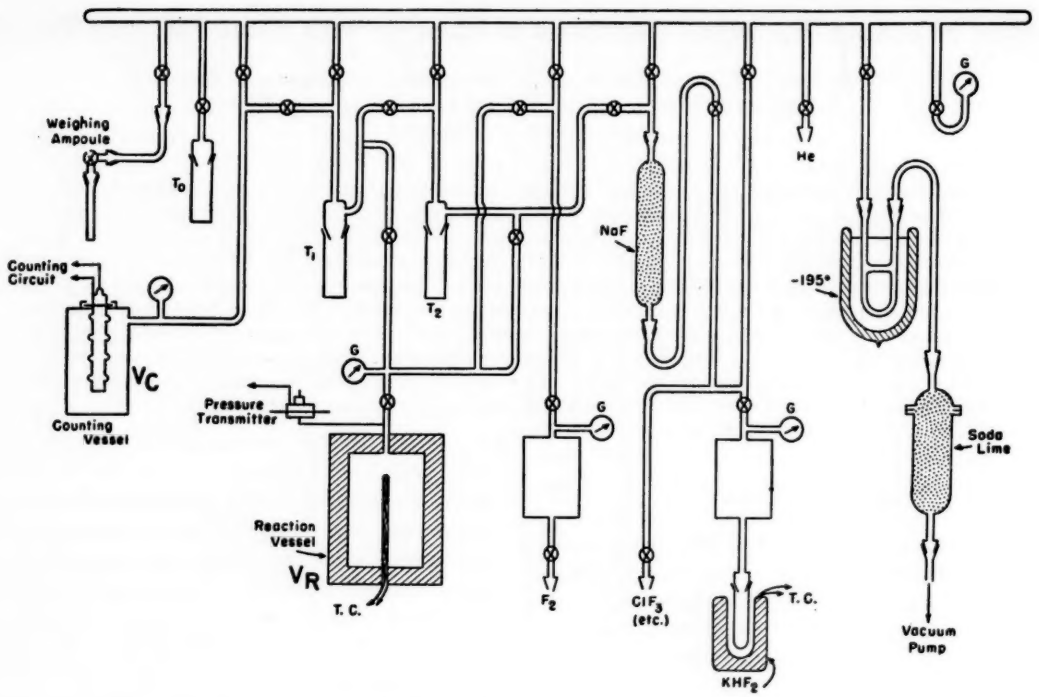

FIG. 1. Apparatus for studying fluorine exchange reactions.

irradiation to cooling time was adopted in order to minimize the Cl^{38} activity ($t_{\frac{1}{2}}=38$ min) and to maximize the F^{18} activity. By this procedure it was possible to produce at least 5000 counts/min of F^{18} activity at the time of initial counting, with less than 1 percent contamination from the Cl^{38} activity. The radiochemical purity of the activity was determined by following the decay of F^{18}, which gave a half-life of 112 ± 1 minutes, over a period of 4 to 5 half-lives (twice the length of an average experiment). A negligible amount of a long-lived activity with approximately a 30-hour half-life (probably a mixture of Br^{80} and Br^{82}) was observed to be present also.

F^{18} was counted as elemental gaseous fluorine or as the appropriate gaseous halogen fluoride in a 350-ml nickel vessel using a Victoreen 1B85 aluminum Thyrode as a counting tube. A vacuum-tight seal was made between the counting tube and the nickel vessel with a Fluorothene gasket and a compression screw. The solder joint of the Thyrode was protected by Fluorothene wax and, when properly prepared, the tube could be used for 3 or 4 months before failure occurred because of corrosion at the solder joint. A Nuclear Instrument and Chemical Company Scaler, Model 165, was used for counting.

The exchange experiments were all conducted in a vacuum line (see Fig. 1) constructed of copper and nickel with silver-soldered and flared connections. Cold traps T_0, T_1, and T_2 were machined from $\frac{3}{4}$-inch Fluorothene rod. Helicoid gauges equipped with Monel-metal Bourdon tubes were used to read rough pressures. Precise pressure measurements were made using a Booth-Cromer[6] nickel diaphragm null-type pressure transmitter with an external pressure balancing system.

The 2184-ml reaction vessel *VR* was made of nickel with all joints nickel-welded. It was heated electrically and completely insulated with asbestos. Temperature variation along the length of the vessel, observed by means of thermocouples at each end and one in a central thermocouple well, was less than 0.5°C. The temperature in any given experiment was constant to ±0.5°C. A duplicate of this vessel, with a removable gasketed cap on one end through which additional material could be added, was used in certain experiments in which surface effects were studied.

III. EXCHANGE PROCEDURE AND ERRORS

A description of a typical exchange experiment follows. A sample of irradiated $LiF-Al_2O_3$ is placed in Fluorothene trap T_0 and evacuated. The proper amount of purified halogen fluoride, XF_n, is frozen on to the $LiF-Al_2O_3$ mixture and allowed to warm to room temperature under its own vapor pressure. After the solid-liquid exchange is complete (10 to 20 minutes), the XF_n* is removed and further purified if necessary. It is then expanded into the counting vessel *VC*, and the decay of F^{18} is followed for about $\frac{1}{2}$ hour. The XF_n* is transferred to the reaction vessel *VR*, which is at equilibrium at the temperature chosen for reaction, and the desired quantity of F_2 is introduced by expansion from a tank. After a suitable exchange time at a constant temperature, the mixture of gases is separated quanti-

[6] S. Cromer, U. S. Atomic Energy Commission Declassified Document MDDC-803, June, 1944.

tatively by expansion into the evacuated counting vessel through traps T_2 and T_1 immersed in liquid nitrogen baths to remove the halogen fluoride. The activity of the F_2* fraction is determined, after which it is discarded. The XF_n* fraction is then introduced into the counting vessel and its activity determined.

The total inventory of F^{18} was usually better than 95 percent, and the small losses were shown to be due primarily to exchange with the metal fluoride coating. The gas-phase exchange was calculated by means of the recoverable total activity, i.e., the sum of the F_2* and XF_n* activities after exchange.

Assignment of an over-all error to the rate measurements is difficult. Nevertheless, from an estimate of determinate errors, and from a comparison of the results of duplicate experiments, it is believed that those rates obtained in experiments with a contact time greater than 10 minutes are reliable to better than ± 10 percent; those rates obtained with contact times of 10 minutes or less are probably reliable to better than ± 20 percent.

IV. CALCULATIONS

Using the method of McKay,[7] the rate of exchange has been shown[3] to be

$$R=\frac{2.303}{t}\left(\frac{2nab}{na+2b}\right)\log\left(\frac{1}{1-f}\right), \qquad (1)$$

where R = exchange rate; t = contact time; f = fraction exchanged in time t; n = subscript in XF_n; a = moles/liter of XF_n in reaction vessel; and b = moles/liter of F_2 in reaction vessel.

Concentrations of BrF_5 and F_2 have been calculated from observed temperatures and pressures by means of the ideal gas law, which was demonstrated experimentally to be obeyed by these gases. In the case of ClF_3 and IF_7, small corrections have been applied where necessary to the primary data to take into account known facts about their behavior. The data of Schmitz and Schumacher[8] were used to calculate dissociation and association corrections for ClF_3. The data of Bernstein and Katz[3] were used to calculate dissociation corrections for IF_7.

The fraction exchanged was calculated from the relationship $f=G/\beta$, where G is the fraction of the total activity in the fluorine gas, and β is the atomic fraction of fluorine in the form of elemental fluorine in the mixture. The use of this relationship assumes that all the fluorine atoms in the halogen fluoride molecules are exchangeable. This was proved experimentally to be true for all three halogen fluorides used.[9]

TABLE II. ClF_3-F_2 exchange data at 467°K.

Exp.	Temp. (°K)	Time (min)	ClF_3 ($\times 10^3$)	F_2[b] ($\times 10^3$)	Percent exchange	R[c] ($\times 10^5$)
A. Experiments at constant F_2 concentration.[a] $F_2=8.31\pm0.08\times10^{-3}$.						
41	467	37	0.35	8.12	76.9	3.93
36	467	60	0.85	8.48	71.9	4.70
39	467	60	0.85	8.35	78.3	5.65
37	467	32	0.84	8.19	59.6	6.20
34	468	66	1.27	8.36	67.7	5.32
40	467	60	1.73	8.35	52.8	4.96
23	467	60	2.58	8.40	37.3	4.12
26	468	60	4.11	8.31	27.2	3.75
27	468	70	7.37	8.20	22.3	3.40
43	467	69	9.29	8.32	18.3	3.05
29	468	67	11.90	8.26	14.0	2.54
24	467	60	15.76	8.43	12.7	2.81
B. Experiments at constant ClF_3 concentration. $ClF_3=7.41\pm0.03\times10^{-3}$.						
27	468	70	7.37	8.20	22.3	3.40
2	464	35	7.43	11.70	12.5	4.36
30	468	60	7.40	18.13	22.9	5.96
31	468	70	7.42	18.13	24.7	5.58
32	468	72	7.45	27.34	28.6	7.44
33	467	65	7.36	36.20	32.4	10.19

[a] All concentrations given in this paper are in moles liter^{-1}.
[b] All fluorine concentrations have been corrected by the purity factor of the fluorine used.
[c] Units of R throughout this paper are moles liter^{-1} min^{-1}.

TABLE III. ClF_3-F_2 exchange data at 497°K.

Exp.	Temp. (°K)	Time (min)	ClF_3 ($\times 10^3$)	F_2 ($\times 10^3$)	Percent exchange	R ($\times 10^4$)
A. Experiments at constant F_2 concentration. $F_2=8.87\pm0.14\times10^{-3}$.						
35	497	20	0.61	9.02	86.0	1.63
38	498	20	0.61	8.91	88.9	1.83
22	497	20	0.91	8.97	85.1	2.25
13	497	32	2.01	8.75	82.5	2.44
16	498	32	2.47	8.81	76.2	2.34
15	498	32	3.08	8.74	67.3	2.11
12	497	30	4.07	8.85	62.2	2.34
17	497	32	4.88	8.88	53.5	1.92
10	495	31	7.68	8.96	42.9	1.82
11	498	31	10.81	8.74	34.9	1.57
128	496	60	10.91	8.45	51.2	1.41[a]
127	497	30	10.94	8.53	33.0	1.58[a]
14	496	34	15.45	9.39	29.4	1.31[a]
9	497	33	16.23	8.61	35.3	1.77
8	496	42	16.58	8.72	37.0	1.42
129	496	30	38.35	8.43	28.5	1.67[a]
B. Experiments at constant ClF_3 concentration. $ClF_3=3.13\pm0.03\times10^{-3}$.						
21	498	52	3.16	2.84	71.3	0.86
15	498	32	3.08	8.74	67.3	2.11
19	497	32	3.14	9.71	66.9	2.19
18	497	32	3.16	16.58	80.6	3.78
20	498	22	3.11	26.28	78.7	5.57

[a] R values corrected to $F_2=8.87\times10^{-3}$ using a smooth curve drawn through the fluorine-dependence data given in Part B of this table.

[7] H. A. C. McKay, Nature **142**, 997 (1938).

[8] H. Schmitz and H. J. Schumacher, Z. Naturforsch. **2A**, 362 (1947).

[9] Assume an equimolar mixture of F_2 and ClF_3 in which F^{18} is present initially (in small concentration) only in the ClF_3. If all three fluorine atoms in ClF_3 are exchangeable, then after complete exchange, the probability that the F_2 now contains F^{18} is 2/5, and the probability that the ClF_3 now contains F^{18} is 3/5. Thus, $G=2/5$; and since $\beta=2/5$, then $f=1$. If, however, only two of the

TABLE IV. ClF_3-F_2 exchange data at 530°K.

Exp.	Temp. (°K)	Time (min)	ClF_3 ($\times10^3$)	F_2 ($\times10^3$)	Percent exchange	R ($\times10^4$)
A. Experiments at constant F_2 concentration. $F_2=6.99\pm0.11\times10^{-3}$.						
47	533	8.0	0.58	6.97	89.8	4.39
48	530	8.0	0.74	7.15	92.6	6.26
46	529	11	1.43	6.89	95.3	9.09
45	532	11	2.34	5.31[a]	87.0	9.45[a]
44	529	11	5.25	7.10	74.7	9.34
49	528	10	14.19	6.83	57.2	8.78
B. Experiments at constant ClF_3 concentration. $ClF_3=5.25\times10^{-3}$.						
45	532	11	2.34[b]	5.31	87.0	7.87
44	529	11	5.25	7.10	74.7	9.34
50	527	10	5.23	29.39	91.6	30.70

[a] R value for this run corrected to $F_2=6.99\times10^{-3}$ using a smooth curve drawn through the data in Part B of this table.
[b] This run included here because R changes by only about 1 percent from $ClF_3=2.34\times10^{-3}$ to 5.25×10^{-3} (see Fig. 2).

V. RESULTS AND DISCUSSION

The results of the kinetic studies of the exchanges are given in Tables II through X and in Figs. 2 through 7. The dependence of the rate on the XF_n concentration shows a maximum at all three temperatures in the BrF_5-F_2 exchange, with the maximum becoming less pronounced in the ClF_3-F_2 and IF_7-F_2 exchanges until it almost disappears in the latter. The dependence of the rate on the F_2 concentration is linear for all the exchanges, but it is to be noted that there is a nonzero intercept in the case of the ClF_3-F_2 and IF_7-F_2 exchanges.

Since it is known that ClF_3 and IF_7 dissociate, it is reasonable to suppose that a dissociative mechanism is partly responsible for the exchange observed in these cases. Thus, in the case of ClF_3, dissociation and recombination as in

$$ClF_3^* \xrightarrow{k_1} ClF+F_2^*, \tag{1a}$$

$$ClF+F_2 \xrightarrow{k_{-1}} ClF_3 \tag{1b}$$

TABLE V. IF_7-F_2 exchange data at 454°K.

Exp.	Temp. (°K)	Time (min)	IF_7 ($\times10^3$)	F_2 ($\times10^3$)	Percent exchange	R ($\times10^4$)
A. Experiments at constant F_2 concentration. $F_2=13.88\pm0.11\times10^{-3}$.						
108	454	71	3.33	13.82	36.2	0.82
107	454	66	7.25	13.77	31.5	1.02
109	454	74	11.38	14.04	31.6	1.07
B. Experiments at constant IF_7 concentration. $IF_7=7.28\pm0.03\times10^{-3}$.						
107	454	66	7.25	13.77	31.5	1.02
110	454	61	7.30	31.21	28.7	1.56

three fluorine atoms in ClF_3 are exchangeable in the gas phase, there are two important cases to be considered: Case (a), only two F atoms exchange with the solid mixture to introduce F^{18}, and only two exchange in the gas phase with F_2; Case (b), all three F atoms exchange with the solid, but only two exchange in the gas phase. Case (a) would lead to a calculated 125 percent exchange, whereas (b) would lead to 83.4 percent. Experimentally, exchanges calculated on the basis that all the fluorine atoms were exchangeable were observed to range from 98 to 103 percent.

will result in exchange. Moreover, the experimental data reveal that there is some similarity between the ClF_3-F_2 and the IF_7-F_2 exchanges, and that these are different from the BrF_5-F_2 exchange. However, the dissociative mechanism alone cannot account for the entire amount of exchange observed, for if it is assumed that the rate-determining step is (1a), i.e., $k_1 \ll k_{-1}$, then the rate of the exchange would be independent of the (F_2) and linearly dependent on (ClF_3), which is contrary to the experimental facts.

The maximum in the graphs of the rate *vs* XF_n concentration suggests that the mechanism is complex, and that some part of the exchange may be heterogeneous, being surface-catalyzed by the metal fluoride coating always present on the surface of the reaction vessel. Let it be assumed that exchange takes place either by a heterogeneous path or by a combination of a heterogeneous plus a homogeneous path, i.e., that the total rate is the sum of the components

$$R_{tot}=R_{het}+R_{hom}. \tag{2}$$

TABLE VI. IF_7-F_2 exchange data at 467°K.

Exp.	Temp. (°K)	Time (min)	IF_7 ($\times10^3$)	F_2 ($\times10^3$)	Percent exchange	R ($\times10^4$)
A. Experiments at constant F_2 concentration. $F_2=14.89\pm0.28\times10^{-3}$.						
94	469	61	1.40	14.84	80.9	1.95
93	468	61	3.28	14.64	65.7	2.25
91	467	61	3.86	15.11	51.3	1.68
86	467	61	6.78	15.16	56.7	2.53
92	468	56	13.10	14.35	56.3	3.34
95	467	62	19.78	15.21	67.2	4.49
B. Experiments at constant IF_7 concentration. $IF_7=3.73\pm0.21\times10^{-3}$.						
98	468	61	3.67	3.15	78.7	1.29
96	467	61	3.91	6.26	56.9	1.19
93	468	61	3.28	14.64	65.7	2.25
91	467	61	3.86	15.11	51.3	1.68
97	467	61	3.94	28.94	61.3	2.91

If the heterogeneous exchange takes place by the competitive adsorption mechanism (the Langmuir[10]-Hinshelwood[11] type), and the homogeneous exchange occurs via the dissociative mechanism, the total rate becomes

$$R_{tot}=\frac{k_2x(F_2)y(XF_n)}{[1+x(F_2)+y(XF_n)]^2}+k_1(XF_n), \tag{3}$$

where x and y are adsorption coefficients of F_2 and XF_n, respectively, and k_2 is the rate constant for the heterogeneous exchange. This may be simplified if the assumption[12] is made that fluorine is much less strongly adsorbed than the halogen fluorides. Equation (3) may

[10] I. Langmuir, Trans. Faraday Soc. **17**, 621 (1921).
[11] C. N. Hinshelwood, *Kinetics of Chemical Change* (Oxford University Press, New York, 1940), p. 178.
[12] This assumption is justified by the fact that little or no exchange of activity between F_2^* and the metal fluoride coating on the walls was observed (see reference 3).

TABLE VII. IF_7-F_2 exchange data at 497°K.

A. Experiments at constant F_2 concentration. $F_2=8.93\pm0.29\times10^{-3}$.

Exp.	Temp. (°K)	Time (min)	IF_7 ($\times10^3$)	F_2 ($\times10^3$)	Percent exchange	R ($\times10^6$)
100	496	10	3.83	8.97	69.1	1.26
101	497	10	6.13	9.00	72.3	1.62
104	496	8.0	6.66	9.24	61.6	1.59[a]
102	497	8.0	14.00	9.22	84.2	3.59
103	496	4.5	17.42	8.21	66.5	3.52

B. Experiments at constant IF_7 concentration. $IF_7=6.29\pm0.19\times10^{-3}$.

105	497	11	6.15	4.59	89.7	1.56
101	497	10	6.13	9.00	72.3	1.62
104	496	8.0	6.66	9.24	61.6	1.59
106	495	4.8	6.20	25.01	33.4	1.99

[a] 11.0-mm HF added to exchange mixture (4 percent of the total F_2 pressure).

then be written as

$$R_{tot}=\frac{k_2x(F_2)y(XF_n)}{[1+y(XF_n)]^2}+k_1(XF_n). \qquad (4)$$

Qualitatively, Eq. (4) fits the experimental facts; it correctly predicts the observed behavior of the R *vs* (XF_n) curves, and it correctly predicts the linear dependence of the rate on the fluorine concentration. Furthermore, it is to be expected that the temperature dependence of the homogeneous component should be greater than that of the heterogeneous component, and thus that the graphs of R *vs* (XF_n) may flatten out with increasing temperature as in the case of ClF_3, or may even approach a straight line through the origin when the homogeneous component becomes most important, as in the case of IF_7. This is also consistent with the fact that the dissociation-equilibrium constant for IF_7 increases more rapidly with temperature than that for ClF_3, and therefore the homogeneous contribution to exchange in the case of IF_7 could be greater than in the case of ClF_3. In the case of BrF_5 no homogeneous contribution to exchange is expected (except for the possibility that BrF_5 and F_2 may associate to form BrF_7), since BrF_5 is known[3] to be undissociated even at temperatures as high as 400°C. Therefore, the shape of the R *vs* (BrF_5) curves should remain sensibly constant with increasing temperature.

TABLE VIII. BrF_5-F_2 exchange data at 466°K.

A. Experiments at constant F_2 concentration. $F_2=6.32\pm0.05\times10^{-3}$.

Exp.	Temp. (°K)	Time (min)	BrF_5 ($\times10^3$)	F_2 ($\times10^3$)	Percent exchange	R ($\times10^6$)
82	466	60	0.51	6.25	76.6	5.11
81	467	60	0.87	6.26	62.7	5.29
80	466	60	1.47	6.41	46.0	4.80
79	466	60	2.96	6.33	29.8	4.02
78	466	60	5.52	6.35	20.8	3.38

B. Experiments at constant BrF_5 concentration. $BrF_5=5.51\pm0.02\times10^{-3}$.

78	466	60	5.52	6.35	20.8	3.38
84	467	60	5.48	16.39	24.3	6.92
83	466	61	5.54	35.64	33.8	13.49

TABLE IX. BrF_5-F_2 exchange data at 497°K.

A. Experiments at constant F_2 concentration. $F_2=4.62\pm0.11\times10^{-3}$.

Exp.	Temp. (°K)	Time (min)	BrF_5 ($\times10^3$)	F_2 ($\times10^3$)	Percent exchange	R ($\times10^6$)
59	496	15	0.40	4.54	81.4	1.83
57	497	15	0.69	4.54	78.5	2.55
55	497	31	1.25	4.87	83.6	2.22
54	497	31	1.73	4.54	72.2	1.83
51	497	27	4.49	4.54	43.1	1.35
58	496	31	8.45	4.71	39.9	1.27

B. Experiments at constant BrF_5 concentration. $BrF_5=4.48\pm0.01\times10^{-3}$.

51	497	27	4.49	4.54	43.1	1.35
52	495	31	4.48	15.46	64.3	4.31
53	497	31	4.46	32.56	78.7	8.29

Many examples of heterogeneous reactions are known in which the rate is found to decrease with increasing concentration of some component, as is here observed for the dependence of the rate on XF_n concentration. In the combination of ethylene and hydrogen on a copper catalyst, Pease[13] found that the rate decreases with increasing concentration of ethylene, but increases approximately linearly with the hydrogen concentration. More recently, a rate expression similar to the heterogeneous component of Eq. (4) has been postulated by J. Weber and K. J. Laidler[14] to explain the heterogeneous NH_3-D_2 exchange. Their work verified

TABLE X. BrF_5-F_2 exchange data at 529°K.

A. Experiments at constant F_2 concentration. $F_2=3.98\pm0.06\times10^{-3}$.

Exp.	Temp. (°K)	Time (min)	BrF_5 ($\times10^3$)	F_2 ($\times10^3$)	Percent exchange	R ($\times10^6$)
65	529	5.0	0.50	3.96	89.5	8.52
74	529	5.0	0.51	4.10	81.4	6.53
67	528	5.0	0.52	3.80	77.8	5.81
64	529	5.0	0.52	3.98	87.7	8.22
63	530	5.5	0.83	3.82	71.2	6.06
75	529	5.0	1.48	4.10[a]	54.1	6.06
77	529	4.8	1.50	3.94	51.4	5.84
61	528	10	1.82	3.99	78.1	6.46
60	528	10	3.48	4.06	67.9	6.30
73	529	10	3.50	3.98	62.7	5.39
70	529	10	3.48	4.02[a]	58.5	4.84
72	529	10	3.50	4.01[a]	57.3	4.68
66	529	10	8.57	3.95	47.3	4.28
71	529	10	8.62	3.99[a]	47.7	4.36

B. Experiments at constant BrF_5 concentration. $BrF_5=3.49\pm0.01\times10^{-3}$.

60	528	10	3.48	4.06	67.9	6.30
73	529	10	3.50	3.98	62.7	5.39
70	529	10	3.48	4.02[a]	58.5	4.84
72	529	10	3.50	4.01[a]	57.3	4.68
68	529	6.0	3.48	32.07	85.3	43.75

[a] F_2 of 100 percent purity used.

[13] R. Pease, J. Am. Chem. Soc. **45**, 1196 (1923).
[14] J. Weber and K. J. Laidler, J. Chem. Phys. **19**, 1089 (1951).

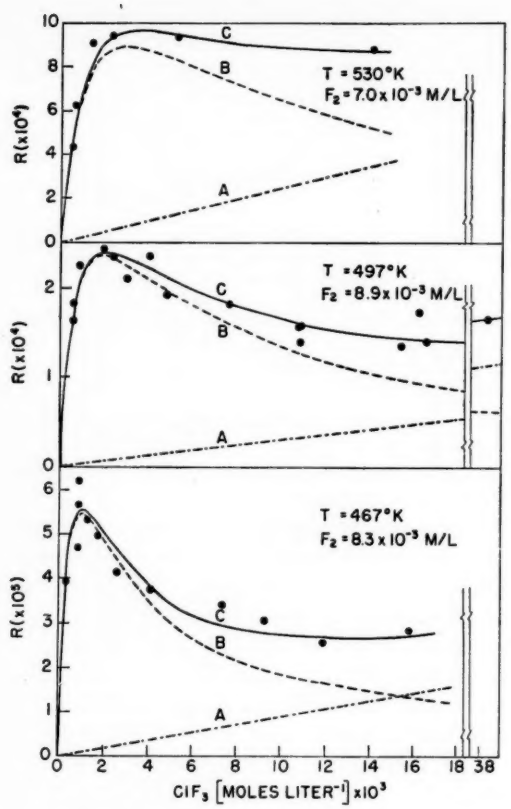

FIG. 2. ClF_3-F_2 exchange. Rate *vs* ClF_3 concentration. A=homogeneous exchange; B=heterogeneous exchange; $C=A+B$; ⊙=experimental data.

the maximum in the dependence of the rate on the ammonia pressure and, incidentally, is considered evidence for the Langmuir-Hinshelwood type of reaction rather than for the Rideal[15] type.

It should be noted that without the homogeneous term in Eq. (4), the R *vs* (F_2) curves should all extrapolate to the origin at zero fluorine concentration. This is not observed in the IF_7 and ClF_3 exchanges whose rates extrapolate to a nonzero intercept. For the BrF_5 exchange, the rate does extrapolate to zero except for the data at the lowest temperature, where, perhaps, the

TABLE XI. Homogeneous and heterogeneous rate constants.

Exchange	T(°K)	k_1(min^{-1})	(k_2x)(min^{-1})
ClF_3-F_2	467	9.4×10^{-4}	0.027
	497	3.0×10^{-3}	0.11
	530	2.5×10^{-2}	0.51
IF_7-F_2	454	1.6×10^{-3}	0.027
	467	2.0×10^{-2}	0.037
	497	2.1×10^{-1}	0.15
BrF_5-F_2	466	···	0.033
	497	···	0.22
	529	···	0.75

[15] E. K. Rideal, Proc. Cambridge Phil. Soc. **35**, 130 (1939); Chemistry and Industry **62**, 335 (1943).

adsorption term for fluorine in the denominator of Eq. (3) may not be negligible. The lower the temperature the more important this term would be.

Since the homogeneous term of Eq. (4) increases linearly with (XF_n), while the heterogeneous term increases to a maximum and then decreases asymptotically to zero, it should be possible at very high XF_n concentrations to find that the rate begins to increase again with increasing (XF_n). An attempt was made to find such behavior in the ClF_3-F_2 exchange at 497°K. Experiment 129 (Table III) was run at a ClF_3 concentration of 38.35×10^{-3} moles liter^{-1}. From Fig. 2 it can be seen that the rate at this concentration is slightly higher than the rate at the flat portion of the curve at lower concentrations. This indicates that the homogeneous contribution to exchange at this temperature

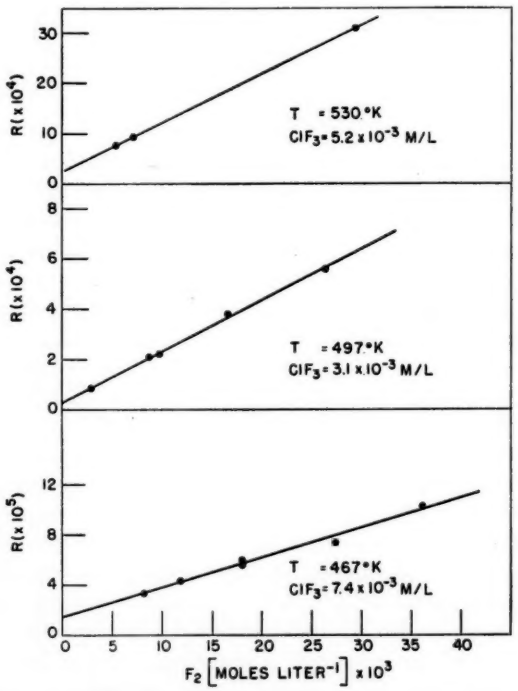

FIG. 3. ClF_3-F_2 exchange. Rate *vs* F_2 concentration.

may be small enough to be neglected in the region of the maximum. It should then be possible to calculate from the observed data the theoretical curve representing the heterogeneous exchange in the following way. Neglecting the homogeneous term, Eq. (4) may be written

$$R=\frac{Ky(XF_n)}{[1+y(XF_n)]^2}, \tag{5}$$

where

$$K=k_2x(F_2). \tag{6}$$

At the maximum, $(XF_n)=1/y$, and therefore

$$R_{max}=0.25K. \tag{7}$$

Knowing the value of R and the XF_n concentration at

the maximum, the value of R at any other concentration may be calculated.

Such a procedure has been followed in calculating the theoretical curves given in Figs. 2 and 4, which show the dependence of the rate on the XF_n concentration in the ClF_3-F_2 and IF_7-F_2 exchanges. It can be seen that the theoretical curves fit the experimental data well. The importance of the homogeneous component increases very rapidly with temperature for the IF_7-F_2 exchange but not for the ClF_3-F_2 exchange. This is probably owing to the fact that the dissociation equilibrium constant for IF_7 increases more sharply with temperature than that for ClF_3.

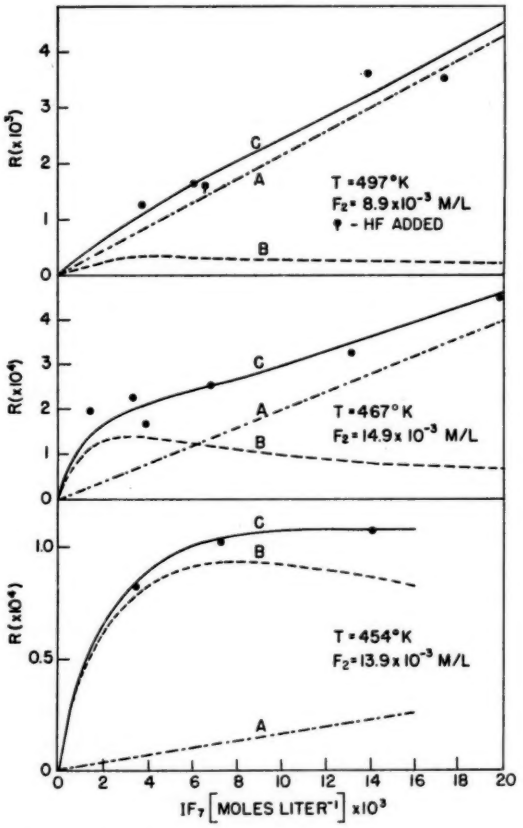

FIG. 4. IF_7-F_2 exchange. Rate *vs* IF_7 concentration. A = homogeneous exchange; B = heterogeneous exchange; $C = A+B$; ⊙ = experimental data.

For the BrF_5-F_2 exchange the theoretical curves given in Fig. 6 represent only the theoretical heterogeneous exchange. The experimental data are represented fairly well on the assumption that all of the exchange is heterogeneous, except at the higher concentrations of BrF_5. The fact that the experimental data all fall above the theoretical curves at high (BrF_5) might indicate that there also exists some homogeneous component to this exchange. A small contribution to exchange of the bimolecular association type would not be inconsistent with the experimental facts, and would also lead to an

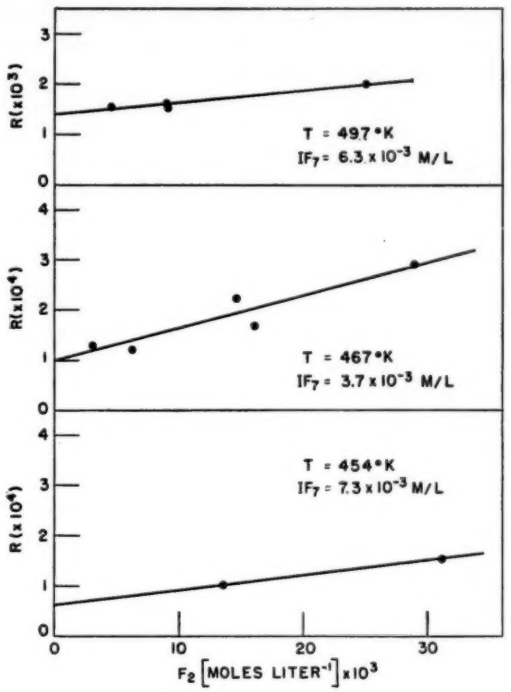

FIG. 5. IF_7-F_2 exchange. Rate *vs* F_2 concentration.

R *vs* (F_2) curve which extrapolates to zero at zero F_2 concentration.

Since the homogeneous and heterogeneous components of the ClF_3-F_2 and IF_7-F_2 exchanges may thus be separated, it is possible to calculate the individual rate constants. The homogeneous rate constant k_1 is the slope of the straight line representing the homogeneous component of the exchange. For the heterogeneous path it is possible to calculate from the theoretical heterogeneous curve only the product of the rate constant times the adsorption coefficient of F_2, k_2x. Values are given in Table XI.

Apparent activation energies may be determined from the variation with temperature of experimental values of R at various concentrations of XF_n. It is also possible to obtain apparent activation energies for the separate homogeneous and heterogeneous components

TABLE XII. Apparent activation energies.

Exchange	E_a(hom) (kcal mole^{-1})	E_a(het) (kcal mole^{-1})	E_a(exp) (kcal mole^{-1})	
			(XF_n)	
ClF_3-F_2	29	24	1×10^{-3}	22.1
			8	26.8
			15	29.0
IF_7-F_2	40	18.5	1×10^{-3}	20.5
			8	33.0
			15	36.4
BrF_5-F_2	...	23	1×10^{-3}	22.2
			5.5	22.4
			10	22.3

of the exchange from the temperature dependence of k_1, and from the temperature dependence of the product (k_2x). These are given in Table XII.

It might be expected that a homogeneous dissociative mechanism should have an activation energy comparable with the heat of dissociation of the halogen fluoride. The heats of dissociation of ClF_3, IF_7, and BrF_5 are 25, 28.5, and >42 kcal per mole.[3] Reference to Table XII shows that E_a(exp) for the ClF_3 and IF_7 exchanges are somewhat lower than ΔH^0 for these halogen fluorides at the lowest concentrations, and much lower than an estimated minimum ΔH^0 for all concentrations in the BrF_5 exchange. The existence of a heterogeneous path for exchange could account for this.

Attempts to find a change in rate due to a change in the nature and/or amount of surface were not entirely successful. A large number of experiments using different surfaces and additional surface area were run. The results were erratic; the largest effect noted was a factor of three in the rate. While the role of the surface in the exchange is not clear, there seems to be no doubt that it is involved in some way. Further work is in progress.

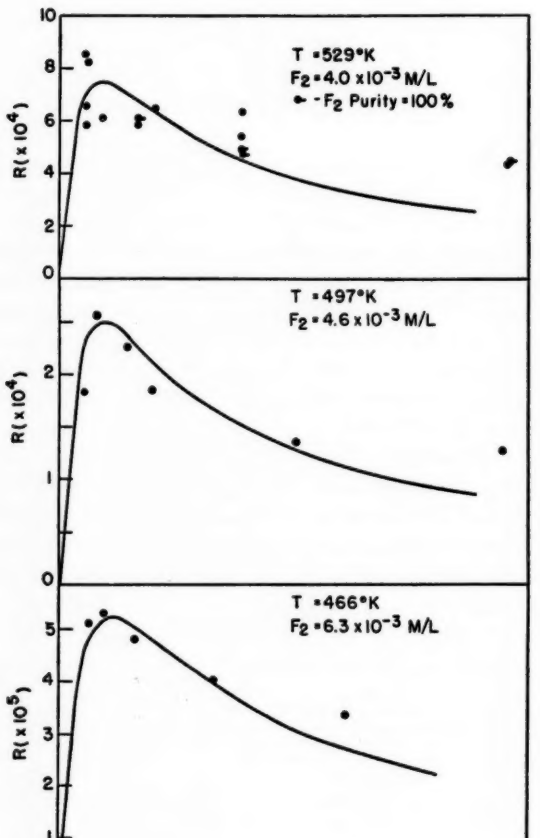

FIG. 6. BrF_5-F_2 exchange. Rate *vs* BrF_5 concentration. —= calculated heterogeneous exchange curve; ⊙ = experimental data.

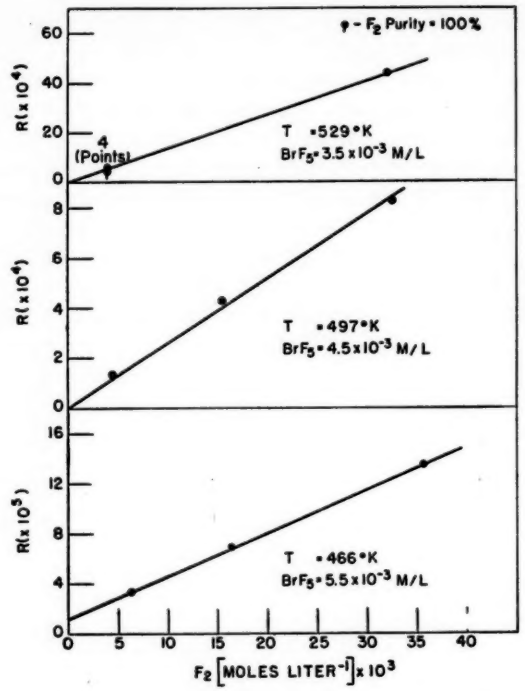

FIG. 7. BrF_5-F_2 exchange. Rate *vs* F_2 concentration.

Similar small surface effects have recently been observed in the deuterium-diborane exchange.[16]

The possibility that the air impurity in the fluorine might be responsible for the observed exchanges was eliminated by the use of fluorine of 100-percent purity in a number of the experiments. The rates thus observed are quite comparable to the rates obtained under similar conditions with the fluorine of 93.5-percent purity. Also, the possibility that some small amount of HF impurity in the fluorine might be responsible for the observed exchanges was eliminated by deliberately adding HF to an exchange mixture to the extent of 4 percent of the fluorine used. Figure 4 shows that the rate thus obtained falls on the smooth curve determined by the other experiments in this series.

A large number of alternative reaction mechanisms of the homogeneous type were considered with no success. For example, a simple homogeneous dissociative mechanism demands that the rate be independent of the fluorine concentration, which is contrary to the observed facts. It is possible, however, to develop a rate equation which qualitatively fits the experimental data by using the method of Spitalsky,[17] which assumes the reversible and simultaneous formation of two different activated complexes between F_2 and XF_n. This approach seems somewhat improbable because, while in the case of the ClF_3-F_2 exchange it might be possible to form a second activated complex between the dimer $(ClF_3)_2$ and F_2, it is difficult to believe that BrF_5 or IF_7 would be capable of forming such complexes.

[16] P. C. Maybury and W. S. Koski, J. Chem. Phys. **21**, 742 (1953).

[17] E. Spitalsky, Z. physik. Chem. **122**, 257 (1926).

A simple atomic mechanism seems likewise improbable, since it would lead to a rate expression involving the square root of the fluorine concentration.[18]

It would thus appear that for the ClF_3-F_2 and IF_7-F_2 reactions the exchange occurs by a combined heterogeneous mechanism of the competitive type and a homogeneous mechanism involving the dissociation of the halogen fluoride. In the case of the BrF_5-F_2 exchange, a competitive heterogeneous mechanism would appear to explain the results.

[18] The concentration of fluorine atoms resulting from thermal dissociation of F_2 may be estimated from the data given by R. N. Doescher [J. Chem. Phys. **20**, 330 (1952)] for the heat of dissociation of F_2. For a F_2 concentration of 12×10^{-3} mole/liter (about 10^{19} molecules/cc at 500°K) in the reaction vessel, there would be about 10^{14} F atoms/cc. This may be compared to the estimate given by Dodgen and Libby (reference 1) of 10^{12} F atoms/cc per 10^{19} F_2 molecules/cc present in the $HF-F_2$ exchange when it is carried out in the presence of ultraviolet light at room temperature, under which conditions no exchange was observed. Although the concentration of fluorine atoms in these exchanges appears to be large enough so that an atomic mechanism might exist, no success has been achieved in devising an atomic mechanism which would give a linear dependence of the rate on the fluorine concentration.

THE JOURNAL OF CHEMICAL PHYSICS VOLUME 22, NUMBER 1 JANUARY, 1954

Symmetry Classification of the Energy Levels of Some Triarylmethyl Free Radicals and Their Cations*

TING LI CHU AND S. I. WEISSMAN
Washington University, St. Louis, Missouri

(Received August 24, 1953)

The absorption and luminescence spectra of triphenylmethyl, tri-p-xenylmethyl, phenyl-di-p-xenylmethyl, diphenyl-p-xenylmethyl, and their cations have been determined. Polarization of the luminescence of each substance under excitation by plane polarized light has been examined. Assignment of symmetry classifications to the energy levels of these substances has been attempted.

IN this paper we describe our studies of the spectra of a set of triarylmethyl free radicals and their positive ions. The experiments consist of observations of the absorption spectra, the fluorescence spectra, and polarizations of the fluorescence spectra under excitation by polarized light. From a combination of these observations and some assumptions which appear to be not excessively bizarre, we have attempted to assign symmetry classifications to the electronic levels of the molecules under study. These molecules are triphenylmethyl, diphenyl-p-xenylmethyl, phenyl-di-p-xenylmethyl, tri-p-xenylmethyl, and their positive ions.

EXPERIMENTAL PROCEDURES

The free radicals were prepared by standard procedures.[1,2] Pure tri-p-xenylcarbinol was provided by Professor Lipkin. Diphenyl-p-xenylcarbinol and phenyl-di-p-xenylcarbinol were prepared by appropriate Grignard reactions. Their melting points were 135°C and 150–151°C (uncorrected), respectively, as compared with the accepted values of 136°C and 151°C. Triphenyl methyl was prepared from commercial triphenyl-chloromethane which had been purified by vacuum sublimation.

The solvent for the free radicals was a mixture of toluene and triethylamine containing 20 percent by volume of triethylamine. The absorption spectra were measured both at room temperature and liquid nitrogen temperature with a Beckman model D. U. spectrophotometer.[3] The spectra at liquid nitrogen temperatures were checked by photography with an A.R.L. grating instrument. The fluorescence spectra were observed only from glassy rigid solutions at liquid nitrogen temperature. These were photographed with a Steinheil spectrograph.

The absorption and luminescence spectra of the free radicals are presented in Figs. 1–5, of the cations in Figs. 6–10.

Polarizations of the fluorescence were determined both by visual observation and by photography. The experimental arrangement, involving excitation in two almost contiguous strips by beams of equal intensity and mutually perpendicular polarization, has been described previously.[4]

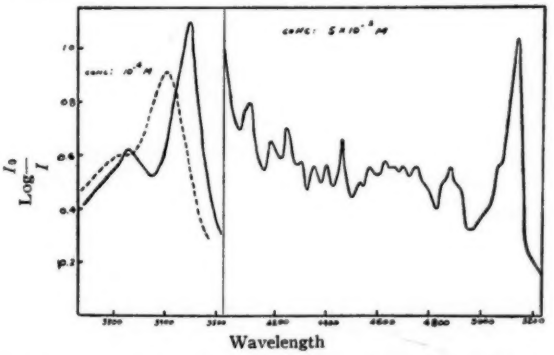

FIG. 1. Absorption spectrum of triphenylmethyl. Dashed curve at room temperature, solid curve at 77°K. One centimeter path length.

* Assisted by the joint program of the U. S. Office of Naval Research and U. S. Atomic Energy Commission.

[1] Lewis, Lipkin, and Magel, J. Am. Chem. Soc. **66**, 1579 (1947).

[2] T. L. Chu and S. I. Weissman, J. Am. Chem. Soc. **73**, 4462 (1951).

[3] The free radicals were prepared under high vacuum. The absorption and fluorescence cells were in every case sealed off.

[4] S. I. Weissman, J. Chem. Phys. **18**, 1258 (1950).

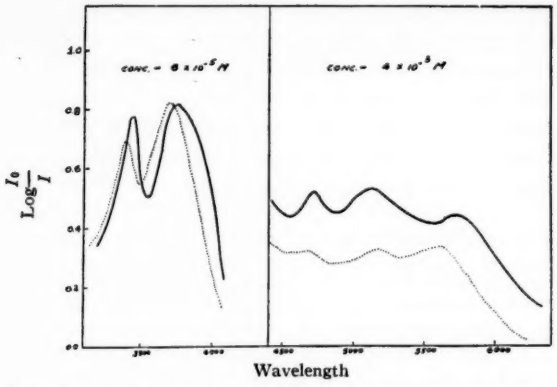

FIG. 2. Absorption spectrum of diphenyl-p-xenylmethyl. Dashed curve at room temperature, solid curve at 77°K. One centimeter path length.

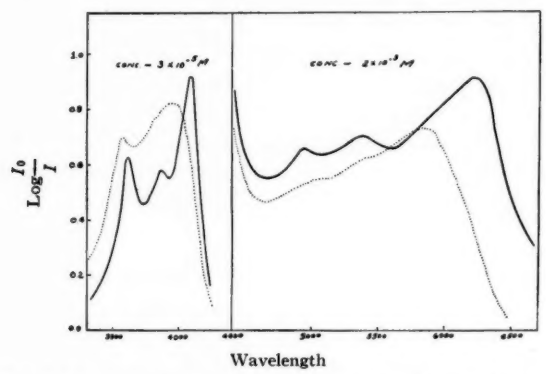

FIG. 3. Absorption spectrum of phenyl-di-p-xenylmethyl. Dashed curve at room temperature, solid curve at 77°K. One centimeter path length.

The solvents employed for the cations were syrupy phosphoric acid (90 percent H_3PO_4) and phosphorus oxychloride. The carbinols were dissolved in the former, the chlorides in the latter. The phosphoric acid solutions form clear rigid glasses at low temperatures; these were used for observations of the luminescences of the cations. Phosphorus oxychloride is not suitable for use at low temperatures, but yields better transparency in the ultraviolet than phosphoric acid.

CLASSIFICATION OF LEVELS

Classification of the electronic levels requires knowledge of the symmetries of the equilibrium configurations of the molecules. In the absence of direct structure determinations we have assumed the following symmetries: for triphenylmethyl, tri-p-xenylmethyl and their cations C_3 (somewhat distorted from D_3h);[5] for the other molecules C_2 (distorted from C_{2V}). Let us consider first the molecules of trigonal symmetry. Both a simple molecular orbital theory[6] and a valence bond treatment[7] lead to the assignment A_2'' (in symmetry D_3h) to the ground state of triphenylmethyl. We accept this assignment (A in symmetry C_3) and make further assignments on this basis. Should this assignment require correction, all the rest of our assignments may be corrected in a straightforward way.

In the absence of detailed calculations we assign the same classification (A_2'' in D_3h, A in C_3) to the normal state of tri-p-xenylmethyl.

The normal states of the cations, since these are even electron molecules, are in all likelihood totally symmetric.

Each free radical possesses a system of weak absorption bands in the visible,[8] and an intense absorption in the near ultraviolet. The strong absorptions we assign to allowed transitions. The only allowed transition from A_2'' consistent with the π electron hypothesis is to an E'' state. Hence we label the excited states responsible

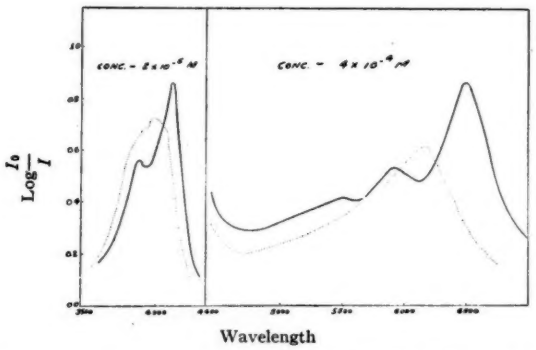

FIG. 4. Absorption spectrum of tri-p-xenylmethyl. Dashed curve at room temperature, solid curve at 77°K. One centimeter path length.

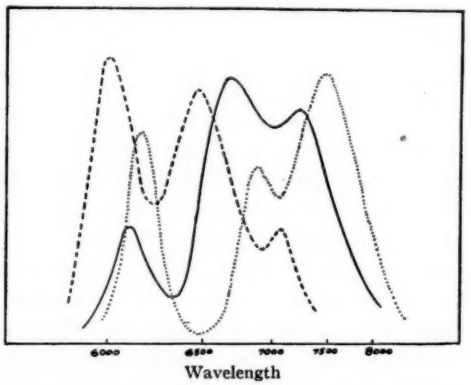

FIG. 5. Densitometer tracings of luminescence of free radicals. ····· tri-p-xenylmethyl; —— phenyl-di-p-xenyl methyl; – – – diphenyl-p-xenyl methyl. (Our curve for triphenylmethyl is indistinguishable from the one given by Lewis, Lipkin, and Magel.)

[5] We have not taken into account the distortion through the Jahn-Teller effect of these molecules from C_3 in some of their excited states. We have chosen the symmetry C_3 rather than D_3, because the latter does not permit mixing of s orbitals with p orbitals. The results of paramagnetic resonance studies of triphenylmethyl require such mixing.

[6] E. Huckel, Z. Physik. 83, 632 (1933).

[7] L. Pauling and G. W. Wheland, J. Chem. Phys. 1, 362 (1933).

[8] The approximate oscillator strengths are: tri-p-xenylmethyl, 0.02 phenyl-di-p-xenylmethyl 0.014; diphenyl-p-xenylmethyl 0.005. The value for triphenylmethyl is uncertain, because of strong association, but it is in the same range as the others.

for the strong near ultraviolet absorption in triphenylmethyl and tri-p-xenylmethyl E' in symmetry D_3h, E in symmetry C_3.

Classification of the states responsible for the weak absorptions in the visible is facilitated by the polarization data. Lewis, Lipkin, and Magel[1] have observed that the triphenylmethyl fluorescence spectrum with its complex vibrational structure and the weak absorption are accurate mirror images of each other. The peak of shortest wavelength in fluorescence and the peak of longest wavelength absorption almost coincide. Hence the short wavelength fluorescence peak probably corresponds to a vibrationless transition. Its polarization is determined by the nature of the electronic states involved, while the polarization of the other peaks involves also the nature of the associated vibrational modes. When the fluorescence is excited by plane polarized light which is absorbed in the intense ultraviolet band, the "vibrationless" fluorescence peak is polarized at right angles to the polarization of the exciting light.[9] Since the intense absorption involves a transition with electric moment perpendicular to the trigonal axis of the molecule we conclude that the O—O transition occurs with electric moment parallel to the trigonal axis. Such a transition is forbidden (under the π-electron hypothesis) if the molecule possesses a reflection plane perpendicular to the trigonal axis. The O—O transition becomes partially allowed by distortion from the completely planar configuration. The propeller distortion or noncoplanarity of the four central carbon atoms or a combination of these effects is probably involved.

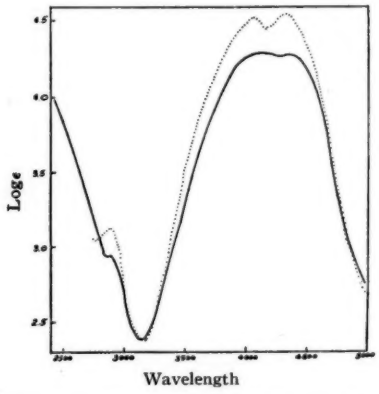

FIG. 6. Absorption spectrum at room temperature of triphenyl carbonium ion. Dashed curve in phosphoric acid, solid curve in phosphorus oxychloride.

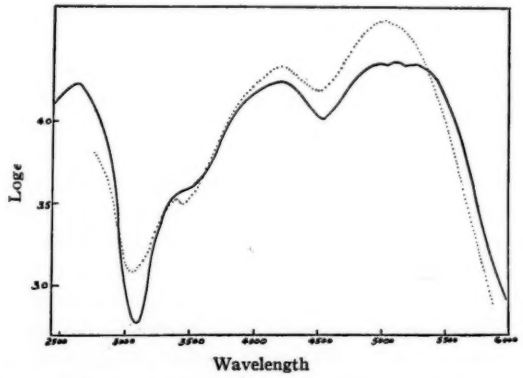

FIG. 7. Absorption spectrum of diphenyl-p-xenyl carbonium ions at room temperature. Dashed curve in phosphoric acid, solid curve in phosphorus oxychloride.

[9] The polarization ratio is approximately 0.9.

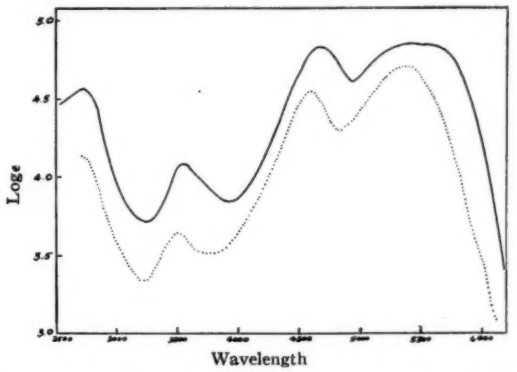

FIG. 8. Absorption spectrum at room temperature of phenyl-di-p-xenyl carbonium ion. Dashed curve in phosphoric acid, solid curve in phosphorus oxychloride.

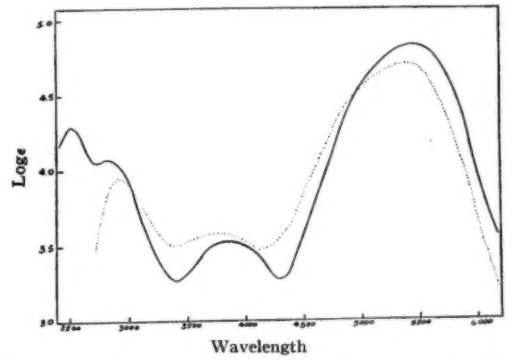

FIG. 9. Absorption spectrum at room temperature of tri-p-xenyl carbonium ion. Dashed curve in phosphoric acid, solid curve in phosphorus oxychloride.

Because of incomplete resolution of the vibrational peaks reliable determination of the polarizations of the individual vibrational transitions is not possible. Nevertheless from the sign of the polarization at each maximum a guess as to the direction of the associated moment may be made. The signs of the polarizations and the guesses as to the nature of the various vibrations are given in Table I. These guesses are based on the assignment of classification A in C_3(A_1'' in D_3h) to the excited electronic state. This assignment in turn is based on the polarization of the vibrationless transition.

For tri-p-xenylmethyl the situation is less clear cut. In the first place we note that the short wavelength fluorescence peak occurs at a considerably shorter wavelength—6200A—than the long wavelength absorption—6500A. Excitation at 6500A leads to no fluorescence. Certainly the fluorescent state and the state responsible

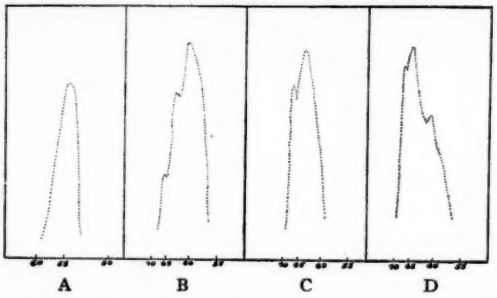

FIG. 10. Densitometer tracings of luminescence spectra of triphenyl carbonium ions. A. Triphenylmethyl carbonium. B. Diphenyl-p-xenyl carbonium. C. Phenyl-di-p-xenyl carbonium. D. Tri-p-xenyl carbonium.

for the absorption at 6500A are distinct. Our conclusions which are dependent on polarization of fluorescence apply to the fluorescent state.

The strong absorption near 4000A ($\epsilon \sim 4\times10^4$) we have associated with an allowed transition to an E'' state. The second peak at a frequency 1500 cm^{-1} higher than the main peak corresponds, we believe, to a transition to one of the vibrational levels of the E state rather than to another electronic state, or to absorption by an isomeric molecule. Excitation in each of the peaks separately yields the same fluorescence spectrum with the same polarization.

The fluorescence, when excited by plane polarized light of wavelength 4000A is positively polarized, with the polarization ratio between 1.2 and 1.3. Since a polarization ratio of 1.33 is anticipated for excitation by an $A_2''\rightarrow E''$ transition with subsequent emission by an $E''\rightarrow A_2''$ transition, we conclude that the weak transition occurs mainly through perturbation by assymetric vibrations of species e. Since the vibrational structure of the fluorescence is not nearly so well resolved as in the case of triphenylmethyl we are unable to make detailed assignments as we did in that case. It seems likely that in C_3 the symmetry of the excited electronic state is A and that e vibrations are responsible for most of the observed transition moment.

For both phenyl di-p-xenylmethyl and diphenyl-p-xenylmethyl, the strong ultraviolet absorption contains two well-separated peaks, which condition we believe corresponds to the "splitting" of the doubly degenerate E state of the triphenylmethyl and tri-p-xenylmethyl under the lower symmetry. The behavior of diphenyl-p-xenylmethyl corresponds well to this supposition. Excitation in the peak at 3850 leads to fluorescence with strong positive polarization; excitation at 3400 leads to fluorescence of negative polarization. Hence absorption in the two bands must occur with transition moments perpendicular to each other. Further, the fluorescence, as in tri-p-xenylmethyl occurs with moment in the plane (since this moment is parallel to one of the "allowed" moments).

Similar behavior is exhibited by phenyl-di-p-xenylmethyl. The absorption in the visible is not forbidden in C_2v or C_2 symmetry. Excitation in the band at 4100A leads to strong positive polarization, at 3800 to weak positive polarization, and at 3600A to practically no polarization.[10] The first two peaks we ascribe to vibrational levels of a single electronic state, the third peak to another electronic state.

A summary of the positions of the electronic levels and the assignments is given in Table II.

TABLE I. Classification of vibrational levels of triphenylmethyl from polarization of luminescence. Symmetry C_3 is assumed. V is the frequency of the peak in question, V_0 the frequency of the O—O peak.

V_0-V (cm^{-1})	Polarization	Species of associated vibration
0	negative	
230	positive	e
670	negative	a
970	uncertain	
1080	uncertain	
1550	negative	a
1850	positive	e
2210	negative	a
2510	negative	a

TABLE II. Classification of the levels of the free radicals. Two classifications are given for each level. The first corresponds to the approximate symmetries D_3h or C_2v, the second in parentheses, to the symmetries C_3 or C_2.

Triphenylmethyl	Tri-p-xenylmethyl	Phenyl-di-p-xenylmethyl	Diphenyl-p-xenylmethyl
0 cm^{-1}: $A_2''(A)$	0 cm^{-1}: $A_2''(A)$	0 cm^{-1}: $B_1(B)$	0 cm^{-1}: $B_1(B)$
19 400 cm^{-1}: $A_1''(A)$	16 400 cm^{-1}: $A_1''(A)$	16 400 cm^{-1}: $A_2(A)$	16 700 cm^{-1}: $A_2(A)$
29 000 cm^{-1} $E''(E)$	23 800 cm^{-1} $E''(E)$	24 400 cm^{-1}: $A_2(A)$	26 700 cm^{-1}: $A_2(A)$
		27 800 cm^{-1} $B_1(B)$	29 000 cm^{-1} $B_1(B)$

THE CATIONS

The luminescence of the triphenylmethyl cation, since it seems to arise exclusively from a triplet state, was no help in classification of the singlet states of this ion. We shall not consider here the nature of this triplet state. Since the broad absorption with peak at 4000A is very intense, there is little doubt that the excited state is an E state. Similarly the strong absorption at 5200A in the tri-p-xenyl cation is ascribed to absorption to an E state. The fluorescence of this ion, because of its position, is ascribed to the reverse electronic transition of the absorption. For excitation by an $A_1\rightarrow E$ transition followed by $E\rightarrow A_1$ luminescence a polarization ratio of 1.33 is expected. Positive polarization of about this magnitude was found when the luminescence was excited by light at 5500A. For both the phenyl-di-p-xenyl and diphenyl-p-xenyl cations the absorption in the visible is split into two bands, separated by about 4000 cm^{-1}. These bands we ascribe to transition to the two states into which the E state of triphenylmethyl or tri-p-xenyl cation splits under the lower symmetry. The polarization of luminescence of the phenyl-di-p-xenyl-

[10] In this case negative polarization is not achieved because of incomplete resolution of the bands.

methyl cations are in complete accord with this assignment. Excitation in the long wavelength absorption peak leads to a high positive polarization. The polarization ratio is about 2.5 as compared with the theoretical maximum of 3.0. Excitation in the next band leads to strong negative polarization of the luminescence. Thus the moments for the two transitions must be at right angles to each other.

The shorter wavelength absorption seems to differ considerably between the triphenylmethyl cation and the cations containing p-xenyl groups. All of the latter exhibit a strong absorption maximum ($\epsilon > 10^4$) in the neighborhood of 2800 angstroms, while the former is relatively transparent ($\epsilon < 10^3$) at this wavelength. A similar phenomenon occurs in the carbinols dissolved in non-ionizing solvents. At 2580 angstroms in methanol solution, triphenyl carbinol shows no absorption peak ($\epsilon = \sim 10^3$) while diphenyl-p-xenyl carbinol, phenyl-di-p-xenyl carbinol, and tri-p-xenyl carbinol each exhibit an absorption maximum with the extinction coefficients approximately in the ratio 1:2:3. (The values are 2.4×10^4, 6×10^4, 9×10^4.) We suggest that absorption at 2800A in the cations as well as the absorption at 2580A in the carbinols is to be ascribed to a "localized" excitation in the p-xenyl group.[11]

[11] We use the term "localized excitation" to mean that the interaction between states in which the excitation energy is in a single p-xenyl group is not great enough to lead to an observable splitting. Thus for a molecule containing two p-xenyl groups, appropriate zero-order functions would be linear combinations of the functions which localize the excitation in single groups. If the energy difference between the state corresponding to these linear combinations is too small for observation, we speak of the excitation energy as "localized."

TABLE III. Classification of the levels of the cations. The classifications are given in symmetry D_3h for triphenyl carbonium and tri-p-xenyl carbonium ions; C_2v for diphenyl-p-xenyl carbonium and phenyl-di-p-xenyl carbonium ions.

Triphenyl carbonium	Tri-p-xenyl carbonium	Phenyl di-p-xenyl carbonium	Di-phenyl-p-xenyl carbonium
0 cm^{-1}: A_1'	0 cm^{-1}: A_1'	0 cm^{-1}: A_1	0 cm^{-1}: A_1
22 000 cm^{-1} E'	17 200 cm^{-1}: E'	17 200 cm^{-1} A_1	17 900 cm^{-1}: A_1
35 000 cm^{-1}: A_2'	25 600 cm^{-1}: A_2'	21 700 cm^{-1}: B_2	23 500 cm^{-1}: B_2
40 000 cm^{-1}?	36 000 cm^{-1}: E', and A_1'	28 200 cm^{-1}: A_1	37 000 cm^{-1}: A_1
		36 000 cm^{-1}: A_1 and B_2	

A consequence of this suggestion may easily be tested. For diphenyl-p-xenyl cations, the state in which excitation is localized in the single-p-xenyl is nondegenerate. Excitation by polarized light at 2800 angstroms should lead to a high positive polarization if emission from the fluorescent state occurs with a transition moment parallel to that of the absorption moment, to negative polarization if the moments are perpendicular. Measurement reveals a high positive polarization.

For phenyl-di-p-xenylmethyl cations, a much smaller degree of polarization is expected since excitation in the two p-xenyl groups may occur both with a moment parallel to the two fold axis and with a moment perpendicular to the axis. Under the assumption that excitation in the p-xenyl group occurs with moment along the long axis, we anticipate a polarization ratio of $13/11 = 1.2$. About 1.1 is observed, as contrasted to a ratio greater than 2 for the ions containing but one p-xenyl group.

If we accept the assumption that the absorption at 2800 angstroms in the p-xenyl group occurs with moment along the long axis, we are led to the assignments given in Table III.

A Note on the Fluorine Resonance Shifts*

A. SAIKA AND C. P. SLICHTER
University of Illinois, Urbana, Illinois

(Received August 28, 1953)

A theoretical analysis is given of the fluorine magnetic resonance shifts in molecules. It is shown that the large range of shifts among different fluorine compounds arises from the effects of binding on the magnetic fields at the nucleus produced by the orbital motion of the electrons in the unfilled valence shell. The simple dependence on ionic character of the bond is also explained. The chemical shift between F_2 and HF is calculated to be 14×10^{-4} compared to the experimentally observed value 6.3×10^{-4}.

GENERAL theoretical expressions for chemical shifts in the magnetic shielding of nuclei in molecules have been developed by Ramsey.[1] The theoretical evaluation of chemical shifts in individual cases has been discouraged by the rather complex nature of the analysis and the sensitive dependence of the results upon the molecular wave functions chosen. A particularly challenging and appealingly simple case is that of the fluorine magnetic resonance. It was found experimentally[2] that a covalently bound fluorine nucleus is paramagnetic relative to the fluoride ion, that is, is less shielded magnetically. The chemical shift found in the fluorine resonance in the highly covalent F_2, referred to the most ionic fluorine molecule HF, is 6.3×10^{-4}; moreover, between these extremes, the fluorine resonance shifts are almost linearly dependent upon the electronegativity of the atom bonded to the fluorine in question. It has proven possible to account at least semiquantitatively for these experimental results by suitable approximations and simplifications of Ramsey's analysis.

ESTIMATE OF THE CHEMICAL SHIFT BETWEEN F_2 AND F^-

Equation (10) in Ramsey's second paper[1] expresses the nuclear magnetic shielding as

$$A\nu_\lambda\sigma_\lambda=(e^2/3mc^2)(0|\sum_k 1/r_k|0)$$
$$-2A\nu_\lambda\sum_{n\lambda}{}'[1/(E_n-E_0)]$$
$$\times[(0\lambda|\sum_k m_{zk}{}^0|n\lambda')(n\lambda'|\sum_k m_{zk}{}^0/r_k{}^3|0\lambda)$$
$$+(0\lambda|\sum_k m_{zk}{}^0/r_k{}^3|n\lambda')(n\lambda'|\sum_k m_{zk}{}^0|0\lambda)]. \quad (1)$$

This expression consists of two types of terms, ordinarily called the diamagnetic and the second order paramagnetic terms, respectively. However, as Ramsey points out, the second term cancels off a good part of the first term for electrons on other atoms. An alternative division would be into three terms: (1) *The diamagnetic correction for the atom in question*. This is the well-known Lamb expression, and differs in different fluorine compounds by an amount that is only about 1 percent of the observed range in chemical shifts. (2) *The paramagnetic term for the atom in question*. This term represents the contribution from magnetic fields set up by the orbital motion of the valence electrons. In the absence of an external static field, the orbital fields have a zero average value, but at any instant produce fields of several thousand gauss at the nucleus. A slight polarization of these enormous fluctuating fields by the static magnetic field produces an appreciable magnetic shielding. (3) *The contribution from other atoms*. Electrons on other atoms are either tightly bound in closed shells, or else are in the valence shells. The former are hard to polarize and clearly give only small fields. The valence electrons will have an effect small compared to item (2) above because of the $1/r^3$ falling off of the interaction.

Item (2) is therefore principally responsible for chemical shifts in fluorine. On this basis we see why the range in chemical shifts of the proton is so much smaller than that of fluorine and phosphorus, since s electrons exert a zero instantaneous orbital magnetic field at the nucleus, whereas p or d electrons exert large ones. Of course our remarks on the relative magnitudes of terms 1, 2, and 3 do not apply to s states, since items 1 and 3 may be dominant here. On the basis of the above considerations, the second-order paramagnetic term would be zero in the completely ionic F^-, because of the filled L shell, and would have its largest value in covalent F_2, as observed.

The chemical shift data we wish to analyze is obtained from studies with liquids, so that the molecule is thought of as jumping from one spatial orientation to another at a rate that is rapid compared with the Larmor frequency, but slow compared with frequencies associated with electronic energies. We therefore must consider the external field to have arbitrary orientation with respect to the molecular axes, compute the shielding for each orientation, and perform an average over all such orientations. It is convenient to choose as our molecular axes a set x, y, z with origin at the fluorine nucleus, the x axis being along the bond formed by the fluorine. It is then easy to show the chemical shielding is the average of that for the three orientations in which the x, y, and z axes respectively are parallel to the static

* Supported in part by the U. S. Office of Naval Research.
[1] N. F. Ramsey, Phys. Rev. **77**, 567 (1950); **78**, 699 (1950); **83**, 540 (1951); **86**, 243 (1952).
[2] H. S. Gutowsky and C. J. Hoffman, J. Chem. Phys. **19**, 1259 (1951).

field. We will outline such a calculation, one for which the external field lies along the z axis of the molecule.

In order to estimate the shielding for F_2, we approximate the ground-state wave function for the molecule, which is considered to be in the $^1\Sigma_g^+$ state, taking the necessary electrons only into account and neglecting overlap,

$$\psi_0=(2)^{-\frac{1}{2}}(6!)^{-\frac{1}{2}}[\det|y_a(1)\alpha(1)y_a(2)\beta(2)x_a(3)\alpha(3)\, x_b(4)\beta(4)y_b(5)\alpha(5)y_b(6)\beta(6)| -\det|y_a(1)\alpha(1)y_a(2)\beta(2)x_a(3)\beta(3)\, x_b(4)\alpha(4)y_b(5)\alpha(5)y_b(6)\beta(6)|], \quad (2)$$

where x and y denote $2p_x$ and $2p_y$ orbitals, α and β are the spin up and down functions, det is the Slater determinant of which the diagonal is given, and the subscripts a and b refer to the given fluorine and the other fluorine respectively. In our model, one $2p_x$ electron may be considered as missing, at a given instant, from the electron shells about each of the fluorines.

The applied magnetic field may then couple any of the $2p_y$ electrons with the unoccupied $2p_x$ orbital, via the operator m_z^0, thus bringing up the polarized $^1\Pi_g$ state. This excited state may be represented as

$$\psi_n=(4)^{-\frac{1}{2}}(6!)^{-\frac{1}{2}}[\det|y_a(1)\alpha(1)x_a(2)\beta(2)x_a(3)\alpha(3)\, x_b(4)\beta(4)y_b(5)\alpha(5)y_b(6)\beta(6)| -\det|x_a(1)\alpha(1)y_a(2)\beta(2)x_a(3)\beta(3)\, x_b(4)\alpha(4)y_b(5)\alpha(5)y_b(6)\beta(6)| +\det|y_a(1)\alpha(1)y_a(2)\beta(2)x_a(3)\alpha(3)\, x_b(4)\beta(4)x_b(5)\alpha(5)y_b(6)\beta(6)| -\det|y_a(1)\alpha(1)y_a(2)\beta(2)x_a(3)\beta(3)\, x_b(4)\alpha(4)y_b(5)\alpha(5)x_b(6)\beta(6)|]. \quad (3)$$

The matrix elements can be calculated directly in terms of ψ_0 and ψ_n if we neglect the m_{zk}^0/r_k^3 terms on the fluorine b as mentioned before, and we arrive at an expression for the shielding contributed by our one orientation of the molecule. The shielding for the other two orientations is calculated in a like manner.

Averaging over all orientations, the chemical shift between F_2 and F^- is found to be

$$\Delta\sigma=-2/3(e^2\hbar^2/m^2c^2)(\langle 1/r^3\rangle_{Av})_{2p}1/\Delta E, \quad (4)$$

where $(\langle 1/r^3\rangle_{Av})_{2p}$ is the average of $1/r^3$ for $2p$ electrons and where ΔE is the average excitation energy from the $^1\Sigma_g^+$ state to the $^1\Pi_g$ state. The observed excitation energy to the $^1\Pi_u$ state is about 4.3 ev.[3] We shall employ this value as ΔE assuming the $^1\Pi_g$ and $^1\Pi_u$ states have about the same energy level. Sternheimer[4] gives a value for $(\langle 1/r^3\rangle_{Av})_{2p}$ of $8.89/a_H^3$, where a_H is the Bohr radius. Introducing these values, Eq. (4) reduces to

$$\Delta\sigma=-20\times10^{-14}, \quad (5)$$

which will be compared with the observed values later.

If we were not particularly interested in what the excited states would be, Eq. (4) could be obtained more readily by use of Eq. (14) in Ramsey's second paper.[1]

$$\Delta\sigma=-(4/3\Delta E)(0|\sum_{jk}\mathbf{m}_j^0\cdot\mathbf{m}_k^0/r_k^3|0). \quad (6)$$

As has been pointed out earlier, we need take into account only the fluorine atom in question in performing the sums. We shall approximate this fluorine atom by an isolated fluorine atom with one p electron missing from the closed shell. Denoting the total angular momentum of the atom by $\mathbf{M}$, (6) becomes

$$\Delta\sigma=-(4/3\Delta E)(e/2mc)^2(0|\mathbf{M}\cdot\mathbf{M}/r^3|0) =-2/3(e^2\hbar^2/m^2c^2)(\langle 1/r^3\rangle_{Av})_{2p}1/\Delta E, \quad (7)$$

in agreement with (4).

IONIC CHARACTER AND THE CHEMICAL SHIFTS

The effect upon the fluorine shift of the atom bonded to the fluorine may be ascribed mainly to the associated change in the ionic character of the A—F bond. This ionic change will effect $\Delta\sigma$ in two ways: namely, (1) the change in the matrix elements, and (2) the change in the excitation energies. In our approximation, as can be seen from (7), the matrix element may be considered to decrease by the factor $(1-i)$ by the introduction of the ionic character i into the bond since the ionic terms correspond to a closed shell on the fluorine. No simple way of theoretically predicting the change in the excitation energies with ionic character has been found, nor is there sufficient data to make any general statement. However, it would not be too bad an approximation to assume that the excitation energies would generally be of the same order of magnitude. In HF, the most ionic molecule whose shift was experimentally measured, we may take the excitation energy to be 7.7 ev from the ultraviolet spectral data.[5] Then using $i=0.43$ for HF,[6] the shift between F_2 and HF becomes -14×10^{-4}, which is somewhat larger than the observed value -6.3×10^{-4}. In any case we may expect that the shifts vary between the extremes HF and F_2 according to the ionic character of the bond as observed experimentally. The rather small experimental value -5.5×10^{-4} for F^- seems to indicate the shift for F^- ions in the aqueous solution is no longer that for ideal F^- on account of hydration. The general trend that the higher oxidation states have the lower F shielding in the case of halogen fluorides might be also ascribed to the less ionicity of the bonds of the higher oxidation states.

Though hybridization could have the same effect as the ionic character, we have neglected it and ascribed the effect solely to the ionic character, because the general trend of the experimental values seems to favor

[3] G. Herzberg, *Molecular Spectra and Molecular S... e* (D. Van Nostrand Company, Inc., New York, 1950), Vol. I, ...nd edition.
[4] R. Sternheimer, Phys. Rev. **84**, 244 (1951).
[5] Safary, Romand, and Vodar, J. Chem. Phys. **19**, 379 (1951).
[6] Coulson, *Valence* (Oxford University Press, New York, 1952), p. 128.

this and the ambiguity in the excitation energies hinders any numerical estimate of the hybridization. It is interesting, however, to note the close resemblance with nuclear quadrupole coupling effects in molecules[7] in that both of them are essentially dependent upon the fraction of the unbalanced p electrons on the atom in question.

We have benefited from many interesting discussions with Dr. H. S. Gutowsky. In addition, Dr. Gutowsky's encouragement and help to one of us (A.S.) while at Illinois is deeply appreciated and gratefully acknowledged.

[7] C. H. Townes and B. P. Dailey, J. Chem. Phys. **17**, 782 (1949).

THE JOURNAL OF CHEMICAL PHYSICS VOLUME 22, NUMBER 1 JANUARY, 1954

Bromination of Hydrocarbons. VII. Bromination of Isobutane. Bond Dissociation Energies from Bromination Kinetics*

BERNARD H. ECKSTEIN, HAROLD A. SCHERAGA, AND ERVIN R. VAN ARTSDALEN†
Department of Chemistry, Cornell University, Ithaca, New York

(Received July 2, 1953)

The kinetics of the gas phase photochemical bromination of isobutane to yield 2-bromo 2-methylpropane was investigated in the temperature range 40–95°C and the reaction found to proceed through an atom and radical chain mechanism analogous to that observed with a number of other hydrocarbons. The thermal reaction was studied at 112 and 130°C and shown to have the same mechanism except for the mode of production of bromine atoms. Bromination was inhibited by hydrogen bromide, a product of the reaction, and also by oxygen. The dissociation energy of the tertiary C−H bond in isobutane was found to be 89.6 kcal/mole at 0°K, in agreement with the idea that tertiary bonds are considerably weaker than primary bonds. A general review of activation energies of bimolecular reactions involved in bromination is given as well as a recapitulation of values of C−H and C−C bond dissociation energies derived from bromination studies.

INTRODUCTION

FROM studies of the kinetics of the gas phase bromination of hydrocarbons and the accompanying inhibition of the reaction by hydrogen bromide it has been possible to determine carbon-hydrogen bond dissociation energies and also enthalpies of formation of the corresponding radicals.[1–4] In addition, it was possible to compute carbon-carbon bond dissociation energies from these data.[3–5] Thus far these studies have been confined to the bromination of primary carbon-hydrogen bonds in several aliphatic compounds[1–3] and also in the alkyl side chain of toluene.[4,6] It was of interest, therefore, to extend this method to a hydrocarbon containing another type of carbon-hydrogen bond. The compound selected was isobutane which contains a tertiary C−H bond. This would be expected to brominate at a much faster rate than the primary bonds.

MATERIALS

Because of the sensitivity of gas-phase bromination to traces of oxygen, all materials used in the kinetic studies were purified and degassed in a grease-free high vacuum system by the procedure described previously.[4] The starting materials were: Phillips Petroleum Company research grade isobutane having a purity of 99.88 ±0.06 mole percent,[7] Baker and Adamson analytical reagent grade bromine, and Mathieson anhydrous hydrogen bromide of a stated purity of 99.5 percent.

The products of the reaction were identified by means of their infrared spectra obtained with a Perkin-Elmer Model 21, double beam, recording infrared spectrophotometer using a 0.1-mm sodium chloride absorption cell. For comparison spectra the following compounds were purified by fractional distillation: Eastman Kodak Company 2-bromo 2-methylpropane (b. pt. 72.9° at 740 mm), Columbia Organic Chemicals Company 1-bromo 2-methylpropane (b. pt. 37.0°C at 115 mm), and Eastman Kodak Company 1,2-dibromopropane (b. pt. 47.0°C at 30 mm). 1,2-dibromo 2-methylpropane (b. pt. 66°C at 50 mm) was prepared by a procedure suggested by J. Howald. The solvent for all spectrophotometer measurements was Baker and Adamson reagent grade

* This paper is adapted from part of a Ph.D. thesis submitted to Cornell University, February, 1953, by Bernard H. Eckstein, who would like to thank the Cornell University Department of Chemistry and the Proctor and Gamble Company for the grant of fellowships.

† Present address: Oak Ridge National Laboratory, Oak Ridge, Tennessee.

[1] G. B. Kistiakowsky and E. R. Van Artsdalen, J. Chem. Phys. **12**, 469 (1944).

[2] H. C. Andersen and E. R. Van Artsdalen, J. Chem. Phys. **12**, 479 (1944).

[3] E. I. Hormats and E. R. Van Artsdalen, J. Chem. Phys. **19**, 778 (1951).

[4] Anderson, Scheraga, and Van Artsdalen, J. Chem. Phys. **21**, 1258 (1953).

[5] E. R. Van Artsdalen, J. Chem. Phys. **10**, 653 (1942).

[6] Swegler, Scheraga, and Van Artsdalen, J. Chem. Phys. **19**, 135 (1951).

[7] According to the manufacturer's certificate quoting the determination of purity by the National Bureau of Standards.

carbon disulfide dried with anhydrous magnesium sulfate.

The reaction mixtures from a considerable number of photochemical runs were combined for the infrared analysis. The brominated product was freed of isobutane, hydrogen bromide, and bromine by washing with aqueous sodium bisulfite and water. This aqueous mixture was extracted with carbon disulfide and dried with anhydrous magnesium sulfate. The resulting solution contained approximately 1 mole percent of brominated hydrocarbon.

EXPERIMENTAL

The design of the apparatus was based on that used previously in the investigation of the bromination of neopentane.[3] The reaction was carried out in a cylindrical Pyrex cell having a volume of 103 cc and a surface area of 122 cm^2. It was kept in an air thermostat in which the temperature could be maintained constant within ± 0.1°C.

The rate of both the photochemical and thermal reactions was determined by following the rate of disappearance of bromine photometrically, using a system in which a pair of calibrated polaroids was "in series" with the reaction cell. The photometer employed light at 4358A from a General Electric AH-4 mercury vapor lamp as a measuring beam and an RCA 931A photomultiplier tube as light sensitive element. The light intensity from the AH-4 lamp was sufficiently low so that no measureable photochemical activation was induced by the measuring system. The *photochemical* reaction was interrupted at regular time intervals by means of a shutter to permit making the photometric determination of the amount of bromine remaining. In these experiments the light intensity on the photomultiplier tube was kept constant by decreasing the transmission of the polaroids as the transmission through the cell increased because of the disappearance of bromine during the course of the reaction. The bromine concentration at any time was therefore obtainable from the polaroid setting required to maintain constant light intensity on the photomultiplier tube. The system was calibrated before each run by determining the polaroid settings at a series of bromine pressures. An alternate reference optical path served to check on the constancy of the light intensity of the photometer lamp. Because the *thermal* reaction could not be interrupted for transmission measurements the rate of disappearance of bromine was followed by measuring the increase in photocell output at constant polaroid setting. Again each run was preceeded by a calibration.

The photochemical reaction was initiated by light from a General Electric AH-5 mercury vapor lamp. Corning filters were used in conjunction with a water filter to yield light of which 96 percent was between 4047 and 5780A. It has been shown[8] that light absorbed at wavelengths shorter than 5780A is effective in dissociating bromine molecules and that bromine atoms produced by predissociation show about the same reactivity as those dissociated in a primary act. In the temperature range employed here the absorption coefficient of bromine is essentially independent of temperature.[9] The activating beam was at right angles to the measuring beam, and it could be interrupted at will by a shutter so that the bromine pressure at any time during the reaction could be determined. It was established that the total amount of reaction depended only on the total time of illumination, and not on the frequency of the interruptions, other things being constant. This is of course true only as long as the periods of illumination and of darkness are very long compared to the time required to attain the steady-state concentrations of atoms and radicals, which was the case in this investigation. To assure constant light intensity for all the photochemical experiments, the output of the AH-5 lamp was monitored by means of a circuit similar to that described by Wood.[10]

The reaction cell was attached to an all-glass high-vacuum system in which all stopcocks exposed to either bromine or hydrogen bromide were lubricated with Du Pont Perfluorolube FCX-334. All other stopcocks were lubricated with Apiezon "N." Initial pressures of all reactants were measured using a quartz spiral manometer as a null point instrument.

No pyrolysis of isobutane[11,12] or tertiary butyl bromide[13] occurs in the temperature range employed here. Also no appreciable thermal reaction occurred at the highest temperatures used in the photochemical experiments.

Initial rates of reaction were determined by short extrapolations to zero time of reaction; these initial rates of reaction were used in all subsequent calculations of rate constants, inhibition effects, and temperature coefficients. Thus, the effects of secondary bromination were eliminated.

RESULTS

According to the work of Hass, McBee, and Weber[14] on the chlorination of simple paraffin hydrocarbons it may be expected that bromination of isobutane would take place predominantly at the tertiary carbon atom at the temperatures employed here. The work of Vaughan and Rust[15] on the oxidation of aliphatic hydrocarbons and the studies of Moore and Wall[16] on the reaction

[8] W. Jost, Z. Physik. Chem. **B3**, 95 (1929). See also reference 1.

[9] Acton, Aickin, and Bayliss, J. Chem. Phys. **4**, 474 (1936).

[10] L. A. Wood, Rev. Sci. Instr. **7**, 157 (1936).

[11] A. D. Stepukhovich, J. Gen. Chem. (USSR) **15**, 341 (1945).

[12] E. W. R. Steacie and I. E. Puddington, Can. J. Research **16B**, 260 (1938).

[13] G. B. Kistiakowsky and E. H. Stauffer, J. Am. Chem. Soc. **59**, 165 (1937).

[14] Hass, McBee, and Weber, Ind. Eng. Chem. **27**, 1190 (1935); **28**, 333 (1936).

[15] W. E. Vaughan and F. R. Rust, U. S. Patent No. 2,395,523 (1945).

[16] W. J. Moore and L. A. Wall, J. Chem. Phys. **17**, 1325 (1949).

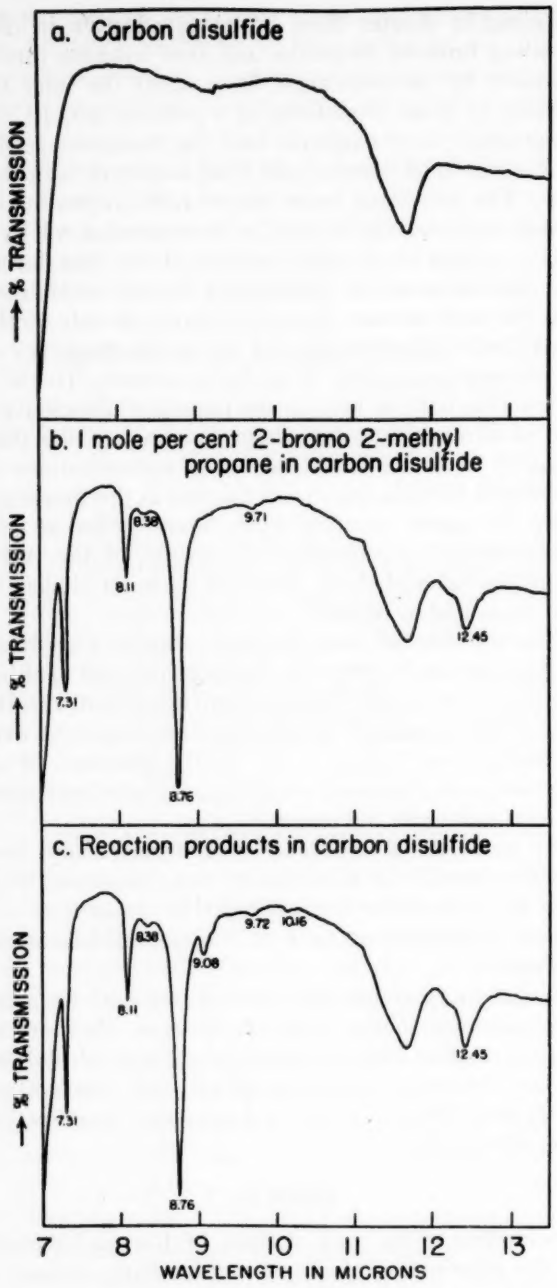

FIG. 1. Infrared spectra.

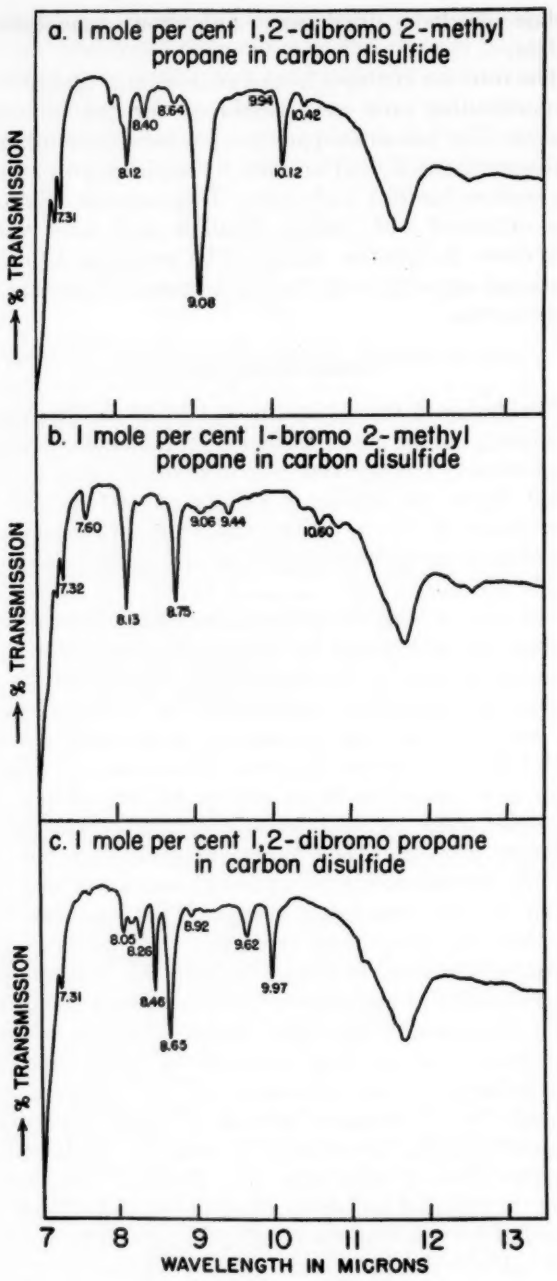

FIG. 2. Infrared spectra.

between hydrogen atoms and isobutene gave further support to the feeling that the principal point of attack would be the tertiary carbon atom. This anticipated result was borne out by infrared analysis[17] of the products of the photochemical reaction.

If the tertiary hydrogen is replaced by bromine the product is 2-bromo 2-methylpropane. If the bromination were allowed to continue some of this product would be converted to 1,2-dibromo 2-methylpropane. On the other hand, if bromination takes place on a primary carbon 1-bromo 2-methylpropane would be formed. Another possible product could arise if the tertiary butyl radical, postulated as an intermediate in the free radical bromination at the tertiary carbon atom, were unstable and decomposed into methyl radicals and propylene. If so, the latter, upon bromination, would yield 1,2-dibromopropane. The infrared spectra of 1 mole percent solutions of each of these brominated hydrocarbons in carbon disulfide are reproduced in part in Figs. 1 and 2. Several peaks were readily identified and quantitative criteria were established for the smallest concentrations of each of these brominated hydrocarbons in carbon

[17] We are indebted to Professor D. F. DeTar and Mr. T. Wentink for aid in the infrared analyses.

disulfide which would give unambiguously discernible peaks. Their wavelengths, good to $\pm 0.02\mu$, are shown next to the peaks in Figs. 1 and 2.

A comparison of the several curves leads to the conclusion that the principal product of the reaction between bromine and isobutane is 2-bromo 2-methylpropane (see Figs. 1b and 1c). The two extra peaks at 9.08μ and 10.16μ of Fig. 1c indicate that between 5 and 10 percent of the main product was brominated further to give 1,2-dibromo 2-methylpropane (see also Fig. 2a). Since the reaction was generally allowed to proceed until about one-fourth of the initial amount of bromine was used up, this result is not unreasonable.

From the established limits of detectability it may further be concluded that much less than 5 percent of the brominated product is 1,2-dibromopropane on the basis of the peaks at 8.46μ and 9.97μ (Fig. 2c), and that much less than 5 percent is 1-bromo 2-methylpropane on the basis of the peak at 7.60μ (Fig. 2b). No trace of any of these peaks was visible in the reaction products although they were discernible in reference solutions at the corresponding concentrations.

On the basis of these results the gas phase bromination of isobutane may be represented by the following over-all reaction

$$tB\text{H}+\text{Br}_2=tB\text{Br}+\text{HBr}, \qquad \text{(I)}$$

where tB represents the tertiary butyl radical $(CH_3)_3C\cdot$, and tBH and tBBr represent isobutane and tertiary butyl bromide, respectively. It is, therefore, valid to base the kinetic study on the observed rate of disappearance of bromine in light of Eq. (I).

The empirical rate law for the initial part of the photochemical reaction at constant light intensity was determined at 78.3°C and found to be

$$-d(\text{Br}_2)/dt=k_p(\text{Br}_2)^{\frac{1}{2}}(tB\text{H})(P)^{-\frac{1}{2}}, \qquad \text{(II)}$$

where k_p is the photochemical rate constant and P is the total pressure of reactants. Values of k_p at several temperatures are given in Table I. The two series of measurements correspond to different apparatus constants, involving also changes in incident light intensity, which appear in k_p.

The bromination was found to be inhibited by HBr, and the rate law was modified to

$$-\frac{d(\text{Br})_2}{dt}=\frac{k_p(\text{Br}_2)^{\frac{1}{2}}(tB\text{H})(P)^{-\frac{1}{2}}}{1+n(\text{HBr})/(\text{Br}_2)}. \qquad \text{(III)}$$

Data on the inhibited reaction are presented in Table II, where the values of n were computed from the known values of k_p at each temperature from the data of series B of Table I. Both the measurements in series B for uninhibited runs and those of Table II for inhibited runs were made at the same light intensity and with the same apparatus constant.

The temperature dependence of k_p and n are shown in Figs. 3 and 4, respectively. The data have been treated

TABLE I. Photobromination of isobutane at constant light intensity (wavelength 4047–5780A).

t°C	Initial pressures (mm at t°C) Br_2	Initial pressures (mm at t°C) tBH	Initial rate $(-d[Br_2]/dt)$ (mm/min)	k_p (min$^{-\frac{1}{2}}$)
		Series A, light intensity I_0'		
49.9	29.2	147.8	1.22	0.0203
	29.1	143.6	1.21	0.0205
	17.2	242.9	1.25	0.0200
	17.3	241.7	1.24	0.0198
				0.0202±0.0002
64.1	30.9	141.3	2.65	0.0443
	30.1	139.9	2.50	0.0425
	30.0	138.5	2.55	0.0436
	29.7	136.5	2.52	0.0437
				0.0435±0.0005
78.3	29.8	104.4	4.40	0.0894
	30.0	106.7	4.37	0.0874
	30.0	158.7	5.55	0.0877
	30.0	219.0	6.55	0.0862
	30.3	220.5	6.63	0.0865
	29.9	323.8	8.30	0.0882
	29.5	324.2	8.20	0.0876
	14.5	154.1	3.90	0.0863
	18.0	157.4	4.45	0.0883
	18.4	157.4	4.55	0.0894
	43.1	147.4	6.15	0.0877
	49.2	147.0	6.50	0.0883
				0.0878±0.0008
94.9	31.3	143.7	11.20	0.184
	30.7	140.2	10.68	0.180
	31.3	138.9	12.30	0.206
	30.5	138.8	10.40	0.177
	18.7	199.6	11.00	0.188
	18.4	189.6	11.50	0.204
	18.2	189.2	10.20	0.182
				0.189±0.007
		Series B, light intensity I_0		
40.3	29.2	226.1	2.60	0.0340
	29.6	165.4	2.38	0.0369
	28.0	162.8	2.03	0.0325
	28.5	162.8	2.08	0.0331
	29.6	161.8	2.17	0.0341
				0.0341±0.0009
48.7	28.7	185.8	3.75	0.0552
	27.9	182.7	3.85	0.0579
	30.1	181.9	3.93	0.0573
	27.9	181.3	3.85	0.0581
	27.9	181.6	3.80	0.0573
				0.0572±0.0008
66.2	32.2	115.0	8.45	0.157
	29.7	116.5	8.00	0.152
	30.0	215.5	10.05	0.133
	31.5	213.9	10.70	0.140
				0.146±0.009
84.9	29.6	160.7	22.4	0.353
	30.3	160.3	22.8	0.356
	30.9	160.3	22.9	0.355
				0.354±0.001

TABLE II. Photobromination of isobutane at constant light intensity, I_0 (wavelength 4047–5780A); inhibition by hydrogen bromide.

	Initial pressure (mm at t°C)			Initial rate $(-d[Br_2]/dt)$	
t°C	Br_2	HBr	tBH	(mm/min)	n[a]
40.3	28.2	48.6	209.7	1.34	0.391
	27.1	59.4	199.3	1.51	0.176
	27.5	47.1	145.7	0.975	0.467
	28.7	61.7	139.8	1.00	0.318
	29.1	58.8	200.0	1.19	0.407
	29.0	60.3	138.3	0.950	0.371
					0.355±0.072
48.7	27.6	61.3	163.4	1.57	0.436
	28.2	59.6	165.3	1.48	0.535
	28.5	57.0	161.4	1.52	0.531
	29.0	61.0	158.6	1.55	0.475
	29.3	46.6	160.4	1.84	0.475
					0.490±0.034
66.2	28.7	65.3	197.7	2.85	0.957
	28.8	65.4	198.3	2.95	0.916
	29.4	47.1	212.1	4.10	0.881
	29.0	51.9	200.7	3.26	1.053
					0.952±0.053
84.9	29.8	63.0	214.0	5.00	1.76
	29.4	61.5	212.4	5.20	1.67
	29.9	60.7	211.2	5.10	1.78
	29.9	25.2	209.6	10.05	1.76
	30.1	109.6	189.7	2.85	1.68
	18.5	60.6	201.4	2.65	1.80
	47.2	45.1	200.3	10.75	1.73
					1.74±0.04

[a] The values of n were calculated using the values of k_p given in series B, Table I, for the corresponding temperatures.

by the method of least squares and the following equations were obtained:

For series A

$$\log_{10}k_p = 6.3101 - 2588/T. \quad \text{(IV)}$$

For series B

$$\log_{10}k_p = 6.6463 - 2541/T. \quad \text{(V)}$$

It should be noted that Eqs. (IV) and (V) give k_p in min^{-1}. For n

$$\log_{10}n = 5.1062 - 1742/T. \quad \text{(VI)}$$

From Eqs. (IV) and (V) the experimental activation energy is 11.7±0.1 kcal/mole. From Eq. (VI) the apparent activation energy of inhibition is 8.0±0.2 kcal/mole.

The effect of change of incident light intensity on the rate of the photochemical reaction was investigated at 78.3°C by introducing a calibrated screen of 25.9 percent transmission into the light path. The results are shown in Table III. Assuming that $k_p = kI^a$, where k is independent of light intensity and a is the experimental order in light intensity, then the ratio of rate constants at light intensities I_0' and $0.259I_0'$ is $(I_0')^a/(0.259I_0')^a = 0.0878/0.0438$ giving a value of $a = 0.53$, which indicates a half-power dependence on light intensity.

Oxygen in small amounts inhibited the reaction. In large amounts the initial inhibition was followed by a rapid disappearance of bromine.

The thermal reaction was studied at two temperatures with no HBr present initially. Values of the specific

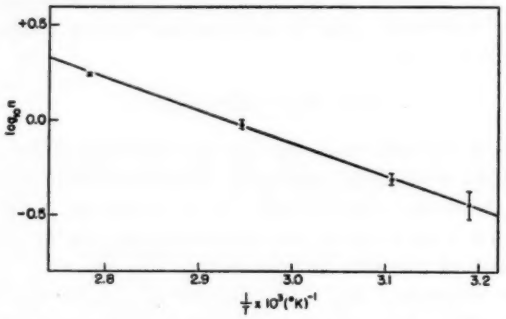

FIG. 4. Temperature dependence of inhibition by hydrogen bromide of photobromination of isobutane.

reaction rate constant k_t for the thermal reaction were computed from the empirical rate law

$$-d(Br_2)/dt = k_t(Br_2)^{\frac{1}{2}}(tBH) \quad \text{(VII)}$$

and are given in Table IV. These data give an activation energy of 35.6 kcal/mole which must be regarded as only an approximate value since only 3 runs were carried out at 112.4°C and data at only 2 temperatures are available for this computation.

Three thermal runs were carried out with HBr added initially, the inhibition constant n being computed from the equation

$$-\frac{d(Br_2)}{dt} = \frac{k_t(Br_2)^{\frac{1}{2}}(tBH)}{1+n(HBr)/(Br_2)}. \quad \text{(VIII)}$$

The data are shown in Table V. n was found to be approximately 4.3. Subsequent discussion will show that at any given temperature the value of n should be the same for both the thermal and the photochemical reaction. Extrapolation of the photochemical data would lead to a value of 6.1 for n at 130.2°C, the temperature

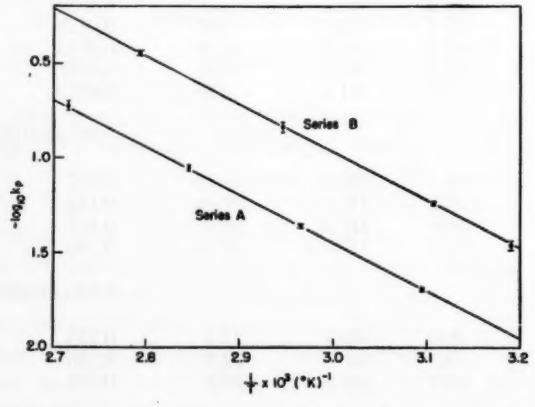

FIG. 3. Temperature dependence of photobromination of isobutane for two series of measurements.

of these experiments. Since so few runs were carried out on the inhibited thermal reaction more confidence must be placed in the value of n obtained photochemically. It should also be pointed out that even in the photochemical experiments the value of n is not determinable with high precision. The agreement shown here between the values 4.3 and 6.1 is therefore quite good.

DISCUSSION

The experimental data presented above can be accounted for by the following mechanism:

$$Br_2+h\nu=2Br \quad (1)$$

or

$$Br_2+M=2Br+M \quad (1a)$$

$$Br+tBH=HBr+tB \quad (2)$$

$$tB+Br_2=tBBr+Br \quad (3)$$

$$tB+HBr=tBH+Br \quad (4)$$

$$2Br+M=Br_2+M. \quad (5)$$

The usual steady-state assumption for the concentrations of Br atoms and tB radicals leads to the following rate expressions:

For the photochemical reaction initiated by step (1)

$$-\frac{d(Br_2)}{dt}=\frac{k_2k_1^{\frac{1}{2}}}{k_5^{\frac{1}{2}}}\frac{(tBH)(Br_2)^{\frac{1}{2}}(M)^{-\frac{1}{2}}}{[1+k_4(HBr)/k_3(Br_2)]}. \quad (IX)$$

For the thermal reaction initiated by step (1a)

$$-\frac{d(Br_2)}{dt}=\frac{k_2k_{1a}^{\frac{1}{2}}}{k_5^{\frac{1}{2}}}\frac{(tBH)(Br_2)^{\frac{1}{2}}}{[1+k_4(HBr)/k_3(Br_2)]}. \quad (X)$$

These rate expressions derived from the postulated mechanisms agree with the empirical rate laws [Eqs. (III) and (VIII)] if one sets $M=P$, $n=k_4/k_3$, $k_p=k_2(k_1/k_5)^{\frac{1}{2}}$, and $k_t=k_2(k_{1a}/k_5)^{\frac{1}{2}}$. It should be noted that $k_{1a}/k_5=K$, the equilibrium constant for the thermal dissociation of bromine molecules, and one may therefore write $k_t=k_2K^{\frac{1}{2}}$. Also, k_1 is used here as a short-hand notation for the expression $k_{app}\alpha I_0$ where k_{app} is a temperature-independent apparatus constant and α is the absorption coefficient of Br_2 for light of incident intensity I_0 for the wavelength range employed.

The reasons for not considering other possible elementary reactions in the over-all mechanism have been discussed previously.[1,3,4] Also, while the infrared analyses indicated that about 5 to 10 percent of the 2-bromo 2-methylpropane was further brominated to give 1,2-dibromo 2-methylpropane, this secondary bromination does not influence the rate constants since the latter were calculated from the *initial* rate of disappearance of bromine. In addition, these analyses show that no consideration need be given to products other than tBBr.

It is readily apparent that on the basis of the proposed mechanism the value of $n=k_4/k_3$ should be the same for both the photochemical and thermal bromination at any given temperature. Within the large experimental error involved in the determination of this inhibition constant this similarity is seen to exist.

As shown previously,[1-4] the experimental activation energy of 11.7 kcal/mole for the photochemical reaction may be assigned to step (2). Since the thermal rate constant is $k_t=k_2K^{\frac{1}{2}}$ it follows that the experimental activation energy, $E_A=35.6$ kcal/mole, of the thermal reaction may be written

$$E_A=E_2+\tfrac{1}{2}\Delta H \quad (XI)$$

where ΔH is the heat of dissociation of Br_2. At 394°K, the mean temperature of the thermal runs, $\Delta H=46.2$

TABLE III. Photobromination of isobutane at reduced light intensity, $0.259I_0'$ (wavelength 4047–5780A).

t°C	Initial pressure (mm at t°C) Br_2	tBH	Initial rate $(-d[Br_2]/dt)$ (mm/min)	k_p (min^{-1})
78.3	30.0	144.6	2.60	0.0434
	30.2	144.2	2.65	0.0441
				0.0438

TABLE IV. Thermal bromination of isobutane.

t°C	Initial pressure (mm at t°C) Br_2	tBH	Initial rate $(-d[Br_2]/dt)$ (mm/sec)	k_t([cc/mole]$^{\frac{1}{2}}$ sec^{-1})
130.2	33.4	171.0	0.0460	0.233
	34.5	168.6	0.0430	0.218
	34.6	164.6	0.0465	0.241
	33.9	166.3	0.0490	0.258
	21.8	164.9	0.0350	0.228
	21.7	165.7	0.0360	0.234
	53.4	154.1	0.0565	0.252
	65.4	145.4	0.0560	0.239
	45.4	152.7	0.0480	0.234
	33.8	120.6	0.0325	0.232
	33.0	260.4	0.0720	0.241
	34.0	371.0	0.1025	0.238
				0.237±0.007
112.4	32.7	242.9	0.0089	0.0314
	32.0	204.7	0.0071	0.0301
	32.4	203.3	0.0072	0.0305
				0.0307±0.0005

TABLE V. Thermal bromination of isobutane at 130.2°C; inhibition by hydrogen bromide.

Br_2	Initial pressure (mm at 130.2°C) HBr	tBH	Initial rate $(-d[Br_2]/dt)$ (mm/sec)	n*
34.2	64.5	198.7	0.00685	3.79
34.1	59.3	197.6	0.00580	4.83
32.8	61.8	198.9	0.00604	4.20

* n was calculated using the value $k_t=0.237$ (cc/mole)$^{\frac{1}{2}}$ sec^{-1}.

TABLE VI. Activation energies of bimolecular reactions involved in brominations.[a]

Reaction	E_A (kcal/mole)	Temp. range (°C)	Reference
H_2+Br	17.2±0.6	160–218	b
$H+HBr$	0	160–218	b
CH_4+Br	17.8±0.4	150–230	c
CH_3+HBr	about 2	150–230	c
CH_3Br+Br	15.6±1.0	150–230	c
C_2H_6+Br	13.3±0.5	35– 90	d
C_2H_5+HBr	assumed 0.8		d
$C_5H_{12}+Br$	17.8±0.3	98–152	e
$C_5H_{11}+HBr$	9.6±2	98–152	e
$C_6H_5CH_3+Br$	7.2±0.6	82–132	f
$C_6H_5CH_2+HBr$	5.0±1.2	82–132	f
i-$C_4H_{10}+Br$	11.4±0.2	40– 95	this work
t-C_4H_9+HBr	7.7±0.3	40– 85	this work

[a] All activation energies have been obtained from photochemical reactions. They have been corrected for the temperature dependence of the frequency factor by subtracting $RT/2$ from the experimental activation energies.
[b] M. Bodenstein and H. Luetkemeyer, Z. Physik. Chem. **114**, 208 (1925).
[c] See reference 1.
[d] See reference 2.
[e] See reference 3.
[f] See reference 4.

kcal/mole[18] giving a value of 12.5 kcal/mole for E_2. Considering the small number of thermal runs at 112.4°C, the appreciably different temperature regions, and the fact that only two temperatures were employed, this may be considered good agreement with the more reliable photochemically determined value of 11.7 kcal/mole.

It has also been shown [1–4] that the apparent activation energy of inhibition by HBr, 8.0 kcal/mole, is equal to E_4-E_3 and that E_3 may be regarded as negligibly small. Therefore, we may write

$$E_4-E_3\cong E_4=8.0 \text{ kcal/mole}.$$

The activation energies for steps 2 and 4 are listed, together with the analogous steps involved in previous bromination studies in this series, in Table VI.

The mechanisms proposed here for the photochemical and thermal reactions appear to be well substantiated by (a) the analysis of the reaction products, (b) the good precision of the rate constants, and (c) the agreement between the values of E_2 and n obtained from both the photochemical and thermal experiments. An interesting aspect of the reaction mechanism is made evident if one attempts to compute a steric factor on the basis of the collision theory. If the thermal rate constant k_t is represented in terms of K and k_2, and if k_2 is written in the Arrhenius form, it is found that the frequency factor A_2 is 3.76×10^{17} (cc/mole) sec^{-1} at 403.4°K (130.2°C). Using 3.0A as the collision diameter of the bromine atom[3] and 4.6A for that of the isobutane molecule,[19] the collision number at that temperature is found to be $Z_2=1.37\times10^{14}$ (cc/mole) sec^{-1}. Then if one introduces a steric factor s_2 to account for the discrepancy ($A_2=s_2Z_2$), s_2 is found to be 2740, an abnormally high result. One may explain this large steric factor on a basis similar to that used to account for the extremely large rates of many unimolecular gas reactions. If several vibrational degrees of freedom can contribute to the energy of activation of the bimolecular reaction step 2 then the fraction of the molecules activated on collision will be *greater*[19a] than $e^{-E/RT}$. If approximately 4 degrees of vibrational freedom contribute, then k_2 will be several thousand times larger than that computed from the collision number and the simple factor $e^{-E/RT}$, in agreement with the value 2740. The computed factor, s_2, would not be regarded as a steric factor in light of such an explanation but rather as a manifestation of the contribution of vibrational degrees of freedom to the energy of activation.

TABLE VII. Heats of formation and dissociation in isobutane.

T°K	$\Delta H_f(tB)$ kcal/mole	$D(tB-H)$ kcal/mole
0	13.4±0.6	89.6±0.6
298	7.5±0.5	91.1±0.5
335	7.1±0.5	91.3±0.5

TABLE VIII. Carbon-hydrogen bond dissociation energies at 0°K.

Bond	Dissociation energy (kcal/mole)	Reference
CH_3-H	101.6±1.0[a]	b
CH_2Br-H	99 ±2.5[a]	b
C_2H_5-H	98.5±2.0[a]	c
$(CH_3)_3CCH_2-H$	94.0±2.5[a]	d
$(CH_3)_3C-H$	89.6±0.6	this work
$C_6H_5CH_2-H$	88.1±1.4	e

[a] Recomputed from original data using the more recently determined heat of formation of HBr (see reference 18).
[b] See reference 1.
[c] See reference 2.
[d] See reference 3.
[e] See reference 4.

BOND DISSOCIATION ENERGIES

As used here the term "bond dissociation energy" refers to the enthalpy change for the dissociation of a particular bond in a molecule to yield two atomic or molecular fragments.

Since the number of molecules of reactants and products are equal for the reaction $tB\text{H}+\text{Br}=tB+\text{HBr}$, we may equate the enthalpy change to E_2-E_4 to obtain $\Delta H_{335}=3.7$ kcal/mole at 335°K, the mean temperature of the photochemical experiments. This may be combined with the heat of formation of hydrogen bromide[18] in the following manner:

$tB\text{H}+\text{Br}=tB+\text{HBr}$	$\Delta H_{335}=$ 3.7 kcal/mole
$\text{HBr}=\text{H}+\text{Br}$	$=87.6$ kcal/mole
$tB\text{H}=tB+\text{H}$	$\Delta H_{335}=91.3$ kcal/mole

[18] U. S. National Bureau of Standards, *Selected Values of Chemical Thermodynamic Properties*, Series III, Washington, D. C., 1948, and Circular 500, Washington, D. C., 1952.

[19] T. Titani, Bull. Chem. Soc. Japan, **5**, 98 (1930).

[19a] See, for example, L. S. Kassel, *Kinetics of Homogeneous Gas Reactions*, Chemical Catalog Company, Inc., Chap. II, III (1932).

to give the bond dissociation energy $D(tB-H)=91.3$ kcal/mole at 335°K. The tertiary C−H bond dissociation energies in isobutane at several temperatures are given in Table VII. In computing enthalpy changes at temperatures other than 335°K National Bureau of Standards data[18] were used, and it was assumed that the heat capacities of isobutane and the tertiary butyl radical are approximately equal. The value at 0°K is compared in Table VIII to those for primary C−H bonds which were also determined from bromination kinetics.

It is of interest to consider further the value for isobutane. As expected it is considerably lower than that for the various aliphatic primary C−H bonds and is roughly comparable to the strength of that bond in the aliphatic side chain of toluene. Numerous investigators, e.g., Kossiakoff and Rice,[20] have concluded on the basis of such evidence as thermal decompositions, resonance stabilization, the isomerization of free radicals, etc. that the strength of the tertiary C−H bond should be about four kilocalories lower than that of the primary. This conclusion is borne out by the present work.

TABLE IX. Heats of formation of radicals at 0°K from bromination kinetics.

Radical	ΔH_f kcal/mole	Reference
methyl	34.0±1.0[a]	b
ethyl	30.4±2.0[a]	c
t-butyl	13.4±0.6	this work
neopentyl	11.1±2.5[a]	d
benzyl	53.9±1.4	e

[a] Recomputed from original data and more recent heats of formation.
[b] See reference 1.
[c] See reference 2.
[d] See reference 3.
[e] See reference 4.

The value of 89.6 kcal/mole agrees well with the value of 89.5 kcal/mole (3.8_8±0.1 ev) which Stevenson[21] obtained for the same bond by the electron impact method. Both of these values are somewhat higher than the 86.0 kcal/mole reported by Butler and Polanyi,[22] based upon extensive studies of the rate of pyrolysis of certain alkyl halides. The difference may be due to their assumption about the dependence of the heat of substitution on the nature of the R group in the reaction $RH+X=RX+H$ as R varies in the alkane series. This discrepancy has also been discussed by Stevenson.[21]

Using the value of 89.6 kcal/mole for the dissociation energy of the tertiary carbon-hydrogen bond in isobutane the heat of formation of the *t*-butyl radical can be calculated.

$$\Delta H_f(tB)=\Delta H_f(tB\text{H})-\Delta H_f(\text{H})+D(tB-\text{H})$$
$$=-24.6-(+51.6)+89.6$$
$$=+13.4 \text{ kcal/mole at } 0°\text{K}.$$

For this computation the heats of formation of isobutane and hydrogen were obtained from the data of the Bureau of Standards.[18,23] The low value of the heat of formation of the *t*-butyl radical at 335°K (Table VII) indicates that this radical is fairly stable. The decomposition of *t*-butyl radicals into methyl radicals and propylene is improbable since the reaction is endothermic to the extent of about 29 kcal/mole at 0°K. Even the slight increase in entropy which probably accompanies this reaction will not make the free energy change favorable for decomposition. Also, the rearrangement of *t*-butyl to isobutyl radical is unlikely; in fact, according to the work of Moore and Wall[16] it is likely that the rearrangement of isobutyl to *t*-butyl radicals is favored. All of these factors are in accord with the absence of bromides other than tBBr in the reaction products as found in the infrared analyses.

The heats of formation of other radicals have been calculated in the same manner and are given in Table IX.

It is now also possible to calculate various carbon-carbon bond dissociation energies. For example, in neopentane (NpH)

$$D(tB-\text{CH}_3)=\Delta H_f(tB)+\Delta H_f(\text{CH}_3)-\Delta H_f(\text{Np}H)$$
$$=+13.4+34.0-(-31.3)$$
$$=+78.7 \text{ kcal/mole}.$$

Similar calculations can be carried out for other compounds and the results are shown in Table X. Again, the heats of formation were obtained from data of the National Bureau of Standards.[18,23] It is interesting to observe the magnitude of the lowering of the dissociation energy of aliphatic carbon-carbon bonds by the introduction of chain branching or a phenyl group.

TABLE X. Carbon-carbon bond dissociation energies at 0°K.

Bond	Dissociation energy (kcal/mole)
CH_3-CH_3	84.5±2.0
$C_2H_5-CH_3$	83.9±3.0
$C_2H_5-C_2H_5$	84.1±4.0
Np$-CH_3$	79.7±3.5
Np$-C_2H_5$	79.5±4.5
$tB-CH_3$	78.7±1.6
$tB-C_2H_5$	78.4±2.6
$tB-tB$	67.9±1.2
$C_6H_5CH_2-CH_3$	74.0±2.4
$C_6H_5CH_2-C_2H_5$	74.5±3.4

[20] A. Kossiakoff and F. O. Rice, J. Am. Chem. Soc. **65**, 590 (1943).
[21] D. P. Stevenson, Discussions Faraday Soc. **10**, 35 (1951).
[22] E. T. Butler and M. Polanyi, Trans. Faraday Soc. **39**, 19 (1943).
[23] U. S. National Bureau of Standards Circular 461, *Selected Values of Properties of Hydrocarbons*, Washington, D. C., 1947.

The Infrared Spectrum and Molecular Constants of $C^{14}O_2$

ALVIN H. NIELSEN AND ROBERT T. LAGEMANN*
Department of Physics, The University of Tennessee, Knoxville, Tennessee
(Received June 3, 1953)

A detailed account of the appearance of and the constants derivable from the infrared absorption spectra of the active fundamentals ν_2 and ν_3 of $C^{14}O_2$ is given. The following constants have been determined: $\nu_2=632.20\ cm^{-1}$, $\nu_3=2225.85\ cm^{-1}$, $B_{000}=0.39078\ cm^{-1}$, $\alpha_3=0.00293\ cm^{-1}$. The harmonic frequencies ω_i and the anharmonic constants x_{ij} for the three isotopic species have been determined. Excellent agreement is obtained between observed and calculated band centers.

INTRODUCTION

IN 1949 R. K. Sheline and W. J. Weigl[1] investigated the infrared prism spectrum of a 30 percent enriched sample of radioactive carbon dioxide. They observed the two active fundamentals ν_2 and ν_3 and listed their band centers as 632 and 2220 cm^{-1}, respectively. The grating spectra of these two fundamentals were later observed by Nielsen and Lagemann.[2] In this preliminary report they described the appearance of the bands and gave the band centers, as determined from analyses of the rotational structures of the bands. The present paper contains a detailed account of the experiment, and values of the harmonic frequencies, the anharmonic constants, and the rotational constants of the molecule.

EXPERIMENTAL WORK

The high-dispersion measurements on ν_2 and ν_3 of $C^{14}O_2$ were made on the prism-grating spectrometer[3] at the University of Tennessee. A 7200 lines-per-inch replica grating was used to record ν_3 at about 4.5μ, and 1800 lines-per-inch replica was used to record ν_2 at about 15.8μ. The dispersed infrared radiation was detected and recorded by means of a Golay pneumatic detector and amplifier, constructed by the Eppley Laboratories, coupled to a type-G Leeds and Northrup Speedomax recorder.

The $C^{14}O_2$ was prepared from $BaCO_3$ which had been enriched in the Oak Ridge Pile. Two samples, 4.2 percent and 16 percent enrichment, respectively, were used for the work described herein. For the observations on ν_3 an 8-cm long cell closed with KBr windows and filled with the 4.2 percent enriched sample to a pressure of 14 cm of mercury was found satisfactory. Several records were made across the entire region from 2160 cm^{-1} to 2260 cm^{-1} with slit widths including a spectral interval of about 0.4 cm^{-1}. The recorded spectral interval includes all of the $C^{14}O_2$ band as well as a few overlapping lines in the P branch of ν_3 for $C^{13}O_2$.[4] Excellent agreement between the line frequencies of the new records and the earlier ones of Nielsen and Yao was obtained. Figure 1 shows a trace of a typical record of ν_3 of $C^{14}O_2$ with the first few lines of the P and R branches labeled with the appropriate J value for the ground state. The lines are well resolved, and the frequencies in cm^{-1}, corrected to vacuum, are listed along with the correct assignments in Table I.

The spectrum of ν_2 was recorded for both the 4.2

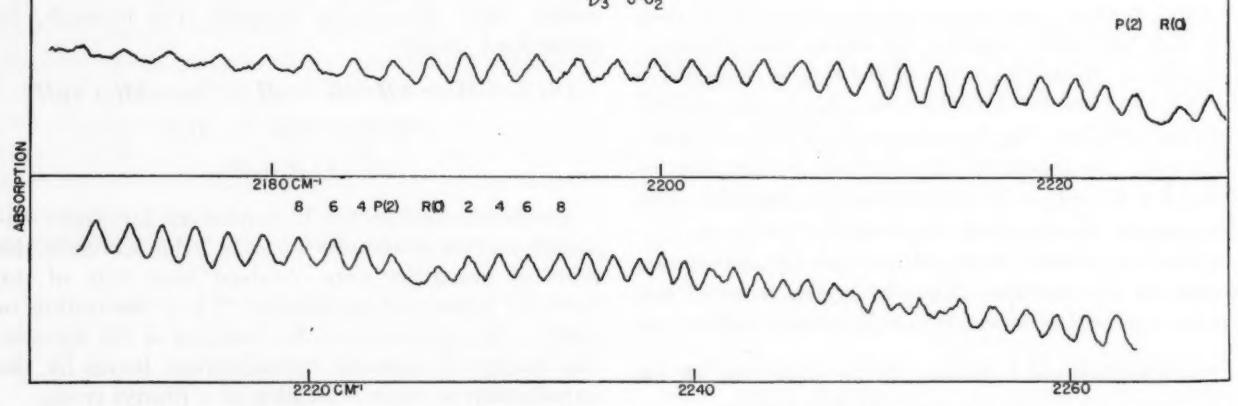

FIG. 1. Trace of the vibration-rotation band ν_3 for 4.2 percent enriched $C^{14}O_2$.

* Department of Physics, Vanderbilt University, Nashville, Tennessee.
[1] R. K. Sheline and W. J. Weigl, J. Chem. Phys. **17**, 747 (1949).
[2] A. H. Nielsen and R. T. Lagemann, Phys. Rev. **83**, 245 (1951).
[3] A. H. Nielsen, J. Tenn. Acad. Sci. **22**, 241 (1947).
[4] Alvin H. Nielsen and Y. T. Yao, Phys. Rev. **68**, 173 (1945); **71**, 825 (1947).

percent and the 16 percent enriched samples using the same cell but with the pressure increased to about 20 cm of mercury. Several records were made with each sample over the spectral interval 600 cm^{-1} to 670 cm^{-1}. This includes ν_2 of $C^{14}O_2$, some overlapping lines in the P branch of $C^{12}O_2$, the extremely weak ν_2 of $C^{13}O_2$, and the difference band $2\nu_2^0-\nu_2^1$ of $C^{12}O_2$. In addition to these records, the background with the cell removed from the beam was also recorded. Traces of typical records of ν_2 and the background, drawn to the same scale, are shown in Fig. 2a, b, c. With the relatively small enrichments of 4.2 and 16 percent the $C^{14}O_2$ molecules in the beam are, of course, a small minority, and it is to be expected that the rotation lines ascribable to $C^{14}O_2$ will be much less intense than those for $C^{12}O_2$. This is not serious in the case of ν_3 because the isotopic shifts $\Delta\nu(C^{13}O_2-C^{14}O_2)$ and $\Delta\nu(C^{12}O_2-C^{14}O_2)$ are 65 cm^{-1} and 130 cm^{-1}, respectively, and the overlapping of lines only becomes confusing near the extreme edge of the R branch of $C^{14}O_2$ where the P lines of $C^{13}O_2$ are rapidly weakening. In the case of ν_2, however, $\Delta\nu(C^{12}O_2-C^{14}O_2)$ is only 35 cm^{-1}. The P branch of $C^{12}O_2$, as may be seen in Fig. 2c, is still quite intense in the region of the Q branch of $C^{14}O_2$ and the overlapping of the isotopic lines is quite confusing. Elimination of atmospheric $C^{12}O_2$ from the spectrometer box was of very little, if any, help because of the overwhelming concentration of $C^{12}O_2$ in the cell itself. To lessen the confusion of the overlapping of lines, records of the two available samples were made, keeping the amount of $C^{14}O_2$ essentially the same in both cases. This had the effect of weakening the $C^{12}O_2$ lines relative to the $C^{14}O_2$ lines and made it possible to distinguish between them. That this was indeed the case may be seen in Fig. 2a, b, c, as the relative intensities have changed sufficiently from Fig. 2a to Fig. 2b to make the identification quite certain, and to make it possible to determine the

TABLE I. Observed and calculated frequencies (cm^{-1}) for ν_3 of $C^{14}O_2$.

Identification	Obs freq. (ν_3 = 2225.85 cm^{-1})	Calc freq.	Δ(O−C)
$P(62)$	2166.81	2166.31	+0.50
$P(60)$	2168.98	2168.58	+0.40
$P(58)$	2170.92	2170.83	+0.09
$P(56)$	2173.18	2173.06	+0.12
$P(54)$	2175.44	2175.26	+0.18
$P(52)$	2177.77	2177.44	+0.33
$P(50)$	2179.73	2179.59	+0.14
$P(48)$	2181.91	2181.73	+0.18
$P(46)$	2184.08	2183.83	+0.25
$P(44)$	2186.08	2185.92	+0.16
$P(42)$	2188.01	2187.98	+0.03
$P(40)$	2190.10	2190.02	+0.08
$P(38)$	2192.12	2192.03	+0.09
$P(36)$	2194.10	2194.02	+0.08
$P(34)$	2196.06	2195.99	+0.07
$P(32)$	2197.98	2197.93	+0.05
$P(30)$	2199.85	2199.85	0.00
$P(28)$	2201.81	2201.75	+0.06
$P(26)$	2203.68	2203.63	+0.05
$P(24)$	2205.45	2205.48	−0.03
$P(22)$	2207.33	2207.30	+0.03
$P(20)$	2209.10	2209.11	−0.01
$P(18)$	2210.90	2210.89	+0.01
$P(16)$	2212.67	2212.64	+0.03
$P(14)$	2214.45	2214.38	+0.07
$P(12)$	2216.07	2216.08	−0.01
$P(10)$	2217.74	2217.77	−0.03
$P(8)$	2219.42	2219.43	−0.01
$P(6)$	2221.17	2221.07	+0.10
$P(4)$	2222.73	2222.69	+0.04
$P(2)$	2224.23	2224.28	−0.05
$R(0)$	2226.66	2226.63	+0.03
$R(2)$	2228.24	2228.16	+0.08
$R(4)$	2229.75	2229.67	+0.08
$R(6)$	2231.10	2231.16	−0.06
$R(8)$	2232.65	2232.62	+0.03
$R(10)$	2234.11	2234.06	+0.05
$R(12)$	2235.42	2235.48	−0.06
$R(14)$	2236.96	2236.87	+0.09
$R(16)$	2238.19	2238.34	−0.14
$R(18)$	2239.50	2239.59	−0.09
$R(20)$	2240.90	2240.91	−0.01
$R(22)$	2242.18	2242.21	−0.03
$R(24)$	2243.45	2243.48	−0.03
$R(26)$	2244.70	2244.74	−0.04
$R(28)$	2245.90	2245.97	−0.07
$R(30)$	2247.22	2247.17	+0.05
$R(32)$	2248.25	2248.34	−0.09

Identification	Obs freq.	Calc freq.	Nielsen-Yao[a] freq.	Δ(O−C)
$P(38)C^{13}O_2$; $R(34)C^{14}O_2$	2249.61	2249.51	2249.39	
$R(36)C^{14}O_2$	2250.61	2250.65		−0.04
$P(36)C^{13}O_2$; $R(38)C^{14}O_2$	2251.68	2251.76	2251.47	
$R(40)C^{14}O_2$	2252.94	2252.85		+0.09
$P(34)C^{13}O_2$; $R(42)C^{14}O_2$	2253.82	2253.91	2253.35	
$P(32)C^{13}O_2$; $R(44)C^{14}O_2$	2255.66	2254.96	2255.42	
$P(30)C^{13}O_2$;	2257.62	2255.97	2257.40	
$R(46)$, $R(48)C^{14}O_2$		2256.97		
$P(28)C^{13}O_2$	2259.46		2259.11	
$P(26)C^{13}O_2$	2261.36		2261.20	
$P(24)C^{13}O_2$	2263.06		2263.09	
$P(22)C^{13}O_2$	2264.91		2264.94	

[a] See reference 4.

TABLE II. Observed and calculated frequencies (cm^{-1}) for ν_2 of $C^{14}O_2$.

Identification	Obs freq. (ν_2 = 632.20 cm^{-1})	Calc freq.	Δ(O−C)
$P(28)$	610.54	610.46	+0.08
$P(26)$	611.99	611.92	+0.07
$P(24)$	613.59	613.57	+0.02
$P(22)$	615.13	615.03	+0.10
$P(20)$	616.73	616.59	+0.14
$P(18)$	618.16	618.25	−0.09
$P(16)$	619.70	619.71	−0.01
$P(14)$	621.29	621.27	+0.02
$P(12)$	622.80	622.83	−0.03
$P(10)$	624.35	624.39	−0.04
$P(8)$	625.97	626.05	−0.08
$P(6)$	627.49	627.51	−0.02
$P(4)$	629.05	629.08	−0.03
$P(2)$	630.73	630.64	+0.09
$R(0)$		632.89	
$R(2)$	634.57	634.55	+0.02
$R(4)$	636.12	636.11	+0.01
$R(6)$	637.60	637.67	−0.07
$R(8)$	639.26	639.24	+0.02
$R(10)$	640.77	640.81	−0.04
$R(12)$	642.43	642.37	+0.06
$R(14)$	644.02	643.94	+0.08
$R(16)$	645.49	645.51	−0.02
$R(18)$	647.07	647.07	0.00
$R(20)$	648.60	648.64	−0.04
$R(22)$	650.04	650.21	−0.17

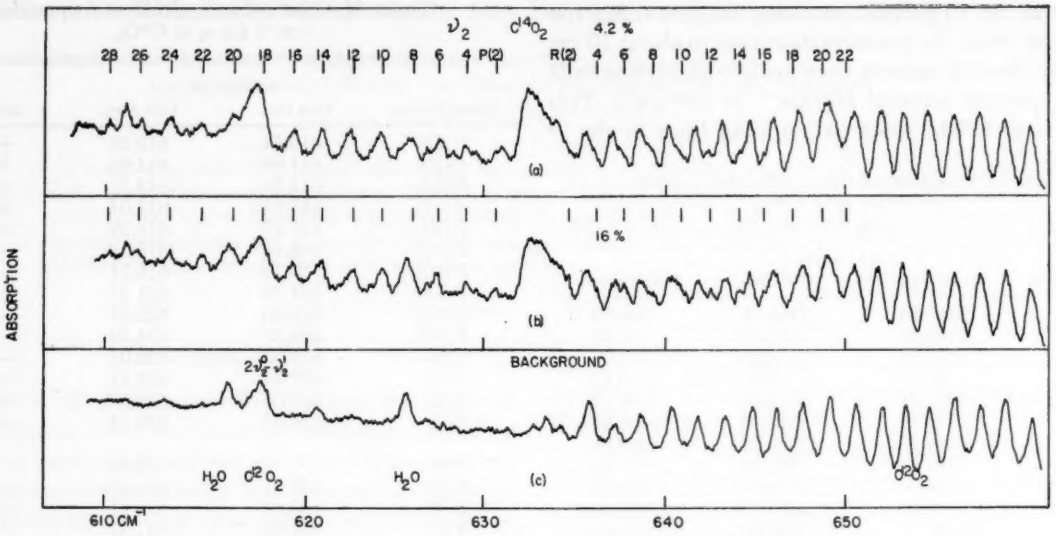

FIG. 2. Traces of vibration rotation band ν_2 for (a) 4.2 percent enriched $C^{14}O_2$ and (b) for 16 percent enriched $C^{14}O_2$. (c) Background of atmospheric absorption in the region of ν_2 for $C^{14}O_2$.

frequencies. Table II gives a list of the observed frequencies and the identification in terms of the J value for the ground state. It is clear from the appearance of the Q branch of $2\nu_2^0-\nu_2^1$ at 618 cm^{-1} in Fig. 2b that the concentration of $C^{12}O_2$ in the 16 percent sample has been appreciably reduced over that in the 4.2 percent sample.

BAND ANALYSES AND RESULTS

With the observed frequencies listed in Table I an analysis of the vibration-rotation band ν_3 was carried out along the usual lines utilizing well-known combination relations. The relation $[R(J-1)-P(J+1)]/2(2J+1)$ was plotted *versus* $(2J+1)^2$. This results in a straight line, the intercept of which is B_{000}, and the slope of which is the centrifugal expansion. In this case, the centrifugal expansion is negligible. As data are available for a great many bands originating in the ground state for the various isotopic species the points for the aforementioned curve were obtained by averaging $[R(J-1)-P(J+1)]/2(2J+1)$ for the bands $\nu_3(C^{12}O_2, C^{13}O_2, C^{14}O_2)$ and from $\nu_2(C^{12}O_2$ and $C^{14}O_2)$. The value of B_{000} thus obtained is 0.39078 cm^{-1}. This is in excellent agreement with the average of values given by Nielsen and Yao[4] for $C^{12}O_2$ and $C^{13}O_2$, $B_{000}=0.39085$ cm^{-1}, and with a more recent value $B_{000}=0.39063$ cm^{-1} given by Goldberg, Mohler, McMath, and Pierce,[5] and with a $B_{000}=0.39037$ cm^{-1} as-

TABLE III. Harmonic frequencies and anharmonic constants for ν_3 of $C^{12}O_2$, $C^{13}O_2$, and $C^{14}O_2$. Constants in cm^{-1}.

Isotopic species	ω_3	x_{13}	x_{23}	x_{33}	ν_3(calc)	ν_3(obs)	Δ(O−C)
$C^{12}O_2$	2396.4	−21.9	−11.0	−12.5	2349.4	2349.4	0.00
$C^{13}O_2$	2328.20	−21.81	−10.30	−11.77	2283.45	2283.53	+0.08
$C^{14}O_2$	2268.33	−20.88	− 9.70	−11.11	2225.97	2225.85	−0.12

[5] Goldberg, Mohler, McMath, and Pierce, Phys. Rev. **76**, 1848 (1949).

cribed by these authors to Herzberg. The band center ν_3 was determined from a plot of $R(J)+P(J)$ *versus* $2J(J+1)$ and was found to be 2225.85 cm^{-1}. The vibration-rotation constant α_3 was found to be 0.00293 cm^{-1}.

From the theoretical expressions for the ω_i and the x_{ij} given by Dennison,[6] the values of ω_3, x_{13}, x_{23}, and x_{33} were computed for $C^{13}O_2$ and $C^{14}O_2$ by making appropriate mass conversions. These quantities, together with the observed and computed band centers for the three isotopic species are given in Table III.

TABLE IV. Harmonic frequencies and anharmonic constants for ν_2 of $C^{12}O_2$, $C^{13}O_2$, and $C^{14}O_2$. Constants in cm^{-1}.

Isotopic species	ω_2	x_{12}	x_{23}	x_{22}	x_{11}	ν_2(calc)	ν_2(obs)	Δ(O−C)
$C^{13}O_2$	672.2	5.7	−11.0	−1.3	1.7	667.3	667.3	
$C^{13}O_2$	653.07	5.54	−10.30	−1.23	1.65	648.65	...	...
$C^{14}O_2$	636.23	5.40	− 9.70	−1.17	1.61	632.18	632.20	−0.02

The agreement between the observed and computed band centers is seen to be quite satisfactory. Table I also lists the computed frequencies using the vibration and rotation constants. With the exception of a few lines in the P branch the calculated line frequencies agree quite well with the observed ones.

ν_2

A rotational analysis similar to the one for ν_3 was also performed for ν_2 of $C^{14}O_2$ in order to determine the band center and rotational constants. Fewer lines were observed in this band than in ν_3, and in nearly all cases the lines were obscured, to some extent, by lines in the P branch of $C^{12}O_2$. In spite of this, the calculated line

[6] D. M. Dennison, Revs. Modern Phys. **12**, 175 (1940).

positions agree very well with the observed ones, as may be seen in Table II. The harmonic frequencies ω_2, and the x_{ij} for the three isotopic species were calculated from the expressions of Dennison[6] and some expressions given by Goldberg *et al.*[5] They are tabulated in Table IV, in which it may be seen that the observed band center 632.20 cm^{-1} agrees very well with the calculated one.

ACKNOWLEDGMENT

The authors are greatly indebted to Dr. C. J. Collins and Dr. O. K. Neville, of the Chemistry Division of the Oak Ridge National Laboratory, for active assistance in the preparation of the samples and for much helpful advice. They are also grateful to Dr. M. T. Clark, of the Oak Ridge Institute of Nuclear Studies, for his kind assistance.

THE JOURNAL OF CHEMICAL PHYSICS VOLUME 22, NUMBER 1 JANUARY, 1954

Kinetics of the Reaction of Ethyl Bromomalonate with Thiosulfate*

WILSON J. BROACH† AND EDWARD S. AMIS
Department of Chemistry, University of Arkansas, Fayetteville, Arkansas

(Received June 29, 1953)

The effect of changing the dielectric constant and the effect of changing the ionic strength on the reaction between thiosulfate ion and ethyl bromomalonate have been studied. The rates of the ion-molecule reaction could be accounted for on the basis of the simple second-order mechanism between the dipolar ester molecule and the thiosulfate ion represented by the equation

$$C_2H_5OOCCHBrCOOC_2H_5+S_2O_3^{=}=C_2H_5OOCCH(S_2O_3)^{-}COOC_2H_5+Br^{-}$$

and considering the change of ionic strength with extent of reaction to be secondary in importance.

The reactions of thiosulfate ion and ethyl bromomalonate was studied at 0.1°C and at 25°C. The specific reaction rates for this reaction conformed to the prediction of the Amis-Jaffe equations with respect to changing ionic strength and conformed to the Amis equation with respect to changing dielectric constant.

IT was thought to be of interest to investigate the rates of the reactions of ethyl bromomalonate with sodium thiosulfate since such rates could be used to check equations now extant for rates of reaction between ions and dipolar molecules.

EXPERIMENTAL

Eastman No. 898 ethyl bromomalonate was used without purification. The sodium thiosulfate, iodine, and methyl alcohol were all of C. P. reagent quality. Soluble starch solution was made up according to procedure given in Kolthoff and Sandell.[1]

The iodine solution was made up in 3 percent KI solution and was standardized against an As_2O_3 standard solution. It was checked at intervals for changes in concentration. The standard arsenic acid solution was prepared according to Kolthoff and Sandell.[1]

A 0.1000 M solution of sodium thiosulfate was prepared and standardized against the iodine solution. The ethyl bromomalonate solution was made so that 25 ml would contain 0.00500 mole. The solvent was methyl alcohol. Weights were calibrated against Bureau of Standard weights. All glassware was calibrated.

The runs using the ethyl bromomalonate were made at 0.10°C ±0.02 and at 25.00°C ±0.02. A calibration run was made first at each dielectric constant to find out the exact quantities of chemicals to be used in the reaction flask, so that the reaction could be studied in the shortest time possible. For the calibration run methyl alcohol, 50.00 ml of thiosulfate solution and almost the requisite amount of water were measured into a 500-ml volumetric flask. Enough room was left to add 25 ml of ethyl bromomalonate solution and a small measured volume of water. The flask containing the thiosulfate in the alcohol-water solution was brought to the thermostat temperature and 25 ml of ethyl bromomalonate, which had also been brought to the same temperature, was pipetted from a bottle and drained into the 500-ml volumetric flask containing the thiosulfate solution. Each reactant was, therefore, 0.0100 molar. This concentration was used for both reactants in all the runs recorded in this paper. A small amount of water, which was carefully measured, was then added to bring the total volume up to exactly 500 ml. The mixture was quickly dumped into a wide mouth bottle which had been placed in the thermostat. Since the reaction went to completion in only a few minutes, 50.00-ml samples were taken consecutively in as short a time as possible and delivered to flasks each containing 10.00 ml of I_2 solution which was in excess. The time of the reaction was

---

* Presented before the Division of Physical Chemistry at the Eighth Southwest Regional Meeting of the American Chemical Society, Little Rock, Arkansas, December, 1952.

† Presented by Wilson J. Broach to the Graduate Faculty of the Department of Chemistry of the University of Arkansas in partial fulfillment of the requirements for the degree of Doctor of Philosophy, February, 1953.

[1] I. M. Kolthoff and A. B. Sandell, *Textbook of Quantitative Inorganic Analysis* (Macmillan Company, New York, 1936), pp. 589–593.

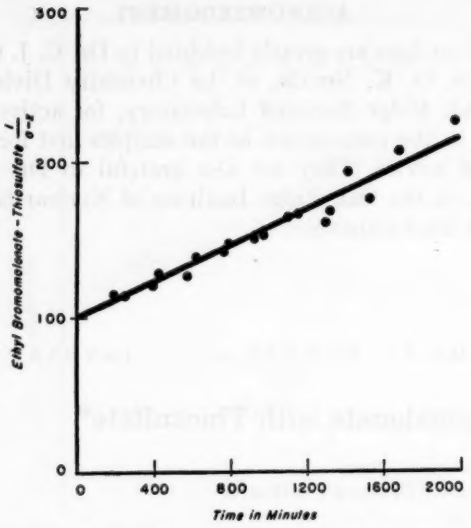

FIG. 1. Data for typical duplicate runs for the reaction of ethyl bromomalonate and thiosulfate at 0.10°C and at a dielectric constant of 54.0.

checked with a stop watch beginning when the last drop of ethyl bromomalonate was added and ending when the last drop of the 50-ml sample was delivered into the iodine solution. A total of nine samples was drawn from each run and the excess iodine titrated as soon as possible with standard thiosulfate solution. Starch was used as an indicator in runs of low alcohol concentration but was discarded in runs of higher alcohol concentration because of erroneous results. At higher alcohol concentrations the titration was made using the disappearance of the iodine color as the end point. The end point was checked by a potentiometric titration and proved to be the correct end point.

After the calibration run the quantities of water and alcohol to be used were known exactly, thus permitting one to obtain earlier data in these runs than in the calibration runs. The water, alcohol, and thiosulfate were measured into a reaction flask and brought to thermostatic temperature. The ethyl bromomalonate solution was added and the timing begun as the last drop entered. The reaction flask was equipped with a stirrer which was turned on for a few seconds just as the last of the malonate entered. The procedure from here was similar to that of the calibration run.

The rate of the reaction at 25.00°C ±0.02 was found to be so rapid that it was necessary to modify the procedure used at 0.10°C ±0.02. For these reactions a reaction flask was devised from a 500 ml erlenmeyer flask. The flask was equipped with a 29/40 ground glass stopper and a center well approximately 3 cm in height and 6 cm in diameter. Methyl alcohol, water and thiosulfate solution were pipetted into that portion of the flask outside of the well. Methyl alcohol, water, and ethyl bromomalonate were pipetted into the center compartment. The methyl alcohol-water concentration were the same both in the well and in the portion outside of the well, thus preventing temperature changes when the two solutions were mixed. The substances were added to the flask in such quantities that when mixed the solution contained the desired concentration of each component.

The flask was stoppered and placed in a thermostat for a sufficient length of time to allow all materials to reach an equilibrium temperature. The reaction flask was then suddenly inverted and shaken insuring an instantaneous mixing of the reactants. The timing of the reaction was started with the inversion of the flask. A measured amount of standard I_2 solution was dumped into the flask to stop the reaction. At this point, the timing of the reaction was completed. The small flask which had contained the I_2 solution was thoroughly washed and the washings poured into the reaction flask. The progress of the reaction was followed by a titration of the excess I_2 with a standard thiosulfate solution. An electric timer, calibrated to 1/100 of a second, was used in timing these reactions.

In order to study the effect of changing ionic strength of the medium on the two reactions discussed above, the required amounts of 1.0000 N KNO_3 solution were added to the reaction flask in place of an equal quantity of water to give the desired ionic strengths.

DIELECTRIC CONSTANT AND SALT EFFECTS UPON THE ETHYL BROMOMALONATE-THIOSULFATE REACTION

In Fig. 1 are plotted the data of duplicate sample runs at 0.10°C ±0.02 and a dielectric constant of 54.0. The plot is the reciprocal of the concentration of one of the two reactants present at equal concentrations *versus* the time in minutes. From the slope of this line the specific velocity constant was calculated in liters per mole per minute. This method and these units were used in evaluating the specific velocity constants of all runs. The plot is indicative of the precision and accuracy of the measurements.

In Table I are the data for the reaction of ethyl

TABLE I. Dielectric constant effect on the reaction between ethyl bromomalonate and thiosulfate ion.

Weight percent methyl alcohol	Dielectric constant	$1/D$	Specific velocity constant k'	Logk'
		0.10°C		
20.3	71.4	0.0142	58.4	1.766
28.6	67.5	0.0148	56.0	1.748
37.3	63.3	0.0158	48.8	1.688
56.0	54.2	0.0184	23.6	1.373
66.2	49.2	0.0203	17.0	1.230
72.3	46.2	0.0216	12.0	1.079
		25.00°C		
20.4	69.0	0.0144	393	2.594
37.8	60.9	0.0164	256	2.408
57.3	51.4	0.0195	140	2.146
67.5	46.6	0.0215	120	2.079
79.4	40.9	0.0244	72.2	1.865

bromomalonate and thiosulfate ion at 0.10°C and at 25.00°C and at varying dielectric constants.

These data are plotted in Fig. 2 where values of $\log k'$ are used as ordinates and reciprocals of D are used as abscissas. The plots are straight lines of a negative slope in agreement with the requirements of the equation.[2]

$$\ln k'_{D=D} = \ln k'_{D=\infty} + \frac{z\epsilon\mu}{DkTr^2}. \quad (1)$$

From Eq. (1) the slope S of the line of a plot of $\log k'$ *versus* $1/D$ is given by

$$S = z\epsilon\mu/kTr^2, \quad (2)$$

and assuming a radius r for the complex of 2.5×10^{-8} cm the moment of the ethyl bromomalonate molecule μ may be calculated. The value found at 0.10°C is 5.45×10^{-18} and for 25.00°C the value is 4.60×10^{-18} giving an average value of 5.03×10^{-18} which is a reasonable value. In Eq. (1) $k'_{D=D}$ is the specific velocity constant for the reaction at any selected dielectric constant D; $k'_{D=\infty}$ is the velocity constant at infinite dielectric constant; $Z\epsilon$ is the charge on the ionic reactant; k is the Boltzmann gas constant; T is the absolute temperature, and the other quantities have been defined.

In Table II is presented energies of activation, ΔE, Arrhenius frequency factors, $\log Z$, and entropy change, ΔS, at constant dielectric and at constant composition of the solvent. The frequency factor is for a bimolecular reaction and its units are liters per mole per minute, that is, it has the same units as the specific velocity constant.

The following equations were used in the calculation of the values in Table II:

$$\Delta E = \frac{2.303RT_2T_1\,(\log k_2' - \log k_1')}{T_2 - T_1}, \quad (3)$$

$$\mathrm{Log}Z = \frac{\Delta(T\log k')}{\Delta T}, \quad (4)$$

$$\Delta S = \frac{R}{2.303} \times \left(\log Z - \log \frac{kT}{h}\right). \quad (5)$$

TABLE II. ΔE, $\log Z$, and ΔS for the reaction between ethyl bromomalonate and thiosulfate at constant dielectric constant and at constant composition.

Constant D				Constant composition			
D	ΔE calories per mole	$\log Z$	ΔS calories per mole per degree	Percent MeOH	ΔE calories per mole	$\log Z$	ΔS calories per mole per degree
69.0	12 130	11.4	−1.21	20.3	11 700	11.1	−1.47
64.5	12 280	11.5	−1.12	28.6	11 500	11.0	−1.55
58.8	12 870	11.8	−0.86	37.3	11 800	11.1	−1.47
52.6	13 470	12.1	−0.60	56.0	12 100	11.1	−1.47
46.0	14 370	12.6	−0.17	72.3	13 300	11.7	−0.95

[2] E. S. Amis, J. Chem. Educ. **30**, 351 (1953).

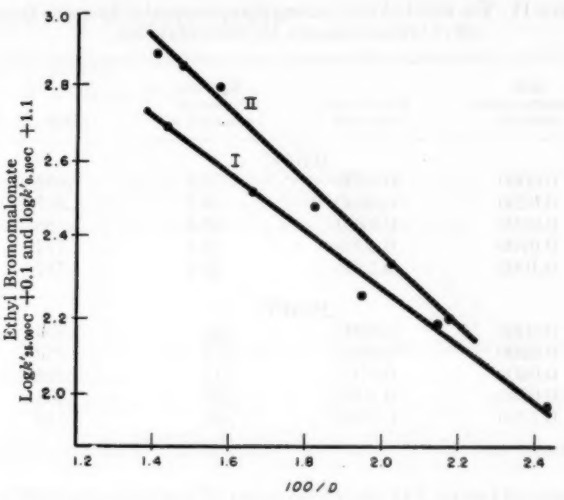

FIG. 2. Plot of $\log k'$ *vs* $100/D$ for the ethyl bromomalonate-thiosulfate reaction. Curve I, 25.00°C; Curve II, 0.10°C.

In Eq. (5) k is the Boltzmann gas constant and h is Planck's constant.

In both cases when the dielectric constant is decreased the energy of activation increases and ΔS increases. This energy increase could be expected from a decrease in specific velocity at lower dielectrics.

From the equation,[3]

$$\Delta E_c = \frac{Z\epsilon\mu\cos\theta}{D_1D_2r^2}\Delta D, \quad (6)$$

the Coulombic energy of activation may be calculated over a range of dielectric constant of the solvent and can be compared with the observed values. In Eq. (6) if we consider a head on approach of the ion to the molecule, then $\cos\theta$ (where θ is the angle of approach) becomes 1. In the calculation μ is taken as 5.03×10^{-18} and r as 2.5×10^{-8} cm. Results of these calculations are presented in Table III.

The calculated values of Coulombic energies of activation agree with observed values at the high dielectric constants, but as the dielectric constants become lower the differences between calculated and observed values become greater, but never differ by as much as a factor of two. Similar trends have been

TABLE III. Calculated changes of Coulombic energies of activation in kilocalories per mole as a function of dielectric constant of the solvent compared with observed changes of energy of activation.

Dielectric range ΔD = diff.	ΔE_c kcal change of Coulombic energy	ΔE_o kcal observed
69.0—64.5	−0.174	−0.150
69.0—58.8	−0.415	−0.740
69.0—52.6	−0.765	−1.340
69.0—46.0	−1.220	−2.240

[3] E. S. Amis, J. Am. Chem. Soc. **63**, 1606 (1941).

TABLE IV. The effect of ionic strength on removal of bromine from ethyl bromomalonate by thiosulfate ion.

Salt concentration molarity	Total ionic strength	Specific velocity constant k'	logk'
	0.10°C		
0.0000	0.0300	70.8	1.844
0.0200	0.0500	64.2	1.807
0.0400	0.0700	61.2	1.786
0.0700	0.1000	59.5	1.774
0.1000	0.1300	60.6	1.782
	25.00°C		
0.0000	0.0300	393	2.594
0.0200	0.0500	357	2.552
0.0400	0.0700	312	2.494
0.0700	0.1000	288	2.438
0.1200	0.1500	330	2.518

observed before.[3] It might be pointed out that the differences between observed and calculated values of coulombic energies could have been markedly reduced by a slight decrease in the value of r used in Eq. (6). However, it was felt that the same r should be used in coulombic energy calculation that was used in calculation of the moment of the molecule from the logk' *vs* $1/D$ relationship.

The effect of the ionic strength on the removal of bromine from ethyl bromomalonate by the thiosulfate ion was studied in 20.3 and 20.4 percent methyl alcohol solvents, respectively, at 0.10°C ±0.02 and at 25.00°C ±0.02. Table IV shows the results from these runs at 0.10°C and 25.00°C, respectively.

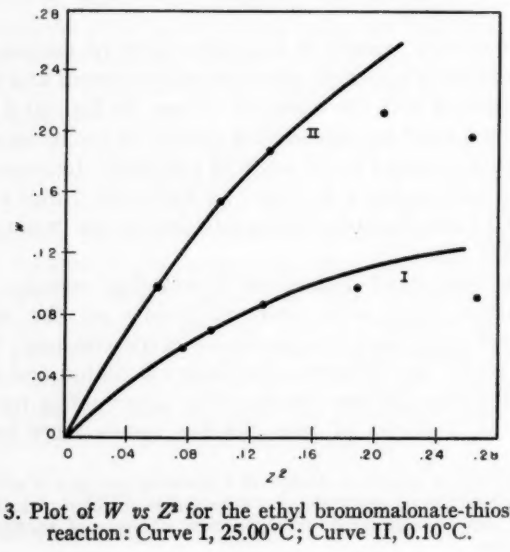

FIG. 3. Plot of W *vs* Z^2 for the ethyl bromomalonate-thiosulfate reaction: Curve I, 25.00°C; Curve II, 0.10°C.

It can be seen from this table that, as the ionic strength increases, the velocity constant decreases except in the case of higher ionic strength. This effect of the ionic strength is in agreement with the Amis-Jaffe equation,[4] mentioned earlier in this paper. Values of W and Z^2 (dimensionless variables defined by Amis and Jaffe, and functions, respectively, of the logrithm of the velocity constant and of the ionic strength) derived from data are fitted to the theoretical curve of the Amis-Jaffe equation and are presented in Fig. 3 using 4×10^{-8} cm as the distance of closest approach. It can be observed from this graph that in regions of higher ionic strength the data fall away from the theoretical curve. This deviation from theoretical curve has been noted by other investigators.[5]

In Table V are presented data to show the effect of ionic strength on the energy of activation, Arrhenius frequency factor, and entropy. Low energies of activation are to be expected from the great velocity of the reaction.

TABLE V. Energies of activation (ΔE), entropies (ΔS), and Arrhenius frequency factors (log$Z$) for the reaction of ethyl bromomalonate and thiosulfate ion is a function of ionic strength.

Ionic strength	ΔE	Log$Z$	ΔS
0.0400	11 500	11.0	−1.5
0.0500	11 200	10.7	−1.8
0.0700	10 600	10.3	−2.2
0.1000	10 300	9.9	−2.5
0.1500	10 900	10.4	−2.1

Thus, it is evident that the neutralization of the electron-repelling CO_2^- substituent by ester formation favors the bimolecular mechanism for the substitution of the halogen by a negative ion. The reaction of ethyl bromomalonate with thiosulfate ion is then a S_N2 reaction as one would guess from the work of Hughes and associates[6,7] on the hydrolysis of halogen substituted carbon compounds. The mechanism is apparently the simple second order mechanism given in the abstract.

[4] E. S. Amis and G. Jaffe, J. Chem. Phys. **10**, 598 (1942).
[5] Amis, Jaffe, and Overman, J. Am. Chem. Soc. **66**, 1823 (1944).
[6] Cowdrey, Hughes, Ingold, Masterman, and Scott, J. Chem. Soc. (London), 1252 (1937).
[7] E. D. Hughes and A. T. Taher, J. Chem. Soc. (London), 956 (1940).

Structure of the Monomer of Formic Acid

I. L. KARLE AND J. KARLE
Naval Research Laboratory, Washington, D. C.
(Received April 27, 1953)

The structure of the monomer of formic acid was determined by the sector-microphotometer method in electron diffraction. The equilibrium distances are C=O=1.23±0.01A, C−O=1.36±0.01A, O−O=2.27 ±0.005A, and angle OCO=122.4°±1°. The average displacements from equilibrium due to the molecular vibrations are listed in Table I.

THE monomer of formic acid has been previously studied by electron diffraction[1,2] and by infrared[3,4] and microwave spectroscopy.[5] Recently the crystal structure of formic acid has been determined.[6] The results for the interatomic distances or the principal moments of inertia have differed in each case. In this paper, the monomer of formic acid has been investigated using the sector-microphotometer method in electron diffraction,[7–9] and the results for the structural parameters are different from any of the other investigations. These results are contained within the limits of error assigned to the Schomaker and O'Gorman results;[2] however, their specific model lies outside our limits of error.

PROCEDURE

Electron diffraction photographs were taken through an s and an s^2 sector at a camera length of ~11 cm and a wavelength near 0.06A. Two different procedures were used to obtain the monomer of the acid. In the first,[1] not more than 0.2 g of acid was placed in a liter flask and the flask and nozzle were maintained at 150–160°C during the electron diffraction exposures. Under these conditions the degree of the dissociation of the dimer was at least 0.93 (using the equilibrium constant and heat of dissociation data of Coolidge).[10] The second procedure was the one described by Schomaker and O'Gorman[2] in which the acid was dissociated by passing through a nozzle about 70 mm long which was packed with $\frac{1}{16}$-in. nichrome helices and heated to 250°C. The photographs obtained from these two procedures were indistinguishable. The photographic plates were rotated while being scanned by a microphotometer,[7] the density readings were converted to relative intensity,[9] and a molecular scattering curve was obtained. The radial distribution function $f(r)$ was computed from the molecular scattering curve.

In practice the peaks of the computed $f(r)$ curves often are composed of peaks for several distances. The two criteria used to decompose composite peaks into individual peaks for each distance are that the peaks should be Gaussian in shape and that the areas under the peaks multiplied by their respective equilibrium distances should be proportional to the scattering powers of the pairs of atoms involved. These criteria are found to be quite restrictive. The permissible range of distances and amplitudes of vibration are most conveniently obtained from a comparison of theoretical intensity curves with the experimental curve. A detailed discussion of the procedure and an evaluation of experimental accuracy can be found in previous papers.[7–9]

ANALYSIS AND RESULTS

The radial distribution curve $f(r)$ for formic acid is illustrated in Fig. 1. It is essentially zero everywhere except in the vicinity of the interatomic distances. There is no indication of a significant amount of dimer present in the molecular scattering curve since there are no peaks beyond the one at ~2.27A. Furthermore, the absence of a peak at ~3A in the $f(r)$ curve implies that the equilibrium position for the hydrogen atom in the hydroxyl group is not the *trans* position. The first composite peak was decomposed most satisfactorily into peaks for two C−O distances at 1.23 and 1.36A, with average displacements from equilibrium of about 0.02 and 0.046A, respectively, and O−H and C−H distances at 0.97 and 1.09A, respectively. The second composite

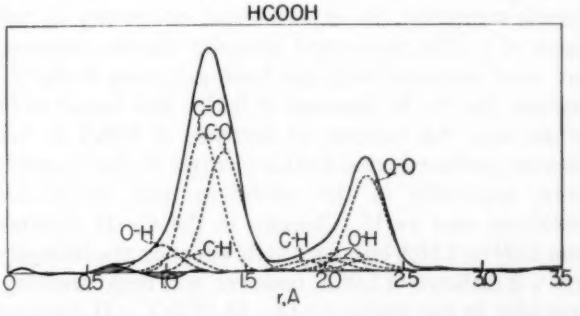

FIG. 1. The solid line is the computed radial distribution curve $f(r)$. The dashed lines indicate the individual peaks for each interatomic distance. The shaded portion is the difference between the computed curve and the sum of the component peaks.

[1] J. Karle and L. O. Brockway, J. Am. Chem. Soc. **66**, 574 (1944).
[2] V. Schomaker and J. M. O'Gorman, J. Am. Chem. Soc. **69**, 2638 (1947).
[3] S. H. Bauer and R. M. Badger, J. Chem. Phys. **5**, 852 (1937).
[4] V. Z. Williams, J. Chem. Phys. **15**, 232 (1947).
[5] J. D. Rogers and D. Williams, American Physical Society Meeting, Washington, D. C., April, 1951.
[6] Holtzberg, Post, and Fankuchen, Acta Cryst. **6**, 127 (1953).
[7] I. L. Karle and J. Karle, J. Chem. Phys. **17**, 1052 (1949).
[8] J. Karle and I. L. Karle, J. Chem. Phys. **18**, 957 (1950).
[9] I. L. Karle and J. Karle, J. Chem. Phys. **18**, 963 (1950).
[10] A. S. Coolidge, J. Am. Phys. Soc. **50**, 2166 (1928); **52**, 1874 (1930).

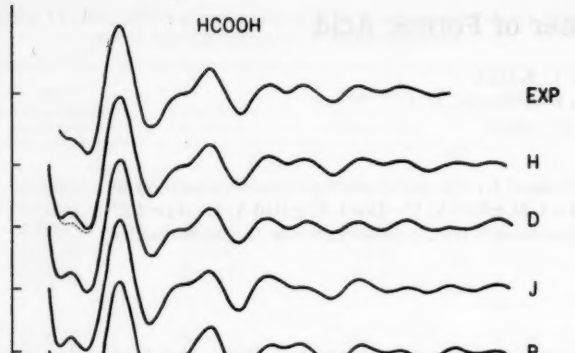

FIG. 2. The experimental and computed molecular intensity curves.

peak is due mostly to the O−O distance at 2.27A with an average displacement of about 0.042A. All the remaining area under the second peak is accounted for by the one long C−H and three long O−H distances where the two HCO angles were assumed to be equal and the COH angle was chosen to be 105°. These angles can be varied considerably without destroying the agreement, so that no accurate conclusions can be drawn about the angles involving hydrogen atoms. No chemical decomposition is suggested by the $f(r)$ curve since no area is left over for any H_2O, CO, or CO_2, which are possible decomposition products of formic acid.

Theoretical intensity curves were computed for comparison with the experimental curve, Fig. 2. The intensity curves were found to be relatively insensitive to considerable change in the angles and bond lengths containing hydrogen atoms. Changes of the order of ten degrees in the HCO angles had almost no effect on the intensity curves; hence these angles were assumed to be equal in all the models. Changes in the COH angle had a small effect on intensity curves below $s=7$, and curves with a COH angle near 105° were somewhat better than those with angles near 95° or 115°. The main effect of placing the hydrogen atom in the hydroxyl group in the *trans* position instead of the *cis* was to decrease the intensity of the maximum at $s=6$ by 10 percent, which exceeds somewhat the experimental inaccuracy in this region of s. The theoretical intensity curves presented here were computed with the hydrogen atom in the *cis*-position. An O−H distance of 0.97A was found to be satisfactory. An increase or decrease of 0.06A in this distance produced considerable changes in the intensity curve, especially in the minimum near $s=13$ and maximum near $s=15$. Changes in the C−H distance from 1.09 to 1.18A had very little effect on the intensity curve. A distance of 1.06A, however, was unsatisfactory, especially in the region $s=14-18$. The C−H distance was assumed to be 1.09A. The addition of 3.6 percent of the dimer of formic acid, the maximum amount which could have been present under the conditions at which the photographs were taken, does not change to any extent the appearance of the intensity curves.

Curve *H*, Fig. 2, which is based on the parameters determined from the radial distribution curve reproduces the experimental curve satisfactorily. The average s/s_{exp} for twelve maxima and minima is 0.999 ± 0.0042 where the largest individual deviation from the average is 0.008. Intensity curves were also computed for the models indicated on the parameter chart, Fig. 3. Values of $\langle l_{ij}^2\rangle_{Av}^{\frac{1}{2}}$ were chosen to be most consistent with the $f(r)$ curve. Models *E*, *F*, *H*, and *L* reproduce the experimental curve sufficiently well to be included in the acceptable range of parameters. Curves *D*, *J*, and *P* illustrate various unacceptable features encountered in the theoretical intensity curves such as a shelf at $s=10$ which is too high in curve *J* and too low in curve *P* (- - - - line on the parameter chart), a too low maximum at $s=11.5$ in curve *D* (— — line on parameter chart), and a too shallow minimum in curve *D* and a misplaced minimum in curve *J* at $s=13$ (—·—·—· line on the parameter chart). The portion of the curve between $s=15$ and 25 consists of a deep minimum between two shallow minima and four maxima approximately equal in height. Curves *D*, *J*, and *P* do not reproduce these features (——— line on parameter chart). Beyond $s=26$ the molecular scattering as compared to the background scattering was so weak that reliable measurements of the intensity could not be made. It should be noted that the theoretical curves *H* (our model) and *D* (model of Schomaker and O'Gorman) differ in the intensities of a pair of maxima in the region of $s=25\rightarrow30$. Model *D* is in better agreement in this region with the visually estimated intensity curve appearing in the paper of Schomaker and O'Gorman. Our microphotometer data do not extend this far and consequently no comparison can be made. However, the elimination of model *D* from this experiment was based on the disagreements in the more accurate experimental

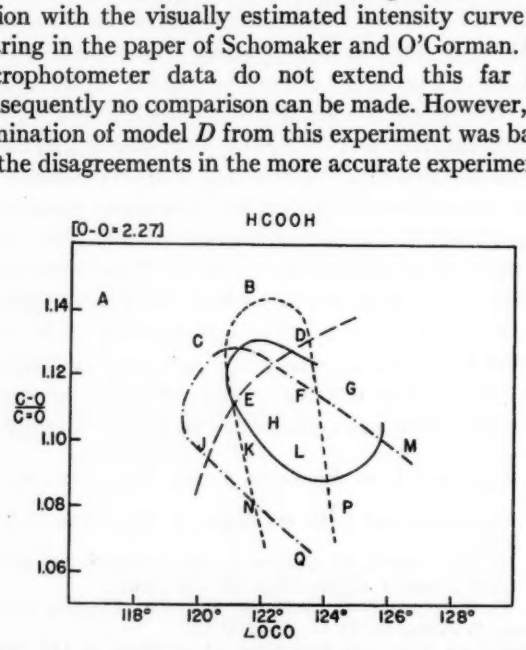

FIG. 3. Parameter chart for HCOOH. The positions of the letters indicate the parameters of the models for which intensity curves were computed. The dashed and dotted lines indicate when particular features of the intensity curves were sufficiently different from the experimental curve to make them unacceptable.

region $8<s<25$ which were indicated above and illustrated in Fig. 2.

All the computed curves of models in Fig. 3 differ from the experimental curve in the region of $s=2\rightarrow5$. This difference can be largely eliminated by using variable instead of constant coefficients in the intensity formula. This change produces the dotted curve H.

Variations in the $\langle l^2\rangle_{Av}^{\frac{1}{2}}$ values for the C−H and O−H distances had little effect on the intensity curves and no definite values could be assigned. The over-all damping of the intensity curve was quite sensitive to the $\langle l^2\rangle_{Av}^{\frac{1}{2}}$ value for the O−O distance. The heights of some of the maxima were sensitive to the $\langle l^2\rangle_{Av}^{\frac{1}{2}}$ values of the C−O and C=O distances. For every model, better curves were obtained for $\langle l_{C-O}{}^2\rangle_{Av}^{\frac{1}{2}}$ larger than $\langle l_{C=O}{}^2\rangle_{Av}^{\frac{1}{2}}$. All experimental $\langle l_{ij}{}^2\rangle_{Av}^{\frac{1}{2}}$ values need a small correction as a result of the spreading of the gas about the nozzle during an exposure to an electron beam.[9] This correction has been taken into account in the reported values. The best values as determined from the intensity curves are near the values obtained from the radial distribution curve.

The structure of HCOOH as obtained from the microphotometer method is given in Table I.

The best models of the earlier electron diffraction investigations which were performed by the visual method are model A (Karle and Brockway)[1] and model D (Schomaker and O'Gorman),[2] which are indicated on the parameter chart. The values of the principal moments of inertia obtained from the infrared spectra[4] are $I_A=86.38\times10^{-40}$, $I_B=75.27\times10^{-40}$, and $I_C=11.11\times10^{-40}$ gm cm², whereas those obtained from the microwave spectra[5] are $I_A=80.05\times10^{-40}$, $I_B=70.00\times10^{-40}$ and $I_C=10.05\times10^{-40}$ gm cm² (assuming that HCOOH is planar and that the relation $I_A=I_B+I_C$ is applicable). The values of the principal moments of inertia of the best model in the present investigation are $I_A=81.61\times10^{-40}$, $I_B=70.11\times10^{-40}$, and $I_C=11.50\times10^{-40}$ gm cm². The value of I_B is almost entirely dependent upon the O−O distance which has been determined to be 2.27–2.275A in all three electron-diffraction investigations of HCOOH. On the other hand, the value of I_C is somewhat sensitive to the O−H and C−H distances, which could not be determined precisely in this experiment. The value of I_C can easily be changed by several tenths with small changes (0.01–0.02A) in these two distances and/or variations within the permitted range of other distances in the molecule. For instance, with C−H =1.08A and O−H=0.95A, model L duplicates the I_C of V. Z. Williams.[4]

TABLE I. Equilibrium distances and average displacements from equilibrium for HCOOH obtained from quantitative electron diffraction data.[a]

	r, A	$\langle l^2\rangle_{Av}^{\frac{1}{2}}$, A
C=O	1.23±0.01	<0.030
C−O	1.36±0.01	0.044±0.008
O−O	2.27±0.005	0.040±0.008
O−H	0.97±0.05	
C−H	1.09 (assumed)	
∠OCO=122.4°±1°		

[a] The uncertainties in the distances and angles are interrelated. Consequently, models in which the parameters have the extremes of the values listed above may be quite unsatisfactory.

The results of the recent crystal structure determination[6] of formic acid show that in the solid the molecules are arranged in the form of infinite chains and that the C=O bond length is 1.23±0.03A, the C−O bond length is 1.26±0.03A, and that the O−C=O angle is 123±1°. It is interesting to note that the C=O distance and the O−C=O angle are the same (within limits of error) in the vapor and solid states but that the C−O distance is reported to be reduced by 0.10A in the solid state. The agreement between the results of Schomaker and O'Gorman and those of this paper establishes the fact that the C−O distance is 1.36±0.01A in the vapor state.

We wish to thank Mr. P. O'Hara of the National Bureau of Standards for performing the IBM computations of the $f(r)$ and intensity curves.

Temperature Gradients in Reacting Systems*†

SIDNEY W. BENSON
Department of Chemistry, University of Southern California, Los Angeles 7, California
(Received July 16, 1953)

A study of the heat conduction equation for reactions going on in a spherical flask leads to a calculation of three parameters, τ the mean lifetime for the establishment of stationary states, ΔT_m the maximum temperature difference between the walls of the vessel and the reacting gas, and the average temperature difference $\langle \Delta T_m \rangle_{Av}$. These are given by

$$\tau = \frac{\rho c_v r_0^2}{\pi^2 K}, \quad \Delta T_m = \frac{RHr_0^2}{6K}, \quad \langle \Delta T_m \rangle_{Av} = \frac{RHr_0^2}{15K}$$

in which ρ is the density, c_v the specific heat at constant volume, r_0 the radius of the vessel, K the coefficient of thermal conductivity, R the specific rate of reaction, and H the heat of reaction.

In liquid systems under usual conditions τ is of the order of r_0^2 minutes (r_0 in cm) while $\langle \Delta T_m \rangle_{Av}$ is about ± 0.2°C (for $H = \pm 10$ kcal, half-life = 1 hour, $r_0 = 5$ cm) so that such effects are usually negligible. In gases on the other hand $\langle \Delta T_m \rangle_{Av}$ can be of the order of magnitude of 2°C or higher depending on the various conditions, resulting in significant errors in observed rate constants and activation energies. The effects of added inert gases, pressure, vessel packing, and other parameters are discussed. A very crude treatment of convection shows that it is not expected to alter appreciably the magnitude of $\langle \Delta T_m \rangle_{Av}$.

INTRODUCTION

WHILE there has been a considerable amount of work done on the temperature gradients in chemically reacting systems prior to and during explosions,[1–3] relatively little attention has been given to the much smaller, but still possibly important gradients which may occur in normally "slow" reactions.[4] Such gradients may be expected to occur during chemical reactions going on in closed vessels[5] when the usual processes of temperature equilibration, convection, and conduction are insufficiently fast to compensate for temperature changes arising from the heat of the reaction. Because of the large temperature coefficients of most reactions (35 percent per percent change in T), temperature gradients of as little as 1°C across a reaction vessel can cause a 5-percent error in measurements of the rate constant and even greater errors in estimations of the activation energies of the reaction.[6]

In the following sections I shall first calculate the approximate gradients which may be expected in "slow" reaction systems and then go on to estimate the extent to which convection may play a role in diminishing them.

Conduction Gradients

Let us assume that in a "slow" reaction the only mechanism for establishing temperature equilibrium is via conduction. Then the well known equation for the temperature distribution in a closed reaction vessel will be

$$\frac{\partial T}{\partial t} = \frac{K}{\rho c_v} \nabla^2 T + \frac{R \cdot H}{\rho c_v}, \tag{1}$$

in which K = coefficient of thermal conductivity, ρ = density, c_v = specific heat, R = specific rate of the reaction, and H = the heat of the reaction.[7] For a spherical vessel of radius r_0, T will be a function of r and t only and $\nabla^2 T = (1/r)(\partial^2/\partial r^2)(rT)$ so that defining $\theta = rT$, Eq. (1) becomes

$$\partial\theta/\partial t = (K/\rho c_v)\partial^2\theta/\partial r^2 + (RH/\rho c_v)r. \tag{2}$$

For periods of time which are short compared to the half-life of the reaction we may consider R to be independent of time and for very small temperature gradients, neglect as a first approximation the dependence of R on T.[8] Under these conditions R is a constant and the

* This work was supported by the U. S. Office of Ordnance Research under Contract No. DA-04-495-Ord-345 with the University of Southern California.

† Presented before the Division of Physical and Inorganic Chemistry, at the meeting of the American Chemical Society in Chicago, September, 1953.

[1] B. Lewis and G. von Elbe, *Combustions, Flames and Explosions of Gases* (Academic Press Inc., New York, 1951), Chap. I (especially Section 3).

[2] O. K. Rice, J. Chem. Phys. **8**, 727 (1940).

[3] P. L. Chambré, J. Chem. Phys. **20**, 1795 (1952).

[4] W. S. Horton, J. Phys. Colloid Chem. **52**, 1129 (1948) has made similar calculations of the temperature gradients in liquid systems arising from improper attainment of temperature equilibrium across the walls of a reaction vessel at the start of the reaction.

[5] These problems are, as we shall see, usually negligible in flow systems because of the flow velocities employed. Much more important problems in these latter systems arise from the slowness of heat transfer from the vessel walls to an initially cooled gas.

[6] It is generally assumed that the effects of such small temperature gradients will tend to cancel in making comparisons of the rate constants. As will be shown later this may be quite far from the actual case.

[7] In this equation we have approximated $\nabla \cdot (K\overrightarrow{\nabla T}/\rho c_v) = (K/\rho c_v)\nabla^2 T$, thus neglecting the dependence on temperature of the ratio $K/\rho c_v$. This is a valid approximation for small temperature gradients.

[8] Rice (reference 2) has checked the original work of D. A. Frank-Kamenetzky, Acta Physicochimica U.R.S.S. **10**, 365 (1939) by making a numerical integration of the stationary state equation (obtained by equating $\partial\theta/\partial t = 0$ in Eq. (2)) for the case in which the exponential dependence of R on T is included. The conditions for an explosion (that the temperature not have a finite value) can be obtained from this equation.

A simpler approach under the conditions of the present calculations (i.e., small temperature gradients) is to assume $R = R_0[1 + \alpha(T - T_0)]$ where α is the temperature coefficient of the

temperature gradients calculated will be less than those obtaining under real conditions.

The solution to Eq. (2) is then well known[9] and we can write it directly in terms of $T(r,t)$:

$$T(r,t)-T(r_0)=\frac{RHr_0^2}{6K}\left[1-\frac{r^2}{r_0^2}+\frac{12r_0}{\pi^2 r}\times\sum_1^\infty\frac{(-1)^n}{n^3}\sin\left(\frac{\pi nr}{r_0}\right)\exp\left(-\frac{n^2t}{\tau}\right)\right], \quad (3)$$

where $T(r_0)$ is the constant temperature at the walls of the flask ($r=r_0$) and is independent of time; $\tau=\rho c_v r_0^2/\pi^2 K$ a positive quantity and the boundary conditions are $T(r,0)=T(r_0)$ throughout the sphere.

The maximum temperature will exist at the center of the vessel $T(0,t)$ and the maximum temperature difference at any time t is given by $T(0,t)-T(r_0)=\Delta T_m(t)$ which can be shown to be:

$$\Delta T_m(t)=\frac{RHr_0^2}{6K}\left[1+\frac{12}{\pi^2}\sum_1^\infty\frac{(-1)^n}{n^2}\exp(-n^2t/\tau)\right]. \quad (4)$$

For times $t>\tau$, the series in Eq. (4) converges very rapidly to zero and we reach an asymptotic limit for the maximum temperature difference:[10]

$$\Delta T_m(\infty)=\frac{RHr_0^2}{6K}. \quad (5)$$

The mean time needed to establish this temperature distribution is given by τ:

$$\tau=\frac{\rho c_v r_0^2}{\pi^2 K}. \quad (6)$$

A final parameter of importance is the average maximum difference in temperature $\langle\Delta T_m\rangle_{Av}$ between the walls of the vessel and the reacting medium. Since the temperature distribution is parabolic we can average ΔT_m over a spherical flask. We find:

$$\langle\Delta T_m\rangle_{Av}=\frac{3}{r_0^3}\int_0^{r_0}r^2\Delta T_m dr$$

$$=0.4\Delta T_m(\infty)=\frac{RHr_0^2}{15K}. \quad (7)$$

reaction and T_0 is the wall temperature. The resulting equations are only slightly more complicated to deal with than Eq. (2) and the stationary state solutions will be either a sine function or a hyperbolic sine function depending on the sign of H.

[9] H. Bateman, *Partial Differential Equations of Mathematical Physics* (Dover Publications, New York, 1944), p. 353.

[10] Inspection of Eq. (3) shows that under these conditions (i.e.—at the stationary state) the temperature gradient in the flask is parabolic:

$$\Delta T(r,\infty)=\Delta T_m(\infty)[1-r^2/r_0^2].$$

Conduction Gradients in Liquid Systems

The two parameters essential to a discussion of the conduction temperature gradients are $\Delta T_m(\infty)$ (henceforth ΔT_m) and τ, given by Eqs. (5) and (6), respectively. For most liquids the product ρc_v lies between 0.3 and 1.0 cal/cc-°C while K is found in the range 0.5 to 1.5 cal/cm-sec-°C$\times10^{-3}$. If we choose as probable values, 0.6 cal/cc-°C and 1.0×10^{-3} cal/cm-sec-°C, respectively we find that stationary states in liquid systems will be reached in a time $\tau=60r_0^2$ seconds$=r_0^2$ minutes (r_0 in cm).

For a 500-cc vessel ($r_0\sim5$ cm) τ will be about 25 minutes while for a 50-cc vessel ($r_0\sim2.3$ cm) and $\tau\sim5.3$ minutes. We see that in liquid systems stationary states are approached only very slowly so that it may be expected that simple stirring will tend to minimize gradients.[11]

To compute the expected order of magnitude of the maximum temperature difference in liquids, let us calculate ΔT_m for a reaction of half-life ~1 hour ($k\sim2\times10^{-4}$ sec^{-1}) with reactive concentrations of 0.05 mole/liter such that the initial specific rate of reaction $R=1\times10^{-8}$ mole/cc-sec. If the heat of reaction H is taken to be ±10 kcal/mole and $K=1\times10^{-3}$ cal/cm-sec-°C. Then we calculate for a 500-cc vessel, $\Delta T_m=\pm0.42$°C or for a 50-cc vessel, $\Delta T_m=\pm0.08$°C. The average temperature differences $\langle\Delta T_m\rangle_{Av}$ (Eq. (7)) are, respectively, ±0.17°C and ±0.03°C.

In view of the fact that most liquid reactions are run in small vessels and that the normal range of the appropriate physical properties of liquids are rather limited, we can see that the expected temperature gradients will be rather small unless the heats of reactions are much larger than ±10 kcal, the reacting concentrations are greatly in excess of 0.05 M or the half-lives are much smaller than 1 hour.

Conduction Gradients in Gas Systems

The situation for gases is quite different than that for liquids since the relevant physical properties of gases show a much greater range of variation and heat conductivities are much smaller. Thus c_v lies in the range 0.1 to 0.4 cal/g-°C for most gases, ρ(STP)$=4.5\times10^{-5}M$ g/cc (M=molecular weight) and K is about 7×10^{-5} cal/cm-°C-sec except for H_2 and He which are higher by about a factor of 5.

Taking $c_v=0.25$ cal/g-°C and $K=7\times10^{-5}$ cal/cm-°C-sec we find for the mean time to establish a stationary state; $\tau=1.6\times10^{-2}Mr_0^2$ sec at STP. For a mean molecular weight of 60 and a 500-cc vessel $\tau=25$ seconds while for a 50-cc vessel under the same conditions $\tau=5.3$ seconds. Thus we see that stationary states can be

[11] R. P. Bell and J. C. Clunie, Proc. Roy. Soc. (London) **A212**, 16 (1952) have shown how the rate constants of first order fast reactions can be measured experimentally in liquid systems from the maximum change in temperature observed. Their calculations are based on the consideration of conduction.

established much more quickly in gases than in liquids and moreover that these times will be much more sensitive to the particular gases studied and the conditions employed.[12]

We also find that the maximum temperature differences are larger than in liquid. Thus for a gas reaction at STP ($\sim 4.5\times10^{-5}$ mole/cc) with a half-life of 1 hour, $R=9.0\times10^{-9}$ mole/cc-sec. Again choosing $H=\pm10$ kcal/mole this gives $RH=9\times10^{-5}$ cal/cc-sec and if we take $K=7\times10^{-5}$ cal/cm-°C-sec we find ΔT (500 cc) $=\pm5.3$°C and for the mean temperature difference $\langle\Delta T_m\rangle_{Av}$ (500 cc) $=\pm2.1$°C. These are rather significant temperature differences and they can have important bearings on measured rate constants and activation energies.[13] In particular if the half-lives are much shorter than 1 hour then these values will be proportionately larger.

It is interesting to look at the dependence of $\langle\Delta T_m\rangle_{Av}$ and τ on physical properties in some greater detail. $\langle\Delta T_m\rangle_{Av}$ is proportional to the specific rate of reaction and the heat of the reaction. If the reaction is studied at lower concentrations the specific rate decreases and ΔT_m decreases proportionately. Since, however, K is independent of pressure, rate constants measured in the same vessel at constant temperature but at decreasing initial pressures might be expected to show a systematic decrease for exothermic reactions and an increase for endothermic reactions.[13a] By similar reasoning if we compare the same reaction at constant density at two different temperatures, ΔT_m will be greater in absolute magnitude at the higher temperature because of the difference in half-life and we should find that the observed activation energies will appear too great for exothermic reactions and too small for endothermic reactions.

The effect of added inert gases is also rather interesting. ΔT_m will be affected by inert gases only if their heat conductivities are notably different than that of the reacting gas. In general only H_2 and He show marked differences, having thermal conductivities some 5 times greater than most other gases. Therefore the addition of H_2 or He to a reacting gas will lower ΔT_m and so appear to speed up endothermic reactions and slow down exothermic reactions.[14]

The results of packing a vessel with, for example solid glass rod or tubes, will be to lower the effective value of r_0^2 and so swamp out the temperature gradients. This result arises from the fact that for normally slow reactions the subsequent heating of the added glass by the heat of the reaction will in general be quite small because of the relatively large heat capacity of solids compared to gases. Such effects allow us generally to neglect in the heat Eq. (2) the conduction through the glass walls.[15] On the other hand they are a limiting factor which makes almost impossible the direct measurements of small changes in gas temperatures by means of thermocouples, etc.

The mean life time of stationary gradients is similarly very sensitive to reaction conditions. Thus τ will decrease with decreasing concentration and molecular weight. At pressures of 10-mm Hg, τ is of the order of 0.1 second so that gradients are quickly established at low pressures. In many reaction studies attempts are made to avoid wall effects by using large vessels. Such efforts will increase τ but simultaneously increase ΔT_m so that if the reactions are not thermoneutral wall effects may be diminished at the expense of adding errors due to gradients.[16] Finally it may be noted that the addition of inert gases will increase τ in proportion to their molecular weights while their effects on K will be negligible except for H_2 and He which have already been noted (reference 12).

Effects of Convection

While conduction effects are relatively simple to treat, the effect of free convection due to gravity introduces complexities into the problem which make only the simplest of approximations possible.

One such approach is to calculate the maximum possible gradients to be expected in a reacting system. If the system reaches a steady state then we can write the following energy balance equation for a spherical vessel of radius r_0:

$$\langle\Delta T\rangle_{Av}\cdot h\cdot 4\pi r_0^2=(4/3)\pi r_0^3\cdot R\cdot H, \tag{8}$$

where the product RH represents as before the specific rate of heat evolution, $\langle\Delta T\rangle_{Av}$ is the mean difference in temperature between the reaction mixture and the vessel walls and h is some average heat transfer coefficient for the system. Solving for $\langle\Delta T\rangle_{Av}$ we find

$$\langle\Delta T\rangle_{Av}=\frac{RH}{3h}r_0, \tag{9}$$

which can be compared with $\langle\Delta T_m\rangle_{Av}$ for the conduction

[12] The effect of H_2 is quite spectacular because of its low molecular weight and high thermal conductivity. For H_2 at STP we find τ (500 cc) $=0.16$ second and τ (50 cc) $=0.03$ second.

[13] As typical examples we find for the reaction $N_2O\rightarrow N_2+1/2O_2-20$ kcal, $\bar{M}=44$ so that for a 1 hour half-life τ (500 cc) $=80$ sec and $\langle\Delta T_m\rangle_{Av}=+4.2$°C. For $C_2H_5\rightarrow CH_4+C_2H_4-16$ kcal; $\bar{M}=44$, τ is the same and $\langle\Delta T_m\rangle_{Av}=-3.4$°C.

[13a] The effects will be in opposite directions because of the difference in sign in ΔT_m. At sufficiently low pressures ΔT_m becomes negligible.

[14] It seems quite possible that the unique affects of H_2 on the rates of some pyrolytic decompositions at low pressures in bringing the rate constant up to their high-pressure limits may be a reflection of the above considerations. Such speculation however must be treated very cautiously in view of the complex chain character of these decompositions.

[15] For example in a 500-cc Pyrex glass vessel, the volume of glass in the walls is about 75 cc and the total heat capacity of the walls is then about 38 cal/°C. For other typical cases considered above the total heat evolved in 10 minutes is 16 cal so that if we neglected entirely the heat flow from the walls to the thermostat their total temperature rise would not exceed 0.4°C.

[16] This is of course compensated for by the decrease in the total amount of heat liberated as a result of the lower pressures.

process Eq. (7), namely $RHr_0^2/15K$. The ratio of $\langle\Delta T\rangle_{Av}/\langle\Delta T_m\rangle_{Av}=5K/r_0h=5/Nu(r_0)$ where $Nu(r_0)$ is the dimensionless quantity used in engineering calculations called the Nusselt number. For laminar flow in tubes of diameter d, average Nusselt numbers are in the range of 5,[17] so that if we can assume that the flow distribution which may be set up in a spherical flask is laminar and similar to that in a cylinder we see that the net effect of convection is to cause some central stirring and so diminish the maximum temperature differences but not otherwise appreciably affect the mean temperatures in the system. The reason for this is the large thicknesses associated with boundary layers of gases moving at low velocities.

A crude method of estimating the appropriateness of the approximation to laminar flow is to calculate the maximum velocities in the system and see if they are near the values expected for turbulence. A simple model for such a calculation is to assume that the laminar flow consists of a central column of low-density gas moving upwards in the reaction vessel compensated by an equal outer flow of high-density gas moving downwards.[18] The average resistance over the entire path can be estimated by Poiseuille's formula for flow and we find that the mean pressure drop per unit length of such a path is given approximately by

$$\frac{dp}{dx}=\frac{160\eta\bar{V}}{r_0^2}, \tag{10}$$

where η is the viscosity and $\bar{V}$ is the mean velocity over the path. This can now be equated to the mean driving force for the convection which is crudely $\frac{1}{2}g(\Delta\rho_m)$ where g is the acceleration of gravity and $\Delta\rho_m$ is the maximum density difference in the vessel. We then find solving for $\bar{V}$:

$$\bar{V}=\frac{r_0^2g(\Delta\rho_m)}{320\eta}=\frac{r_0^2\cdot 980}{320}\left(\frac{\Delta\rho_m}{\rho}\right)\left(\frac{\rho}{\eta}\right)$$

$$=3.1r_0^2\left(\frac{\Delta\rho_m}{\rho}\right)\left(\frac{\rho}{\eta}\right). \tag{11}$$

If we assume that the maximum temperature differences are of the order of 1 percent so that $\Delta\rho_m/\rho\sim 0.01$, then since for most gases at STP, the kinematic viscosity $(\eta/\rho)\sim 0.1$ cm^2/sec, we see that for $r_0=5$ cm, $V\sim 8$ cm/sec which is below the critical velocities expected for turbulence in such systems. This can be expressed in terms of the Reynold's number for the vessel

$$R=2r_0\frac{\bar{V}\rho}{\eta}=6.2r_0^3\left(\frac{\Delta\rho_m}{\rho}\right)\left(\frac{\rho}{\eta}\right)^2, \tag{12}$$

which using the above magnitudes has the value $R=775$. The critical value for turbulent flow corresponds to $R\sim 2000$.

We see then from the above considerations that we might expect convection to be relatively unimportant unless the densities exceed those at STP or the vessels are increased in size or the density differences exceed 1 percent.[19] On the other hand for pressures of 100 mm Hg or less or for smaller vessels the Reynold's numbers decrease rapidly and we may expect that conduction plays the major role in heat transport.[20]

These considerations receive some support from the work of Rice *et al.*[2,21] who found that in 200 cc vessels at 371°C and 32 mm Hg pressure of azomethane ($C_2H_6N_2$) the experimentally calculated value of the heat transfer coefficient is 1.6×10^{-4} cal/cm^2-sec-°C. This is very close to the value that one would calculate for this system using a Nusselt number of 5,[22] showing that even under the gradients of some 15°C occurring in these incipient explosions the flow conditions must be close to laminar.

ACKNOWLEDGMENTS

I would like to express my thanks to Dr. Charles Cousin, Postdoctoral Research Fellow from Paris at University of Southern California for many helpful discussions during the preparation of this paper and also to the U. S. Office of Ordnance Research for their enthusiastic support of the present project.

Note added in proof.—Professor O. K. Rice has called to my attention the alternative methods used by himself and co-workers [A. O. Allen and O. K. Rice, J. Am. Chem. Soc. **57**, 313 (1935) and O. K. Rice and D. V. Sickman, J. Chem. Phys. **4**, 242 (1936)] for calculating the temperature effects to be expected for thermally explosive reactions and it is of some interest to compare the two methods in the case of azomethane for which data are available. Using the data of Table III (reference 1) for $T=341.0$°C, an initial pressure of 140 mm Hg (3.66×10^{-6} moles/cc) in a 200 cc vessel ($V_0=3.86$ cm) and a rate constant of 5.6×10^{-3} sec^{-1} and $H=50$ kcal/mole, we find that $R=2.05\times 10^{-8}$ mole/cc-

[17] E. R. G. Eckert, *Introduction to the Transfer of Heat and Mass* (McGraw Hill Book Company, Inc., New York, 1950), p. 104. Note that we can also write $\Delta T=RHr_0^2/3K\cdot Nu(r_0)$ and that $\langle\Delta T\rangle_{Av}\ll\langle\Delta T_m\rangle_{Av}$ only for $Nu(r_0)\gg 5$.

[18] This flow would be expected for exothermic reactions while the reverse would be obtained in endothermic reactions.

[19] Even with much larger Reynold's numbers the Nusselt's numbers in the system do not grow too rapidly and they do not exceed values of 10 until the Reynolds numbers are in excess of 10 000.

[20] W. G. Kannuluick and E. H. Carman, Proc. Phys. Soc. (London) **B65**, 701 (1952) have shown that in a vertical tube with central heated filament, convection is experimentally undetectable for temperature differences of 3°C (internal diameter of 7 mm and a length of 12 cm).

[21] Rice, Allen, and Campbell, J. Am. Chem. Soc. **57**, 2212 (1935).

[22] The authors state that the above cited heat transfer coefficient is in excess of what one would compute for heat conduction. Since they do not give any calculations or quantitative explanations for such a conclusion, it is my feeling that the above calculation shows to the contrary that this is not the case and that convection is not too important in these experiments. They do find that the heat transfer coefficient increases with increasing pressure and this does indicate that there is probably some laminar flow at the higher densities. The results are still not very different from what one would compute purely on the basis of conduction. [Note: in the second paper (reference 2) Rice seems to have reversed his earlier statements (above) on the importance of convection.]

sec and $RH=1\times10^{-3}$ cal/cc-sec. If we now take K for azomethane to be 1.2×10^{-4} cal/cm-deg-sec (estimated from n-pentane data) at this temperature we find $\langle\Delta T_m\rangle_{Av}=7.3°C$ (a value of 1.5×10^{-4} for K gives $\langle\Delta T_m\rangle_{Av}=5.8°C$). Using the activation energy of 50.2 kcal/mole given by Rice and Sickman this leads to a value of the ratio of the experimentally observed rate constant, k_e, to that expected in the absence of heating effects, k_0 of 1.62. (For $\langle\Delta T_m\rangle_{Av}=5.8°C$, $k_e/k_0=1.47$.)

We can now compare this with the values of k_i/k_0 given by Rice and Sickman for a relative pressure $P_i/P^*=0.73$ (P^* = explosion limit at 341°C = 191-mm Hg) which is 1.52. The agreement is certainly better than would have been expected considering the differences in the two methods, the nature of the extrapolation from the explosion limits and the difficulty of the experiments and can be taken as lending further support to the considerations presented in this paper.

THE JOURNAL OF CHEMICAL PHYSICS VOLUME 22, NUMBER 1 JANUARY, 1954

Raman Spectra of Chlorofluoromethanes in the Gaseous State*

HOWARD H. CLAASSEN†
Department of Physics, University of Oklahoma, Norman, Oklahoma
(Received July 8, 1953)

Raman spectra of gaseous CCl_4, CCl_3F, CCl_2F_2, $CClF_3$, and CF_4 are presented in the form of microphotometer traces. All but one of the fundamental frequencies of these molecules have been observed.

INTRODUCTION

THE series of halogenated methanes, CCl_4, CCl_3F, CCl_2F_2, $CClF_3$, and CF_4, have all been studied earlier both by infrared absorption and by the Raman effect. The infrared spectra have been observed in several laboratories, most completely by Plyler and Benedict,[1] who observed the absorption from 2 to 38μ for four of these methanes in the gaseous state and for CCl_4 over part of this range. The Raman spectrum of gaseous CCl_4 has been obtained by Morino, Watanabe, and Mizushima[2] and by Welsh[3] *et al.* Yost, Lassettre, and Gross[4] observed one Raman band of CF_4 in the gaseous state. Other Raman data for these compounds are limited to the liquid state. The data for CCl_3F have been summarized by Zietlow, Cleveland, and Meister.[5] Raman data for liquid CCl_2F_2 have been reported by Bradley;[6] for liquid $CClF_3$ by Kahovec and Wagner[7] and by Delwaulle and Francois;[8] for liquid CF_4 by Yost, Lassettre, and Gross.[4] Only in the case of CCl_4 have all fundamentals been previously observed for the gaseous state. Thus, a study of the Raman spectra of this series of molecules in the gaseous state seemed desirable.

EXPERIMENTAL

The spectrograph used and the method of measuring Raman frequencies have been described earlier.[9] Some of the weak diffuse Raman bands of the present investigation were difficult to see on enlarged prints, and could be located more precisely on microphotometer traces. Frequencies of these bands were measured on the microphotometer traces as well as on prints.

A new Raman tube and an irradiation apparatus, especially designed for gases,[10] were used. For CCl_4 it was necessary to heat the sample to increase the vapor pressure. The tube was sealed off with enough CCl_4 in it to exert six atmospheres pressure at 150°C. The whole Raman tube was then wrapped with No. 26 Nichrome wire (one-cm spacing) and a sample temperature of about 175°C achieved by electric heating.

The spectra were recorded on Kodak Tri-X Panchromatic Film, developed in Dk 60a for eight minutes at 20°C. Microphotometer traces were made with a Leeds and Northrup photoelectric instrument.

The sample of CCl_4 was Merck, C. P. The other four compounds were furnished by Dr. W. S. Murray and Dr. R. C. McHarness of the Jackson Laboratory of E. I. du Pont de Nemours and Company.

RESULTS AND DISCUSSION

Photographs of microphotometer traces of the spectra for the gaseous state are given in Fig. 1 for the two

* This work has been supported by the U. S. Atomic Energy Commission under Contract No. AT-(40-1)-1074.
† Present address: Wheaton College, Wheaton, Illinois.
[1] E. K. Plyler and W. S. Benedict, J. Research Natl. Bur. Standards **47**, 202 (1951).
[2] Morino, Watanabe, and Mizushima, Sci. Papers Inst. Phys. Chem. Research, Tokyo **39**, 348 (1942).
[3] Welsh, Crawford, Thomas, and Love, Can. J. Phys. **30**, 577 (1952).
[4] Yost, Lassettre, and Gross, J. Chem. Phys. **4**, 325 (1936).
[5] Zietlow, Cleveland, and Meister, J. Chem. Phys. **18**, 1076 (1950).
[6] C. A. Bradley, Jr., Phys. Rev. **40**, 908 (1932).
[7] L. Kahovec and J. Wagner, Z. physik. Chem. **B48**, 188 (1941).
[8] L. Delwaulle and F. Francois, Compt. rend. **214**, 828 (1942); J. phys. et radium VIII **7**, 15, 53 (1946).
[9] Smith, Nielsen, and Claassen, J. Chem. Phys. **18**, 326 (1950).
[10] H. H. Claassen and J. Rud Nielsen, J. Opt. Soc. Am. **43**, 352 (1953).

molecules of tetrahedral symmetry, in Fig. 2 for the molecules of symmetry C_{3v}, and in Fig. 3 for CCl_2F_2 of symmetry C_{2v}. Frequency shifts from the Hg 4358A exciting line are given in the figures, as well as sample pressures and temperatures. The first three columns of Table I give the frequencies and descriptions of the observed Raman bands and the Hg exciting lines with which each shift was observed. The next two columns list corresponding frequencies from earlier Raman and infrared studies.

TABLE I. Raman and infrared spectral data for CCl_4, CCl_3F, CCl_2F_2, $CClF_3$, and CF_4.

Present Raman Data, Gaseous State			Previous Raman data	Previous infrared data gaseous state	Interpretation
Wave number	Description	Exciting Hg lines			
		CCl_4, Symmetry T_d			
			Gas (ref. 3)	(ref. 1)	
216	m[a]	e	221	···	e fundamental
311	m,d	e	310.0	···	f_2 fundamental
431	w, sh	e	434	···	$2\times216 = 432 (A_1 \div E)$
457	s	e, k	459.0	···	a_1 fundamental
···	···	···	756	778[b]	$311 \div 457 = 768$ F_2
798	m, d	e	794.3	795[b]	f_2 fundamental
		CCl_3F, Symmetry C_{3v}			
			Liquid (ref. 5)	(ref. 1)	
241	s, d	e	244.6	···	e fundamental
349.5	s, sh	e, k	350.5	350	a_1 fundamental
394	m, d	e	397.8	401	e fundamental
535.2	vs, sh	e, k	535.8	535	a_1 fundamental
847	m, d	e	835.4	847	e fundamental
1090	vw	e	1068.1	1085	a_1 fundamental
		CCl_2F_2, Symmetry C_{2v}			
			Liquid (ref. 6)	(ref. 1)	
261.5	m, sh[a]	e, k	260	···	a_1 fundamental
322	w, d	e	320	···	a_2 fundamental
433	m	e, k	433	437	b_1 fundamental
···	···	···	···	446	b_2 fundamental
457.5	s, sh	e, k, i	455	···	a_1 fundamental
640	w	e	···	···	$2\times322 = 644$ A_1
667.2	s, sh	e, f, k, i	664	667	a_1 fundamental
923	w, d	e	919	922	b_1 fundamental
1098	m	e	1082	1101	a_1 fundamental
1167	w, d	e	1147	1159	b_2 fundamental
		$CClF_3$, Symmetry C_{3v}			
			Liquid (ref. 7)	(ref. 1)	
350	m, vd	e	356	···	e fundamental
468.2	m, sh	e, k	···	···	a_1 fundamental Cl^{37}
475.8	s, sh	e, k, i	478	···	a_1 fundamental Cl^{35}
560	w	e	560	563	e fundamental
781.7	vs, sh	e, k, i	784	781	a_1 fundamental
1106	w	e	1092	1105	a_1 fundamental
1217	w, d	e	1205	1212	e fundamental
		CF_4, Symmetry T_d			
			Liquid (ref. 4)	(ref. 1)	
434.5	m	e	437	···	e fundamental
586.3	w	e	···	···	Impurity?
624	m	e	635	630	f_2 fundamental
638	m	e			
865	w	e	···	···	$2\times434.5 = 870 (A_1+E)$
908.2	vs, sh	e, k, i	904	···	a_1 fundamental
1282	w, d	e	···	1277	f_2 fundamental

[a] Apparently a sharp Q branch and rotational branches.
[b] These values are interpolated from Fig. 12 of reference 1.

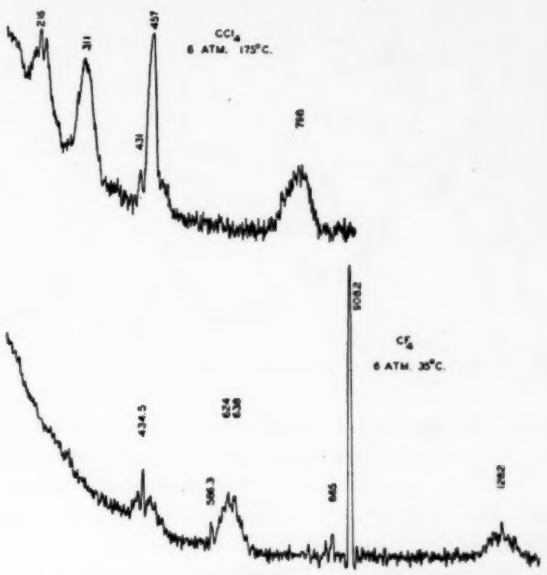

FIG. 1. Raman spectra of gaseous CCl_4 and CF_4.

The accuracy of the frequency values obtained in the present work depends greatly on the shape and intensity of the bands. For the totally-symmetric vibrations the uncertainty is in most cases less than one wave number. For the "breathing" vibration of CF_4, for example, the average shifts measured from Hg, e, i, and k, were 907.9, 908.3, and 908.3, respectively. For the most diffuse bands, on the other hand, the uncertainty may be as high as five wave numbers. The accuracy of the

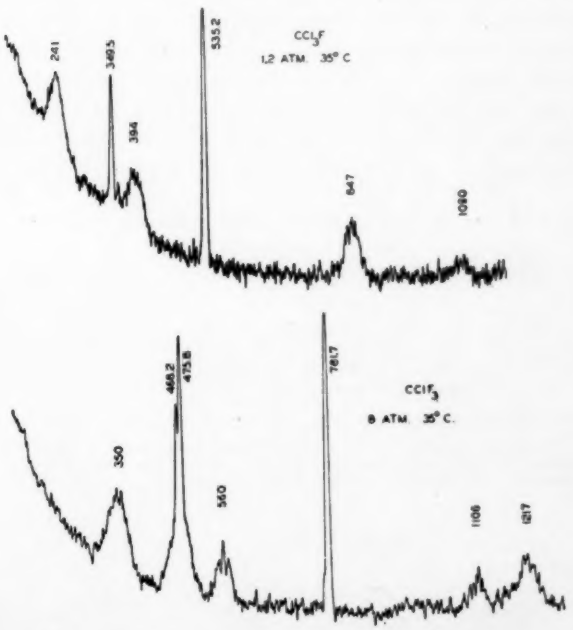

FIG. 2. Raman spectra of gaseous CCl_3F and $CClF_3$.

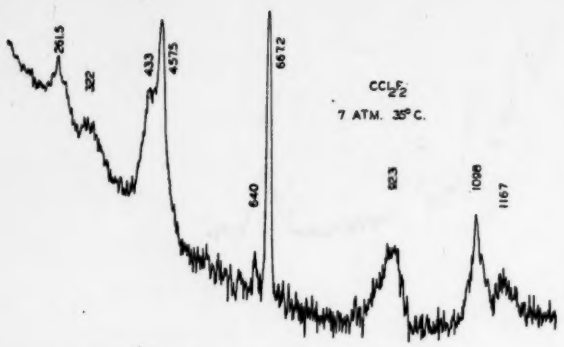

FIG. 3. Raman spectrum of gaseous CCl_2F_2.

infrared frequency measurements also varies greatly, depending on the dispersion, band intensity and shape, etc. A critical comparison of the absorption curves of Plyler and Benedict[1] with the present data, and with those of Welsh *et al.*[3] for CCl_4, has led to the list of estimated most probable fundamental frequencies given in Table II.

The interpretation of the observed bands is given in the last column of Table I. For the two molecules of symmetry T_d and the two of symmetry C_{3v} there are no difficulties of assignment: the band contours of the present data verify earlier assignments. An exception is the weak Raman band at 586.3 cm^{-1} in the spectrum of CF_4. Its interpretation as due to an unknown impurity is the only plausible explanation found.

For CCl_2F_2 there must be nine fundamental frequencies. Nine Raman bands have been measured in the present research, but the one at 640 cm^{-1} is undoubtedly an overtone. This leaves one fundamental in doubt. Calculations by Plyler and Benedict[1] indicate that three frequencies must lie between 400 and 500 cm^{-1}. Their infrared absorption curves show a distinct minimum at 437 cm^{-1}, and slight minima at 446 and 473 cm^{-1}. The Raman data, on the other hand, show strong maxima at 433 and 457.5 cm^{-1}. This leaves a choice between 446 and 473 cm^{-1} as the most likely value for the third fundamental in this region. The Raman data possibly favor the choice of 446 cm^{-1}, because of the absence of indication of a band at 473 cm^{-1}. A Raman band at 446 cm^{-1} would be hidden by the intense neighboring bands. This choice for the ninth fundamental frequency is in close agreement with that of Masi,[11] who proposed a value of 450 cm^{-1} for this frequency on the basis of specific heat measurements on CCl_2F_2.

TABLE II. Estimated best values of fundamental frequencies (in cm^{-1}).

CCl_4	218, 310, 458, 794[a]
CCl_3F	241, 349.5, 398, 535.2, 847, 1085
CCl_2F_2	261.5, 322, 435, 446, 457.5, 667.2, 922, 1099, 1162
$CClF_3$	350, 475.8, 560, 781.7, 1105, 1212
CF_4	434.5, 630, 908.2, 1277

[a] This is undoubtedly shifted somewhat due to resonance, but probably only slightly, since this component is much more intense than the other component as shown clearly in Fig. 12 of reference 1.

The four a_1 fundamentals of CCl_2F_2 can be identified in the Raman spectrum by the sharpness of the bands. The other five have been assigned as shown in Table I by considering correlations with the other molecules in the series as well as the calculations of Plyler and Benedict.[1]

Following the suggestion given by Bernstein[12] that sums of frequencies progress in a regular manner for a series of molecules such as that considered here, we have plotted in Fig. 4 the sum of the fundamental vibration frequencies against the number of fluorine atoms in the molecule. The curve is strikingly smooth. Changing the doubtful fundamental of CCl_2F_2 from the preferred value of 446 to 473 cm^{-1} would cause a noticeable inflection in the curve.

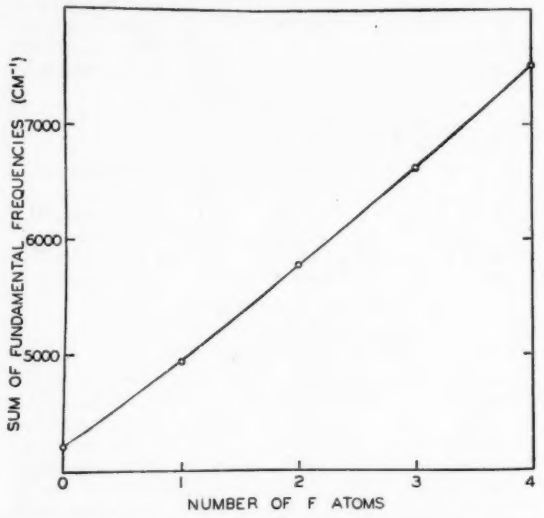

FIG. 4. Plot of the sum of fundamental vibration frequencies against number of fluorine atoms in the molecule.

ACKNOWLEDGMENTS

The writer is indebted to Professor J. Rud Nielsen for valuable suggestions and to Dr. W. S. Murray and Dr. R. C. McHarness and to E. I. du Pont de Nemours and Company for the gift of samples.

[11] J. F. Masi, J. Am. Chem. Soc. **74**, 4738 (1952).
[12] H. H. Bernstein, Symposium on Molecular Structure and Spectroscopy, Ohio State University, June, 1952.

On the Scavenger Effect in the n,γ Reaction in Carbon Tetrachloride*

WILLIAM H. HAMILL AND RUSSELL R. WILLIAMS, JR.
Chemistry Departments of the University of Notre Dame, Notre Dame, Indiana, and the Brookhaven National Laboratory, Upton, Long Island, New York

(Received July 22, 1953)

Neutron bombardment of liquid carbon tetrachloride yields 38.5 min Cl^{38}, and approximately 40 percent of the induced activity is retained in organic form. Dissolved chlorine reduces this retention in a regular fashion to approximately 25 percent at a concentration of 6 mole percent. Allyl chloride increases retention to 53 percent in equivalent concentrations. Neither of these "scavenger effects" is significantly dependent on the intensity of total dose of concomitant nonactivating pile radiation. This rules out the radiation-decomposition theory of scavenger action and supports an atom-radical diffusion-recombination mechanism.

IT has been repeatedly shown that the degree of retention of radioactive halogen in organic form after neutron bombardment of liquid organic halides is significantly altered by the presence of small concentrations of various additives during irradiation. Molecular halogens,[1] hydrocarbons,[2] or aniline[3] present to the extent of a few mole percent have been shown to lower organic retention by 10 to 40 percent in various organic halides. Still smaller amounts of halo-olefins have been shown to increase the organic retention.[4]

At least two distinctly different explanations of this "scavenger effect" have been considered. The view favored by Willard *et al*[1]. and also by Miller and Dodson[2] is that the reactions responsible for the effect occur in a limited volume of liquid located at the end of the track of the recoiling atom. Within this region various reactions involving competition for the active atom between the scavenger and the molecular fragments formed by the recoiling atom are thought to occur in such a fashion as to largely determine the ultimate fate (organic *vs* inorganic) of the active halogen atoms before they diffuse into the main body of liquid to form a homogeneous system.

In contrast to this view, it has been considered possible[5] that the competing reactions responsible for the scavenger effect occur homogeneously throughout the system, after the active halogen atoms have diffused away from the region of original recoil and disruption. In this case the competition for the active atoms is again thought to be between the additive and molecular fragments formed by radiation decomposition of the medium, with the difference that the latter is attributed to the concomitant gamma irradiation of the neutron bombardment. An obvious consequence of this second description of the scavenger effect is that the variation of retention with concentration of additive should depend on the intensity and amount of concomitant radiation decomposition encountered during the neutron bombardment. This explanation has been rejected by Levey and Willard[1] on the basis of calculation and measurement of the rate of radiation induced reaction of iodine with ethyl iodide. We have subjected the question to still more direct experimental test, as reported in the following.

EXPERIMENTAL

The effect of dissolved chlorine and allyl chloride upon the distribution of chlorine activity (Cl^{38}, $t_{\frac{1}{2}}=38.5$ min) between inorganic and organic forms has been determined after bombardment of dilute solutions of these reagents in carbon tetrachloride under varying conditions of neutron flux and radiation intensity.

The solutions bombarded were prepared from carbon tetrachloride which had been prechlorinated, washed, dried, and carefully fractionated. Chlorine solutions were made by gas absorption and their concentration determined by iodimetry. Solutions of allyl chloride (freshly distilled) were prepared volumetrically.

Samples of pure carbon tetrachloride and the various solutions were bombarded in sealed quartz ampoules containing *ca* 20 or *ca* 200 milligrams of liquid. The former size was used for bombardments in the pneumatic tube (PN2) of the Brookhaven reactor, where the thermal neutron flux is 3×10^{12} n/cm²/sec and the radiation intensity (gamma and fast neutron) estimated[6] to be 3×10^{-3} cal/g/sec. The larger size sample was used for bombardments in the thermal column of the Brookhaven reactor where the thermal neutron flux is 10^{9} n/cm²/sec and the radiation intensity (mainly gamma) is estimated to be 2.8×10^{-8} cal/g/sec.[7]

After bombardment and appropriate decay the capsules were opened in separatory funnels containing equal volumes of carbon tetrachloride and an aqueous solution 1*N* in sodium hydroxide and 0.01*N* in sodium chloride. The capsule, its contents, and the two phases were thoroughly agitated, and after separation of the

* Work supported in part by the U. S. Atomic Energy Commission under contract At(11-1)-38. Presented at the 123rd National Meeting of the American Chemical Society, Los Angeles, California, March 19, 1953.

[1] G. Levey and J. E. Willard, J. Am. Chem. Soc. **74**, 6161 (1952).
[2] J. M. Miller and R. W. Dodson, J. Chem. Phys. **18**, 865 (1950).
[3] C. Lu and S. Sugden, J. Chem. Soc. **1939**, 1273.
[4] Hamill, Williams, and Schwarz, J. Am. Chem. Soc. **72**, 2813 (1950).
[5] W. H. Hamill and R. R. Williams, Jr., U. S. Atomic Energy Commission AECU-2057.
[6] Information supplied by A. O. Allen, Chemistry Department, Brookhaven National Laboratory.
[7] Information supplied by S. Person, Biology Department, Brookhaven National Laboratory.

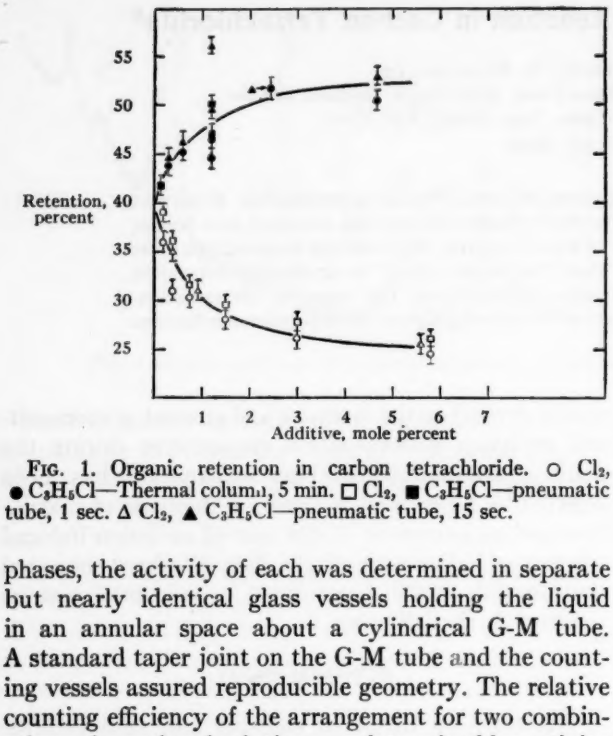

FIG. 1. Organic retention in carbon tetrachloride. ○ Cl_2, ● C_3H_5Cl—Thermal column, 5 min. □ Cl_2, ■ C_3H_5Cl—pneumatic tube, 1 sec. △ Cl_2, ▲ C_3H_5Cl—pneumatic tube, 15 sec.

phases, the activity of each was determined in separate but nearly identical glass vessels holding the liquid in an annular space about a cylindrical G-M tube. A standard taper joint on the G-M tube and the counting vessels assured reproducible geometry. The relative counting efficiency of the arrangement for two combinations of vessel and solution was determined by activity measurements on Cl^{38} (with carrier) extracted from the organic to the inorganic phase. Corrections for this effect, radioactive decay between measurements, dead-time losses in the G-M tube, and background counts have been made in computing the retentions reported below. 4096 counts were collected in each activity measurement and the corresponding uncertainty in count rate, together with uncertainties in liquid volume measurements, etc., indicate that the standard deviation of the reported retention is approximately one percent for retentions in the range (25–50 percent) encountered. The samples were bombarded in groups of ten, and in most instances the sample weights were measured and the specific activity of the samples compared within the group. Gross failure to recover all activity was avoided by discarding all individual experiments in which the specific activity was more than ten percent less than the maximum for the group, but precise reproducibility could not be expected due to self-shadowing by Cl^{35} ($\sigma_t = 50$ barns).

RESULTS

The percent organic retention of chlorine activity in bombardment of pure carbon tetrachloride was measured in 19 instances: in five the purified carbon tetrachloride was used without further treatment; in seven samples were distilled and bombarded in vacuum; two were dried with phosphorus pentoxide just prior to bombardment; two were shaken with mercury prior to bombardment; and three were washed with caustic solution, water and dried with anhydrous calcium chloride prior to bombardment. All samples in this group were bombarded five minutes in the thermal column. No systematic variation of retention according to treatment was observed. The mean value of the retention was 39.5 percent and the average deviation from the mean was 1.5 percent (39.5±1.5 percent retention). Previous workers have given the retention in pure carbon tetrachloride as 43 percent.[2,8] We presume that this discrepancy is due to a systematic error which will not influence our conclusions.

The percent organic retention has been measured for solutions of chlorine in carbon tetrachloride ranging in concentration from 0.0002 mole percent to 5.8 mole percent after five minutes bombardment in the thermal column as shown in Fig. 1. At concentrations of 0.02 mole percent or less, the retention of the solutions was experimentally indistinguishable from the value for pure carbon tetrachloride, and these values are not given in the figure. The retention has also been measured for one-second and fifteen-second bombardment in the pneumatic tube, over a range of chlorine concentration from 0.02 mole percent to 5.8 mole percent. Most of the points given represent the mean values from two experiments, and in no case do the results of such pairs differ by more than two percent.

A test for failure to extract all activity from the bombardment capsule was made as follows: a group of eight capsules, after the usual treatment, was placed in small breakers containing hot $6M$ sodium hydroxide solution. After 15–20 minutes these solutions were diluted to $1M$, and their activity was determined in the counting vessel previously used for the inorganic phase. The activities observed, in terms of the total activity for each sample, were 0.2, 1.5, 2.8, 0.6, 0.8, 0.8, 0.0, 0.0 percent.

The percent organic retention was also measured after bombardment of solutions of allyl chloride ranging in concentration from 0.31 mole percent to 4.68 mole percent under three different conditions of bombardment as shown in Fig. 1. Again, each point in the figure usually represents the mean of two determinations, except at a concentration of 1.22 mole percent, where an unusually great scatter in the results has lead us to plot the individual values.

DISCUSSION

The experiments on the scavenger effect of chlorine and allyl chloride in carbon tetrachloride show little or no dependence on radiation intensity. In these tests, the radiation dose rate on the sample from the pile was varied by a factor of *ca* 10^5 and the integrated dose by a factor of *ca* 5×10^3. In chlorine compounds, however, the self-irradiation due to the capture gammas from the reaction $Cl^{35}(n,\gamma)Cl^{36}$ ($\sigma_t = 50$ barns) may be more important than the radiation from the pile. Assuming that each capture produces two 4-Mev gammas, and that these will have mass absorption

[8] Goldhaber, Chiang, and Willard, J. Am. Chem. Soc. **73**, 2271 (1951).

coefficients of 0.04, it is possible to estimate the effect of this source of radiation to be 5×10^{-3} cal/g/sec in the pneumatic tube and 2×10^{-8} cal/g/sec in the thermal column (self-shadowing of the sample is neglected). Therefore the actual range of dose rate may have been as small as a factor of *ca* 3×10^{3} and the range of integrated dose as small as a factor of *ca* 1.5×10^{2}.

Although the data shown in Fig. 1 leave room for doubt as to the complete absence of a radiation effect, it is clear that the major portion of the scavenger effect is not influenced by this experimental variable. A mechanism involving homogeneous competition between the scavenger and the radiation decomposition products would seem to require[5] that a 150-fold increase in radiation dose should be accompanied by a 150-fold decrease in the effectiveness of a given amount of scavenger, which is not observed.

The results of these experiments lead us to a conclusion in general agreement with that of Willard *et al.*[1] and of Miller and Dodson,[2] namely, that the competing processes responsible for the scavenger effect do not occur homogeneously throughout the system, but rather in a limited region near the end of the path of the recoiling halogen atom. The fate of the majority (*ca* 70 percent for carbon tetrachloride) of the recoil atoms is determined in *bona fide* hot atom reactions not influenced by small amounts of additives. (Failure to rupture the original bond may make a small contribution to this fraction.) We conclude that in the remaining cases the recoil atoms are either moderated to near thermal energies without entering into stable combination or receive only a little more than enough energy to break the original bond and remain in the vicinity of the original bond partner. Chemical evidence for low energy recoils in the n,γ process is present in (1) the finite yield of active carbon tetrachloride at infinite dilution in cyclohexane or benzene[2] and in (2) an apparent finite lower limit in retention by iodate and periodiate in dilute aqueous solution.[9] In either event, the controlling factor in the scavenger effect would seem to be the probability of encounter of the active halogen atom with some nearby molecular fragment *versus* the probability of encounter with a scavenger molecule.

A similar situation, namely, the probability of diffusion to infinite distance *versus* recombination of iodine atoms formed by photodissociation of molecular iodine in solution has been treated by Noyes.[10] He has shown that the chance of recombination, even when the atoms are separated by more than one liquid lattice position, is quite significant. The present case is comparable in that we are concerned with the probability of recombination of an active halogen atom with nearby organic radical, but in addition the presence of reactive scavenger molecules in the vicinity and the dependence of the fate of the active atoms on their concentration must be considered. An analytical expression describing this diffusion-recombination process for a single atom-radical pair will be developed and compared with Noyes' treatment[10] and with retention data in a succeeding publication.

In the present case, qualitative explanation of the scavenger effect must suffice, since it appears that more than one atom-radical pair must be formed in close proximity as the initial act in the diffusion-recombination process. While this is not inconsistent with the nature of the n,γ process, we have not been able to develop a simple expression to describe the effect.

In pure carbon tetrachloride, we conceive that the active atoms which escape hot atom reaction become thermalized in the vicinity of one or more each of CCl_3 radicals and Cl atoms, formed by impact of the Cl* atom. As these particles diffuse away from each other in the liquid, we fix our attention on the fate of the radioactive atom. If the encounter

$$CCl_3+Cl^*\rightarrow CCl_3Cl^* \qquad (1)$$

occurs, organic activity is produced (retention); or if the encounter

$$Cl+Cl^*\rightarrow ClCl^* \qquad (2)$$

occurs, inorganic activity is produced. These recombinations occur in fixed proportion on the average and determine the observed retention in the pure liquid. Addition of Cl_2 consumes organic radicals

$$CCl_3+Cl_2\rightarrow CCl_4+Cl, \qquad (3)$$

decreases the probability of reaction (1), and thus lowers the retention to a limiting value near 25 percent. In the absence of direct information on the nature of the active products in the presence of allyl chloride, we adopt the assumption that it lowers the chlorine atom concentration

$$Cl+C_3H_5Cl\rightarrow C_3H_5Cl_2 \qquad (4)$$

and thus decreases the probability of reaction (2) and thus increases the retention to a limiting value near 55 percent. The concentration region in which these effects are evident (*ca* 1 mole percent) clearly rules out processes competing homogeneously with radiation decomposition products. Reference to Noyes' calculations[10] indicates that diffusion-recombination occurs mainly between particles which have been separated by no more than a very few molecule diameters and therefore interference of solute molecules with such processes will occur at relatively high concentrations as is observed.

It appears that three degrees of solute action distinguish three general types of reactions of radioactive atoms produced by neutron capture:

I. A fraction of the events (*ca* 70 percent in carbon tetrachloride) is not subject to solute influence and can be called hot atom reactions. They must occur in

[9] Cleary, Hamill, and Williams, J. Am. Chem. Soc. **74**, 4675 (1952).

[10] R. M. Noyes, J. Chem. Phys. **18**, 999 (1950).

the first collisions made by the recoiling atoms and may lead to either organic or inorganic products (25 and 45 percent in carbon tetrachloride).

II. A fraction of the events produces thermalized atoms (*ca* 30 percent in carbon tetrachloride) lying initially near one or more radicals or atoms formed by collisions of the hot atom. Diffusion-recombination may occur between these particles, and solute concentrations in the region of 1 mole percent may alter these reactions and change retention.

III. A fraction of the thermal atoms may escape the diffusion-recombination reactions and diffuse rather large distances in the liquid, eventually to react with the solvent, if that is possible, as with Br atoms in alkyl bromides, with impurities, or with radiation decomposition products. This class of events is distinguished by extreme sensitivity of retention to solute additions as is observed with bromo-olefin in alkyl bromides, which are effective at concentrations less than 0.01 mole percent. It is only in this class of reaction that an influence of concurrent radiation damage might be observed. Neither high solute sensitivity nor the radiation intensity effect has been observed in carbon tetrachloride.

THE JOURNAL OF CHEMICAL PHYSICS VOLUME 22, NUMBER 1 JANUARY, 1954

The Theory of Radioactive Ion Exchange*

E. Pitts
Research Laboratories, Kodak Limited, Harrow, Middlesex, England
(Received April 17, 1953)

Experiments reported by other workers have shown that when a precipitate of silver bromide is shaken with a solution containing either silver or bromide ions, some of which are radioactive, the radioactive strength of the solution decreases. The final value reached corresponds to a uniform distribution of the active material throughout both solid and solution. No agreement on the interpretation of these results has up until now been reached. Two possible mechanisms for this exchange are described, and their consequences are examined. A new theoretical treatment is given which includes a consideration of the effect of the spread in crystal sizes, which was neglected in previous discussions of the problem. From those results, a new method of comparison between theory and experiment is suggested. This shows unambiguously that the exchange of silver ions is in agreement with predictions based on the hypothesis that the ions diffuse through the solid. It is shown that the exchange of bromide ions cannot be explained in this way. Values obtained for the diffusion constant of silver are in fair agreement with those from other sources. The relation of these results to the various suggestions put forward by other workers is discussed.

INTRODUCTION

THE question of whether the ions in the silver halide lattice are mobile or not is of obvious interest in the theory of the photographic process. One answer to this question was given by experiments in which the electrical conductivity of large crystals of silver bromide prepared from the melt was measured. The results showed that the silver ions were mobile but that, within the limits of experimental error, the bromide ions were not. Recently, however, suggestions have been made that the bromide ions are mobile in crystals of precipitated silver bromide. These suggestions were put forward in the light of certain experiments (described briefly below) and have been challenged by alternative explanations. It is the purpose of this paper to re-examine the theory on which the arguments have been based and to give the necessary extensions to enable an unambiguous interpretation of the experimental results to be made.

The work which prompted the suggestion of bromide-ion mobility was part of a series of investigations on the exchange of radioactive ions in solution with ions of a precipitate. If a solution of silver nitrate containing radioactive silver ions is shaken with a precipitate of silver bromide, it is found that the radioactivity of the solution decreases with time, eventually approaching a constant value.[1,2] This final value agrees with that calculated on the assumption that the ratio of the numbers of radioactive ions to inactive ions is constant throughout both the solid and the liquid. The extent of the exchange after a given length of time is found to depend on the previous treatment of the precipitate. A similar exchange of ions occurs when an electrolytically deposited layer of silver chloride or bromide is immersed in the solution.

If the precipitate is shaken with a solution of sodium bromide containing radioactive bromide ions, a decrease in the radioactivity of the solution is again observed, with the end point corresponding to homogeneous distribution of the active ions throughout the system.[1,2] The rate of exchange again depends on the previous treatment of the precipitate. On the other

* Communication No. 1533H from the Kodak Research Laboratories.

[1] A. Langer, J. Chem. Phys. **10**, 321 (1942); **11**, 11 (1943).
[2] I. M. Kolthoff and A. S. O'Brien, J. Chem. Phys. **7**, 401 (1939); J. Am. Chem. Soc. **61**, 3409 (1939).

hand, if layers of silver bromide are used, no exchange of bromide ions can be detected.[3]

In Langer's work, the effect of dyes adsorbed on the precipitate was studied. They were found to have no effect on the silver exchange but greatly reduced the amount of bromide exchanged in a given length of time.

As an explanation of these phenomena, Kolthoff and O'Brien suggested that recrystallization of the precipitate was responsible for the exchange of bromide ions shown by their experiments. Langer considered this to be of minor importance and suggested that both the radioactive silver and bromide ions were entering the precipitate by diffusion through the solid lattice. He presented quantitative evidence which appeared to show that theoretical predictions based on this model were in accord with his results. Zimen regarded the silver exchange as occurring by diffusion in the solid but considered that the bromide exchange was due to recrystallization. This would explain the absence of exchange of bromide ions when silver bromide layers are used and the reduction of the rate of exchange when dyes are added to the precipitate since their addition would be expected to slow down, or even stop, the recrystallization.

Finally, Grimley[4] discussed the results, assuming that diffusion through the solid occurs with both bromide and silver ions. The value of the diffusion constant which he obtained for silver ions was smaller than that derived from electrical conductivity measurements whereas, as has already been stated, the same measurements suggest that the bromide ion is immobile. From the comparison of theory and experiment, Grimley also inferred that the value of the diffusion constant depended on the size of the crystal in the precipitate.

Thus, it appears that the experimental facts are agreed, but their interpretation remains a subject for dispute. A detailed description of the process of recrystallization, which could account quantitatively for the experimental results, was not given by Kolthoff and O'Brien. Zimen criticized Langer's work on the grounds that the latter used the wrong solution of the theoretical problem. This, however, is not the case, for Langer only quotes, correctly, the form which the solution must have, without giving its details. Grimley derived a value for the diffusion constant of the silver ion using Langer's work, yet Zimen states that this experimental work is not in accord with the theory based on diffusion.

In attempting to decide among these several interpretations, it is necessary first to remove a restriction in the extant theoretical treatment, namely, that all the crystals in the precipitate are spheres of equal size. This is a poor approximation to the actual state of the system, and to some extent makes the previous theoretical considerations of the problem of doubtful relevance. We shall consider spheres having a range of sizes. No advantage would be gained in examining crystals of other geometrical shape, for example, ellipsoids, since the approximation of the model to the physical state of the precipitate would not be greatly improved, and extreme complexity would result. Two mechanisms of the exchange reaction will be discussed, one based on diffusion and the other on a reaction whose rate is determined by the extent of the solid-liquid interface, both of which appear plausible. A method of comparing experiment with theory in a way which allows a clear interpretation of the results will then be described and the conclusions drawn.

THE MECHANISM OF EXCHANGE

At the beginning of the experiment, the total mass (I^*) of the radioactive ion is present in the liquid; and if $C(t)$ is the concentration of active ion in the solution at time t, $C(0)$ will be proportional to the total amount of radioactive material present. It will be supposed that at the end of the experiment ($t=\infty$) the radioactive ions are distributed between the solution and the precipitate in such a way that a homogeneous distribution is attained. Writing suffixes s and p to denote presence in solution and precipitate, respectively, and an asterisk to denote radioactivity, in the equilibrium state,

$$\frac{I_s^*}{I_s+I_s^*}=\frac{I_p^*}{I_p+I_p^*}.$$

Obviously

$$\frac{I_s^*}{I_s+I_s^*}=\frac{I_s^*+I_p^*}{I_s+I_p+I_s^*+I_p^*}=\frac{\text{total } I^* \text{ in system}}{\text{total } (I+I^*) \text{ in system}}.$$

From this it follows that

$$\frac{C(\infty)}{C(0)}=\frac{I_s^*}{I_s^*+I_p^*}=\frac{\text{total } (I+I^*) \text{ in solution}}{\text{total } (I+I^*) \text{ in system}} \quad (1)$$

It is found that the experimentally observed value $C(\infty)/C(0)$ agrees with this expression, for both silver- and bromide-ion exchange.

Let us first consider the exchange to occur by diffusion through the solid. The concentration of radioactive ion in the liquid $C(t)$ will be assumed to be a function of time only, that is, we assume that the concentration remains constant in the liquid up to the solid surface. This is a good approximation to conditions in all the experiments since the precipitates were shaken with the solution. We then suppose that the ions diffuse into

[3] K. E. Zimen, in *Fundamental Mechanisms of Photographic Sensitivity* (Butterworth's Scientific Publications, Ltd., London, 1951), p. 53.

[4] T. B. Grimley, reference 3, p. 46; [See also Proc. Roy. Soc. (London) **A201**, 60 (1950)].

the solid, with a diffusion constant D, thus causing the gradual decrease in the radioactive strength of the solution. Let us suppose that there are present n_i spheres, each with radius a_i; let us suppose the concentration of the active ion in these is c_i. Then c_i will be a function of both t and r, the distance from the center of the sphere. Let V be the volume of solution and V_p the volume of the precipitate; then

$$V_p=\frac{4\pi}{3}\sum n_i a_i^3. \tag{2}$$

At any moment during the reaction, the surface layer is assumed to be in equilibrium with the solution, so that

$$\left(\frac{\text{concentration of active ions in solution}}{\text{concentration of inactive ions in solution}}\right)=\left(\frac{\text{concentration of active ions in surface layers of crystal}}{\text{concentration of inactive ions in surface layers of crystal}}\right),$$

i.e.,

$$C(t)=\left(\frac{\text{concentration of } I \text{ ions in solution}}{\text{concentration of } I \text{ ions in surface layers of crystal}}\right)c_i(a_i,t).$$

Now, the actual number of radioactive ions in the whole system is only a very small fraction of all the ions present, and thus the ratio in brackets above is practically constant throughout the reaction. We may therefore write

$$C(t)=fc_i(a_i,t), \tag{3}$$

where f is a constant. The fact that the total amount of radioactive substance in the system is constant throughout the course of the reaction gives the equation

$$VC(t)+4\pi\sum n_i\int_0^{a_i} r^2c_i\,dr=VC(0); \tag{4}$$

the first term on the left-hand side is the quantity present in solution whereas the second is that in the precipitate, and their sum equals the amount originally present. Apart from obvious initial conditions, Eqs. (3) and (4) are the boundary conditions which the solution of the diffusion equation,

$$\frac{\partial c_i}{\partial t}=D\left(\frac{\partial^2 c_i}{\partial r^2}+\frac{2}{r}\frac{\partial c_i}{\partial r}\right), \tag{5}$$

must satisfy.

A second theoretical possibility must also be examined. It could be imagined that the mobility of the ions within the crystal was high enough to maintain a uniform concentration throughout the interior, and that the rate of the exchange depended only on the numbers crossing the solid-liquid interface. (It is not possible to obtain this solution as a special case corresponding to $D=\infty$ of Eqs. (4) and (5), since their derivation assumed an infinite rate of surface interchange.) In this case, c_i is a function of t alone. It is reasonable to suppose that the number of ions leaving the sphere of radius a_i may be written $\alpha_i c_i$, where α_i is a constant proportional to the surface area of the sphere. Likewise, the number entering the sphere may be written $\alpha_i C(t)/\eta_i$, where η_i is another constant. Hence, we may write

$$V_i\frac{dc_i}{dt}=\frac{\alpha_i C}{\eta_i}-\alpha_i c_i,$$

where V_i is the volume of the sphere. After infinite time, the concentration in the sphere becomes constant, and so

$$C(\infty)=\eta_i c_i(\infty).$$

Since $c_i(\infty)$ is constant for all spheres, it follows that η_i does not depend on the size of the sphere. Thus, putting $\sigma_i=\alpha_i/V_i$, $\eta_i=\eta$,

$$\frac{dc_i}{dt}=\sigma_i(C/\eta-c_i). \tag{6}$$

The equation expressing conservation of radioactive material becomes

$$VC(t)+\frac{4\pi}{3}\sum n_i a_i^3 c_i(t)=VC(0). \tag{7}$$

The solution of Eqs. (6) and (7) and the usual initial conditions are therefore required.

This completes the description of the physical properties of the two models which will be examined. In the next section, the above equations will be solved.

MATHEMATICAL TREATMENT

It will be convenient to introduce the mean radius a, defined by the relation,

$$a=\frac{\sum n_i a_i}{\sum n_i}.$$

Dimensionless variables may be defined as follows:

$$\xi=r/a,\quad \tau=Dt/a^2,\quad x_i=a_i/a.$$

Putting

$$\theta_i=\xi c_i(\xi,\tau),$$

the diffusion Eq. (5) may be written

$$\frac{\partial\theta_i}{\partial\tau}=\frac{\partial^2\theta_i}{\partial\xi^2}, \tag{8}$$

and the boundary conditions are

(a) θ_i/ξ finite when $\xi\rightarrow 0$,
(b) $\theta_i=0$ when $\tau=0$, $(0\leq\xi\leq x_i)$,
(c) $x_iC(\tau)=f\theta_i(x_i,\tau)$. This follows from Eq. (3),
(d) From Eq. (4)

$$Vf\theta_i(x_i,\tau)/(x_i)+4\pi a^3\sum n_i\int_0^{x_i}y\theta_i dy=VC(0).$$

To solve Eq. (8), we make use of the Laplace transformation. Putting

$$\chi_i=\int_0^\infty e^{-p\tau}\theta_i d\tau,$$

taking the transform of Eq. (5) in the usual way, and using the boundary conditions corresponding to (a) and (b) above, there results

$$\chi_i=hx_i\frac{\sinh(\xi p^{\frac{1}{2}})}{\sinh(x_ip^{\frac{1}{2}})},$$

where h is a constant to be found by using the boundary condition corresponding to (d). This gives

$$\chi_i=x_iVC(0)\frac{\sinh(\xi p^{\frac{1}{2}})}{\sinh(x_ip^{\frac{1}{2}})}$$
$$\times\{pfV+4\pi a^3\sum n_ix_i[x_ip^{\frac{1}{2}}\coth(x_ip^{\frac{1}{2}})-1]\}^{-1}. \tag{9}$$

The solution may be obtained by the evaluation of the contour integral

$$\theta_i=\frac{1}{2\pi_i}\int_{\gamma-i\infty}^{\gamma+i\infty}\chi_i(p)e^{p\tau}dp. \tag{10}$$

Unfortunately, the presence of the summation over sizes in the denominator of χ_i makes a direct evaluation of (10) impossible, and we shall derive an approximate solution which is very convenient for the values of τ occurring in the experiments.

Using the expansion of cothy in terms of $\exp(-2y)$, we obtain

$$\chi_i=x_iVC(0)\frac{\{\exp[-(x_i-\xi)p^{\frac{1}{2}}]-\exp[-(x_i+\xi)p^{\frac{1}{2}}]\}}{(pfV+4\pi a^3p^{\frac{1}{2}}\sum n_ix_i^2-4\pi a^3\sum n_ix_i)}F_{(p)},$$

where

$$F(p)=[1-\exp(-2x_ip^{\frac{1}{2}})]^{-1}$$
$$\times\left[1+\frac{8\pi a^2p^{\frac{1}{2}}\sum_i n_ix_i^2\sum_{m=1}^{\infty}\exp(-2mx_ip^{\frac{1}{2}})}{(pfV+4\pi a^3p^{\frac{1}{2}}\sum n_ix_i^2-4\pi a^3\sum n_ix_i)}\right]^{-1}.$$

Now, the volume of the precipitate is given by (2), and so we may write

$$\chi_i=\frac{x_iVC(0)}{3V_p}$$
$$\times\left\{\frac{\exp[-(x_i-\xi)p^{\frac{1}{2}}]-\exp[-(x_i+\xi)p^{\frac{1}{2}}]}{\alpha p+k_2p^{\frac{1}{2}}-k_1}\right\}F_{(p)},$$

where

$$\alpha=\frac{fV}{3V_p},\quad k_1=\frac{\sum n_ix_i}{\sum n_ix_i^2},\quad k_2=\frac{\sum n_ix_i^2}{\sum n_ix_i^2}. \tag{11}$$

As an approximation we shall put

$$F_{(p)}=1, \tag{12}$$

and so

$$\chi_i=\frac{x_iVC(0)}{3V_p(k_2^2+4\alpha k_1)^{\frac{1}{2}}}\left[\frac{z_1}{p^{\frac{1}{2}}(p^{\frac{1}{2}}-z_1)}-\frac{z_2}{p^{\frac{1}{2}}(p^{\frac{1}{2}}-z_2)}\right]$$
$$\times\left[\exp[-(x_i-\xi)p^{\frac{1}{2}}]-\exp[-(x_i+\xi)p^{\frac{1}{2}}]\right],$$

where

$$2\alpha z_1=-k_2+(k_2^2+4\alpha k_1)^{\frac{1}{2}},$$
$$2\alpha z_2=-k_2-(k_2^2+4\alpha k_1)^{\frac{1}{2}}.$$

Writing

$$E(x)=\frac{2\exp(x^2)}{\pi^{\frac{1}{2}}}\int_x^\infty\exp(u^2)du=\frac{1}{x\pi^{\frac{1}{2}}}\left[1-\frac{1}{2x^2}+O\left(\frac{1}{x^4}\right)\right],$$

then

$$\int_0^\infty e^{-p\tau}\exp(-x^2/4\tau)E(x/2\tau^{\frac{1}{2}}-z\tau^{\frac{1}{2}})d\tau=\frac{\exp(-xp^{\frac{1}{2}})}{p^{\frac{1}{2}}(p^{\frac{1}{2}}-z)},$$

and we obtain the approximate result

$$\theta_i=\frac{x_iVC(0)}{3V_p(k_2^2+4\alpha k_1)^{\frac{1}{2}}}\Big\{\exp[-(x_i-\xi)^2/4\tau]$$
$$\times\{z_iE[(x_i-\xi)/2\tau^{\frac{1}{2}}-z_1\tau^{\frac{1}{2}}]-z_2E[(x_i-\xi)/2\tau^{\frac{1}{2}}-z_2\tau^{\frac{1}{2}}]\}$$
$$-\exp[-(x_i+\xi)^2/4\tau]\{z_1E[(x_i+\xi)/2\tau^{\frac{1}{2}}-z_1\tau^{\frac{1}{2}}]$$
$$-z_2E[(x_i+\xi)/2\tau^{\frac{1}{2}}-z_2\tau^{\frac{1}{2}}]\}\Big\}.$$

Evaluating this when $\xi=x_i$, it is seen that

$$\theta_i(x_i,\tau)=\frac{x_iVC(0)}{3V_p(k_2^2+4\alpha k_1)^{\frac{1}{2}}}\{z_1E(-z_1\tau^{\frac{1}{2}})-z_2E(-z_2\tau^{\frac{1}{2}})$$
$$-\exp(-x_i^2/\tau)[z_1E(x_i/\tau^{\frac{1}{2}}-z_1\tau^{\frac{1}{2}})$$
$$-z_2E(x_i/\tau^{\frac{1}{2}}-z_2\tau^{\frac{1}{2}})]\}.$$

Now, for a large number of the crystals in the precipitate, $x_i>\frac{1}{2}$, and if $\tau<0.1$, then

$$\exp(-x_i^2/\tau)E(x_i\tau^{\frac{1}{2}})\ll 1 \tag{13}$$

and may be neglected. Using the boundary condition

(c) and the definition of α [Eq. (11)], we find, to a sufficient approximation,

$$\frac{C(\tau)}{C(0)}=\frac{\alpha}{(k_2^2+4\alpha k_1)^{\frac{1}{2}}}\{z_1\exp(z_1^2\tau)[1+erf(z_1\tau^{\frac{1}{2}})]$$
$$-z_2\exp(z_2^2\tau)[1+erf(z_2\tau^{\frac{1}{2}})]\}. \quad (14)$$

It is easily shown that in making the approximation (12), we have neglected terms like (13) in the final solution, and hence Eq. (14) is an adequate approximation.

The value of $C(\infty)$ may be found as follows: In the contour integral (10), one pole of χ_i occurs at the origin. Other poles give rise to a series of terms, each of which has the form $A\exp(-s^2\tau)\sin(s\xi+\phi)$, where A, s, and ϕ are real constants. Thus, when τ tends to infinity, these terms vanish, leaving only the contribution from the pole at the origin. Expanding χ_i in powers of p, it is found that

$$\chi_i=\frac{\xi VC(0)}{(Vf+V_p)}\cdot\frac{1}{p}[1+O(p)].$$

The contribution to (10) from the pole at the origin therefore gives

$$\frac{C(\infty)}{C(0)}=\frac{fV}{fV+V_p}=\frac{3\alpha}{3\alpha+1}. \quad (15)$$

By inserting the definition of f given in Eq. (3), we obtain

$$\frac{C(\infty)}{C(0)}=\frac{VC(\infty)}{VC(\infty)+V_pc_i(\infty)}$$
$$=\frac{\text{amount of tracer left in solution}}{\text{total amount of tracer in system}}.$$

On physical grounds we expect that in the equilibrium state

$$\frac{\text{amount of tracer left in solution}}{\text{amount of ion in solution}}$$
$$=\frac{\text{total amount of tracer in system}}{\text{total amount of ion in system}}.$$

From this it follows that Eq. (15) is equivalent to Eq. (1).

The approximate solution of the problem has now been found. To compare this with experimental results, it is first necessary to investigate the influence of the spread in sizes of the crystals. This enters the result through the quantities k_1 and k_2, which would both be unity if spheres of only one size were present. In the Appendix, values of k_1 and k_2 are evaluated on the assumption that the spheres have a log-normal distribution, which is often a close approximation to the truth.

The distribution function contains an adjustable parameter β which determines the spread in sizes about the mean. If σ is the standard deviation and a the mean radius, from the Appendix we find that, for a log-normal distribution,

$$\sigma/a=[\exp(\beta^2)-1]^{\frac{1}{2}}=\beta\left[1+\frac{\beta^2}{4}+\frac{5\beta^4}{96}+O(\beta^6)\right],$$

and

$$k_1=\exp(-3\beta^2),\quad k_2=\exp(-2\beta^2).$$

Let us suppose that we consider precipitates, all with the same total volume, and all having the same average radius a. Then by changing β, we alter the size distribution of the precipitate, and the total surface of the precipitate is proportional to $\exp(-2\beta^2)$. Taking α equal to 0.07543 (corresponding to one of Langer's series of experiments), the expression

$$Q(\tau)=\frac{C(0)-C(\tau)}{C(0)-C(\infty)} \quad (16)$$

has been calculated as a function of τ for different values of β. The resulting curves are shown in Fig. 1 plotted against $\log_{10}(10^3\tau)$. It will be seen that on increasing β, the amount of exchange occurring within a given time decreases. This is to be expected in view of the corresponding decrease in surface area. Thus, the degree of dispersion of the precipitate has a considerable influence on the rate of the exchange process. Suppose, however, that the total surface area of the

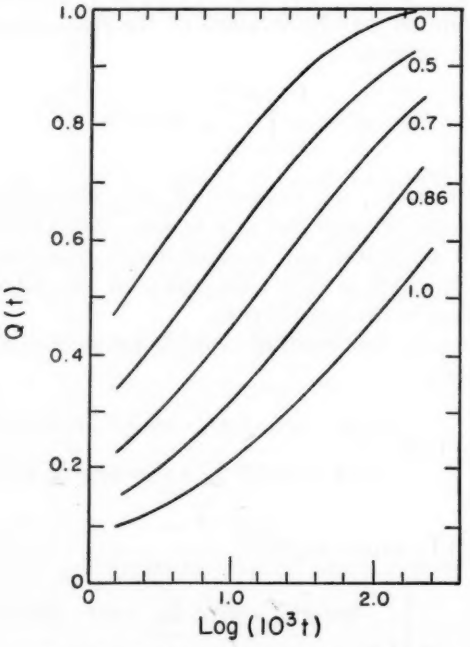

FIG. 1. Function $Q(\tau)$, for different values of β, assuming volume and average radius are constant.

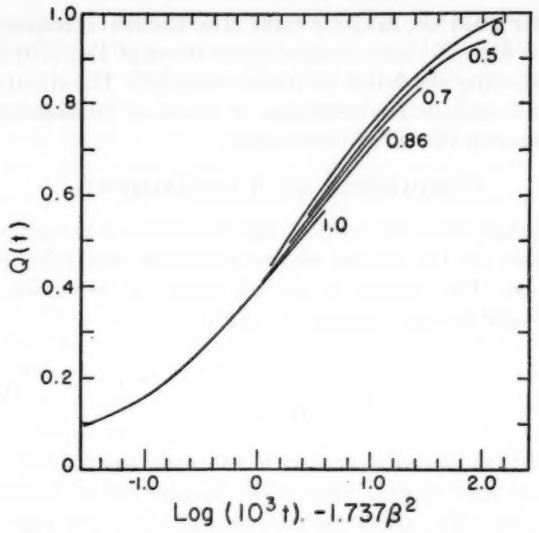

FIG. 2. Function $Q(\tau)$, for different values of β, assuming volume and surface area are constant.

precipitate is kept constant, together with the total volume. Then from the Appendix we find that the mean radius is given by

$$a=\mathrm{K}\exp(-2\beta^2)$$

where K is a constant. Then

$$\tau=Dt\mathrm{K}^{-2}\exp(4\beta^2).$$

Thus, the curve corresponding to β equal to zero has Dt/K^2 as argument. The curve corresponding to a different value of β will, in effect, be plotted against the same argument if an appropriate shift of abscissa is made. In Fig. 2, the curves of Fig. 1 are redrawn, making these shifts; each curve is plotted against $\log_{10}(10^3\tau)-4\beta^2\log_{10}e$. It will be seen that the curves are very close together. This implies that the rate of exchange is almost directly proportional to the surface area throughout a large part of the reaction. Proportionality is no longer found toward the end. This result is to be expected, since in the early stages of the exchange the ions only penetrate the surface layers of the precipitate with the result (provided the total surface area is constant) that the actual sizes of the individual spheres have little importance. But at later stages, the ions have penetrated more deeply, and the relative numbers of large and small crystals must then influence the course of the reaction. This result shows that for precipitates of differing total surface area, the form of the function Q remains practically constant, but the time scale is shifted by varying amounts.

We now turn to the solution of Eqs. (6) and (7). Remembering that C is a function of t, we may write the solution of (6)

$$c_i(t)=\frac{\sigma_i}{\eta}\int_0^t \exp(-\sigma_i(t-x)]C(x)dx,$$

so that

$$c_i(0)=0,$$

as required by the boundary conditions. From Eq. (7) it follows that

$$C(t)=C(0)-(\eta V)^{-1}\sum v_i n_i\sigma_i\int_0^t \exp[-\sigma_i(t-x)]C(x)dx.$$

Writing

$$C^*(p)=\int_0^\infty e^{-pt}C(t)dt,$$

and using a well-known theorem, we find

$$C^*(p)=p^{-1}C(0)-(\eta V)^{-1}\sum v_i n_i\sigma_i(p+\sigma_i)^{-1}C^*,$$

whence

$$C^*(p)=C(0)p^{-1}[1+(\eta V)^{-1}\sum v_i n_i\sigma_i(p+\sigma_i)^{-1}]^{-1}. \quad (17)$$

If there are grains of only one size present, the inversion of (17) is elementary. Writing

$$\lambda=V_p\sigma/V_\eta,$$

then

$$C^*/C(0)=\sigma/p(\sigma+\lambda)+\lambda/(\sigma+\lambda)(p+\sigma+\lambda),$$

whence

$$C(t)/C(0)=\sigma/(\sigma+\lambda)+\lambda\exp[-(\sigma+\lambda)t]/(\sigma+\lambda).$$

From this it follows that

$$\frac{C(\infty)}{C(0)}=\frac{V\eta}{V\eta+V_p},$$

and thus η has the same meaning as f in Eq. (3). Defining

$$P(t)=1-Q(t), \quad (18)$$

we obtain

$$P(t)=\exp[-(\sigma+\lambda)t],$$

which shows that $\log P$ is a linear function of t.

Again, the presence of the summation in Eq. (17) makes it impossible to obtain the inversion in closed form. We shall use the following approximation. From the definition of σ_i it is obvious that we may write

$$\sigma_i=k/a_i,$$

where k is a constant independent of the size of the crystal. Then

$$\sum v_i n_i\sigma_i/(p+\sigma_i)=4\pi k\sum n_i a_i^3/3(k+a_i p),$$

and by developing in partial fractions

$$\sum v_i n_i\sigma_i/(p+\sigma_i)=\frac{4\pi k}{3}\sum n_i\left(\frac{a_i^2}{p}-\frac{ka_i}{p^2}+\frac{k^2}{p^3}-\frac{k^3}{p^3(k+a_i p)}\right). \quad (19)$$

As an approximation, we replace a_i in the last term in the bracket by the mean value a. Making use of the results given in the Appendix for the case in which

TABLE I. Values of $\log_{10}(10P)$.

μt \ β	0	0.5	0.7	0.86	1.0
0.2	0.826	0.830	0.836	0.841	0.844
0.4	0.653	0.673	0.686	0.694	0.690
0.6	0.479	0.520	0.539	0.536	0.502
0.8	0.306	0.369	0.380	0.336	0.227

total volume and total surface area are kept constant, we find

$$\sum \frac{v_i n_i \sigma_i}{(p+\sigma_i)} \Big/ \sum v_i n_i = \frac{\mu}{p} - \frac{\mu^2 \exp(\beta^2)}{p^2} + \frac{\mu^3 \exp(3\beta^2)}{p^3} - \frac{\mu^4 \exp(3\beta^2)}{p^3[\mu + p\exp(2-\beta^2)]},$$

where

$$\mu = k/\kappa.$$

Then, after algebraic manipulation, it follows that

$$C^*/C(0) = A/(p+\mu\alpha_+) + B/(p+\mu\alpha_-),$$

where

$$A = \frac{\alpha_+ - \exp(2\beta^2)}{\alpha_+ - \alpha_-}$$

$$B = \frac{\exp(2\beta^2) - \alpha_-}{\alpha_+ - \alpha_-}$$

and

$$\alpha_\pm = \tfrac{1}{2}\{\exp(2\beta^2) + r \pm [(\exp(2\beta^2) - r)^2 + 4r\exp(2\beta^2)]^{\frac{1}{2}}\},$$

$$r = V_p/V_\eta.$$

We therefore obtain

$$C(t)/C(0) = A\exp(-t\mu\alpha_+) + B\exp(-t\mu\alpha_-). \quad (20)$$

This solution behaves correctly when t tends to zero, but breaks down for large values of t. As before, we find the limiting value $C(\infty)/C(0)$ by considering the contribution from the pole at the origin to the contour integral which is the inversion of (17). It is unnecessary to give the details; the result is the same as Eq. (15) with f in that equation replaced by η.

If the total volume and the mean radius are kept constant, then on evaluating (19), using results from the Appendix, we find

$$C(t)/C(0) = A\exp[-t\mu\alpha_+\exp(2\beta^2)] + B\exp[-t\mu\alpha_-\exp(2\beta^2)], \quad (21)$$

with A and B as before. It is clear that Eq. (21) is equivalent to Eq. (20) with a shift in the time scale.

In Table I the function $\log_{10}(10P)$ obtained from Eq. (20) is given as a function of (μt). It will be seen that values corresponding to different values of β are not greatly different, and so $\log_{10}(10P)$ is roughly a linear function of the time. Thus, provided the total surface and total volume are kept constant, the exchange proceeds at approximately the same rate no matter what the range of sizes. The results corresponding to Eq. (21) are obtained from those of Eq. (20) by transferring the latter to times $t\exp(2\beta^2)$. The diminution of surface on increasing β causes a considerable decrease in the rate of exchange.

COMPARISON WITH EXPERIMENT

In the preceding section, the influence of the spread in sizes on the course of the exchange has been examined. The course of the exchange is conveniently expressed by the fraction Q, where

$$Q = \frac{C(0) - C(t)}{C(0) - C(\infty)}, \quad (16)$$

and it has been shown that the form of the function Q is only very slightly altered by changes in the size distribution. The small deviations occurring (see Fig. 2) are within the limits of experimental error. However, the time at which a given value of Q is reached is profoundly affected by the distribution, since it is closely related to the extent of the surface area of the precipitate. This is related to the value of the mean radius, which occurs in the definition of τ.

Having obtained the important result that the form of the function Q is effectively the same for all distributions likely to occur in practice, we can devise a satisfactory method of comparing experiment and theory. The function Q appropriate to the experimental conditions is calculated; it is assumed for simplicity that crystals of only one size are present. The value of τ corresponding to a certain value of Q observed in the experiment at time t is then found. Supposing that the exchange is proceeding by this type of mechanism, it follows that if $\log t$ is plotted against $\log\tau$, a straight line of slope unity should be found, since

$$\log\tau = \log t + \log(D/a^2).$$

This method of comparison depends on the approximate constancy of the form of the function Q for different distributions of sizes. It has the advantage that the whole course of the exchange-time curve can be used, and no arbitrary values are assigned to any of the parameters occurring in the theoretical expressions.

It should be noticed that slight departures from this behavior may be anticipated. In the first place, the crystals are not true spheres. Secondly, the size distribution does, in fact, slightly modify the function Q, particularly at the later stages of the exchange, when Q is approaching unity. The small effect of the spread can be described in this way. If τ_1 corresponds to a certain small value of Q, and τ to a larger value, then the value of $\log(\tau/\tau_1)$ tends to increase slightly with increasing spread in crystal sizes (increasing β). In the graphs the ordinates are values of $\log\tau$, obtained on the assumption that crystals of only one size are present. It is clear that these values will be slightly too small, the error increasing as the value of τ increases.

Hence, we may anticipate that the plots will show slight curvature, being concave toward the abscissa. This is actually found. Finally, in the performance of the experiment, a not inappreciable quantity of solution is removed during the time of the determination of its radioactive strength and subsequently returned. During the time of measurement, the conditions in the liquid surrounding the crystals are altered. However, since the quantity of liquid used and the time taken in the measurements are both kept fairly small, errors from this cause are likely to be no greater than those already implicit in using the model of spherical crystals.

The method of comparison described above has been carried out for the results given by Langer.[2] In Fig. 3 are shown the results, using data given in Fig. 6 of Langer's 1942 paper, and Curve *a* of Fig. 1 in the 1943 paper. The appropriate theoretical curve is the uppermost curve ($\beta=0$) of Fig. 1 (this paper). It will be seen that all the gradients are close to the value unity, and the plots are usually slightly concave towards the abscissa. Thus, the experimental observations are consistent with the hypothesis that the rate of exchange is determined by diffusion of the silver ions through the solid. Very similar results are found when data from Fig. 3 of Langer's 1942 paper are used; the only cases in which discrepancies occur are for Curves *f* and *g*, where the crystals are probably not nearly spherical (the gradients are about 0.75).

If the same procedure is adopted for the bromide-ion exchange, quite different results are found. In Fig. 4 plots derived from Figs. 1(b), 1(c), and 4(b) of the

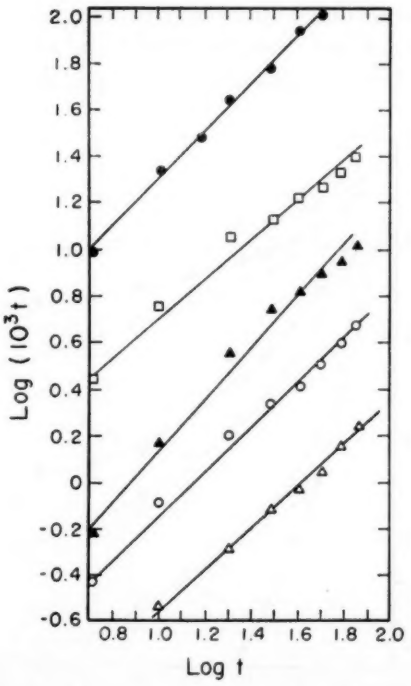

FIG. 3. Silver-ion exchange: from Langer (1943), Fig. 1. ● Curve *a*, slope 1.03; from Langer (1942), Fig. 6. △ 0°C, slope 0.91; ○ 15°C, slope 0.96; ▲ 30°C, slope 1.06; □ 50°C, slope 0.82.

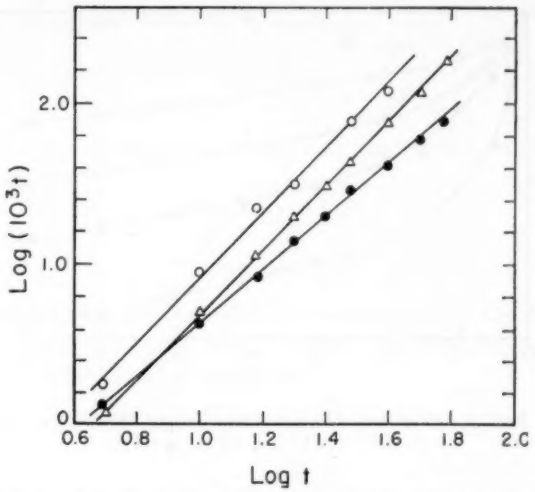

FIG. 4. Bromide-ion exchange: from Langer (1943), Fig. 1. △ Curve *b*, slope 1.99; ○ Curve *c*, slope 2.04; Fig. 4. ● Curve *b*, slope 1.63.

1943 paper are compared with the appropriate theoretical curves (not illustrated). In these cases, the slope is markedly different from the theoretical value unity, being 2.0 and 1.65. Similar results are found using the data of Fig. 3 in that paper, but in this case the gradients of the graphs derived from Curves *e*, *f*, and *g* are nearer to the value unity.

From these results it appears that the silver-ion exchange is fully consistent with the hypothesis of exchange by diffusion through the solid, but that the bromide-ion exchange is, in general, inconsistent with this model.

If τ is plotted against t and the slope found, it results that the average value of (D/a^2) is roughly 3.10^{-5} sec^{-1}. No accurate values of the average radius are quoted by Langer; but if precipitates are prepared by his method, it is found that a very rough value of a appears to be about 0.5×10^{-4} cm, giving a value of D of the order 10^{-13} cm^2 sec^{-1}. This value agrees quite well with the value obtained from conductivity measurements. However, it is possible to obtain another estimate of D, if the results Langer obtained in his study of the effect of dye adsorption, which are displayed in Fig. 5 (Curve *a*) of his 1943 paper, are used. If ρ is the density of the silver bromide, M_p the mass of the precipitate, and N the number of particles each supposed of radius a, then the total surface S of the precipitate is given by

$$S=3M_p/a\rho.$$

For different precipitates, with the same total volume, a given value of Q will be reached at the same value of τ. From the definition of τ it is therefore obvious that the time t at which the given value of Q is reached is related to the surface area of the precipitate S by the equation

$$S^2t=\text{constant},$$

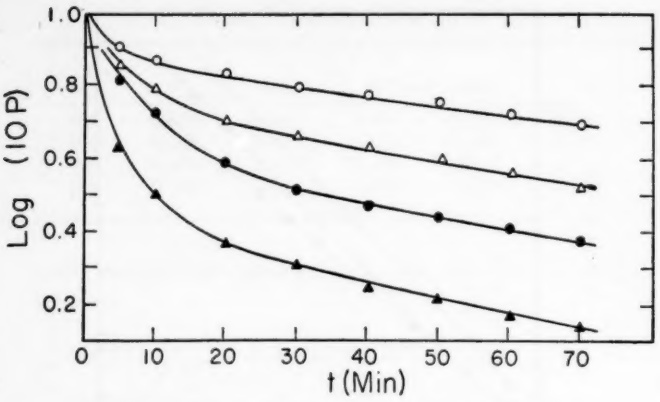

FIG. 5. Silver-ion exchange: from Langer (1942), Fig. 6. ○ 0°C, △ 15°C, ● 30°C, ▲ 50°C.

provided the same value of D holds for all the precipitates.

In Langer's work, M_p is roughly 108 mg, and so approximately

$$S=(20a)^{-1}.$$

Now, if we have a monomolecular layer of adsorbed dye, of total weight in grams, then we can write

$$S=km,$$

where k is the area covered by one gram of dye. From the theoretical curve, the value of τ corresponding to 75 percent total exchange is 9.55×10^{-3}. This value will be increased in practice since the precipitate is non-uniform, and from Fig. 2 it is clear that a given fraction of exchange will then be attained at somewhat larger values of τ. Since τ is equal to (Dt/a^2),

$$Dtk^2m^2=2.4\times10^{-5}.$$

From Langer's graph, which shows the time taken to reach 75 percent exchange as a function of the weight of dye adsorbed by the precipitate, it appears that when t is 40 minutes, 0.1 mg is adsorbed, and it follows that

$$Dk^2=1.0.$$

If we assume that a molecule of methylene blue has an area of 3.10^{-15} cm^2, the area covered by a monomolecular layer of weight one gram is 5.6×10^6 cm^2, which is equal to k. From this we find that D is roughly 3.10^{-14} cm^2 sec^{-1}. It is obvious that if the layer of dye adsorbed were more than one molecule thick, the area covered by one gram would be decreased and hence the value of D would be increased. Again, it is seen that the value of D derived is in fair agreement with that obtained from electrical conductivity measurements on the bulk halide. Further, Langer's figure shows that the experimental results for a number of precipitates are in agreement with the requirement that S^2t is constant. There is no indication whatever of any variation in the value of D between the different precipitates, and the effect quoted by Grimley[4] seems to be largely the result of his inadequate method of comparing theory and experiment.

It is important to examine the alternative mechanism, to see whether it too might give an explanation in as good agreement with experiment as that already found. As has been shown, we expect log$P$ to be approximately a linear function of the time, if the exchange is proceeding by the alternative mechanism. In Fig. 5 are shown the curves obtained on plotting log$P$ against t, for the silver-ion exchange already examined in Fig. 3. It will be seen that straight lines are not found, the plots being in all cases very strongly curved. This shows clearly that the silver-ion exchange does not proceed by this mechanism. Likewise, in Fig. 6 are shown similar plots for the bromide-ion exchange, which are again strongly curved. (Data for this figure are provided by Fig. 3 of Langer's 1943 paper.)

From these results it is clear that the alternative suggestion is incapable of explaining the exchange of bromide or silver ions. Exchange of the latter is fully in agreement with predictions based on exchange by diffusion through the solid, but this mechanism does not explain the bromide exchange. In the latter case, it appears that recrystallization must be the effective mechanism, but the details of the process are far from clear. In particular, the attainment of the end-point given by Eq. (1) after relatively short lengths of time is very difficult to explain. There appears to be no reason why the final amount of radioactive material removed from solution to precipitate should not sometimes be greater than that corresponding to (1). If we assume that the bromide ions are indeed immobile, the final state found experimentally would seem to demand the continual dissolution and reprecipitation of the larger part of the halide. It is difficult to see how Ostwald ripening—the

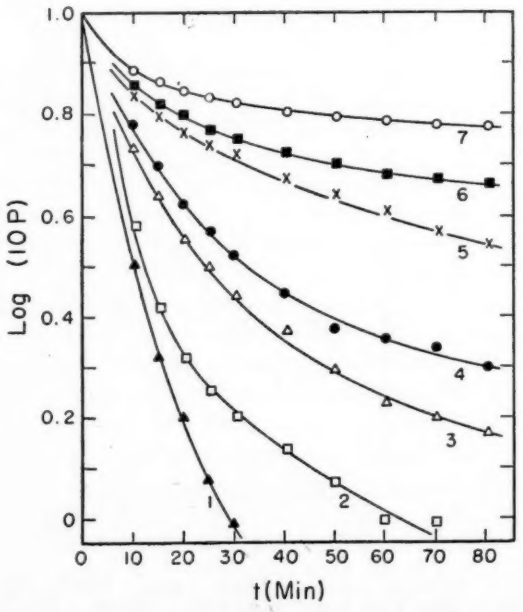

FIG. 6. Bromide-ion exchange: from Langer (1943), Fig. 3.

solution of the smaller crystals and growth of the larger —could in a relatively short time by itself give an end-point which always corresponds to a homogeneous distribution of the radioactive material.

ACKNOWLEDGMENT

Dr. A. Langer, of the Westinghouse Electric Corporation, kindly supplied further information and comments on his experimental work, for which the author wishes to express his gratitude. He is also indebted to Mr. A. Marriage and others of these Laboratories for stimulating discussions.

APPENDIX

Let us suppose that the number of crystals with radii in the range r, $r+dr$ is $f(r)dr$, where

$$f(r)=k\exp\left[-\frac{(\ln r-\ln a_0)^2}{2\beta^2}\right].$$

Here β is a quantity determining the characteristics of the spread of grain sizes, a_0 is the value of the radius most frequently found, and k is a normalizing factor. It is frequently found that the distribution of sizes occurring in a precipitate can be approximated by such a function. Put

$$L_n=\int_0^\infty r^n f(r)dr;$$

then by elementary methods we find

$$L_n=(2\pi)^{\frac{1}{2}}k\beta a_0^{n+1}\exp[(n+1)^2\beta^2/2].$$

The average radius a is given by

$$a=L_1/L_0=a_0\exp(3\beta^2/2).$$

The standard deviation σ is given by

$$\sigma^2=L_2/L_0-a^2=a_0^2[\exp(4\beta^2)-\exp(3\beta^2)],$$

and therefore

$$\sigma/a=[\exp(\beta^2)-1]^{\frac{1}{2}}=\beta\left[1+\frac{\beta^2}{4}+\frac{5\beta^4}{96}+O(\beta^6)\right].$$

We also find that the constants defined in Eq. (11) are given by

$$k_1=\exp(-3\beta^2)$$

and

$$k_2=\exp(-2\beta^2).$$

Two possible cases need to be considered. In the first, the total volume is kept constant, together with the mean radius a. This means that

$$a_0=a\exp(-3\beta^2/2),$$

and

$$L_3=\text{constant}.$$

Thus,

$$(2\pi)^{\frac{1}{2}}\beta k a^4\exp(2\beta^2)=ga^3,$$

where g is a constant; from which one obtains the results

$$L_0=g\exp(-3\beta^2),\quad L_1=ga\exp(-3\beta^2),$$
$$L_2=ga^2\exp(-2\beta^2),\quad L_3=ga^3.$$

Hence, the surface area, which is proportional to L_2, decreases with increasing β.

We now consider that the total volume and the total surface are kept constant. This means that L_2 and L_3 are both constant, and their ratio may be put equal to a constant, say κ:

$$\kappa=L_3/L_2=a_0\exp(7\beta^2/2).$$

From the constancy of the integrals it is easily found that

$$(2\pi)^{\frac{1}{2}}\beta k=g\kappa^{-1}\exp(6\beta^2),$$

where g is a constant. Then

$$L_0=g\exp(3\beta^2),\quad L_1=g\kappa\exp(\beta^2),$$
$$L_2=g\kappa^2,\quad L_3=g\kappa^3,$$
$$a=\kappa\exp(-2\beta^2).$$

Radiation-Induced Reaction between Iodine and Heptane*†

PAUL F. FORSYTH,‡ EDWARD N. WEBER,§ AND ROBERT H. SCHULER‖
Department of Chemistry, Canisius College, Buffalo, New York

(Received May 4, 1953)

The radiation-induced reaction between iodine and *n*-heptane has been studied with a view to its use in the quantitative determination of free radical production in the radiolysis of liquid hydrocarbons. The yield of this reaction has been found to be nearly independent of iodine concentration and of temperature of the sample. The reaction is inhibited by the presence of dissolved oxygen. For each mole of hydrogen produced, 0.6 mole of iodine is absorbed which indicates that free radical production is a major component of the over-all process. The primary decomposition yield is of the order of 10 bonds broken per 100 ev of absorbed energy.

INTRODUCTION

THE principal observations on the radiation decomposition of aliphatic hydrocarbons have been on the production of gaseous products, with little attention paid to processes yielding substances other than hydrogen and the lower hydrocarbons. Such processes include the reactions of free radical intermediates which ultimately form higher molecular weight hydrocarbons. The gas-production reactions, themselves, have been subjected to rather limited scrutiny. The principle studies here include those of Lind and his school using alpha activation,[1] the early work of Schoepfle and Fellows,[2] where the relative yields were examined for a large number of hydrocarbons exposed in the vapor phase to 100-kev cathode rays, and the more recent work of Flanagan, Hochanadel, and Penneman,[3] and Manion and Burton,[4] where the gas production yields were determined for the Mev electron bombardment of cyclohexane and other hydrocarbons.

The relatively large yield of hydrogen in the radiation decomposition has masked to a considerable extent the importance of reactions involving the larger radicals. Recent work in these laboratories[5] has shown that processes are operative which independently produce both hydrogen and free radicals, with the latter capable of being quenched by the iodine present in the reacting system.

Magat and co-workers,[6] and also Wild,[7] have used the reaction of highly colored diphenylpicrylhydrazyl radical as an indication of free-radical formation in the radiolysis of a number of organic substances including cyclohexane, *n*-heptane, and *n*-octane. Styrene polymerization has also been used, with, however, some difficulty because of the necessary changes in the reacting system.[6,8] Schuler and Hamill,[9] in studies of the radiolysis of organic iodides, have observed the radiation induced reaction between iodine and *n*-heptane.[10] A similar reaction, followed by carrier isolation of the products, has been used as the basis for the identification of the various radical fragments formed in the radiation decomposition of the gaseous hydrocarbons.[11]

The purpose of this investigation was to study the characteristics of the radiation-induced reaction between iodine and *n*-heptane and the possibilities of its use in detecting free radicals in hydrocarbon systems. Together with the isolation of the various alkyl iodides formed, it is anticipated that this reaction may then serve to estimate the yield of production of the individual alkyl radicals.

EXPERIMENTAL

Materials

The normal heptane employed in these investigations was obtained from the following sources: experiments 1–10, Eastman Kodak (white label), n_D^{25} 1.3851–2; experiments 11, 12, 14–19, Phillips (pure grade), n_D^{25} 1.3852–3; experiments 13, 20–22, Phillips (research grade), n_D^{25} 1.3851. The Phillips research grade *n*-heptane was used as received. This was from a lot certified as being 99.87±0.05 mole percent *n*-heptane with 3-methyl hexane and 3-ethyl pentane as the most probable impurities. All other samples were distilled through a 60-cm helix-packed column. The center cut boiling at 98.4±0.2°C was further fractionated through

* Supported in part under contract AT(30-1)-1084 with the U. S. Atomic Energy Commission.

† From the M.S. dissertation of P. F. Forsyth, Canisius College, June, 1953.

‡ Present address: Metals Research Laboratory, Union Carbide and Carbon Corporation, Niagara Falls, New York.

§ Present address: St. John Fisher College, Rochester, N. Y.

‖ Present address: Brookhaven National Laboratory, Upton, New York.

[1] S. C. Lind and D. C. Bardwell, J. Am. Chem. Soc. **48**, 2335 (1926); S. C. Lind, *Chemical Effects of Alpha Particles and Electrons* (Reinhold Publishing Company, New York, 1935).

[2] C. S. Schoepfle and C. H. Fellows, Ind. Eng. Chem. **23**, 1396 (1931).

[3] See M. Burton, J. Phys. and Colloid Chem. **51**, 611 (1947).

[4] J. P. Manion and M. Burton, J. Phys. Chem. **56**, 560 (1952).

[5] C. C. Schubert and R. H. Schuler, J. Chem. Phys. **20**, 518 (1952).

[6] Prevost-Bernas, Chapiro, Cousin, Landler, and Magat, Discussions Faraday Soc. **12**, 98 (1952).

[7] W. Wild, Discussions Faraday Soc. **12**, 127 (1952).

[8] A. Chapiro, J. chim. phys. **47**, 747 (1950).

[9] R. H. Schuler and W. H. Hamill, J. Am. Chem. Soc. **74**, 6171 (1952).

[10] G. L. Clark and L. W. Pickett, J. Am. Chem. Soc. **52**, 465 (1930), observed qualitatively that iodine reacted with benzene under the influence of x-radiation.

[11] W. H. Hamill and R. R. Williams, Jr., J. Am. Chem. Soc. **72**, 1857 (1950); L. H. Gevantman and R. R. Williams, Jr., J. Phys. Chem. **56**, 569 (1952).

a 30-cm Podbielniak column. The center cut from this distillation, which has a boiling range of approximately 0.2°C and a refractive index as indicated above, was used in the irradiations.

C.P. resublimed iodine was used without further purification.

Irradiation

Most of the irradiations were carried out using the unfiltered radiation from an industrial x-ray unit operated at 120 pkv and 5 ma. The effective wavelength of this radiation is in the region of 0.2–0.4A. The radiation entered vertically through the bottom of the irradiation cells, 50-ml Florence flasks, placed in a fixed position in the well of the x-ray tube. The control of the instrument and geometry permitted reproducibility in the irradiations to within 2 percent. This arrangement allowed maximum dosage of the sample and is essentially the same as that used in the studies of the radiolysis of methyl iodide.[12]

In the case of the experiments performed for the purpose of measuring the temperature dependence of the reaction, the irradiation cell consisted of a 25-ml flask with an annular jacket through which thermostating water was circulated. The cell assembly, irradiated as described above, absorbed energy at a rate 0.75 times that of the other x-ray experiments.

For the gamma-radiation experiments, three 100 millicurie Co^{60} sources were arranged in a triangle 10 mm on edge and the irradiation vessel was placed in a reproducible position over these sources. The geometry factor is estimated as being of the order of 20 percent. These experimental arrangements were monitored using the radiation-induced oxidation of ferrous sulfate in 0.8N sulfuric acid.

The *n*-heptane (10 ml), containing the appropriate concentration of iodine, was sealed in the irradiation cell after the removal of dissolved air. Degassing was accomplished by freezing the sample in liquid nitrogen, pumping, melting, and briefly boiling the sample, and repeating this procedure again twice before sealing.

For purposes of measuring the iodine concentration, an absorption cell of 1-cm square tubing was sealed to the irradiation vessel. The optical densities, which were measured with the aid of a Beckman DU quartz spectrophotometer, could then be determined during the course of irradiation without opening the sample. These were corrected by subtraction of the value obtained for the pure solvent. The following molar extinction coefficients of iodine in heptane [in units of cm^{-1} $(moles/liter)^{-1}$] were used in these calculations: at 480 mμ, 461; at 500 mμ, 728; at 520 mμ (maximum), 859; and at 550 mμ, 634.

The gas-production measurements were carried out as previously described.[5,13] The sample was frozen in liquid nitrogen and the volatile hydrogen-methane fraction was pumped to a McLeod gauge for measurement, followed by combustion analysis.

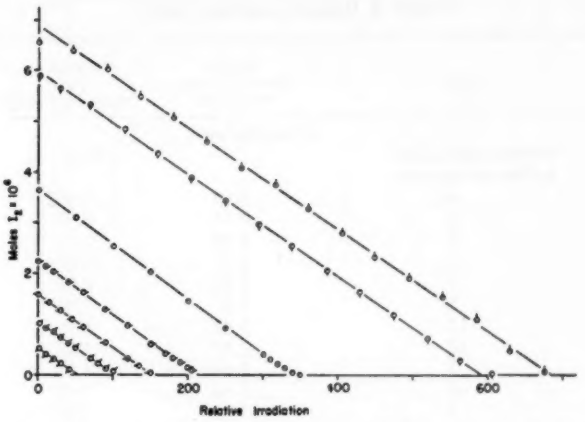

FIG. 1. Absorption of iodine by *n*-heptane induced by x-radiation.

Results

The general nature of the radiation-induced reaction between *n*-heptane and iodine is illustrated in Fig. 1. The reaction appears to be of zero order, depending directly upon the energy absorbed by the reacting system. These kinetics hold both for the case of the individual samples, where the yield is constant over the entire course of reaction, and for the various different experiments, where the yields are substantially constant. The relative yields observed in the individual experiments are listed in Table I.[14] As seen in Fig. 2 there is a slight drop in the yield for iodine concentrations below 2×10^{-4}M. This effect is probably, partially

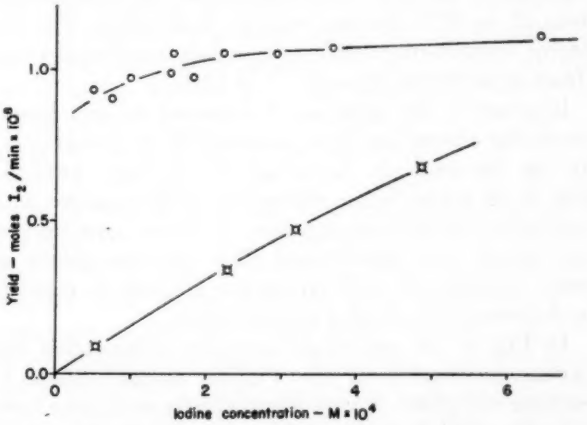

FIG. 2. Relative yields of iodine absorption: ○—degassed samples, ⊗—air saturated samples.

[12] R. C. Petry and R. H. Schuler, J. Am. Chem. Soc. **75**, 3796 (1953).

[13] R. H. Schuler and C. T. Chmiel, J. Am. Chem. Soc. **75**, 3792 (1953).

[14] For the purposes of this investigation, the relative yields are given in terms of the experimental unit, moles of reaction per unit irradiation. The absolute yields are given in the discussion in terms of *G*, i.e., processes produced per 100 ev of absorbed energy.

TABLE I. Relative reaction yields.

Expt. No.	Iodine concentration molar $\times 10^4$	Relative yield moles/min $\times 10^8$
	x-irradiation	
ferrous oxidation		18.0
iodine absorption		
4	0.50	0.93
6	0.74	0.90
7	1.00	0.97
17	1.38	0.99[a]
5	1.52	0.98
8	1.57	1.05
11	1.82	0.97
12	2.22	1.05
3	2.96	1.05
9	3.64	1.07
1	5.87	1.02[b]
13	6.42	1.11
2	5.55	1.01[b]
hydrogen production		
21	...	1.66
22	...	1.72
	gamma irradiation	
ferrous oxidation		0.193
iodine absorption		
20	3.10	0.0295

[a] Thermostated sample; yield normalized by factor of 1/0.75.
[b] Irradiated at 140 pkv and 6 ma; yield normalized by factor of 1/1.505.

at least, due to trace impurities which are difficult to remove in the purifications and are relatively more important at the lower concentrations. The experimental scatter, which is somewhat greater than expected from possible variations in intensity, appears to be due to a similar effect. The yield for the sample of Phillips research-grade heptane (experiment 13) is notably slightly high although the iodine concentration is also high in this case.

In Table II the results of the studies of temperature dependence are given. An increase in the temperature from 25 to 75°C is seen to have little effect. The ten degree temperature coefficient has the maximum value (from experiments 15 and 17) of 1.02.

In general, the presence of dissolved oxygen lowers the iodine absorption yield, presumably by competition for the free radicals. As is seen in the lower curve in Fig. 2, the initial iodine absorption yield increases with increasing iodine concentration. In these experiments, the sample was equilibrated with the atmosphere at room temperature with no further attempt to regulate or determine the oxygen concentration.

In Fig. 3, the results of both the x-irradiation and gamma irradiation of the Phillips research-grade *n*-heptane are given. A very slight curvature is seen here, with the yield decreasing about 10 percent, going from 5×10^{-4}M to 0.5×10^{-4}M as the iodine is used up during the reaction. This appears to be minor and may be, similar to the effects mentioned earlier, the result of the presence of trace impurities. A close examination of the other data indicates that most, but not all, of the runs have very slight tails at the end. The gamma-irradiation data are given here on the assumption that the rate of absorption of energy is 0.0273 of that of the case of x-irradiation.

Figure 4 illustrates the absorption spectrum of the sample of experiment 13 before and after the irradiation. As the irradiation was continued until the iodine was completely absorbed, there is no component of free iodine in the final spectrum. The molar extinction coefficient of ethyl iodide in *n*-heptane is 430 at 260 mμ (the maximum in the absorption). If this value is representative of the alkyl iodides, a yield (which will be somewhat high because of the presence of an unidentified component which absorbs in the region below 300 mμ) of 15×10^{-6} moles of alkyl iodides is estimated. This compares with the 12.8×10^{-6} mole expected for the absorption of the iodine initially present.

DISCUSSION

The general problem of detecting free-radical production in the radiolysis of hydrocarbons can involve much greater complications than are apparent from a cursory review of the situation. This is very well illustrated by Magat's paper[6] and the discussion subsequent to his paper.[15] The present investigation indicates that iodine, as an additive in small concentration, possesses characteristics which make it suitable for radical detection in these systems. In spite of this it is not impossible that certain difficulties, particularly changes caused by electron capture and charge transfer processes caused by differences in the reacting system, may arise to complicate the reactions. For that reason, we can only tentatively propose the radiation-induced reaction between iodine and the hydrocarbons as an indication of free radical production. Only upon cross checking the results of the present work with other systems will its proper position become known.

Molecular iodine can serve as a detector only for radicals which are eventually thermalized because it is necessary that these radicals diffuse relatively long distances before encountering iodine with which they can react. Any products produced directly in the primary decomposition, or via ionic or hot radical processes, cannot be detected by the methods described here.

On the whole, except for minor effects, the kinetics of the iodine-absorption reaction appears to be without serious complication; the total reaction yield is proportional to the energy absorbed by the system. Therefore, it is necessary that no other substances be present which can competitively react with the radicals, as is the case

TABLE II. Effect of temperature.

Expt. No.	Temperature °C	Iodine concentration molar $\times 10^4$	Relative yield moles/min $\times 10^8$
17	25	1.38	0.74
16	50	2.12	0.75
15	75	1.38	0.82

[15] See Discussions Faraday Soc. **12**, 115–116, 125–131 (1952).

when oxygen is present in the system. In the presence of small amounts of iodine and the absence of other reactive species, the principal reaction is

$$R+I_2 \rightarrow RI+I. \quad (1)$$

The iodine atoms must eventually combine and react according to (1). Here it is important that there be no reaction between the atoms and the solvent, which would set up a chain and extend the reaction beyond that of radical detection.

The activation energy for the reaction of the radicals with the substrate must be sufficiently high to render the reactions of the type

$$R+R'CH_3 \rightarrow RH+R'CH_2 \quad (2)$$

improbable. If reaction (2) occurs and is followed by a reaction of type (1), the observed yield will, of course, not be affected, although a change in identity of the product will result. Reaction (2) is, however, also complicated by the possibility of decomposition of this secondary radical along a different reaction path. Assuming, for reactions (2) and (1), an activation energy difference of 8 kcal/mole and a ratio of steric factors of 10^{-2}, then reaction (2) should be of importance for iodine concentrations below 10^{-5}M. It does not appear that these reactions are of more than secondary importance in hydrocarbon systems, although they must be considered where more reactive groups are present.

Similarly, it is also important that the products of the reaction not be susceptible to further attack by free radicals. Little difficulty is expected in this particular case because of the low concentration and relative stability of the alkyl iodides formed.

Yields

The absolute yield for iodine absorption can be estimated from the yield observed in the case of Co^{60} gamma activation (0.0295×10^{-8} mole/min) by comparison with that for ferrous oxidation (0.193×10^{-8} mole/min). Assuming a ferrous oxidation yields of 15.5[16] and an absorption relative to 0.8N sulfuric acid of 0.69, a yield of 3.4 iodine molecules absorbed or 6.8 radicals produced per 100 ev of absorbed energy is calculated. This compares favorably with the value estimated in the electron bombardment studies ($G(RI)=7.3$).[9]

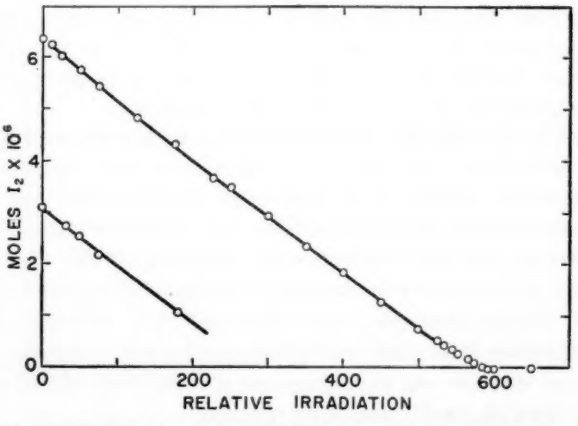

FIG. 3. Iodine absorption—Phillips research-grade *n*-heptane: O—x-irradiation (min), -⊖-—Co^{60} gamma-irradiation (min $\times0.0273$).

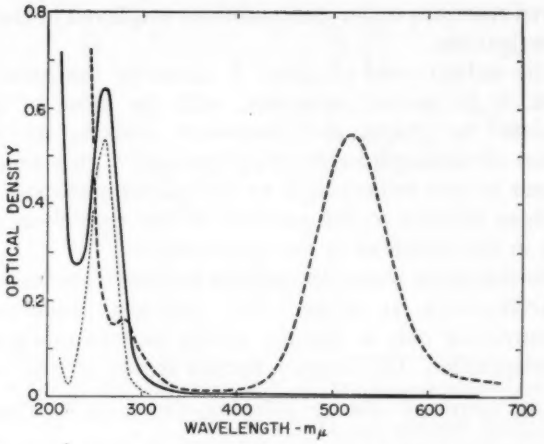

FIG. 4. Absorption spectrum of sample 13: solid curve, after irradiation; dashed curve, before irradiation. Dotted curve represents 12.4×10^{-4}M ethyl-iodide solution.

The relative yields in the case of gamma and x-irradiation may be compared for iodine absorption, $G_{Co^{60}}(-I_2)/G_{x\text{-ray}}(-I_2)=0.0268$, and for hydrogen production, $G_{Co^{60}}(H_2)/G_{x\text{-ray}}(H_2)=0.0273$. It is seen that although the average energy of the primary electron changes from the Mev region to approximately 40 kev and the absorbed intensity decreases by a factor of 39, there is no appreciable effect on the relative yields of these processes.

In the x-ray studies, because the absorption of energy involves both the Compton and photoelectric effect in varying degrees, it is much more difficult to make accurate calculations of the absolute yields. In going from water to the hydrocarbon, the photoelectric contribution is reduced by a factor of ~0.42. If it is assumed (as at 0.3*A*) that in water the absorption is 83 percent photoelectric and 17 percent Compton, then the absorption relative to water, after correction is made for the difference in density of the samples, is estimated to be 0.36 in the case of *n*-heptane. Using this value, comparison with ferrous oxidation gives a yield of 2.8. If hydrogen production is used as the dosimeter, no correction need be made for absorption, and the x-ray yield is seen to be in agreement with the gamma yield. The data, in general, indicate little, if any, effect of energy or intensity on the absolute yields of the ob-

[16] See N. Miller and J. Wilkinson, Discussions Faraday Soc. 12, 50 (1952) for a discussion of the absolute yield of ferrous oxidation. It now appears from accurate calorimetric measurements [C. J. Hochanadel and J. Ghormley, J. Chem. Phys. 21, 880 (1953)] and from charge measurement in the fast electron irradiation of ferrous sulfate solutions [J. Saldick and A. O. Allen (to be published)] that $G(Fe^{++}\rightarrow Fe^{+++})\simeq15.5$.

served reactions under the conditions employed in these investigations.

The radical yield of about 7, given by the present work, is in general agreement with the value of 8.1 obtained by Magat and co-workers utilizing the reaction of diphenylpicrylhydrazyl radical.[17] This would appear to give some weight to the general applicability of these systems to the problem of free radical detection in the radiolysis of the hydrocarbons.

On the above basis, the yield for hydrogen production is $G(H_2)=5.2$. It is seen that hydrogen production accounts for only a fraction of the radiation-induced decomposition. This is given further significance by the observation of Schubert and Schuler[5] that at the concentration of iodine present, under the conditions of the present investigations, the iodine is ineffective in quenching the hydrogen-production reactions. This would also indicate that charge-transfer or electron-capture processes, at least in so far as they affect the reactions producing hydrogen, are not operative in the present case.

The primary yield for bonds being broken must be at least $G(H_2)+G(-I_2)\simeq 8.6$ with an additional yield of 5–10 percent caused by miscellaneous processes. The primary decomposition yield in the radiolysis of heptane is, therefore, very close to 10, or approximately 1 process per 10 ev of absorbed energy. This appears to be somewhat higher than anticipated in earlier work.

[17] See reference 6; also the following discussion, M. Magat, Discussions Faraday Soc. **12**, 129 (1952).

THE JOURNAL OF CHEMICAL PHYSICS VOLUME 22, NUMBER 1 JANUARY, 1954

The Vibrational Spectra of *N*-Dimethylaminodiborane*†

D. E. MANN‡
School of Chemistry, University of Minnesota, Minneapolis, Minnesota
(Received June 5, 1953)

The infrared and Raman spectra of *N*-dimethylaminodiborane, $(CH_3)_2NB_2H_5$, and its deuteriated relative, $(CH_3)_2NB_2D_5$, have been determined. A satisfactory vibrational assignment has been achieved.

THE present study of the infrared and Raman spectra of *N*-dimethylaminodiborane[1,2] was undertaken in an attempt to elucidate its structure further. Hedberg and Stosick have recently published the results of their electron-diffraction investigation of DMADB.[3] They found that their data are in closest accord with a symmetrical structure derived from diborane by replacement of a bridge hydrogen with the nitrogen of the dimethylamino group. This configuration has C_{2v} symmetry, and their intensity curves were calculated for such a model. The electron-diffraction results call attention to several interesting structural features. Apart from the occurrence of a tetrahedrally coordinated nitrogen atom in the bridge, Hedberg and Stosick found that while the C–N distance and C–N–C angle have normal values (1.48A and 111.5°, respectively), the B–N and B–B distances and the B–N–B angle have the rather surprising values 1.55A, 1.92A, and 76.4°, respectively. It will be interesting, therefore, to see how the elongation of the B–B distance over that in ordinary diborane, as well as the other unusual features, are reflected in the vibrational spectra.

EXPERIMENTAL DETAILS

The normal and deuteriated compounds were provided by Professor A. B. Burg. The 4.5 ml sample of the former and the 0.5 ml sample of the latter sufficed for all measurements. The deuteriated compound was contaminated by the normal substance to the extent of between five and ten percent. All filling and emptying operations were carried out with the aid of an all-glass, high-vacuum system so that only negligible decomposition and other losses were sustained.

For the infrared measurements a Perkin-Elmer 12C spectrometer was used. The instrument was equipped with KBr windows, a wavelength drive for the NaCl prism, a G-M breaker-amplifier, and a Brown recorder. During runs the housings were flushed with dry nitrogen. The vapor of the sample, at room temperature and at various pressures, was contained in a 10-cm glass cell whose KBr windows had been sealed with a beeswax-rosin mixture. At each pressure spectra were obtained in the LiF, NaCl, and KBr regions.

The apparatus and methods used to obtain the Raman spectra were essentially those described by

* This research was supported in part by the U. S. Office of Naval Research through Contract N5ori-147, T. O. II.
† Presented at Symposium on Molecular Structure and Spectroscopy, Ohio State University, June 10, 1952.
‡ DuPont Postdoctoral Fellow, 1948–1949; Jewett Postdoctoral Fellow, 1949–1951. Present address: National Bureau of Standards, Washington 25, D. C.
[1] A. B. Burg and C. L. Randolph, J. Am. Chem. Soc. **71**, 3451 (1949).
[2] *N*-dimethylaminodiborane and *N*-dimethylaminodiborane–d_5 will hereafter be abbreviated to DMADB and DMADB–d_5, respectively.
[3] K. Hedberg and A. J. Stosick, J. Am. Chem. Soc. **74**, 954 (1952).

Crawford and Horwitz.[4] Eastman Kodak 103a-O and 103a-J plates were used, and exposures up to 48 hours in length were taken. An iron arc and argon and helium lamps provided the standard comparison spectra. Frequency measurements were made with a Leeds and Northrup microdensitometer and with a D. W. Mann comparator. All recorded infrared and Raman frequencies have been corrected to vacuum. Depolarization ratios were determined by the method of Crawford and Horwitz.[4] Considerable background and the weak-

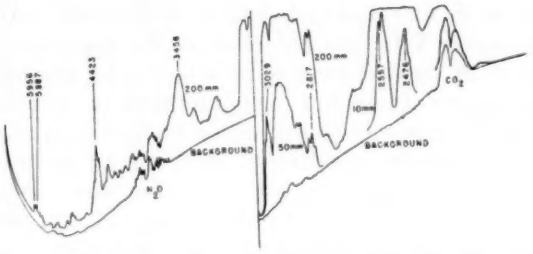

FIG. 1. Infrared absorption spectrum of DMADB (LiF prism).

ness of many lines made precise ratios difficult to obtain, so only rounded factors are given.

The infrared spectra of the two compounds are given in Figs. 1–5. All observed infrared and Raman frequencies are given in Tables I–IV.

INTERPRETATION OF SPECTRA

In view of the unusual structure of DMADB several general remarks about the interpretation of its vibra-

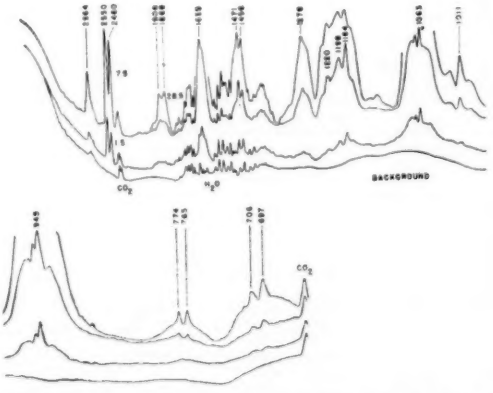

FIG. 2. Infrared absorption spectrum of DMADB (NaCl prism).

tional spectra are relevant. The highest symmetry which DMADB can have is C_{2v}.§ This would apply even if, as Hedberg and Stosick suggest,[3] the BH_2 groups are rotated away from the nitrogen to the extent of 15–20°. The observed spectra are compatible with the assumption of C_{2v} symmetry and have been interpreted on this basis.

[4] B. L. Crawford, Jr., and W. Horwitz, J. Chem. Phys. **15**, 268 (1947).

§ It should be noted that DMADB and DMADB$-d_5$ belong to the same point group.

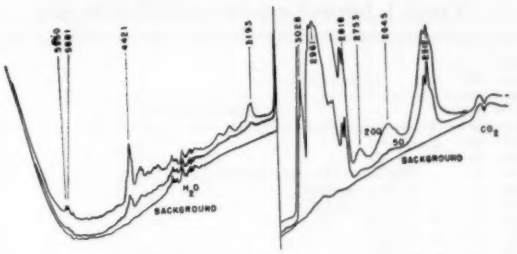

FIG. 3. Infrared absorption spectrum of DMADB$-d_5$ (LiF prism).

Reference to Table VI will show that the 42 fundamental vibrations of DMADB are apportioned among the species as follows: 13 in a_1, 8 in a_2, 10 in b_1, and 11 in b_2. Now at least for the light compound the observed spectra in the region where fundamentals are to be expected can conveniently be grouped in five parts.

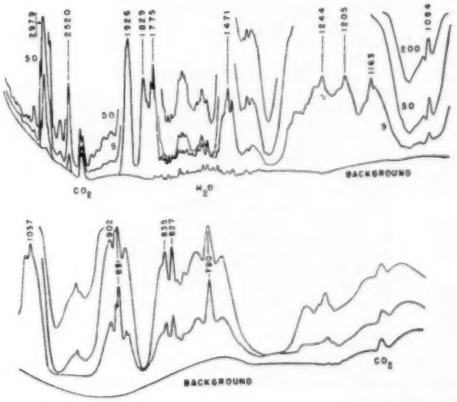

FIG. 4. Infrared absorption spectrum of DMADB$-d_5$ (NaCl prism).

First, the C–H stretching vibrations occur well separated from other vibrations. Second, the B–H stretchings for the end-group and bridge hydrogens occur at about 2400–2500 cm^{-1} and 1600–2000 cm^{-1}, respectively, and are also well removed from other fundamentals. Third, the deformation frequencies char-

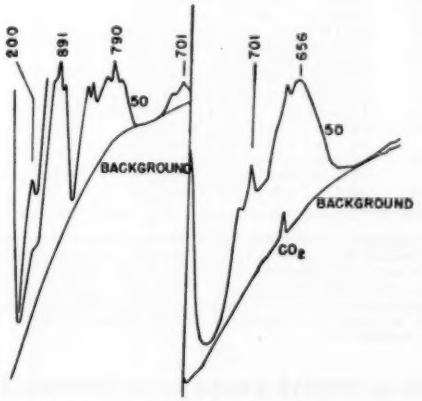

FIG. 5. Infrared absorption spectrum of DMADB$-d_5$ (KBr prism).

TABLE I. Infrared spectrum of DMADB (gas).

Wave number (cm^{-1})	Intensity		Interpretation[a]
697	m	Q	$\nu_{12}(a_1)$
706	m	R	$\nu_{12}(a_1)$
712	w		$950(b_2)-236(a_2)=714(B_1)$
765	w		$\nu_{11}(a_1)$; $\nu_{40}(b_2)$
775	w		$\nu_{11}(a_1)$; $\nu_{40}(b_2)$
935	vs	P	$\nu_{10}(a_1)$
945	vs	Q	$\nu_{10}(a_1)$
950	vs		$\nu_{39}(b_2)$
956	vs	R	$\nu_{10}(a_1)$
1002	w	P	$\nu_9(a_1)$
1011	s	Q	$\nu_9(a_1)$
1024	m		$\nu_{38}(b_2)$
1058	vs	P	$\nu_{29}(b_1)$
1063	vs	Q	$\nu_{29}(b_1)$
1069	vs	Q	$\nu_8(a_1)$
1075	vs	R	$\nu_8(a_1)$; $\nu_{37}(b_2)$
1140	vw		$236(a_2)+896(a_2)=1132(A_1)$
1184	vs		$\nu_{37}(b_1)$
1198	vs		$\nu_7(a_1)$
1220	vs		$\nu_{36}(b_1)$
1232	vs		$325(b_2)+896(a_2)=1221(B_1)$
1278	vs		$325(b_2)+945(a_1)=1270(B_2)$; $325(b_2)+950(b_2)=1275(A_1)$
1387	m		$\nu_{36}(b_2)$
1393	m		$\nu_6(a_1)$; $\nu_{36}(b_2)$
1458	vs		$\nu_{28}(b_1)$
1471	vs		$\nu_5(a_1)$; $\nu_{35}(b_2)$
1530	s		$325(b_2)+1198(a_1)=1523(B_2)$
1539	s		$2\times772(a_1)=1544(A_1)$
1623	vs	P	$\nu_{24}(b_1)$
1635	vs	Q	$\nu_{24}(b_1)$
1708	m		$697(a_1)+1011(a_1)=1708(A_1)$
1868	m		$\nu_4(a_1)$[a]
1908	m		$2\times945(a_1)=1890(A_1)$[b]
1963	vw		$772(a_1)+1184(b_1)=1956(B_1)$; $896(a_2)+1063(b_1)=1959(B_2)$; $772(a_1)+1198(a_1)=1970(A_1)$
2008	vw		$945(a_1)+1063(b_1)=2008(B_1)$
2018	vw		$950(b_2)+1069(a_1)=2019(B_2)$
2072	vw		$1046(a_2)+1024(b_2)=2070(B_1)$; $1011(a_1)+1069(a_1)=2080(A_1)$
2125	vw		$2\times1063(b_1)=2126(A_1)$
2134	vw		$2\times1069(a_1)=2138(A_1)$
2229	vw		$325(b_2)+2\times945(a_1)=2215(B_2)$; $1024(b_2)+1198(a_1)=2222(B_2)$
2268	vw		$1084(b_1)+1184(b_1)=2268(A_1)$
2374	m		$2\times1184(b_1)=2368(A_1)$
2476	vs		$\nu_3(a_1)$
2547	vs		$\nu_{23}(b_1)$; $\nu_{34}(b_2)$
2557	vs		$\nu_{23}(b_1)$; $\nu_{34}(b_2)$
2649	vw		$772(a_1)+1885(a_1)=2657(A_1)$
2743	vw		$2\times772(a_1)+1198(a_1)=2742(A_1)$
2806	w	P	$\nu_2(a_1)$
2817	m	Q	$\nu_2(a_1)$
2830	m	R	$\nu_2(a_1)$
2870	s		$\nu_{33}(b_2)$
2883	s		$\nu_{33}(b_2)$
2964	vs		$\nu_{32}(b_2)$
2978	vs	P	$\nu_1(a_1)$
2990	vs	Q	$\nu_1(a_1)$
3020	m	P	$\nu_{22}(b_1)$
3029	s	Q	$\nu_{22}(b_1)$
3040	m	R	$\nu_{22}(b_1)$
3196	vw		$3\times1063(b_1)=3189(B_1)$; $3\times1069(a_1)=3207(A_1)$
3352	vw		$2\times950(b_2)+1451(a_2)=3351(B_1)$; $2\times945(a_1)+1458(b_1)=3348(B_1)$
3458	vw		$896(a_2)+2552(b_2)=3448(B_1)$
3714	vw		$1011(a_1)+1069(a_1)+1635(b_1)=3715(B_1)$
3937	vw		$950(b_2)+2990(a_1)=3940(B_2)$
4023	vw		$1046(a_2)+2964(b_2)=4010(B_1)$; $1069(a_1)+2964(b_2)=4033(B_2)$
4087	vw		$1063(b_1)+3029(b_1)=4092(A_1)$
4159	vw		$1198(a_1)+2964(b_2)=4162(B_2)$
4252	vw		$2\times1184(b_1)+1885(a_1)=4253(A_1)$
4385	vw		$1393(a_1)+2990(a_1)=4383(A_1)$
4423	vw		$1393(a_1)+3029(b_1)=4422(B_1)$
4472	vw		$1451(a_2)+3019(a_2)=4470(A_1)$
4620	vw		$1635(b_1)+2990(a_1)=4625(B_1)$
4917	vw		$2\times1184(b_1)+2552(b_2)=4920(B_2)$
5023	vw		$2476(a_1)+2547(b_1)=5023(B_1)$; $2476(a_1)+2552(b_2)=5028(B_2)$
5887	vw		$2876(b_2)+2990(a_1)=5866(B_2)$; $2876(b_2)+3019(a_2)=5895(B_1)$
5956	vw		$2964(b_2)+2990(a_1)=5954(B_2)$

[a] In presenting the assignments in Tables I–IV no attempt has been made to list all possible binary-sum explanations for every nonfundamental band, and in only very few instances have ternary sums been invoked. Only those which seem physically reasonable or which are typical have been used.

[b] The fundamental $\nu_4(a_1)$ is placed at about 1885 cm^{-1} and appears to have been shifted as a result of Fermi resonance with the overtone $2\times945(a_1)=1890(A_1)$.

acteristic of methyl groups occur between 1390 cm^{-1} and 1470 cm^{-1} in DMADB (and DMADB$-d_5$ as well) and so are quite distinct from other vibrations. The important point here is that there are no other fundamentals which can reasonably be expected to occur above 1390 cm^{-1}. The spectral region of real interest has therefore been narrowed down to that below about 1390 cm^{-1}. It will be helpful to classify the remaining frequencies as "low" if they occur below 500–600 cm^{-1}, and as "intermediate" otherwise.

The preceding classification effects a marked apparent simplification of the assignment problem. For there now remain in a_1 only one low and six intermediate frequencies. In a_2 there are now only three and two, in b_1 four and two, and in b_2 four and two, respectively. A further reduction in the apparent complexity of the problem can be achieved by considering how many of the low and intermediate frequencies would be expected to undergo a marked isotope shift upon deuterium substitution. With one exception, ν_{42}, all the low frequencies are connected with the gross motions of the dimethylamino group. Hence, almost every one of the interesting, and troublesome, vibrations is confined (in the light compound) to the region 600–1300 cm^{-1}. Furthermore, three of these are in the species a_2 and so do not appear in the infrared spectrum.

TABLE II. Raman spectrum of DMADB (liquid).

Wave number (cm^{-1})	Intensity; depolarization factor	Interpretation
−766[a]	m, ?	
−692	vw, ?	
−590	vw, ?	
−523	?, ?	
−490	?, ?	
−452	w, b, ?	
−389	w, ?	
−315	vw, ?	
−269	vvw, ?	
−232	vvw, ?	
+236	vvw, 0.9	$\nu_{20}(a_2)$
279	vvw, ?	$\nu_{30}(b_1)$
325	vvw, 0.9	$\nu_{42}(b_2)$
399	w, 0.9	$\nu_{13}(a_1)$; $\nu_{41}(b_2)$
488	vvw, 0.6	$2\times236(a_2)=472(A_1)$
599	w, 0.8	$\nu_{19}(a_2)$
702	w, 0.7	$\nu_{12}(a_1)$
772	vvs, 0.1	$\nu_{11}(a_1)$; $\nu_{40}(b_2)$
896	vw, 0.9	$\nu_{18}(a_2)$
940	vvw, 0.9	$\nu_{10}(a_1)$; $\nu_{39}(b_2)$
1012	vw, 0.8	$\nu_9(a_1)$; $\nu_{38}(b_2)$
1046	vw, 0.9	$\nu_{17}(a_2)$
1069	vw, 0.8	$\nu_8(a_1)$; $\nu_{28}(b_1)$; $\nu_{29}(b_1)$; $\nu_{37}(b_2)$
1111	vvw, 0.9	$396(a_1)+697(a_1)=1096(A_1)$
1191	vw, 0.8	$\nu_7(a_1)$; $\nu_{27}(b_1)$
1279	vvw, 0.7	$325(b_2)+950(b_2)=1275(A_1)$; $325(b_2)+945(a_1)=1270(B_2)$
1339	vvw, ?	$279(b_1)+1069(a_1)=1348(B_1)$; $399(a_1)+950(b_2)=1349(B_2)$
1451	w, 0.9	$\nu_{16}(a_2)$; $\nu_{26}(b_1)$
1475	w, 0.9	$\nu_5(a_1)$; $\nu_{35}(b_2)$
1566	vvw, ?	$2\times772(a_1)=1544(A_1)$
1627	vvw, 0.7	$\nu_{24}(b_1)$
1767	?, ?	$697(a_1)+1069(a_1)=1766(A_1)$
1857	w, 0.3	$\nu_4(a_1)$[b]
1900	w, 0.3	$2\times945(a_1)=1890(A_1)$; $2\times950(b_2)=1900(A_1)$[b]
1966	vvw, 0.6	$950(b_2)+1024(b_2)=1974(A_1)$
2113	vvw, 0.7	$2\times1069(a_1)=2138(A_1)$; $2\times1063(b_1)=2126(A_1)$; $2\times1046(a_2)=2092(A_1)$
2366	vvw, 0.5	$2\times1184(b_1)=2368(A_1)$
2475	vvs, 0.1	$\nu_3(a_1)$; $\nu_{15}(a_2)$
2529	m, 0.8	$\nu_{23}(b_1)$; $\nu_{34}(b_2)$
2810	w, 0.3	$\nu_2(a_1)$
2863	w, 0.3	$\nu_{33}(b_2)$; $1393(a_1)+1471(a_1)=2864(A_1)$; $1390(b_2)+1471(b_2)=2861(A_1)$
2950	s, 0.4	$\nu_1(a_1)$
2975	w, ?	$\nu_{32}(b_2)$
3017	w, 0.8	$\nu_{14}(a_2)$; $\nu_{22}(b_1)$

[a] The entries preceded by minus sign are for the observed anti-Stokes lines. The discrepancies between corresponding Stokes and anti-Stokes wave numbers are unexplained.

[b] See footnote a to Table I.

TABLE III. Infrared spectrum of DMADB$-d_5$ (gas).

Wave number (cm^{-1})	Intensity	Interpretation
656	w	$\nu_{10}(a_1)$
660	w	$1054(a_2)-396(b_2)=658(B_1)$
701	w	Q $\nu_{13}(a_1)$
705	vw	$\nu_{12}+\nu_i-\nu_i$
713	w	R $\nu_{13}(a_1)$
729	vw	$\nu_{11}(a_1)$
778	w	P $\nu_{29}(b_1)$
791	m	Q $\nu_{29}(b_1)$
803	w	R $\nu_{29}(b_1)$
815	vw	P $\nu_{26}(b_1)$
822	vw	$1037(a_1)-214(b_2)=823(B_2)$
827	w	Q $\nu_{26}(b_1)$
835	m	$\nu_{37}(b_2)$
838	vw	$\nu_{37}(b_2)$
881	m	P $\nu_7(a_1)$
891	s	Q $\nu_7(a_1)$
895	s	$\nu_7(a_1)+\nu_i-\nu_i$
902	m	R $\nu_7(a_1)$
946	vw	$\nu_{39}(b_2)$
953	w	$\nu_{39}(b_2)$
1031	vs	$\nu_8(a_1)+\nu_i-\nu_i$
1037	vs	Q $\nu_8(a_1)$
1042	vs	$\nu_8(a_1)+\nu_i-\nu_i$
1048	vs	R $\nu_8(a_1)$
1084	w	Q $\nu_{28}(b_1)$
1092	vw	R $\nu_{28}(b_1)$
1158	m	P $\nu_{27}(b_1)$
1163	s	Q $\nu_{27}(b_1)$
1172	m	R $\nu_{27}(b_1)$
1205	s	$396(a_2)+791(b_1)=1187(B_2)$; $566(b_2)+656(a_1)=1222(B_2)$
1230	?	
1236	m	$566(b_2)+669(a_2)=1235(B_1)$
1244	s	$\nu_{24}(b_1)$
1261	m	$566(b_2)+701(a_1)=1267(B_2)$
1275	m	$2\times279(b_1)+721(a_1)=1279(A_1)$
1290	m	$279(b_1)+1011(a_1)=1290(B_1)$; $566(b_2)+721(a_1)=1287(B_2)$
1301	m	P $2\times656(a_1)=1312(A_1)$
1310	m	Q $2\times656(a_1)=1312(A_1)$
1402	w	$\nu_6(a_1)$; $\nu_{36}(b_2)$
1416	w	$\nu_4(a_1)$
1459	m	$\nu_{25}(b_1)$
1471	m	$\nu_5(a_1)$; $\nu_{35}(b_2)$
1477	m	$396(a_1)+1084(b_1)=1480(B_1)$
1486	m	$656(a_1)+827(b_1)=1483(B_1)$; $656(a_1)+830(b_2)=1486(B_2)$
1560	w	$396(a_1)+1163(b_1)=1559(B_1)$; $396(a_2)+1163(b_1)=1559(B_2)$
1638	w	DMADB impurity
1775	s	Q $2\times891(a_1)=1782(A_1)$
1790	s	R $2\times891(a_1)=1782(A_1)$; $701(a_1)+1084(b_1)=1785(B_1)$
1829	s	$\nu_3(a_1)$[a]
1926	vs	$\nu_{23}(b_1)$; $\nu_{34}(b_2)$
2069	vw	$2\times1037(a_1)=2074(A_1)$
2119	vw	$701(a_1)+1042(a_1)=2103(A_1)$; $1037(a_1)+1084(b_1)=2121(B_1)$
2193	vw	$2\times656(a_1)+891(a_1)=2203(A_1)$
2243	vw	$791(b_1)+1459(b_1)=2250(A_1)$
2504	s	DMADB impurity
2512	s	DMADB impurity
2522	s	DMADB impurity
2645	vw	$721(a_1)+1926(b_1)=2647(B_1)$; $721(a_1)+1926(b_2)=2647(B_2)$
2753	vw	$830(b_2)+1926(b_2)=2756(A_1)$
2818	m	Q $\nu_2(a_1)$
2828	m	R $\nu_2(a_1)$
2869	s	$\nu_{33}(b_2)$
2881	s	$\nu_{33}(b_2)$
2946	vs	$2\times1471(a_1)=2942(A_1)$; $2\times1471(b_2)=2942(A_1)$; $1471(a_1)+1471(b_2)=2942(B_2)$
2961	vs	$\nu_{32}(b_2)$
2979	vs	P $\nu_1(a_1)$
2987	vs	Q $\nu_1(a_1)$
3020	s	P $\nu_{22}(b_1)$
3028	s	Q $\nu_{22}(b_1)$
3038	s	R $\nu_{22}(b_1)$
3193	w	$2\times891(a_1)+1416(a_1)=3198(A_1)$; $214(b_2)+2987(a_1)=3201(B_2)$
3241	?	$2\times891(a_1)+1459(b_1)=3241(B_1)$
3253	?	$2\times891(a_1)+1471(a_1)=3253(A_1)$
3334	vw	$1402(b_2)+1926(b_2)=3328(A_1)$
3412	vw	$2\times214(b_2)+2987(a_1)=3415(A_1)$
3985	vw	$1024(b_2)+2961(b_2)=3985(A_2)$
4015	vw	$1054(a_2)+2961(b_2)=4015(B_1)$
4059	vw	$1037(a_1)+3028(b_1)=4065(B_1)$
4146	vw	$1163(b_1)+2987(a_1)=4150(B_1)$
4218	vw	$1402(a_1)+2818(a_1)=4220(A_1)$
4248	vw	$1244(b_1)+3017(a_2)=4261(B_2)$; $566(b_2)+701(a_1)+2987(a_1)=4254(B_2)$
4386	w	$1402(a_1)+2987(a_1)=4389(A_1)$
4421	m	$1471(b_2)+2961(b_2)=4432(A_1)$; $1402(a_1)+3028(b_1)=4430(B_1)$
4472	w	$1451(a_2)+3017(a_2)=4468(A_1)$
5210	?	$791(b_1)+1459(b_1)+2961(b_2)=5211(B_2)$
5315	?	$891(a_1)+1471(b_2)+2961(b_2)=5323(A_1)$
5706	vw	$2818(a_1)+2876(b_2)=5694(B_2)$
5794	?	$2818(a_1)+2987(a_1)=5805(A_1)$
5881	vw	$2876(b_2)+3017(a_2)=5893(B_1)$
5950	vw	$2961(b_2)+2987(a_1)=5948(B_2)$

[a] The fundamental $\nu_3(a_1)$ may interact slightly with the overtone $2\times891(a_1)=1782(A_1)$.

This leaves 14 fundamentals, of which three are methyl rockings, and six are directly involved with hydrogen and would be expected to undergo large isotopic shifts. Finally, six of the 14 should give rise to polarized Raman lines.

In the light of these considerations it is appropriate to consider the utility of the more usual tools for correct assignment. Surprisingly close correlations are possible between the frequencies of DMADB and those of its nearest relatives, *viz.*, diborane,[5] *N*-dimethylaminoborine, $(CH_3)_2NBH_2$[6], dimethylamine,[7,8] and dimethylammonium ion.[8] Analogies with previously studied boron hydrides suggest that several fundamentals will be exceedingly intense and may swamp their weaker neighbors. That there are 14 bands expected in the region 600–1300 cm^{-1} suggests the possibility of considerable overlapping. This, together with the low symmetry and relatively small rotational constants of DMADB (see Table V), indicates that the value of band contours as assignment criteria is less than might otherwise be the case. For related reasons the utility

TABLE IV. Raman spectrum of DMADB$-d_5$ (liquid).

Wave number (cm^{-1})	Intensity; depolarization factor	Interpretation
−701[a]	vw, ?	
−226	vw, ?	
+214	vw, ?	$\nu_{42}(b_2)$
299	vw, ?	$\nu_{30}(b_1)$
396	w, 0.8	$\nu_{13}(a_1)$; $\nu_{19}(a_2)$; $\nu_{41}(b_2)$
477	?, ?	$214(b_2)+279(b_1)=493(A_2)$
566	w, 0.8	$\nu_{40}(b_2)$; $2\times279(b_1)=558(A_1)$
669	w, 0.8	$\nu_{10}(a_1)$; $\nu_{18}(a_2)$
721	vs, 0.3	$\nu_{11}(a_1)$
790	w, 0.8	$\nu_{29}(b_1)$
843	w, 0.8	$\nu_{26}(b_1)$; $\nu_{37}(b_2)$
923	w, 0.3	$\nu_7(a_1)$; $\nu_{39}(b_2)$
1054	w, 0.8	$\nu_8(a_1)$; $\nu_{17}(a_2)$; $\nu_{28}(b_1)$; $\nu_{38}(b_2)$
1209	?, ?	$\nu_{24}(b_1)$; $\nu_{27}(b_1)$
1297	?, ?	$2\times656(a_1)=1312(A_1)$
1410	w, 0.4	$\nu_4(a_1)$; $\nu_6(a_1)$; $\nu_{36}(b_2)$; $2\times721(a_1)=1442(A_1)$
1477	w, 0.8	$\nu_5(a_1)$; $\nu_{16}(a_2)$; $\nu_{25}(b_1)$; $\nu_{35}(b_2)$
1645	?, ?	$2\times287(b_1)=1654(A_1)$; $2\times830(b_2)=1660(A_1)$
1787	w, 0.3	$2\times891(a_1)=1782(A_1)$[b]
1847	s, 0.2	$\nu_3(a_1)$[b]
1936	m, 0.9	$\nu_{22}(b_1)$; $\nu_{34}(b_2)$; $\nu_{18}(a_2)$
2813	vw, 0.9	$\nu_2(a_1)$
2886	w, ?	$\nu_{33}(b_2)$
2975	m, 0.3	$\nu_1(a_1)$; $\nu_{32}(b_2)$
3017	w, ?	$\nu_{14}(a_2)$; $\nu_{22}(b_1)$

[a] See footnote a to Table II.
[b] See footnote a to Table III.

[5] R. C. Lord and E. Nielsen, J. Chem. Phys. **19**, 1 (1951).
[6] Price, Fraser, Robinson, and Longuet-Higgins, Discussions Faraday Soc., No. 9, 131 (1950).
[7] The infrared spectrum of dimethylamine was obtained and studied in this laboratory and will be published at a later date.
[8] K. W. F. Kohlrausch, *Ramanspektren* (J. W. Edwards, Ann Arbor, Michigan, 1945), pp. 215–225.

TABLE V. Approximate calculated rotational constants and branch separations for DMADB and DMADB$-d_5$.

	DMADB (in cm^{-1})	DMADB$-d_5$ (in cm^{-1})
$A(z)$	0.192	0.166
$B(y)$	0.168	0.142
$C(x)$	0.137	0.124
type A band: P–R	ca 21	ca 20
type B band: Q–Q	ca 3–4	ca 3
P–Q, Q–R	ca 11	ca 10
type C band: P–R	ca 26	ca 24

of the product rule is partially nullified since, even if the assignment were essentially correct, overlapping would prevent the determination of some band centers with accuracy. Nevertheless, the relatively small number of frequencies of each species that undergo an isotopic shift means that the product rule may be useful as a criterion for a correct assignment.

Depolarization data are no less suspect than band contours in such a rich spectrum. In the first place, some lines may be too weak to be observed or, if barely seen, still too feeble to yield even qualitatively reliable polarization data. Secondly, several lines may be overlapped or superimposed, and the measured ratios may be composite factors. Thirdly, certain totally symmetric vibrations may give rise to lines which are only slightly polarized and so may be difficult to distinguish from their less favored neighbors. In spite of these doleful contingencies the polarization data proved to be of some assistance in the attempt to unravel the spectrum.

VIBRATIONAL ASSIGNMENT

The analysis will begin with a discussion of the C–H stretching frequencies. The appearance and location of these bands in the LiF traces for the light compound are almost precisely duplicated in those for the heavy so it is sufficient to confine their mention to the former. Six C–H frequencies are to be expected. All of them may appear in the Raman spectrum. Two of these should be polarized and should have type A envelopes in the infrared. In addition, one type C and two type B bands are also to be expected in the LiF region. The Raman data indicate three polarized lines in the C–H region. The infrared spectra suggest that the 2990 cm^{-1} and 2817 cm^{-1} bands be assigned to ν_1 and ν_2, respectively. The polarized character of the line at 2863 cm^{-1} is probably due to the superposition of A_1 combination bands which arise from the methyl-group deformation frequencies. The band at 3029 cm^{-1} is easily assigned as the type C fundamental ν_{22}. The appearance of the 2990 cm^{-1} band indicates overlapping so the shoulder at 2964 cm^{-1} is ascribed to ν_{32}. The appearance of the band at 2876 cm^{-1} suggests a type B fundamental so it is assigned to ν_{33}. The assignment of the 3017 cm^{-1} Raman line to ν_{14} as well as to ν_{22} is somewhat arbitrary.

Next the methyl-group deformation frequencies are considered. Here also the spectra of the heavy compound parallel those for ordinary DMADB. There are six such frequencies and by species and band type they are apportioned just like the C–H stretchings. In the infrared they obviously correspond to the bands at 1390, 1451, and 1471 cm^{-1}. There are only two Raman lines in this region, both weak and both depolarized. It is evident that the polarized line at 1471 cm^{-1} has been fairly swamped and that expected at 1393 cm^{-1} is too weak to be seen at all. The assignment of 1471 cm^{-1} to ν_5 and ν_{35}, 1451 cm^{-1} to ν_{16} and ν_{25}, 1393 cm^{-1} to ν_6, and 1390 cm^{-1} to ν_{36} is quite straightforward and need not be gone into in detail. Except that attention should be drawn to the frequencies of the methyl-group parallel deformation vibrations, ν_6 and ν_{36}. Inspection of the spectra in Figs. 2 and 4 leaves no room for doubting that the assignment given in Table VI for ν_6 and ν_{36} is correct. It is surprising, however, that the frequency for the heavy compound is about 10 cm^{-1} higher than that for the light molecule. This effect, which appears to be real, remains unexplained.

So far 12 fundamental vibrations have been dispatched, none having any special bearing on the main problem at hand. It is through the B–H stretchings that contact is first made with the interesting aspects of the spectra of DMADB. There are four end-group stretchings, one in each species, and two bridge-hydrogen stretchings, one in a_1 and one in b_1. There can be no question about the assignment of the 2476 cm^{-1} band to ν_3 since it is very strong and highly polarized in the Raman spectrum. The band at 2547–57 cm^{-1} is assigned to ν_{23} and ν_{34}. A study of its envelope suggests that a type B and a type C band may be overlapped.

The assignment of the BH and BD stretchings in a_2 is more difficult. For the light compound a depolarized Raman line in the 2400–2600 cm^{-1} region is to be expected, while for the heavy molecule a corresponding line in the range 1800–2000 cm^{-1} may be sought. For this species there should, of course, be no real coincidence of Raman lines with infrared bands. The Raman spectra give no evidence of lines in this region other than those already assigned to ν_3 and the pair ν_{23}, ν_{34}. It may therefore be supposed that the line due to ν_{15} is blended with one of those ascribed to the other end-group stretchings. The product rule may be used to advantage here in conjunction with an otherwise not very convincing analogy with the related diborane frequencies to suggest that ν_{15} for DMADB is probably overlapped by the Raman line at 2475 cm^{-1}, while for DMADB$-d_5$ it is part of the 1936 cm^{-1} line.

In ordinary diborane the bridge-hydrogen stretchings range from 1602 cm^{-1} (b_{3u}) to 2104 cm^{-1} (a_{1g})[5]. Evidently the very strong band at 1636 cm^{-1} in the infrared spectrum of DMADB corresponds quite closely to the former and must perforce be assigned to ν_{24}. Again by analogy with diborane the $\nu_4(a_1)$ fundamental is expected to be weaker in the infrared, stronger in the Raman, and to occur 200–300 cm^{-1} higher than ν_{24}.

TABLE VI. Fundamental frequencies of DMADB and DMADB$-d_5$.

Species (C_{2v})	Number; approximate description[a]	DMADB (cm^{-1})	DMADB$-d_5$ (cm^{-1})	B_2H_6[b] (cm^{-1})	B_2D_6 (cm^{-1})	Product rule obs./theor.
a_1	1 ν–CH	2990	2987			0.260/0.259
IR: type *A*	2 ν–CH	2817	2818			
R: *p*	3 ν–BH	2476	1825*,[c]	(1)2524	1860	
	4 ν–BH′	1885*	1416	(2, 13)2104, 1915	1511, 1465	
	5 δ–$CH_3(\perp)$	1471	1471			
	6 δ–$CH_3(\parallel)$	1393	1402			
	7 δ–BH_2	1198	891	(3)1180	929	
	8 ν–BN	1069	1037	(2, 13)		
	9 ρ–CH_3	1011	(1011)			
	10 β–BH_2	945	656	(14) 973	728	
	11 ν–BB	772	721	(4) 794	726	
	12 ν–CN	697	701			
	13 δ–NMe_2	399	396			
a_2	14 ν–CH	3017	3017			0.386/0.380
IR: inactive	15 ν–BH	2475	1936	(11)2591	1980	
R: *dp*	16 δ–CH_3	1451	(1451)			
	17 ρ–CH_3	1046	1054			
	18 ρ–BH_2	896	669	(12) 920	740	
	19 τ–BH_2	599	396	(5) 829	592	
	20 τ–NMe_2	236	(236)			
	21 *T*					
b_1	22 ν–CH	3029	3028			0.285/0.282
IR: type *C*	23 ν–BH	2547	1926	(16)2525	1845	
R: *dp*	24 ν–BH′	1635	1244	(6, 17)1768, 1602	1273, 1205	
	25 δ–CH_3	1458	1459			
	26 δ–BH_2	1220	827	(18)1177	0.881	
	27 ν–BH	1184	1163	(6, 17)		
	28 ρ–CH_3	(1084)	1084			
	29 β–BH_2	1063	791	(7)1035	870	
	30 β–NMe_2	279	(279)			
	31 *T*					
b_2	32 ν–CH	2964	2961			0.282/0.272
IR: type *B*	33 ν–CH	2876	2876			
R: *dp*	34 ν–BH	2552	1926	(8)2612	1999	
	35 δ–$CH_3(\perp)$	1471	1471			
	36 δ–$CH_3(\parallel)$	1390	1402			
	37 ρ–BH_2	1075	830	(9) 950	705	
	38 ρ–CH_3	1024	(1024)			
	39 ν–CN	950	950			
	40 τ–BH_2	770	566	(15)1012	730	
	41 ρ–NMe_2	399	396			
	42 δ–H′	325	214	(10) 368	262	

[a] The classification of the vibrations is essentially that given by J. W. Linnett, J. Chem. Phys. 6, 692 (1938). Here ν denotes a stretching mode; δ and ρ refer to deformation and rocking, respectively, β means an out-of-plane wag or bend; τ implies a twisting or torsional vibration, and *T* refers to hindered internal rotation. See reference 10 for pictures of the diborane normal vibrations.

[b] The data for B_2H_6 and B_2D_6 are taken from reference 5. The enumeration of the diborane vibrations follows reference 5 and is given by the numbers in parentheses.

[c] Frequencies in parentheses have been estimated. Those marked with an asterisk are presumed to be involved in Fermi resonance and are therefore shifted in the observed spectrum (See Tables I, II, III, IV, and text).

The Raman spectrum displays a pair of polarized, moderately intense lines at 1857 cm^{-1} and 1900 cm^{-1}. Since there can be at most only one polarized fundamental in this region‖ Fermi resonance with the overtone of the strong band at 945 cm^{-1} is at once suggested. Again by analogy with the data for B_2H_6 and B_2D_6 the strong, though ill-defined, band at 1244 cm^{-1} is assigned to the corresponding B—D stretching, ν_{24}, and the weaker one at 1301 cm^{-1} to ν_4.

Now only the so-called intermediate and low frequencies remain to be assigned. As has already been remarked several of these should be more or less independent of deuterium substitution. The methyl rocking vibrations are expected with only moderate intensity in the region 1000–1100 cm^{-1} in both light and heavy DMADB. Unfortunately this region also contains one of the most intense bands in the entire spectrum (1063 cm^{-1} in DMADB, 1037 cm^{-1} in DMADB

‖ In this connection it may, perhaps, be worthwhile to remark that if the dimethylamino group were not in the bridge but attached to one end of the molecule then *four* bridge-hydrogen stretching frequencies would be expected, just as in diborane itself. The very striking correspondence of the two which are actually observed in the spectrum of DMADB with ν_{13} (1915 cm^{-1}, b_{2u}) and ν_{17} (1602 cm^{-1}, b_{2u}) of diborane is equivocal evidence. On the one hand its suggests that it is rather unlikely that there are two additional fundamentals in this region but that they have escaped detection, and so can be said to support the C_{2v} model. On the other hand this same close correspondence can be used to argue that the bridge in DMADB must be very similar structurally to that in diborane and that a low- or no-symmetry model is correct. In support of a low-symmetry model it must further be remarked that the bands at 1708 cm^{-1} and 1535 cm^{-1} in the spectrum of DMADB could be nicely interpreted as bridge-hydrogen stretching fundamentals. Moreover, the very strong absorption around 1200 cm^{-1} in the spectrum of the heavy compound could also be partially explained on this basis.

$-d_5$) so that it is not surprising that only one or two of the rockings should appear in the clear. It is interesting to note that these extremely strong infrared bands appear but feebly in the Raman spectra where their intensities are on a par with those of the methyl rockings. Finally, the marked resemblance between the band at 1011 cm^{-1} in the spectrum of the light compound and that at 1084 cm^{-1} in the heavy suggests similar origins. These considerations lead with safety to the assignment given in Table VI for ν_9, ν_{17}, ν_{28}, and ν_{38}.

Apart from the low-frequency dimethylamino group vibrations only three types of motions which should not be markedly dependent on deuterium substitution remain to be considered. These are the B—N, C—N, and B—B stretchings. According to Lord and Nielsen the last-named vibration gives rise, in light and heavy diborane,[5] to extremely strong, highly polarized Raman lines at 794 cm^{-1} and 726 cm^{-1}, respectively. The Raman spectra of DMADB and DMADB—d_5 reveal similarly strong, polarized lines at 772 cm^{-1} and 721 cm^{-1}, respectively. There can be no doubt whatever that these must be assigned to ν_{11}. It is perhaps significant that the frequency of the B—B stretching vibration is very little shifted from that of its counterpart in ordinary diborane. It is also noteworthy that the corresponding infrared bands are remarkably weak. The 770 cm^{-1} band in the infrared spectrum of DMADB appears to have a definite type B contour which cannot readily be reconciled with its assignment to ν_{11}. Its shape could perhaps be explained on the basis of the overlapped type *A* bands which arise from the $B^{11}—B^{11}$ and $B^{11}—B^{10}$ isotopic species. It seems preferable to assign the observed 770 cm^{-1} infrared band to ν_{40}, a type *B* vibration.

The assignment of 1063 cm^{-1} and 1037 cm^{-1} to the symmetric B—N stretching in the light and heavy compounds respectively, and of 1184 cm^{-1} and 1163 cm^{-1} to the corresponding anti-symmetric motions is also quite direct. In this connection the most closely related molecule for which adequate data are available is *N*-dimethylaminoborine.[6] Its infrared spectrum in the region below 1600 cm^{-1} exhibits three extremely intense bands: 1193.5–1209.6 cm^{-1}, 1148–56 cm^{-1}, and 961–966.5 cm^{-1}. The 964 cm^{-1} band is certainly too low for a B—N stretching. It is not possible, in the absence of additional information, to choose between the two remaining. It is evident, however, that one must correspond to the BH_2 deformation, the other to the B—N stretching. As Price *et al.*[6] have suggested, the unusually high intensity of the B—N band is not surprising in view of the probable distribution of charge among the nitrogen and boron atoms. By comparison the C—N stretchings may be expected to give rise to weaker bands. The striking resemblance between the 1063 cm^{-1} and 1037 cm^{-1} bands, and also between the 1184 cm^{-1} and 1163 cm^{-1} bands, suggests at once that these vibrations are only slightly affected by deuterium substitution. The parallelism in frequency, intensity, envelope, and isotopic shift provides strong evidence in favor of the present assignment.

The problem of the C—N vibrations is a much more perplexing one. These frequencies should show little, if any, dependence on deuterium substitution. On the basis of the data given by Kohlrausch for dimethylamine and dimethylammonium ion[8] the symmetric C—N stretching is to be expected in the neighborhood of 900 cm^{-1}, the antisymmetric stretch around 1000–1050 cm^{-1}. For both the amine and the ion the symmetric vibration appears as a polarized Raman line of moderate intensity whereas the antisymmetric vibration shows up only very feebly. Although there is a moderately strong band in the infrared spectrum of dimethylamine that is very close to the Raman frequency (931 cm^{-1}) for the symmetric mode, the only band within 40 cm^{-1} of the antisymmetric frequency (1078 cm^{-1}) is a very weak one at 1085 cm^{-1}. There is, to be sure, a very strong band at 1022 cm^{-1} and an extremely intense one at 1157 cm^{-1}. But there appear to be no corresponding Raman lines unless those at 1078 cm^{-1} (0) and 1236 cm^{-1} (00) can be said to correspond. In any case it may be concluded that the antisymmetric frequency appears in the Raman spectrum weakly, if at all. As to its appearance in the infrared spectrum nothing definite can be said at this time.

There is still another point about the Raman spectra of the methylamines that deserves mention in this connection. If only the polarized, moderately intense Raman lines which may be safely ascribed to the symmetric stretching mode are considered, then in passing from dimethyl- to tetramethylammonium ion this frequency drops from 895 cm^{-1} to 752 cm^{-1}. It is suggested that the C—N vibrations in DMADB occur at lower frequencies than might have been supposed. The infrared spectrum of N-dimethylaminoborine is not very revealing in this regard except that there do not appear to be any bands above 964 cm^{-1} which may be ascribed to either of the C—N stretching vibrations. In fact it appears more probable that these are to be associated with absorption in the region 750–900 cm^{-1}.

The spectra of DMADB and DMADB—d_5 lend some support to this thesis though it is indeed scant. The slightly polarized Raman line at 702 cm^{-1} in the spectrum of the light compound is ascribed to $\nu_{12}(a_1)$. Its counterpart in the spectrum of the heavy compound is evidently swamped by the exceedingly intense line at 721 cm^{-1} or else belongs to the line at 669 cm^{-1}. The corresponding bands in the infrared spectra of the two compounds do resemble each other rather closely and appear not to have been shifted by deuterium substitution. In a like manner the frequency 950 cm^{-1} is ascribed to ν_{39}, though in the case of the light compound it is much overshadowed by the 945 cm^{-1} band. If in the spectrum of DMADB—d_5 the band at 950 cm^{-1} is not due entirely to the 945 cm^{-1} band of the light compound then it may be assigned to ν_{39}. While there can be no doubt about the assignments for the B—B and

B—N vibrations, those for the C—N modes must be regarded as somewhat suspect.

Next, the deformation, rocking, bending or wagging, and twisting motions of the BH_2 and BD_2 groups are considered.¶ Lord and Nielsen place the deformation vibrations of the BH_2 groups in diborane at about 1180 cm^{-1}.[5] As has been remarked previously this mode corresponds either to the 1152 cm^{-1} or the 1202 cm^{-1} band in the infrared spectrum of *N*-dimethylaminoborine,[6] probably the latter. These considerations restrict the choice for the b_1 mode in DMADB to the bands at 1063 cm^{-1}, the group around 1200 cm^{-1}, and the 1278 cm^{-1} band. The first may, apart from other reasons already alluded to, be rejected as too low. The 1184 cm^{-1} band quite obviously has its image at 1163 cm^{-1} in the spectrum of the heavy compound, and so can be eliminated. The band at 1278 cm^{-1} has not been chosen as ν_{26} because it is considerably higher than analogy with diborane would suggest. Moreover, it may be readily explained as a sum band. The bands around 1200 cm^{-1} provide the most reasonable choices for ν_{26}, and ν_7 as well. The more specific assignment of 1220 to the former and 1198 cm^{-1} to the latter is, however, largely arbitrary. For the heavy compound the choice is again limited by the paucity of bands in a suitable region. Lord and Nielsen place the symmetric mode at 929 cm^{-1} and the antisymmetric vibration at 881 cm^{-1}. The present assignment of 891 cm^{-1} to ν_7 and 827 cm^{-1} to ν_{26} parallels their choice closely. It will be noticed that between 791 cm^{-1}, which is too low, and 1037 cm^{-1}, which is too high, there are no other possibilities than those given. Moreover, the contour of the 891 cm^{-1} band appears to have the required type *A* character whereas that at 791 cm^{-1} seems to be of type *C*. Finally, the low depolarization factor of the 923 cm^{-1} line in the Raman spectrum of the heavy compound must derive largely from the 891 cm^{-1} vibration.

The bending or wagging modes are also expected to give rise to rather intense infrared bands, though at somewhat lower frequencies than the deformations. For diborane they are placed at 1036 cm^{-1} and 973 cm^{-1} by Lord and Nielsen.[5] For *N*-dimethylaminoborine the obvious choice is the strong band at 964 cm^{-1}.[6] These considerations, when applied to the spectrum of DMADB, emphasize an important point. There are simply not enough strong bands in this region to go around! Hence several are required to do double or triple duty. For example, there are no bands of even medium intensity below the one at 945 cm^{-1}. And between it and 1278 cm^{-1} there is only the group at 1200 cm^{-1} and the extremely strong one at 1063 cm^{-1}. For these reasons the assignment of 945 cm^{-1} to ν_{10} and 1063 cm^{-1} to ν_{29} seems unavoidable for DMADB, and respectively 656 cm^{-1} and 791 cm^{-1} for the heavy molecule. Here it should be noticed that the contour of the strong 945 cm^{-1} band in the light spectrum closely resembles that of the 891 cm^{-1} band in the spectrum of DMADB—d_5.

The rocking and twisting frequencies very probably show up only weakly in the infrared spectra, if at all. In any event it would be inconsiderate to place still another burden on the so-called strong bands. In ethylene the rocking frequencies are known to occur at 1236 cm^{-1} (b_{1g}) and at 810 cm^{-1} (b_{2u}).[9] In ordinary diborane they are placed at 920 cm^{-1} (b_{2g}) and 950 cm^{-1} (b_{1u}). For DMADB only the b_2 (type B) rocking may appear in the infrared spectrum. If it is in fact strong enough to appear at all it may presumably be expected between the rather wide limits 800–1200 cm^{-1}. In the spectrum of the heavy compound the band at 830 cm^{-1} has, to some extent, the appearance of a type *B* band overlaid, perhaps, by either a type *A* or a type *C* band. If ν_{37} is placed at 830 cm^{-1} then a reasonable choice for this fundamental in DMADB may be 1075 cm^{-1}. A correspondingly reasonable pair for ν_{18} is 896 cm^{-1} and 669 cm^{-1}. This assignment of the rocking vibrations, as well as that below for the twisting modes, is somewhat doubtful. They may be partially justified *a posteriori* by the agreement between the observed and theoretical product-rule ratios, and also by their occurrence in combination bands.

The type *B* twisting fundamental ν_{40} is placed at 770 cm^{-1} for DMADB. This is in accord with the apparent character of the infrared band at this frequency. Analogy with similar isotopic shifts in related molecules places ν_{40} for the heavy compound at 566 cm^{-1}. The corresponding frequencies for ν_{19} are 599 cm^{-1} and 396 cm^{-1}. It must be admitted that the a_2 twisting frequency is unconventionally low. It should be remembered, however, that the twisting modes are probably more affected by the presence of the nitrogen atom in the bridge than are any of the other angular motions. Further, it is difficult to explain the Raman line at 599 cm^{-1}, which is of medium intensity, as other than a fundamental. It is undoubtedly too high for the gross motions of the dimethylamino group, and it is probably too low for most of the other fundamental vibrations of the DMADB molecule.

There still remain seven fundamentals to be assigned. Four of these are the angular motions of the dimethylamino group considered as a three particle system. Two are methyl-group hindered rotations, and the last is essentially a ring-bending motion. Only the last may be expected to show a marked deuterium shift and is analogous to $\nu_{10}(b_{1u})$ of diborane,[10] shifting from 368 cm^{-1} in the light to 262 cm^{-1} in the heavy molecule. The only one of the so-called angular motions which has an analogue in dimethylamine itself is the deforma-

¶ The classification of these motions is that given by J. W. Linnett, J. Chem. Phys. **6**, 692 (1938).

[9] R. L. Arnett and B. L. Crawford, Jr., J. Chem. Phys. **18**, 118 (1950).

[10] For pictures of the normal modes of vibration of diborane see R. P. Bell and H. C. Longuet-Higgins, Proc. Roy. Soc. (London), **A183**, 357 (1945).

tion mode. Kohlrausch's Raman data place this frequency at 390 cm^{-1} for dimethylamine and 412 cm^{-1} for the corresponding ammonium ion. Of the lines below about 500 cm^{-1} in the Raman spectra of *both* DMADB and its deuteriated relative the strongest is that at about 400 cm^{-1}. This then is the obvious choice for ν_{13}. The assignments for the remaining vibrations are dictated largely by the abundance of low-frequency lines available for this purpose. It must be emphasized at this point that all of these lines also appear as anti-Stokes shifts in the spectrum of DMADB. Their assignment as overtones, combination or difference tones does not seem plausible.

The ring frequency, ν_{42}, is placed at 325 cm^{-1} in the light molecule and at 214 cm^{-1} in heavy DMADB by analogy with its diborane counterparts. Again, the close correspondence of many of the DMADB frequencies with their diborane counterparts deserves special emphasis. The remaining frequencies are assigned in accord with a more or less conventional sequence. This completes the assignment (Table VI).

CONCLUSIONS

The most striking, and perhaps the most significant, feature of the spectra of DMADB is the close resemblance in frequency and relative intensity of certain bands with their counterparts in the diborane data. There can be no question whatever of the correspondence of the B—B and bridge-hydrogen stretchings in the two molecules. In view of the bond distances and assumed structure of DMADB[3] the almost exact duplication of the diborane B—B frequency is hard to understand. A less symmetrical structure in which the nitrogen atom is not in the bridge but attached as part of an end-group would seem to be indicated.[11]

While a serious attempt to interpret the observed vibrational spectra of DMADB on the basis of a model of lower symmetry has not been made, it would certainly be feasible and would in fact have some attractive features. Not only would the previously mentioned frequency correspondence be more readily understood but it would be necessary to assign only *one* set of BH_2 angular motions, only one B—N stretching, and so on. On this basis the limited number of strong infrared bands and their similarity to those of *N*-dimethylaminoborine (and diborane) would be more easily explicable.

On the other hand many of the features of the spectra which appear to support the C_{2v} model have already been mentioned in connection with the assignment. It must be emphasized that the suggestion that the relatively small number of polarized Raman lines indicates a symmetrical structure does not really constitute a convincing argument. For a configuration of sufficiently low symmetry the distinction between certain polarized and depolarized lines is, even qualitatively, hazardous. In fact if the model has only C_1 symmetry any such argument would be essentially meaningless.

In order to avoid imputing significance to our data out of proportion with our ability to interpret them correctly it must be said that they appear neither to prove nor to disprove with conviction the C_{2v} configuration. We are content to suggest that the data do contain interesting implications in regard to the valence structure and bonding of DMADB but that it would be rash, or at least premature, to attempt at this time to detail them.

ACKNOWLEDGMENTS

The author is indebted to Professor A. B. Burg for the samples of DMADB and DMADB—d_5, and to Professor Bryce L. Crawford, Jr., for suggesting this project and for helpful advice and encouragement. To the fellowship committees of E. I. Du Pont de Nemours and Company and the Bell Telephone Research Laboratories and to the U. S. Office of Naval Research we wish to express our appreciation of the financial support which made this study possible.

[11] Compare, for example, with the structure of bromodiborane as determined from its microwave spectrum: C. D. Cornwell, J. Chem. Phys. 18, 1118 (1950).

Pressure Broadening of Linear Molecules. I*

HAROLD FEENY, HENRY LACKNER, PAUL MOSER, AND WILLIAM V. SMITH
Department of Physics, University of Delaware, Newark, Delaware

(Received September 8, 1953)

A microwave spectroscope, especially designed for studies of the temperature dependence of microwave line widths is described. With this spectroscope, the line width of the $J=1-2$ OCS line has been measured over a temperature range from 195°K to 476°K. Over this range, the line width varies as $T^{-0.9}$. An interpretation in terms of intermolecular forces is deferred, pending work with other linear molecules and other transitions.

INTRODUCTION

THIS work is a continuation of microwave pressure broadening investigations initiated at Duke.[1-3] The original work was primarily a survey of the pressure broadening of ammonia in mixtures of different types of molecules. Partly as a result of this survey it seemed desirable to do more precise work on simpler classes of molecules. The present paper is the first of a series dealing with the pressure broadening of linear molecules. An improved microwave spectroscope, designed particularly for measuring the temperature dependence of line widths is described, along with the measured temperature dependence of the $J=1-2$ OCS line width parameter.

SPECTROSCOPE DESIGN

The block diagram of the microwave spectroscope is shown in Fig. 1. The absorption cell A (Fig. 2) is a thirty-nine foot length of coin silver K-band wave guide coiled in a helix of 15 inch diameter. For temperature control the cell is placed in an electric oven which can be maintained at temperatures up to 300°C or, by filling the oven with dry ice, can be brought to −78°C. The K band klystron B is a battery operated low voltage $2K50$. It is frequency modulated by a low-amplitude sine wave (usually 90 kc, block C) applied to the reflector electrode. The microwave energy is detected by a silicon crystal D. The rf component of the crystal output is amplified and detected by a National HRO "Sixty" radio receiver E tuned to the modulation frequency. Superimposed on the high-frequency modulation is a low-frequency (about 30 cps) saw tooth voltage F of sufficient amplitude to sweep a frequency range of several line widths. With this type of detection system, the audio-frequency component of the detected rf signal is the magnitude of the first derivative of the line shape.[4a] To minimize distortion, the audio amplifier of the receiver is replaced by a battery operated Ballantine decade amplifier (model 220-A) G with a flat output over the range of 20 cps to 100 kc. The output of the audio amplifier is applied to the vertical plates of a DuMont type 304-A oscilloscope H.

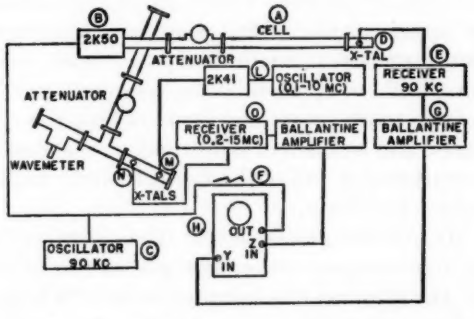

FIG. 1. Block diagram of spectrograph.

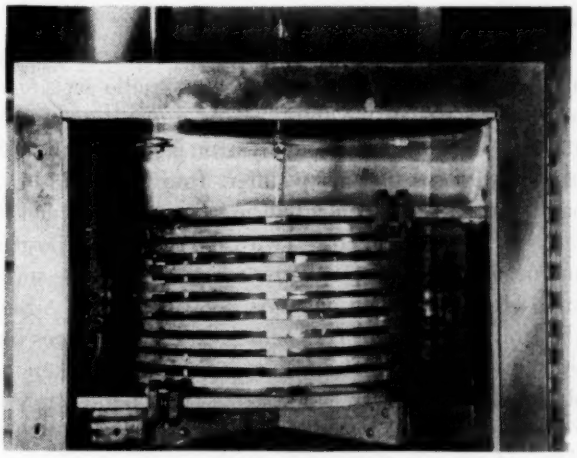

FIG. 2. Absorption cell.

A typical absorption line, with OCS in the cell at 28°C and under a pressure of 78 microns of mercury, is shown in Fig. 3(a). This direct reproduction of the line results from omitting the 90-kc modulation and detection stages in the spectroscope. The magnitude of the derivative of the line, obtained by including these stages, is shown in Fig. 3(b). Frequency markers are superimposed on the half-power points of Fig. 3(a) and the maxima of Fig. 3(b), which are separated by $1/\sqrt{3}$ times the line width $2\Delta\nu$.[4d] These markers are generated

* Supported by the U. S. Air Force Office of Scientific Research.

[1] R. R. Howard and W. V. Smith, (a) Phys. Rev. **77**, 840 (1950); (b) **79**, 128 (1950).
[2] W. V. Smith and R. R. Howard, Phys. Rev. **79**, 132 (1950).
[3] R. M. Hill and W. V. Smith, Phys. Rev. **82**, 451 (1951).

[4] Gordy, Smith, and Trambarulo, *Microwave Spectroscopy* (John Wiley and Sons, Inc., New York, 1953), (a) pp. 7–8; (b) pp. 76–79; (c) pp. 35–36; (d) pp. 73–74.

FIG. 3(a). Absorption line.

by mixing the 8th harmonic of a battery operated *S*-band klystron *L* with a fraction of the output of the *K*-band klystron by crystal *N*. This harmonic is produced by crystal *M*.

The rf output of crystal *N* is amplified and detected by a radio receiver *O*, again with its audio section replaced by a Ballantine amplifier. An audio signal results at those parts of the *K* band klystron mode where the *K*-band klystron's frequency differs from that of the *S*-band harmonic frequency by the frequency to which the radio receiver is tuned.[4b] Two pips result (for positive and negative frequency difference), which may be superimposed on the line maxima by tuning the *S*-band klystron and receiver *O*. For frequency differences outside of the range of the receiver, auxiliary markers are obtained by frequency modulating the *S*-band klystron. Several sideband markers are thereby generated on both sides of the fundamental markers. These sideband markers are spaced at intervals equal to the modulating frequency.

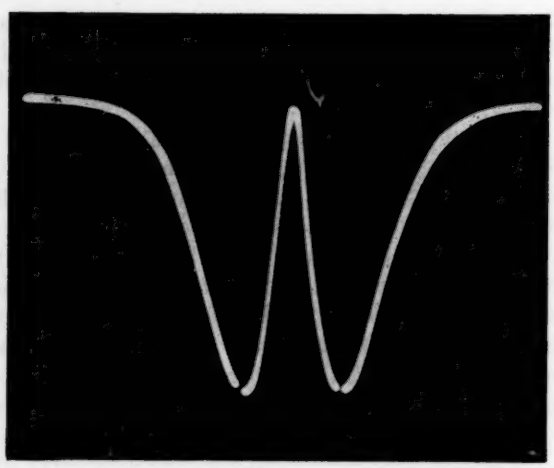

FIG. 3(b). Derivative of line.

VACUUM SYSTEM AND CHEMICAL PREPARATION

A diagram of the vacuum system is shown in Fig. 4. During the runs the pressure is measured both by McLeod gauge *A*, isolated from the rest of the vacuum system by a trap immersed in dry ice, and by thermocouple gauge *B*. An ionization gauge was used to test the ultimate obtainable vacuum.

The OCS sample was prepared by[5] the action of sulfuric acid on ammonium thiocyanate. It was purified by passage through two bubbling towers containing a 40 percent aqueous KOH solution and a third tower containing concentrated H_2SO_4. It was further purified by two fractionations and two condensations with the use of liquid nitrogen and dry ice.

After preparation, the sample was stored in trap *C* maintained at dry ice temperature. Sample purity was checked by infrared analysis and by consistency of microwave data using two sample batches.

EXPERIMENTAL PROCEDURE

Runs of line width *versus* pressure were taken at temperatures near −80°, 30°, 100°, and 200° centigrade.

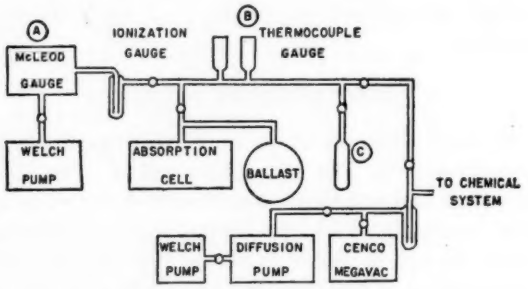

FIG. 4. Vacuum system block diagram.

Data were taken for the two separate sample batches and for a mixture of the two samples. All the data agreed within experimental error. The greatest precision was obtained in the final data. These data, corrected for systematic errors introduced by the 90-kc frequency modulation, as discussed below, are plotted in Fig. 5.

The apparent line width may be a function of a number of variables: microwave power level, frequency and amplitude of rf modulation, frequency and amplitude of saw tooth sweep, curvature of klystron mode, or amplitude and location of reflections on the mode, jitter in the marker pips. All of these effects were checked and minimized as follows.

1. Microwave power level: Excessive microwave power may saturate either the gas or the crystal detector. The klystron was operated with a PRD precision attenuator generally set at 20 db. Assuming a 20-milliwatt klystron output, this corresponds to 200 microwatts incident on the gas. The cell introduces an extra 6-db attenuation, so that about 50 microwatts are

[5] Farkas and Melville, *Experimental Methods in Gas Reactions* (Macmillan Company, New York, 1939).

incident on the crystal. At these power levels the crystal's response does depart slightly from square law behavior.[4c] The departure is minimized by terminating the crystal with an rf impedance in the vicinity of 400 ohms, the input impedance of the receiver. Furthermore, the maximum gas absorption is so low (about five percent) that variations in the rectified crystal current are proportional to variations in incident rf power for any reasonable functional relation of crystal current *versus* rf power; i.e., only the first term of a Taylor's expansion need be retained for small variations of rf power.

2. Rf modulation: When the frequency of rf modulation is comparable with the line width, the apparent width is increased by the modulation.[6] This instrumental error was corrected for by obtaining curves of apparent width *versus* modulation frequency at a series of pressures (Fig. 6). The extrapolated values of these widths at zero modulation frequency are the true widths. The difference between the true width and the

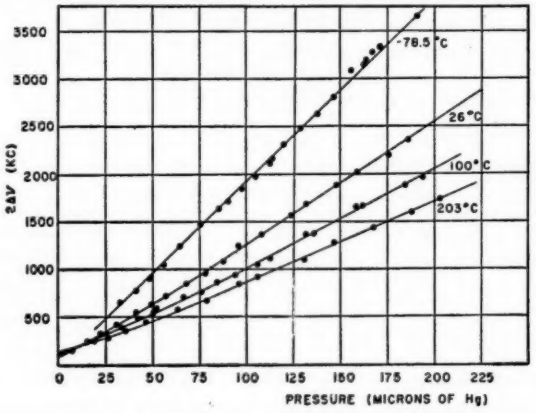

FIG. 5. Graph of line width *versus* pressure.

apparent width for a 90-kc modulation frequency is plotted in Fig. 7. These corrections have been applied to the data of Fig. 5.

The apparent line width is also a function of the rf modulation amplitude; only for small rf amplitudes is the line contour a reproduction of the magnitude of the first derivative of the line. A calibrated rf attenuator was used in series with the rf modulation and adjusted so that the observed line width was independent of rf amplitude over ±5-db variation of the attenuator. A cross check of the smallness of the modulation used is the fact that 90-kc sideband frequency markers were unobservably small for modulations used.

3. Frequency and amplitude of saw tooth sweep: These effects are interrelated. For high sweep frequency or amplitude, markers and line are distorted by the relatively small i.f. band pass of the radio receiver (about 10 kc). Furthermore, the markers, being sharper than the line, are delayed more and are shifted relative to the peak of the line. These effects are minimized by

[6] R. Karplus, Phys. Rev. **73**, 1027 (1948).

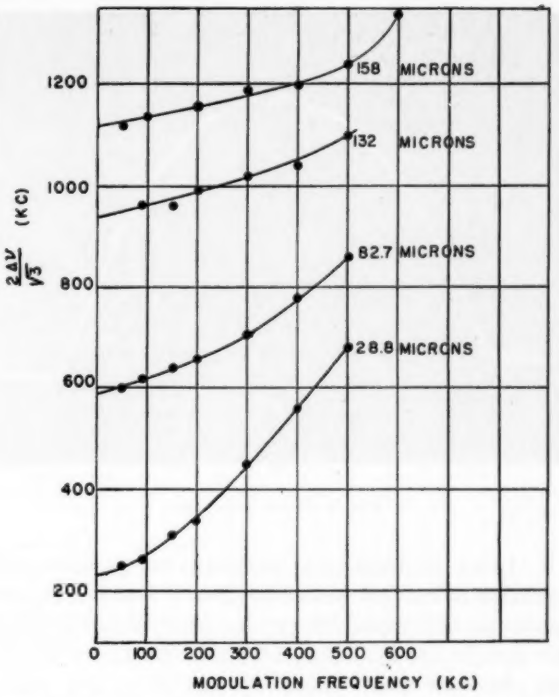

FIG. 6. Graph of $2\Delta\nu/\sqrt{3}$ *versus* modulation frequency.

using low sweeps and checking that variations in sweep by a factor of ±2 does not change the observed line width.

4. Curvature of klystron mode and amplitude and location of reflections: Calculations showed that effects of mode curvature with the wide klystron mode of the 2*K*50 (120 Mc) and the narrow lines used (200 kc—3.5 Mc) should be negligible. Reflections were minimized by careful cell construction. A typical mode, seen at the crystal beyond the 39-foot cell, is shown in Fig. 8. An experimental check of the lack of distortion in line widths by reflections was obtained by deliberately detuning the crystal to superimpose the line first upon a maximum, then upon a minimum of the reflection. Over a wide range of reflection variations no change in apparent line width was observed even for the widest lines used.

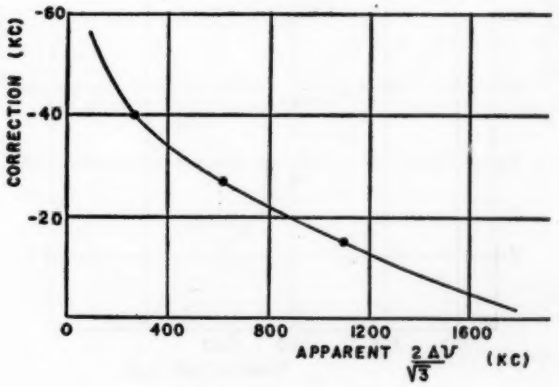

FIG. 7. Correction curve.

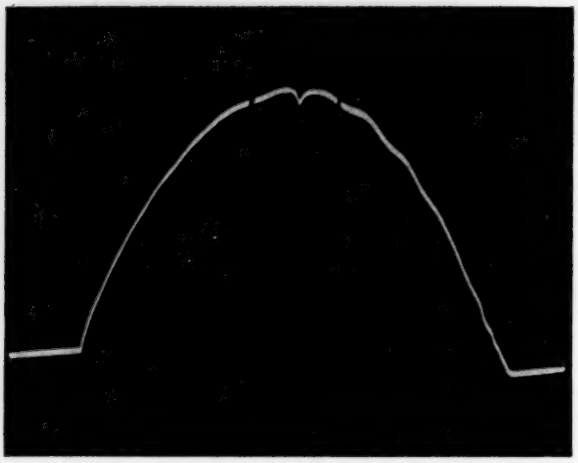

FIG. 8. Mode with line.

5. Jitter in frequency markers: ac power supply operation of marker sources, either K band or S band, was found to introduce excessive jitter. While stabilization circuits are available, adequate frequency stability was obtained most simply by operating the marker klystron as well as the K-band klystron from batteries. After an initial warm up period, markers were easily maintained in coincidence with the line maxima during observations.

DATA ANALYSIS

For line widths greater than 800 kilocycles the curves of Fig. 5 are linear. Within the accuracy of the data, the linear portions of the curves can be so chosen that their extrapolated portions intersect the origin, as expected from widths arising exclusively from pressure broadening. In Table I, the line width parameters are estimated both from the slope obtained by a judged best fit of the data, and from the intercept of this curve with the 150-micron pressure point, corresponding to a best fit of the data to straight line curves through the origin. The two sets of line width parameters agree within maximum errors of three percent. Also listed in Table I is the collision diameter b calculated from the kinetic theory relation.[1,4,7]

$$2\Delta\nu=\sqrt{2}N\bar{v}b^2,$$

where $\bar{v}$ is the mean velocity of the molecules. A logarithmic plot of $\Delta\nu$ and b *versus* temperature is shown in Fig. 9. The data can be represented quite well by the relations $\Delta\nu \propto T^{-0.9}$; $b \propto T^{-0.2}$. The room temperature line breadth parameter agrees with Johnson's value[8] within the combined experimental errors. Johnson's published temperature variation has been revised[9] and now agrees with ours.

It is interesting to note that the curves of Fig. 5 all intersect at a pressure near 10 microns, and yield intercepts at zero pressure that increase with temperature as do the Doppler width and the contribution to the line width arising from collisions with the walls.[4] The extrapolated room temperature width of 80 kc compares satisfactorily with the calculated wall-collision width of 74 kc and the Doppler width of 38 kc. Exact agreement is not to be expected as the detailed line shapes differ from that due to collision broadening, and the different line width contributions are not linearly additive.

TABLE I. Temperature dependence of OCS line width parameter $\Delta\nu$ and collision diameter b.

Temperature (°K)	$\Delta\nu$ [from slope, Fig. 5] (Mc/mm)	$\Delta\nu$ [from 150μ intercept, Fig. 5] (Mc/mm)	$\Delta\nu$ [Avg.] (Mc/mm)	b (cm)
194.5	9.58	9.57	9.58	10.24×10^{-8}
299	6.46	6.33	6.40	9.28×10^{-8}
373	5.21	5.07	5.14	8.78×10^{-8}
476	4.21	4.27	4.24	8.55×10^{-8}

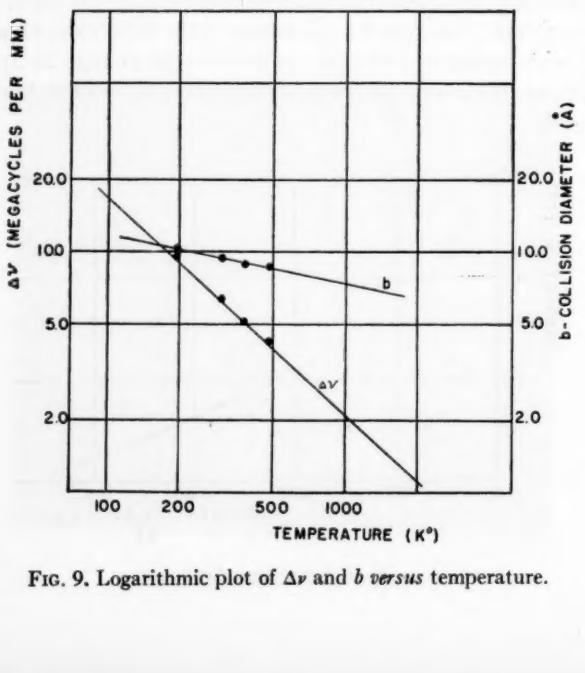

FIG. 9. Logarithmic plot of $\Delta\nu$ and b *versus* temperature.

CONCLUSIONS AND ACKNOWLEDGMENTS

A complete picture of the pressure broadening of linear molecules must encompass variation of line width with dipole moment, requiring the study of different molecules, and with rotational transition. Johnson's work on OCS indicates a pronounced increase in line breadth parameter for higher rotational states,[8] and a somewhat different temperature dependence for these higher states.[9]

The variation of collision diameter with temperature can arise in two ways: from variation in the velocity of the colliding molecules, or from variation in the rotational state population of the average molecule with which the molecule in the specific rotational state under

[7] W. V. Smith, Ann. N. Y. Acad. Sci. **55**, 891 (1952).
[8] C. M. Johnson, Phys. Rev. **87**, 677 (1952).
[9] C. M. Johnson, private communication.

investigation collides. Johnson's work indicates that the latter effect is important. Pending confirmation of his results, no conclusions as to the nature of the molecular interactions will be drawn from the present investigation.

Finally, we wish to acknowledge the help of several people. Particularly important was the careful cell construction accomplished by Martin Mealey and Melvin Weaver. We are grateful to the chemistry department for help in several items, especially to Eugene Levy and Dr. Harold Beachell for their infrared analysis of our sample. We have also benefited from discussions with Dr. Ralph Trambarulo and Dr. Charles M. Johnson.

THE JOURNAL OF CHEMICAL PHYSICS VOLUME 22, NUMBER 1 JANUARY, 1954

The Effect of Nonrigidity on the Line Strengths of Vibrational-Rotational Transitions*

HARRY C. ALLEN, JR.†
Mallinckrodt Chemical Laboratory, Harvard University, Cambridge, Massachusetts
[Received July 20, 1953]

The effect of the difference in asymmetry of the ground and excited states of a vibrttional band on the line strengths of the vibrational-rotational transitions has been investigated. It is found that for sufficiently large $\Delta\kappa$ ($\sim$0.1–0.2) in A- and C-type bands there is an enhancement of the line strengths of either the R or P branch, depending on whether or not κ of the ground state is greater or less than κ of the excited state. In B-type bands certain sub-bands are enhanced, but in general no branch of the band is enhanced as a whole.

INTRODUCTION

IN the early analyses of the rotational fine structure of vibrational bands of asymmetric rotors, the intensities of the fine structure components were estimated from the intensities of the transitions in the closer symmetric limit. Cross, Hainer, and King[1] have shown that such a procedure is dangerous. CHK have published a very useful table of line strengths for the rigid asymmetric rotor. It is well known, however, that molecules are not rigid rotors. In fact, in those cases where complete analyses of the rotational-fine structure have been made, it has been necessary to use effective moments of inertia for each vibrational state. This difference of asymmetry in the two vibrational states, the asymmetry being measured by $\kappa=(2b-a-c)/(a-c)$,[2] can have marked effect on the line strengths of various transitions if $\Delta\kappa$ between the two vibrational states is large. If $\Delta\kappa$ is small, then the line strengths calculated for the rigid approximation are sufficient. However, for some of the higher combination bands of light molecules such as water and hydrogen sulfide $\Delta\kappa$ can be as large as 0.1 or 0.2 and in free radical spectra even larger changes can occur.[3] In these cases the intensity pattern calculated for the rigid approximation breaks down.

THEORY

The problem of the asymmetric rotor has been treated in great detail.[1,2]

In setting up the energy matrix, Wang combinations of symmetric rotor wave functions must be used.[2] Then an orthonormal transformation can be found which diagonalizes the energy, i.e., such that

$$E(\kappa)=T'X'EXT, \tag{1}$$

where X is defined as in reference 2, Eq. (29), and serves to give the Wang combinations of the symmetric rotor wave functions, and T is the transformation which diagonalizes the energy matrix.

The line strengths are obtained by squaring the matrix elements of the direction cosine matrix of the asymmetric rotor. If the direction cosine matrix is also set up in terms of symmetric rotor wave functions, then the asymmetric rotor direction cosine matrix is obtained by[1]

$$\Phi_{F_0}{}^{A}=T_1'X'\Phi XT_2, \tag{2}$$

where T_1 and T_2 are the transformations which diagonalize the ground and excited states, respectively. The case where $T_1=T_2=T$ was considered by Cross,

TABLE I. Summary of sub-bands whose intensity is enhanced.

	Case I $\kappa_G<\kappa_e$	Case II $\kappa_e<\kappa_G$
Stronger Sub-bands	${}^{be}R_{1,1}$ ${}^{be}P_{\bar{1},1}$ ${}^{be}Q_{1,\bar{1}}$ ${}^{bo}Q_{1,\bar{1}}$ ${}^{ae}P_{0,\bar{1}}$ ${}^{ao}P_{0,\bar{1}}$ ${}^{ae}Q_{0,\bar{1}}$ ${}^{ao}Q_{\bar{2},1}$ ${}^{co}Q_{\bar{1},0}$ ${}^{ce}Q_{\bar{1},2}$ ${}^{ce}R_{1,0}$ ${}^{co}R_{1,0}$	${}^{bo}R_{1,\bar{1}}$ ${}^{bo}P_{\bar{1},1}$ ${}^{be}Q_{\bar{1},1}$ ${}^{bo}Q_{\bar{1},1}$ ${}^{ae}R_{0,\bar{1}}$ ${}^{ao}R_{0,1}$ ${}^{ao}Q_{0,\bar{1}}$ ${}^{ae}Q_{2,\bar{1}}$ ${}^{ce}Q_{1,0}$ ${}^{co}Q_{1,\bar{2}}$ ${}^{co}P_{\bar{1},0}$ ${}^{ce}P_{\bar{1},0}$

κ_G = ground state
κ_e = excited state
Sub-band labeling is that suggested in reference 1.

* The research reported herein was supported in part by the U. S. Office of Naval Research under ONR Contract N5ori 76, Task Order V.

† U. S. Atomic Energy Commission Postdoctoral Fellow, now at Department of Physics, Michigan State College, East Lansing, Michigan.

[1] Cross, Hainer, and King, J. Chem. Phys. 12, 210 (1944).

[2] King, Hainer, and Cross, J. Chem. Phys. 11, 27 (1943).

[3] This was kindly pointed out by Dr. Herzberg at the "Symposium on Molecular Structure and Spectroscopy," Columbus, Ohio, 1953.

TABLE II. Calculated line strengths of A- and B-type bands.

			A type band				
	$^{a}Q_{01}$				$^{a}Q_{0\bar{1}}$		
Transition	$\Phi^2(1)$	$\Phi^2(0.5\text{–}7)$	$\Phi^2(0.5)$	Transition	$\Phi^2(1)$	$\Phi^2(0.5\text{–}7)$	$\Phi^2(0.5)$
1_1-1_0	15 000	15 000	15 000	1_0-1_1	15 000	15 000	15 000
2_2-2_1	25 000	28 223	28 223	2_1-2_2	25 000	26 926	28 223
3_3-3_2	35 000	44 966	45 104	3_2-3_3	35 000	41 498	45 104
4_4-4_3	45 000	63 926	64 494	4_3-4_4	45 000	58 949	64 494
2_0-2_{-1}	8333	8333	8333	$2_{-1}-2_0$	8333	8333	8333
3_1-3_0	14 583	16 278	16 278	3_0-3_1	14 583	15 514	16 278
4_2-4_1	20 250	26 100	26 168	4_1-4_2	20 250	23 431	26 168
$3_{-1}-3_{-2}$	8750	7730	7403	$3_{-2}-3_{-1}$	8750	7505	7403
4_0-4_{-1}	15 750	13 893	13 221	$4_{-1}-4_0$	15 750	12 987	13 221
$4_{-2}-4_{-3}$	9000	8087	7587	$4_{-3}-4_{-2}$	9000	7616	7587
	$^{a}Q_{2\bar{1}}$				$^{a}Q_{\bar{2}1}$		
$2_{-2}-2_1$	8333	5110	5110	2_1-2_{-2}	8333	6405	5110
$3_{-1}-3_2$	14 583	5395	5722	3_2-3_{-1}	14 583	9328	5722
4_0-4_3	20 250	3691	4363	4_3-4_0	20 250	9896	4363
$3_{-3}-3_0$	8750	7055	7055	3_0-3_{-3}	8750	7819	7055
$4_{-2}-4_1$	15 570	10 714	11 214	4_1-4_{-2}	15 750	13 952	11 214
$4_{-4}-4_{-1}$	9000	7565	7558	$4_{-1}-4_{-4}$	9000	8138	7558
	$^{a}R_{01}$				$^{a}P_{0\bar{1}}$		
0_0-1_{-1}	10 000	10 000	10 000	$1_{-1}-0_0$	10 000	10 000	10 000
$1_{-1}-2_{-2}$	15 000	16 159	16 934	$2_{-2}-1_{-1}$	15 000	16 934	16 934
$2_{-2}-3_{-3}$	25 000	25 351	25 893	$3_{-3}-2_{-2}$	25 000	25 968	25 893
$3_{-3}-4_{-4}$	35 000	35 373	35 773	$4_{-4}-3_{-3}$	35 000	35 793	35 773
1_1-2_0	15 000	15 000	15 000	2_0-1_1	15 000	15 000	15 000
2_0-3_{-1}	16 667	20 381	22 500	$3_{-1}-2_0$	16 667	22 500	22 500
$3_{-1}-4_{-2}$	26 250	27 225	29 261	$4_{-2}-3_{-1}$	26 250	29 554	29 261
2_2-3_1	20 000	18 530	18 636	3_1-2_2	20 000	19 229	18 636
3_1-4_0	18 750	25 684	29 055	4_0-3_1	18 750	29 431	29 055
3_3-4_2	25 000	19 832	20 331	4_2-3_3	25 000	22 214	20 331
	$^{a}R_{01}$				$^{a}P_{0\bar{1}}$		
1_0-2_{-1}	15 000	15 000	15 000	$2_{-1}-1_0$	15 000	15 000	15 000
$2_{-1}-3_{-2}$	25 000	25 445	25 710	$3_{-2}-2_{-1}$	25 000	25 710	25 710
$3_{-2}-4_{-3}$	35 000	35 406	35 758	$4_{-3}-3_{-2}$	35 000	35 765	35 758
2_1-3_0	16 667	16 667	16 667	3_0-2_1	16 667	16 667	16 667
3_0-4_{-1}	26 250	27 566	28 252	$4_{-1}-3_0$	26 250	28 258	28 252
3_2-4_1	18 750	18 171	18 207	4_1-3_2	18 750	18 414	18 207

Hainer, and King. In this paper the case will be considered where $T_1 \neq T_2$.

The transformations for $\kappa=0.5$ and $\kappa=1$ have been evaluated up through $J=4$ and applied to the direction cosine matrix in the order

$$\Phi_{P_0}{}^{A} = T(0.5)X'\Phi XT(1). \tag{3}$$

This order assumes that $\kappa=0.5$ in the ground state and $\kappa=1$ in the excited state. A change this large is likely to be encountered only in the case of free radical spectra, but the large change was used in order to emphasize any regularities which might appear. The resulting elements were squared and multiplied by 10^4 in order to be consistent with reference 1. The transitions were then sorted into sub-branches in order to find any regularities which occurred.

DISCUSSION

The regularities found are summarized in Table I. It was found necessary to consider two cases; (1) κ of ground state less than κ in the excited state, and (2) κ of ground state greater than κ in the excited state. The conclusions for case 2 are the converse of the conclusions for case 1, so only case 1 will be discussed.

The most striking regularities are found in the A- and C-type bands, i.e., the dipole moment change along the least and largest inertial axes, respectively. In the A-type band it is found that the P-branch line strengths are enhanced, quite generally, with respect to the R branch, while in the C-type bands it is the R branch which is enhanced. Certain of the Q-branch sub-bands are also enhanced under these conditions.

An inspection of the table of line strengths in reference 1 shows that it is not always necessary to consider the difference of asymmetry of the two vibrational states. For an A type band, the change of line strength with κ, is very small in the region $-1 \leqslant \kappa \leqslant 0$. Hence $a\,\Delta\kappa$ in this region would not lead to pronounced effects. However, for $0 \leqslant \kappa \leqslant 1$ the change in line strength with κ is quite steep; hence in this region of κ one might expect quite pronounced effects. For C-type bands the pronounced effects are to be expected in the region $-1 \leqslant \kappa \leqslant 0$. The line strengths of Q-branch transitions have a much greater κ dependence than either the P- or R-branch transitions. Such unexpected intensity patterns as can arise from these Q-branch transitions could become a useful tool in the analysis of vibrational-rotational bands.

TABLE II—*Continued*.

B type band

Transition	$^{be}Q_{1,\bar{1}}$ $\Phi^2(1)$	$\Phi^2(0.5\text{–}7)$	$\Phi^2(0.5)$	Transition	$^{be}Q_{\bar{1},1}$ $\Phi^2(1)$	$\Phi^2(0.5\text{–}7)$	$\Phi^2(0.5)$
$1_{-1}-1_1$	15 000	15 000	15 000	1_1-1_{-1}	15 000	15 000	15 000
2_0-2_2	25 000	22 912	21 289	2_2-2_0	25 000	21 289	21 289
3_1-3_3	35 000	27 961	23 196	3_3-3_1	35 000	23 041	23 196
4_2-4_4	45 000	29 930	22 157	4_4-4_2	45 000	21 541	22 157
$2_{-2}-2_0$	8333	12 044	12 044	2_0-2_{-2}	8333	10 422	12 044
$3_{-1}-3_1$	14 583	25 529	24 417	$3_{-1}-3_1$	14 583	19 652	24 417
4_0-4_2	20 250	40 243	36 119	4_2-4_0	20 250	28 245	36 119
$3_{-3}-3_{-1}$	8750	11 750	10 583	$3_{-1}-3_{-3}$	8750	9471	10 583
4_2-4_0	15 750	21 904	20 622	4_0-4_{-2}	15 750	16 498	20 622
$4_{-4}-4_{-2}$	9000	10 655	10 617	$4_{-2}-4_{-4}$	9000	9776	10 544
	$^{bo}Q_{1,\bar{1}}$				$^{bo}Q_{\bar{1},1}$		
$2_{-1}-2_1$	8333	8333	8333	2_1-2_{-1}	8333	8333	8333
3_0-3_2	14 583	14 583	13 160	3_2-3_0	14 583	13 160	13 160
4_1-4_3	20 250	20 171	16 126	4_3-4_1	20 250	16 092	16 126
$3_{-2}-3_0$	8750	10 173	10 173	3_0-3_{-2}	8750	9592	10 173
$4_{-1}-4_1$	15 750	19 977	18 280	4_1-4_{-1}	15 750	16 716	18 280
$4_{-3}-4_{-1}$	9000	10 515	10 584	$4_{-1}-4_{-3}$	9000	9839	10 584
	$^{be}R_{1,1}$				$^{bo}P_{\bar{1},1}$		
0_0-1_0	10 000	10 000	10 000	1_0-0_0	10 000	10 000	10 000
$1_{-1}-2_{-1}$	15 000	15 000	15 000	$2_{-1}-1_{-1}$	15 000	15 000	15 000
$2_{-2}-3_{-2}$	25 000	24 330	24 086	$3_{-2}-2_{-2}$	25 000	24 183	24 086
$3_{-3}-4_{-3}$	35 000	34 421	34 083	$4_{-3}-3_{-3}$	35 000	34 114	34 083
1_1-2_1	15 000	15 000	15 000	2_1-1_1	15 000	15 000	15 000
2_0-3_0	16 667	16 667	16 667	3_0-2_0	16 667	16 667	16 667
$3_{-1}-4_{-1}$	26 250	24 034	23 550	$4_{-1}-3_{-1}$	26 250	23 941	23 550
2_2-3_2	20 000	21 295	21 383	3_2-2_2	20 000	20 414	21 383
3_1-4_1	18 750	19 506	19 563	4_1-3_1	18 750	19 182	19 563
3_3-4_3	25 000	29 205	29 580	4_3-3_3	25 000	27 992	29 580
	$^{be}R_{1,\bar{1}}$				$^{bo}P_{\bar{1},1}$		
1_0-2_2	5000	6253	7226	2_2-1_0	5000	7226	7226
2_1-3_3	10 000	14 021	16 667	3_3-2_1	10 000	16 667	16 667
3_2-4_4	15 000	23 369	27 406	4_4-3_2	15 000	27 337	27 406
$2_{-1}-3_1$	1667	2245	2792	3_1-2_{-1}	1667	2792	2792
3_0-4_2	3750	5675	7602	4_2-3_0	3750	7602	7602
$3_{-2}-4_0$	1250	1185	1537	4_0-3_{-2}	1250	1705	1537

In *B*-type bands, i.e. for a dipole moment change along the intermediate inertial axis, no particular branch is generally enhanced. It is found that certain sub-bands in the *P*, *Q*, and *R* branches are enhanced. It is again to be hoped that the intensity patterns found in this special case of large $\Delta\kappa$ will become a useful analytical tool. In order to give some idea of the size of these effects, in Table II are shown the calculated line strengths for the main sub-bands for both *A*- and *B*-type selection rules through $J=4$. No *C*-type examples are given for the effect is very small in the κ region chosen, as pointed out earlier. A ground state of 0.5 and an excited state κ of 0.7 have been used in the calculations. The line strengths for the rigid approximations in which $\kappa=0.5$ and 1.0 have been included for comparison.

In many instances these effects are small, of the order of 1 or 2 percent for a $\Delta\kappa=0.2$. However, for many *Q* branch transitions in the appropriate κ range these effects can be as much as 10 percent even at low *J*. In the case of free radicals[4] where $\Delta\kappa$ may be as high as 0.6–0.8, these effects will be pronounced in practically all transitions.

ACKNOWLEDGMENTS

The author wishes to express his appreciation to Professor Paul C. Cross, who originally suggested this problem, and to Professor E. Bright Wilson, Jr., in whose laboratory the work was carried out.

[4] D. A. Ramsay, private communication.

Dipole Moments, Nuclear Quadrupole Coupling, and the Bonding Orbitals in Group V—Trihalides*

PAUL KISLIUK†
Columbia University, New York, New York
(Received April 10, 1953)

By means of microwave spectral measurements the following molecular parameters have been determined: 1. The dipole moment of NF_3 is 0.235 ± 0.007 Debye. 2. The nuclear quadrupole coupling of arsenic in $AsCl_3$ is -173 ± 20 Mc. 3. The internuclear distance Sb−Cl and the bond angle Cl−Sb−Cl are 2.325 ± 0.005A and $99.5\pm1.5°$, respectively, in $SbCl_3$.

The measured molecular parameters of the group V-trihalides are assembled and interpreted in terms of $s-p$ hybridization, partial ionic, and partial multiple bond character. In particular, certain regularities in the dipole moments are pointed out which indicate that apparent anomalies in the dipole moments of these molecules can be understood in terms of $s-p$ hybridization.

From the evidence of nuclear hyperfine structure, it appears that NF_3 and AsH_3, as was previously suggested for NH_3, have an $s-p$ hybridization which is not simply related to the bond angles. The quadrupole coupling per p-electron of N^{14}, previously reported to have been established by the measurements on NF_3, has been again thrown open to question.

I. INTRODUCTION

THE trihalides of the group V elements are exceptions to the empirical rules for estimating electric dipole moments.[1,2] Robinson, for HCl,[3] and Coulson, for carbon bonds,[4] have shown that the calculation of molecular dipole moments depends strongly on the assumed amount of $s-p$ hybridization in the wave functions of the electrons of the valence shell. The anomalies in the dipole moments of the group V trihalides can be partially understood in these terms, as suggested by Schomaker and Lu, for the case of NF_3.[5]

Furthermore, evidence of $s-p$ hybridization, in addition to that of the bond angles, may be obtained from the electric quadrupole coupling of the nucleus.[6] Multiple bonding, which may be estimated from the bond distances, also affects the nuclear quadrupole coupling. The dipole moments, nuclear quadrupole couplings, bond angles, and bond distances may all be measured by the techniques of microwave spectroscopy. In the succeeding sections microwave measurements are presented for the dipole moment of NF_3, the quadrupole coupling of arsenic in $AsCl_3$, and the structural parameters of $SbCl_3$. The bonding orbitals are then considered in the light of the available evidence.

In an attempt to gain further evidence regarding this class of molecules, unsuccessful search has been made for the microwave spectra of NCl_3 and SbF_3. Failure in the former case is probably due to a small dipole moment and, therefore, very weak lines. In the latter case, the apparatus to be described in the section on $SbCl_3$ was utilized in the search at temperatures on the order of 100°C, and failure is attributed to the high reactivity of SbF_3.

II. THE DIPOLE MOMENT OF NF_3

The $J=1\rightarrow2$ transition in NF_3 has been reported at 42 724 Mc, and the quadrupole coupling of the N^{14} nucleus found to be -7.07 Mc.[7] In a recently published paper[8] the value $\mu=0.234\pm0.004$ is found for $N^{15}F_3$, in excellent agreement with the measurement reported below and earlier measurements.[8a]

The three components of the $J=0\rightarrow1$ transition, resulting from the nuclear quadrupole interaction of N^{14}, have been observed, and the Stark effect of the strongest of these ($F=1\rightarrow2$), measured.

The theory of the Stark effect in symmetric top molecules with appreciable quadrupole coupling has been treated by Low and Townes,[9] but for $K=0$, as in this case, Fano's treatment for linear molecules[10] is applicable, and the particular case required is worked out in detail. The frequency shifts measured for various applied voltages are plotted in Fig. 1, together with the theoretical curve appropriate to the geometry of the Stark cell used[11] for the value of the dipole moment giving the best fit: namely, $\mu=0.235\pm0.007$ Debye.

III. THE QUADRUPOLE COUPLING OF ARSENIC IN $AsCl_3$

The number of lines in the hyperfine structure due to the arsenic nuclear quadrupole coupling in $AsCl_3$ is large

* Work supported jointly by the U. S. Signal Corps and the U. S. Office of Naval Research.
† Present address: Bell Telephone Laboratories, Murray Hill, New Jersey.

[1] J. G. Malone, J. Chem. Phys. **1**, 197 (1933).
[2] L. Pauling, *The Nature of the Chemical Bond* (Cornell University Press, Ithaca, 1945), p. 67.
[3] D. Z. Robinson, J. Chem. Phys. **17**, 1022 (1949).
[4] C. A. Coulson, Trans. Faraday Soc. **38**, 433 (1942).
[5] V. Schomaker and C. S. Lu, J. Am. Chem. Soc. **72**, 1182 (1950).
[6] C. H. Townes and B. P. Dailey, J. Chem. Phys. **17**, 782 (1949).
[7] J. Sheridan and W. Gordy, Phys. Rev. **79**, 513 (1950).
[8] Ghosh, Trambarulo, and Gordy, J. Chem. Phys. **21**, 308 (1953).
[8a] Watson, Kane, and Ramaswamy, Proc. Roy. Soc. (London) **156**, 130 (1936).
[9] W. Low and C. H. Townes, Phys. Rev. **76**, 1295 (1949).
[10] U. Fano, J. Research Nat. Bur. Standards **40**, 215 (1948).
[11] R. G. Shulman, thesis, Columbia University (1949).

for the transitions in the convenient microwave region, and the spectrum is not easily resolved.[12] Further complications might be expected from the chlorine nuclear quadrupole couplings, but the chlorine coupling in covalently bonded compounds is ordinarily about $\frac{1}{3}$ of that of arsenic, and averaging over the rotational motion of the molecule reduces the chlorine splitting by a factor of $\frac{1}{6}$, so that the resulting effect is small. In fact, the chlorine hyperfine structure has not been resolved at all in PCl_3, where there can be no quadrupole splitting due to the phosphorus nucleus; nor does it appear to broaden the lines appreciably.[12]

In order to measure the quadrupole coupling of the arsenic nucleus, the dependence of the Stark effect on the quantum number K was used to suppress a number of lines, and thus to resolve the remaining lines. A very small modulating field was used in a Stark modulation microwave spectrometer,[13] so that lines of low K were not seen. The lines of greatest intensity ($\Delta F=+1$) of the $J=5\rightarrow6$ transition of $AsCl_3^{35}$ are plotted in Fig. 2 and labeled with the appropriate K values. The experimental traces obtained for various magnitudes of the modulating voltage are shown in Fig. 3. By measuring the frequency separation of the most widely split lines ($K=5$, $F=11/2\rightarrow13/2$ and $7/2\rightarrow9/2$) one finds $(eqQ)_{As}=-173\pm20$ Mc.

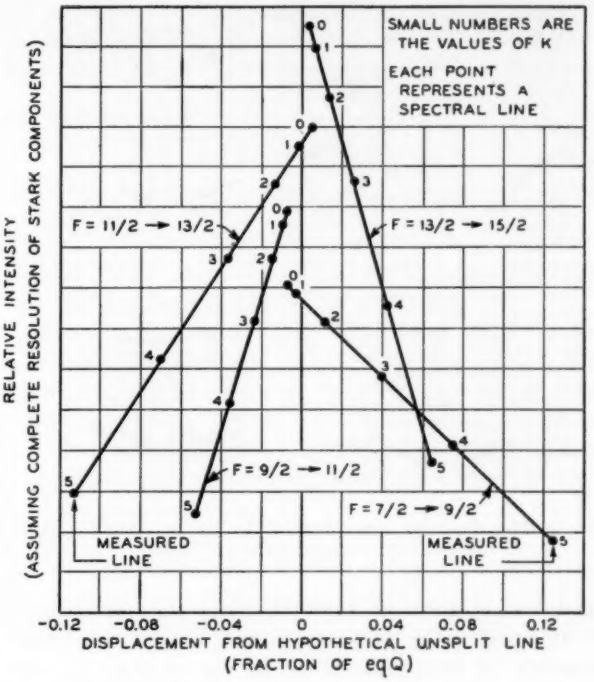
SMALL NUMBERS ARE THE VALUES OF K
EACH POINT REPRESENTS A SPECTRAL LINE
F = 11/2 → 13/2
F = 13/2 → 15/2
F = 9/2 → 11/2
F = 7/2 → 9/2
MEASURED LINE
MEASURED LINE
RELATIVE INTENSITY (ASSUMING COMPLETE RESOLUTION OF STARK COMPONENTS)
-0.12 -0.08 -0.04 0 0.04 0.08 0.12
DISPLACEMENT FROM HYPOTHETICAL UNSPLIT LINE (FRACTION OF eqQ)

FIG. 2. Theoretical quadrupole hyperfine structure for $J=5\rightarrow6$; $I=\frac{3}{2}$; $\Delta F=+1$.

IV. THE BOND DISTANCE AND ANGLE IN $SbCl_3$

For $Sb^{121}Cl_3^{35}$ and $Sb^{123}Cl_3^{35}$ the large molecular angular momentum encountered in the convenient microwave region and the high spins of the two antimony isotopes result in two broad groups of unresolved lines which do not yield to the method of resolution used for arsenic trichloride. The groups of lines due to the $J=6\rightarrow7$ transition of $Sb^{121}Cl_3^{35}$ and $Sb^{123}Cl_3^{35}$, centered at 24 554 and 24 510 Mc, respectively, are only partially resolved, but with the additional check provided by the groups of lines due to the asymmetric molecules including either one or two Cl^{37} nuclei, it is possible to determine the bond angle and internuclear distance. These are given in Table I, together with earlier electron diffraction results, with which the agreement is poor.

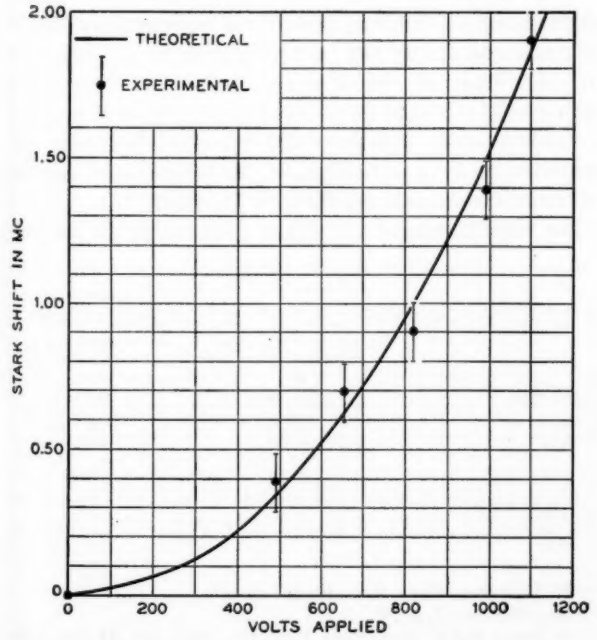

FIG. 1. Stark shift of $N^{14}F_3$, $J=0\rightarrow1$, $F=1\rightarrow2$. Theoretical curve for $\mu=0.235$ Debye; $(eqQ)_{N^{14}}=-7.07$ Mc.

To obtain sufficient vapor pressure ($\sim10^{-2}$ mm Hg) for this experiment and for the unsuccessful search for the spectrum of SbF_3, it was necessary to raise the apparatus above room temperature. This was accomplished by immersing the entire waveguide absorption cell in an electrically heated oil bath. The cell was isolated from the pump with metal bellows-type valves within the oil bath, and the sample tube was heated independently, so that the vapor pressure of the sample could be easily controlled. Teflon insulators supported the Stark electrode, and lead-gasketed mica windows terminated the absorption cell. The spectrum of $SbCl_3$ was observed at 35°C, and the search for SbF_3 spectrum was made at about 120°C. At temperatures approaching 150°C gas was evolved within the system, apparently from the Teflon, at a rate which made it impossible to maintain a pressure of 10^{-2} mm Hg in the closed system for any appreciable time.

V. DIPOLE MOMENTS AND $s-p$ HYBRIDIZATION

The best available values of the internuclear distances, bond angles and dipole moments of the group V

[12] P. Kisliuk and C. H. Townes, J. Chem. Phys. **18**, 1109 (1950).
[13] McAfee, Hughes, and Wilson, Rev. Sci. Instr. **20**, 821 (1949).

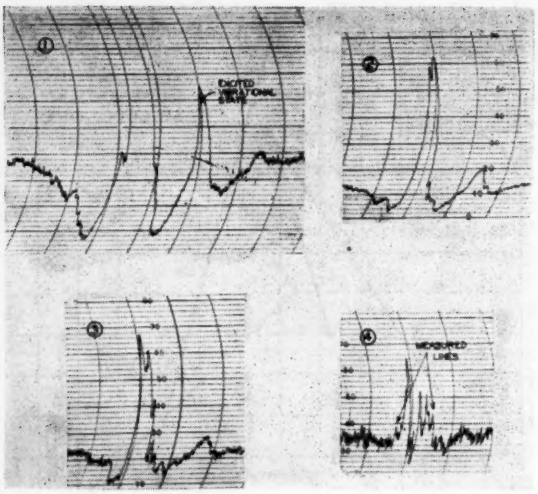

FIG. 3. The $J=5\rightarrow6$ transition of $AsCl_3^{35}$ at $-40°C$, under successively smaller Stark modulation.

trihalides are given in Table II. Since the bond angles are all roughly the same, one might expect the dipole moments to be proportional to the product of the electronegativity difference[14] and the internuclear distance if hybridization were not of importance. The ratios of the observed moments to this quantity are given in Table III. This ratio is approximately constant for each group V nucleus, and increases steadily from the lighter to the heavier ones, suggesting that the dipole moments can be explained in terms of the hybridization of the bonding orbitals of the group V element, rather than in terms of the relative size of the atoms, the polarization of the core electrons, or partial multiple bonding, all of which would depend upon the halogen as well as the group V element. In the light of this regularity, the low value of the dipole moment of NF_3 does not appear exceptional. In the remainder of this section dipole moment measurements will be interpreted in terms of $s-p$ hybridization; possible contributions of the d orbitals are neglected.

The dipole moment due to the hybridization of the nonbonding orbitals of the valence shell of the group V element will detract from that due to partial ionic character.[5,15] A similar effect takes place in the valence shell of the halogen atom, but the effect is reduced because:

(1) the nonbonding orbitals of the halogen have less p character than those of the group V atom since there is only one bonding orbital requiring partial s character.

(2) the resulting dipole moment is in the direction of the bond and must be projected onto the figure axis.

The total moment is thus less than the contribution of the ionic form when the latter is predominant. The over-all moment tends to be small when the s character of the bonding orbital is large, since the p character of the nonbonding orbital is then correspondingly large.

The relatively small dipole moments observed for the trihalides of the lighter group V elements are expected from these considerations to correspond to larger bond angles, since the angle is related to the $s-p$ hybridization by[16]

$$\alpha+\beta\cos\theta=0, \tag{1}$$

where α and β are the fractions of s and p character, respectively, $(\alpha+\beta=1)$, and θ is the bond angle. A slight tendency in this direction may be noted in Table II and is to be expected because of the tighter binding of the penetrating s orbitals by nuclei of larger atomic number. The elementary group V substances exhibit the tendency for heavy nuclei to exhibit small bond angles more strongly than do the trihalides,[17] but the angles of the latter are complicated by steric forces, and by the coulombic forces of the ions with each other and with the charge imbalance due to $s-p$ hybridization,[5] all of which might result in "bent" or "strained" bonds, i.e. bonds in which the nuclei are not along the line of greatest electron density of the orbitals of the nuclei to which they are bonded.

Bending of the bonds has been shown to take place during the bending vibration of ICN,[18] where, as in all molecules, the electronic motion is presumed to adjust adiabatically to the nuclear positions (Born-Oppenheimer approximation). There is also some evidence of bending of the bonds in methylene chloride,[19] but it is probably on the order of one degree.[20] Except in certain ring compounds,[19] there is apparently no clear-cut evidence of sufficient bending of bonds to invalidate the rough calculations of $s-p$ hybridization by means of Eq. (1). This will be of some importance in a later section (VII), in that large bond strains will not be used to explain away apparent discrepancies between the estimates of $s-p$ hybridization from the bond angles and from the nuclear quadrupole coupling.

The significance of the dipole moment in estimating

TABLE I.

	Internuclear distance Sb–Cl (*A*)	Bond angle Cl–Sb–Cl
Microwave	2.325±0.005	99.5°±1.5°
Gregg *et al.*[a]	2.37 ±0.02	104° ±2°
Swingle[b]	2.37 ±0.02	96° ±4°

[a] Gregg, Hampson, Jenkins, Jones, and Sutton, Trans. Faraday Soc. **33**, 852 (1937).
[b] S. M. Swingle, quoted by P. W. Allen and L. E. Sutton, Acta Cryst. **3**, 46 (1950).

[14] See reference 2, p. 58 ff.
[15] Gordy, Smith, and Trambarulo, *Microwave Spectroscopy* (John Wiley and Sons, Inc., New York, 1953), pp. 293–294.
[16] R. Hultgren, Phys. Rev. **40**, 891 (1932).
[17] See reference 2, p. 80.
[18] A. Javan and C. H. Townes, Bull. Am. Phys. Soc. **27**, No. 1, 33 (1952).
[19] E. B. Wilson, Jr., Ann. N. Y. Acad. Sci. **55**, No. 5, 943 (1952), p. 947.
[20] R. J. Myers and W. D. Gwinn, J. Chem. Phys. **20**, 1420 (1952).

partial ionic character is greatly reduced by the uncertainties due to $s-p$ hybridization, polarization of the core electrons, and the overlapping of the wave functions of atoms of unequal size, but some information can, nevertheless, be obtained. In the molecules under consideration, the first two of these effects tend to reduce the dipole moment, so that for AsF_3 and $SbCl_3$, which attain 73 percent and 75 percent, respectively, of the dipole moment attributed to the ionic form

$$X^+—Y^-$$

, it seems clear that each bond is approximately 33 percent ionic. Pauling's graph[14] of ionic character *vs* electronegativity difference indicates about 5 percent ionic character for the bond in PI_3, and only about 60 percent for the AsF_3 bond. The revised estimate of Townes and Dailey[21] indicates somewhat more ionic character for AsF_3.

VI. MULTIPLE BONDING

Multiple bonding is expected to be important in the lighter molecules, especially in NF_3.[22,23] While Skinner and Sutton[24] have shown from a comparison of the arsenic trihalides and similar methylated compounds that bond shortening due to double bonds is negligible for $AsCl_3$, $AsBr_3$, and AsI_3, the surprisingly short bond distance in PF_3 is evidence that multiple bonding does indeed contribute to the lighter molecules.

TABLE II.

Molecule XY_3	Distance $X-Y$(A)	Reference	$\angle YXY$	Reference	Dipole moment, μ, in Debye units (10^{18} esu cm)	Reference
NF_3	1.371±0.003	a	102°9′±10′	a	0.234±0.005	l
PF_3	1.551±0.006	b	102°±3°[h]	b	1.025±0.009	j
AsF_3	1.712±0.005	c	102°±2°	i	2.815±0.025	j
PCl_3	2.043±0.005	d	100°7′±20′	d	0.80±0.1	k
$AsCl_3$	2.161±0.004	d	98°25′±30′	d	2.1±0.3	k
$SbCl_3$	2.325±0.005	e	99.5°±1.5°	e	3.9±0.4	k
PBr_3	2.20±0.04	f	101°±1.5°	f	0.61±0.1	k
$AsBr_3$	2.33±0.04	g	101°±1.5°	g	1.7±?	k
$SbBr_3$	2.50±0.03	g	97°±2°	g	2.8±0.4	k
PI_3	2.47±0.05	g	100°±2°	g	0.0±0.3	k
AsI_3	2.55±0.04	g	100.5°±2°	g	0.96±0.4	k
SbI_3	2.72±0.05	g	98.5°±2°	g	1.58±0.4	k

[a] See reference 7.
[b] Gilliam, Edwards, and Gordy, Phys. Rev. **75**, 1014 (1949).
[c] Dailey, Rusinow, Shulman, and Townes, Phys. Rev. **74**, 1245 (1949).
[d] See reference 12.
[e] Measurements presented in this paper.
[f] See reference g. The values computed from the microwave data of Q. Williams and W. Gordy, Phys. Rev. **79**, 225 (1950) (P−Br=2.45Å, θ=89°40′) are so far removed from both reasonable estimated values and the electron diffraction results that it has been assumed that an error was made in identifying the lines, and the electron diffraction value is given.
[g] P. W. Allen and L. E. Sutton, Acta Cryst. **3**, 46 (1950).
[h] Assumed.
[i] P. Kisliuk and S. Geschwind, J. Chem. Phys. **21**, 828 (1953).
[j] Shulman, Dailey, and Townes, Phys. Rev. **78**, 145 (1950).
[k] L. G. Wesson, *Tables of Electric Dipole Moments* (The Technology Press, Cambridge, Massachusetts, 1948).
[l] See reference 8.

TABLE III.

Ratio $K=\mu/d(\Delta X)$, where μ is the electric dipole moment in Debye units, d is the internuclear distance (A), and ΔX is the electronegativity difference.[a]

NF_3 0.17±0.01	PF_3 0.35±0.01	AsF_3 0.82±0.01		
	PCl_3 0.44±0.06	$AsCl_3$ 0.93±0.14	$SbCl_3$ 1.3±0.2	
	PBr_3 0.42±0.07	$AsBr_3$ 0.86±?	$SbBr_3$ 1.2±0.2	
	PI_3 0.0±0.3	AsI_3 0.94±0.5	SbI_3 0.83±0.2	

[a] See reference 14.

Microwave measurements have been made of the bond distances in PF_3,[25] AsF_3,[26] PCl_3,[12] and $AsCl_3$,[12] as shown in Table II. One finds the differences in bond distances $d_{As-F}-d_{P-F}=0.161\pm0.011$ and $d_{As-Cl}-d_{P-Cl}=0.118\pm0.007$. If the concept of covalent single bond radii were applicable, these quantities would be identical and equal to $R_{As}-R_P[=0.11]$ whether or not the present table of radii is correct. Furthermore, if a correction for partial ionic character which is linear in the electronegativity difference were applicable,[27] these differences would remain identical and would be equal to

$$R_{As}-R_P-\beta(X_{As}-X_P)[=0.12]$$

whether or not the constant β and the electronegativities are correctly given in the existing tables. The discrepancy between the two differences (0.043±0.018) is in such a direction that the PF bond is shortened more relative to the AsF bond than the PCl bond is shortened relative to the AsCl bond. Since the difference is correctly given by existing tables of radii for the chlorides, it appears that multiple bonding is negligible for the chlorides, but quite significant for PF_3. However, the possible influence of d orbitals and $p-d$ hybridization has not been considered, although this would not be expected to affect the bond distances drastically. Furthermore, the short PF distance may possibly be satisfactorily explained by the reduced repulsive forces to be considered subsequently.

The fact that the fluorides do not appear to have exceptional dipole moments on the meager evidence of Table III, in spite of apparent multiple bonding, probably is due to contributions of structures of the type

$$\begin{matrix} F^+ \\ \| \\ X \\ \diagdown \\ F \end{matrix} \quad F^-, \text{ rather than } \quad X^-—\begin{matrix} F^+ \\ \| \\ F \end{matrix} .$$

The multiple bonds in the group V trifluorides may not be simple double bonds. Pauling[28] gives a formula which enables one to compute the fraction, f, of the double bond character:

$$f=(R_1-R)/(R_1+2R-3R_2), \qquad (2)$$

[21] C. H. Townes and B. P. Dailey, Phys. Rev. **78**, 346 (1950).
[22] N. V. Sidgwick, *Chemical Elements and Their Compounds* (Oxford University Press, New York, 1950), Vol. I, p. 654, and Vol. II, p. 1099.
[23] L. Pauling, *The Nature of the Chemical Bond* (Cornell University Press, Ithaca, New York, 1945).
[24] H. A. Skinner and L. E. Sutton, Trans. Faraday Soc. **40**, 164 (1948).
[25] See reference b of Table II.
[26] See reference c of Table II.
[27] V. Schomaker and D. P. Stevenson, J. Am. Chem. Soc. **63**, 37 (1941).
[28] See reference 2, p. 175.

where R_1 and R_2 are pure single and double bond distances, respectively, and R is the measured bond distance. The values to be used for R_1 and R_2 are not obvious for the molecules under consideration. One might use the sums of the single and double bond radii, or perhaps modify them for partial ionic character according to the formulas of Schomaker and Stevenson[27] and Gordy.[29] There is, however, a further shortening due to the attraction of the F^- and F^+ ions in structures of the type

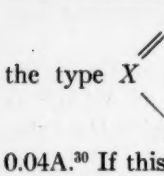

X F^-, estimated by Pauling to be about 0.04A.[30] If this correction were not taken into account, the PF distance would be less than the pure double bond distance. Using all of the above corrections, one finds the following values for the percentage of double bonds: NF—7 percent, PF—83 percent, AsF—40 percent. Values in excess of 33 percent would involve seemingly improbable structures like

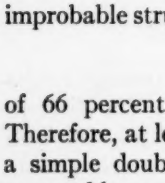

X^- F^-, and values in excess of 66 percent are meaningless for these molecules. Therefore, at least in PF_3, the structure is probably not a simple double bond if the accepted bond radii are reasonably correct.

Furthermore, it may be surprising that NF_3 does not appear to exhibit as much multiple bonding as PF_3.[22] Evidence of some multiple bonding, however, is afforded by a comparison with N_2F_2, where the most probable structure is F—N=N—F, confining the NF linkage largely to a single bond. The NF distance is 1.46A in N_2F_2,[31] as compared to 1.37A in NF_3, indicating considerable multiple bonding in the latter.

Pitzer[32] explains the short bond distances in row 1—row 2 molecules, like PF_3, SiF_4, and P_4O_6 in terms of unusually small repulsive forces between the nonbonding electrons in the valence shells of one atom, with those in the inner shells of the other. He shows this repulsion to be much smaller in row 1—row 2 molecules than in row 1—row 1 molecules. Mulliken[33] gives approximate calculations showing that Pitzer has probably underestimated the outer shell—outer shell repulsions in these molecules, but finds the argument to have some validity. Mulliken attributes the greatly reduced tendency toward the formation of multiple bonds in the second row atoms as compared to the first row atoms, to the greater stability of the single bonds in the former case. It therefore does not seem unreasonable to assume that there is considerable multiple bonding in both NF_3 and PF_3 and that the extremely short bond distance in the latter is due to the reduced repulsive forces pointed out by Pitzer.

On the other hand, the suggestion has also been made that the short bond lengths in these compounds may be due to double bonds utilizing d orbitals, which cannot exist for row 1—row 1 molecules, and may not contribute significantly to the bonds of atoms heavier than those of row 2.[34]

Thus, by comparison with N_2F_2 and by other less direct considerations, the multiple bonding in NF_3 appears to be appreciable. The agreement of the bond distance with that predicted from the Schomaker-Stevenson rule[27,7,35] may be coincidental. Multiple bonding is probably considerable for NF_3 and PF_3, and perhaps also for AsF_3 and NCl_3, but it is not of importance in the other group V trihalides.

VII. NUCLEAR QUADRUPOLE COUPLING

Townes and Dailey have shown that the nuclear quadrupole coupling in molecules is primarily dependent on the manner in which the p orbitals of the valence shell are filled. Their procedure is outlined in reference 15, Chapter VII.

Assuming a fraction η of s character in each of the single bonds and in the σ orbitals of the double bonds, the following numbers of unbalanced p electrons are found for the types of structures considered thus far, using the correction for the formal charge on the X ion suggested in reference 6.

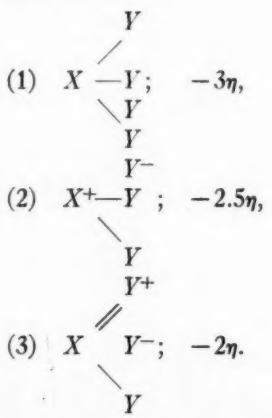

(1) X—Y; -3η,

(2) X^+—Y^-; -2.5η,

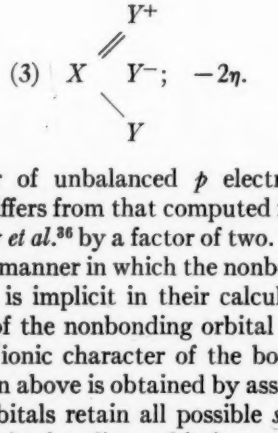

(3) X Y^-; -2η.

The number of unbalanced p electrons given for structure (2) differs from that computed from a formula given by Gordy *et al.*[36] by a factor of two. This difference arises from the manner in which the nonbonding orbitals are treated. It is implicit in their calculation that the hybridization of the nonbonding orbital is not affected by the partial ionic character of the bonding orbitals. The result given above is obtained by assuming that the nonbonding orbitals retain all possible s character not demanded by the bonding orbitals, so that when an electron is partially absent from the bonding orbital

[29] W. Gordy, J. Chem. Phys. **15**, 81 (1947).
[30] See reference 2, p. 234.
[31] S. H. Bauer, J. Am. Chem. Soc. **69**, 3104 (1948).
[32] K. S. Pitzer, J. Am. Chem. Soc. **70**, 2140 (1948).
[33] R. S. Mulliken, J. Am. Chem. Soc. **72**, 4493 (1950).
[34] See reference 15, p. 320.
[35] See reference 15, p. 319.
[36] See reference 15, p. 281.

(partial ionic character) the unused s character is gained by the nonbonding orbital. This assumption is implicit in the treatment of AsF_3 by Townes and Dailey,[6] and seems most reasonable from energy considerations.

In structure (3) it has been assumed that the π orbital of the double bond is perpendicular to the figure axis.

Since η may be estimated from the bond angles of most of the group V trihalides as roughly 0.17, the number of unbalanced p electrons is estimated for the above structures to be -0.51, -0.42, and -0.34, respectively.

For arsenic, the quadrupole coupling for a p-electron is estimated at 600 Mc, but this is subject to a possible error of about 20 percent. For AsF_3, the measured coupling (-236 Mc)[37] is in reasonable agreement with the evidence from the dipole moment that the structure is largely ionic,[6] but a considerable contribution of the double bonded structure is by no means excluded.

The lower coupling in $AsCl_3$ (-173 Mc) indicates less s character in the bonding orbitals than in those of AsF_3. The Cl—As—Cl angle yields 12.8 percent s character in the bonding orbital. If all other factors were the same, the ratio of the quadrupole couplings would indicate that the AsF bonds have 17.4 percent s character, leading to a bond angle of 102°10′, a value which is by no means unreasonable. However, since $AsCl_3$ probably contains more of the single bonded structure (1) than AsF_3, the angle and percentage s character for AsF_3 are both probably somewhat larger than the above estimate.

The arsenic nuclear quadrupole coupling in a closely related compound, AsH_3, is -164 Mc.[38] This value is surprisingly large for the measured bond angle of only 92°[38,39] which would lead one to expect a coupling of about -63 Mc. Hence one must assume either that d orbitals are of importance and affect the bond angles in this particular way, or that the approximation of isolated directed bonds breaks down for this hydride. The latter possibility and some evidence for it in the case of NH_3, where no d hybridization is to be expected, has already been discussed by Townes and Dailey[6] who indicated this type of bond by $N{\equiv}H_3$. The antimony nuclear quadrupole coupling in stibine[38] is also surprisingly low and may be similarly explained.

Townes and Dailey[6] indicate some doubt as to the quadrupole coupling per p electron to be assigned to N^{14}, the possibilities lying between 10 and 24 Mc. The measured bond angle in NF_3 indicates 17 percent s character in bonding orbitals of types considered earlier, leading to the results given in Table IV.

The measured value is close either to structure (1) with a coupling constant of 10 Mc per p electron, or to (3) with 24 Mc per p electron. Structure (1) does not seem very likely, in that it does not involve the expected large amount of multiple bonding discussed earlier. The measured coupling constant is in fact not satisfyingly close to any value obtainable from Table IV. This may indicate that again the amount of $s-p$ hybridization cannot be directly obtained from the bond angles. NF_3 is similar to NH_3 and AsH_3 in having three very short bonds where perhaps the isolated bond approximation is not satisfactory. If 24 Mc per p electron is assumed for N^{14}, the measured coupling constant can be obtained with $\eta=0.08$. AsH_3 requires $\eta=0.09$, a similar amount of hybridization.

TABLE IV. $(eqQ)_{N^{14}}$ in NF_3 [measured value, -7.07 Mc (see reference 7)].

Structure	Of unbalanced p electrons	Quadrupole coupling if 10 Mc per p electron	Quadrupole coupling if 24 Mc per p electron
(1) $X(Y)(Y)(Y)$	−0.52	−5.2 Mc	−12.5 Mc
(2) $X^+(Y^-)(Y)(Y)$	−0.43	−4.3	−10.4
(3) $X(Y^+)(Y^-)(Y)$	−0.35	−3.5	−8.3

Mulliken[33] points out that hydrides are likely to have a multiply bonded structure, which may correspond to that designated $N{\equiv}H_3$, calling this "a sort of hyperconjugation." Arsine and stibine may be further examples of such hydrides, and NF_3 an extension to row 1-row 1 compounds.

Thus the question of which of the two proposed values of the quadrupole coupling for p electron is to be assigned to N^{14} remains in doubt. This is contrary to the conclusion of Sheridan and Gordy,[7] who indicate that structure (2) is the most important one for NF_3, and that the NF_3 quadrupole coupling constant then definitely determines the coupling per p electron of N^{14} to be near 10 Mc.

VIII. CONCLUSION

Dipole moment and bond angle measurements, together with comparisons of the bond distances in group V trichlorides with those of similar methylated compounds[20] indicate that the group V trihalides, with the exception of the fluorides, probably contain hybridized $s-p$ single covalent bonds of about 17 percent s character, and with varying degrees of partial ionic character.

From structural parameters, dipole moments, and quadrupole coupling, AsF_3 appears to be 33 percent ionically bonded,[6] perhaps with some multiple character. From its extremely short bond distance, phosphorus trifluoride appears to be multiply bonded, but other explanations are possible,[27,34] and since the phosphorus nucleus has a spin of one-half, there can be no evidence from quadrupole hyperfine structure as to what form the

[37] See references c and i in Table II.
[38] C. C. Loomis and M. W. P. Strandberg, Phys. Rev. **81**, 798 (1951).
[39] H. H. Nielsen, J. Chem. Phys. **20**, 1955 (1952).

bonds may take. It is suggested from the evidence of nuclear quadrupole hyperfine structure, that for nitrogen trifluoride, arsine, and stibine as well as for ammonia, the approximation of isolated directed valence bonds is not valid.

It is shown that the value to be assigned to the quadrupole coupling per p electron of N^{14} has not been uniquely established by the measurement of the coupling in NF_3 as was previously reported.[7] Thus the estimate of the quadrupole moment of N^{14} from nuclear quadrupole coupling in molecules remains doubtful in the range $0.01-0.03\times10^{-24}$ cm^2.[6]

In conclusion, the author would like to thank Professor B. P. Dailey for helpful discussions and Professor C. H. Townes for his guidance during much of this research.

THE JOURNAL OF CHEMICAL PHYSICS VOLUME 22, NUMBER 1 JANUARY, 1954

Microwave Spectra and Structures of Methyl Mercury Chloride and Bromide*

WALTER GORDY AND JOHN SHERIDAN†
Department of Physics, Duke University, Durham, North Carolina
(Received June 22, 1953)

From the pure rotational spectra of several different isotopic species of CH_3HgCl it is shown that $d_{CH_3}=2.061\pm0.02$A, $d_{HgCl}=2.282\pm0.005$A, and $\angle CHgCl=180°$. Similarly, for CH_3HgBr it is shown that $d_{CH_3}=2.074\pm0.015$A, $d_{HgBr}=2.406\pm0.005$A, and $\angle CHgBr=180°$. Nuclear quadrupole couplings evaluated are $Cl^{35}=-42$ Mc, $Cl^{37}=-33$ Mc in CH_3HgCl, and $Br^{79}=350$ Mc, $Br^{81}=290$ Mc in CH_3HgBr. These indicate ionic character of 62 percent for the HgCl and 55 percent for the HgBr bond in these molecules, and lead to a value of 1.7 to 1.8 for the electronegativity of divalent mercury.

INTRODUCTION

STUDIES of crystal structures,[1] electric dipole moments,[2] and spectra[3] of mercuric derivatives have all indicated that the two covalencies of the mercury atom are oppositely directed in a linear configuration. In addition, a number of such substances have been studied by electron diffraction.[4] When the attached atoms are heavy, as in mercuric iodide, the linear configuration can be approximately established from the patterns, but it has normally been necessary to assume linearity in interpreting these, on account of the reduction in precision caused by the excessive mercury scattering. We have found the pure rotation spectra of methyl mercury chloride and bromide to be characteristic symmetric-top spectra, which shows unquestionably that the C-Hg-Hal configuration is strictly linear. It has also been possible to determine the C-Hg and Hg-Hal distances with good precision and to obtain a value for the effective covalent radius of divalent mercury. The nuclear quadrupole couplings of the halogens obtained from an analysis of the hyperfine structures yield a value for the electronegativity of divalent mercury.

When the work here described was begun, no previous structural studies of methyl mercury halides were known, but an x-ray investigation of the solid chloride[5] has since been stated[6] to indicate the expected axial symmetry of the molecule and a C-Hg bond length in good agreement with the present results. The Hg-Hal distances reported from this x-ray study, however, are not in agreement with the findings from the microwave spectra of the gaseous molecules.

EXPERIMENTAL DETAILS

Methyl mercuric bromide was made by the method of Slotta and Jacobi.[7] Their method for the preparation of methyl mercuric chloride gave a product which contained much bromide, and hence the following method was preferred for preparation of the chloride free from other halides. Methyl mercuric iodide was made by the method of Hinkel and Angel.[8] This was then shaken for 48 hours in alcoholic solution with dry silver chloride, which was renewed until no further deposition of silver iodide occurred. Methyl mercuric chloride was obtained by evaporation of the filtered solution. The samples of the halides used in the microwave studies were recrystallized several times from alcohol and dried in vacuum.

The microwave spectra were observed with a frequency sweep spectrometer having a video type detector described elsewhere.[9] The hyperfine compo-

* This research was supported by the U. S. Air Force under Contract No. AF18(600)-497 monitored by the Office of Scientific Research, Air Research and Development Command.

† Present address: Department of Chemistry, University of Birmingham, Birmingham, England.

[1] H. Braekken and W. Scholten, Z. Krist. **89**, 448 (1934); **81**, 152 (1932).

[2] H. Braune and R. Linke, Z. physik. Chem. **B31**, 12 (1935).

[3] H. S. Gutowsky, J. Chem. Phys. **17**, 128 (1949).

[4] P. W. Allen and L. E. Sutton, Acta Cryst. **3**, 46 (1950).

[5] D. R. Grdenich and A. I. Kitaigorodskii, Zhur. Fiz. Khim. **23**, 1161 (1949).

[6] Chem. Abs. **44**, 1301 (1950).

[7] K. H. Slotta and K. R. Jacobi, J. prakt. Chem. **20**, 272 (1928).

[8] L. E. Hinkel and T. H. Angel, J. Chem. Soc. **1927** (1948).

[9] Gordy, Smith, and Trambarulo, *Microwave Spectroscopy* (John Wiley and Sons, Inc., New York, 1953), p. 6.

nents of a single transition for the different isotopes were measured with a frequency standard calibrated by comparison with the standard 5-Mc signal of Station WWV. The stronger components of several other transitions were measured with a cavity wavemeter.

The substances were allowed to evaporate into the evacuated wave-guide cell at room temperature (25 to 30°C). This should ultimately place in the cell the saturated vapor pressures of the solids, which are known[10] to be 1.6×10^{-2} mm at 27°C in each case. The pressures attained in the cell were, in practice, barely sufficient to allow observation of the spectra at room temperature and were probably somewhat less than the saturated vapor pressures, although they sustained a blue discharge when the glass apparatus was sparked. Nevertheless, a better resolution of the fine structure was sometimes attained by a slight reduction of pressure by pumping the cell.

When methyl mercuric bromide was admitted to the cell, the spectrum of methyl mercuric chloride was usually observed in addition to that of the bromide. This was almost certainly due to the presence, inside the silver waveguide cell, of traces of silver chloride which reacted with vapor of methyl mercuric bromide to

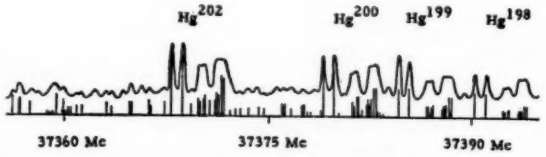

FIG. 1. Calculated and observed pattern of the 8→9 rotational transition of methyl mercury chloride. Theoretical patterns are not plotted for Hg^{201} and Hg^{204}.

produce some of the corresponding chloride. These observations suggest a way in which this reaction between a solid and a gas at low pressure can conveniently be studied. As expected if the above is the case, the spectrum of methyl mercuric bromide is best observed after the guide has been repeatedly treated with the vapor of the bromide to reduce the exposed amount of silver chloride in the cell.

SPECTRAL CONSTANTS

The large number of abundant mercury isotopes combine with the nuclear quadrupole hyperfine structure to make the spectra of mercury methyl bromide and chloride exceedingly complicated. This will be readily apparent from Fig. 1, in which the calculated spectra for the isotopic species $CH_3Hg^{198}Cl^{35}$, $CH_3Hg^{199}Cl^{35}$, $CH_3Hg^{200}Cl^{35}$, and $CH_3Hg^{202}Cl^{35}$ are compared with a section of the observed spectrum. It did not prove possible to unravel the $CH_3Hg^{201}Cl^{35}$ spectrum, and no calculated spectrum for this species is given because the required Hg^{201} quadrupole coupling factor could not be assigned. Several observed lines not

[10] T. Charnley and H. A. Skinner, J. Chem. Soc. **1951** (1921).

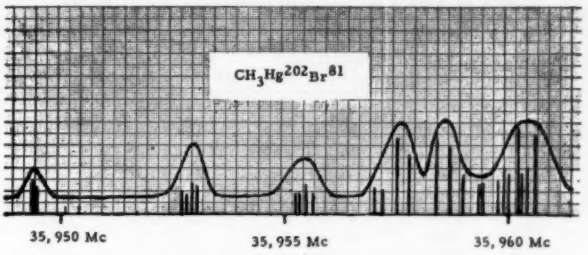

FIG. 2. Calculated and observed pattern of the 15→16 rotational transition of $CH_3Hg^{200}Br^{81}$ for $K\leq6$.

appearing in the calculated spectrum are no doubt due to $CH_3Hg^{201}Cl^{35}$. Others probably arise from molecules in excited vibrational states. The Hg^{201} quadrupole moment is known to be rather large (0.3×10^{-24} cm^2), and it is probable that the $CH_3Hg^{201}Cl$ hyperfine structure is intermingled with that of other isotopes. Even for the closely spaced Cl hyperfine structure it is only at the relatively high J transitions ($\sim J=8\rightarrow9$) that the major Cl hyperfine components of the different species are sufficiently separated for indentification. For CH_3HgBr it was necessary to go to still higher transitions ($\sim J=15\rightarrow16$) to achieve this result. Here a change in Hg of one mass number shifts the transition by about 24 Mc whereas the stronger Br hyperfine components fall within a span of about 15 Mc. Figure 2 shows the observed and theoretical pattern for $CH_3Hg^{200}Br^{81}$ at the saturation vapor pressure for room temperature. The theoretical pattern for $K>6$ is not plotted. The higher K lines lie to the left of the pattern shown and mix to some extent with the lines of the neighboring isotopic species. They are too weak to be observed with the spectrometer employed. The Cl and Br couplings so obtained are not accurate, but the fitting of the observed spectrum is sufficiently good to indicate that they are approximately correct.

In Table I are listed the spectral constants of methyl mercury chloride as determined from the $J=8\rightarrow9$ rotational transition. Table II gives similar constants for methyl mercury bromide obtained from an analysis of the $J=15\rightarrow16$ transition. In each case the ν_0 represents the frequency of the hypothetical pure rotational transition after correction is made for nuclear quadrupole perturbations. The B's were calculated from

TABLE I. Observed spectral constants of CH_3HgCl.

Cl	Hg	ν_0(Mc/sec) $J=8\rightarrow9$	B_0(Mc/sec) (assuming $D_J=0$)	D_{JK}(kc/sec)
35	198	37 394.00	2077.44	21.5
	199	37 388.40	2077.13	21.5
	200	37 382.80	2076.82	21.5
	202	37 371.60	2076.20	21.5
	204	37 360.62	2075.59	21.5
37	198	36 110.53	2006.14	19.5
	199	36 104.30	2005.79	19.5
	200	36 098.07	2005.45	19.5
	202	36 085.75	2004.76	19.5
	204	36 073.62	2004.09	19.5

TABLE II. Observed spectral constants of CH_3HgBr.

Br	Hg	ν_0(Mc/sec) $J=15\rightarrow16$	B_0(Mc/sec) (assuming $D_J=0$)	D_{JK}(kc/sec)
79	198	36 571.55	1142.86	8.2
	199	36 547.33	1142.10	8.2
	200	36 523.48	1141.36	8.2
	202	36 476.28	1139.88	8.2
81	198	36 008.79	1125.28	8.0
	199	35 984.46	1124.51	8.0
	200	35 960.40	1123.76	8.0
	202	35 912.50	1122.27	8.0

the usual symmetric top formula,

$$\nu_0=2B(J+1)-4D_J(J+1)^3-2D_{JK}(J+1)K^2,$$

by neglecting the small constant D_J. It is hoped that the latter constant can be obtained later from measurements in the very short millimeter wave region.

NUCLEAR QUADRUPOLE COUPLINGS

Table III lists the nuclear quadrupole couplings of the halogen nuclei which were obtained from an analysis of the hyperfine structure. From these an estimate of the ionic character of the Hg-Hal bonds can be made. On account of the late position of mercury in the periodic classification, it is not expected that it will form bonds with any significant amount of double bond character and we have therefore assumed that any double bond character present can be neglected. It can also be assumed that bonds are formed with pure p orbitals of the halogen.[11] To a good approximation, it can also be assumed that, in the electronic ground state, the Hg to Hal bond resonates between the covalent and ionic forms, CH_3Hg-Hal and $CH_3Hg^+Hal^-$. In the purely covalent form, the halogen coupling is essentially that of one unbalanced p electron, and in the ionic form it is essentially zero because of the spherical symmetry of the electron cloud around Hal^-. To a first approximation, therefore, one might assume that the actual coupling is the coupling per p electron multiplied by the fractional contribution of the covalent form CH_3Hg-Hal to the ground state. The coupling per unbalanced p electron for Cl^{35} has been determined from atomic beam experiments[12] as -109 Mc. This value with the observed Cl^{35} coupling in CH_3HgCl indicates an ionic character of 62 percent for the HgCl bond. Similarly, the observed Br^{79} coupling in CH_3HgBr with the coupling per unbalanced p electron (770 Mc) observed from atomic beam experiments[13] indicates 55 percent ionic character for the Hg-Br bond. It has been shown that the ionic character as obtained in this way from quadrupole data is related approximately to the electronegativity difference of the two atoms by the simple relation,[11a]

$$\text{ionic character}\approx(x_A-x_B)/2.$$

Since the electronegativity (x) values for Cl and Br are known to be 2.8 and 3.0, this relation allows the determination of the electronegativity value of divalent Hg from the quadrupole coupling data. The values thus obtained are 1.8 from CH_3HgCl and 1.7 from CH_3HgBr. They are in agreement with the values 1.7 to 1.9 estimated for divalent Hg from a relation[14] between force constant and electronegativity applied to $Hg(Hal)_2$ molecules and with the value 1.8 obtained by Haissinsky[15] from data on heats of reaction.

TABLE III. Halogen quadrupole couplings.

	Nucleus	eQq(Mc/sec)
CH_3HgCl	Cl^{35}	-42
	Cl^{37}	-33
CH_3HgBr	Br^{79}	$+350$
	Br^{81}	$+290$

TABLE IV. Molecular structures.

CH_3HgCl	$d_{CH_3}=2.061\pm0.02$A	with $d_{CH}=1.10$A and $\angle HCH=110°42'$ assumed
	$d_{HgCl}=2.282\pm0.005$A, $\angle CHgCl=180°$	with no assumptions
CH_3HgBr	$d_{CH_3}=2.074\pm0.015$A	with $d_{CH}=1.10$A and $\angle HCH=110°42'$ assumed
	$d_{HgBr}=2.406\pm0.005$A, $\angle CHgBr=180°$	with no assumptions

MOLECULAR STRUCTURES

The molecular dimensions obtained are given in Table IV. No assumed parameters are involved in the determination of the mercury-halogen distance. This distance is obtained unambiguously from the moments of inertia of the different isotopic forms. Simplified formulas for these calculations are given elsewhere.[16]

The carbon-mercury distances are calculated with the configuration of the methyl group assumed to be close to that found in the methyl halides and similar substances. This configuration does not vary appreciably from molecule to molecule, and the value of d_{C-Hg} is not greatly dependent on reasonable variations in the assumed parameters, but further uncertainties arise from the fact that slight inconsistencies in the data, partly at least connected with small isotopic shifts of the mercury substitutions, are reflected, with this method of calculation, chiefly as variations in d_{C-Hg}. The errors quoted, however, are believed to be sufficient to include possible errors in both assumptions and measurements.

[11] (a) W. Gordy, J. Chem. Phys. **19**, 792 (1951). (b) R. Livingston, J. Chem. Phys. **19**, 803 (1951).
[12] V. Jaccarino and J. G. King, Phys. Rev. **83**, 471 (1951).
[13] V. Jaccarino and J. G. King, North Carolina Meeting, American Physical Society, 1953.
[14] W. Gordy, J. Chem. Phys. **14**, 305 (1946).
[15] M. Haissinsky, J. phys. et radium **7**, 7 (1946).
[16] See reference 4, p. 301.

More precise determination of d_{C-Hg} will be possible from measurements of spectra of species containing C^{13}. Through the lines were too weak for such spectra to be observed with C^{13} in natural abundance, it is hoped that studies will ultimately be made with enriched samples.

No precise masses for the mercury atoms are known, and it was necessary to estimate the most probable values from the packing-fraction curves for atoms in the immediate vicinity of mercury.[17] It should be mentioned, however, that uncertainties arising from this are of relatively small importance.

From the fact that the several different transitions which were observed fall into harmonic series, it is evident that CH_3HgCl and CH_3HgBr are strictly symmetric tops, i.e., the CHgHal configuration is linear. Evidently the bonding orbitals are

$$\psi_1 = 1/\sqrt{2}(\psi_{6s}+\psi_{6p})$$
$$\psi_2 = 1/\sqrt{2}(\psi_{6s}-\psi_{6p}).$$

The lobes of these two sp hybrids are oppositely directed in agreement with the Hg bond angles.

From a consideration of the interatomic distances obtained in the present study as well as data on other molecules, Gordy, Smith, and Trambarulo[18] have assigned the value of 1.34A to the sp hybridized covalent radius of Hg. Furthermore, from a consideration of a large number of molecular studies with microwave spectroscopy they revised downward from 0.09 to 0.06 the value of the constant β in the Schomaker-Stevenson equation.[19] In Table V the present observed bond lengths are compared with those calculated from the revised Schomaker-Stevenson rule

$$d_{AB} = r_A + r_B - 0.06|x_A - x_B|.$$

The Hg radius is taken as 1.34A and x_{Hg} as 1.8. In the same table comparisons with the mercury di-halides are made.

The general agreement is good. Mention should, however, be made of the importance in this connection of an accurate determination of the Hg−C bond distance in mercury dimethyl. Electron diffraction data[4] have been interpreted to indicate a value in this molecule somewhat greater than that found for d_{Hg-C} in the methyl mercury halides. It would appear, however, that the precision of these rather early measurements of mercury dimethyl is not sufficient to prove this point beyond doubt, and a reinvestigation would be valuable.[20] Also relevant are the recent thermochemical studies by Skinner and co-workers,[21] which show that the Hg−C bond in the methyl mercury halides is less easily dissociated than the Hg−C bonds in mercury dimethyl. For comparison with distance data the bond energies are needed, and these cannot be allocated so readily as the heats of dissociation. If, however, it is assumed that the heats of formation of Hg−Hal bonds in the methyl mercury halides are the same as those in the mercury dihalides, as is supported by the similarity of their lengths, the heats of formation computed for Hg−C appear likely to be a few kcal/mole more for bonds in methyl mercuric halides than for those in mercury dimethyl. Since the heat of formation of C−Hg is small (not over 30 kcal/mole[22]) such a difference might correspond to a measurable difference in length. The uncertainty regarding the equality of Hg−Hal bond energies, however, and the possible errors inherent in computations of this type, do not allow certainty in this conclusion. Since, moreover, the force constants found for the Hg−C stretching mode in mercury dimethyl[23] favor stronger bonds than otherwise anticipated and have evoked consideration of the possibility of hyperconjugation of the methyl groups, we regard the problem of the relation of the structure of mercury dimethyl to the present results as indeterminate at the present time. Should it ultimately be proved that d_{C-Hg} exceeds 2.1A in mercury dimethyl, this would favor a somewhat larger mercury bond-radius than that used here.

TABLE V. Comparison of bond lengths in some mercury halides.

Molecule	Bond	Distance in A Observed	Calculated[a]
CH_3HgCl	CHg	2.06	2.09[c]
	HgCl	2.28	2.26
CH_3HgBr	CHg	2.07	2.09[c]
	HgBr	2.40	2.42
$HgCl_2$	HgCl	2.28[b]	2.26
$HgBr_2$	HgBr	2.43[b]	2.42
HgI_2	HgI	2.61[b]	2.63

[a] Calculated with $d_{AB} = r_A + r_B - 0.06|x_A - x_B|$, with $r_{Hg} = 1.34$A and $x_{Hg} = 1.8$.
[b] From electron diffraction review by Allen and Sutton, Acta Cryst. 3, 46 (1950).
[c] The radius used here for carbon is 0.79A. A better fitting value, 2.07, is obtained with the Pauling value of r_C of 0.77A.

[17] We are grateful to Dr. H. E. Duckworth for a discussion of the probable values of the mercury masses.
[18] See reference 4, p. 308.
[19] V. Schomaker and D. P. Stevenson, J. Am. Chem. Soc. 63, 37 (1941).
[20] We are indebted to Dr. L. E. Sutton for a discussion of the electron diffraction data on mercury dimethyl.
[21] Hartley, Pritchard, and Skinner, Trans. Faraday Soc. 46, 1019 (1950).
[22] N. V. Sidgwick, *The Chemical Elements and their Compounds* (Oxford University Press, London, 1950), p. 300.
[23] H. S. Gutowsky, reference 3, and J. Am. Chem. Soc. 71, 3194 (1949).

Ion-Exchange and Adsorption Column Kinetics with Uniform Partial Presaturation

THEODORE VERMEULEN AND NEVIN K. HIESTER*
Division of Chemical Engineering, University of California, Berkeley 4, California
(Received July 28, 1953)

The available mathematical solutions for fixed-bed concentration histories apply primarily to one-component systems in adsorption and to two-component systems in ion exchange. Thomas has developed explicit general relations for the saturation of an adsorbent bed initially free of saturating component by a fluid phase containing only this component; as well as for the converse elution situation.

These results are extended here to cases of mixed binary feeds (in ion exchange), and cases of columns that are uniformly partially saturated prior to the run under study. New definitions of the dimensionless parameters that characterize the sorption processes render the existing numerical framework applicable for evaluating this broadened range of operating conditions. From the theoretical standpoint, these new parameters clarify the mathematical interrelationships between adsorption and ion exchange, between saturation and elution, and between sorption of trace components and sorption of gross or bulk components. A method is suggested for calculating physical-adsorption operations which do not conform to Langmuir isotherms.

Calculation procedures based upon this approach are illustrated by an idealized but representative example.

THE most general calculation method that has become available for prediction and interpretation of adsorption column performance is that of Thomas[1] which is based upon reversible second-order reaction kinetics as an approximation to the diffusional processes actually involved. The present authors have presented Thomas's result in graphical form,[2,3] and have shown its applicability for ions of unequal valence; its inclusion of the constant-pattern, linear, and unfavorable equilibrium conditions as special cases;[2,4] and its utilization in trace chromatography.[5,6]

Recently Opler and Hiester[7] have obtained extensive tables of numerical solutions to Thomas's equations, by punched-card calculation. This paper will show how the available solutions can be used in a more complicated situation which has not previously been solved explicitly. Analysis of this situation will also serve to clarify the interrelation between the theories for ion exchange and for physical adsorption.

Thomas's result has greater generality than that of other analyses because of his provision for a full range of variation of both the rate constant and the mass-action equilibrium constant for the sorption process. So far, it has been applied mainly to two-component ion exchange systems in which a fluid containing only one component interacts with a solid phase containing initially only the other component; or to one-component adsorption systems involving solid that initially is entirely free of adsorbed material. However, Thomas[4] also showed that elution from a completely saturated bed and saturation of a completely eluted bed are complementary processes, each of which has an equilibrium constant that is the reciprocal of the constant for the other. Amundson[8] has extended Thomas's methods to obtain an algebraic framework for numerical integration of the binary case in which the initial solid-phase composition varies with position in the column, and the feed composition varies with time (but also under the restriction of constant total flow rate). However, derivation of the present results from Amundson's solution framework is not direct or obvious, even in the simplest special case of linear equilibrium.

A derivation somewhat similar to the following one for ion exchange was obtained independently by Nelson.[9]

The problem to be considered is of intermediate complexity. The initial solid-phase and entering fluid-phase compositions are each to be uniform (independent of position or time, respectively), but may each involve any desired proportion of the component of interest (component A).

ION-EXCHANGE SATURATION

This process is governed by the rate equation,

$$\left(\frac{\partial q_A}{\partial \tau}\right)_h = k\left[c_A q_B - \frac{1}{K} q_A c_B\right]$$

$$= k\left[c_A(Q-q_A) - \frac{1}{K} q_A (C_0 - c_A)\right], \qquad (1)$$

* Present address: Stanford Research Institute, Stanford, California.

[1] H. C. Thomas, J. Am. Chem. Soc. **66**, 1664 (1944).

[2] N. K. Hiester and T. Vermeulen, Chem. Eng. Progr. **48**, 505 (1952).

[3] Hiester, Radding, Nelson, and Vermeulen, paper submitted to Chem. Eng. Progr.

[4] See also H. C. Thomas, Ann. N. Y. Acad. Sci. **49**, 161 (1948); E. R. Gilliland and R. A. Baddour, Ind. Eng. Chem. **45**, 330 (1953).

[5] N. K. Hiester and T. Vermeulen, J. Chem. Phys. **16**, 1087 (1948).

[6] T. Vermeulen and N. K. Hiester, Ind. Eng. Chem. **44**, 636 (1952).

[7] A. Opler and N. K. Hiester, "Tables for Predicting Performance of Fixed-Bed Ion Exchange," Stanford Research Institute (1954).

[8] N. R. Amundson, J. Phys. Colloid Chem. **54**, 812 (1950).

[9] H. W. Nelson, Ph.D. thesis in chemical engineering, University of Wisconsin (1949).

where c_A, c_B=concentration of A (or B) in the fluid phase at a particular point; q_A, q_B=concentration of A (or B) in the solid phase at the same point; C_0=concentration of total solute in the fluid phase. (This replaces the symbol c_0 used in references 2 and 6); Q=total sorbent capacity (exchange capacity) of the solid phase; k=kinetic rate constant. As discussed elsewhere,[2,3] k can be related to $(k_F a_F)$ and $(k_P a_P)$, the external and internal diffusional rate constants; $K(=K^{II})$=mass-action constant for equilibrium between exchanging ions that have the same valence; τ=time measured from start of run; h=height or length of column. This equation may be transformed into one containing only dimensionless variables:

$$\left(\frac{\partial y}{\partial t}\right)_s = x_A(1-y_A) - r y_A(1-x_A), \tag{2}$$

where $x_A=c_A/C_0$; $y_A=q_A/Q$; $r=1/K$, the equilibrium parameter; $t=kC_0(\tau-vf_E/R)$, the "solution-capacity" parameter; $s=kQ\rho_b v/R$, the "column-capacity" parameter, and where v=packed volume of resin in the column; f_E=fraction of voids in the column, external to the resin particles; R=volumetric flow rate of solution through the column; and ρ_b=bulk density of resin as packed in the column. It is solved in combination with the material-balance relation

$$\left(\frac{\partial y}{\partial t}\right)_s = -\left(\frac{\partial x}{\partial s}\right)_t \tag{3}$$

to give solutions of the form $x=x(r,s,t)$ and $y=y(r,s,t)$. The exact form of the functions is given in Eqs. (23) and (24) of reference 2. These results are based upon a pure A solution interacting with a pure B resin, and hence are bounded by $0\leq x\leq 1$, $0\leq y\leq 1$.

In a column that is uniformly presaturated with component A to any specified level (for example, by mixing A-resin and B-resin; or by saturating completely with a solution containing both A and B ions), the initial concentration $(q_A)_0$ corresponds to an equilibrium concentration $(c_A)_0{}^*$ in the solution phase at a given total solution concentration C_0. With a feed at $(c_A)_0$, only the amount $[(c_A)_0-(c_A)_0{}^*]$ will be removed from each unit volume of solution under the most favorable conditions. Likewise, if $(q_A)_0{}^*$ is the resin concentration that would be in equilibrium with feed solution at $(c_A)_0$, the resin at most will accumulate only $[(q_A)_0{}^*-(q_A)_0]$ moles of A per unit weight. The equilibrium relations between c_A and q_A are obtained from Eq. (1) by setting the rate equal to zero; there results

$$\frac{(q_A)_0{}^*}{Q} = (y_A)_0{}^* = \frac{K(c_A)_0}{(K-1)(c_A)_0+C_0} = \frac{K(x_A)_0}{(K-1)(x_A)_0+1}. \tag{4}$$

A relation of similar form evidently exists between $(y_A)_0$ and $(x_A)_0{}^*$.

In order to utilize the saturation functions derived for pure feed and pure resin we define a solution saturation-fraction,

$$\lambda = \frac{c_A-(c_A)_0{}^*}{(c_A)_0-(c_A)_0{}^*} = \frac{x_A-(x_A)_0{}^*}{(x_A)_0-(x_A)_0{}^*} \tag{5^B}[10]$$

and a resin saturation-fraction,

$$\omega = \frac{q_A-(q_A)_0}{(q_A)_0{}^*-(q_A)_0} = \frac{y_A-(y_A)_0}{(y_A)_0{}^*-(y_A)_0}, \tag{6^B}$$

where

$$(x_A)_0=(c_A)_0/C_0, \quad (x_A)_0{}^*=(c_A)_0{}^*/C_0,$$
$$(y_A)_0=(q_A)_0/Q, \quad (y_A)_0{}^*=(q_A)_0{}^*/Q.$$

The numerical solutions for $\lambda=\lambda(r,s,t)$ and $\omega=\omega(r,s,t)$ will correspond exactly to those derived for x and y, if the parameters r, s, and t can be redefined so that λ and ω, respectively, will replace x and y in Eqs. (2) and (3) and will obey, as they do, the saturation boundary conditions:

$$\left(\frac{\partial \omega}{\partial t}\right)_s = \lambda(1-\omega) - r\omega(1-\lambda) = -\left(\frac{\partial \lambda}{\partial s}\right)_t. \tag{7^B}$$

The new defining equations can be obtained by modifying Eq. (1) so as to incorporate λ and ω, and then comparing the respective coefficients of the λ, ω, and $\lambda\omega$ terms. This leads to the relations:

$$r = \frac{(K-1)(c_A)_0{}^*+C_0}{(K-1)(c_A)_0+C_0} = \frac{(K-1)(x_A)_0{}^*+1}{(K-1)(x_A)_0+1} \tag{8^B}$$

and

$$t = \frac{k}{K}[(K-1)(c_A)_0+C_0](\tau-vf_E/R),$$
$$= \frac{kC_0}{K}[(K-1)(x_A)_0+1](\tau-vf_E/R). \tag{9^B}$$

Incorporating ω and λ into Eq. (3) leads also to

$$s = \frac{kQ\rho_b C_0}{(K-1)(c_A)_0{}^*+C_0}\cdot\frac{v}{R} = \frac{kQ\rho_b}{(K-1)(x_A)_0{}^*+1}\cdot\frac{v}{R}. \tag{10^B}$$

It will be seen that Eqs. (7) through (10) include the definitions for r, s, and t in the case where $(c_A)_0{}^*=0$ and $(c_A)_0=C_0$, as given following Eq. (2). Under these conditions, Eq. (5) indicates that λ reduces to x; and, by Eq. (6) with $(q_A)_0=0$ and $(q_A)_0{}^*=Q$, ω reduces to y.

[10] The superscript B (for "binary") will be used to identify equations which apply expressly to partial-presaturation conditions and mixed feeds.

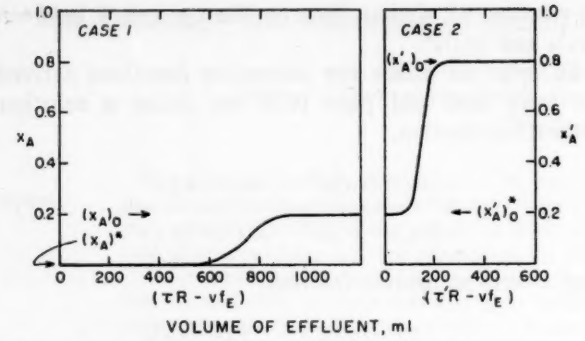

FIG. 1. Saturation curves at two levels of feed concentration. Case 1, solid phase initially empty. Case 2, solid phase initially partly saturated. Column void volume, 50 ml.

Also, Eqs. (5)–(10) are equally applicable to negative ranges of $[(c_A)_0-(c_A)_0^*]$.

The physical significance of the foregoing treatment can best be illustrated by considering the concentration history curves for some sample cases. The usual way of obtaining uniform partial saturation of a column is by treating a fixed bed, initially free of A, with a feed containing both A and B. This case will be illustrated numerically. Suppose that

$$(c_A)_0/C_0=0.2=(x_A)_0$$
$$(q_A)_0/Q=0=(y_A)_0,$$

and that the system and column variables are

$$K=6$$
$$kC_0/R=0.12\ \text{ml}^{-1}$$
$$Q\rho_b/C_0f_E=5$$
$$vf_E=50\ \text{ml}.$$

From the equilibrium relation, Eq. (4),

$$(x_A)_0^*=0$$
$$(y_A)_0^*=0.6.$$

Thus, from Eq. (5),

$$x_A=(x_A)_0\lambda=0.2\lambda.$$

Calculation of r, s, and t from Eqs. (8)–(10) shows that

$$r=0.5$$
$$s=30$$
$$t=0.04(\tau R-vf_E);\quad \text{or}\quad (\tau R-vf_E)=25t,$$

the volume of effluent. The numerical solution of $\lambda(r,s,t)$ for these values of the parameters can be obtained from the tables of Opler and Hiester,[7] or less precisely from the graphical solutions.[2] For instance, at the given r and s, with $t=30$, or $(\tau R-vf_E)=750$ ml, the tables show $\lambda=0.501$ and therefore $x_A=0.100$. The complete concentration history for this example is shown in Fig. 1 as Case 1.

This uniformly partially saturated column can be treated with a different mixed feed to obtain another saturation level, either higher or lower in A content than before. Case 2 in Fig. 1 will consider a feed that is higher in A content. Let the system and column variables be the same as before; also,

$$(y_A')_0=0.6=(y_A)_0^*\ \text{for Case 1}$$
$$(x_A')_0=0.8.$$

The primes denote the second case. Use of Eqs. (4) and (5) now gives

$$(x_A')_0^*=0.2=(x_A)_0\ \text{for Case 1}$$
$$(y_A')_0^*=0.96,$$

and

$$x_A'=[(x_A')_0-(x_A')_0^*]\lambda'+(x_A')_0^*$$
$$=0.6\lambda'+0.2.$$

The dimensionless parameters are

$$r'=0.4$$
$$s'=15$$
$$t'=0.1(\tau' R-vf_E),$$

so that

$$(\tau' R-vf_E)=10t'.$$

The concentration history calculated from these values is shown in Fig. 1. The shapes of saturation curves can thus be related quantitatively to differences in the presaturation condition of the resin and in the feed composition.

GAS-ADSORPTION SATURATION

This process can often be assumed to conform to the Langmuir rate equation,

$$\left(\frac{\partial q_A}{\partial \tau}\right)_h=k\left[c_A(Q-q_A)-\frac{1}{K^{ad}}q_A\right],\qquad(11)$$

where K^{ad} = equilibrium constant for a Langmuir isotherm and the other variables have comparable definitions to those given following Eq. (1). This relation transforms to

$$\left(\frac{\partial q_A}{\partial \tau}\right)_h=k\left[\frac{1+K^{ad}(c_A)_0}{K^{ad}(c_A)_0}\right]\left[c_A\{(q_A)_0^*-q_A\}-\frac{1}{1+K^{ad}(c_A)_0}q_A\{(c_A)_0-c_A\}\right].\qquad(12)$$

For the simple case of initially empty adsorbent, i.e., with $(q_A)_0=0$, Eq. (12) takes the form of Eq. (2) and the same numerical solutions can be used, provided the dimensionless variables are defined in the following

manner:

$$x_A = c_A/(c_A)_0$$

$$y_A = q_A/(q_A)_0{}^*$$

$$r = 1/\{1+K^{ad}(c_A)_0\}$$

$$l = k(c_A)_0\left[\frac{1+K^{ad}(c_A)_0}{K^{ad}(c_A)_0}\right]\left(\tau - \frac{vf_E}{R}\right)$$

$$s = kQ\rho_b v/R.$$

The results for physical adsorption can be extended to the case of uniform partial presaturation of the column, in the same way as for ion exchange. As before, the general rate relation is given by Eqs. (5)–(7). It is simplest to utilize the results for the corresponding case of ion exchange by substituting $(1+K^{ad}(c_A)_0)$ for K, and $(c_A)_0$ for C_0, to indicate probable expressions for adsorption which can then be confirmed by algebraic trial.

Use of Eqs. (8) – (10), in conjunction with the definitions following Eq. (12) which apply in the limiting case of $(q_A)=0$ and $c_A{}^*=0$, leads to

$$r = \frac{1+K^{ad}(c_A)_0{}^*}{1+K^{ad}(c_A)_0} \tag{13^B}$$

$$s = \frac{kQ\rho_b v/R}{1+K^{ad}(c_A)_0{}^*} \tag{14^B}$$

$$l = k(c_A)_0\left[\frac{1+K^{ad}(c_A)_0}{K^{ad}(c_A)_0}\right]\left(\tau - \frac{vf_E}{R}\right). \tag{15^B}$$

These definitions suffice to make the algebraic,[1,2] graphical,[2] and tabulated numerical[7] solutions of the second-order-rate equation available for Langmuir-type adsorption with uniform partial saturation of the adsorbent. Thus Fig. 1 equally well describes this case.

ADSORPTION AS AN "EXCHANGE" PHENOMENON

In the foregoing calculation, the results for ion-exchange are seen to represent an idealized system of two adsorbable components and an inert fluid carrier, with a fixed concentration of total solutes in the solid phase and also in the fluid phase. Likewise, the results for adsorption apply to a system with only one adsorbable component in an inert fluid carrier; here the solid-phase concentration has a limiting value that is related to the entering fluid-phase concentration by a Langmuir equilibrium isotherm. A method will now be outlined whereby second-order kinetics (with its basis in the diffusional mechanisms) may be utilized for adsorption operations that do not conform to a Langmuir isotherm.

First, it can be shown that Langmuir adsorption corresponds to a particular instance of "exchange adsorption." In order to establish this correspondence, it is necessary to suppose that the empty sites on the adsorbent are fully occupied by an imaginary component B. This component will have an initial concentration $(c_B)_0$, which will contribute to a hypothetical total concentration $C_0(=(c_A)_0+(c_B)_0)$ of adsorbable material in the fluid feed. The equilibrium relation in the Langmuir case is, from Eq. (11),

$$\frac{(q_A)_0{}^*}{(c_A)_0[Q-(q_A)_0{}^*]} = K^{ad}. \tag{16}$$

The corresponding relation for "exchange adsorption" is, from Eq. (1),

$$\frac{(q_A)_0{}^*}{(c_A)_0[Q-(q_A)_0{}^*]} = \frac{K}{C_0-(c_A)_0}. \tag{16a}$$

As has been noted, the mathematical solutions for exchange and for Langmuir adsorption correspond if $K=1+K^{ad}(c_A)_0$, or hence if $K^{ad}=(K-1)/(c_A)_0$. Under these conditions,

$$C_0 = 2(c_A)_0 + \frac{1}{K^{ad}} = \frac{(2K-1)(c_A)_0}{K-1} \tag{17}$$

or

$$(c_B)_0 = \frac{1+K^{ad}(c_A)_0}{K^{ad}} = \frac{K}{K^{ad}}. \tag{17a}$$

Many types of adsorption which do not follow a Langmuir isotherm should still prove amenable to an "exchange adsorption" method of calculation, but with different assumptions regarding the precise behavior of the unoccupied sites. Particularly in adsorption from the liquid phase, the sites not filled by solute may readily be occupied by the solvent, so that competition for the sites becomes a reality.

In order for the equations of "exchange adsorption" to apply, it is necessary only that K and C_0 in Eq. (1)—and also Q if an experimental value is lacking—be selected to describe the change in driving force for adsorption that results from changes in q_A and c_A.

The driving force is determined by the differences between the local concentration in each phase and the concentration that phase would assume if it were in equilibrium with the actual concentration of coexisting phase. The selection of appropriate K, Q, and C_0 values involves curve-matching of the experimental adsorption isotherm with all possible theoretical isotherms for "exchange adsorption," as given by Eq. (15a) and plotted in Fig. 2.[11] The procedure is to plot the q_A (or q_A/Q) *vs* c_A (or c_A/C_0) isotherm on logarithmic coordinates, and to match the resulting curve against the master plot.

[11] Figure 2 offers a method of evaluating K[11] for the case of ion exchange between ions of unequal valence that is alternative to the procedure suggested in reference (2).

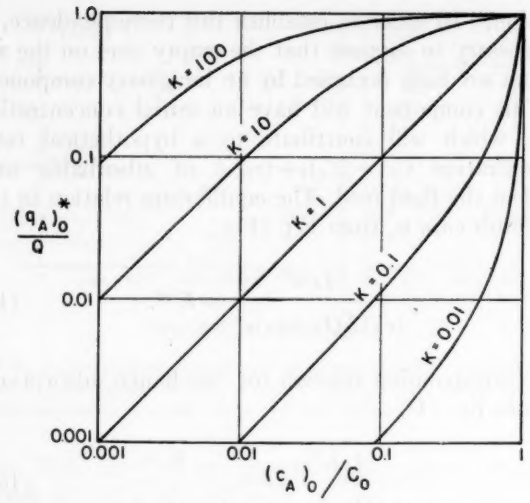

FIG. 2. Dependence of isotherms upon equilibrium constant K (or K^{II}), for ion exchange or "exchange adsorption."

The experimental isotherm in terms of q_A *vs* c_A can be adjusted horizontally (if C_0 is not specified) and/or vertically (if Q is not specified), over the master plot drawn to the same scale. Division of any q_A value by the corresponding q_A/Q, and of c_A by the corresponding c_A/C_0, gives directly the apparent values of Q and C_0.

Adsorption isotherms corresponding to the Langmuir equation will be similar in shape to the "exchange" isotherms for $K \gg 1$. For gas-phase adsorption from an inert carrier component, the "exchange adsorption" treatment should be used only if the true isotherm deviates markedly from Langmuir behavior.

When the effective values of Q and C_0 are purely empirical, rate constants evaluated empirically should be used in preference to those evaluated from diffusional principles, because of possible systematic errors. However, the diffusional theory will still be useful to estimate relative (or extrapolated) values of the rate constants under varying flow conditions.

LIMITING CASES

The theory for partially presaturated columns serves to unify the calculation methods for exchange adsorption and Langmuir adsorption, by including within its framework several situations which, in the absence of this framework, have had to be solved separately as isolated problems. These situations are those of elution of a completely saturated column, saturation and chromatography of trace components (the trace-linear-equilibrium situation), and the simplification of the exchange-adsorption equations in the bulk linear-equilibrium case which is relatively unrelated to the trace-linear situation.

Elution from a Completely Saturated Column

This case corresponds to $(c_A)_0=0$, $(c_A)_0^*=C_0$. The parameters will be designated by $(^+)$ to distinguish them from the saturation case. For ion-exchange, Eqs. (8) to (10) give

$$r^+=K=\frac{1}{r} \tag{18}$$

$$t^+=(k/K)C_0(\tau-vf_E/R)=rt \tag{18a}$$

$$s^+=(k/K)Q\rho_b v/R=rs, \tag{18b}$$

where r, t, and s for saturation have the values given following Eq. (2). For adsorption, Eqs. (13 to 15) give

$$r^+=1+K^{ad}(c_A)_0^*=\frac{1}{r} \tag{19}$$

$$t^+=(k/K^{ad})(\tau-vf_E/R)=rt \tag{19a}$$

$$s^+=\frac{kQ\rho_b v/R}{1+K^{ad}(c_A)_0^*}=rs. \tag{19b}$$

Here $(c_A)_0^*$ is the feed concentration in the period of complete saturation that precedes the elution, and r, t, and s are given following Eq. (12). These results are well known from Thomas's work,[4] but serve to confirm the correctness of the present uniform-partial-saturation theory.

Behavior of Trace Components

The trace situation represents a linear equilibrium, because of the small extent of saturation of the adsorbent by the trace component (A). For ion exchange, with $c_A \ll C_0$, it follows that $C_0=c_A+c_G\approx c_G$, where c_G is the concentration of the gross or carrier ion. For adsorption, $K^{ad}(c_A)_0 \ll 1$. In both processes, generally $(c_A)_0^*=0$, although this limitation is not a necessary one and either Eq. (2) or (7) is applicable. There results

$$r=\frac{C_0}{(K-1)(c_A)_0+C_0} \quad \text{or} \quad \frac{1}{1+K^{ad}(c_A)_0}$$

$$\approx 1 \tag{20}$$

$$t\approx\frac{kC_0}{K}\left(\tau-\frac{vf_E}{R}\right) \quad \text{or} \quad \frac{k}{K^{ad}}\left(\tau-\frac{vf_E}{R}\right)$$

$$\approx\frac{kQ\rho_b}{\mathbf{D}_A f_E}\left(\tau-\frac{vf_E}{R}\right), \tag{20a}$$

since, in either case, $\mathbf{D}_A=(q_A)_0^*\rho_b/(c_A)_0 f_E$ and

$$s=kQ\rho_b v/R. \tag{20b}$$

The practical application of these equations has been dealt with in detail elsewhere.[6]

Linear Equilibrium for Bulk Exchange

This case corresponds simply to $K=1$, for which Eqs. (8)–(10) convert to

$$r=1 \tag{21}$$

$$t=kC_0(\tau-vf_E/R) \tag{21a}$$

$$s=kQ\rho_b v/R, \tag{21b}$$

so that the simplest relations for these parameters apply, even with partial presaturation. This case has no counterpart in Langmuir adsorption; if, in Fig. 2, the curve for $K=100$ is considered to approach a Langmuir isotherm, it is seen that it becomes linear only in the trace region.

This comparison emphasizes the utility of the dimensionless parameters to express the solutions of the governing differential equations. The present treatment for varying levels of saturation is seen to possess a generality that includes the usually encountered situations as special cases.

THE JOURNAL OF CHEMICAL PHYSICS VOLUME 22, NUMBER 1 JANUARY, 1954

Effects of Temperature Gradients, Self-Absorption, and Line Shape on Apparent Rotational Temperatures of OH*

B. H. Elliott† and S. S. Penner
Guggenheim Jet Propulsion Center, California Institute of Technology, Pasadena, California

(Received April 3, 1953)

The effect on apparent rotational temperatures (of OH) of adjacent radiating and absorbing regions at different temperatures and of spectral line shape, coupled with varying degrees of self-absorption, has been studied. The calculations emphasize the fact that definitive conclusions regarding interpretation of flame spectra are difficult to obtain by use of conventional low-resolution spectroscopic studies of flames. Multiple path experiments, or absorption studies with a discrete line source, appear promising provided they are restricted to conditions under which the spectral line shape is known.

In earlier publications the influence of spectral line shape[1] and of self-absorption[1,2] on apparent rotational temperatures of OH has been studied. It is the purpose of the present calculations to amplify the conclusions drawn previously, particularly as regards distortion produced by adjacent radiating and absorbing regions at different temperatures.

I. EFFECT OF LINE SHAPE AND OF SELF-ABSORPTION ON THE USE OF THE ISOINTENSITY METHOD[3] FOR ISOTHERMAL SYSTEMS

According to the isointensity method the temperature of a radiator is obtained from a comparison of two spectral lines which are of equal intensity. Let $A(a,K)$ be the total intensity of the line identified by the index K. The line shape for combined Doppler and collision broadening is described by the parameter

$$a=(b_N+b_C)(\ln 2)^{\frac{1}{2}}/b_D, \tag{1}$$

where b_N, b_C, and b_D denote, respectively, the natural, the collision, and Doppler half-widths. In general $b_N \ll b_C$ and $a \simeq 0$ for pure Doppler broadening. The effect of line shape, under isothermal conditions, on the use of the isointensity method may be determined by evaluating the ratio $A(a,K)/A(a,K')$.[4] The result can be obtained most conveniently by using the "curves of growth."[5]

The results for $K'=1$ of representative calculations at 3000°K for the P_1-branch, (0,0) band, $^2\Sigma \rightarrow {}^2\Pi$ transitions of OH are plotted in Figs. 1 and 2 for $a=0.005$, and $a=2$, respectively. The self-absorption parameter ϵ' refers to the value of $1-\exp(-P_{\max}X)$ for the first line of the P_1 branch.[4] In order to illustrate the combined effects of line shape and self-absorption on lines of equal intensity, from which conclusions might be drawn concerning the "temperature," the results listed in Table I may be consulted. In Table I the lines of intensity closest to the intensities of the lines with $K=3$ and $K=6$ have been tabulated for different values of ϵ' and of a. Reference to the data shown in Table I indicates a large effect of ϵ' for small a, but the results are quite insensitive to ϵ' for large a. Hence the conclusion is reached that self-absorption errors become more im-

* Supported by the U. S. Office of Naval Research under Contract Nonr-220(03), NR 015-210.

† This article is based, in part, on a thesis submitted by Lt. Colonel Elliott to the Graduate School of the California Institute of Technology, in partial fulfillment of requirements for the degree of Aeronautical Engineer, June, 1953.

[1] S. S. Penner, J. Chem. Phys. **21**, 686 (1953).

[2] S. S. Penner, J. Chem. Phys. **21**, 31 (1953).

[3] G. H. Dieke and H. M. Crosswhite, *The Ultraviolet Bands of OH, Fundamental Data* (Bumblebee Series Report No. 87, November, 1948).

[4] For discussions of terms which are not considered in detail in the present publication, references 1 and 2 should be consulted.

[5] E. M. F. van der Held, Z. Physik **70**, 508 (1931); A Unsöld, Physik der Sternatmosphären (J. W. Edwards Company, Ann Arbor, Michigan, 1948), p. 168; for an extension of the curves of growth to larger values of the line-shape parameter a, see S. S. Penner and R. W. Kavanagh, Technical Report No. 6, Contract Nonr-220(03), NR 015 210, California Institute of Technology, Pasadena (September, 1952).

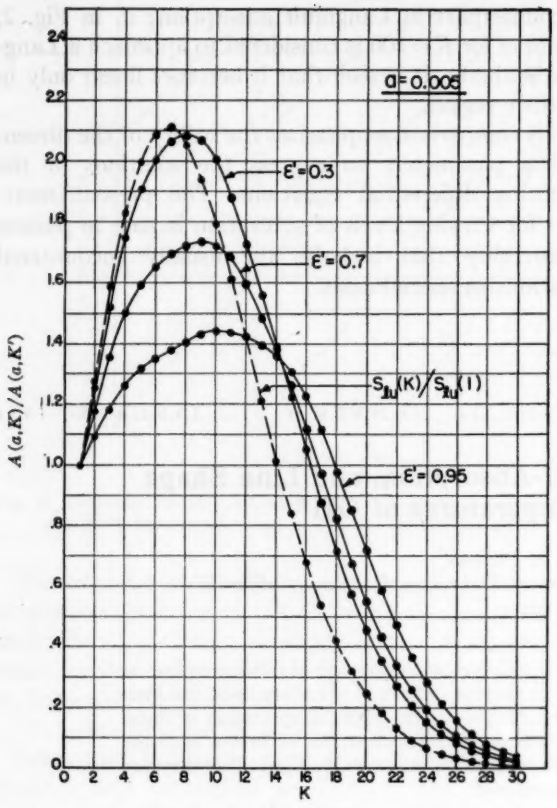

FIG. 1. The quantity $A(a,K)/A(a,K')$ as a function of K for $K'=1$, $a=0.005$.

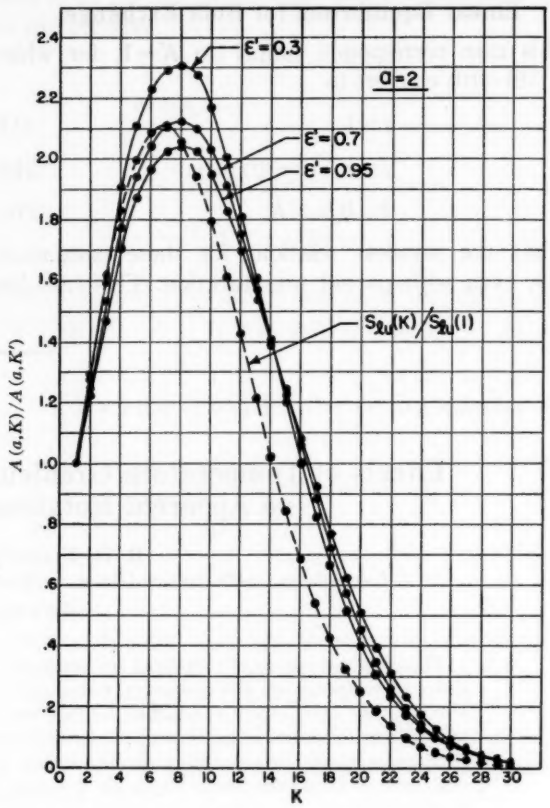

FIG. 2. The quantity $A(a,K)/A(a,K')$ as a function of K for $K'=1$, $a=2$.

portant as the pressure is reduced, i.e., as a is decreased.[1] A more definite conclusion is justified only if absolute values are known for a in flames, which is not the case at the present time.

II. TWO-PATH EXPERIMENTS FOR TWO ADJACENT ISOTHERMAL REGIONS (SPECTRAL LINES WITH DOPPLER CONTOUR, PEAK INTENSITIES)

Calculations which are made in this section correspond to the assumed experimental arrangement illustrated in Fig. 3. The OH concentration is treated as a variable parameter both in the hot region $[\epsilon=1-\exp(-P_{\max}X)]$ and in the cool region $[\epsilon'=1-\exp(-P_{\max}'X')]$. It is physically reasonable to assume $\epsilon'\ll\epsilon$. Calculations have been carried out for *peak* intensities and for spectral lines with Doppler contour. Peak intensities, even for low-pressure flames with Doppler-broadened lines, have not been measured; such measurements might be possible with an interferometer.

TABLE I. Effect of ϵ' and a on lines of equal total intensity.

	K value of line with intensity closest to $K=3$ for		
	$\epsilon'=0.3$	$\epsilon'=0.7$	$\epsilon'=0.95$
$a=0.005$	13	14	16
$a=0.05$	13	14	16
$a=2$	13	13	14
	K value of line with intensity closest to $K=6$ for		
	$\epsilon'=0.3$	$\epsilon'=0.7$	$\epsilon'=0.95$
$a=0.005$	10	11	14
$a=0.05$	10	11	13
$a=2$	10	10	10

Referring to Fig. 3, the peak intensity I for the spectral line whose center lies at ν_{lu} may be written as

$$I\simeq R(\nu_{lu})\epsilon(1-\epsilon')[1+(1-\epsilon)(1-\epsilon')^2] \qquad (2)$$

for unit reflectivity of the mirror, if $\exp(-h\nu_{lu}/kT')\ll\exp(-h\nu_{lu}/kT)$. If I' represents the intensity for the single path, then $I'\simeq R(\nu_{lu})\epsilon(1-\epsilon')$ whence

$$I/I'\simeq 1+(1-\epsilon)(1-\epsilon')^2. \qquad (3)$$

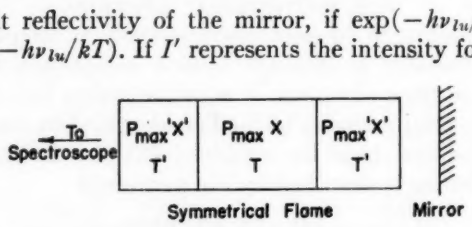

FIG. 3. Schematic arrangement of two-path experiment for a flame represented by two isothermal regions.

The observable ratio I/I' has been calculated as a function of K for various values of $\epsilon(K=1)$ and $\epsilon'(K=1)$ for the P_1 branch, (0,0) band, and $^2\Sigma\rightarrow{}^2\Pi$ transitions of OH. Representative results are plotted in Figs. 4 and 5. Reference to these figures shows that the intensity ratio $I(K)/I'(K)$ is a sensitive function of the self absorption

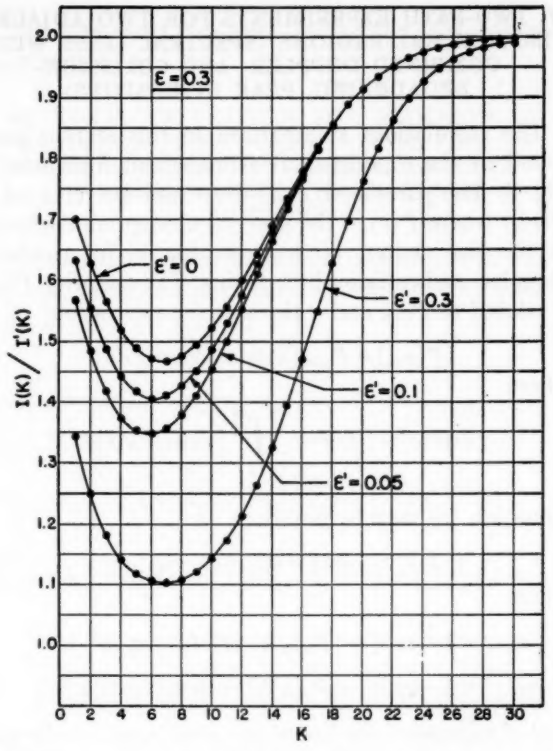

FIG. 4. The quantity $I(K)/I'(K)$ as a function of K for $\epsilon=0.3$, $\epsilon'=0$, 0.05, 0.10, and 0.3.

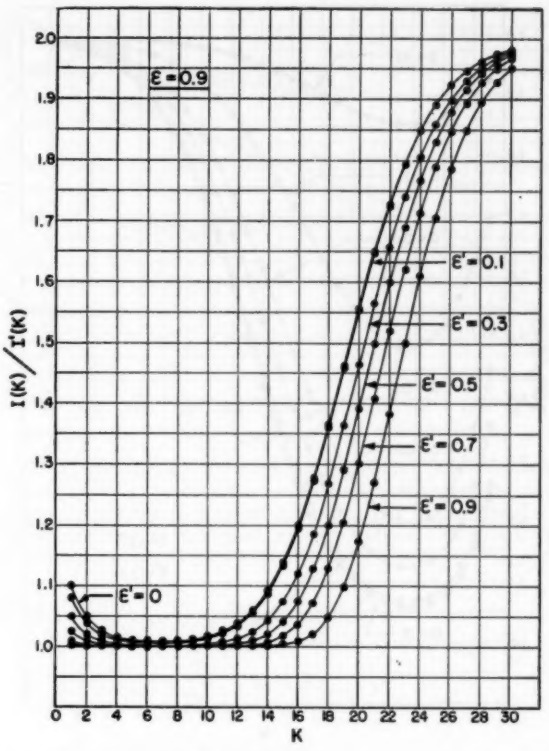

FIG. 5. The quantity $I(K)/I'(K)$ as a function of K for $\epsilon=0.9$, $\epsilon'=0$, 0.1, 0.3, 0.5, 0.7, and 0.9.

parameters ϵ and ϵ'. It is clear that the intensity ratio for two-path experiments will be a somewhat less sensitive function of ϵ and ϵ' for measurements of total intensity.

The important result derived from the present calculations is that even for values of ϵ as small as 0.3, the ratio $I(K)/I(K')$ is appreciably less than two for the stronger lines. In other words, a two-path experiment measuring peak intensities is a relatively sensitive device for studying self-absorption and temperature distortion, quantitatively. As will be shown in Sec. III, this last conclusion applies also to absorption experiments in which peak intensities are measured.

III. ABSORPTION EXPERIMENT FOR TWO ADJACENT ISOTHERMAL REGIONS (SPECTRAL LINES WITH DOPPLER CONTOUR, PEAK INTENSITIES)

Because of the experimental difficulties arising from inadequate resolving power in the measurement of peak intensities for two-path experiments, it is of interest to consider the use of absorption experiments using discrete line sources. Calculations which are made in this section correspond to the assumed experimental arrangement illustrated in Fig. 6. The light source is assumed to radiate at the center of a given spectral line as a blackbody at the temperature T_s, i.e., with intensity $R(T_s)$. For the same conditions for which Eq. (2) applies it is found that

$$I^*/R(T_s)\simeq(1-\epsilon')^2(1-\epsilon), \qquad (4)$$

where I^* denotes the transmitted intensity at ν_{lu}.

Comparison of Eqs. (3) and (4) shows that the transmitted intensity divided by the incident intensity from a discrete line source is nearly equal to $I/I'-1$ where I/I' is the ratio of the intensity of the flame for a double-path experiment to the intensity of the flame for a single-path experiment. Figures 4 and 5 may then be reinterpreted in such a way that $I/I'-1$ represents the transmissivity of the flame for discrete radiation.

Since I/I' or $I/I'-1$, for measurements of peak intensities, are very sensitive functions of the self-

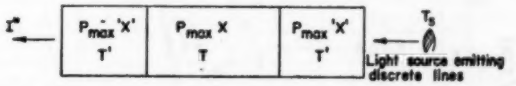

FIG. 6. Schematic arrangement of absorption experiment for a flame represented by two isothermal regions.

absorption parameters ϵ and ϵ', it follows that $I^*/R(T_s)$ is also a sensitive function of ϵ and ϵ'. Unlike peak-intensity determinations in two-path experiments, the discrete line source experiment may be feasible with ordinary spectroscopic apparatus by using as source OH in a discharge tube, or else an excited metal line which coincides exactly with a line of OH.[6] In this connection it is of interest to note that the 3063.97A line of tungsten

[6] Absorption experiments using discrete lines as source have been considered at various times by most of the active workers in combustion spectroscopy. See also Kane and Broida, J. Chem. Phys. 21, 347 (1953).

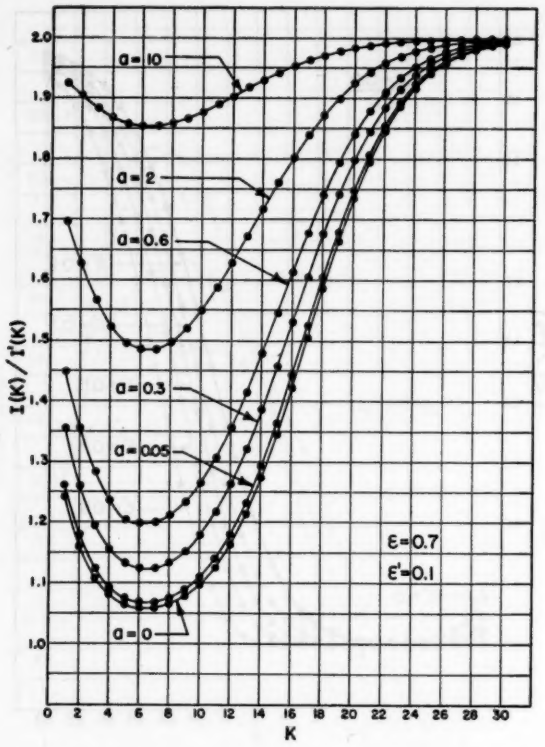

FIG. 7. The quantity $I(K)/I'(K)$ as a function of K for $\epsilon=0.7$, $\epsilon'=0.1$, $a=0$, 0.05, 0.3, 0.6, 2, and 10.

coincides with the 10′ line of the (0,0) band, $^2\Sigma\rightarrow{}^2\Pi$ transitions of OH.

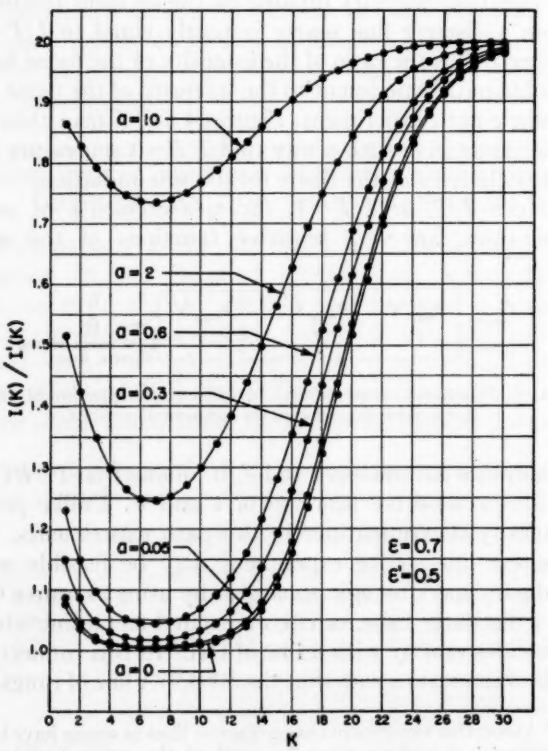

FIG. 8. The quantity $I(K)/I'(K)$ as a function of K for $\epsilon=0.7$, $\epsilon'=0.5$, $a=0$, 0.05, 0.3, 0.6, 2, and 10.

IV. TWO-PATH EXPERIMENTS FOR TWO ADJACENT ISOTHERMAL REGIONS (SPECTRAL LINES WITH COMBINED DOPPLER- AND COLLISION-BROADENING, PEAK INTENSITIES)

The calculations summarized in this section correspond to the experimental arrangement illustrated in Fig. 3. The parameter $P_{\max}$ must now be replaced by $P(\nu_{lu})$ where $P(\nu_{lu})$, the spectral absorption coefficient at the line center, is to be evaluated for combined Doppler- and collision-broadening. The quantity $P(\nu_{lu})$ is related to $P_{\max}$ and a through the expression[5]

$$P(\nu_{lu})=P_{\max}[\exp(a^2)][\operatorname{erfc}(a)], \tag{5}$$

where

$$\operatorname{erfc}(a)=[2/\pi^{(1/2)}]\int_a^\infty[\exp(-x^2)]dx.$$

Equation (3) may be rewritten as

$$I/I'\simeq 1+(1-\epsilon_{D-C})(1-\epsilon_{D-C}')^2, \tag{3a}$$

where

$$\epsilon_{D-C}=1-\exp[-(P_{\max}X)\operatorname{erfc}(a)\exp(a^2)], \tag{6}$$

$$\epsilon_{D-C}'=1-\exp[-(P_{\max}'X')\operatorname{erfc}(a')\exp(a'^2)], \tag{6a}$$

and a' represents the line-shape parameter for the gases at the temperature T'.

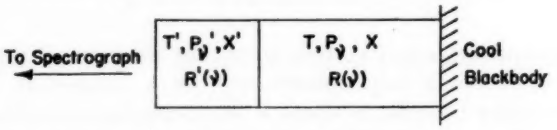

FIG. 9. Schematic arrangement for emission experiment from two adjacent isothermal regions.

The ratio I/I' has been calculated for $a'=a$ ranging from 0 to 10, $\epsilon(K=1)=0.7$, $\epsilon'(K=1)=0.1$ and 0.5, for the P_1 branch, (0,0) band, and $^2\Sigma\rightarrow{}^2\Pi$ transitions of OH. Results are plotted in Figs. 7 and 8. Reference to Figs. 7 and 8 shows that two-path experiments will yield results which are sensitive functions of the line-shape parameter a with distortion of experimental data by self-absorption diminishing as the numerical value of a is increased, under otherwise comparable experimental conditions.

V. PEAK ABSORPTION EXPERIMENTS FOR TWO ADJACENT ISOTHERMAL REGIONS (SPECTRAL LINES WITH COMBINED DOPPLER- AND COLLISION-BROADENING)

Calculations in this section correspond to the experimental arrangement illustrated in Fig. 6 with $P_{\max}$ replaced by $P(\nu_{lu})$. Equation (4) now becomes

$$I^*/R(T_s)\simeq(1-\epsilon_{D-C})(1-\epsilon_{D-C}')^2. \tag{4a}$$

Comparison of Eqs. (3a) and (4a) shows that $I^*/R(T_s)=I/I'-1$ is obtained simply by reinterpreting the ordinates of Figs. 7 and 8. Hence the same conclusions apply to absorption experiments with discrete sources as

to measurements of peak intensities for two-path experiments.

VI. TOTAL INTENSITIES FOR EMISSION OF RADIATION FROM FLAMES CONSISTING OF TWO ADJACENT ISOTHERMAL REGIONS (SPECTRAL LINES WITH DOPPLER CONTOUR)

The experimental arrangement is sketched in Fig. 9. The total observable intensity A for the line with center at ν_{lu} is

$$A\equiv\int_{-\infty}^{\infty} I_\nu d\nu \simeq R(\nu_{lu}) \times\int_{-\infty}^{\infty}[1-\exp(-P_\nu X)][\exp(-P_\nu' X')]d\nu, \quad (7)$$

where the intensity of radiation emitted from the cool

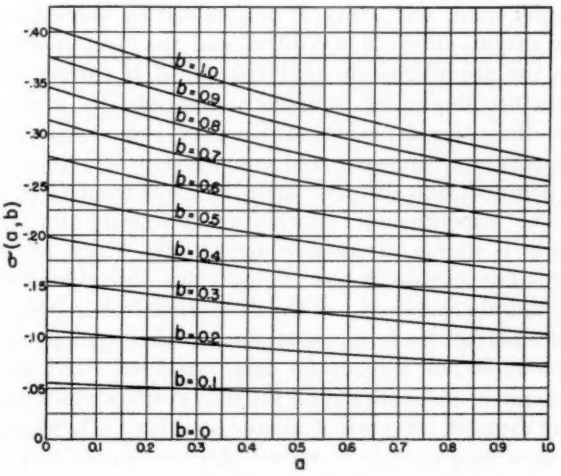

FIG. 10. The double sum $\sigma(a,b)$ for $c=2$ as a function of a and b.

gas layer has been neglected. But, for spectral lines with Doppler contour, $P_\nu=a\exp[-\beta(\nu-\nu_{lu})^2]$, $P_\nu'=b\exp[-\beta'(\nu-\nu_{lu})^2]$, where $a=P_{\max}X$, $b=P_{\max}'X'$, $\beta=mc^2/2kT\nu_{lu}^2$, $\beta'=mc^2/2kT'\nu_{lu}^2$. Replacing P_ν and P_ν' and making the substitutions, $x^2=\beta(\nu-\nu_{lu})^2$, $d\nu=\beta^{-(1/2)}dx$, $\beta'(\nu-\nu_{lu})^2=(\beta'/\beta)x^2\equiv cx^2$, and expanding the exponentials, it follows that

$$A/R(\nu_{lu})=P_{\max}X(\pi/\beta)^{(1/2)}\sum_{n=0}^{\infty}[(-1)^n(P_{\max}X)^n]/[(n+1)!(n+1)^{(1/2)}]+P_{\max}X(\pi/\beta)^{(1/2)} \times\sum_{n=0}^{\infty}\sum_{m=1}^{\infty}(-1)^{n+m}(P_{\max}X)^n(P_{\max}'X')^m \times[(n+1)!m!(n+1+mc)^{(1/2)}]^{-1}. \quad (8)$$

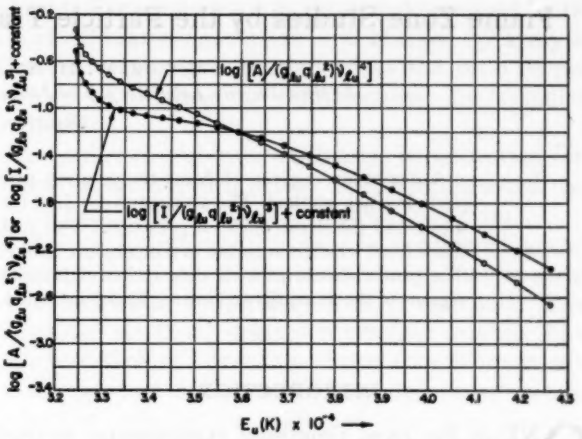

FIG. 11. Comparison of conventional plots for the determination of rotational temperatures of OH for measurements of total emitted intensities A and of peak emitted intensities I. Two adjacent isothermal regions at temperatures of 3000 and 1500°K, respectively; spectral lines with Doppler contour; $\epsilon=0.5$, $\epsilon'=0.3$.

But $S_{lu}X=P_{\max}X(\pi/\beta)^{\frac{1}{2}}$, whence

$$A/R(\nu_{lu})=S_{lu}X\{\sum_{n=0}^{\infty}(-1)^n(P_{\max}X)^n \times[(n+1)!(n+1)^{\frac{1}{2}}]^{-1} +\sum_{n=0}^{\infty}\sum_{m=1}^{\infty}(-1)^{n+m}(P_{\max}X)^n(P_{\max}'X')^m \times[(n+1)!m!(n+1+mc)^{(1/2)}]^{-1}\}. \quad (9)$$

The value of the first sum appearing on the right-hand side of Eq. (9) has been determined by Ladenburg as a function of $P_{\max}X$.[7] It therefore remains to calculate the value of the double sum, $\sigma(a,b,c)$, as a function of $a=P_{\max}X$ and $b=P_{\max}'X'$. For small values of a and b the double sum given in Eq. (9) can be evaluated conveniently by direct summation of the rapidly convergent series. The results of the calculations for $c=T/T'=2$ are plotted in Fig. 10 where the ordinate, $\sigma(a,b)$, represents the double sum appearing on the right-hand side of Eq. (9) for $c=2$.

The ratio $A/R(\nu_{lu})$ has been computed from Eq. (9) as a function of a and b for $\epsilon=1-\exp(-a)=0.5$ and $\epsilon'=1-\exp(-b)=0.3$ for the P_1 branch, (0,0) band, $^2\Sigma\rightarrow{}^2\Pi$ transitions of OH. The results of these calculations are contrasted in Fig. 11 with the corresponding data applying to peak intensities.[1] Reference to Fig. 11 shows that, for spectral lines with Doppler contour, distortion of data for measurements of total intensity is smaller than the distortion calculated for peak intensities. For rotational temperatures derived from emission experiments on isothermal regions, very similar results had been obtained previously for measurements of total and of peak emission intensities.[2]

[7] R. Ladenburg, Z. Physik 65, 200 (1930).

Flame Zone Studies by the Particle Track Technique. I. Apparatus and Technique*

R. M. FRISTROM, W. H. AVERY, R. PRESCOTT AND A. MATTUCK†
Applied Physics Laboratory, The Johns Hopkins University, Silver Spring, Maryland
(Received May 29, 1953)

A discussion is given of flame temperature profiles of laminar premixed Bunsen flames derived by the particle track method. The apparatus required for the study is described. A critical discussion of the technique and the flame model is presented. This method allows the derivation of a temperature profile for a flame front which is accurate in temperature and relative position to a few percent depending on the pressure. The profile should provide description of translational temperature within the flame front. The singular regions of the flame tip and burner lip are excluded from this discussion.

INTRODUCTION

ONE of the most promising experimental methods used in the study of the structure of flames is the particle track method of visualizing flow patterns. Analysis of this streamline pattern yields a density *vs* position function which can, with certain limitations, be converted directly into a temperature profile. Essentially the method utilizes the flame gases themselves as a gas thermometer.

The experimental technique was suggested by Smith[1] in 1932 and extended in 1943 by Lewis and von Elbe.[2] It was applied to quantitative temperature determinations by Andersen and Fein[3] in 1948, and Fristrom, Prescott, Neumann, and Avery[4] in 1952. Temperature profiles were derived by assuming a linear change in gas velocity parallel to the flame front. Direct measurement of velocity by use of stroboscopic illumination has made it possible to avoid this assumption. We will discuss in some detail the corrections necessary for the quantitative application of this method, together with a description of improved experimental techniques. As an example, the results obtained from a propane-air flame are presented.

EXPERIMENTAL

Premixed laminar Bunsen flames were chosen for study. In order to visualize and study streamline flow through these flame fronts, it is necessary to have a picture representing a cross section of known geometry.

The presently accepted model for this type of flame pictures it as a stationary conical reaction surface (flame front) in a flowing gas stream.

The geometry of this reaction surface is determined by burner geometry, the rate of propagation of the combusion reaction (burning velocity) and the rate of gas flow. This model has been discussed by a number of authors[5,6] and appears to be an excellent approximation outside the singular regions of the flame tip and the burner lip. The gases flowing through the flame front obey the laws of hydrodynamic flow.

In addition to these macroscopic properties, the flame front which we have described has a microscopic structure which appears to be independent of the type of burner used, and which is determined by the rates of the various chemical and diffusional processes involved. To the approximation that the model is correct, this structure should be completely described by a set of one-dimensional profiles which give the variation of temperature, pressure, and composition as a function of perpendicular distance from the flame front (Fig. 1).

The experimental information necessary for this study is derived from flow streamlines which are recorded by focusing a fast photographic objective on the diametral cross section of the flame and stroboscopically illuminating from the side during the passage of a number of fine magnesium oxide particles. Particles in the field of focus appear on the film as spots which indicate the path traversed while the light is on. The shutter is open long enough to record also the burner and the luminous zone of the flame. Measurement of position

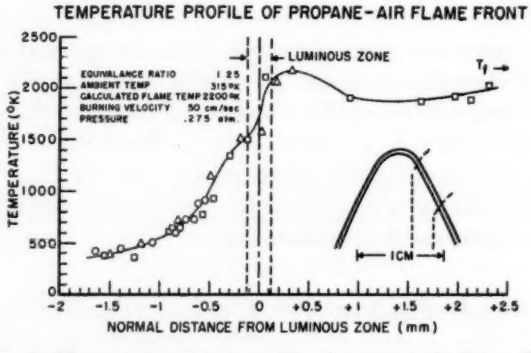

FIG. 1. Flame temperature profile of propane-air flame. This illustrates the results obtained by this method in the case of a flame at one-quarter atmosphere pressure. The equivalence ratio is 1.25 (5.02-percent propane by volume). This is a composite of measurements on seven streamlines from the central region.

* This work was done under Contract NOrd 7386 with the Bureau of Ordnance of the U. S. Navy.
† Present address: Department of Mathematics, Princeton University, New Jersey.
[1] F. Smith, Chem. Revs. **21**, 389 (1932).
[2] B. Lewis and G. von Elbe, J. Chem. Phys. **11**, 75 (1943).
[3] J. W. Andersen and R. S. Fein, J. Chem. Phys. **17**, 1268 (1949).
[4] Fristrom, Prescott, Neumann, and Avery, *Fourth International Combustion Symposium* (Williams Wilkins and Company, Baltimore, 1953), pp. 267.
[5] W. Jost, *Explosions and Combustion Processes in Gases* (McGraw-Hill Book Company, Inc., New York, 1946), p. 74.
[6] B. Lewis and G. von Elbe, *Combustion, Flames and Explosions in Gases* (Academic Press, New York, 1952), Chap. VII.

and time in these photographs constitutes the primary data of this experiment.

In order to transform these velocity and positional measurements into temperatures, we consider the infinitesimal volume generated by rotating the area between two adjacent streamlines about the axis of the flame. Conservation of mass dictates that within the streamtube so defined, the product of density, velocity, and cross section is constant.

$$\rho v A = \text{const.} \tag{1}$$

Velocity and cross section have been measured in a number of cases where adjacent streamlines were recorded. In each case, the observation of Anderson and Fein[3] that the streamline separation is constant was confirmed. Therefore, area as defined by the intersection of the streamtube and the family of cones parallel to the flame front, e.g., the luminous zone, is a function only of the horizontal distance from the axis of the flame. The component of velocity normal to this surface is parallel to the burning velocity and is initially equal to it. These considerations allow us to calculate the velocity and relative streamtube cross section from measurements on a single representative streamline.

Thus, change in density with position along a streamline can be determined and application of the perfect gas law allows us to calculate the corresponding temperature profile. The molecular weight changes to some extent as the reaction proceeds and must be estimated independently.

At point i the temperature T_i is given by

$$T_i = T_o[v_i/v_o][r_i/r_o][M_o/M_i]. \tag{2}$$

(See Table I for a list of symbols used.)

TABLE I. Symbols used.

Symbol	Subscripts	
T	o, i, f	Temperature in degrees Kelvin, at points o, i. T_f—maximum flame temperature
ρ		Gas density
v	o, i	Gas velocity in centimeters per second, at points o and i
A		Cross-sectional area in square centimeters
r	o, i	Horizontal distance in millimeters measured from the axis of the flame[a]
M	o, i	Average molecular weight at points o, i
Δv		Slippage velocity in centimeters per second
η		Viscosity of air in poises
a		Acceleration in centimeters per second per second

[a] r_0 must be referred to the base of the burner.

The methods used to correct this temperature for the effects of change in average molecular weight and velocity lag of the particle are described in the next section.

The propane used in these studies was Phillips' Petroleum pure grade 99 mole percent. Dry compressed air was used, and as an additional precaution cylinders were discarded as soon as their pressure fell below 600 lb/in.^{2} The moisture content should be below 0.1 percent. The equivalence ratios were determined by the use of calibrated flowmeters[7] and checked by analysis. The equivalence ratio is defined as the ratio of percentage of propane to that required for complete combustion.

A number of problems which arise in connection with this work are outlined below. They are discussed elsewhere relative to a somewhat different analysis.[4]

The first question which must be considered is what meaning to attach to the temperature that is measured. Because of the rapidity of flame reactions, vibrational and electronic degrees of freedom may not have sufficient time to come into thermal equilibrium with translation and rotation. We may deduce an average molecular velocity or collisional rate and hence a "translational" temperature, but may not deduce directly the population distribution within the other degrees of freedom.

The second question concerns the effect of change in average molecular weight which enters in Eq. (3). The initial and final values which differ by about 2 percent are known, and the intervening changes have been estimated using a preliminary composition profile obtained by use of a fine probe in conjunction with a mass spectrometer.[8]

The third question concerns the effect of particles on the flame reactions. By use of our improved illumination system, we have been able to reduce the particle size and the number necessary so that the heat capacity of the particles abstracts less than 0.01 percent of the total output of the flame. Upon introducing the particles no change in burning velocity or in the appearance of the flame front has been detected.

Next is the problem of how closely the particles actually follow the streamlines. This is governed by the relative importance of viscous drag and inertial forces and is described approximately by Stokes' law. In practice, available illumination sets the lower limit of usable particle diameter at a few microns. The accuracy with which a particle track approximates a streamline has been calculated by a method similar in principle to that of Wright.[9] In this case it is found that a particle with a "Stokes' law" diameter smaller than 4 microns will require a velocity correction smaller than 2 percent in the region of maximum acceleration. This diameter was determined by time of fall experiments and checked photographically and by microscopic examination.

$$4/3\pi r^3 \rho a = 6\pi\eta r \Delta v, \tag{3}$$

(See Table I for a list of symbols used.)

$$v = \frac{2}{9}\frac{r^2 \rho a}{\eta}.$$

[7] J. W. Andersen and R. Friedman, Rev. Sci. Instr. **20**, 61–66 (1949).

[8] Prescott, Foner, Avery, and Hudson, "Composition profiles in flame fronts," J. Chem. Phys. (to be published).

[9] F. H. Wright, Progress Report 3–23, Jet Propulsion Laboratory, California Institute of Technology (1951).

The error in radial position produced by this slippage is negligible outside the tip region. The only acceleration not directed normal to the flame front is that due to gravity, which results in negligible error.

The thermomechanical effect, that is, the force on a particle in a nonuniform temperature field, is discussed by Saxton and Rant.[10] Calculations dictate a maximum correction at the point of maximum temperature gradient of the order of one quarter percent at one quarter atmosphere.

The effect of optical inhomogeneities in the gas has been considered. The gradients change uniformly throughout the flame front[11] so no abrupt distortions were expected. Experimentally, photographs of a small probe immersed in the flame showed no visible distortion.

Several aberrations could affect the optical system: if the focal plane did not coincide with the flame center, or if the depth of field were too great,[12] tracks of particles outside the diametral plane would appear in focus. Film shrinkage could also be a source of error; it was minimized by careful handling and held well below 1 percent. Film was read on a two-coordinate comparator which was reproducible to one micron. Settings on the film could be reproduced to five microns. The average distance between successive points was several hundred microns and the total thickness of the reaction zone was several thousand microns.

A further source of error lies in the asphericity of the particles. Microscopic study shows an irregular particle outline which is oriented at random; therefore, the position of the leading edge of the image which was measured could be displaced by a fraction of the particle diameter due to change in the distance from the leading edge to the center of gravity and due to local variation in scattering. An effect of this type was detected in measurements. This might be attributed to small scale turbulence, but we are inclined to accept the former explanation. Brownian motion is an order of magnitude smaller than this effect.

In order that a temperature profile be meaningful, we must also know position accurately. This is limited by two factors: (1) experimental errors in measurement and (2) superimposability of temperature profiles derived from different pictures and positions within the flame. The former set the limit of positional resolution to one-hundredth of a millimeter. It was found that the superimposition of two temperature profiles did not lead to a large increase in the experiment scatter, and further, when this was done, that the position of the center of the luminous zone was independent of the section of the flame from which the profile was derived. It should be pointed out that because of the sharp plane of focus of our optical system, the blurring of the luminous zone was minimized. These pictures show that the thickness of the luminous zone is independent of position in the flame even at the tip. All pictures were taken at the same speed and the position and thickness of the luminous zone are reproducible to about three-hundredths of a millimeter.

APPARATUS

The instrumentation for this project is sufficiently novel to warrant description in some detail. The apparatus can be divided into two categories: (1) the burner system and (2) the optical system. The first includes (Fig. 2) a gas handling system, a particle segregator and introducer, a burner, and a constant pressure reaction chamber.[13] The second (Fig. 3) includes an illumination system of timed flash lamps and a camera for recording the results.

Burner System

The burner was a $\frac{1}{2}$-inch constant-velocity-profile nozzle of the Mache-Hebra type[14,15] surrounded by a second nozzle which supplied a protective sheath of gas. The resulting jet had an essentially uniform velocity profile. Gas flows were handled by a set of critical orifice flowmeters[7] which delivered flows constant to within 0.03 percent. The particles of magnesium oxide were introduced from a segregation chamber which kept the average particle size below four microns.[16]

Optical System

The optical system consisted of two parts—the camera and the illumination system. The camera was a

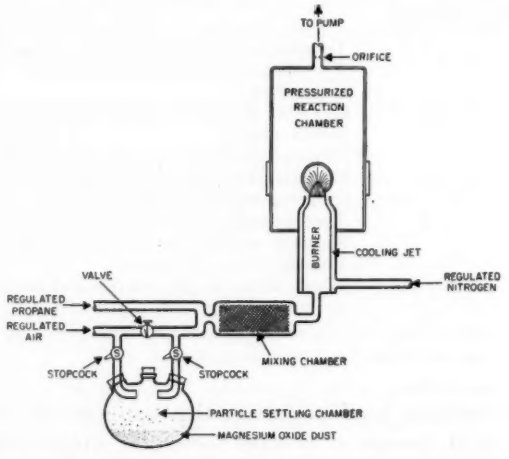

FIG. 2. Burner system schematic.

[10] R. L. Saxton and W. E. Rant, J. Appl. Phys. **23**, 917 (1951).
[11] G. Dixon-Lewis and M. J. G. Wilson, Trans. Faraday Soc. **47**, 1106 (1951).
[12] A change of focal length of 0.5 mm noticeably broadened a fine line observed in the diametral plane of the nozzle. If a particle track 0.5 mm from the diametral plane were selected, an error of one-half percent would result.
[13] This chamber makes it possible to study flames at pressures other than atmospheric; for an example of such studies see reference 4.
[14] H. Mache and A. Hebra, Österr. Akad. Wiss. Math.-naturw. Kl. Sitzber. Abt. IIa **150**, Band 157–74 (1941).
[15] J. W. Andersen, Rev. Sci. Instr. **19**, (1948).
[16] Reference 4 has further details of this apparatus.

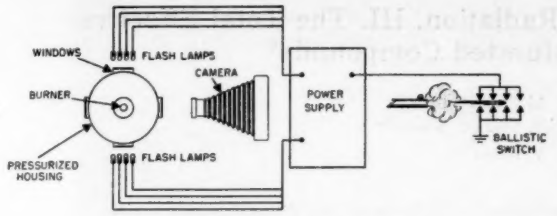

FIG. 3. Optical system schematic.

Nu Vue 4 in.×5 in. camera using a Xenon Special *f*/2 12.5-cm focal length coated lens and Ilex shutter. Operation was at magnification ratios up to three and one-half to one with a resolution of 40 lines per millimeter on the film.[17] Both Eastman Triple-S Ortho and Contrast Process Ortho films were used. The latter proved to be the more satisfactory film with high intensity illumination.

The critical equipment for these studies was the illumination system. Photographing particles smaller than 5 microns in diameter by scattered light at equivalent exposure speeds of 5 microseconds requires light intensities of the order of megalumens per square centimeter. The realization of this light flux required average power dissipation as high as a megawatt. Such power dissipations, of course, cannot be realized continuously, but are quite feasible for transient operation.

The stroboscopic illumination system devised for this work consisted of an illuminator giving a series of twelve flashes of 5-microseconds duration at a repetition rate of 20 kilocycles. Two types of electronic flash lamps were used successfully—the General Electric GE FT 2340 and the Edgerton, Germeshausen, and Grier "Cloud Chamber" flash tube. Both of these lamps could dissipate 200 wattsecond flashes. Since it was necessary to use several lamps for this purpose, the compactness of the E.G.G. tube (6 in. long, $\frac{1}{4}$ in. diameter) recommended itself over the bulkier GE tube.

Power supply control proved to be a formidable problem under these conditions. An attempt to provide electronic control of spark gap switches was frustrated by coupling through the grounds.[18] To avoid these problems a ballistic switch[19] was devised for this study capable of handling the very high powers and repetition rates required. The ballistic switch is a series of spark gap switches aligned in the path of a rifle bullet. Each spark gap is in series with a charged condenser and lamp so that when a bullet passes between the gaps these condensers are successively discharged through the lamps.

[17] As might be expected, appreciably better resolution was obtained by reversing the lens under these conditions.

CONCLUSION

The temperature profile presented herein is for a propane-air flame with an equivalence ratio of 1.25 and a pressure of 0.275 atmosphere. It is taken from seven streamlines in the flame covering the region indicated in the accompanying sketch of the flame. Based on the center of the luminous zone as the origin of the coordinate system, a very satisfactory congruence was obtained among several temperature profiles derived from the central section of the flame front. Correlation with the temperature profiles obtained previously by the streak method is satisfactory; the principal differences were as a result of the discovery that the unburned gases had been preheated by contact with the burner walls and the indication that a slow rise of the order of a 50° per millimeter occurs beyond the luminous zone. These effects were not previously detected because of the assumptions necessary in the streak analysis. The presence of the temperature maximum just outside the luminous zone is of considerable interest, but final conclusions should await composition profile information which is becoming available.

ACKNOWLEDGMENTS

We would like to express our appreciation to Dr. H. Lowell Olsen, Captain E. L. Gayhart, and Mr. Clyde Holliday for a number of helpful suggestions, to Mr. William Badders, to the members of the Laboratory staff who provided much of the instrumentation, and to Miss Betty Gross who reduced the data presented herein.

[18] Because of the high currents carried by the lamps during discharge, ground pulses of the order of 1000 volts were encountered.

[19] R. M. Fristrom, "A high intensity, high speed illuminator," J. Soc. Photo. Engr. 4, No. 2, 74 (1953).

The Quenching of Mercury Resonance Radiation. III. The Total Effective Cross Sections of Some Saturated Compounds*

B. deB. Darwent† and M. K. Phibbs‡
National Research Laboratories, Ottawa, Canada
(Received August 3, 1953)

Total effective cross sections have been measured for 22 compounds in the processes $^3P_1 \rightarrow {}^3P_0$ and $^3P_1 \rightarrow {}^1S_0$, by which mercury resonance radiation is quenched. The compounds include the methylamines, methyl halides, methyl alcohol, dimethyl ether, H_2S, ethyl mercaptan, dimethyl sulfide, ethylene oxide, cycloparaffins, and dimethyl mercury. The cross sections varied from less than $0.01A^2$ (fluoroform) to $46A^2$ (dimethyl mercury). In general σ_Q^2 is increased when a carbon atom is replaced by oxygen and even larger increases occur when the substituting atom or group is, or contains, nitrogen, sulfur, or mercury. The presence of halogens, except fluorine, increases σ_Q^2; the introduction of fluorine reduces the cross section.

INTRODUCTION

In part I of this series the effects of molecular weight and branching of the carbon skeleton on the total effective cross sections of parafinic hydrocarbons was investigated[1] and, in part II, evidence was presented[2] that some compounds including ethane, ethylene and hydrogen quenched λ2537 by the process $^3P_1 \rightarrow {}^3P_0$ as well as by $^3P_1 \rightarrow {}^1S_0$. In the present paper we have extended the measurements of total effective cross sections to some substituted paraffinic compounds to obtain information about the effect of substituents, other than carbon atoms, on the sum of the efficiencies of the processes $M+\mathrm{Hg}(^3P_1) \rightarrow M+\mathrm{Hg}(^1S_0)$ and $\rightarrow M+\mathrm{Hg}(^3P_0)$ as well as to provide data of value to studies of the mercury photosensitized reactions of those compounds.

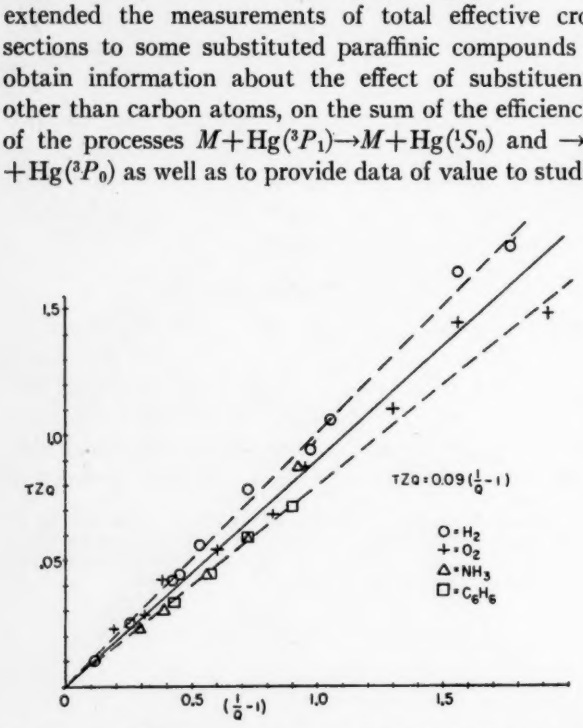

FIG. 1. Calibration experiments. The relationship between $1/Q-1$ and τZ_Q. The broken lines represent a 10-percent deviation from the mean.

EXPERIMENTAL

The apparatus and general technique of measurement were similar to those used previously.[1] The absorption cell was 10.0 mm thick and 50 mm in diameter. The mercury supply to the resonance lamp was maintained at 20°C, instead of 0°C, to provide a greater intensity and so improve the accuracy of the measurements. In this way small random fluctuations and the zero drift of the dc amplifier were rendered much less important than when the incident intensity was low (Hg at 0°C). This change did not affect the magnitude of σ_Q^2, since it was found that the values of σ_Q^2 for hydrogen and *n*-butane were independent of the concentration of mercury in the resonance lamp and did increase the accuracy. The low pressure mercury exciting lamp was placed in a water bath at 32°C and was operated, as was the dc amplifier, from the constant voltage output of a 3-kw Sorenson regulator. The dc amplifier was the same one that was used previously.[1]

The gases were the purest available and were subjected to repeated bulb to bulb distillations, thawing, and freezing in vacuum to remove air which might have been introduced with the sample. The hydrogen and oxygen were purified as previously.[1]

Calibration

The value of the constant α in the relationship $\tau Z_Q=\alpha(1/Q-1)$ was evaluated by measuring the quenching (Q) as a function of pressure using com-

TABLE I. Results of calibration experiments.

Compound	Expt. no.	$(1/Q-1)/P$	$\tau Z_Q/P$	α [c]
H_2	9, 10	10.4	1.10[a]	0.106
O_2	15, 16	7.4	0.68[a]	0.092
NH_3	35	2.3[8]	0.19[a]	0.080
C_6H_6	61	17.6	1.42[b]	0.082
Average				0.09±0.01

[a] M. W. Zemansky, Phys. Rev. **36**, 919 (1930).
[b] J. R. Bates, J. Am. Chem. Soc. **54**, 569 (1932).
[c] $\alpha=\tau Z_Q/(1/Q-1)$.

* Contribution No. 3135 from the National Research Council, Ottawa, Canada.
† Present address: Olin Industries, Inc., New Haven, Connecticut.
‡ Present address: E. I. du Pont de Nemours, Wilmington, Delaware.
[1] B. deB. Darwent, J. Chem. Phys. **18**, 1532 (1950).
[2] B. deB. Darwent and F. G. Hurtubise, J. Chem. Phys. **20**, 1684 (1952).

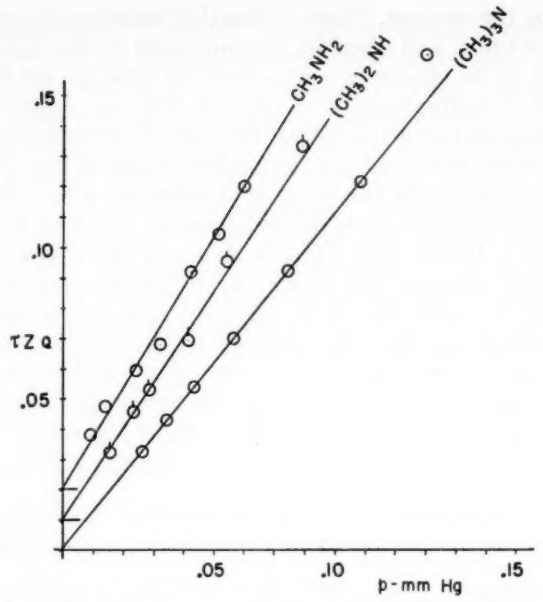

FIG. 2. Quenching by methylamines. The abscissas have been displaced vertically, as shown, to avoid overlapping.

pounds for which τZ_Q had already been measured as a function of pressure. The initial measurements were made with hydrogen and oxygen and, in subsequent experiments, benzene and ammonia were also used. These compounds should be equally satisfactory as standards since very pure samples of all of them have been available for several years.

RESULTS

The relationship between τZ_Q and $(1/Q-1)$ is shown in Fig. 1. The results fall, within ± 10 percent, on a straight line through the origin with a slope of

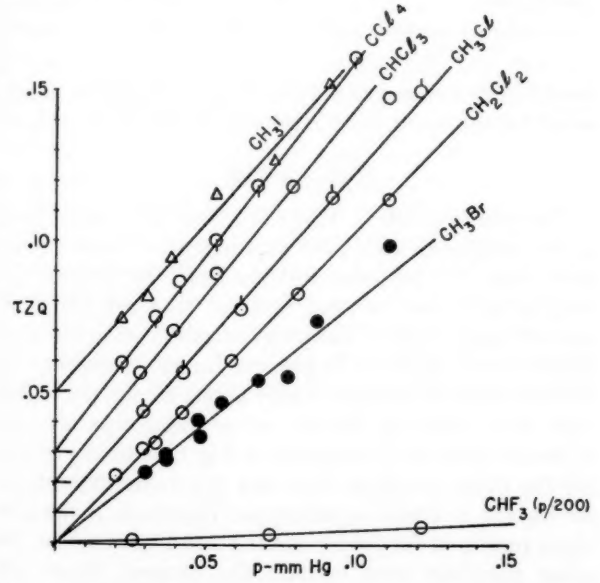

FIG. 3. Quenching by methyl halides (Series I experiments). Some abscissas have been displaced vertically as shown.

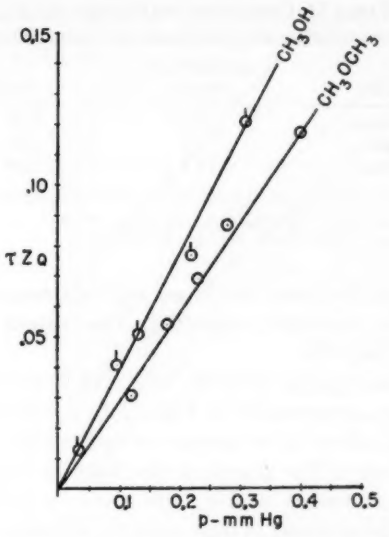

FIG. 4. Quenching by methanol and dimethyl ether.

0.09. In general, the hydrogen results lie consistently above, and those for ammonia and benzene below, this line. Nearly all of the points fall within the stated limits of error as represented by the broken lines. The values of $(1/Q-1)/P$, as measured for the standard compounds, of $\tau Z_Q/P$, and the constant α are given in Table I.

The quenching cross sections of the compounds under investigation were calculated, as described previously,[1] by measuring the quenching Q as a function of pressure. The values of Q so obtained were then converted to the corresponding values of τZ_Q. The cross sections were calculated from the relationship

$$\sigma_Q^2 = 3.0 \times 10^{-4} \mu^{-\frac{1}{2}} (\tau Z_Q/P).$$

The effective cross sections of propane, butane, and pentane were also measured. This allows a comparison

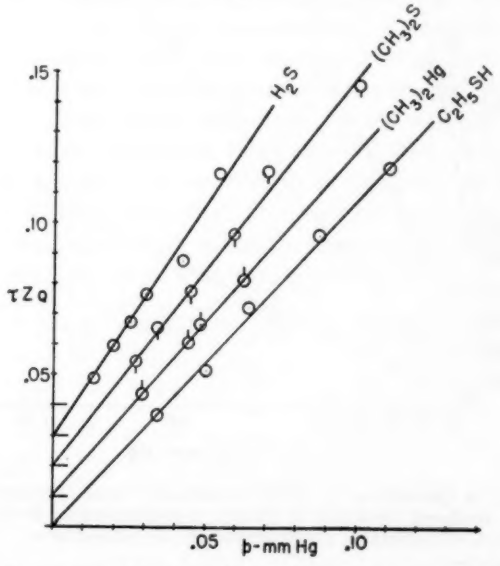

FIG. 5. Quenching by sulfur and mercury compounds.

TABLE II. Comparison with earlier results.

Substance	$\sigma_Q^2 \times 10^{16}$ cm² Present	Previous
Propane	1.6	1.3[a]
Butane	5.1	3.0[a], 4.1[b]
Pentane	10.3	8.6[a]

[a] B. deB. Darwent, J. Chem. Phys. **18**, 1532 (1952).
[b] J. R. Bates, J. Am. Chem. Soc. **54**, 569 (1932).

to be made between the cross sections measured now with those previously reported. The values are compared in Table II.

The relationships between τZ_Q and P are shown for the various compounds in Figs. 2 to 6, which demonstrate that there is no serious or systematic departure from linearity. The slopes of the lines in Figs. 2 to 6, the reduced masses, and σ_Q^2 are given in Table III.

A surprising result is that methyl bromide was found to have a smaller cross section than methyl chloride although methyl iodide was much larger. This is unexpected and was further investigated by carrying out another series of experiments§ with those three compounds in the same apparatus, altered only by more thorough screening of the photocell and refocusing and recollimating the light.

In the new experiments the values of α, measured with hydrogen, oxygen, and ammonia, were found to be 0.17 (H_2), 0.16 (O_2), and 0.15 (NH_3). The average value was 0.16 and, when τZ_Q was plotted against $(1/Q-1)$, it was found that again the hydrogen results appeared, in general, to be higher and ammonia lower

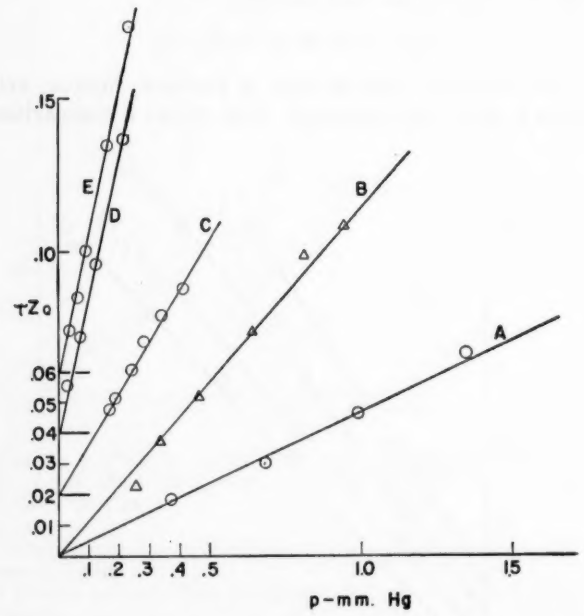

FIG. 6. Quenching by cyclic compounds. Some abscissas have been displaced vertically as shown. *A*–cyclopropane; *B*–ethylene oxide; *C*–cyclobutane; *D*–cyclopentane; *E*–cyclohexane.

§ We are indebted to Mr. F. G. Hurtubise for these experiments.

than the average. These calibration experiments were done before and after the measurements on the halides and, as no change in α was observed between the two sets of calibrations, it is obvious that no significant change had occurred during this series of measurements. However, the reason for the marked change in the value of α between the two series of experiments is not clear. The relationship now derived between τZ_Q and P for CH_3Cl, CH_3Br, and CH_3I is shown in Fig. 7, and the actual values of $\tau Z_Q/P$ and σ_Q^2 for those compounds given in Table IV. It is seen that now σ_Q^2 increases progressively from the chloride to the iodide. These second series experiments were done rather more thoroughly than the previous ones, and we consider the results to be more reliable. Accordingly the results for these compounds from the series one experiments are

TABLE III. Experimental results and quenching cross sections.

Compound	Expt. no.	$\tau Z_Q/P$	$\mu^2 \times 10^{-11}$	$\sigma_Q^2 \times 10^{16}$ (cm²)
CH_3NH_2	32	1.68	1.50	33.5
$(CH_3)_2NH$	33	1.52	1.28	36
$(CH_3)_3N$	34	1.24	1.15	32
CH_3OH	36	0.38	1.48	8
$(CH_3)_2O$	38	0.29	1.27	7
H_2S	52	1.50	1.93	23
C_2H_5SH	54	1.09	1.12	29
$(CH_3)_2S$	55	1.29	1.12	34.5
CF_4	37	Nil	...	...
CHF_3	41	0.0002	1.08	0.005
CCl_4	42	1.31	0.85	46
$CHCl_3$	43	1.25	0.90	42
CH_2Cl_2	44	1.04	1.01	31
CH_3Cl	45	(1.14)	(1.23)	(28)
CH_3Br	47	(0.81)	(1.03)	(24)
CH_3I	46	(1.13)	(1.48)	(39)
$(CH_3)_2Hg$	60	1.15	0.75	46
Ethylene oxide	48	0.12	1.30	2.7
Cyclopropane	19	0.048	1.32	1.1
Cyclobutane	56	0.175	1.18	4.4
Cyclopentane	21	0.47	1.08	13
Cyclohexane	20	0.47	1.01	14

placed in parentheses in Table II and should be superseded by the more reliable data of Table IV.

DISCUSSION

The results given in Table II allow the present data to be compared with past experiments. These results show that, for propane and pentane, the present determinations lead to cross sections that are about 20 percent larger than in the previous publication but that butane is as much as 70 percent larger. However, the present value for butane is only about 25 percent higher than that found by Bates,[3] whose value was actually in better agreement (reference 1, Fig. 6) with the results for the other paraffins than was the value determined for butane in those experiments. Therefore, if the previous results of Bates[3] for butane and Darwent[1] for the other paraffins were correct, the present values are

[3] J. R. Bates, J. Am. Chem. Soc. **52**, 3825 (1930).

approximately 20 percent too high. From this it appears likely that the reproducibility of these measurements by different workers is not better than ±10 to 15 percent.

Irrespective of the validity of the absolute values of these cross sections, we may still assume that the relative values are correct. By comparing monomethylamine with ethane and methanol, and dimethylamine with propane and dimethyl ether, the physical size of the three compounds in each group being approximately the same, we find that in both cases the presence of the nitrogen atom leads to a very much larger cross section than does the presence of either the carbon or the oxygen atom. We find further that trimethylamine, which contains no N−H bond, is about as efficient as mono- and dimethylamine. It, therefore, appears likely that the high quenching efficiency of these amines is not necessarily caused by the presence of an N−H bond.

The results obtained with the cyclic compounds show that cyclopropane has a relatively small cross section and gives no indication that it behaves as a compound with even incipient unsaturation. As was found with methanol and dimethyl ether, the substitution of O for CH_2 increases the cross section. The effective size of the ring compounds increases, as was found[1] for the paraffins, with increasing physical size although the ratio of the cross sections of cyclohexane and cyclopropane is far greater than would have been expected. Hence it appears likely that the efficiency of quenching increases with increasing size of the ring, and this may result from a progressive decrease in the C−H bond dissociation energy. The fact that the cross sections of cyclopentane and cyclohexane are approximately equal suggests that the physical sizes of those molecules as well as their C−H bond energies are essentially the same.

No less striking is the wide variation in the quenching cross sections of the halogen substituted methanes. The very small cross sections of the fluorine compounds suggests that, with those compounds, quenching does not occur as the result of an interaction between Hg ($^3P_1$) and the fluorine atom whereas such is possibly the case with methyl chloride[4] and, presumably, with the other chloromethanes and methyl bromide and iodide. However, in spite of this, one would have expected that fluoroform, because of its weak C−H bond, would have quenched more efficiently than found here since Bates[3] has shown that methane has a cross section of about 0.06×10^{-16} cm^2.

TABLE IV. Methyl halides—re-investigation (Series B).

Substance	$(1/Q-1)/P$	$\tau Z_Q/P$	$\sigma_Q^2\times10^{16}$ (cm^2)	Expts. no.
CH_3Cl	6.10	0.98	24	B23, B24, B26, B27
CH_3Br	5.95	0.95	28	B24, B26
CH_3I	6.95	1.11	41	B24, B25, B26

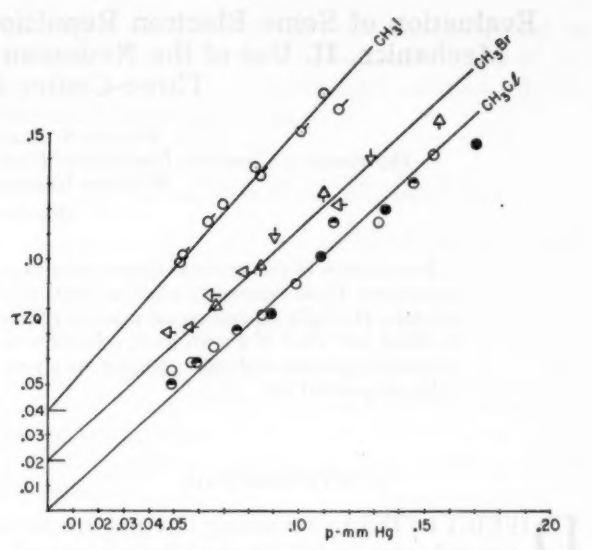

FIG. 7. Quenching by methyl chloride, bromide and iodide (Series II experiments). Some abscissas have been displaced vertically as shown.

Masson and Steacie[4] measured the effect of the addition of CO_2 on the rate of the mercury photosensitized decomposition of methyl chloride. They assumed that the only effect of CO_2 was to compete with CH_3Cl for the Hg($^3P_1$) atoms and so derived a cross section of 5.7×10^{-16} cm^2 for CH_3Cl. Their value is very much lower than that (24×10^{-16} cm^2) obtained by us. Their treatment is not entirely unambiguous, since CO_2 may have exerted other effects on the reaction, and we consider our more direct measurement to be preferable.

The comparatively large cross sections of the sulfur compounds and dimethyl mercury is also worthy of note. However, when allowance is made for the large physical size of these compounds, it appears probable that they are not significantly more efficient than, say, methylamine. Further discussion of these compounds should be postponed until more is known about the mechanism by which they react with excited mercury.

[4] C. R. Masson and E. W. R. Steacie, J. Chem. Phys. **19**, 183 (1951).

Evaluation of Some Electron Repulsion Integrals Needed in Molecular Quantum Mechanics. II. Use of the Neumann Expansion in Evaluation of Two Electron Three-Center Repulsion Integrals*

ROLAND S. BARKER AND HENRY EYRING
Department of Chemistry, University of Utah, Salt Lake City, Utah, and Department of Chemistry, Princeton University, Princeton, New Jersey

(Received May 4, 1953)

Formulation of two types of three-center electron interaction integrals in convergent series is explicitly considered. These expressions place no restrictions on the effective nuclear charges of the composite atomic orbitals. The basic expansions are made in elliptical coordinates. The auxiliary functions used are discussed in detail and when of known form, references to the original literature are cited. Examples arising in the triatomic hydrogen molecular complex are given. Possibilities of extension of the method to complex molecules are pointed out.

1. INTRODUCTION

DIFFICULTIES in evaluating electron interaction integrals may well be said to have appeared at the very inception of molecular quantum mechanics. The classical work of Heitler and London[1] on the diatomic hydrogen molecule contained an approximate evaluation of such an integral (the two-center resonance or exchange integral) which was later exactly evaluated by Sugiura.[2] Three-center electron interaction integrals have been less thoroughly investigated. New methods for evaluating such three-center ones are described in this and our two earlier papers[3,4] on this subject. Specific application of these general methods allow the evaluation of all integrals occurring in the energy calculations of the H_3 activated complex molecule without restriction as to effective charges of the composite atomic orbitals of the variational trial function.

Methods previously proposed for integrals of this type[5–7] expand $1/r_{12}$ and at least two of the exponential factors in the integrand in terms of double infinite series of spherical harmonics about one of the centers. The resulting integrations are then carried through by using the orthogonality properties of the spherical harmonics. The individual terms are ponderous even for the simplest of the three-center integrals. This made the computation of such integrals, as Coolidge and James[8] pointed out, "exceedingly laborious." References to work on such integrals has been cited in a previous communication of this series.[4] In that paper we treated particular types of these integrals by a method not requiring the Neumann expansion of $1/r_{12}$ and obtained single series solutions. Two types of three-center electron interaction integrals not readily accessible to our previous method are the subject of this article. Use of the Neumann expansion in conjunction with either the Maclaurin or the Taylor series expressions of the previous development is here employed. The necessary auxiliary functions required are for the most part known and tabulated[9,10] over large ranges of the parameters.

2. THE THREE-CENTER ELECTRONIC REPULSION INTEGRAL FOR LINEAR MOLECULES WITH A SINGLE ORBITAL CENTERED ON THE MIDDLE NUCLEUS

The general formula for such integrals may be written,

$$L_{cm,ee}=\int \chi_e(1)\chi_m(1)(1/r_{12})\chi_e'(2)\chi_e''(2)d\tau \equiv (\chi_e\chi_m|1/r|\chi_e'\chi_e''), \quad (2.1)$$

where the functions $\chi_e(1)$, $\chi_e'(2)$, $\chi_e''(2)$, $\chi_m(1)$ represent the general AO's (atomic orbitals) on the exterior nuclei and the middle nucleus of electrons 1 and 2, and where "r_{12}" is the distance between electron 1 and 2. The integration is over the position coordinates of both electrons. If the centers of the exterior orbitals of electron two, $\chi_e'(2)$ and $\chi_e''(2)$, are identical as for example in $L_{ab,cc}$ the integral is best handled by the method given in the previous communication.[4]

When the centers of the exterior orbitals of electron two are different as for example in $L_{ab,ac}$ the initial integration using this method would involve a three-center integration[11] and this and subsequent steps would

* This work was assisted in part by a grant from the National Science Foundation.

[1] W. Heitler and F. London, Z. Physik **44**, 455 (1927).
[2] Y. Sugiura, Z. Physik **45**, 484 (1927).
[3] R. S. Barker and H. Eyring, J. Chem. Phys. **21**, 912–917, (1953).
[4] R. S. Barker and H. Eyring (to be published).
[5] A. S. Coolidge, Phys. Rev. **42**, 189 (1932).
[6] S. O. Lundquist and P. O. Lowdin, Arkiv Fysik (Stockholm) **3**, 147 (1951).
[7] M. P. Barnett and C. A. Coulson, Trans. Roy. Soc. (London) **A243**, 221 (1951).
[8] A. S. Coolidge and H. M. James, J. Chem. Phys. **2**, 816 (1934).
[9] Kotani, Ishiguro, Hijikata, Nakamura, and Amemiya, J. Phys. Soc. Japan, **8**, 463 (1953).
[10] Kotani, Amemiya, and Simose, Proc. Phys. Math. Soc. Japan, **20**, Extra No. 1 (1938); **22**, Extra No. 1 (1940). We wish to thank Professor Kotani (Tokyo Imperial University) for the privilege of examining, in mimeographed form, range extensions of certain of these useful auxilary functions.
[11] For the restriction of the composite AO's to those of equal effective charges the formula of Hirschfelder, Eyring, and Rosen could be used. See Hirschfelder, Eyring, and Rosen, J. Chem. Phys. **4**, 121 (1936).

be difficult. The general case of unrestricted effective nuclear charges is accessible to the new method outlined below.

For illustrative purposes a specialized integral occurring in calculations of the triatomic hydrogen activated complex D·H·H will be formulated. Restriction to 1*s* hydrogenic atomic orbitals (with equal or unequal effective charges) is thus assumed. It may be well to point out that more general Slater-type orbitals with even powers of "r" before the exponential expressions of the middle nucleus' orbital would serve equally well as an example. The selected illustrative integral is,

$$L_{ab,\,ac}=\int \chi_a\chi_b(1/r_{12})\chi_a'\chi_c d\tau\equiv(\chi_a\chi_b|\,1/r\,|\chi_a'\chi_c). \quad (2.2)$$

The 1*s* hydrogenic orbitals are,

$$\chi_a(1)=(\zeta_0^3/\pi)^{\frac{1}{2}}\exp(-\zeta_0 r_{a1});$$
$$\chi_a'(2)=(\zeta_0^3/\pi)^{\frac{1}{2}}\exp(-\zeta_0 r_{a2});$$
$$\chi_b(1)=(\zeta_m^3/\pi)^{\frac{1}{2}}\exp(-\zeta_m r_{b1});$$
$$\chi_c(2)=(\zeta_0^3/\pi)^{\frac{1}{2}}\exp(-\zeta_0 r_{c2}),$$

where ζ_0=effective charge on nucleus of orbital "a" or "c," ζ_m=effective charge on nucleus of orbital "b," r_{a1}=distance of nucleus "a" from electron 1, r_{b1}=distance of nucleus "b" from electron 1, r_{a2}=distance of nucleus "a" from electron 2, and r_{c2}=distance of nucleus "c" from electron 2. The integral then is,

$$L_{ab,\,ac}=(\zeta_0^9\zeta_m^3)^{\frac{1}{2}}/(\pi)^2\int\int(1/r_{12})$$
$$\exp(-\zeta_0 r_{a1}-\zeta_m r_{b1}-\zeta_0 r_{a2}-\zeta_0 r_{c2})d\tau_1 d\tau_2, \quad (2.3)$$

in which, r_{12}=distance between electron 1 and 2, $d\tau_1$=volume element of electron 1 and $d\tau_2$=volume element of electron 2.

Elliptical coordinates are introduced. Choice of centers "a" and "c" as the foci of the coordinate system being made for simplification of the nuclear-electronic distance expressions. The interfoci distance D is then equal to $2R$ where R is the distance between the interior and exterior orbital centers. The coordinate expressions are,

$$\mu=\frac{r_a+r_c}{2R};\quad \nu=\frac{r_a-r_c}{2R};$$

ϕ=azimuthal angle of the electron.

The nuclear-electronic distances become,

$$r_{a1}=R(\mu_1+\nu_1);\quad r_{b1}=R(\mu_1^2+\nu_1^2-1)^{\frac{1}{2}};$$
$$r_{a2}=R(\mu_2+\nu_2);\quad r_{c2}=R(\mu_2-\nu_2).$$

In these coordinates the volume elements of the electrons are,

$$d\tau_1=R^3(\mu_1^2-\nu_1^2)d\mu_1 d\nu_1 d\phi_1$$

and

$$d\tau_2=R^3(\mu_2^2-\nu_2^2)d\mu_2 d\nu_2 d\phi_2.$$

The inverse electron-electron distance, $1/r_{12}$, may be expressed in terms of the elliptical coordinates of the two electrons in the conventional manner by the Neumann[12] expansion. Thus,

$$1/r_{12}=\frac{2}{D}\sum_{\tau=0}^{\infty}\sum_{\eta=0}^{\tau}L_{\tau\eta}Q_\tau^\eta(\mu_+)P_\tau^\eta(\mu_-)P_\tau^\eta(\nu_1)P_\tau^\eta(\nu_2)$$
$$\times\cos\eta(\phi_2-\phi_1) \quad (2.4)$$

where $L_{\tau 0}=(2\tau+1)$;

$$L_{\tau\eta}=(-1)^\eta 2(2\tau+1)\{(\tau-\eta)!/(\tau+\eta)!\}^2(\eta>1)$$

and $\mu_+(\mu_-)$ is the larger (smaller) of μ_1 and μ_2. The functions P_τ^η and Q_τ^η are the associated Legendre functions of the first and second kind. Introduction of the elliptical coordinate expressions and (2.4) into (2.3) then gives,

$$L_{ab,\,ac}=C'\int\int\int\int\int\int$$
$$\times\left[\sum_{\tau=0}^{\infty}L_{\tau\eta}Q_\tau^\eta(\mu_+)P_\tau^\eta(\mu_-)P_\tau^\eta(\nu_1)P_\tau^\eta(\nu_2)\right]$$
$$\times\{[\exp[-\zeta_0 R(\mu_1+\nu_1)-\zeta_m R(\mu_1^2+\nu_1^2-1)^{\frac{1}{2}}]$$
$$\times\exp[-\zeta_0 R(\mu_2+\nu_2)-\zeta_0 R(\mu_2-\nu_2)]\}$$
$$\times[(\mu_1^2\mu_2^2-\mu_1^2\nu_2^2-\mu_2^2\nu_1^2+\nu_1^2\nu_1^2)d\mu_1 d\mu_2 d\nu_1 d\nu_2 d\phi_1 d\phi_2, \quad (2.5)$$

where

$$C'=\frac{R^5(\zeta_0^9\zeta_m^3)^{\frac{1}{2}}}{(\pi)^2};\quad C=C'(\pi)^2;$$

and

$$d\tau=R^6(\mu_1^2\mu_2^2-\mu_1^2\nu_2^2-\mu_2^2\nu_1^2+\nu_1^2\nu_2^2)d\mu_1 d\mu_2 d\nu_1 d\nu_2 d\phi_1 d\phi_2.$$

Simplification of (2.5) is at once possible. The angles ϕ_1 and ϕ_2 enter the integrand only through the Neumann expansion (2.4) and the differentials in the volume elements. Integration over these angles will reduce all terms to zero except that for which $\eta=0$ when such integration gives $4(\pi)^2$. A third integration over ν_2 results in termination of the series from the Neumann expansion. This last statement is readily verified from the definition of the well-known auxiliary function[13] $G_\tau(p,0)$, the orthogonal property of Legendre polynomials, and the fact that ν to any power p may be expressed as a sum of Legendre polynomials of degrees no greater than p. Thus $G_\tau(p,0)=0$ for all $\tau>p$ and the four term volume derived expression in (2.5) will become zero for all $\tau>2$. After such alterations the ex-

[12] Conventions and nomenclature used here are consistent with that used before (see reference 3).

[13] This auxiliary function is defined as

$$G_\tau(p,\beta)=\int_{-1}^{1}\nu^p P_\tau(\nu)e^{-\beta\nu}d\nu.$$

It has well-known recurrence relations and tabulated values, $\beta=0.0(0.25)5.50$ and $\beta=6.0(0.50)7.0$, have been given by Kotani (see reference 10).

pression becomes,

$$L_{ab,ac}=4C\int\int\int\sum_{\tau=0}^{2}([L_{\tau 0}Q_\tau(\mu_+)P_\tau(\mu_-)P_\tau(\nu_1)]$$
$$\times\{\exp[-\zeta_0R(\mu_1+\nu_1)]\exp[-\zeta_mR(\mu_1^2+\nu_1^2-1)]^{\frac{1}{2}}$$
$$\times\exp(-2\zeta_0R\mu_2)\}[\mu_1^2\mu_2^2\cdot G_\tau(0,0)-\mu_1^2\cdot G_\tau(2,0)$$
$$-\mu_2^2\nu_1^2\cdot G_\tau(0,0)+\nu_1^2\cdot G_\tau(2,0)])d\mu_1d\mu_2d\nu_1. \quad (2.6)$$

Expression (2.6) may be further simplified by evaluating the $G_\tau(p,0)$'s in the equation. From the function definition[13] and elementary integration it follows that,

$$G_0(0,0)=2;\quad G_1(0,0)=0;\quad G_2(0,0)=0;$$
$$G_\tau(0,0)=0\quad(\tau>0);$$
$$G_0(2,0)=2/3;\quad G_1(2,0)=0;\quad G_2(2,0)=4/15;$$
$$G_\tau(2,0)=0\quad(\tau>2).$$

Insertion of these values then reduces (2.6) to (2.7).

$$L_{ab,ac}=8C\int\int\int Q_0(\mu_+)P_0(\mu_-)P_0(\nu_1)\{\cdots\}$$
$$\times[\mu_1^2\mu_2^2-\tfrac{1}{3}\mu_1^2-\mu_2^2\nu_1^2+\tfrac{1}{3}\nu_1]d\mu_1d\mu_2d\nu_1$$
$$+16C\int\int\int Q_2(\mu_+)P_2(\mu_-)P_2(\nu_1)\{\cdots\}$$
$$\times[-\tfrac{1}{3}\mu_1^2+\tfrac{1}{3}\nu_1^2]d\mu_1d\mu_2d\nu_1. \quad (2.7)$$

To perform the remaining integrations the irrational exponential function $\exp[-\zeta_mR(\mu_1^2+\nu_1^2-1)]^{\frac{1}{2}}$ in braces is expanded by the Maclaurin series employed before.[4] Thus letting $(\nu_1^2-1)=x$ and expanding about the point $x=0$ one obtains,

$$\exp[-\zeta_mR(\mu_1^2+\nu_1^2-1)^{\frac{1}{2}}]$$
$$=\exp(-\zeta_mR\mu_1)\Big[1-\frac{\zeta_mR}{2\mu_1}(\nu_1^2-1)$$
$$+\sum_{p=2}^{\infty}\Big\{\frac{(-1)^p(2p-3)!(\zeta_mR)}{(p-2)!2(2p-2)\mu_1(2p-1)}$$
$$+\sum_{q=2}^{p}\frac{(-1)^p(2p-q-1)!(\zeta_mR)^q}{(q-1)!(p-q)!2(2p-q)\mu_1(2p-q)}\Big\}\frac{(\nu_1^2-1)^p}{p!}\Big]$$
$$=e^{-k\mu_1}[\sum_{t=0}^{\infty}u_t\cdot(\nu_1^2-1)^t], \quad (2.8)$$

where $k=\zeta_mR$, and the coefficients, u_t, of the Maclaurin series are functions of μ_1 only and may be expressed in terms of constants times inverse powers of μ_1. Expression (2.5) may now be rewritten as,

$$L_{ab,ac}=8C\int\int Q_0(\mu_+)P_0(\mu_-)\exp[-(\zeta_0+\zeta_m)R\mu_1]\exp(-2\zeta_0R\mu_2)[\mu_1^2\mu_2^2-\tfrac{1}{3}\mu_1^2]$$
$$\times\sum_{t=0}^{\infty}u_t\Big\{\int_{-1}^{1}\exp(-\zeta_0R\nu_1)[(\nu_1^2-1)^tP_0(\nu_1)d\nu_1]\Big\}d\mu_1d\mu_2$$
$$+8C\int\int Q_0(\mu_+)P_0(\mu_-)\exp[-(\zeta_0+\zeta_m)R\mu_1]\exp(-2\zeta_0R\mu_2)[-\mu_2^2+\tfrac{1}{3}]$$
$$\times\sum_{t=0}^{\infty}u_t\Big\{\int_{-1}^{1}\nu_1^2\exp(-\zeta_0R\nu_1)[(\nu_1^2-1)^tP_0(\nu_1)d\nu_1]\Big\}d\mu_1d\mu_2$$
$$-\frac{16}{3}C\int\int\mu_1^2Q_2(\mu_+)P_2(\mu_-)\exp[-(\zeta_0+\zeta_m)R\mu_1]\exp(2\zeta_0R\mu_2$$
$$\times\sum_{t=0}^{\infty}u_t\Big\{\int_{-1}^{1}\exp(-\zeta_0R\nu_1)[(\nu_1^2-1)^tP_2(\nu_1)d\nu_1]\Big\}d\mu_1d\mu_2$$
$$+\frac{16}{2}C\int\int Q_2(\mu_+)P_2(\mu_-)\exp[(\zeta_0+\zeta_m)R\mu_1]\exp(2\zeta_0R\mu_2)$$
$$\times\sum_{t=0}^{\infty}u_t\Big\{\int_{-1}^{1}\nu_1^2\exp(-\zeta_0R\nu_1)[(\nu_1^2-1)^tP_2(\nu_1)d\nu_1]\Big\}d\mu_1d\mu_2. \quad (2.9)$$

The coefficients u_t are not functions of ν_1 so the integration over ν_1 may now be performed by use of the $G_\tau(p,\beta)$ auxiliary functions in the manner described for the ν_2 integration. The remaining integrations may

now be expressed in terms of the functions,

$$W_\tau(p,\gamma_1,q,\gamma_2)=\int_1^\infty\int_1^\infty \exp(-\gamma_1\mu_1-\gamma_2\mu_2)\times\mu_1{}^p\mu_2{}^qQ_\tau(\mu_+)P_\tau(\mu_-)d\mu_1d\mu_2. \quad (2.10)$$

When the power of μ_1 is positive (2.10) is the same auxiliary function as that occurring in the two-center exchange integral. Recurrence formulas and use of this function have been dealt with by H. M. James.[14] For $\gamma_1=\gamma_2$ tabulated values are available.[10] The power of μ_1 occurring in (2.10) is the sum of the power of μ_1 entering from the volume element term (always positive) and that from the Maclaurin expansion (0 for the first term, -1 for the second, etc.). Thus the large terms of the above method lead to no new auxiliary functions. For precise work one may wish to include higher terms from the Maclaurin expansion which lead to negative powers of μ_1 in the $W_\tau(p,\gamma_1,q,\gamma_2)$ expressions. These may be evaluated by use of the method described in the next section.

3. EVALUATION OF AUXILIARY FUNCTIONS

Evaluation of the type integrals of section 2 depend on known auxiliary functions[10,14] for the larger terms of the final series expression. For precise work however it is desirable to include higher terms of the series which introduce the complication of negative powers of the variable, μ_1, in the auxiliary function,

$$W_\tau(p,\gamma_1,q,\gamma_2)=\int_1^\infty\int_1^\infty \mu_1{}^p\mu_2{}^qe^{-\gamma_1\mu_1}e^{-\gamma_2\mu_2}Q_\tau(\mu_+)\times P_\tau(\mu_-)d\mu_1d\mu_2. \quad (3.1)$$

Recurrence relations exist for the Legendre polynomials of the first and second kind, which enable one to express $W_\tau(p,\gamma_1,q,\gamma_2)$ in terms of $W_0(p,\gamma_1,q,\gamma_2)$ and $W_1(p,\gamma_1,q,\gamma_2)$. These functions may be reduced as follows:

$$W_\tau(p,\gamma_1,q,\gamma_2)=\int_1^\infty \mu_1{}^pe^{-\gamma_1\mu_1}Q_\tau(\mu_1)d\mu_1\times\int_1^{\mu_1}\mu_2{}^qe^{-\gamma_2\mu_2}P_\tau(\mu_2)+\int_1^\infty\mu_2{}^qe^{-\gamma_2\mu_2}Q_\tau(\mu_2)d\mu_2\times\int_1^{\mu_2}\mu_1{}^pe^{-\gamma_1\mu_1}P_\tau(\mu_1)d\mu_1. \quad (3.2)$$

Known methods were previously developed[3] for evaluation of

$$\int_1^{\mu_1}\mu_2{}^qe^{-\gamma_2\mu_2}P_\tau(\mu_2)d\mu_2$$

in linear terms of products of $e^{-\gamma_2\mu_1}$ and positive powers of μ_1. The remaining consideration for the first part of (3.2), after combining terms from the first integration with those initially present, is the second integration. This has the form

$$\int_1^\infty \mu_1{}^ne^{-\alpha\mu_1}Q_\tau(\mu_1)d\mu_1,$$

where $\alpha=(\gamma_1+\gamma_2)$. Known methods are available[10] when n is positive. If n is negative use of the recurrence relationship for $Q_\tau(\mu)$ already cited reduces consideration to terms involving only $Q_0(\mu)=\frac{1}{2}\ln\mu+1/\mu-1$. Thus interest is centered on integrations of the type,

$$\frac{1}{2}\int_1^\infty \mu^ne^{-\alpha\mu}\ln\left(\frac{\mu+1}{\mu-1}\right)d\mu=\frac{1}{2}\int_1^\infty\{e^{-\alpha\mu}\ln(\mu+1)\}\mu^nd\mu-\frac{1}{2}\int_1^\infty\{e^{-\alpha\mu}\ln(\mu-1)\}\mu^nd\mu. \quad (n<0) \quad (4.3)$$

Such integrals may be integrated by parts. For example,

$$\frac{1}{2}\int_1^\infty \mu^ne^{-\alpha\mu}\ln(\mu+1)d\mu=\frac{1}{2}\frac{\mu^{n+1}}{n+1}e^{-\alpha\mu}\ln(\mu+1)\Big]_1^\infty-\frac{1}{2}\int_1^\infty\frac{\mu^{n+1}}{n+1}\left\{e^{-\alpha\mu}\frac{d\mu}{\mu+1}-\alpha e^{-\alpha\mu}\ln(\mu+1)d\mu\right\}.$$

Successive application of the above process followed by use of elementary integration methods enables one to evaluate the necessary terms. In the second part of (4.2) the possibility of negative powers of μ_1 in the integral

$$\int_1^{\mu_2}\mu_1{}^pe^{-\gamma_1\mu_1}P_\tau(\mu_1)d\mu_1$$

may be dealt with by use of given recurrence relations and by use of the elementary integration formula,

$$\int\frac{e^{-\alpha x}}{x^n}dx=\frac{-1}{n-1}\left[\frac{e^{-\alpha x}}{x^{n-1}}+\alpha\int\frac{e^{-\alpha x}}{x^{n-1}}dx\right].$$

Interest is thus reduced to evaluation of

$$\int_1^\mu\frac{e^{-\alpha x}}{x}dx$$

in a form which will enable one to carry through the second integration. Known series expressions may be adapted[15] for this needed initial evaluation which give terms for the second integration of the form already considered.

[14] H. M. James, J. Chem. Phys. 2, 794 (1934).

[15] See the series used in reference 10, p. 21 for evaluation of the exponential integral.

4. NUMERICAL CALCULATIONS

A numerical example using the proposed Maclaurin series, showing rapidity of the series convergence, and indicating the labor required in numerical calculation through its use has been given elsewhere.[4] Numerical evaluation of the spherical harmonic expressions conjunctionally used in this paper is illustrated below. Since the proposed method doesn't depend upon the effective nuclear charges of the orbitals the particular integral with equal effective nuclear charge orbitals, $L_{ab,\,ac}(R,\zeta)$, will be used to illustrate the numerical calculations of the proposed general method. Hirschfelder,[16] using special numerical integration methods applicable to equal effective nuclear charge orbitals only, secured after several months of hard work a few values for the integrals $L_{ab,\,ac}$ and $L_{ab,\,bc}$. He obtained the value $L_{ab,\,ac}=0.051214$ for $R=2.0$ and $\zeta_0=\zeta_m=1$. For comparative and illustrative purposes one may then use these parametric values in the general expression (2.6) or (2.9). Restricting detailed consideration to the spherical harmonic expressions, one may illustrate the evaluation of (2.9) by explicitly writing out only terms from the first member of the Maclaurin series as below,

$$\begin{aligned}L_{ab,\,ac}=&\,8CW_0(2,2,4)\cdot G_0(0,2)-\frac{8C}{3}W_0(2,0,4)\cdot G_0(0,2)\\&-8CW_0(0,2,4)\cdot G_0(2,2)+\frac{8C}{3}W_0(0,0,4)\cdot G_0(2,2)\\&-\frac{16}{3}CW_2(2,0,4)\cdot G_2(0,2)+\frac{16}{3}CW_2(0,0,4)\cdot G_2(2,2)\\&+(\text{expressions from higher terms of the Maclaurin expansion}).\end{aligned}\tag{4.1}$$

Values of $W_\tau(p,q,\gamma)$ and $G_\tau(p,\beta)$ may be obtained from the tabulations[9–11] of Kotani and his associates. Upon inserting the above values into (4.1) one obtains, $L_{ab,\,ac}=0.024\ 81875+$(higher terms from the Maclaurin series).

5. THE GENERAL THREE-CENTER ELECTRONIC REPULSION INTEGRAL FOR SYMMETRICAL LINEAR MOLECULES

The formula for such integrals may be written,

$$\begin{aligned}L_{e\gamma,\,\nu\nu}=&\int\chi_e(1)\chi_\gamma(1)(1/r_{12})\chi_\nu'(2)\chi_\nu''(2)d\tau\\&\equiv(\chi_e\chi_\gamma|1/r|\chi_\nu'\chi_\nu''),\end{aligned}\tag{5.1}$$

where the function χ_e represents an AO on an exterior nucleus and χ_γ, χ_ν', χ_ν'' represent AO's on either exterior or interior nuclei. The other symbols are as before defined. If the "γ" centers of electron two are the same as for example in $L_{ac,\,bb}$ or $L_{ab,\,cc}$, the integral is best handled by the method given in a previous paper.[4] If only one of the three "γ" centers is on the interior nucleus as for example in the integral $L_{ab,\,ae}$ one may use the method of Sec. 2. If, as in the integral $L_{ab,\,bc}$, interior orbital centers for both electron 1 and 2 are present (the only possibility not already considered) the method of this section applies.

Again for illustrative purposes an integral occurring in calculations of the triatomic hydrogen complex may be used. The integral may be written,

$$\begin{aligned}L_{ab,\,bc}=&C_1\int\frac{1}{r_{12}}\\&\times\exp(-\zeta_0r_{a1}-\zeta_mr_{b2}-\zeta_mr_{b2}-\zeta_0r_{c2})d\tau_1d\tau_2,\end{aligned}\tag{5.2}$$

where

$$C_1=\frac{(\zeta_m{}^3\zeta_0{}^3)}{(\pi)^2}.$$

Elliptical coordinates are again introduced but this time choice of centers "b" and "a" as foci of the coordinate system is made so the "b" nuclear-electronic distances will be simplified. The interfoci distance D is now equal to R the distance of the interior orbital center from the exterior ones. The orbital-center electron distances are,

$$r_{a1}=\frac{\zeta_0R}{2}(\mu_1+\nu_1);\quad r_{b2}=\frac{\zeta_mR}{2}(\mu_2-\nu_2)$$

$$r_{b1}=\frac{\zeta_mR}{2}(\mu_1-\nu_1);\quad r_{c2}=\frac{\zeta_0R}{2}(\mu_2{}^2+\nu_2{}^2-6\mu_2\nu_2+8)^{\frac{1}{2}}.$$

The interfoci distance, D, in the Neumann expansion (2.4) is this time just R. Substitution in the manner of Sec. 2 leads, after integration over the angles ϕ_1 and ϕ_2 to the equation,

$$\begin{aligned}L_{ab,\,bc}=&C_2\int\int\int\int\\&\times\left[\sum_{\tau=0}^{\infty}L_{\tau0}Q_\tau(\mu_+)P_\tau(\mu_-)P_\tau(\nu_1)P_\tau(\nu_2)\right].\\&\times[\exp[\zeta_0R/2(\mu_1+\nu_1)-\zeta_mR/2(\mu_1-\nu_1)]\\&\times\exp[-\zeta_mR/2(\mu_2-\nu_2)-\zeta_0R/2(\mu_2{}^2+\nu_2{}^2-\mu_2\nu_2+8)^{\frac{1}{2}}]]\\&\times[(\mu_1{}^2\mu_2{}^2-\mu_1{}^2\nu_2{}^2-\mu_2{}^2\nu_1{}^2+\nu_1{}^2\nu_2{}^2)d\mu_1d\nu_1d\mu_2d\nu_2]\end{aligned}\tag{5.3}$$

TABLE I. Particular values of $W_\tau(p,q,\gamma)$.

$W_0(2,2,4)$	$4.970\ 5855\times10^{-5}$
$W_0(2,0,4)$	$3.308\ 9750\times10^{-5}$
$W_0(0,2,4)$	
$W_0(0,0,4)$	$2.231\ 9390\times10^{-5}$
$W_2(0,2,4)$	$6.080\ 7286\times10^{-6}$
$W_2(2,0,4)$	
$W_2(0,0,4)$	$4.454\ 1796\times10^{-6}$

[16] J. O. Hirschfelder (Ph.d. thesis, Princeton University, 1935).

where

$$C_2=\frac{(\zeta_0^3\zeta_m^3)R^5}{4}.$$

Letting $\alpha=(R/2)(\zeta_m+\zeta_0)$; $\beta=(R/2)(\zeta_m-\zeta_0)$; $\gamma=\zeta_m R/2$, integration over ν_1 may be accomplished as before by use of the auxiliary functions $G_\tau(p,\beta)$. To perform the remaining integrations, one is this time faced with the exponential function,

$$\exp(-\zeta_0 r_{c2})=\exp[-\zeta_0 R/2(\mu_2^2+\nu_2^2-6\mu_2\nu_2+8)]^{\frac{1}{2}}.$$

This may be expanded by the Taylor series before developed.[4] Thus expanding about $\nu=-1$,

$$\begin{aligned}f(\nu_2)&=\exp[-\zeta_0 R/2(\mu_2^2+\nu_2^2-6\mu_2\nu_2+8)^{\frac{1}{2}}]\\&=f(-1)+f'(-1)\frac{(\nu_2+1)}{1!}\\&\qquad+f''(-1)\frac{(\nu_2+1)^2}{2!}+\cdots\\&=\exp[-(\zeta_0 R/2)(\mu_2+3)]\\&\qquad\times\left[1+\left(\frac{1+3\mu_2}{\mu_2+3}\right)(\nu_2+1)+\cdots\right]\\&=\exp[-k_2(\mu_2+3)][\sum_{m=0}^{\infty}u_m(\nu_2+1)^m],\end{aligned}\tag{5.4}$$

where $k_2=\zeta_0 R/2$, and the coefficients, u_m, of the Taylor series are functions of μ_2 only and may be further decomposed. Integration over ν_1 may be performed by use of the ${}_mG_\tau(p,\gamma)$ auxiliary functions. Expression (5.3) may now be rewritten

$$\begin{aligned}L_{ab,\,bc}=C_2&\sum_{\tau=0}^{\infty}L_{\tau 0}Q_\tau(0,\beta)\\&\times\sum_{m=0}{}_mG_\tau(m,\gamma)\cdot{}_mW_\tau(u_m,2,2,\alpha)\\&+C_2\sum_{\tau=0}L_{\tau 0}Q_\tau(2,\beta)\\&\times\sum_{m=1}{}_mG_\tau(m,\gamma)\cdot{}_mW_\tau(u_m,0,2,\alpha)\\&+C_2\sum_{\tau=0}L_{\tau 0}Q_\tau(0,\beta)\\&\times\sum_{m=0}{}_mQ_\tau(m,\gamma)\cdot{}_mW_\tau(u_m,0,2,\alpha)\\&+C_2\sum_{\tau=0}L_{\tau 0}Q_\tau(2,\beta)\\&\times\sum_{m=0}{}_mQ_\tau(m,\gamma)\cdot{}_mW_\tau(u_m,0,0,\alpha),\end{aligned}\tag{5.5}$$

Table II. Particular values of $G_\tau(p,\beta)$.

$G_0(0,2)$	3.626 86041
$G_0(2,2)$	1.678 09492
$G_2(0,2)$	0.703 71218
$G_2(2,2)$	0.866 08322

where one defines,

$${}_mQ_\tau(p,\beta)=\int_{-1}^{1}(\nu+1)^m P_\tau(\nu)\cdot\nu^p e^{-\beta\nu}d\nu\tag{5.6}$$

and

$${}_mW_\tau(u_m,p,q,\alpha)=\int_1^\infty\int_1^\infty u_m\mu_1^2\mu_2^2\times\exp(-\alpha\mu_1-\alpha\mu_2)Q_\tau(\mu_+)P_\tau(\mu_-)d\mu_1 d\mu_2.\tag{5.7}$$

The first term in the Maclaurin series ($m=0$) gives the well-known two-center exchange integral auxiliary function $W_\tau(p,q,\alpha)$.

Evaluation of the higher terms, used in precise work, of the auxiliary function ${}_mW_\tau(p,q,\alpha)$ are much the same as those already described. The single complication arising here not discussed before is the presence of terms in $z=\mu+3$. Thus for example one may examine integrals of the type,

$$\int_0^\infty\frac{e^{-\alpha z}}{z^n}Q_\tau(\mu)d\mu.$$

This expression may be reduced, by the recurrence relation for $Q_\tau(\mu)$, to consideration of the form,

$$\frac{1}{2}\int_0^\infty\frac{e^{-\alpha z}}{z}\ln\left(\frac{z-2}{z-4}\right)dz,$$

This term may be readily evaluated by use of the exponential integral[16] (or integral logarithm) which is defined as

$$Ei(-z_0)=-\int_0^\infty(e^{-z}/z)dz.$$

Other modifications needed are of the same type.

ACKNOWLEDGMENTS

We would like to thank Professor C. J. Thorne (Mathematics Department, University of Utah) for taking part in discussions of certain phases of this problem and D. A. Baker for independently verifying the numerical calculations.

[16] For values of the exponential integral see the two volumes "Tables of Sine, Cosine and Exponential Integral" prepared by the Federal Works Agency under the Sponsorship of the National Bureau of Standards (N.Y.M.T.P., 1940).

Unified Orbital Treatment of Ethylene

C. R. MUELLER
Chemistry Department, Purdue University, Lafayette, Indiana
(Received May 18, 1953)

Quantum-mechanical calculations of the properties of pi and sigma bonds in ethylene were carried out using atomic, molecular, and semilocalized orbital methods. Theoretical values were obtained for binding, and singlet-triplet separation energies. The polarizabilities of these bonds were also calculated, as were the charge distributions.

The electronic structure of the π bond was found to be largely localized contrary to the assumptions of molecular orbital theory, but the sigma bond was found to have molecular orbital structure.

On the basis of calculations of bond polarizability it was concluded that π bond accounts for about 90 percent of total bond polarizability. This result is due to the sp^2 hybridization of the sigma bond.

The results of extended orbital treatments of π-electron systems are also discussed.

QUANTUM-MECHANICAL calculations of the properties of pi and sigma bonds were carried out using the atomic, molecular, and semilocalized orbital methods. Theoretical values were obtained for the binding energies, polarizabilities, singlet-triplet energy separation, and charge distributions. In addition the results of extended orbital treatments of π-electron systems are also considered.

PART I. PROPERTIES OF THE SIGMA BOND

The calculation of the properties of the sigma bond was made by application of the variational theorem to a two-electron problem. The two valence electrons are in a coulombic and exchange field of each other and the effect of electrons not in this bond was treated as a coulomb potential.

The Hamiltonian operator for a field of this type is

$$H=-\tfrac{1}{2}(\nabla_1^2+\nabla_2^2)-\frac{Z_a}{R_{a1}}-\frac{Z_a}{R_{a2}}-\frac{Z_b}{R_{b1}}-\frac{Z_b}{R_{b2}}+\frac{1}{R_{12}}+\frac{Z_aZ_b}{R_{ab}}+C. \quad (1)$$

C is the Coulombic potential due to the electrons outside the bond. In the computation of C the effect of the hydrogen atoms on the carbon-carbon bond was not considered. We have neglected such effects for the reason that we wished to compare the results of this calculation with those made on benzene with a similar approximation. The interaction between the carbon-carbon bond and the attached hydrogen atom has been estimated by Mulliken[1] to be about 0.1 ev and, if this estimate is correct, could properly be neglected.

The eigenfunction for such a problem has the form

$$\Psi=\psi_1(1)\psi_2(2)+\psi_1(2)\psi_2(1). \quad (2)$$

The number in brackets indicates the electron which is assigned to ψ_1 and ψ_2, where ψ_1 has the form

$$\psi_1=\varphi_a+\lambda\varphi_b \quad (3)$$

and ψ_2 has the form

$$\psi_2=\lambda\varphi_a+\varphi_b. \quad (4)$$

φ_a and φ_b are Slater atomic orbitals with an exponential charge of 3.18. λ is a parameter determined by use of the variational theorem.

The energy of such a system is given by the equation

$$E=\frac{\int\Psi H\Psi d\tau}{\int\Psi\Psi d\tau}. \quad (5)$$

On substituting (2) into Eq. (5) we obtain the energy of the valence electron in terms of various kinds of integrals and the variational parameter.

Two approximations were used in the evaluation of the integrals both of which have been extensively applied by Mulliken.[1]

The first of these is that the integral

$$\int\varphi_a\left(-\tfrac{1}{2}\nabla^2-\frac{Z_a}{R_a}\right)\varphi_a d\tau$$

is equal to the ionization potential of an electron in the state of the free atom represented by φ_a. Since φ_a for the sigma bond represents an electron in a trigonal state of hybridization, an ionization potential of 0.4865 atomic unit (1 atomic unit = 27.205 electron volts) was used for the sigma bonding electrons. This value is calculated using the self-consistent field results of Ufford[2] for the carbon atom.

The second approximation used is that the integral

$$\int\varphi_a\left(-\tfrac{1}{2}\nabla^2-\frac{Z_a}{R_a}\right)\varphi_b=SI_p,$$

where S is the overlap integral between φ_a and φ_b, and I_p is the ionization potential.

The remaining integrals were evaluated using the integral tables of Kopineck.[3]

[1] R. S. Mulliken, J. chim. phys. **46**, 497 (1949).

[2] C. W. Ufford, Phys. Rev. **53**, 568 (1938).

[3] H. Kopineck, Z. Naturforsch. **5a**, 420 (1950).

All of the calculations in the paper were carried out using an internuclear distance of 1.33 Ångstrom units.

Using these integrals and the variational theorem one can now find the best eigenfunction for such a two-electron system. The value of λ for the sigma bond was then found to be 1.00, and the sigma valence orbitals have molecular orbital form. When $\lambda=0$, the orbitals are forced into atomic orbital form.

Binding energy calculations were made using the formula of Mulliken,[1]

$$E_B=\frac{2\beta}{1+S}, \tag{6}$$

where E_B is the binding energy, β is the resonance integral, and S is the overlap integral.

This formula is valid only for molecular orbitals and the binding energies for other cases were obtained by calculating the difference between the total electronic energies of the various methods. The binding energy for the sigma bond was found to be 128 kcal for the molecular orbital method and 69 kcal for the atomic orbital method.

PART II. PROPERTIES OF THE PI BOND

A similar calculation was carried out for the pi bond. The experimental ionization potential for the carbon atom was used, and φ_a and φ_b are in this case Slater atomic p_x orbitals with an exponential charge of 3.18.

In sharp contrast the valence electrons in this case are largely localized on the carbon atoms. The eigenfunctions obtained from the variational method have the form

$$\varphi_a+0.282\varphi_b; \quad 0.282\varphi_a+\varphi_b,$$

and λ has the value 0.282, instead of 0 in the atomic orbital method and one in the molecular orbital method.

The calculated binding energies are 90 kcal for the molecular orbital method, 103 for the semilocalized orbital method ($\lambda\neq 0$, $\lambda\neq 1.00$), and 75 kcal for the atomic orbital method. There is considerable doubt as to the experimental energy but Mulliken[1] gives a value of 100 or 127 kcal depending on whether or not the heat of sublimation of carbon is 125 or 175 kcal. These values are at least twice those given by Pauling.

PART III. BOND POLARIZABILITIES

The bond polarizabilities are also very interesting. There are, of course, no experimental observations on the π and σ bonds separately, but one expects the bond polarizability of the σ bond in ethylene to be about the same as that in saturated hydrocarbons. If we subtract this σ-bond polarizability from the polarizability of the carbon-carbon double bond, we should have an estimate of the π-bond polarizability. The data of Denbigh leads one to conclude that $\frac{2}{3}$ of the double bond polarizability is due to the sigma bond and $\frac{1}{3}$ to the π bond. Quantum-mechanical discussions of systems containing π electrons have always assumed a negligible sigma bond polarizability, and we had expected to disprove this.

The bond-polarizability calculations were made by finding the dipole moment of the bond in a uniform electric field directed along the internuclear axis. The polarizability α is related to the dipole moment, μ, by means of the defining relationship

$$\boldsymbol{\mu}=\alpha\mathbf{E}. \tag{7}$$

The calculations were carried out for the sigma bond using the standard secular equation technique.[4] A special form of the secular equation must be used for the π bond because of exchange energy terms. The derivation starts with an expression for the total energy, including exchange.

The expression for the total energy is

$$E=(Q+K)/(I+S^2). \tag{8}$$

In order to take advantage of the secular equation technique, we have calculated the effect of the applied electric field on only one orbital at a time, and have not included the second-order interactions which arise through changed charge distribution of electrons other than the one in the orbital under consideration.

We wish to calculate the distortion of an orbital $a\varphi_a+b\varphi_b$. Let Φ represent the second orbital, which has been previously determined; then substituting into the total energy expression:

$$\begin{aligned}Q=&a^2\int\varphi_a(1)\Phi(2)H\varphi_a(1)\Phi(2)d\tau_1d\tau_2\\&+b^2\int\varphi_b(1)\Phi(2)H\varphi_b(1)\Phi(2)d\tau_1d\tau_2\\&+2ab\int\varphi_a(1)\Phi(2)H\varphi_b(1)\Phi(2)d\tau_1d\tau_2\\&=a^2(aa/H/\Phi\Phi)+b^2(bb/H/\Phi\Phi)\\&\qquad+2ab(ab/H/\Phi\Phi).\end{aligned} \tag{9}$$

In the abbreviated notation

$$\begin{aligned}K=&a^2(a\Phi/H/a\Phi)\\&+2ab(a\Phi/H/b\Phi)\\&+b^2(b\Phi/H/b\Phi).\end{aligned} \tag{10}$$

Letting

$$I=a^2+2abS+b^2$$

and

$$S=a^2Sa^2\Phi+2abS_{a\Phi}S_{b\Phi}+b^2S_{b^2\Phi}.$$

Minimization with respect to the energy results in the secular equation,

$$\begin{vmatrix}A_{11}&A_{12}\\A_{21}&A_{22}\end{vmatrix}=0. \tag{11}$$

$$A_{11}=(a^2/H/\Phi^2)+(a\Phi/H/a\Phi)-(I+S_{a^2\Phi})E$$

$$A_{21}=A_{12}=(ab/H/\Phi^2)+(a\Phi/b\Phi)-(S_{ab}+S_{b\Phi}S_{a\Phi})E$$

$$A_{22}=(b^2/H/\Phi^2)+(b\Phi/b\Phi)-(I+S_{b^2\Phi})E.$$

[4] C. A. Coulson, *Valence* (Oxford University Press, London, 1953), p. 61.

TABLE I.

π and σ bond	Polarizabilities	
$E\times10^{-16}$ (e.s.u. units)	$\alpha\times10^{24}$ cm^3	
	π bond	σ bond
0.1715	2.86	0.26
0.8575	2.82	0.26
1.715	2.64	0.26

The major difference between this and the usual molecular orbital secular equation is the presence of exchange integrals in each matrix element.

The results of this calculation are given in Table I.

The calculated values attribute over 90 percent of the polarizability to the π bond.

While the total is in excellent agreement with calculation from experiment (2.86), the ratio is in flagrant disagreement. The reason for the small sigma bond polarizability is directly attributable to hybridization. The charge centroid of the sp^2 orbital is too near the bond center for effective distortion. Either it is necessary to give up this concept or else one must reinterpret the experimental evidence. The theoretical calculations are concerned only with the bonding electrons. It is, perhaps, possible that the value obtained from the interpretation of experiment are simply values of the component of the total molecular polarizability along the bond axis.

The accuracy of the eigenfunction for the π bond was checked by calculating the singlet-triplet energy separation for ethylene. This includes a calculation for both the perpendicular and parallel excited states. The results are give in Table II.

PART IV. RESULTS OF EXTENDED ORBITAL TREATMENTS OF π-ELECTRON SYSTEMS

It is perhaps an opportune moment to discuss the results obtained by transcending the molecular and atomic orbital methods. Essentially there are at least three methods of doing this. The method utilized in the preceding calculations has been called a semilocalized or unified oribital approach. The same goal may be achieved in the molecular orbital method by mixing in excited configurations, and in the atomic orbital method by mixing in other canonical structures, notably ionic ones. In this case the three methods are very closely related, if not mathematically identical. The ionic configurations are probably the most important addition but some improvement results if other excited states are included.

A number of calculations have been performed by Craig and his co-workers. Additional work has also been done by a group of Japanese physicists, particularly on acetylene. Primarily all of the papers mentioned are concerned with a study of the excited states. The details of the approximations used in each case vary but there is general agreement as to the magnitude of the improvement of the extended orbital methods over the traditional molecular and atomic orbital approaches.

The most pertinent comparison of the calculations in this paper are with the work by Craig[5] on ethylene. Craig reports that the addition of ionic terms to the atomic orbitals ground-state eigenfunction results in a 0.624-ev improvement of the best orbitals over the atomic orbitals, and a 1.663-ev improvement over molecular orbitals. Craig has used a much higher effective nuclear charge (3.432) for the π electrons, and the effect of this charge should be to reduce delocalization of the atomic orbitals during bond formation. This is reflected in the lower λ value found by Craig. The coefficient of the ionic terms is 0.264 that of the covalent term. The corresponding λ value is 0.134. The difference in effective nuclear charge is apparently responsible for the reversal of the atomic and molecular orbitals methods in order of accuracy. It is safe to conclude the extended orbital treatments lead to improvement of 0.5 to 1.7 ev in accuracy for the ethylene ground state and that the π electrons are largely localized on the atoms.

TABLE II. Excitation energies for ethylene.

	$\perp$ State	$\parallel$ State
Atomic orbital method	1.36 ev	2.97 ev
Molecular orbital method	1.99 ev	3.60 ev
Semilocalized orbital method	2.57 ev	4.174 ev
Observed		5.4 ev

An interesting calculation on acetylene has been done by Nakamura and co-workers.[6]

In this molecule, where the approximations used are similar to those made here, the molecular orbital method appears to be more accurate than the atomic orbital method. The best ground state orbitals show a 3.16-ev improvement over atomic orbitals and a 2.37-ev improvement over molecular orbitals. The singlet-triplet separation energies are quite close to ours.

Some of the excited states in acetylene are improved by as much as 4.4 ev.

Craig[7] has reported improvements of about 5 ev in some of the excited states of benzene.

In view of the enormous amount of work using the primitive molecular and atomic orbital theories, and the rather large improvement resulting from extended orbital treatments, it seems imperative that a searching analysis is in order of the previous explanations of the reactivities of aromatic systems. It is too early to say whether any drastic alteration in these explanations will be forthcoming.

[5] D. P. Craig, Proc. Roy. Soc. (London) **A200**, 272 (1950).
[6] Nakamura, Ohno, Kotani, and Hyikata, Progr. Theoret. Phys. (Japan) 8, 387 (1952).
[7] D. P. Craig, Proc. Roy. Soc. (London) **A200**, 474 (1950).

Steady-State Diffusion into a Streaming Sphere at Low Reynolds Number*

H. L. FRISCH†
Department of Chemistry, Polytechnic Institute of Brooklyn, Brooklyn, New York
(Received July 3, 1953)

A solution of the steady-state Smoluchowski equation, describing diffusion into a spherical sink streaming with constant velocity relative to the fluid, is obtained as a power series in a parameter which is directly proportional to the Reynolds number of the flow. For small values of Reynolds number the series converges. The concentration and flux to a freely-falling cloud droplet (aerosol particle) in air is calculated. The effect of the motion of the droplet on the flux is proportional to a first approximation to the square of Reynolds number and consequently except for very large times of observation exerts a negligible influence on the diffusion controlled growth of the droplet. An extension of the method to nonstationary diffusion problems is indicated.

INTRODUCTION

IN recent[1,2] papers dealing with the diffusional processes in the growth of aerosol particles, e.g., cloud droplets in the atmosphere, the motion of the particles relative to the medium in which they are suspended is neglected. In the case of cloud droplets whose radius varies from 10^{-5} cm to 10^{-3} cm in still air, this motion is caused by the action of the earth's gravitational field, imparting to a particle of radius R the constant terminal velocity V_0 given by the Stokes[3]-Cunningham[4] law. The diffusion of water vapor in the surrounding air to such a "streaming" droplet is then no longer governed by Fick's Second Law but is determined to a sufficient approximation by Smoluchowski's equation.[5,6]

More generally, consider a spherical aerosol particle of radius R streaming with a constant velocity—V_0, parallel to say the x axis, in an incompressible fluid of infinite extent. The fluid consists of two components, the first present in excess; the second or "diffusing" component having initially a constant concentration, a, throughout. The spherical aerosol particle acts as a sink for the molecules of the diffusing component. The density, ρ_0, of the fluid, the viscosity, μ, of the fluid and the diffusion constant, D, of the diffusing component are to be unaffected by the diffusion; i.e., they remain constant with changes in time and location. We choose the center of the streaming sphere as the origin of an (r',θ,ϕ) coordinate system. The concentration $c(\mathbf{r}',t)$ of the diffusing component of the fluid at $\mathbf{r}'$ at time t satisfies the Smoluchowski equation

$$\frac{\partial c}{\partial t}=\operatorname{div}(D\ \operatorname{grad}c-\mathbf{v}c), \tag{1}$$

where the velocity of disturbance of the fluid relative to the sphere, $\mathbf{v}$, due to its motion is given to an excellent approximation by a suitable solution of the Navier-Stokes equation and the continuity equation, $\operatorname{div}\mathbf{v}=0$. Since we are interested in solutions which are symmetric in ϕ, such a suitable $\mathbf{v}=V_0\mathbf{f}=V_0f_{(r')}\mathbf{a}+V_0f_{(\theta)}\mathbf{b}$ (with $\mathbf{a}$ and $\mathbf{b}$ "unit vectors" in the increasing r' and θ directions, respectively), which satisfies the boundary condition

$$f_{(r')}=\cos\theta,\quad f_{(\theta)}=\sin\theta\quad\text{at}\quad r'=R \tag{2a}$$

and

$$f_{(r')},\quad f_{(\theta)}=O(1/r'^n),\quad n\geq 1 \tag{2b}$$

as r' becomes infinitely large, e.g., Stokes flow,[3] where

$$f_{(r')}(r',\theta)=\left(-\frac{3}{2}\frac{R}{r'}+\frac{1}{2}\frac{R^3}{r'^3}\right)\cos\theta$$

$$f_{(\theta)}(r',\theta)=\left(\frac{3}{4}\frac{R}{r'}+\frac{1}{4}\frac{R^3}{r'^3}\right)\sin\theta.$$

At steady state, i.e., when $\partial c/\partial t=0$, Eq. (1) reduces to

$$D\nabla^2 c=\mathbf{v}\cdot\operatorname{grad}c \tag{3a}$$

in the region $R<r'<\infty$, $0\leq\theta\leq\pi$. At the surface of the sink (aerosol particle), partial absorption and reflection of the molecules of the diffusing component occurs. If λ is the "boundary parameter" then

$$-\mathbf{Q}\cdot\mathbf{a}=(D\ \operatorname{grad}c-\mathbf{v}c)\cdot\mathbf{a}=\lambda Dc. \tag{3b}$$

As λ varies from zero to infinity, the aerosol particle changes from a perfect reflector to a perfect absorber. The concentration at points in the fluid at very great distances from the sphere is undisturbed,

$$c\to a\quad\text{as}\quad r'\to\infty. \tag{3c}$$

Finally, we require that the boundary condition

$$c(r',0)=c(r',\pi) \tag{3d}$$

be satisfied. Introducing the dimensionless quantities

$$u(r,\theta)=\frac{c(r',\theta)}{a}-1, \tag{4a}$$

$$\xi=\lambda R, \tag{4b}$$

$$\epsilon=V_0R/D \tag{4c}$$

* The research reported in this paper has been sponsored by the Geophysics Research Directorate of the U. S. Air Force Cambridge Research Center under Contract No. AF 19(122)-412.

† Present address: Department of Physics, Syracuse University, Syracuse, New York.

[1] H. Reiss and V. K. LaMer, J. Chem. Phys. **18**, 1 (1950); H. Reiss, J. Chem. Phys. **19**, 482 (1951).

[2] H. L. Frisch and F. C. Collins, J. Chem. Phys. **20**, 1797 (1952).

[3] G. B. Stokes, Mathematical and Physical Papers (Cambridge University Press, Cambridge, 1880-1905), Vol. I, p. 75; Vol. III, p. 59.

[4] E. Cunningham, Proc. Roy. Soc. (London) **A83**, 357 (1910).

[5] M. von Smoluchowski, Physik. Z. **17**, 557, 585 (1916).

[6] N. Fuchs, Physik. Z. Sowjetunion **6**, 224 (1934).

with $r=r'/R$, into Eqs. (3), we obtain the dimensionless "model" equations

$$\nabla^2 u(r,\theta)=\epsilon f\cdot \text{grad} u(r,\theta) \tag{5a}$$

in the region $1<r<\infty$, $0\leq\theta\leq\pi$ with

$$u(r,\theta)\to 0 \quad \text{as} \quad r\to\infty, \tag{5b}$$

$$\frac{\partial u}{\partial r}=\xi(u+1)+\epsilon f_{(r)}(u+1) \quad \text{at} \quad r=1, \tag{5c}$$

$$u(r,0)=u(r,\pi), \quad r>1. \tag{5d}$$

The parameter ϵ is interesting. From kinetic theory, the diffusion constant D is given by $D=\kappa^{-1}\nu$, where κ is the Schmidt number which is constant at constant temperature, e.g., κ for water vapor in air at room temperature is 0.60, and ν is the kinematic viscosity μ/ρ_0. Substituting D into ϵ, we find $\epsilon=[V_0R/\nu]\kappa=[Re]\kappa$, where $[Re]$ is the Reynolds number of the flow. Since stable, fully-grown cloud droplets rarely exceed a radius of 10 microns we will be interested in solutions of Eqs. (5) for values of $\epsilon\leq 0.1$, i.e., for small values of $[Re]$.

THE SOLUTION OF THE STEADY-STATE SMOLUCHOWSKI EQUATION FOR SMALL REYNOLDS NUMBERS

The method of separation of variables cannot, in general, be applied directly to the solution of Eq. (5a). Since u occurs linearly, one may construct a nontrivial solution by an infinite sum of functions $u_k(r,\theta)$, $k=0, 1, 2, \cdots$ such that

$$u(r,\theta)=u_0(r,\theta)+\epsilon u_1(r,\theta)+\epsilon^2 u_2(r,\theta)+\cdots \tag{6}$$
$$=\sum_{k=0}^{\infty}\epsilon^k u_k(r,\theta).$$

Alternatively, one may regard Eq. (6) as a perturbation series in the parameter ϵ, ($\epsilon<1$). Substituting Eq. (6) into Eqs. (5) we find

$$\nabla^2 u_0=0,$$
$$\nabla^2 u_j=f(r,\theta)\cdot\text{grad}u_{j-1}=-B_{j-1}(r,\theta), \tag{7a}$$

$j=1, 2, \cdots$ with

$$u_k\to 0 \quad \text{as} \quad r\to\infty, \tag{7b}$$

$$\frac{\partial u_0}{\partial r}=\xi(u_0+1); \quad \frac{\partial u_1}{\partial r}=\xi u_1+f_{(r)}(u_0+1); \tag{7c}$$
$$\frac{\partial u_i}{\partial r}=\xi u_i+f_{(r)}u_{i-1}=\xi u_i+F_{i-1}(r,\theta)$$

$i=2, 3, \cdots$ at $r=1$ and

$$u_k(r,0)=u_k(r,\pi). \tag{7d}$$

The original problem is thus separated into finding solutions of Laplace's and Poisson's equations with simple boundary conditions, solutions which can be found by separation of variables.

The solution of Eqs. (7) is

$$u_0(r)=-(\xi/\xi+1)1/r,$$

$$u_j(r,\theta)=2\pi\int_0^{\pi}\int_1^{\infty}B_{j-1}(r_0,\theta_0)g(r,r_0;\theta,\theta_0)$$
$$\times r_0^2 dr_0\sin\theta_0 d\theta_0. \tag{8}$$

The function $g(r,r_0;\theta,\theta_0)$ is the Green's function satisfying

$$\nabla^2 g=-\frac{\delta(r-r_0)\delta(\theta-\theta_0)}{2\pi r^2\sin\theta} \tag{9}$$

and the boundary conditions given by Eqs. (7b)–(7d). We found g to be

$$g=\frac{1}{2\pi}\sum_{n=0}^{\infty}\left(\frac{2n+1}{2}\right)a_n(r,r_0)P_n(\cos\theta)P_n(\cos\theta_0), \tag{10}$$

where $P_n(\cos\theta)$ is the nth Legendre polynomial in $\cos\theta$ and $a_n(r,r_0)$ is

$$a_n(r,r_0)=-\frac{[A_n(1)r^n+r^{-(n+1)}](r_0)^{-(n+1)}H(r_0-r)}{(2n+1)A_n(1)}$$
$$-\frac{r^{-(n+1)}[A_n(1)(r_0)^n+(r_0)^{-(n+1)}]H(r-r_0)}{(2n+1)A_n(1)}$$

with $H(x)$ the Heaviside unit function of argument x,

$$A_n(1)=\frac{n+\xi}{n-\xi}+\frac{G_n(1)+1}{n-\xi}$$

and

$$G_n(1)=\lim_{r\to 1}\int_0^{\pi}\left(\frac{2n+1}{2}\right)^{\frac{1}{2}}F_{j-1}(r,\theta)P_n(\cos\theta)\sin\theta d\theta.$$

The series, Eq. (6), converges to the desired solution of Eqs. (5) for $\epsilon<1/\pi$. This is shown by proving that the individual terms of Eq. (6) are identical with the convergent Neumann expansion in ϵ of the linear integral equation of the second kind which corresponds to Eqs. (5). For example, when $\lambda\to\infty$, i.e., the sink is a perfect absorber, a condition often met in applications, this integral equation is

$$u(r,\theta)=u_0(r)+2\pi\epsilon\int_0^{\pi}\int_1^{\infty}K(r,r_0;\theta,\theta_0)u(r_0,\theta_0)dr_0 d\theta_0,$$

where the kernel function K is found to be

$$K=\frac{\partial}{\partial r_0}(r_0^2\sin\theta_0 f_{(r_0)}g)+\frac{\partial}{\partial\theta_0}(r_0\sin\theta_0 f_{(\theta_0)}g)$$

and g is the limit as λ approaches infinity of the Green's function given by Eq. (10). Finally the concentration

$c(r',\theta)$ of the diffusing component is

$$c(r',\theta)=a\left[1-\left(\frac{\lambda R}{\lambda R+1}\right)\frac{R}{r'}+\sum_{i=1}^{\infty}\epsilon^i u_i\left(\frac{r'}{R},\theta\right)\right]. \quad (11)$$

DISCUSSION AND APPLICATIONS

Even though the series Eq. (24) converges, it is useful if and only if the first few terms are a sufficient approximation for $c(r',\theta)$. This is realized if ϵ is sufficiently small. In the particular case of diffusion of water vapor in air to a freely falling cloud droplet ($R\leqq 10^{-3}$ cm), where v is given by Stokes flow,[3] $c(r',\theta)$ is very well represented by the first two terms of the series Eq. (11). Performing the quadratures shown in Eq. (8) we find

$$\begin{aligned}\frac{c(r',\theta)}{a}&=1+u_0(r)+\epsilon u_1(r,\theta)+\cdots\\&=1-\left(\frac{\xi}{\xi+1}\right)\left\{\frac{1}{r}+\frac{\epsilon}{3}\left[\frac{9}{4r}-\frac{\beta}{r^2}+\frac{3}{8r^3}\right]\cos\theta+\cdots\right\}\\&=1-\left(\frac{\lambda R}{\lambda R+1}\right)\left\{\frac{R}{r'}+\frac{1}{3}\left(\frac{V_0R}{D}\right)\right.\\&\qquad\left.\times\left[\frac{9R}{4r'}+\frac{\beta R^2}{r'^2}+\frac{3R^3}{8r'^3}\right]\cos\theta+\cdots\right\}, \quad (12)\end{aligned}$$

where

$$\beta=2+\frac{5(\lambda^2R^2-1)}{8\{\lambda^2R^2+3\lambda R+[2-(\frac{2}{3})^{\frac{1}{2}}]\}}$$

and $1+u_0(r)$ is the concentration when the droplet is at rest.

If $R=10^{-3}$ cm, $\lambda\geqq 10^4$ cm^{-1}, $T=10$°C, $D=0.2$ cm^2/sec, and $V_0=1.6$ cm/sec., then the percentile error in the concentration made in neglecting higher terms in ϵ in Eq. (11) is less than 0.6 percent. Under the same conditions the percentile error in $c(r',\theta)$ made in neglecting the motion of the droplet (i.e., neglecting the term in ϵ) is at most 3 percent.

The integral flux at $r'=R$, $\Phi(R)$, is

$$\begin{aligned}\Phi(R)&=-2\pi R^2\int_0^{\pi}\mathbf{Q}\cdot\mathbf{a}\sin\theta d\theta\\&=2\pi R^2D\lambda\int_0^{\pi}c(R,\theta)\sin\theta d\theta, \quad (\lambda<\infty)\end{aligned} \quad (13)$$

and can in turn be expanded in a power series in ϵ,

$$\Phi(R)=\Phi_0(R)+\epsilon\Phi_1(R)+\epsilon^2\Phi_2(R)+\cdots. \quad (14)$$

The term $\Phi_0(R)$ is the flux to a stationary droplet. We find that $\Phi_1(R)=0$, since the integral of u_1 over θ is zero. The first term which makes a contribution to the flux is the term proportional to the square of ϵ or $[Re]^2$. Thus

$$\begin{aligned}\Phi(R)&=\Phi_0(R)+\epsilon^2\Phi_2(R)+\cdots\\&=4\pi DR^2\lambda a\left\{1-\left(\frac{\lambda R}{\lambda R+1}\right)\left[1-\left(\frac{89}{72}-\frac{11}{48}\beta\right)\left(\frac{V_0R}{D}\right)^2\right.\right.\\&\qquad\left.\left.\times\left\{1-\frac{\lambda R(\lambda R+1)}{(\lambda R+1)^2+\frac{2^{\frac{1}{2}}\lambda^2R^2}{3}\left(\frac{21}{8}-\beta\right)}\right\}+\cdots\right]\right\}. \quad (14b)\end{aligned}$$

If the droplet grows in such a manner that its spherical shape is preserved, then the rate of its mass increase, $\rho 4\pi R^2dR/dt$, is directly proportional to the flux given by Eq. (14b). Under these conditions the motion of the droplet exerts a negligible influence on its growth except at very long times of observation, a conclusion which Fuchs[6] has surmised.

The experimental measurements of Kramers[7] on the analogous transport process, heat conduction from spheres of radius 10^{-1} to 2 cm in laminarly flowing air streams show that the flux of heat per unit temperature difference, more properly the Nusselt number, is a linear function of $[Re]^{\frac{1}{2}}$. The measurements were carried out in the absence of free convection in the range $540\leqq[Re]\leqq 1460$. Extrapolating these results to mass transfer and comparing with Eq. (14b) we see that the calculated series cannot conform with the experimental observation. The explanation of the discrepancy is the breakdown of Stokes flow for $[Re]\geqq 0.5$.[8] Similarly it is not expected that Eqs. (12) and (14b) hold for particles whose radius is much below 10^{-5} cm because of molecular slip.[8] Finally the assumption made in treating air as an incompressible fluid is justified since in the case of free fall of cloud droplets ($R\leqq 10^{-3}$ cm) the ratio of the fall velocity to the local velocity of sound is at most 10^{-5}.[9]

The outlined perturbation method may be applied to the nonstationary transport problem, i.e., to Eq. (1) directly. The equations which then determine the successive approximations to the desired solution are the ordinary diffusion equation and diffusion equations with a time and space-dependent source function. The latter can be again solved using Green's function.[10]

The author wishes to express his indebtedness to Professor B. Friedman of the Institute for Mathematics and Mechanics, New York University, for many helpful discussions particularly in connection with the convergence proof. He also thanks Professor F. C. Collins of the Polytechnic Institute of Brooklyn for interest in the work as evidenced in their discussions.

[7] H. Kramers, Physica **12**, 61 (1946).
[8] A. Sommerfeld, *Mechanics of Deformable Bodies* (Academic Press, Inc., New York, 1952), p. 246 ff.; see also T. Sexl, Ann. Physik **81**, 855 (1926).
[9] A. Sommerfeld, Ann. Physik **81**, p. 101 ff.
[10] See for example H. L. Frisch, Z. Elektrochem. **56**, 324 (1952).

Mass Spectrometric Study of the Molecular Sublimation of Graphite

RICHARD E. HONIG
RCA Laboratories Division, Radio Corporation of America, Princeton, New Jersey
(Received July 24, 1953)

The emission of neutral and charged carbon molecules from spectroscopically pure graphite has been studied by rate of vaporization experiments in a 180° mass spectrometer. Small filaments (diameter: 0.015 in.), heated by ac up to 2600°K, yielded neutral particles which were converted into positive ions by bombardment with low-energy electrons. C_3^+, C_2^+, and C_1^+ ions were found. Although the effects of fragmentation and of differences in ionization cross sections may not be negligible, it is believed that carbon vapor consists largely of C_3 molecules. Graphite was found to emit negative ions containing from one to eight carbon atoms. C_2^-, C_4^-, and C_3^- were the most abundant species, in that order. A search was made for carbon particles emitted as positive ions, but none were found.

Heats of activation were obtained for the neutrals and the more abundant negative ions from the slopes of $\log p$ *vs* $1/T$ plots. Identical heats measured for C_1 and C_3 (178±10 kcal/mole at 2400°K) suggest that these two species may sublime at rates that are interdependent. Thus, this value may not be representative of the true heat of sublimation of C_1. For C_2, a heat of 199±20 kcal/mole was measured at 2400°K. Electron affinities have been computed for C_1, C_2, and C_3, and estimated bond energies deduced for C_2 and C_3. Some of the earlier measurements of the heat of sublimation of graphite, obtained from rates of vaporization and equilibrium effusion, but without mass analysis, have been reinterpreted, taking into account the complex character of the sublimation processes.

I. INTRODUCTION

A RECENT investigation of germanium, tin, and lead showed[1] that these Group IVB elements vaporize, in part, as polyatomic clusters. It seemed of interest to extend the mass spectrometric method employed to a study of carbon, the lightest Group IVB element, particularly since the sublimation of graphite has been such a controversial subject for many years.[2] Preliminary results obtained in this manner, including the predominance of the C_3 species, have already been briefly reported.[3] This paper will deal in more detail with the various neutral and charged carbon particles emitted from graphite at elevated temperatures, specifically with their relative intensities, heats of activation, electron affinities, and bond energies. The results obtained by Chupka and Inghram in recent parallel studies[4,5] will be compared with the present investigation. Finally, an attempt will be made to reinterpret the results of some of the more recent, direct measurements of the heat of sublimation of graphite,[6–10] obtained without the benefit of mass analysis.

II. EXPERIMENTAL PROCEDURE

The mass spectrometer used in this investigation has been described elsewhere.[11] Its ion source was modified (see Fig. 1) to permit easy installation and replacement of graphite filaments. Preliminary tests showed that a filament holder made of molybdenum was more suitable than one made of graphite. The molybdenum holder did not react noticeably at the contact points with the graphite filament, whereas the graphic holder, which could not be thoroughly degassed, turned out to be a copious source of CO which interfered with the C_1 measurements (see below).

In the course of this work, a variety of filaments was used. Initial tests were carried out with carbon filaments* (diameter: between 0.005 and 0.010 in.) prepared from pyrolyzed cellulose material. Subsequent electron diffraction studies showed that the center sections of these filaments became, upon prolonged

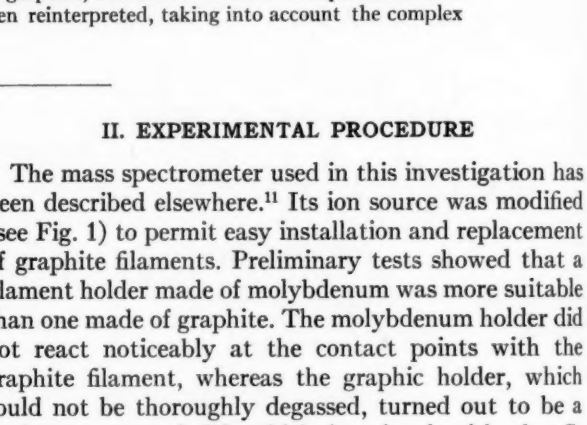

FIG. 1. Scale drawing of mass-spectrometer ion source.

[1] R. E. Honig, J. Chem. Phys. **21**, 573 (1953).
[2] For an inclusive review, see H. B. Springall, Research **3**, 260 (1950).
[3] R. E. Honig, American Physical Society Meeting, Washington, 1953, Abstract L8.
[4] W. A. Chupka and M. G. Inghram, J. Chem. Phys. **21**, 371 (1953).
[5] W. A. Chupka and M. G. Inghram, J. Chem. Phys. **21**, 1313 (1953).
[6] Brewer, Gilles, and Jenkins, J. Chem. Phys. **16**, 797 (1948); L. Brewer and D. E. Mastick, UCRL-572 (1949).
[7] Simpson, Thorn, and Winslow, ANL-4264 (1949).
[8] A. L. Marshall and F. J. Norton, J. Am. Chem. Soc. **72**, 2166 (1950).
[9] [a] Doehaerd, Goldfinger, and Waelbroeck, J. Chem. Phys. **20**, 757 (1952); [b] F. Waelbroeck, J. Chem. Phys. **20**, 757 (1952).
[10] M. Farber and A. J. Darnell, J. Am. Chem. Soc. **74**, 3941 (1953).
[11] R. E. Honig, Anal. Chem. **25**, 1530 (1953).
* Supplied by Filament Supply Company, Hoboken, New Jersey.

heating, graphitic in character. Most of the later experiments were made with spectroscopically pure graphite from two different sources (United Carbon Products Company, Inc., "Cenco Certified Grade"; National Carbon Company, Grades "AGKS" and "AGKSP"). These filaments were turned down from $\frac{1}{4}$-in. stock to about 0.015-in. diameter in a single operation on a well-adjusted lathe.

Direct, electrical heating was employed to raise the filament temperature to the range where emission of carbon particles was observed (2200 to 2600°K). Preliminary runs soon established that dc heating produces hot spots which severely curtail the useful life of a filament. For this reason, a well-stabilized ac source was used in all final experiments. Since temperature measurements by optical pyrometry could not be made reliably through the mass spectrometer envelope during a sublimation experiment, an indirect method was resorted to. Before and after a series of sublimation runs, temperature calibrations were made on each filament, mounted in its regular holder, in a suitable vacuum system. To convert brightness temperatures, measured at the filament center, into absolute values, appropriate corrections were made for the emissivity of graphite and the reflectivity of the Pyrex window. It was found that the parameter best-suited for these temperature calibrations was the voltage drop across the filament. Changes in effective diameter, in resistivity, and possibly also in emissivity occurring during the life of a filament resulted in a slight shifting of the inverse temperature *vs* voltage curves taken before and after a series of sublimation runs. For a given filament, this vertical translation amounted to less than 100° at 2400°K and produced a negligible uncertainty in the measured heats of activation. In addition, however, one must consider possible effects on filament temperature due to different surrounding structures in the actual mass spectrometer tube and in the system used for pyrometric measurements. Finally, there was observed a considerable temperature gradient along the filament. Taking all these effects into account, an over-all uncertainty in the temperature scale resulting in a ±10-kcal/mole error for the absolute values of measured heats has been assumed here.

Neutral particles vaporizing from the graphite filaments were converted into positive ions by electron impact. Initially, relatively high electron energies (70 volts) were employed since the electron gun used did not lend itself to the production of intense electron beams of low energy. After the installation of a more efficient gun design (as shown in Fig. 1), it was possible to work with 23-volt electrons and still obtain sufficient ion beam intensities. Negative ions were observed simply by reversing the electric and magnetic field and readjusting slightly the ion-focusing electrodes in the source.

In a series of runs, the filament temperature was raised in suitable steps, and a background spectrum taken at each level. As soon as the emission of carbon particles could be observed, the peaks of interest were studied, one at a time, by recording their intensity as a function of filament voltage. Data were taken for increasing and decreasing temperatures so as to eliminate any effects due to thermal lag.

TABLE I. Approximate heat capacity coefficients for different carbon species.

Species	D	10^3B
C_1	+2.5	−2.6
C_2	+1.5	−4.6
C_3	+2.0	−6.5

III. CALCULATIONS

For a system in equilibrium, heats of sublimation are obtained from the well-known Van't Hoff equation

$$d\ln p/p = L(T)/RT^2 \cdot dT, \tag{1}$$

where R = gas constant = 1.987 cal/mole-°K; p = equilibrium vapor pressure, in atmos; $L(T)$ = heat of sublimation, in cal/mole; T = absolute temperature, in °K. The dependence of the heat of sublimation on temperature is defined by the Kirchhoff equation

$$L(T) = L(T_1) + \int_{T_1}^{T} \Delta C_p dT$$

$$= L(T_1) + \int_{T_1}^{T} (D + BT) dT, \tag{2}$$

where T_1 = a measured temperature; ΔC_p = change in specific heat at constant pressure, $= C_p$ (gas) $- C_p$ (solid) $= D + BT$ (approximately). For the sublimation of C_1, C_2, and C_3, coefficients D and B can be estimated from Kelley's data[12] for graphite and heat capacity data for typical monatomic, diatomic, and triatomic gases given by Glasstone.[13] Their values have been collected in Table I. When these values are substituted into Eq. (2), it is found that over the experimental temperature range, from 2200 to 2600°K, the heats of sublimation at the extremes differ from the average value L_{2400} by less than ±1.6 percent for C_3, ±1.0 percent for C_2, and 0.5 percent for C_1. Since these errors amount to less than the estimated over-all uncertainty in the temperature scale, the two correction terms in Eq. (2) may be neglected. Thus, Eq. (1) integrates simply to

$$R \ln p = -L(T_1)/T + K, \tag{1a}$$

where T_1 = mean temperature of the range studied (2400°K in these experiments).

When positive ions are produced from neutral species by electron impact, the current collected, I^+, is given by

$$I^+ = \eta Q I^e l n_i, \tag{3}$$

[12] K. K. Kelley, U. S. Bur. Mines Bull. 373, 33 (1935).
[13] S. Glasstone, *Textbook of Physical Chemistry* (D. Van Nostrand Co., Inc., New York, 1946), p. 331.

TABLE II. Relative ion intensities, heats of activation, and electron affinities of molecular species subliming from graphite.

Species	Relative ion intensities at $T=2400°K$		Heats of activation (kcal/mole)		Electron affinities A (ev)	
	$E^e=70$ ev	$E^e=23$ ev	L_{2400}	L_0	Difference value	Ratio value
C_1	35	15	177±10	179±10		1.2
C_2	13		199±20	210±20	4.0	3.1
C_3	*100*	*100*	177±10	190±10	2.5	1.8
C_1^-		28				
C_2^-	*100 000*		209±10			
C_3^-	1 150		230±20			
C_4^-	4 710		240±20			
C_5^-	390					
C_6^-	260					
C_7^-	23					
C_8^-	7					

where η = efficiency of positive ion collection, i.e., the ratio of ions collected to ions formed in the ionizing region; Q = ionization cross section, in cm^2; I^e = electron beam current, in units consistent with those of I^+; l = active path length of electrons, in cm; and n_i = concentration of neutral species in ionizing region, in cm^{-3}. Substituting for n_i from the ideal gas equation, one finds readily for the pressure of neutrals

$$p=K_2I^+T. \tag{4}$$

For negative ions, which are emitted directly from the filament, the pressure is related to the current density I^-/A' by the expression well known in gas kinetics

$$p^-=(I^-/A')(2\pi kmT)^{\frac{1}{2}}=K_3I^-T^{\frac{1}{2}}. \tag{5}$$

Thus, if equilibrium may be assumed, heats of sublimation of neutral species are obtained directly from the slopes of plots $\ln(I^+T)$ *vs* $1/T$, whereas for negative ions $\ln(I^-T^{\frac{1}{2}})$ is plotted *vs* $1/T$.

Simple considerations show that the electron affinity A of a carbon molecule containing x atoms is obtained from the heats of sublimation of the negative ion C_x^- and its neutral counterpart C_x and the work function of the solid

$$A(C_x)=L(T_1,C_x)-L(T_1,C_x^-)+\phi, \tag{6}$$

where ϕ = work function of graphite = 4.4 ev.[14] If Eq. (1a) is applied to C_x^- and C_x and combined with Eq. (6), one obtains

$$R\ln\frac{p(C_x^-)}{p(C_x)}=-\frac{L(T_1,C_x^-)-L(T_1,C_x)}{T}+K(C_x^-)-K(C_x)$$

$$=(A(C_x)-\phi)/T+K(C_x^-)-K(C_x). \tag{7}$$

The constants K include a number of logarithmic terms that are identical for a given negative ion and its neutral counterpart, except for log g, where g is the statistical weight of the particle. This latter quantity is not known in all the cases, but any differences existing will be negligibly small compared to other uncertainties, such as ionization cross sections and fragmentation patterns, which are encountered when $p(C_x)$ is computed from the positive ion current. Thus, assuming that $K(C_x^-)=K(C_x)$, a rough estimate of the electron affinity may be obtained from Eq. (7). On the other hand, electron affinities computed from Eq. (6) are as accurate as the heats of sublimation used.

IV. RESULTS

Relative ion intensities, heats of activation, and electron affinities of the carbon species observed have been collected in Table II. Inspection of the positive ion spectrum shows at once that polyatomic carbon molecules play an important role in the sublimation of graphite. By themselves, the positive ion intensities shown are not sufficient to yield relative concentrations of neutral species, since neither ionization cross sections nor fragmentation patterns are known. Without additional information, such as ionization efficiency curves, one cannot even decide whether the prominent C_3^+ peak is the "parent ion" of the C_3 molecule or an ionized fragment of a larger molecule. However, the first choice is supported by a proposal recently made by Douglas[15] that the 4050A band spectrum observed in carbon arcs should be assigned to a linear C_3 molecule. Similar problems arise in connection with the C_2^+ and C_1^+ peaks. Relative intensities of positive ions are shown at ionizing energies (E^e) of 70 ev, as used initially, and of 23 ev, the value used in later experiments. Chupka and Inghram's[4] results for C_1^+ and C_2^+, as well as their latest values[5] which include C_3^+, agree in order of magnitude with the positive ion spectrum of Table II. They also state[5] that "the appearance potentials of all three species appear to be roughly equal." This suggests that these ions may be *parent ions*, yet it does not eliminate the possibility that positively and negatively charged *fragments* are formed simultaneously in one process.

The negative ion spectrum shown in Table II provides proof that polyatomic molecules containing up to eight carbon atoms participate in the sublimation process. The distribution of intensities is more clearly seen in Fig. 2, which is a semilogarithmic plot of negative ion currents *vs* the number of carbon atoms per ion. Odd-numbered and even-numbered points fall on two separate curves (shown dashed) that approach each other at higher carbon numbers. Differences either in electron affinities or in neutral concentrations could account for the alternating intensities observed. The first explanation is compatible with the electron affinities computed for C_1, C_2, and C_3, as shown below, and is based on the assumption that the positive ions observed are parent ions. If the second explanation, suggested by similar

[14] A. Braun and G. Busch, Helv. Phys. Acta **20**, 33 (1947).

[15] A. E. Douglas, Astrophys. J. **114**, 466 (1951).

odd-even alternations in the positive ion spectra of germanium and tin,[1] were correct, one would be forced to conclude that the positive ion spectrum of carbon consists of fragments rather than parent ions. In any event, the curves of Fig. 2 are seen to converge rapidly for $x>4$ and should therefore represent, in order of magnitude, relative concentrations of the larger neutral molecules. Extrapolation of the curves leads to the conclusion that ions with more than eight atoms exist, but at concentrations below the threshold of detection. Even though C_2^-, the most intense peak in the negative ion spectrum, is considerably stronger than the corresponding C_2^+ peak (taken at $I^e=10\,\mu$A), the computed pressure ratio $p(C_2^-)/p(C_2)$ shows that only one out of about 400 diatomic molecules is emitted as a negative ion.

In the third and fourth columns of Table II are listed heats of activation for six species, at 2400° and 0°K, respectively. The term "activation" rather than "sublimation" is used here because these experiments measured rates of vaporization under nonequilibrium conditions. Possible differences in these heats will be discussed more fully below. Heats of activation at 2400°K (L_{2400}) were determined graphically from plots of $\log p$ *vs* $1/T$, using Eq. (1a). The L_0 values were computed from the corresponding L_{2400} values by Eq. (2). The errors quoted for C_1, C_3, and C_2^- (± 10 kcal/mole) represent the estimated uncertainty in temperature scale, as mentioned before. For these species, the actual uncertainties in slope due to scattering of points were found to lie well within ± 2 kcal/mole. Furthermore, the slopes obtained from successive runs of C_1 and C_3 were found to be identical, within the same limits. For the other three species (C_2, C_3^-, and C_4^-), low ion intensities produced additional uncertainties in slope, estimated at 10 kcal/mole, thus raising the total to perhaps ± 20 kcal/mole. Early attempts to determine $L_{2400}(C_1)$, made initially with 70-volt electrons, showed that a sizeable portion of the mass 12 peak was due to the C^+ fragment from CO, a gas which is produced in high concentration during the sublimation process. For this reason, the ionizing energy was subsequently reduced to about 23 volts, a value sufficiently low to suppress the bulk of the CO contribution, yet high enough to yield the desired C_1^+ ions in sufficient intensity. The slight CO contribution left over under these conditions was readily removed from the mass 12 peak by an appropriate correction.

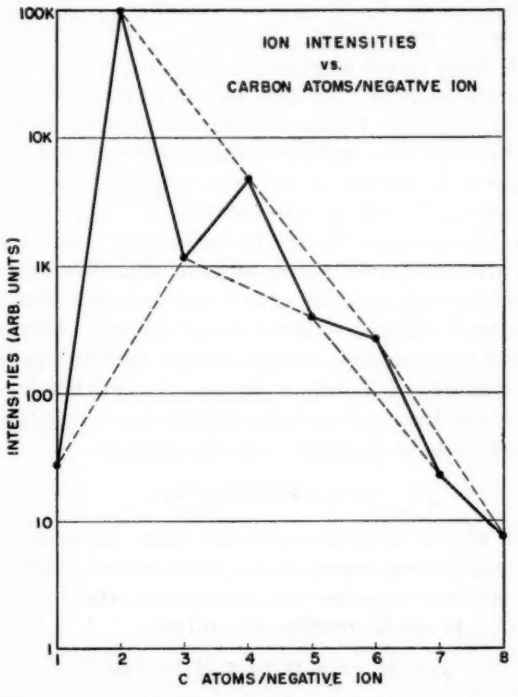

FIG. 2. Intensities of negative ions *vs* number of carbon atoms per ion.

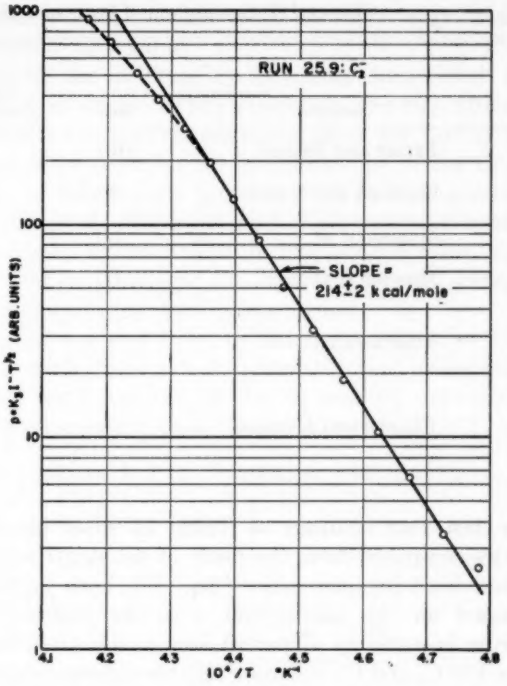

FIG. 3. Plot of observed partial pressure of C_2^- ions *vs* $10^4/T$.

A typical semilogarithmic plot of vapor pressure (in terms of $I^-T^{\frac{1}{2}}$) *vs* inverse temperature is shown for the C_2^- ion in Fig. 3. Except for a systematic deviation at the high-temperature end, most points are seen to fall, over a pressure range of two decades, on a straight line whose slope is 214 ± 2 kcal/mole. The deviation, which is observed for all negative ions, is explained as follows. As the temperature is raised, thermionic electrons are emitted in increasing concentrations but are constrained by the strong magnetic field to stay near the filament surface. The resulting potential depression rejects all negative ions with initial energies below a critical value. Since this critical energy increases with temperature, the ratio of ions collected to ions formed decreases steadily, thus resulting in the curved, dotted portion.

TABLE III. Comparison of heats of activation obtained in some of the more recent studies.

	Authors	Ref.	Rate of vaporization	Equil. effusion	Heats of activation (kcal/mole) Fictitious L_F	Individual L_{2400}	L_0
I	Farber and Darnell	(10)	*R*		190±5		
II	Marshall and Norton	(8)	*R*		178±5		
III	Simpson *et al.*	(7)	*R*		(187)		
IV	Simpson *et al.*	(7)		*E*	(174)		
V	This research		*R*		180	$C_1=177\pm10$ $C_2=199\pm20$ $C_3=177\pm10$	179 ± 10 210 ± 20 190 ± 10
VI	Chupka and Inghram	(5)	*R*		198	$C_1=177\pm6$ $C_2=200\pm10$ $C_3=200\pm10$	176 ± 6 211 ± 10

The last two columns of Table II show electron affinities computed from the heats of sublimation (Eq. (6)) and from pressure ratios (Eq. (7)); both methods are based on the assumption that the positive ion spectrum is made up of parent ions rather than fragments. For C_2 and C_3, the more reliable difference values are larger than the ratio values by about one third. The electron affinity of C_1 could be obtained only from the pressure ratio and might well be on the low side. Even so, it falls within the range of published electron affinities, computed from an extrapolation of the isoelectronic series (Bates:[16] 0.9; Wicke:[17] 1.2 (average); Massey:[18] 1.5 (estimated); Glockler and Sausville:[19] 2.2 volts). Glockler and Sausville's *experimental* values[19] based on negative ion and electron currents measured in a magnetron structure, are believed to be in error since these authors assumed C_1^- to be the predominant ion.

V. DISCUSSION

The heats of activation obtained in the previous section, though of considerable interest, cannot by themselves answer the central question: what is the true heat of sublimation of graphite into atomic carbon. Even if it is assumed that the C_1^+ ion observed actually derives from the atomic species C_1, rather than from any of the many polyatomic species that were found to exist, these experiments measure rates of vaporization, not the equilibrium state. If the accommodation coefficient for C_1 is much smaller than unity, as indicated by Doehaerd *et al.*,[9a] and depends on temperature in an exponential manner, the slope measured in a rate of vaporization experiment would be a straight line and represent a heat of activation that is much larger than the true heat of sublimation. Since Chupka and Inghram state in their first report[4] that the C_1^+ ions have kinetic energies of less than 0.3 ev, this would limit any excess heat due to a potential hill to about 8 kcal/mole. On the other hand, the hypothesis advanced by Herzberg, Herzfeld, and Teller[20] for the sublimation of atomic carbon might well apply here if it were generalized to include molecular species. For example, one might speculate that, in the sublimation of graphite, C_3 and C_1 particles are emitted alternately from the edges of the plane. Either of the two processes might be the rate-controlling one so that the heats measured for C_1 and C_3 would appear identical—which indeed is observed. Thus $L_0(C_1)$ could be considerably higher than the true heat of sublimation. However, such alternating processes should not apply to the emission of C_2, as already pointed out by Waelbroeck.[9b] Therefore, $L_0(C_2)$ could represent a true heat of sublimation.

The more recent attempts to measure directly, without mass analysis, the heat of sublimation of carbon include studies by Farber and Darnell[10] and by Marshall and Norton,[8] who measured rates of vaporization; experiments by Brewer *et al.*,[6] who employed an effusion method; and work by Doehaerd *et al.*[9a] and Simpson *et al.*,[7] who used both. Unfortunately, the values computed from the thermodynamic equation were incorrect in every case because it was assumed that only monatomic carbon sublimes from graphite. However, some of these reports contain enough information for a plot of $\log p_F$ *vs* $1/T$, whose slope L_F is a fictitious heat of activation. Here, p_F has been defined as a fictitious total pressure, and is obtained from the relation

$$p_F=(2\pi RT/M_F)^{\frac{1}{2}}\dot{m}_t, \tag{8}$$

where M_F = a fictitious molecular mass (assumed to be 12 a.m.u. in these reports), $\dot{m}_t$ = total rate of weight loss, in g/cm²/sec = $\dot{m}_1+\dot{m}_2+\dot{m}_3$ (subscripts refer to C_1, C_2, and C_3). It can be readily shown that

$$p_F=M_F^{-\frac{1}{2}}(p_1M_1^{\frac{1}{2}}+p_2M_2^{\frac{1}{2}}+p_3M_3^{\frac{1}{2}}). \tag{9}$$

[16] D. R. Bates, Proc. Roy. Irish Acad. **A51**, 151 (1947).
[17] E. Wicke, Landolt-Börnstein *Zahlenwerte und Funktionen* (Springer, Berlin, 1950) Vol. I, Part 1, p. 213.
[18] H. S. W. Massey, *Negative Ions* (Cambridge University Press, Cambridge, 1950), p. 19.
[19] G. Glockler and J. W. Sausville, Trans. Electrochem. Soc. **95**, 282 (1949).
[20] Herzberg, Herzfeld, and Teller, J. Phys. Chem. **41**, 325 (1937).

The relative partial pressures p_1, p_2, and p_3, obtained from the positive ion spectrum of Table II (assuming equal ionization cross sections and accommodation coefficients of unity), together with the individual heats of activation yield a plot of $\log p_F$ *vs* $1/T$, whose slope L_F can then be compared with the slope of the weight loss data. Table III lists the authors whose data could be plotted, a classification of their experiments, and the fictitious heats obtained. For comparison are given the mass spectrometric results of the present research, and those of Chupka and Inghram.[5]

For the fictitious slopes in lines 1 and 2, errors are quoted that are rough estimates, obtained by inspection from the scattering of data. In the experiments of Simpson *et al.* (lines 3 and 4), the scattering of points is much less severe, but here large additional uncertainties were encountered. Their pyrometric measurement of carbon deposited on the quartz target involved not only a condensation coefficient, but also the possible re-evaporation of particles from neighboring walls. Thus, the slopes shown in lines 3 and 4 are probably no more than rough estimates. However, the difference between them should be quite accurate since the assumptions made were the same. It is found that the value of L_F computed from the present data (line 5) is compatible with previous rate of vaporization measurements (lines 1, 2, and 3). Chupka and Inghram's data[5] lead to a higher value because they found a high heat of activation for the predominant C_3 species.

A comparison of the available equilibrium effusion data with rate of vaporization results allows some conclusions to be drawn concerning the heat of sublimation of atomic carbon. Simpson's effusion data lead to a L_F that lies about 13 kcal/mole below the rate value. If his effusion experiments represent a true equilibrium state, the effusion value is compatible only with $L_0(C_1) = 170$ kcal/mole, the highest of the allowed spectroscopic values. Similar conclusions are reached when the fictitious pressures obtained by Brewer[6] at about 2600°K under equilibrium conditions are compared with the rate values of Marshall and Norton[8] and Farber and Darnell.[10] The equilibrium pressures lie about one order of magnitude above the rate pressures, and this again can be reconciled only with $L_0 = 170$. Finally, one may combine the relative partial pressures obtained in the present research with the absolute weight loss data of Marshall and Norton's at 2357°K to get a rate value for p_1, which then can be compared with the equilibrium value computed thermodynamically on the assumption that $L_0(C_1) = 170$. The computed equilibrium partial pressure of C_1 is found to be 20 times larger than the measured rate value.

Since the alternating processes mentioned above should not apply to the C_2 molecule, one may attempt to compute thermodynamically a value for $L_0(C_2)$, if the vibrational contribution to the entropy of the C_2 molecule is taken into account and an accommodation coefficient of unity is assumed. This computed heat (213 kcal/mole) agrees well with the observed slope value of 210 and suggests that the observed partial pressure of C_2 is close to the equilibrium value.

If one assumes the true heats of sublimation for C_1, C_2, and C_3, to be 170, 210, and 190 kcal/mole, respectively, bond energies of the C_2 and C_3 molecules are readily estimated from the following cycles:

$$\left.\begin{array}{l} 2C(s) \rightarrow 2C_1(g) \\ 2C(s) \rightarrow C_2(g) \end{array}\right\} - \qquad \begin{array}{l} 2L_0(C_1) = 340 \\ -L_0(C_2) = -210 \end{array}$$

$$C_2(g) \rightarrow 2C_1(g) \qquad D(C-C) = 130 \text{ kcal/mole} \quad (C_2)$$

$$\left.\begin{array}{l} 3C(s) \rightarrow 3C_1(g) \\ 3C(s) \rightarrow C_3(g) \end{array}\right\} - \qquad \begin{array}{l} 3L_0(C_1) = 510 \\ -L_0(C_3) = -190 \end{array}$$

$$\begin{array}{ll} C_3(g) \rightarrow 3C_1(g) & 2D(C-C) = 320 \\ & D(C-C) = 160 \text{ kcal/mole} \quad (C_3) \end{array}$$

Although the values obtained are, necessarily, very approximate, they nevertheless suggest C−C linkages of double-bond character for both molecules.

ACKNOWLEDGMENTS

Thanks are due Mr. O'Keefe of the Filament Supply Company, Hoboken, New Jersey, for a generous supply of carbon filaments. The writer is indebted to Dr. J. Turkevich, of Princeton University, for bringing reference 15 to his attention. It is a pleasure to acknowledge the help rendered by Mr. M. A. Colacello who mounted the filaments and first showed that small filaments could be turned out of graphite rod. The author wishes to thank Dr. J. Hillier for taking and interpreting electron micrographs and diffraction patterns of several filaments. Associates within the Physical Research Laboratory, in particular Dr. D. O. North, have contributed greatly to this research by many stimulating discussions.

Note added in proof.—After this paper had been accepted for publication in its final form, Professor P. Goldfinger sent a private communication and a copy of F. Waelbroeck's thesis. In answer to his comments, some textual changes were made, but it is unfortunately not possible to discuss fully the interesting points raised.

Theory of Dielectric Relaxation for a Single-Axis Rotator in a Crystalline Field

JOHN D. HOFFMAN* AND HEINZ G. PFEIFFER
General Electric Research Laboratory, Schenectady, New York

(Received June 2, 1953)

The dielectric relaxation times associated with a single-axis polar rotator which may occupy several sites as it turns about its axis are calculated in terms of the probabilities of transition from one site to another. Two special cases are considered in detail: (a) that in which all of the sites are equivalent, and (b) that in which one site is stable with respect to the others. It is assumed that the only important elementary process is a rotational jump to an adjacent site (*single-jump hypothesis*). Fluctuations of barrier height are ignored.

If the dipole has three or more accessible sites, and one is more stable than the others, a distribution of relaxation times develops naturally. The corresponding dielectric loss peak will be somewhat asymmetric. If the sites are all equivalent, only a single dielectric relaxation time is found, and the corresponding dielectric loss peak will be of the simple Debye type. The theory predicts that the dielectric loss peaks in certain polar crystals will become narrower and more symmetrical as the temperature is raised.

I. INTRODUCTION

DIELECTRIC loss data on a number of crystals consisting of polar molecules indicate the existence of a distribution of dielectric relaxation times. Several theoretical discussions of this phenomenon based on the assumption that fluctuations of activation energy are the principal cause of the distribution have been given.[1,2] On the other hand, it has been suggested that an asymmetry of the local free energy barrier restricting rotation of rigid molecules in solids might lead to more than one relaxation time (see for instance reference 3). In the present paper, we undertake a detailed mathematical investigation of certain possible models from the latter point of view.

1. Preliminary Relationships

Let the polarization of a system of dipoles approach equilibrium, after the abrupt removal of a static field, according to the decay function

$$P(t)=P_0\exp(-t/\chi\tau). \tag{1}$$

If the measuring field is sinusoidal, it may be shown that the familiar Debye equations[4] with a single relaxation time

$$\epsilon''(\omega)=(\epsilon_0-\epsilon_\infty)\chi\omega\tau/(1+\chi^2\omega^2\tau^2) \tag{2}$$

and

$$\epsilon'(\omega)=\epsilon_\infty+(\epsilon_0-\epsilon_\infty)/(1+\chi^2\omega^2\tau^2), \tag{3}$$

describe the system.[1,4,5] In the above equations, τ is the molecular relaxation time in the absence of the internal field, t the time, ω the angular frequency, $\epsilon'(\omega)$ and $\epsilon''(\omega)$ the dielectric constant and dielectric loss factor as a function of frequency, and ϵ_0 and ϵ_∞ the dielectric constant well below and well above the observed critical frequency, $\omega_c=1/\chi\tau$. The numerical factor χ is a result of the difference between the applied field and the internal field. The internal field of Lorentz[1,4] leads to the factor $\chi=(\epsilon_0+2)/(\epsilon_\infty+2)$. O'Dwyer and Sack[6] have shown to a first approximation that $\chi\cong 3\epsilon_0/(2\epsilon_0-\epsilon_\infty)$ for the Onsager field; Powles[7] obtained the same result by a different procedure. It should be emphasized that $\chi\tau$ (sometimes called the *decay time*, **T**), and not τ, is the quantity obtained directly from dielectric loss measurements.

If the polarization decays according to the relation

$$P(t)=\sum_\beta P_\beta\exp(-t/\chi_\beta\tau_\beta) \tag{4}$$

after a static field is removed, it follows that

$$\epsilon''(\omega)=\sum_\beta \Delta\epsilon_\beta\chi_\beta\omega\tau_\beta/(1+\chi_\beta^2\omega^2\tau_\beta^2) \tag{5}$$

for alternating fields. In Eq. (5), $\Delta\epsilon_\beta$ is the increment of dielectric constant associated with the βth mode of relaxation. The numerical constants χ_β refer to the internal field correction for each of the modes.

The Onsager internal field is probably reasonable for solids consisting of orienting dipoles. If the Onsager field is assumed, the variation of the χ values in Eq. (5) will be quite small since the maximum possible range of χ is only unity to $\frac{3}{2}$. Little error will be involved, therefore, if τ and $\chi\tau$ are assumed to be identical;[7] this is particularly the case if the dielectric constant is low.

The usual plot of ϵ'' against $\log\omega$ for a substance which shows a distribution of relaxation times, such as that given by Eq. (5), will exhibit a broader dielectric loss peak than a substance which possesses but one relaxation time [Eq. (2)]. Equation (5) can lead to asymmetric loss peaks, for example if $\Delta\epsilon_1\neq\Delta\epsilon_2\neq\Delta\epsilon_3\cdots$.

It is evident from the above that the most important factor influencing the frequency dependence of the dielectric constant and dielectric loss factor, namely, the distribution of relaxation times, may be obtained for a given model by an investigation of $P(t)$.

* Now at National Bureau of Standards, Washington, D. C.

[1] W. Kauzmann, Revs. Modern Phys. **14**, 12 (1942).

[2] H. Fröhlich, *Theory of Dielectrics* (Oxford University Press, London, England, 1949), p. 180, see pp. 90–98.

[3] J. D. Hoffman, J. Chem. Phys. **20**, 541 (1952).

[4] P. Debye, *Polar Molecules* (Dover Publications, New York, 1945), pp. 170, see pp. 104–106.

[5] Reference 2, pp. 70–73.

[6] J. J. O'Dwyer and R. A. Sack, Australian J. Sci. Research **5**, 647 (1952).

[7] J. G. Powles, J. Chem. Phys. **21**, 633 (1953).

It is the principal object of this paper to calculate the distribution of relaxation times associated with a rigid single-axis rotator which may possess a number of equilibrium orientations. The case where the orientational sites are not equivalent is of special interest.

2. The General Model

The four-position model diagrammed in Fig. 1 illustrates the general features of the "site" model we consider. The dipoles in one of the type 2 sites (i.e., one of the sites of higher local free energy such as 2, 3, and 4), experience a barrier to reorientation of magnitude W, while a dipole in site 1 (unique) experiences a local free energy barrier of $W+V$. Two values of V, 0 and $V>W$ are considered in detail for each of the models. The condition $V=0$ corresponds to the case where all the possible orientational sites are equivalent, while the condition $V>W$ corresponds to the case where site 1 is stable with respect to the others. The form of the local free energy barrier is assumed to be determined by the crystalline field.

The transition probability (in jumps per second) for an elementary process in which a dipole vacates site 1 and enters an adjacent type 2 site is given by

$$k=A\exp[-(W+V)/\mathbf{k}T] \tag{6}$$

and the corresponding transition probability (see Fig. 1)

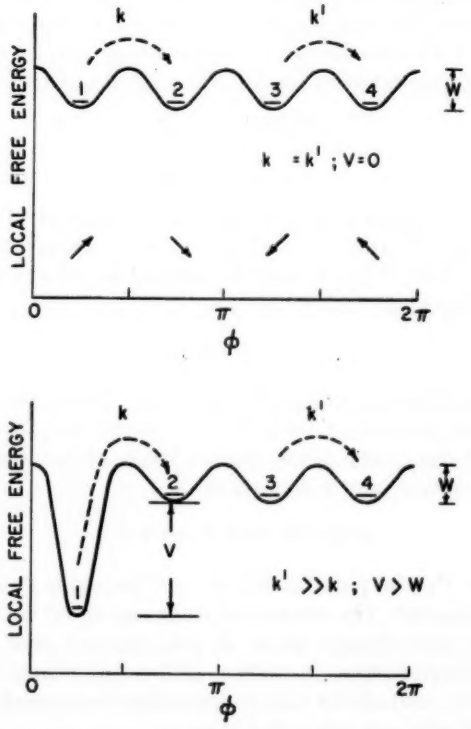

FIG. 1. Assumed local free energy barrier as a function of angle of rotation for a single-axis rotator with four sites. Upper: all sites equivalent. Solid arrows indicate equilibrium dipole orientations. Lower: case where site 1 is the preferred position. k and k' are the transition probabilities for jumps over barriers of magnitude $(W+V)$ and W, respectively.

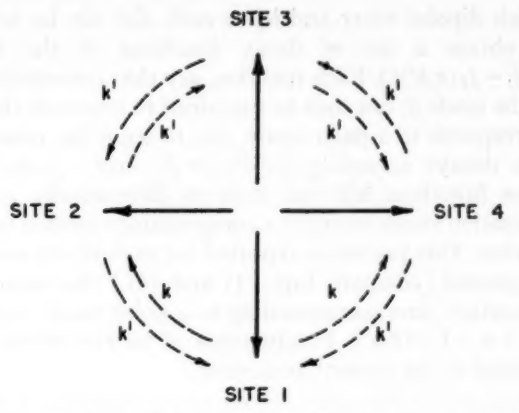

FIG. 2. Rate processes for the four-position model using the single-jump restriction. Heavy arrows indicate equilibrium dipole orientations, dashed arrows show allowed transitions. k and k' are the elementary process transition probabilities.

that a dipole in a type 2 site will shift to an adjacent type 1 or type 2 site is given by

$$k'=A\exp(-W/\mathbf{k}T). \tag{7}$$

In the above equations, A is a constant in the units of frequency, $\mathbf{k}$ is Boltzmann's constant, and T the absolute temperature. W and $(W+V)$ are regarded as the local free energies of activation of the elementary processes. The condition $k'=k$ corresponds to $V=0$, while $k'\gg k$ corresponds to $V>W$. The equilibrium properties of the system depend only on V.[3]

3. Hypothesis Regarding the Nature of the Elementary Reorientation Process

The concept that a dipole occupies a definitely assignable site is strictly valid only when the local free energy barrier between possible positions is considerably greater than $\mathbf{k}T$. It seems reasonable to assume that a dipole jump to an *adjacent* site is the most probable single event in such a system. The concept that the elementary dipole reorientation process consists entirely of individual jumps to adjacent sites is called the *single-jump hypothesis*. The treatment of the three- to six-position models give in Sec. II is based on this assumption.

The rate processes controlling the orientation of dipoles are illustrated in Fig. 2 for the four-position model for the case where the elementary process is a jump to an adjacent site.

4. Mathematical Method

The dielectric relaxation times associated with the single-axis rotator model discussed above can be calculated by expressing the rates at which dipoles enter and leave each site in terms of the transition probabilities k and k'. In general, k is the probability that a dipole will leave site 1 in unit time, while k' is the corresponding transition probability for a type 2 site. The simultaneous differential equations obtained by equating the rate at

which dipoles enter and leave each site can be solved to obtain a set of decay functions of the form $\exp[-f_\beta(k,k')t]$. Each function, say that corresponding to the mode β, can then be examined to ascertain that it corresponds to a polar mode, i.e., to see if the polarization decays according to $P(t)=P_\beta \exp[-f_\beta(k,k')t]$; some functions will not lead to dielectrically active relaxation times owing to a compensatory motion of the dipoles. This process is repeated for each of the modes. In general [compare Eqs. (1) and (4)] the molecular relaxation time corresponding to a polar mode is given by $\tau=-1/f(k,k')$. Fluctuations of barrier height are ignored in the present treatment.

5. The Two-Position Model

Owing to certain of its unique properties, and as an introduction to the methods used in the body of this paper, we shall give below the calculation of the dielectric properties associated with the two-position model. The dielectric relaxation times for this model (or one closely related to it) have been treated previously by Debye[8] and later Fröhlich.[9]

The model consists of two non-equivalent rotational positions 180° apart. k is the probability/sec that a dipole will undergo a jump from site 1 to site 2 (in one direction) and k' is the probability/sec that a dipole will jump from site 2 to site 1. N_1 and N_2 are the number of dipoles in type 1 and type 2 sites in the lattice at any given time; the only restriction on N_1 and N_2 is that their sum shall always equal the total number of molecules in the system, N.

The net rate at which dipoles enter any given site, dN_i/dt, is obtained by algebraically summing the number/sec entering and leaving the site. Thus,

$$dN_1/dt=-2kN_1+2k'N_2, \tag{8a}$$

$$dN_2/dt=-2k'N_2+2kN_1. \tag{8b}$$

The factor 2 appears before each term involving k since each dipole may leave a site in either of two directions.

We will repeatedly encounter sets of equations of the form

$$dN_i/dt=\sum_{j=1}^{\Omega} a_{ij}N_j, \quad i=1, 2, \cdots \Omega. \tag{9}$$

In our problems Ω will be the number of sites. General solutions of such linear simultaneous differential equations are of the form

$$N_i=\sum_{\beta=1}^{\Omega} C_{i\beta}\exp[-f_\beta(a)t], \quad i=1, 2, \cdots \Omega. \tag{10}$$

where $f_\beta(a)$ is in general a function of all the a_{ij}. In our applications one of the $f_\beta(a)$ will be zero; this mode is always designated $\beta=1$. The corresponding constants, C_{i1} will represent equilibrium values of N_i.

[8] Reference 4, p. 105.
[9] Reference 2, p. 103.

The functions $\psi_\beta=\exp[-f_\beta(a)t]$ are referred to as "decay functions" or "modes of decay" and are obtained as eigenfunctions of the operator $\mathbf{D}=d/dt$ corresponding to the eigenvalues $-f_\beta(a)$, by a formal procedure to be illustrated shortly. The βth decay function is then characterized by a relaxation time which is the negative reciprocal of the corresponding eigenvalue. Only those decay functions which correspond to a net change of polarization with time give relaxation times observable in the dielectric relaxation spectrum. It follows from Eqs. (9) and (10) that

$$\sum_i C_{i\beta}=N\delta\beta 1 \tag{11}$$

where δ is the Kronecker symbol, since the total number of dipoles N, must remain constant. This provides a convenient check of the solutions.

Returning to the two-position example, we illustrate the calculations in detail. The characteristic determinant[10] of Eqs. (8) is

$$\begin{vmatrix} (\mathbf{D}+2k) & -2k' \\ -2k & (\mathbf{D}+2k') \end{vmatrix}=0$$

or

$$\mathbf{D}^2+2k\mathbf{D}+2k'\mathbf{D}=0,$$

whence

$$\mathbf{D}=0; \quad -2(k+k'). \tag{12}$$

The root zero leads to the equilibrium time-independent solutions C_{11} and C_{21} for sites 1 and 2, and the root $-2(k+k')$ contributes a term $C_{i2}\exp[-2(k+k')t]$ to the general solution for N_i. Thus we may write

$$N_1=C_{11}+C_{12}\psi_2, \tag{13a}$$

$$N_2=C_{21}+C_{22}\psi_2, \tag{13b}$$

where C_{11} and C_{12} are the equilibrium number of dipoles in sites 1 and 2, and ψ_2 is the decay function $\exp[-2(k+k')t]$. It may be verified by substitution of the term $C_{i2}\psi_2$ in Eq. (8) that

$$C_{12}=-C_{22}. \tag{14}$$

Comparison of Eqs. (14) and (13) shows that equilibrium is attained by a flow of dipoles from one rotational site to the other. Such a mode of decay is obviously active, and it follows that

$$P(t)=P_2\exp[-2(k+k')t], \tag{15}$$

where P_2, the polarization at $t=0$ for mode 2, is as yet unevaluated. The relaxation time associated with mode 1 (the equilibrium mode) is infinity, and need not be considered further. Equation (15) has the same form as Eq. (1), and shows that the two-position model always yields only one relaxation time,

$$\tau_2=1/2(k+k'). \tag{16}$$

[10] E. L. Ince, *Ordinary Differential Equations* (Dover Publications, New York, 1944), p. 558, see p. 144.

Thus, in the absence of fluctuations of barrier height, the two-position model leads to the simple Debye formulas [Eqs. (2), (3)] for $\epsilon'(\omega)$ and $\epsilon''(\omega)$ even in the general case where one site is more stable than the other. Our result [Eq. (16)] differs from that of Debye[8] and Fröhlich[9] by a factor of 2 owing to the fact that we have defined k and k' to be the transition probability for a jump in one direction only.

Although the procedure outlined above shows that mode 2 will be active in the dielectric relaxation spectrum, it is instructive to compute the polarization and polarizability actually associated with τ_2. We proceed as follows. First, an electric field F is applied to the system as shown in Fig. 3, and the new equilibrium values of N_1 and N_2 in Eqs. (13), C_{11}^F and C_{21}^F, obtained using the Boltzmann distribution law. Application of the distribution law yields

$$(1-\mu F\cos\theta/\mathbf{k}T)C_{21}^F = C_{11}^F\exp(-V/\mathbf{k}T)(1+\mu F\cos\theta/\mathbf{k}T),$$

which may be converted to

$$C_{11}^F = C_{11}(1-2C_{21}\mu F\cos\theta/N\mathbf{k}T), \tag{17a}$$

$$C_{21}^F = C_{21}(1+2C_{11}\mu F\cos\theta/N\mathbf{k}T), \tag{17b}$$

using $C_{11}+C_{21}=C_{11}^F+C_{21}^F=N$ and $C_{21}/C_{11}=\exp(-V/\mathbf{k}T)$. μ is the component of the permanent dipole moment perpendicular to the axis of rotation, i.e., the component in the plane of the diagram shown in Fig. 3. In the above and all similar calculations we have assumed that $\mu F\ll kT$.

Next, let the field F be removed at $t=0$. We note that $N_1=C_{11}^F$ and $N_2=C_{21}^F$ at $t=0$, while $N_1=C_{11}$ and $N_2=C_{21}$ at $t=\infty$. It is readily found by comparison of Eqs. (13) and (17) that these conditions are met if

$$N_1=C_{11}-(2C_{11}C_{21}\mu F\cos\theta/N\mathbf{k}T)\psi_2, \tag{18a}$$

$$N_2=C_{21}+(2C_{11}C_{21}\mu F\cos\theta/N\mathbf{k}T)\psi_2. \tag{18b}$$

These results conform with Eq. (11). Equations (18) show formally that the change of polarization with time is a result of a net flow of charge from site 1 to site 2 or vice versa. This result is consistent with that deduced from Eq. (14).

Finally, we compute the polarization in the x, y, and z directions (Fig. 3) at $t=0$ from Eqs. (18) using

$$P_x=(-N_1\mu+N_2\mu)\cos\theta,$$

$$P_y=0;\quad P_z=0.$$

P_x is found to be $4C_{11}C_{21}\mu^2F\cos^2\theta/NkT$. The average value in the x direction, $\bar{P}_x$, is $4C_{11}C_{21}\mu^2F\langle\cos^2\theta\rangle_{Av}/NkT$ where $\langle\cos^2\theta\rangle_{Av}$ is $\frac{1}{3}$. The total polarization associated with mode 2 at $t=0$ is then

$$P_2=\bar{P}_x+\bar{P}_y+\bar{P}_z=(4C_{11}C_{21}\mu^2F/N)(\mu^2/3\mathbf{k}T).$$

Using $\alpha\equiv P/NF$, the polarizability associated with mode 2 is found to be

$$\alpha_2=(4C_{11}C_{21}/N^2)(\mu^2/3\mathbf{k}T). \tag{19}$$

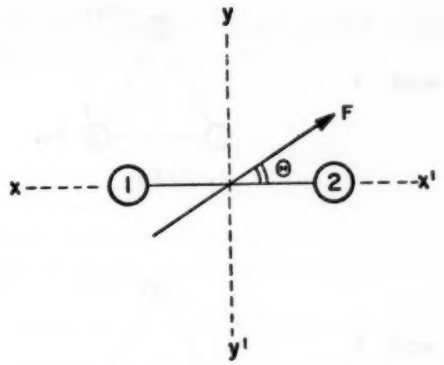

FIG. 3. Coordinate system used in the calculation of the polarizability of the two-position model. The z axis is perpendicular to the plane of the diagram.

Recalling that C_{11} and C_{21} are the equilibrium number of dipoles in sites 1 and 2, respectively, the polarizability may now be evaluated for the special cases $k=k'$ (equivalent sites) and $k'\gg k$ (site 1 stable). When the two sites are equivalent $C_{11}/N=C_{21}/N=\frac{1}{2}$, and the polarizability[11] is $\mu^2/3\mathbf{k}T$. When V is large so that most of the dipoles are in site 1, $C_{11}/N\cong 1$, and the polarizability is given approximately by $(4C_{21}/N)\mu^2/3\mathbf{k}T$ or $4\exp(-V/\mathbf{k}T)(\mu^2/3\mathbf{k}T)$; this shows that the polarizability will be considerably less that $\mu^2/3kT$ when one site is stable with respect to the other.

II. PROPERTIES OF MODELS WHERE JUMPS TO ADJACENT SITES ONLY ARE PERMITTED

1. Three-Position Model

In this model we consider the case where each of the dipoles may occupy any of three sites 120° apart. Sites 2 and 3 are always equivalent, but site 1 is more stable than these if $V>0$. In calculating the properties of this model, we make the first explicit use of the concept that only a jump to an *adjacent* site is permitted as an elementary process. Thus, the rate at which dipoles leave site 1 is $-2kN_1$, since dipoles may turn to sites 2 and 3 from 1, but the number entering site 1 from site 2 is $k'N_2$ (and not $2k'N_2$) since the double jump $2\rightarrow 3\rightarrow 1$ is forbidden as a single step. Bearing this restriction in mind, the rate equations are

$$dN_1/dt=-2kN_1+k'N_2+k'N_3, \tag{20a}$$

$$dN_2/dt=kN_1-2k'N_2+k'N_3, \tag{20b}$$

$$dN_3/dt=kN_1+k'N_2-2k'N_3. \tag{20c}$$

The roots of the characteristic determinant of these equations are found to be

$$\mathbf{D}=0;\ -3k';\ -(2k+k'). \tag{21}$$

[11] It should be noted that μ is the component of the permanent dipole moment perpendicular to the axis of rotation. Thus $\mu=\mu_0\sin\psi$ where μ_0 is the permanent dipole moment and ψ is the angle subtended by the dipole and the axis of rotation. Thus, if a dipole is at a right angle to the axis of rotation, the polarizability will be $\mu_0^2/3\mathbf{k}T$ (see reference 3).

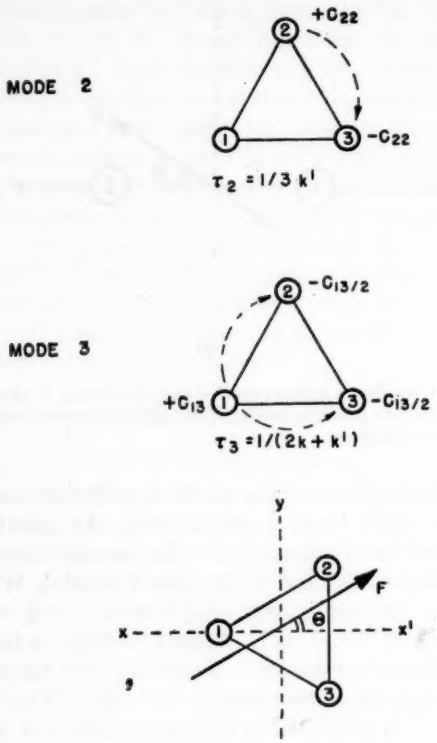

FIG. 4. Upper diagrams: Nature of modes of decay exhibited by three-position model. Lower: coordinates used in polarizability calculations. The z axis is perpendicular to the plane of the diagram.

This suggests that the two relaxation times

$$\tau_2=1/3k', \tag{22a}$$

$$\tau_3=1/(2k+k') \tag{22b}$$

will appear when $k'\neq k$. The root zero leads to the equilibrium time-independent solutions C_{i1} (mode 1).

Substitution of the terms $C_{i2}\exp(-3k't)$ and $C_{i3}\exp[-(2k+k')t]$, which correspond to the time-dependent modes of decay 2 and 3, into Eqs. (20) yields

$$C_{22}=-C_{32};\quad C_{12}=0, \tag{23a}$$

$$C_{23}=C_{33};\quad C_{13}=-2C_{23}. \tag{23b}$$

Thus we obtain

$$N_1=C_{11}+0+C_{13}\psi_3, \tag{24a}$$

$$N_2=C_{21}+C_{22}\psi_2-(C_{13}/2)\psi_3, \tag{24b}$$

$$N_3=C_{31}-C_{22}\psi_2-(C_{13}/2)\psi_3, \tag{24c}$$

where ψ_2 and ψ_3 are the decay functions $\exp(-3k't)$ and $\exp[-(2k+k')t]$.[12]

[12] When $k=k'$ the decay functions ψ_2 and ψ_3 become degenerate, and Eqs. (24) then have the form $N_i=C_{i1}+C_{i2}\psi_2'+tC_{i3}\psi_2'$ where $\psi_2'=\exp(-3kt)$. However, the constants C_{i3} associated with the t term are all zero when evaluated by Eqs. (20). Thus, only one decay function (and hence only one relaxation time) appears for $k=k'$. Similar degeneracies in decay functions for cases involving more sites all lead to trivial solutions for terms of the type $tC_{i\beta}\psi_\beta'$, so that only one relaxation time appears when $k=k'$.

These equations show that mode 2 involves a net shift of dipoles from site 2 to 3, while mode 3 involves a net shift of dipoles from site 1 to both sites 2 and 3, or vice versa.

The nature of the modes of relaxation are illustrated in Fig. 4 (upper two diagrams). These diagrams were constructed by assigning the C values in Eqs. (24) for each mode to the appropriate site. A given mode is polar if the vector sum of the C values for that mode, $\mathbf{C}_\beta$, is not zero; it may be seen by inspection that $\mathbf{C}_\beta\neq 0$ for modes 2 and 3. This method of determining whether a given mode will be active in the dielectric relaxation spectrum will be particularly useful in dealing with models with five or more sites where our principal interest is the distribution of relaxation times, and not the precise value of the polarizability associated with each mode. In the present case, however, it is of interest to evaluate the $C_{i\beta}$ and compute the polarizability associated with modes 2 and 3.

The polarizations P_2 and P_3 associated with each of the modes of decay may be obtained in a manner analogous to that illustrated for the two-position model. The coördinates used are shown in Fig. 4, where the arrow is the projection of the field on the $x-y$ plane. Application of the Boltzmann distribution law yields

$$[1-\mu F\cos(\theta-60°)/\mathbf{k}T]C_{21}{}^F = C_{11}{}^F\exp(-V/\mathbf{k}T)[1+\mu F\cos\theta/\mathbf{k}T],$$

$$[1-\mu F\cos(\theta+60°)/\mathbf{k}T]C_{31}{}^F = C_{11}{}^F\exp(-V/\mathbf{k}T)[1+\mu F\cos\theta/\mathbf{k}T].$$

Using $C_{11}{}^F+C_{21}{}^F+C_{31}{}^F=C_{11}+C_{21}+C_{31}=N$ and $C_{21}=C_{31}=C_{11}\exp(-V/\mathbf{k}T)$ it is readily found that

$$C_{11}{}^F=C_{11}(1-3C_{21}\mu F\cos\theta/N\mathbf{k}T),$$

$$C_{21}{}^F=C_{21}\left\{1+\frac{N\mu F\cos(\theta-60°)-\frac{1}{2}N\mu F\cos\theta+\frac{3}{2}C_{11}\mu F\cos\theta}{N\mathbf{k}T}\right\},$$

$$C_{31}{}^F=C_{21}\left\{1+\frac{N\mu F\cos(\theta+60°)-\frac{1}{2}N\mu F\cos\theta+\frac{3}{2}C_{11}\mu F\cos\theta}{N\mathbf{k}T}\right\}.$$

Using the conditions $N_i=C_{i1}{}^F$ at $t=0$ and $N_i=C_{i1}$ at $t=\infty$ it is found that

$$N_1=C_{11}+\quad 0\quad -\frac{3C_{11}C_{21}\mu F\cos\theta\psi_3}{N\mathbf{k}T}, \tag{25a}$$

$$N_2=C_{21}+\frac{\sqrt{3}C_{21}\mu F\sin\theta\psi_2}{2\mathbf{k}T}+\frac{3C_{11}C_{21}\mu F\cos\theta\psi_3}{2N\mathbf{k}T}, \tag{25b}$$

$$N_3=C_{21}-\frac{\sqrt{3}C_{21}\mu F\sin\theta\psi_2}{2\mathbf{k}T}+\frac{3C_{11}C_{21}\mu F\cos\theta\psi_3}{2N\mathbf{k}T}. \tag{25c}$$

The polarization associated with each mode of decay at $t=0$ may be found from the above using

$$P_x=(-N_1\mu+\cos 60°N_2\mu+\cos 60°N_3\mu)\cos\theta\sin\xi,$$
$$P_y=(\cos 30°N_2\mu-\cos 30°N_3\mu)\sin\theta\sin\xi,$$
$$P_z=0,$$

where ξ is the angle between the z axis and the field F. For mode 2 at $t=0$ it is found that

$$P_2=\bar{P}_x+\bar{P}_y+\bar{P}_z=C_{21}\mu^2F/2\mathbf{k}T$$

so that

$$\alpha_2=(3C_{21}/2N)(\mu^2/3kT). \tag{26a}$$

The analogous calculation for mode 3 yields

$$\alpha_3=(9C_{11}C_{21}/2N^2)(\mu^2/3kT). \tag{26b}$$

In the above equations C_{11} is the equilibrium number of dipoles in site 1, while C_{21} is the corresponding number in sites 2 or 3. In the above we have made use of $\langle\cos^2\theta\sin\xi\rangle_{Av}=\langle\sin^2\theta\sin\xi\rangle_{Av}=\frac{1}{3}$.

When $k'=k$ (equivalent sites) we have $C_{11}/N=C_{21}/N=\frac{1}{3}$ so that the total orientational polarizability, $\alpha_2+\alpha_3$, is given by $\mu^2/3kT$; both modes contribute equally to this result. The relaxation time for $k'=k$ (Eqs. (22)) is $\tau=1/3k$.

In the event that $k'\gg k$ (site 1 deep) it is found from Eqs. (22) that

$$\tau_2\cong 1/3k', \tag{27a}$$
$$\tau_3\cong 1/k'. \tag{27b}$$

Also, when $k'\gg k$, we find using Eqs. (26) that

$$\alpha_3/\alpha_2\cong 3, \tag{28}$$

since $C_{11}/N\cong 1$ under these conditions. Thus the longer relaxation time, τ_3, is associated with the higher polarizability. This means that $\Delta\epsilon_3\cong 3\Delta\epsilon_2$ in Eq. (5) with the result that the dielectric loss peak, in addition to being broadened by the presence of two relaxation times, will be somewhat asymmetric when $k'>k$. It is easily shown that $\alpha_2+\alpha_3$ is approximately $6\exp(-V/kT)(\mu^2/3kT)$ when $k'\gg k$ so that the absolute value of the total orientational polarizability, and hence $\epsilon_{\max}''$, will be quite small when one site is considerably more stable than the others.

2. Four-Position Model

This is the model shown in Figs. 1 and 2. Proceeding as before, and noting that only jumps to adjacent sites are permitted, the rate equations are

$$dN_1/dt=-2kN_1+k'N_2+k'N_4, \tag{29a}$$
$$dN_2/dt=kN_1-2k'N_2+k'N_3, \tag{29b}$$
$$dN_3/dt=k'N_2-2k'N_3+k'N_4, \tag{29c}$$
$$dN_4/dt=kN_1+k'N_3-2k'N_4. \tag{29d}$$

The roots of the characteristic determinant are

$$D=0;\ -2k';\ -(2k'+k-\sqrt{Q});\ -(2k'+k+\sqrt{Q}), \tag{30}$$

where $Q=2k'^2-2kk'+k^2$. These results suggest that three relaxation times given by

$$\tau_2=1/2k', \tag{31a}$$
$$\tau_3=1/(2k'+k-\sqrt{Q}), \tag{31b}$$
$$\tau_4=1/(2k'+k+\sqrt{Q}), \tag{31c}$$

will appear when $k'\neq k$. As in previous cases, the root zero leads to the time-independent equilibrium values of N_i, C_{i1}.

Substitution of the terms $C_{i2}\exp(-2k't)$,

$$C_{i3}\exp[-(2k'+k-\sqrt{Q})t]$$

and

$$C_{i4}\exp[-(2k'+k+\sqrt{Q})t],$$

which correspond to modes of decay 2, 3, and 4, into Eqs. (29) yields the relations

$$\text{Mode 2:}\quad C_{22}=-C_{42};\quad C_{12}=C_{32}=0, \tag{32a}$$
$$\text{Mode 3:}\quad C_{33}=C_{13}(\sqrt{Q}-2k'+k)/(\sqrt{Q}-k), \tag{32b}$$
$$C_{23}=C_{43}=C_{13}(\sqrt{Q}-2k'+k)/2k',$$
$$\text{Mode 4:}\quad C_{24}=C_{44}=C_{14}(k-2k'-\sqrt{Q})/2k', \tag{32c}$$
$$C_{34}=-C_{14}(k-2k'-\sqrt{Q})/(\sqrt{Q}+k).$$

The above relationships have been used to construct equations for the four-position model analogous to Eqs. (24). The C values were then computed for the two special cases $k'=k$ and $k'\gg k$. We have also obtained the vector sum of the $C_\beta\,\mathbf{C}_\beta$, in terms of a reference site,

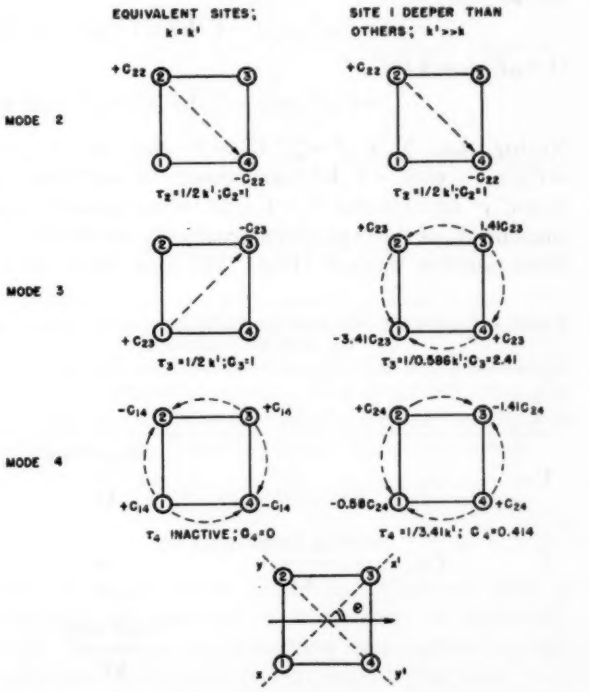

FIG. 5. Upper diagrams: Nature of the modes of decay of the four-position model for $k'=k$ and $k'\gg k$. Lower: coordinates used in calculation of the polarizability. The z axis is perpendicular to the plane of the diagram.

using the convention that when a plus and a minus C value are separated by a distance equal to the diameter of a circle passing through the sites, $\mathbf{C}_\beta=1$. The nature of the modes of decay are shown in Fig. 5.

It is interesting to note that when $k'=k$ that mode 4 is inactive owing to a compensatory motion of the dipoles. Such dielectrically inactive modes will lead to a large permanent dipole Kerr effect. Modes 2 and 3 are both active since $\mathbf{C}_\beta\neq 0$, and have the same relaxation time,

$$\tau=1/2k'. \tag{33}$$

It may be seen in Fig. 5 that $\mathbf{C}_\beta\neq 0$ for modes 2, 3, and 4 when site 1 is stable; the corresponding relaxation times calculated from Eqs. (31) for $k'\gg k$

$$\tau_2\cong 1/2k', \tag{34a}$$

$$\tau_3\cong 1/(2-\sqrt{2})k'=1/0.586k', \tag{34b}$$

$$\tau_4\cong 1/(2+\sqrt{2})k'=1/3.41k', \tag{34c}$$

are all active in the dielectric relaxation spectrum. A calculation of the polarizability associated with each mode follows.

Using the coordinates shown in Fig. 5 (lower) and applying the Boltzmann distribution law for the case where an electric field F is imposed on the system, we obtain

$$(1-\mu F\sin\theta/\mathbf{k}T)C_{21}{}^F = C_{11}{}^F\exp(-V/\mathbf{k}T)(1+\mu F\cos\theta/\mathbf{k}T),$$

$$(1-\mu F\cos\theta/\mathbf{k}T)C_{31}{}^F = C_{11}{}^F\exp(-V/\mathbf{k}T)(1+\mu F\cos\theta/\mathbf{k}T),$$

$$(1+\mu F\sin\theta/\mathbf{k}T)C_{41}{}^F = C_{11}{}^F\exp(-V/\mathbf{k}T)(1+\mu F\cos\theta/\mathbf{k}T).$$

Noting that $\sum_i C_{i1}{}^F=\sum_i C_{i1}=N$ and that $C_{21}=C_{31}=C_{41}=C_{11}\exp(-V/\mathbf{k}T)$, and using the conditions that $N_i=C_{i1}{}^F$ at $t=0$ and $N_i=C_{i1}$ at $t=\infty$, general expressions for N_i of the type given previously for the two- and three-position models (Eqs. (18) and (25)) may be obtained. Since the general expressions for N_i in terms of C_{11}, C_{21}, μ, F, and θ are rather complicated they will not be given here. Instead, we summarize the results in Tables I and II for the special cases $k'=k$ and $k'\gg k$.

TABLE I. $C_{i\beta}$ for the four-position model for $k'=k$. $C_{i1}=C_{11}$ when the sites are equivalent.

i \ β	1	2	3	4
1	C_{11}	0	$\dfrac{-C_{11}\mu F\cos\theta}{\mathbf{k}T}$	0
2	C_{11}	$\dfrac{C_{11}\mu F\sin\theta}{\mathbf{k}T}$	0	0
3	C_{11}	0	$\dfrac{C_{11}\mu F\cos\theta}{\mathbf{k}T}$	0
4	C_{11}	$\dfrac{-C_{11}\mu F\sin\theta}{\mathbf{k}T}$	0	0

The polarization associated with each mode at $t=0$ may be obtained using

$$P_x=(-N_1\mu+N_3\mu)\cos\theta\sin\xi,$$
$$P_y=(+N_2\mu-N_4\mu)\sin\theta\sin\xi,$$
$$P_z=0.$$

By employing the $C_{i\beta}$ values given in Table I in conjunction with the above equations, it is easily shown that

$$\alpha_2=(2C_{11}/N)(\mu^2/3\mathbf{k}T), \tag{35a}$$

$$\alpha_3=(2C_{11}/N)(\mu^2/3\mathbf{k}T), \tag{35b}$$

$$\alpha_4=0 \tag{35c}$$

for $k'=k$. Noting that $C_{11}/N=\frac{1}{4}$ when $k'=k$, it is seen that the total orientational polarizability is $\mu^2/3\mathbf{k}T$. Mode 4 does not contribute to the polarizability when the sites are equivalent (compare Fig. 5). The relaxation time associated with both modes 2 and 3 is given by Eq. (33).

By a similar procedure, the $C_{i\beta}$ in Table II lead to the following polarizabilities for the case $k'\gg k$:

$$\alpha_2=(2C_{21}/N)(\mu^2/3\mathbf{k}T), \tag{36a}$$

$$\alpha_3=[C_{21}(3+2\sqrt{2})/N](\mu^2/3\mathbf{k}T), \tag{36b}$$

$$\alpha_4=[C_{21}(3-2\sqrt{2})/N](\mu^2/3\mathbf{k}T). \tag{36c}$$

These polarizabilities indicate the relative importance in the dielectric relaxation spectrum of the relaxation times given by Eqs. (34) for the case $k'\gg k$. It is seen that longer relaxation time is always associated with the higher polarizability. Thus, as the relaxation times increase as 1/3.41, $\frac{1}{2}$, and 1/0.586, the corresponding polarizabilities increase as $(3-2\sqrt{2})$, 2, and $(3+2\sqrt{2})$. As a consequence, the dielectric loss peaks will be asymmetric when $k'>k$. When site 1 is deep, C_{21}/N, the fraction of dipoles in a type 2 site, will be small so that the total orientational polarizability, and hence $\epsilon_{\max}''$, will be quite low when k' is appreciably greater than k.

The four-position model with one deep site yields a distribution of relaxation times which is broader than that given by the three-position model; the maximum spread of the relaxation times is increased from a factor of 3 to a factor of 5.8 (compare Eqs. (22) with (34)). The dielectric loss peak exhibited by the four-position model will be somewhat more asymmetric than that of the three-position model.

It is convenient to point out here that $\mathbf{C}_\beta{}^2$ is a rough measure of the *relative* importance of the various τ_β for any given ratio of k'/k. For instance, consider the four-position model for the cases $k'=k$ and $k'\gg k$. When $k'=k$, it is seen that $\mathbf{C}_\beta{}^2$ for modes 4, 3, and 2 are 0, 1, and 1. The actual polarizabilities are in the same order

TABLE II. $C_{i\beta}$ for the four-position model for $k'=k$. C_{11} is the equilibrium number of dipoles in site 1, and C_{21} is the corresponding number for sites 2, 3, or 4.

i \ β	1	2	3	4
1	C_{11}	0	$\frac{-C_{21}(3\sqrt{2}+4)\mu F\cos\theta}{2\mathbf{k}T}$	$\frac{+C_{21}(3\sqrt{2}-4)\mu F\cos\theta}{2\mathbf{k}T}$
2	C_{21}	$\frac{C_{21}\mu F\sin\theta}{\mathbf{k}T}$	$\frac{+C_{21}(\sqrt{2}+1)\mu F\cos\theta}{2\mathbf{k}T}$	$\frac{+C_{21}(1-\sqrt{2})\mu F\cos\theta}{2\mathbf{k}T}$
3	C_{21}	0	$\frac{+C_{21}(\sqrt{2}+2)\mu F\cos\theta}{2\mathbf{k}T}$	$\frac{+C_{21}(2-\sqrt{2})\mu F\cos\theta}{2\mathbf{k}T}$
4	C_{21}	$\frac{-C_{21}\mu F\sin\theta}{\mathbf{k}T}$	$\frac{+C_{21}(\sqrt{2}+1)\mu F\cos\theta}{2\mathbf{k}T}$	$\frac{+C_{21}(1-\sqrt{2})\mu F\cos\theta}{2\mathbf{k}T}$

0, $\frac{1}{2}(\mu^2/3\mathbf{k}T)$, and $\frac{1}{2}(\mu^2/3\mathbf{k}T)$. When $k'\gg k$, $\mathbf{C}_\beta^2$ for the same modes in order are 0.181, 1, and 5.82. The corresponding polarizabilities are $0.172C_{21}(\mu^2/3N\mathbf{k}T)$, $2C_{21}(\mu^2/3N\mathbf{k}T)$, and $5.82C_{21}(\mu^2/3N\mathbf{k}T)$. A similar approximate parallelism between α_β and $\mathbf{C}_\beta^2$ is to be expected in other cases. Therefore, in the five- and six-position models to follow, we carry the calculations only to the stage necessary to obtain the mode diagrams.

3. Five-Position Model

The roots of the characteristic determinant of the differential equations of the five-position model are

$$\mathbf{D}=0;\ -(5\pm\sqrt{5})k'/2;\ -(3k'+2k\pm\sqrt{R})/2, \quad (37)$$

where $R=5k'^2-4kk'+4k^2$.

Substitution of the terms $C_{i2}\exp[-(5+\sqrt{5})k't/2]$, $C_{i3}\exp[-(3k'+2k+\sqrt{R})t/2]$, $C_{i4}\exp[-(5-\sqrt{5})\times k't/2]$, and $C_{i5}\exp[-(3k'+2k-\sqrt{R})t/2]$ corresponding to modes of decay 2 to 5 yield relationships between the C values for each mode of the type given for other models (Eqs. (14), (23), and (32)). These values were calculated for the cases $k'=k$ and $k'\gg k$. The diagrams indicating the nature of the modes of decay obtained from the C values are depicted in Fig. 6.

When $k'=k$ it is seen that $\mathbf{C}_\beta=0$ for modes 2 and 3. These modes are therefore inactive in the dielectric relaxation spectrum. Modes 4 and 5 each lead to $\mathbf{C}_\beta$ values of 1.54, and are therefore active in the dielectric relaxation spectrum. Inspection of the decay function part of the terms given above for modes 4 and 5 reveals that

$$\tau=1/[(5-\sqrt{5})k'/2]=1/1.138k', \quad (38)$$

when the sites are all equivalent.

In the event that site 1 is stable with respect to the others, three active relaxation times are found:

$$\tau_3\cong 1\Big/\left(\frac{3-\sqrt{5}}{2}\right)k'=1/0.382k';\quad \mathbf{C}_3=2.13, \quad (39a)$$

$$\tau_4\cong 1\Big/\left(\frac{5-\sqrt{5}}{2}\right)k'=1/1.38k';\quad \mathbf{C}_4=2.13, \quad (39b)$$

$$\tau_5\cong 1\Big/\left(\frac{3+\sqrt{5}}{2}\right)k'=1/2.62k';\quad \mathbf{C}_5=0.68. \quad (39c)$$

The maximum spread of τ is now 6.9 as compared with 5.8 for the four-position case.

4. Six-Position Model

The significant results follow: When all six sites are equivalent, the only active relaxation time is

$$\tau=1/k', \quad (40)$$

when site 1 is deep, four active relaxation times are found:

$$\tau_2=1/(2-\sqrt{3})k'=1/0.268;\quad \mathbf{C}_2=10.2, \quad (41a)$$

$$\tau_3=1/k';\quad \mathbf{C}_3=3.4, \quad (41b)$$

$$\tau_4=1/2k';\quad \mathbf{C}_4=1, \quad (41c)$$

$$\tau_5=1/(2+\sqrt{3})k'=1/3.73k';\quad \mathbf{C}_5=0.20. \quad (41d)$$

The maximum spread of relaxation times is now 13.9.

In the five- and six-position models it should be noted that the larger $\mathbf{C}_\beta$ values are in general associated with the longer relaxation times. This suggests that the longer relaxation times will contribute more strongly to the dielectric loss than the shorter relaxation times.

III. DISCUSSION

1. Equivalent Sites

Only a single active dielectric relaxation time is obtained for the case where all the sites are equivalent ($k'=k$). The dielectric relaxation time for the two- to six-position models may be expressed in the form

$$\tau=(\gamma/A)\exp(W/\mathbf{k}T), \quad (42)$$

where γ is a numerical factor which involves the number

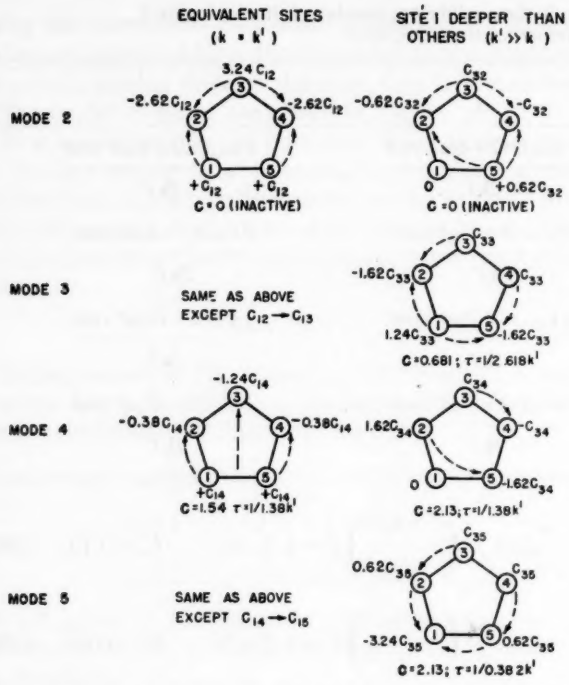
EQUIVALENT SITES
(k = k')
SITE 1 DEEPER THAN OTHERS (k' >> k)
MODE 2
MODE 3
MODE 4
MODE 5
SAME AS ABOVE EXCEPT C12 → C13
SAME AS ABOVE EXCEPT C14 → C15
C = 0 (INACTIVE)
C = 0 (INACTIVE)
C = 0.681; τ = 1/2.618k'
C = 1.54 τ = 1/1.38k'
C = 2.13; τ = 1/1.38k'
C = 2.13; τ = 1/0.382k'

FIG. 6. Nature of modes of decay for the five-position model for $k'=k$ and $k'\gg k$.

of sites (compare Eqs. (16), (22), (33), (38), and (40), with (7)). The factor γ increases as 0.25, 0.33, 0.5, 0.725, and 1.0 as γ increases from 2 to 6. Equation (42) is exact for the models considered.

A simple criterion for distinguishing between "free" and "hindered" rotation in solids consisting of single-axis rotators can be obtained by estimating the dielectric relaxation time associated with a freely rotating molecule with moment of inertia I. It may be shown that the average rate of rotation in radians/sec., $\bar{\phi}^{\cdot}$, for a molecule with one degree of freedom is $(\mathbf{k}T/2\pi I)^{\frac{1}{2}}$. The time required for a complete revolution, $2\pi/\bar{\phi}^{\cdot}$, will be of the same order of magnitude as the dielectric relaxation time. Thus

$$\tau_{\text{free}} \cong 2\pi(2\pi I/\mathbf{k}T)^{\frac{1}{2}}. \tag{43}$$

At ordinary temperatures and reasonable moments of inertia, τ_{free} falls in the range 10^{-10} to 10^{-12} sec. If the observed dielectric relaxation time is considerably longer than that given by Eq. (43), it follows that a local free energy barrier (such as that postulated for our "site" models) is hindering the turning of the dipoles.[13] The observation of a polarizability close to $\mu_0^2/3\mathbf{k}T$ for a solid is sometimes considered to be an indication of "free" rotation, but it should be noted that any equivalent site (hindered) rotator where the permanent dipole moment is at a right angle to the axis of rotation[11] leads to the same value.

The present derivation of a single dielectric relaxation time for polar crystalline solids consisting of single-axis rotators with equivalent sites leads to the simple Debye equations for dielectric behavior (Eqs. (2) and (3)). Our calculations differ significantly from Debye's original derivation of Eqs. (2) and (3)[14] which deals with liquids consisting of large spherical polar molecules, in that we make no reference to viscosity, but use an energy barrier picture instead. Debye evidently recognized the fictitious nature of an "internal" viscosity for polar solids, as he also gave the first derivation of Eqs. (2) and (3) using a "site" model with two-positions.[8] Our work is an extension of Debye's two-position theory. It should be noted, however, that one of the unique features of the "site" model (namely, that it can lead to a distribution of relaxation times in a natural way without the assumption of fluctuations of barrier height) emerges only when models with more than two positions are considered. This brings us to a discussion of the models which are characterized by an asymmetry in the local free energy.

2. Nonequivalent Sites

When a single-axis rotator has three or more sites, and $k'\neq k$, a distribution of relaxation times is predicted (Eqs. (27), (34), (39), and (41)). The width of the distribution is a maximum when $k'\gg k$. This distribution is a natural result of the asymmetry of the local free energy barrier and the single-jump hypothesis. The present calculations show that a definite and fairly marked broadening of dielectric loss peaks can be predicted under certain conditions without the introduction of the concept of fluctuations[15] of barrier height.

The distribution of relaxation times calculated for the three- to six-position models with the use of the single-jump approximation for the case where one site is stable with respect to the others will generally lead to *slightly asymmetric* loss peaks. This arises from two causes: (a) except for the three-position model, the relaxation times are not evenly spaced, and (b) the polarizability (or $\mathbf{C}_\beta^2$ values) associated with each relaxation time are generally higher for the longer relaxation times (compare Eqs. (27) and (28), (34), and (36); also, compare $\mathbf{C}_\beta$ and τ_β values in Eqs. (39) and (41)). Since a high

[13] The familiar rate theory of Eyring leads to Eq. (43) for a free rotator. According to this formulation $\tau \equiv 1/k = (h/\mathbf{k}T)\exp(W/\mathbf{k}T) = (h/\mathbf{k}T)(\mathbf{Q}_A/\mathbf{Q}^*)\exp(E/\mathbf{k}T)$, where $\mathbf{Q}_A$ is the partition function of the initial state, $\mathbf{Q}^*$ the partition function of the "activated complex" with one degree of freedom of *rotation* removed, and E the activation energy. For a free rotator $E=0$, and $\mathbf{Q}_A/\mathbf{Q}^* = 2\pi(2\pi I\mathbf{k}T)^{\frac{1}{2}}/h$, so we recover Eq. (43).

[14] Reference 4, pp. 77–102.

[15] In the present paper, we use the term *fluctuation* in the usual sense of a local change of barrier height with time. A distribution of barrier height resulting from molecular complexity (as in polymers where one can readily imagine a difference in the environment of dipoles on different parts of a molecule on a quasi-equilibrium basis) is not to be considered as a fluctuation in the sense defined above. As Kauzmann has pointed out (reference 1) a distribution of activation energies resulting from molecular complexity (or the "polyphase" nature of polymers) will surely lead to a distribution of dielectric relaxation times in polymers. The calculations presented here apply to monophase dipolar crystals consisting of rigid molecules; no significant distribution of barrier height of the type mentioned above for polymers is to be expected in such a system.

polarizability always implies a high $\Delta\epsilon$ value, it follows from Eq. (5) that the three- to six-position models will lead to dielectric loss peaks which are somewhat steeper on the low frequency side (Fig. 7).

The present theory also leads to an interesting prediction regarding the change of width of the distribution of dielectric relaxation times with temperature. In general, energy barriers of the type shown in Fig. 1 (lower) will become more symmetrical as the temperature is raised, i.e. V will diminish with increase of temperature. This is particularly the case if the system is subject to a cooperative effect.[3] This fact, when combined with the present theory leads to the prediction that *the distribution of relaxation times will become narrower as the temperature increases.* The condition $k' \gg k$ corresponds to the strongly asymmetric local free energy barrier expected at low temperatures, while the condition $k' > k$ or $k' \sim k$ corresponds to the more symmetrical barrier expected at higher temperatures. A single relaxation time is not generally to be expected for solids consisting of single-axis hindered rotators (where there are three or more accessible sites) since it is doubtful that the barriers hindering rotation become completely symmetrical before the material melts. The suggested change from the condition $V > W$ at low temperatures to $V \sim W$ or $V \sim 0$ at higher temperatures leads in a similar way to the concept that the polarizability will increase with temperature until the sites are very nearly equivalent; at this point the $1/T$ part of the polarizability term will then lead to a slowly decreasing polarizability.[16]

The general predictions given above should be observable for substances which may be regarded as single-axis rotators with a number of accessible orientational sites, although very careful work will probably be required to detect the asymmetry of the loss peaks. The dielectric properties of certain types of polar long-chain compounds may prove useful in checking the theory. It should be remembered that the present theory deals only with the dielectric loss resulting from the turning

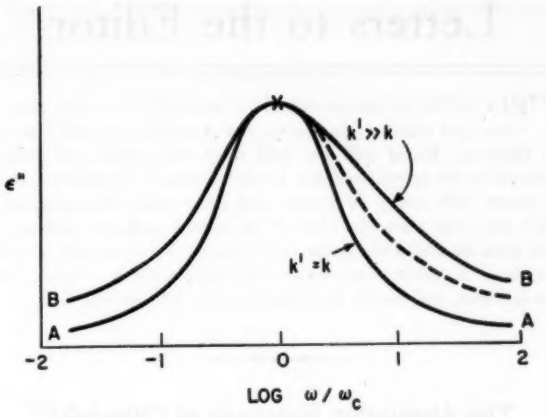

FIG. 7. Shape of the dielectric loss peaks as a function of frequency for the three- to six-position models (schematic). Curve $A-A$: typical Debye-type loss peak with single relaxation time predicted for the case of equivalent sites. Curve $B-B$: slightly asymmetric loss peak for case where one site is more stable than the others. Dashed line is mirror-image of left-hand-side of curve $B-B$.

of dipoles from one equilibrium site to another. Dielectric loss regions due to this cause will generally occur at frequencies of about 10^9 cycles/sec or less; they frequently occur in the audio region.[3] Resonance absorption[17] resulting from rotational oscillations of dipoles in a given site, or a "wagging" motion of a dipole not rigidly coupled to a molecule may lead to dielectric loss peaks which will appear at frequencies considerably higher than 10^9 cycles/sec, and which may be narrower than the Debye-type peak.

In conclusion we must emphasize that the models treated here do not necessarily correspond to any real solid. For example, more than two rate constants may be involved. Nevertheless, the important features of the theory emerge as soon as two rate constants and at least three sites are assumed (together with the single jump hypothesis). More complex models involving more than two rate constants will yield qualitatively similar results.

ACKNOWLEDGMENT

The authors are deeply indebted to Drs. Bruno H. Zimm and John K. Bragg for their advice on this problem. We also wish to thank Dr. Julian Gibbs for helpful discussions.

[16] Sharp solid-state transitions, where V diminishes suddenly as the temperature is raised, often occur in substances consisting of single-axis hindered rotators. At such a transition the polarizability will undergo an *abrupt* increase (reference 3) and the distribution of relaxation times will, according to the theory presented here, *suddenly* become more narrow. The theory given in this paper for the distribution of relaxation times is intended to supersede the oversimplified version given in reference 3.

[17] Reference 2, pp. 98–103.

Letters to the Editor

THIS section will accept reports of new work, provided these are terse and contain few figures, and especially few half-tone cuts. The Editorial Board will not hold itself responsible for opinions expressed by the correspondents. Contributions to this section should not exceed 600 words in length and must reach the office of the Editor not later than the 15th of the second month preceding that of the issue in which the Letter is to appear. No proof will be sent to the authors. A publication charge of $10.00 per Letter is made which, when honored, will entitle the Institution to 100 free reprints.

The Absorption Spectrum of Chlorophyll *a* Crystals

EARL E. JACOBS AND A. STANLEY HOLT
Photosynthesis Research Project, Department of Botany, University of Illinois, Urbana, Illinois
(Received August 3, 1953)

THE position of the red absorption band of chlorophyll and ethyl chlorophyllide depends on the state of association of the molecules. In the crystalline form, ethyl chlorophyllide *a* has an absorption peak in the neighborhood of 730 mμ,[1,2] whereas in acetone and other organic solvents it shows maximum absorption in the region of 660 mμ. Using this absorption band shift as an experimental criterion for condensation, we have brought about the successful crystallization of chlorophyll *a*. A description of the crystals (photographs and x-ray diffraction patterns) and the techniques used in their preparation appear in an accompanying communication to this journal.

The true absorption spectrum of chlorophyll *a* crystals was obtained by correcting the apparent absorption spectrum of a suspension of dispersed microcrystals for selective scattering. Figure 1 shows the apparent absorption spectrum (solid line) of a

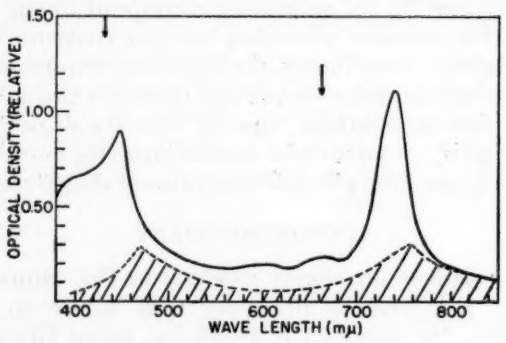

FIG. 1. The apparent absorption spectrum of chlorophyll *a* microcrystals (solid line). The shaded area is the estimated contribution to the apparent absorption by selective scattering.

suspension of the dispersed microcrystals in petroleum ether. The shaded area is the estimated contribution to the apparent absorption by selective scattering. The arrows designate the wavelength positions of the red and blue absorption peaks of chlorophyll *a* in acetone.

A comparison of these curves with those in reference 1 shows a remarkable similarity between the crystalline absorption spectra of chlorophyll *a* and ethyl chlorophyllide *a*. The presence of the long phytyl side chain in chlorophyll *a* does not seem to interfere with interaction between the conjugated ring systems in the molecules of the crystal. Studies on the absorption spectra of monomolecular films of these pigments have shown that chromophore interactions are mostly confined within a single plane. Our results with phytyl chlorophyllide *a* (chlorophyll *a*) are therefore quite reasonable since the long phytyl chain will not obstruct close packing of the planar ring systems in two dimensions. A full report on this work will be given at a later date.

This work has been carried out with the assistance of the U. S. Office of Naval Research.

[1] E. E. Jacobs and A. S. Holt, J. Chem. Phys. **20**, 1326 (1952).
[2] Rabinowitch, Jacobs, Holt, and Kromhoul, Z. Physik **133**, 261 (1952).

The Absorption Spectra of Monomolecular Layers of Chlorophyll *a* and Ethyl Chlorophyllide *a*

EARL E. JACOBS, A. STANLEY HOLT, AND EUGENE RABINOWITCH
Photosynthesis Research Project, Department of Botany, University of Illinois, Urbana, Illinois
(Received August 3, 1953)

RECENT evidence,[1] based on electron microscopy, suggests the possible existence of monomolecular layers of chlorophyll in chloroplasts and grana. With this in mind, an investigation into the spectral properties of monomolecular layers of chlorophyll *a* and its derivatives has been carried out. The feasibility of using pigment monolayers for spectral studies was suggested by two facts. Firstly, monolayers of these pigments on water surfaces had been successfully prepared by Hanson,[2] and secondly, the calculated optical density of a single monolayer (in the red absorption peak) is of the order of 0.01, a measurable quantity.

Hanson's technique for preparing monolayers was found to be unsatisfactory. He spread an acetonic solution of the pigments onto a water surface by means of a micropipette. Acetone does not spread well on water, and consequently it was difficult to avoid the formation of a colloid. Petroleum ether spreads well on a water surface; and, although neither chlorophyll nor chlorophyllide is soluble in pure petroleum ether, both may easily be made to dissolve in this solvent by the intermediary of pyridine. When a droplet of such a mixture, containing the pigment, was allowed to fall on a water surface, monolayers covering 100 square centimeters or more could be produced.

If talcum powder was spread on the water surface, and the droplet allowed to fall in its center, the talcum was pushed to a sharply defined boundary. A sudden contraction of the area within the boundary indicated final solidification of the monolayer. The surface of the water within the pigment-covered area was then quite rigid, and talcum blown onto this surface could not easily be laterally displaced. A drop of solvent placed on the monolayer would not wet it. The monolayer could be lifted up on a small wire loop, or picked up on a glass surface. The latter method was used for the determination of absorption spectra.

In the case of chlorophyll *a*, the presence of Ca^{++} ions in the water resulted in the formation of a layer whose absorption spec-

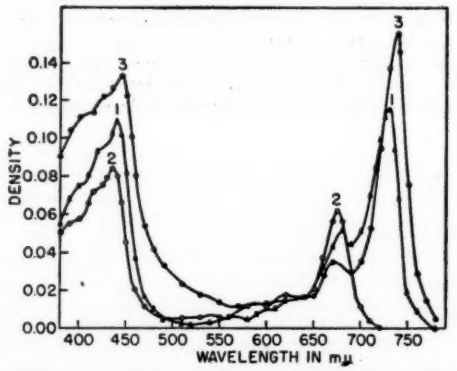

FIG. 1. Absorption spectra of monomolecular layers of chlorophyll *a* and ethyl chlorophyllide *a*. Curve 1 is ethyl chlorophyllide *a*, curve 2 is chlorophyll *a* without added Ca^{++}, and curve 3 is chlorophyll *a* with added Ca^{++}.

trum was quite different from that of a monolayer of the same pigment formed on a distilled water surface.

Figure 1 shows the absorption spectra of the monolayers of ethyl chlorophyllide *a* and chlorophyll *a* obtained by means of a Beckman spectrophotometer, using a stack of six cover glasses, on each of which one monolayer had been deposited. The shift of the red absorption band in curves 1 and 3 by 70–75 mμ towards the longer waves, from its position in acetone solution (660 mμ), indicates considerable resonance interaction between pigment molecules in the monolayers. This shift is about 90–100 percent of those observed in three-dimensional crystals of the same pigments.[2] We infer that resonance interaction in three-dimensional crystals is confined predominantly to the layer planes from which the crystals are built. (See Fig. 1A in reference 3b.)

The approximate optical densities of the individual monolayers in the peak of the red band were found to be

Pigment	$\epsilon = \log(I_0/I)$ for one layer	Surface requirement[2] of a molecule
Ethyl chlorophyllide *a*	0.019	$69A^2$
Chlorophyll *a* (without Ca^{++} ions)	0.011	$106A^2$
Chlorophyll *a* (with Ca^{++} ions)	0.026	($\sim 45A^2$??)

The first two ϵ values are in satisfactory agreement with estimates based on absorption coefficients of the pigments in solution and the molecular surface areas determined by Hanson; but the third one is more than could be attributed to the denser packing (or reorientation) of molecules in a monomolecular layer. This is more than twice as high as expected. Possibly, the presence of Ca^{++} ions causes the formation of two molecular layers instead of true monolayers. Preliminary x-ray studies of three-dimensional chlorophyll *a* crystals support this interpretation since these crystals appear to be built up from stacked bimolecular layers. Three-dimensional crystals of ethyl chlorophyllide *a* are known to consist of stacked monolayers.[2]

Comparison of curves 1 and 3 in Fig. 1 with the absorption curves of chloroplasts and grana shows that the latter contain no close-packed monomolecular (or bimolecular) chlorophyll layers. The possibility that chlorophyll monolayers of the "loose" type may be present *in vivo* is, however, not ruled out, since curve 2 is not unlike a typical chloroplast spectrum.

A full report on this work, including an extension to other pigments, will be presented later.

This work has been carried out with the assistance of the U. S. Office of Naval Research.

[1] See for example E. Rabinowitch, Ann. Rev. Plant Physiol. **4** (1952).
[2] E. A. Hanson, Rec. trav. botan. néerl. **36**, 180 (1939).
[3] (a) E. E. Jacobs and A. S. Holt, J. Chem. Phys. **20**, 1326 (1952); (b) Rabinowitch, Jacobs, Holt, and Kromhout, Z. Physik **133**, 261 (1952).

Nonequivalence of Chlorine Atoms in Phosphorus Pentachloride

JAMES DOWNS AND ROWLAND E. JOHNSON
Department of Chemistry, Florida State University, Tallahassee, Florida
(Received October 19, 1953)

THE phosphorus pentachloride molecule has been shown to be a trigonal bipyramid in the liquid and vapor phase,[1,2] and it seems quite reasonable to assume that this structure persists in nonpolar liquid media. It would seem that the structural nonequivalence of chlorine positions and P—Cl bond lengths[3] may, under certain conditions, be reflected in a differing reactivity between atoms differently located.

The suggestion has been advanced[4] that homogeneous exchange reactions for the system PCl_5-Cl_2, using radioactive chlorine as the tracer atom, may define this difference. Koskoski and Fowler[4] have studied this reaction in carbon tetrachloride solution, using radiochlorine-38 as the tracer, and from their results have inferred that all chlorines in phosphorus pentachloride possess the same degree of reactivity. Further studies on this system have been made by us, using radiochlorine-36 as the tracer atom, and first-order exchange rates have been observed.

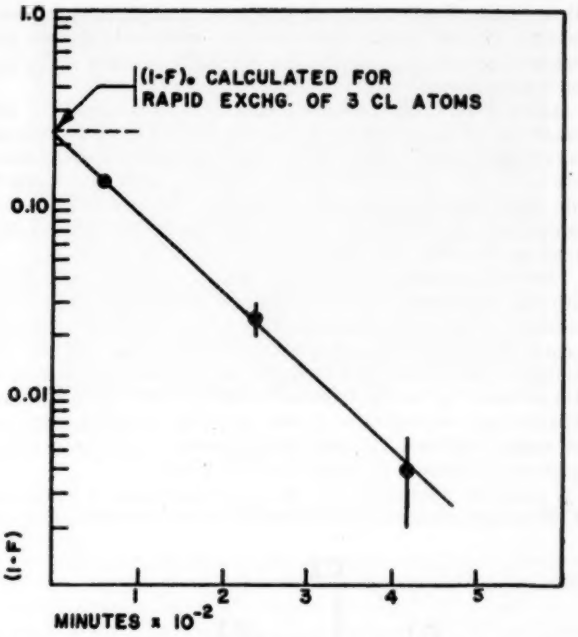

FIG. 1. A typical run showing exchange of Cl_2^* with PCl_5. Fiducial marks indicate the uncertainty arising from expected standard deviation in counting.

For the purpose of measuring the exchange reaction, carbon tetrachloride solutions of known concentrations in reactants were mixed at room temperature, aliquot portions extracted at measured time intervals, and reactants separated by a mechanical method which minimizes separation-induced exchange. Precautions against intrusion of water vapor were observed. Specific activities of separated reactants were determined for the purpose of estimating the fraction exchange.

A plot of (1−fraction exchange) *vs* time (Fig. 1) shows two characteristics for the exchange reactions we have carried out:

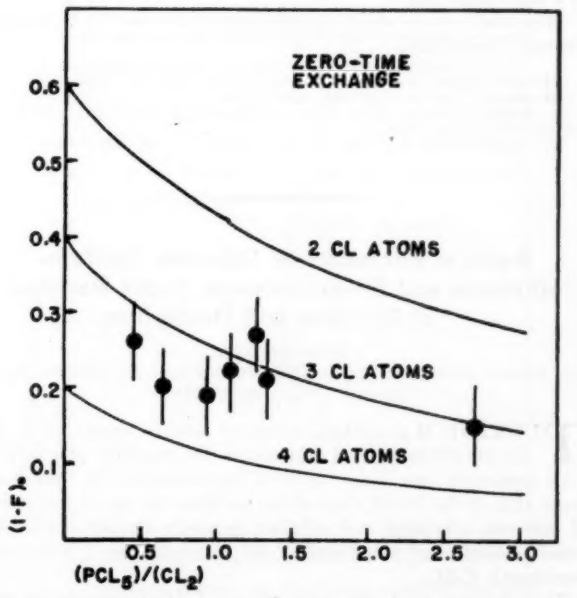

FIG. 2. Extrapolated zero-time exchanges for a series of runs. Fiducial marks indicate the average uncertainty arising from expected standard deviation in counting.

(1) a straight line is observed, indicating a single homogeneous reaction; (2) the straight line does not extrapolate to zero exchange at zero time, indicating a rapid initial reaction which has not been measured.

Apparent zero-time exchanges have been determined by extrapolation to zero time for a series of reactions using different concentration ratios $(PCl_5)/(Cl_2)$. Figure 2 shows expected zero-time exchanges, assuming rapid initial exchange with two chlorines only (upper line) and with three chlorines only (middle line). For comparison, the lower line is calculated assuming rapid initial exchange with four chlorines only.

The experimental points are seen to be in reasonable agreement with the assumption that three chlorines in the molecule undergo rapid initial exchange. Assuming further that these three chlorines occupy the equatorial positions, we conclude that: (1) the exchange of phosphorus pentachloride with molecular chlorine is characterized by a rapid initial exchange with the equatorial chlorines and a comparatively slow exchange involving atoms in the apical positions; (2) rapid intramolecular exchange between apical and equatorial positions is not indicated.

A plausible mechanism for the initial exchange of equatorial chlorines is an atom-transfer process involving the transition state:

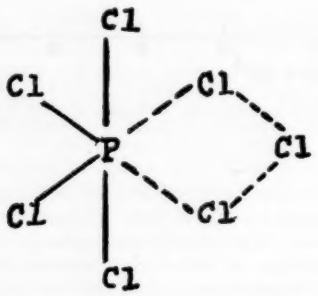

which decomposes rapidly and reversibly into phosphorus pentachloride and chlorine.

Similar experiments on the system PCl_3-Cl_2 in carbon tetrachloride solution indicate that for the reaction $PCl_3+Cl_2\rightarrow PCl_5$, molecular chlorine adds predominantly into the equatorial positions.

A more detailed account of these results and others will appear in a later publication.

This work was done under the auspices of the U. S. Atomic Energy Commission.

[1] Moureu, Magat, and Wetroff, Compt. rend. **205**, 276 (1937).
[2] M. Roualt, Compt. rend. **207**, 620 (1938).
[3] L. Pauling, *Nature of the Chemical Bond* (Cornell University Press, Ithaca, New York, 1944).
[4] W. Koskoski and R. Fowler, J. Am. Chem. Soc. **64**, 850 (1942).

Rates of Formation of Different Deuteroethylenes and Deuteroethanes in the Reaction of Ethylene and Deuterium

TOMINAGA KEII
The Research Institute for Catalysis, Hokkaido University, Sapporo, Japan
(Received September 15, 1953)

TURKEVICH *et al.*[1] have observed rates of formation of different ethylenes and ethanes in the reaction of ethylene with deuterium over nickel at 90°C and obtained the important result that at the initial stage of the reaction the rate of formation of different ethylenes and ethanes decreases regularly with increasing deuterium substitution, the ethanes formed being predominantly C_2H_6.

They remark that the predominant C_2H_6 formation is surprising, but this is rather a natural consequence of the mechanism of the ethylene hydrogenation reaction proposed by Horiuti.[2]

Horiuti concluded, applying his "structure theory"[3] to the scheme,

$$\left.\begin{matrix} C_2H_4 \xrightarrow{I_a} C_2H_4(a) \\ H_2 \xrightarrow{I_b} \begin{cases} H(a) \\ H(a) \end{cases} \end{matrix}\right\} \xrightarrow{II} C_2H_5(a) \Bigg\} \xrightarrow{III} C_2H_6, \qquad (1)$$

where $H(a)$, etc., denotes chemisorbed hydrogen atom, etc., that the rate-determining step is I_b or III at temperatures below or above the so-called optimum temperature of the reaction. With regard to the particular region of partial pressures corresponding to that of Turkevich *et al.* the following conclusions also have been made:

(A) The optimum temperature lies at 130°C,

(B) (i) $v_L(I_b)\ll v_R(I_b)\simeq v_R(III)\ll v_L(II)\simeq v_R(II)$

below the optimum,

(ii) $v_R(III)\ll v_L(II)\simeq v_R(II)\ll v_R(I_b)\simeq v_L(I_b)$

above it, and

(C) (i) $v_R(r),\ v_L(r)\ll v_R(I_a)\simeq v_R(I_a),\ r=I_b,\ II$, and III

(ii) $v_L(III)\ll v_R(III)\ll v_R(II)\simeq v_L(II)$

either below or above, where $v_L(I_b)$, $v_R(I_b)$ etc., denotes the forward and backward rates of I_b, etc. This mechanism is hence coincident with the earlier "associative mechanism"[4] above the optimum temperature but not below.

As the temperature of their experiment was below the optimum, the chemisorbed hydrogen atom originates practically from C_2H_4 only, i.e., it consists predominantly of $H(a)$, $D(a)$ formed from D_2 being instantly replaced by $H(a)$. This explains the predominant formation of C_2H_6, as observed.

The writer develops the "fine structure" of the reaction for explaining their results more closely and deriving some theoretical predictions as follows.

It is assumed that the isotopic replacement does not alter the rate of any elementary reaction and the steady state is established with respect to the intermediate.

Scheme (1) appears, if written with distinction of individual deutero-compound as,

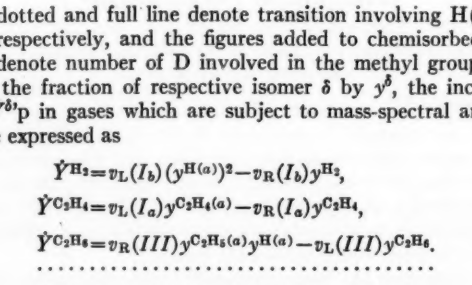

(2)

where dotted and full line denote transition involving $H(a)$ and $D(a)$, respectively, and the figures added to chemisorbed ethyl group denote number of D involved in the methyl groups. Denoting the fraction of respective isomer δ by y^{δ}, the increasing rates $\dot{Y}^{\delta}$p in gases which are subject to mass-spectral analysis, may be expressed as

$$\begin{aligned} \dot{Y}^{H_2} &= v_L(I_b)\,(y^{H(a)})^2 - v_R(I_b)\,y^{H_2}, \\ \dot{Y}^{C_2H_4} &= v_L(I_a)\,y^{C_2H_4(a)} - v_R(I_a)\,y^{C_2H_4}, \\ \dot{Y}^{C_2H_6} &= v_R(III)\,y^{C_2H_5(a)}\,y^{H(a)} - v_L(III)\,y^{C_2H_6}. \\ &\cdots\cdots\cdots\cdots\cdots\cdots\cdots\cdots \\ &\cdots\cdots\cdots\cdots\cdots\cdots\cdots\cdots \end{aligned} \qquad (3)$$

Steady-state conditions may be stated as

$$(2v_L(I_b)+v_R(II)+v_R(III))\,y^{D(a)} = v_R(I_b)\,(2y^{D_2}+y^{HD}) + v_L(II)\sum_i \sum_l \frac{l}{3} y^{C_2H_5-iD_i(a,l)} + v_L(III)\sum_i \frac{i}{6} y^{C_2H_6-iD_i},$$

$$(v_L(I_a)+v_R(II))y^{C_2H_4(a)}=v_R(I_a)y^{C_2H_4}+v_L(II)(y^{C_2H_5(a,0)}+\tfrac{1}{5}y^{C_2H_4D(a,1)}), \quad (4)$$

$$(v_L(II)+v_R(III))y^{C_2H_5(a,0)}=v_R(II)y^{C_2H_4(a)}y^{H(a)}+v_L(III)(y^{C_2H_6}+\tfrac{1}{6}y^{C_2H_5D}).$$

. . . . . .

. . . . . .

Putting $y^{C_2H_4}=y^{D_2}=1$ in the foregoing equations and eliminating $y^{\delta(a)}$'s among them, we have $\dot{Y}^{H_2}$, etc., at the initial stage of the reaction. From those results,

$$\dot{Y}^{H_2}:\dot{Y}^{HD}=1:2\Omega, \quad \Omega=y^{D(a)}/y^{H(a)} \quad (5)$$

is derived exactly and the following are obtained with use of conclusion (C):

$$\dot{Y}^{C_2H_3D}:\dot{Y}^{C_2H_2D_2}:\dot{Y}^{C_2HD_3}:\dot{Y}^{C_2D_4}=1:R/2:R^2/6:R^3/36, \quad (6)$$

$$\dot{Y}^{C_2H_6}:\dot{Y}^{C_2H_5D}:\dot{Y}^{C_2H_4D_2}:\dot{Y}^{C_2H_3D_3}:\dot{Y}^{C_2H_2D_4}:\dot{Y}^{C_2HD_5}:\dot{Y}^{C_2D_6}$$
$$=1:2\Omega:\Omega^2:2R\Omega^2/3:R^2\Omega^2/3:R^3\Omega^2/9:R^4\Omega^2/54, \quad (7)$$

where

$$R=y^{D(a)}v_L(II)/v_L(I_a)\ll 1 \quad (8)$$

and

$$\Omega=v_R(I_b)/(v_L(I_b)-v_R(I_b))+\tfrac{1}{3}v_L(II). \quad (9)$$

Applying this to the experimental condition of Turkevich *et al.* (below the optimum temperature), we have from conclusion (B)(i),

$$\Omega=3v_R(I_b)/v_L(II)\ll 1. \quad (10)$$

It follows from (8) and (10) that relations (6) and (7) both decrease regularly with increasing substitution of deuterium, just as observed by Turkevich *et al.*

We might now add a few theoretical predictions. Above the optimum temperature, when (B)(ii) is valid, we have from (9), $\Omega\gg 1$, and hence

(a) $$\dot{Y}^{H_2}<\dot{Y}^{HD} \quad \text{or} \quad \dot{Y}^{H_2}>\dot{Y}^{HD},$$

according to whether or not temperature is above or below the optimum. On the other hand (7) predicts

(b) $$\dot{Y}^{C_2H_6}<\dot{Y}^{C_2H_5D}<\dot{Y}^{C_2H_4D_2}>\dot{Y}^{C_2H_3D_3}>\dot{Y}^{C_2H_2D_4}>\dot{Y}^{C_2HD_5}>\dot{Y}^{C_2D_6}$$

above the optimum.

Details of this work will soon appear in J. Research Inst. for Catalysis, Hokkaido University. The writer wishes to express his thanks to Professor Horiuti, Director of the Institute, for his interest in this work.

[1] Turkevich, Schissler, and Irsa, J. Phys. Colloid. Chem. **55**, 1078 (1951).
[2] Horiuti, Catalyst **2**, 1 (1947).
[3] Horiuti, J. Research Inst. for Catalysis, Hokkaido Univ. (to be published).
[4] Horiuti and Polanyi, Trans. Faraday Soc. **30**, 1164 (1934).

Composition Profiles in Pre-Mixed Laminar Flames*

ROCHELLE PRESCOTT, R. L. HUDSON, S. N. FONER, AND W. H. AVERY
Applied Physics Laboratory, The Johns Hopkins University, Silver Spring, Maryland

(Received November 9, 1953)

TO implement a study of temperature and reaction rates of hydrocarbon-air flames a technique has been developed for determining composition profiles through a pre-mixed laminar flame front. By means of a fine probe, samples are taken at various distances normal to the flame front using the center of the luminous zone as a reference surface. These samples are analyzed by means of a rapid-scanning mass spectrometer.[1] Only stable chemical components can be analyzed with the probe technique; therefore, the combustion gases were fed into the ion source of the mass spectrometer in a conventional manner.

A half-inch diameter Bunsen burner was used identical to that previously described by Fristrom, Prescott, Neumann, and Avery[2] and was operated in a small chamber exhausted through a critical flow nozzle.

FIG. 1. Photograph of a fused-quartz sampling probe immersed in a propane-air Bunsen flame. (Probe retouched for clarity.)

The probes are made of fused quartz and carefully tapered to allow the pressure of the sample to drop rapidly after it enters the probe tip. Probes have been made with the tip as small as 2-microns inside diameter and up to greater than 0.1-mm inside diameter. As it was considered that the larger probes would cause less pyrolysis of the sample these have been used in the preliminary experiments and the sampling system has been designed to handle the flows associated with these larger probes. The probe used for the data herewith was *ca* 0.05-mm inside diameter and

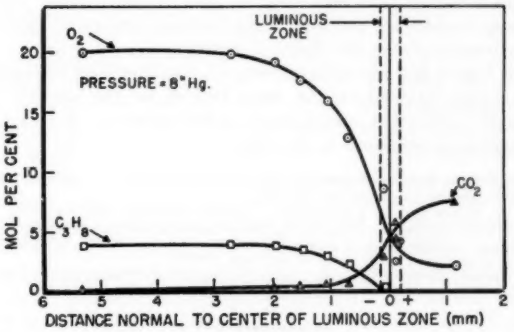

FIG. 2. (a) Mole percent of O_2, CO_2, and C_3H_8 as a function of position in the flame front of a propane-air flame (fuel-to-air ratio 0.93 of the stoichiometric value, pressure 8.0 inches of Hg absolute).

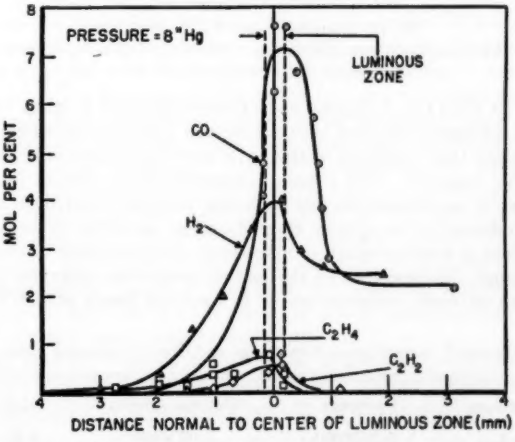

FIG. 2. (b) Mole percent of CO, H_2, C_2H_4, and C_2H_2 as a function of position in the flame front of a propane-air flame (fuel-to-air ratio 0.93 of the stoichiometric value, pressure 8.0 inches of Hg absolute).

0.02-mm wall thickness. From nonviscous, potential flow theory the sampling zone for such a probe is estimated as roughly 1.4 mm in diameter and 0.18 mm in depth. Quenching is accomplished by the rapid drop in pressure of the sample gases which enter the probe tip at sonic speed. The pressure in the sample line is kept at approximately 1 mm Hg, and a fraction of the sample is bled into the mass spectrometer for analysis. Fig. 1 shows a probe in the flame.

Masses from 2 to 100 have been examined, and no appreciable peaks were found above mass 44. Consequently, our analysis was restricted to the mass range 2 to 44. Qualitative tests with heated probes indicated that pyrolysis was negligible in properly drawn probes, and the data shown herewith strengthen the inference that quenching by expansion is effective. A number of runs have been made on a propane-air flame at a pressure of 8 inches of mercury absolute with fuel-to-air ratio 0.93 of the stoichiometric value. Preliminary results are given in Figs. 2 (a) and 2 (b).

In these analyses the following principal components were found: N_2, O_2, A, C_3H_8, C_2H_4, C_2H_2, CO_2, CO, H_2O, and H_2. The present techniques do not permit an accurate determination of H_2O concentration because of adsorption in the sampling system. C_3H_6, C_2H_6, and CH_4 among others were present in quantities less than 0.1-mole percent and are not shown in the accompanying data. To eliminate the effect of temperature on the rate of gas flow into the probe, all the peaks were compared with the argon intensity. The mole fractions were computed from the known concentration (0.90 percent) of argon in the pre-mixed gases using the approximation that the argon mole fraction remained constant, thus neglecting diffusion flows and the change in mole numbers resulting from the combustion reactions.

By passing the gases through a liquid N_2 trap to remove interfering hydrocarbons, H_2, CH_4, and CO were determined with greater accuracy than was possible with unfractionated samples.

These techniques are now being refined, and experiments are under way to obtain the limits of accuracy.

It is hoped that these measurements together with temperature data being obtained on the same system by the particle track method[2,3] will yield quantitative information on the rate and mechanism of reactions in the flame.

* This work was supported by Bureau of Ordnance, U. S. Department of the Navy, under Contract NOrd 7386.

[1] S. N. Foner and R. L. Hudson, J. Chem. Phys. **21**, 1374 (1953).

[2] Fristrom, Prescott, Neumann, and Avery, *Fourth International Symposium on Combustion, Cambridge, Massachusetts 1952*, (Williams and Wilkins Company, Baltimore, Maryland, 1953).

[3] Fristrom, Avery, Prescott, and Mattuck, J. Chem. Phys. **12**, 106 (1954).

The Homomolecular Exchange of Nitrogen in a Glow Discharge*†‡

W. H. JOHNSTON AND R. M. ANSTETT
Department of Chemistry, Purdue University, Lafayette, Indiana
(Received November 19, 1953)

RECENTLY Johnston and O'Shea[1] reported a study of the exchange reaction between oxygen molecules in which they proposed that reactions of this type be called homomolecular exchange reactions. The present communication reports the discovery of an homomolecular exchange reaction in nitrogen under the influence of an electric glow discharge. In order to study this reaction it was necessary to investigate the possibility of thermal exchange. As expected, no thermal exchange was observed in one month at room temperature or in nineteen hours at 850°C. In the experiments with glow discharge, a mass spectrometer was used to follow the approach to isotopic equilibrium in a mixture of N_2^{28}, N_2^{29}, and N_2^{30} molecules containing fifteen percent nitrogen −15. A nitrogen afterglow was not observed because metal electrodes were used in the reaction cell.

TABLE I. Actual rates of exchange and effective electron yields.

Pressure	Exchange	Electron current	Yield
2	5.78×10^{15}	7.09×10^{15}	0.82
4	12.0×10^{15}	10.4×10^{15}	1.15
6	5.37×10^{15}	6.55×10^{15}	0.82

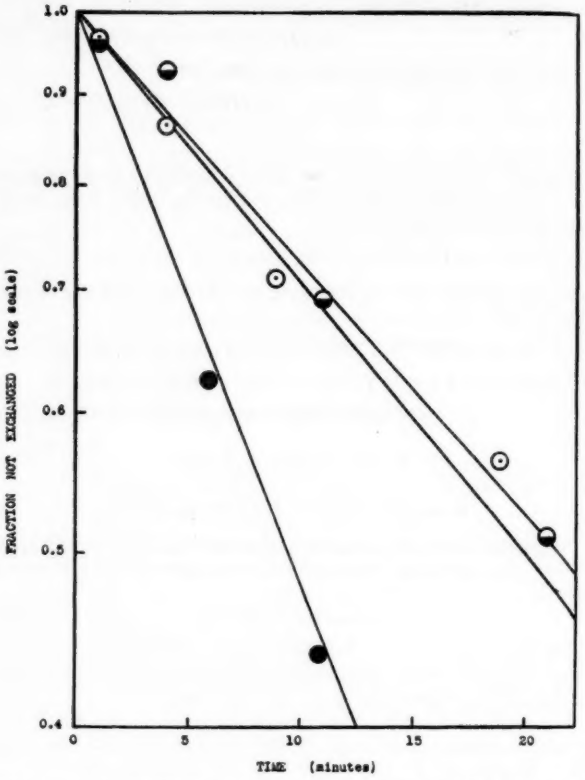

FIG. 1. Homomolecular exchange of N_2 by electric discharge. ⊙ =2-mm pressure; ● =4-mm pressure; ◒ =6-mm pressure.

As shown in Fig. 1 first-order rate laws were obtained in glow discharges at pressures of 2, 4, and 6 mm Hg. The half-times at these pressures were 20.0, 9.6, and 21.5 minutes, respectively. The actual rates of exchange, independent of isotopic change, were calculated from these half-times by the equation of Johnston and O'Shea.[1]

An "effective electron yield" was determined for each pressure in units of molecules exchanged per electronic-charge transferred between the electrodes. The actual rates of exchange and the "effective electron yield" are summarized in Table I.

As shown in Table I the "effective electron yield" is essentially unity within experimental error over the pressure range covered and for a range of two-fold in half-time.

If Mitra's[2] dissociative recombination of N_2^+ ions and electrons is responsible for the majority of the charge transfer at the cathode, then recombination of the nitrogen atoms on the metal electrodes or walls would produce exchange with an "effective electron yield" of essentially unity. On the other hand, an atomic chain reaction, $N+N_2$, could reasonably be expected to have an "effective electron yield" from 0 to 10^{+6} depending upon the rate of the chain-breaking reaction and the rate of exchange. The improbability of finding a yield of unity by this mechanism suggests that the experimental value favors the atom-recombination mechanism of exchange.[3]

* This work was supported in part by the U. S. Atomic Energy Commission under contract with Purdue University.
† Abstracted from the Master of Science thesis of R. M. Anstett, Purdue University, June 1953.
‡ Presented before the Physical and Inorganic Division of the 124th Meeting of the American Chemical Society, Chicago, September 11, 1953.

[1] W. H. Johnston and C. J. O'Shea, J. Chem. Phys. **21**, 2080 (1953).

[2] F. K. Mitra, Phys. Rev. **90**, 516 (1953).

[3] Further work by W. H. Johnston and E. F. Neuzil will be reported soon.

Light Scattering Determination of the Absolute Turbidity of Water

D. A. I. GORING AND P. G. NAPIER
Maritime Regional Laboratory, National Research Council, Halifax, Nova Scotia, Canada
(Received November 2, 1953)

THE absolute turbidity, τ_w, of water is difficult to measure directly because of the high transmission of the liquid. A fairly accurate estimate of τ_w can be made from the light scattering of water and dilute salt solutions.

Such light scattering measurements have been made on distilled water and 1 percent sodium acetate solution by a technique previously described.[1] By enclosing the incident beam in a blackened tube, the small irregular reflections previously noted were completely eliminated. Liquids were purified by centrifuging at 27 000 g for one hour at room temperature and poured directly into the light scattering cells. Unpolarized incident light (5461 A) was used. Intensities were measured from $\theta=37\frac{1}{2}°$ to $\theta=135°$ and were normalized by the factor $\sin\theta/(1+\cos^2\theta)$. The horizontal and vertical components were multiplied by $\sin\theta$.

Reproducibility with water was poor. The most symmetrical distribution obtained is shown in Fig. 1. Except for an increase

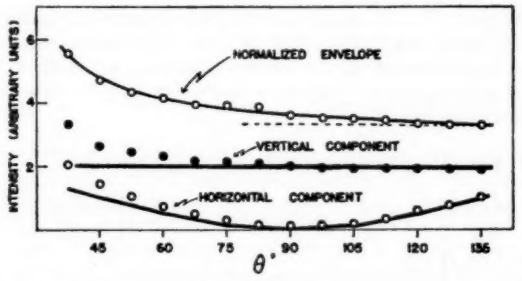

FIG. 1. Distribution of intensity of scatter for water. The interrupted line gives the corrected value of I_{90}. The heavy lines for the vertical and horizontal components are a theoretical Rayleigh distribution.

in intensity at small θ, the vertical and horizontal components fit the theoretical Rayleigh distribution. In this respect water differs markedly from nonpolar liquids such as toluene which show a large depolarization.[2,3]

Thus water may be regarded as a system of small isotropic scatterers in which the observed dissymmetry arises from the dissymmetrical scatter of larger foreign particles. As suggested by Goring and Johnson,[2] in such cases a more correct value for the intensity at 90°, I_{90} is the normalized intensity at high values of θ. From Fig. 1 the corrected value of I_{90} was 3.30 which corresponded to a turbidity of 1.7×10^{-5} cm^{-1}.

With 1 percent aqueous sodium acetate removal of dust particles was more complete and much better reproducibility was obtained. For seven separate solutions the mean value of I_{45}/I_{135} was 1.22 (±0.04) and the mean corrected value of I_{90} was 3.58 (±0.06). The vertical and horizontal components fitted the Rayleigh distribution as shown in Fig. 2. From these results the

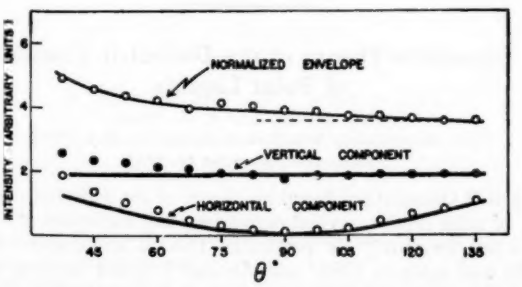

FIG. 2. Distribution of intensity of scatter for 1 percent sodium acetate in water. The lines have the same significance as in Fig. 1.

turbidity was calculated to be 1.84×10^{-5} cm^{-1}. The excess turbidity due to the salt can be computed to be approximately 0.08×10^{-5} cm^{-1}, which leaves a value of 1.76×10^{-5} cm^{-1} for water.

Although the mean deviation in I_{90} for the sodium acetate solutions was less than 2 percent, errors in the calibration of the apparatus and in the assumptions involved may increase the possible error.

[1] D. A. I. Goring, Can. J. Chem. (to be published).
[2] D. A. I. Goring and P. Johnson, Trans. Faraday Soc. **48**, 367 (1952).
[3] W. H. Martin and S. Lehrman, J. Phys. Chem. **26**, 75 (1922).

The Nuclear Spin Quantum Number of Si^{29} Isotope

RICHARD A. OGG, JR., AND JAMES D. RAY
Department of Chemistry, Stanford University, Stanford, California
(Received October 19, 1953)

THE assignment of nuclear-spin quantum number of the Si^{29} isotope has apparently remained a matter of some uncertainty, although on various grounds a probable value of $\frac{1}{2}$ is indicated.[1] In connection with other work on nuclear magnetic resonance, it occurred to the authors that this question could be most simply resolved by study of the spin-spin interaction splitting[2] of the nuclear magnetic resonance of an atomic species chemically bonded to Si. For various practical reasons the most attractive possibility appears to be offered by study of proton resonance in silane, SiH_4. Because of the tetrahedral symmetry of molecules of this substance, a unique proton resonance is expected, except for fine structure due to spin-spin interaction between the proton and Si nucleus.

Silane was prepared by reduction of $SiCl_4$ with $LiAlH_4$ in tetrahydrofurane solution in a closed system. The product was carefully fractionated, the low boiling silane (N.B.P.-112°C) being condensed with liquid nitrogen in the vessel used for nuclear magnetic resonance studies. This vessel, of Pyrex glass, was a cylinder of some 50 cm^3 volume, provided with a slender tip some 5 mm in diameter. After condensation of a quantity of SiH_4 corresponding to about two atmospheres pressure of gas at room temperature, the vessel was sealed off. Immersion of the slender tip in liquid nitrogen resulted in condensation of the silane sample. The tip was then inserted into the probe of the nuclear magnetic resonance instrument, and the proton spectrum was recorded as quickly as possible. Rapid evaporation of the liquid sample necessitated frequent repetition of the operation before satisfactorily reproducible spectra were obtained. The instrument employed was the 30-megacycle high-resolution nuclear magnetic resonance spectrometer at the research and development laboratories of Varian Associates.

With the highest resolution obtained (separations of the order of one milligauss), the proton magnetic resonance spectrum of silane appeared as a single sharp peak flanked symmetrically by two weak, equally-spaced side peaks, at approximately twenty milligauss from the center. The equal amplitudes of these side peaks, compared to that of the central peak, agreed satisfactorily with the known abundance of the Si^{29} isotope—namely some 4.7 percent. The central peak corresponds to silane molecules containing the Si^{28} and Si^{30} isotopes, both of nuclear-spin quantum number zero. Since the nuclear spin quantum number of Si^{29} is necessarily half integral, the observation of a splitting of the attached proton magnetic resonance into only two components excludes all values except $\frac{1}{2}$. Thus the tentative assignment already made appears unequivocally confirmed.

The authors wish to express their gratitude to Dr. Martin Packard and Dr. James Shoolery, both of Varian Associates, for their assistance in the proton magnetic resonance studies.

[1] H. E. Weaver, Jr., Phys. Rev. **89**, 923 (1953); J. R. Holt and T. N. Marsham, Phys. Rev. **89**, 665 (1953).
[2] See, for example, Gutowsky, McCall, and Slichter, J. Chem. Phys. **21**, 279 (1953).

Infrared Absorption Spectra of Complex Cobalt Salts

DOUGLAS G. HILL AND ALEXANDER F. ROSENBERG
Department of Chemistry, Duke University, Durham, North Carolina
(Received November 16, 1953)

ALTHOUGH the near infrared spectra of a number of inorganic salts have been obtained, those with octahedral symmetry seem to have been studied primarily to determine the effect of coordination on the vibrations in the ligand group.[1]

We have obtained the spectra of a number of cobalt (III) ammines in the rock-salt region of the near infrared and have found that these salts show bands probably arising from the octahedral vibrations of the cation, in addition to the expected N−H frequencies. The compounds have been observed as dry powders, deposited by sedimentation upon salt plates from propanol-2 suspensions. We have found the dry powders superior to the Nujol suspensions commonly used. The deposit obtained is more uniform and lends itself to better control of particle size since the salt plate may be placed in the suspension after the larger particles have settled. In addition, the strong absorption bands of Nujol mask regions of interest.

In Table I we list the positions of the two strong bands which appear in the same region for all the salts examined, both hexammines and pentammines. The ligand frequencies are not included at this time, since they are of lesser interest.

A totally symmetrical octahedral molecule should possess two fundamental vibrations active in the infrared so that the bands observed in the hexammines are probably to be identified with these fundamentals. We have been surprised to find these same bands still present and with much the same intensity after the symmetry has been altered by substituting for one of the ammonias. In the aquopentammines the new group differs little in size, but the other pentammines involve a decrease in net charge and the replacement of ammonia with a charged ion. When the ion is Br^- or N_3^-, the size is such that very considerable distortion might be expected.

TABLE I. Strong absorption bands of cobalt ammines.

Salt	Vibration frequencies in cm^{-1}	
$Co(NH_3)_6\,Cl_3$	826	1319
$Co(NH_3)_6\,Br_3$	816	1321
$Co(NH_3)_6\,I_3$	801	1319
$Co(NH_3)_5H_2O\,Cl_3$	837	1312
$Co(NH_3)_5H_2O\,Br_3$	832	1319
$Co(NH_3)_5H_2O\,I_3$	817	1316
$Co(NH_3)_5N_3\,Cl_2$	840	1311
$Co(NH_3)_5N_3\,Br_2$	829	1304
$Co(NH_3)_5N_3\,I_2$	820	1299
$Co(NH_3)_5F\,Cl_2$	845	1305
$Co(NH_3)_5F\,Br_2$	820	1309
$Co(NH_3)_5F\,I_2$	806	1304
$Co(NH_3)_5Cl\,Cl_2$	852	1305
$Co(NH_3)_5Br\,Cl_2$	841	1304
$Co(NH_3)_5Br\,Br_2$	832	1300

It is also noteworthy that, in all the compounds examined, a change in the *anion* causes a shift in the position of the 820 cm^{-1} peak, in every case shifting it to longer wavelength as the anion increases in size. The anion can not be supposed to play any direct part in the vibration frequencies of the ligand groups, although its field must influence the frequencies. It is of interest that calculations[2] have been attempted for certain hexammines which, though doubtful, seem to show that the larger anion decreases the Co−N distance. This would seem to be in the wrong direction to account for a decrease in frequency.

A later report will cover compounds with other substituents and will include the weak bands, some of which may be interpreted as partially resolved fine structure in the strong absorptions discussed.

[1] F. A. Miller and C. H. Wilkins, Anal. Chem. **24**, 1253 (1952).
[2] R. W. Parry, Chem. Revs. **46**, 507 (1949).

Gaussian Functions in Molecular Integrals

RYOICHI KIKUCHI
Institute for the Study of Metals, The University of Chicago, Chicago, Illinois
(Received November 18, 1953)

THE usual procedure of evaluating many-center integrals appearing in molecular problems is to expand functions around one common center. On the other hand, Boys[1] has shown that if one uses functions of the Gaussian type instead of the ordinary exponential ones, the many-center integrals can be evaluated in closed forms. This note is to show a method, which might be worth being exploited, to transform integrals including exponential functions into ones including Gaussian functions.

The following relation holds for a non-negative r:

$$e^{-r}=\frac{2}{\sqrt{\pi}}\int_0^\infty \exp[-(r/2t)^2-t^2]dt. \tag{1}$$

By putting $r=\sqrt{s}$ and $4t^2=1/z$, one sees that this is a modification of the Laplace transformation. In order to prove Eq. (1) straightforwardly, the following integral is shown to be independent of $r(\geqq 0)$ by differentiation with respect to r:

$$\int_0^\infty \exp\left[-\left(\frac{r}{2t}-t\right)^2\right]dt.$$

The procedure of transforming into Gaussian functions becomes helpful particularly when dealing with two-electron wave functions which depend on the relative distance. As an illustration, a case of four-center integrals is shown below to be reduced to a quadrupole integral.

$$\begin{aligned}&\int d\mathbf{r}_1\int d\mathbf{r}_2(1/r_{12})\exp(-ar_{1A}-br_{1B}-cr_{2C}-dr_{2D}-4\alpha r_{12}^2)\\&=\frac{abcd\sqrt{\pi}}{64}\int_0^\infty \rho^5 d\rho\int_0^{\pi/2}d\theta\cos^4\theta\sin^4\theta\exp\left\{-\frac{1}{\rho^2}\left[\frac{\langle AB\rangle_{Av}^2}{\cos^2\theta}\right.\right.\\&\left.\left.+\frac{\langle CD\rangle_{Av}^2}{\sin^2\theta}\right]-\frac{\rho^2}{8}[(a^2+b^2)\cos^2\theta+(c^2+d^2)\sin^2\theta]\right\}\\&\times\int_{-1}^1 du(1-u^2)\exp\left\{-\frac{\rho^2}{8}(a^2-b^2)u\cos^2\theta\right\}\\&\times\int_{-1}^1 dv(1-v^2)\exp\left\{-\frac{\rho^2}{8}(c^2-d^2)v\sin^2\theta\right\}\\&\qquad\times(1+\alpha\rho^2K)^{-1}K^{-\frac{1}{2}}F(4\langle PQ\rangle_{Av}^2\{1+\alpha\rho^2K\}^{-1}\rho^{-2}K^{-1}),\end{aligned} \tag{2}$$

where

$$K=1-u^2\cos^2\theta-v^2\sin^2\theta,$$

$$F(z)=\frac{1}{\sqrt{z}}\int_0^{\sqrt{z}}e^{-t^2}dt,$$

and

$$4\langle PQ\rangle_{Av}^2=[\mathbf{r}_A+\mathbf{r}_B-\mathbf{r}_C-\mathbf{r}_D-(\mathbf{r}_A-\mathbf{r}_B)u-(\mathbf{r}_C-\mathbf{r}_D)v]^2.$$

When one puts $\alpha=0$, Eq. (2) reduces to an ordinary four-center integral. As the integrand of Eq. (2) is a fairly well-behaved function of the variables, except for the values near the upper and the lower limits, it may not be impracticable to carry out the numerical quadrature.

[1] S. F. Boys, Proc. Roy. Soc. (London) **200**, 542 (1950).

Onsager's Theory of the Dielectric Constant of Polar Liquids

R. O. DAVIES AND B. K. SCAIFE
Queen Mary College, Mile End Road, London, E. 1., England
(Received November 17, 1953)

SINCE Onsager[1] published his theory of the dielectric constant of polar liquids, several derivations and variations of it have been put forward.[2–7] In particular, Piekara and Zakrzewski, in 1939[2] and again in 1950,[5] used Onsager's model but proposed a new formula for the dielectric constant. In our view the Piekara formula is not well founded. The purpose of this note is to state

as clearly as possible the difference between the formulas of Onsager and Piekara and to prove that Onsager's form is a correct deduction from his model.

If N denotes the number density of molecules, Ee the potential gradient inside the fluid, m' the total instantaneous moment of a molecule, and ϵ the dielectric constant, then quite generally one has

$$\epsilon-1=4\pi N\langle m'\cdot e\rangle/E. \tag{1}$$

Onsager's idea was to treat an average molecule as a polarizable point dipole of permanent moment μ, free to rotate and situated at the center of a spherical hole of radius "a" ($4\pi Na^3/3=1$) in a continuous medium having the dielectric properties of the bulk liquid. The total field f, acting instantaneously on the molecule is the sum of the cavity field, $G(=3\epsilon E/(2\epsilon+1))$ and the reaction field R $(=gm'$, where $g=2(\epsilon-1)/[a^3(2\epsilon+1)])$. The total instantaneous moment can thus be written as $m'=\mu+\alpha f$, α being the polarizability which is eliminated by using the Clausius-Mossotti formula $(\epsilon_\infty-1)/(\epsilon_\infty+2)=4\pi N\alpha/3$. If we combine these relations we find

$$\epsilon-\epsilon_\infty=4\pi N(\epsilon_\infty+2)\langle\mu\cdot e\rangle/3E. \tag{2}$$

It is at this stage that the treatments diverge: Onsager argues that

$$\langle\mu\cdot e\rangle=[\epsilon(\epsilon_\infty+2)/(2\epsilon+\epsilon_\infty)][E\mu^2/3kT], \tag{3}$$

whereas Piekara and Zakrzewski assert (without proof) that

$$\langle\mu\cdot e\rangle=[\epsilon(\epsilon_\infty+2)^2(2\epsilon+1)/3(2\epsilon+\epsilon_\infty)^2][E\mu^2/3kT]. \tag{4}$$

We wish to show that, for the model under discussion, Eq. (3) is correct.

The procedure is to regard the angles specifying the orientation of the permanent dipole as "external coordinates" for the statistical system consisting of (molecule+surroundings). The distribution function for orientation is then proportional to $\exp(F/kT)$, where F is the free energy of the system for the given orientation.[8] It is convenient to imagine that the molecule (and its hole) is placed at the center of a large sphere of dielectric of radius "b" set in a uniform external field of $(\epsilon+2)E/3$. F can then be split into three parts: (a) $F_1=\frac{1}{2}\alpha f^2$ is the energy required to induce the dipole αf, (b) $F_2=-(\epsilon+2)m'\cdot E/3$ is the energy of the total instantaneous dipole moment in the external field, and (c) F_3 is the energy required to surround a *fixed* dipole m' in the external field with a spherical shell of dielectric.

It can be shown[9] that

$$F_3=-(\epsilon-1)\int_{\text{diel.}}A_0\cdot A_1dv/8\pi,$$

where A_0 and A are, respectively, the fields before and after the introduction of the dielectric. Denoting the field due to a dipole m by $D(m)$ one finds for the problem in hand

$$A_0=(\epsilon+2)E/3+D(m')$$

$$[(2\epsilon+1)(\epsilon+2)-2(\epsilon-1)^2(a/b)^3]A$$
$$=(2\epsilon+1)(\epsilon+2)E-6(\epsilon-1)m'/b^3+(\epsilon+2)D[3m'-a^3(\epsilon-1)E].$$

Note that if g and h are constant vectors,

$$\int_{\text{diel.}}g\cdot hdv=4\pi(b^3-a^3)g\cdot h/3,$$

$$\int_{\text{diel.}}g\cdot D(m)dv=0,$$

and

$$\int_{\text{diel.}}D(m)\cdot D(n)dv=8\pi(b^3-a^3)m\cdot n/3a^3b^3.$$

F_3 can then be evaluated and one finds that, for $a/b\to0$,*

$$F=F_1+F_2+F_3=-E\epsilon(\epsilon_\infty+2)\mu\cdot e/(2\epsilon+\epsilon_\infty)$$
$$+\text{terms independent of orientation.}$$

When this value is inserted into the distribution function, Onsager's result (3) is recovered.

The above value for F is equivalent to assuming an instantaneous torque acting on the molecule of $m'\Delta f$.† Piekara and Zakrzewski take $m'\Delta f/(1-\alpha g)$ for the torque and thus arrive at Eq. (4). We can find no justification for this, and hence, as Van Vleck[10] has said, "We are unable to agree with their contention."

It is interesting to note that Harris and Alder[11] have recently given a formula which, neglecting short range forces, reduces to Piekara's result. For reasons which will be discussed elsewhere we do not accept their argument.

* This condition occurs, either explicitly or implicitly, in all derivations of Onsager's formula. See, in particular, reference 3, p. 914.

† If $m'\Delta f$ is the torque on the molecule, the energy is not just $-m'\cdot f$ since m' and f depend on orientation. Odelevskii made this error [V. I. Odelevskii, Compt. rend. acad. sci. U.R.S.S. **69**, 349 (1949).] which he subsequently corrected [V. I. Odelevskii, J. Tech. Phys. Moscow, **20**, 1511 (1950).]

[1] L. Onsager, J. Am. Chem. Soc. **58**, 1486 (1936).
[2] A. Piekara and K. Zakrzewski, Nature **144**, 250 (1939).
[3] J. G. Kirkwood, J. Chem. Phys. **7**, 911 (1939).
[4] H. Fröhlich, *Theory of Dielectrics* (Clarendon Press, Oxford, 1949).
[5] A. Piekara, Acta Phys. Polonica **10**, 37 (1950).
[6] C. J. F. Böttcher, *Theory of Electric Polarization* (Amsterdam, 1952).
[7] D. G. Frood and A. J. Dekker, J. Chem. Phys. **20**, 1030 (1952).
[8] See, for example, R. C. Tolman, *The Principles of Statistical Mechanics* (Clarendon Press, Oxford, 1938).
[9] See reference 6, or J. A. Stratton, *Electromagnetic Theory* (McGraw-Hill Book Company, Inc., New York, 1941).
[10] J. H. Van Vleck, Ann. New York Acad. Sci. **40**, 293 (1940), footnote on p. 302.
[11] F. E. Harris and B. J. Alder, J. Chem. Phys. **21**, 1031 (1953).

On the Use of Atomic Term Values in Molecular Wave Functions*

CHARLES W. SCHERR

Laboratory of Molecular Structure and Spectra, Department of Physics, The University of Chicago, Chicago, Illinois

(Received November 2, 1953)

THE well-known, approximate, hydrogen molecule wave function,[1]

$$\Phi(H_2)=1s_a(1)1s_b(2)+1s_b(1)1s_a(2)$$
$$+\lambda[1s_a(1)1s_a(2)+1s_b(1)1s_b(2)], \tag{1}$$

[where $1s_a(1)$ for example represents the hydrogen-like $1s$ atomic orbital occupied by electron one about center a] is employed here to test certain approximations with a view to their applicability in more complicated molecular wavefunctions. These approximations are (A) the preselection of suitable, not necessarily the same, ζ's (orbital exponents)[2] for the atomic and ionic parts of the wavefunction (1); (B) the substitution of experimental atomic term values for certain integrals which arise in the energy calculations;[3] and (C) a substitution similar to the substitution in (B), using theoretical atomic term values.

The following atomic units will be used throughout this note: lengths in units of the Bohr radius, $a_H=0.5293$A; energies in units of $e^2/a_H=27.204$ ev.

For the hydrogen molecule problem the suggested choice of the ζ's in (A) is simple; unity for the atomic terms and 0.6875 for that of the ionic terms. This latter has been chosen for the ionic terms since it is the result which arises from a simple application of the variational method to systems with two electrons about a single nucleus.[4]

In order to make the substitutions indicated in (B) and (C), note that by definition the $X(A)$ (electron affinity of particle A) is

$$X(A)=E(A+e)-E(A^-), \tag{2}$$

where $E(A^-)$ represents the energy of the A minus-ion, and $E(A+e)$ represents the energy of particle A and an electron at infinite separation. Also,

$$\mathcal{H}(A^-)\Phi(A^-)=E(A^-)\Phi(A^-), \tag{3}$$

where $\Phi(A^-)$ represents the wavefunction of the A minus-ion, and $\mathcal{H}(A^-)$, the Hamiltonian for the A minus-ion. For the hydrogen minus-ion,

$$\mathcal{H}(H^-)=-\tfrac{1}{2}(\Delta_1+\Delta_2)-(1/r_1+1/r_2-1/r_{12}), \tag{4}$$

where $-\frac{1}{2}\Delta_i$ represents the kinetic energy operator for the ith electron; r_i, the distance of the ith electron from the nucleus;

and r_{12}, the separation of the two electrons. Using the "experimental" $X(H)$,[5] it is found from Eq. (2) that $E(H^-)$ is -0.52615. If the ionic part of the wave function (1) is used as an approximation for the correct hydrogen minus-ion wave function at infinite separation, it is easily found that the value to be used for $E(H^-)$ is -0.47265625. Each of these values [for approximations (B) and (C), respectively] is then substituted for the integrals arising from

$$\int\Phi(H^-)\mathcal{H}(H^-)\Phi(H^-)d\tau \quad \text{and} \quad \int\Phi(H)\mathcal{H}(H^-)\Phi(H^-)d\tau,$$

where $\Phi(H^-)$ is the ionic part of wave function (1) and $\Phi(H)$, the atomic part. This substitution eliminates the calculation of all the two-electron integrals except those arising from the atomic terms alone, which latter necessarily have τ equal zero (all ζ equal) in this case.

The equilibrium internuclear separations and dissociation energies were found by fitting a Morse curve to the potential energy curves in the usual manner.[6] The results are presented in Table I, along with other data for comparison.

The use of 0.6875 instead of unity for the ζ value of the ionic terms represents a moderate improvement of the energy values,

TABLE I. The maximum binding energy of the H_2 molecule.[a]

Method	ζ atomic	ζ ionic	D_e	R_e	λ
Heitler-London[b]	1.0	...	0.1160	1.642	0
Weinbaum[c]					
Molecular orbital	1.193	1.193	0.127	1.38	1.0
Variational method	1.0	1.0	0.1186	1.668	0.159
Variational method	1.193	1.193	0.148	1.417	0.256
Present paper					
Variational method					
approximation (A)	1.0	0.6875	0.1263	1.491	−0.214
approximation (B)	1.0	1.0	0.1753	1.464	0.533
approximation (A) and (B)	1.0	0.6875	0.1175	1.689	0.096
approximation (A) and (C)	1.0	0.6875	0.1231	1.531	−0.181
Experiment			0.174	1.40	

[a] All data in atomic units. D_e represents the dissociation energy; R_e, the equilibrium internuclear separation; ζ atomic and ζ ionic, the orbital exponents of the atomic and ionic terms, respectively, in wave function (1). All old data involving ζ atomic $=\zeta$ ionic $=1$ have been recalculated by the present author.
[b] W. Heitler and F. London, Z. Physik **44**, 455 (1927).
[c] S. Weinbaum, thesis, California Institute of Technology, 1933.

but as an *a priori* guess it is fairly good. In larger molecules it[7] might be close to the best value in terms of the results to be obtained. The use of the theoretical electron affinity seems to be a good approximation to the explicit evaluation of the integrals involved, and might be profitably used. The results obtained from the use of the experimental electron affinity seem to be sensitive to the choice of the ζ's. The outstanding success of approximation (B) alone was unexpected.

The necessary integrals were evaluated for ρ values in steps of 0.2ζ by the methods of Roothaan, Ruedenberg, and Jaunzemis;[8] the numerical values will be published elsewhere.

I would like to thank Professor C. C. J. Roothaan for suggesting this investigation and for his helpful advice, also Mr. Boris Musulin for permission to compare some unpublished data of his.

* This work was assisted by the U. S. Office of Naval Research under Task Order IX of Contract N6ori–20 with the University of Chicago.
[1] S. Weinbaum, J. Chem. Phys. 1, 593 (1933).
[2] This term, introduced by C. C. J. Roothaan and K. Ruedenberg, represents the effective nuclear charge divided by the principal quantum number.
[3] This approximation has been strongly urged by W. Moffitt; see, e.g., Proc. Roy. Soc. (London) **A210**, 245 (1951).
[4] G. W. Kellner, Z. Physik **44**, 91, 110 (1927).
[5] No experimental data are available for the electron affinity of hydrogen, but the theoretical value [E. A. Hylleraas, Z. Physik **65**, 209 (1930)] is generally regarded as being quite accurate and is used here as the experimental value.
[6] In those cases where a comparison could be made, the fundamental frequencies were found to be quite different from those reported by other investigators (e.g., 3800 cm^{-1} for the Heitler-London calculation). The discrepancies are probably attributable to the closer spacing of the ρ values in the present calculations.
[7] I.e., $\zeta=Z-0.3125$, where Z represents the atomic number.
[8] C. C. J. Roothaan, J. Chem. Phys. **19**, 1445 (1951); K. Ruedenberg, J. Chem. Phys. **19**, 1459 (1951); Roothaan, Ruedenberg, and Jaunzemis (to be published).

Equations of State and Detonation Theory

S. PATERSON AND J. M. DAVIDSON
Imperial Chemical Industries Limited, Nobel Division, Research Department, Stevenston, Ayrshire, Scotland
(Received November 13, 1953)

IN a recent letter,[1] Murgai describes calculations for detonation in PETN, based on Lennard-Jones and Devonshire's equation of state.[2] Comparisons are made with the results of other workers, and in particular with those deduced by Cottrell and Paterson[3] for the same explosive.

We have applied the state equation of Cottrell and Paterson to various explosives covering a wide range of loading density and reaction energy. It is hoped to publish details of this work elsewhere. The calculated velocities agreed well with experiment except for explosives of low reaction heat at low loading density; for such explosives the velocity was overestimated. This was attributed to the neglect of intermolecular attractions in the equation of state.

As a preliminary to further study, we then tried out the Lennard-Jones–Devonshire equation with force constants for nitrogen,[4] which correspond, per mole of PETN, to $v^0=340$ cm^3 and $\epsilon/k=96.7^0$. These values are rather similar to the ones used by Murgai in his first calculations, and our theoretical velocities (9950 m/sec at 1.5 g/cm^3, 6685 m/sec at 1.0 g/cm^3) are consistent with his figure of 8100 m/sec at 1.25 g/cm^3. Because of the known limitations of the Lennard-Jones–Devonshire theory, we did not carry these calculations any further, but it is interesting to find that a plausible adjustment of v^0 such as that made by Murgai can lead to close agreement in velocity.

There is some reason[5] to believe that at very high densities a (9,6) potential will be preferable to a (12,6). When the above calculations for PETN were repeated with the (9,6) nitrogen potential, agreement in velocity was appreciably improved, the calculated values now being 8520 m/sec at 1.5 g/cm^3 and 6170 m/sec at 1.0 g/cm^3. These are about 10–12 percent too high.

[1] M. P. Murgai, J. Chem. Phys. **21**, 1403 (1953).
[2] J. E. Lennard-Jones and A. F. Devonshire, Proc. Roy. Soc. (London) **A165**, 1 (1938).
[3] T. L. Cottrell and S. Paterson, Proc. Roy. Soc. (London) **A213**, 214 (1952).
[4] J. E. Lennard-Jones, Proc. Phys. Soc. (London) **43**, 461 (1931).
[5] R. H. Fowler, *Statistical Mechanics* (Cambridge University Press, Cambridge, 1936), p. 325.

Erratum: Relation Between Critical Temperature and Pressure of Normal Paraffins

[J. Chem. Phys. **21**, 1400 (1953)]

YATENDRA PAL VARSHNI
Department of Physics, Allahabad University, Allahabad, India

IN Eqs. (4) and (5) and Table II, T_c/P_c should be replaced by $T_cP_c^{\frac{1}{3}}$.

Thus the correct equation is

$$T_cP_c^{\frac{1}{3}}=\text{const.}$$

The Number of X-Ray Diffraction Groups

C. D. WEST
Polaroid Corporation, Cambridge, Massachusetts
(Received September 12, 1953)

THE x-ray diffraction groups were first defined and listed by Buerger.[1] The same groups were reproduced by Zhdanov and Pospelov[2] (1945), by Nowacki,[3] and by the *International Tables for X-ray Crystallography*.[4] All four references have the same list of 120 different diffraction groups. It is practical to count the 11 pairs of enantiomorphous space groups as units, leaving a total of 230−11=219 practical space groups. Under this manner

of counting 59 of the 120 diffraction groups were considered "unique" by reason of uniquely defining 59 of the 219 practical space groups.

A re-examination of the diffraction groups for crystals which belong to the Voigt-Laue group here designated $\{\bar{3}p2\bar{1}\}$, and which are described by hexagonal primitive lattice vectors, leads to the new results that there are actually 120+2 or 122 diffraction groups, of which 59+2 or 61 are "unique."

The "unique" groups now comprise 28 acentric plus 33 centric groups. The remaining 219−61=158 space groups are distributed over the remaining 61 nonunique diffraction groups.

The new results can be inferred by inspection of Table I. The diffraction group designated No. 81 in Nowacki's list is here split into two groups 81a and 81b; and his No. 82 is split into 82a and 82b, both of which are now "unique." His No. 83 and No. 84 remain unchanged, as do the diffraction groups 85 and 86 for crystals in the same Voigt-Laue group but described by rhombohedral primitive lattice vectors.

TABLE I. Subgroups of the Voigt-Laue group $\{\bar{3}p2\bar{1}\}$ which are referred to hexagonal primitive lattice vectors caa'.

Nowacki number	Diffraction groups	Point groups and space groups $3p21$	$3p\bar{2}1$	$\bar{3}p2\bar{1}$
81a	$\{\bar{3}2\bar{1}\}P\cdots$	$P321-D_3^2$	$P3m1-C_{3v}^1$	$P\bar{3}m1-D_{3d}^3$
81b	$\{\bar{3}\bar{1}2\}P\cdots$	$P312-D_3^1$	$P31m-C_{3v}^2$	$P\bar{3}1m-D_{3d}^1$
82a	$\{\bar{3}2\bar{1}\}P3_{1,2}\cdot\cdot$	$P3_{1,2}21-D_3^{3,5}$		
82b	$\{\bar{3}\bar{1}2\}P3_{1,2}\cdot\cdot$	$P3_{1,2}12-D_3^{4,6}$		
83	$\{\bar{3}2\bar{1}\}P\cdot c\cdot$		$P3c1-C_{3v}^3$	$P\bar{3}c1-D_{3d}^4$
84	$\{\bar{3}\bar{1}2\}P\cdot\cdot c$		$P31c-C_{3v}^4$	$P\bar{3}1c-D_{3d}^2$

The foregoing revisions also necessitate the revision of the table on p. 163 of Nowacki[3] downward from 12 pairs to 8 pairs of space groups. These revisions can be considered as in a favorable direction especially for the purposes of structure crystallography.

The previous miscounts may have arisen from overlooking, first, that among the crystals in question the lattice vectors aa', whose lengths are related by $a\sqrt{3}=a'$, and whose index triples are [01.0] and [12.0], respectively, sometimes take the orientation $\{\bar{2}\bar{1}\}$ and sometimes $\{\bar{1}2\}$ with relation to the horizontal symmetry elements; and further, that x-ray diffraction by single crystals absolutely determines axial Laue *symmetries* such as $\{2\}$ and $\{\bar{1}\}$, as well as the *lengths* of lattice vectors such as a and a'.

A situation quite similar to the foregoing one described for the Voigt-Laue group $\{\bar{3}p2\bar{1}\}$ exists in the point groups $\bar{4}p2\bar{2}$ and $\bar{6}p2\bar{2}$; but no revision of the diffraction groups is needed here. On the other hand, it is justified to consider modifying the presentation of a considerable amount of material in the ITX.

In setting up Table I, we retain the standard ITX and Schoenflies symbols for the space groups, except for an obvious way of representing an enantiomorphous pair of entities by a single symbol. A perhaps trivial inconsistency of the ITX space-group notation seen in this table is that the symbol 1 stands sometimes for an acentric 1 axis, and at other times for a centric or $\bar{1}$ axis, as in space-group symbols of the point groups $3p21-D_3$ and $\bar{3}p2\bar{1}-D_{3d}$, respectively.

We have introduced in this note, and especially in the table, modified symbols for the Voigt-Laue groups (a total of 11), for the point groups (32) and for the diffraction groups (122). These modified symbols should be at least as self-explanatory as the standard ones of the ITX. Some modification has for a long time seemed to the writer to be desirable in the direction of simplicity and practicality, and not only for experimental and applied crystallography, but also for work of a more general nature. The modified symbols as illustrated here have already found use in a not yet published systematic treatment by the author, in the writing of which the foregoing results unexpectedly fell out.

The preparation of the foregoing material was sponsored by the U. S. Office of Naval Research, and was helped by discussions with Professor Buerger.

[1] M. J. Buerger, *X-ray Crystallography* (1942), Table 34.
[2] Cited by Nowacki (see reference 3), p. 162. Original papers not consulted.
[3] Nowacki, *Fouriersynthese von Kristallen* (1952), Table 19 at end.
[4] *International Tables for X-ray Crystallography*, Vol. I (1952), Table 4.4.3 (here referred to as ITX).

Errata: Free-Electron Network Model for Conjugated Systems. I, II, and IV

[J. Chem. Phys. 21, 1565, 1582, 1413 (1953)]

KLAUS RUEDENBERG AND CHARLES W. SCHERR
Laboratory of Molecular Structure and Spectra, Department of Physics, The University of Chicago, Chicago, Illinois

I

P. 1576: The first line after Eq. (2.62) should read: 'the corresponding wave number, $(1/\lambda)=\Delta E/hc\cdots$." The sixth line after Eq. (2.65) should read: "$D=D_C=1.40000$A (the subscript $C\cdots$)." Similarly in Eqs. (2.66, 2.66', 2.67), E_C, λ_C, D_C should be substituted for E_c, λ_c, D_c.

P. 1580: Line 17 in the first column should read: "$\kappa_n=\frac{1}{3}\pi$ and $\cdots$."

II

P. 1582: The text immediately following Eq. (1) reading: "there exist solutions $\cdots$" to the end of the paragraph is incorrect. It should read: "there exist an infinity of solutions which may be found from the considerations of I, Section 2, parts four and five. The symmetries of these higher levels are reproduced in the same fashion as the energy levels of nonalternant molecules."

P. 1587, Table II: Under the row heading "n-polyenes," $(n+1)/2$ should be corrected to $2/(n+1)$.

P. 1594: The next to last line of Eq. (A.2) should read: "$\phi(1,12)-2\cos\kappa\phi(1)+\phi(2)=0$."

P. 1596: Immediately following Eq. (A.9a), the text should read: "Hence, $0.1799=\phi(1)=a_1\cos(3\kappa/2)=0.5488a_1\cdots$."

IV

P. 1413: The two unnumbered equations following Eq. (3b) should each begin with: "$-DE(\text{kcal})=\cdots$."

The Benzyl-Hydrogen Bond Dissociation Energy from Electron Impact Measurements

D. O. SCHISSLER AND D. P. STEVENSON
Shell Development Company, Everyville, California

(Received October 29, 1953)

SOME years ago Szwarc[1] reported 77.5 kcal/mole for the dissociation energy $D(C_6H_5CH_2-H)$ as determined from studies of the pyrolysis of toluene and related compounds. Quite recently Anderson, Scheraga, and Van Artsdalen[2] have reported the considerably higher value 89.9 kcal/mole based on their studies of the kinetics of the photochemical and thermal bromination of toluene. We wish to report that measurements of the appearance potentials of the ion $C_7H_7^+$ presumably the benzyl ion, in the mass spectra of toluene, ethylbenzene, and dibenzyl, when combined with the appropriate thermochemical data lead to $D(C_6H_5CH_2-H)$ equal to 77±3 kcal/mole in excellent agreement with Szwarc.

If it is assumed that the appearance potentials of the $C_7H_7^+$ ion in the mass spectra of toluene and dibenzyl have the significance,

$$C_6H_5CH_3 = C_7H_7^+ + H + \epsilon^-;$$
$$A_1(C_7H_7^+) = D(C_6H_5CH_2 - H) + I^e(C_6H_5CH_2). \quad (1)$$

$$(C_6H_5CH_2)_2 = C_7H_7^+ + C_6H_5CH_2 + \epsilon^-;$$
$$A_2(C_7H_7^+) = D(C_7H_7 - C_7H_7) + I^e(C_6H_5CH_2) \quad (2)$$

then the difference between Eqs. (1) and (2) is

$$(C_6H_5CH_2)_2 + H = C_6H_5CH_3 + C_6H_5CH_2;$$
$$\Delta H = A_2(C_7H_7^+) - A_1(C_7H_7^+). \quad (3)$$

From the heats of formation of toluene[3] (+11.95 kcal/mole) and dibenzyl[4] (+28.0 kcal/mole), and $D(H-H) = 4.48$ ev/molecule,[5] one computes

$$(C_6H_5CH_2)_2 + 2H = 2C_6H_5CH_3;\ \Delta H = -4.66 \text{ ev/molecule}. \quad (4)$$

If we subtract Eq. (4) from (3), we obtain

$$C_6H_5CH_2 - H = C_6H_5CH_2 + H;$$
$$D(C_6H_5CH_2H) = 4.66 + A_2(C_7H_7^+) - A_1(C_7H_7^+). \quad (5)$$

Taking $A_1(C_7H_7^+) = 11.85 \pm 0.1$ ev/molecule, the weighted average of the direct and two indirect determinations (see below) and $A_2(C_7H_7^+) = 10.5_3 \pm 0.1$ ev/molecule as given in the next paragraph,

$$D(C_6H_5CH_2 - H) = 4.66 + 10.53 - 11.85 = 3.34 \pm 0.14 \text{ ev/molecule}$$

or

$$D(C_6H_5CH_2 - H) = 77._0 \pm 3 \text{ kcal/mole}.$$

Our measurements of $A(C_7H_7^+)$ in the mass spectra of toluene, ethylbenzene and dibenzyl give, 11.8 ± 0.1, $11.2_5 \pm 0.1$, and $10.5_3 \pm 0.1$ ev/molecule, respectively. Franklin and Lumpkin[6] have reported $A(C_7H_7^+) = 11.1_3 \pm 0.1$ ev/molecule for benzyl chloride. Use of the heats of formation of toluene,[3] ethylbenzene,[3] and the methyl radical[7] permit the calculation of an energy $A(C_7H_7^+)$ for toluene from the datum on ethylbenzene and the value so calculated $11.8_5 \pm 0.1$ ev/molecule is in excellent agreement with the direct measurement on toluene. No reliable value for the heat of formation of benzyl chloride could be found in the literature. An old datum of unknown reliability on the heat of combustion of benzyl chloride leads to $11._5$ kcal/mole for the heat of formation, while the constancy of the difference

$$\Delta H_f^0(\text{benzyl } X) - H_f^0(\text{allyl } X) = 4.6 \pm 0.7 \text{ kcal/mole}$$

for X = OH, CN, Br, and I, along with ΔH_f^0(allyl chloride) = +0.6 kcal/mole[4] leads to the heat of formation of benzyl chloride equal to 5.2 kcal/mole. Taking the mean of these estimates as 8.3 ± 5 kcal/mole, the Franklin and Lumpkin appearance potential of $C_7H_7^+$ in the benzyl chloride mass spectrum is equivalent to $11.9_8 \pm 0.3$ ev/molecule for $A(C_7H_7^+)$ in the toluene mass spectrum, in essential agreement with the directly observed value.

[1] M. Szwarc, J. Chem. Phys. **16**, 128 (1948).
[2] Anderson, Scheraga, and Van Artsdalen, J. Chem. Phys. **21**, 1258 (1953).
[3] F. D. Rossini *et al.*, *Selected Values of Physical and Thermodynamic Properties of Hydrocarbons* (Carnegie Press, Pittsburgh, 1953).
[4] J. S. Roberts and H. A. Skinner, Trans. Faraday Soc. **45**, 339 (1949).
[5] G. Herzberg, *Spectra of Diatomic Molecules*, (1950) second edition.
[6] J. Franklin and H. E. Lumpkin, J. Chem. Phys. **19**, 1073 (1951).
[7] D. P. Stevenson, Discussions Faraday Soc. **35**, (1953).

Experiments on Polymer Solution in Inhomogeneous Electrical Fields*

P. DEBYE, P. P. DEBYE,† B. H. ECKSTEIN, W. A. BARBER,‡ AND G. J. ARQUETTE
Department of Chemistry, Cornell University, Ithaca, New York
(Received October 22, 1953)

IT is well known that the effect of ions on the solubility of nonelectrolytes can be explained at least as to its fundamental character by the driving force an inhomogeneous electrical field exerts on uncharged polarizable particles. In these cases we are dealing with strong fields and very large gradients. When we decided to investigate this effect in artificial inhomogeneous fields which are much weaker and much less inhomogeneous, it was clear from the beginning that in order to obtain observable effects, we had to work with particles of high polarizability. Polymer molecules were indicated.

Consider a polymer solution used as a dielectric in a condensor consisting of a larger cylinder with a central fine wire, and let us suppose that the polymer molecules are more polarizable than the solvent. If now a static voltage is applied across the dielectric, polymer molecules will accumulate at places of highest field strength, that is, near the central wire. Since the potential energy of a polymer molecule is proportional to its polarizability and to the square of the local field strength, a Boltzman distribution will be obtained at equilibrium. This enables us to relate observed final concentration changes to the molecular weight of the polymer. Equilibrium is attained after a transition period in which the uncharged particles are moving in an inhomogeneous field according to their combined polarizability and mobility (as ions would move in an homogeneous field according to their charge and mobility). As in sedimentation experiments with the ultracentrifuge, observation of the effect during the transition period should, for instance, give information about the molecular weight distribution of a given polymer.

A first experiment was conceived based on the fact that, as a result of the concentration rearrangement, the capacity of the cylindrical condensor changes. In order to observe this change the capacitor was made part of a resonant circuit, which in our arrangement oscillates at approximately 5 megacycles. Its frequency is compared by a beat method with the constant frequency of a crystal-controlled General Radio Company Frequency-Monitor. Beats are counted by a Berkeley Scientific Company EPUT-meter (Events Per Unit Time).

In our arrangement, a water-jacketed cell is used 30 cm long, 5-cm internal diameter with a central platinum wire of 0.1-mm diameter. In a typical experiment, application of 7000 volts to a 1-percent solution of polystyrene (M. W. 600 000) in cyclohexane gave a change (increase of capacity) of 20 cycles per second. The establishment of the new frequency took about 3 minutes. Beats were counted over 1 second periods at intervals of 3 seconds.

H. S. Sack of the Physics Department kindly furnished apparatus in the exploratory stage. The present arrangement was developed during the fall and winter 1952–1953 by P. P. Debye. In October, 1952, Eckstein became associated with the problem and has since been chiefly occupied with making refinements necessary for quantitative measurements. In this he has the very valuable cooperation of T. McLean of the School of Electrical Engineering.

A second experiment was conceived in order to make the concentration effect visible. Remembering the fact that supersonic waves in a liquid act as a diffraction grating for light, we introduced periodic changes of the concentration leading to corresponding changes of the refractive index in the solution with the help of a grating made of razor blades. About 60 blades were assembled, spaced by thin cover glasses (edge-to-edge distance of the blades 0.5 mm). Opposite this assembly was a flat plate, at a distance of about 3 mm the whole submerged in the liquid (a 1-percent solution of polystyrene, M.W. 600 000, in toluene). Parallel light from a slit and lens combination passing through the cell gives a well-defined diffraction spectrum (many orders) in the focal plain of a second lens. Before applying voltage between blades and plate a second, relatively wide slit (0.5 mm) is introduced in the parallel beam blocking off all the light except the part passing just above the edges of the blades. The diffraction spectra disappear. As soon as the voltage is applied the lower-order spectra return. They are due to periodic accumulations of polymer in the liquid along the edges of the blades, where the electrical field is very strong. Since the path of the light along an edge contains about 10^5 light waves and only a periodic phase-difference of a small fraction of a wavelength is necessary to produce appreciable intensity in the diffraction pattern, very small concentration

changes become observable. In fact we succeeded in obtaining weak diffraction spectra in pure liquids. In this case they must be due to electrostriction. If the optical eyepiece is replaced by the eye of the observer, he can actually see the concentration changes in the liquid. Probably a "Schlieren" method could therefore be developed. Disturbing effects, expected due to heating were minimized by using liquids of high resistivity (above 10^{13} ohm cm). The experimental work was done by Barber starting about 6 months ago.

In order to use this effect for the determination of molecular weights, it is necessary to measure the intensity, say of the first-order spectrum. By a slit in the focal plane of the second lens of the arrangement, the first-order spectrum was isolated and its light directed to a photomultiplier tube, whose output is measured by a cathode-ray oscilloscope. To permit study of time effects, arrangements have been made to apply the voltage in pulses.

The necessary equipment was built by Arquette, who became interested in the work about 3 months ago. Some of the details in the time effects, observed this way, are not yet fully understood.

* The work discussed herein was performed as a part of the Research Project sponsored by the Reconstruction Finance Corporation, Office of Synthetic Rubber in connection with the U. S. Government Synthetic Rubber Program.

† Present address: Raytheon Manufacturing Company, Waltham, Massachusetts.

‡ Present address: American Cyanamid Company, Stamford, Connecticut.

Imperfect Gas as an Association Problem

WILLIAM WELTNER, JR.
Department of Chemistry, The Johns Hopkins University, Baltimore, Maryland

(Received October 29, 1953)

DURING the course of an investigation of the properties of methanol vapor,[1] consideration was given to possible equations of state which would clearly express its highly associative nature beyond the formation of only dimers in the gas phase.[2,3] The quasi-chemical approach, that is, treatment of the imperfect gas as a chemical association problem, had been employed successfully as an interpretation of the second virial coefficient[4,5,6] and was extended by the same methods to the calculation of the higher virial coefficients.

The second virial coefficient expressed in this way is

$$B_v = b_1 - K_2 RT, \tag{1}$$

where, if the notation of Hirschfelder *et al.*[4] is used, $b_1 = 2N\pi r_a^3/3$ is the excluded volume of a single molecule considered as having a spherical effective force field. K_2 is the equilibrium constant for association of two monomers to a dimer and R is the gas constant. The third virial coefficient may be obtained in a similar manner by considering three equivalent molecules within each others field of force. This integral is

$$C_v = -N/3 \int\int f(r_{12}) f(r_{13}) f(r_{23}) d\tau_1 d\tau_2,$$

where $f(r_{ij}) = \exp[-u(r_{ij})/kT] - 1$, $u(r_{ij})$ being the intermolecular potential energy. There then results, after expansion and integration, the formal expression

$$C_v = v_3 - 2v_2 K_2'' RT + 4(K_2' RT)^2 - 2K_3 (RT)^2. \tag{2}$$

Here v_2 and v_3 are terms involving only the volume and K_2', K_2'', and K_3 are the classical equilibrium constants for dimer and trimer (symmetry number = 6):

$$K_2' = N \int \exp(-u/kT) d\tau / 2PV, \text{ same for } K_2'',$$

$$K_3 = N^2 \int\int \exp(-u_{12} - u_{23} - u_{31}/kT) d\tau_1 d\tau_2 / 6P^2V^2,$$

and $PV \cong RT$. K_2', K_2'', and K_2 (in Eq. (1)) are different because the volume elements over which the integrations occur are not the same. v_3 may be determined to be $5N^2\pi^2 r_a^6/18 = 5b_1^2/8$ (b_1 as determined from B_v) by changing to confocal elliptical coordinates before integration. v_2 cannot be determined without saying something about the nature of the intermolecular potential energy. The fourth virial coefficient may be similarly treated, but the resulting expression involves more terms.

It is interesting to note that these same expressions for the virial coefficients, at least in the same functional form, may be obtained by considering a perfect gas made up of clusters of molecules, as Woolley[7] has done. One may include the excluded volume terms (mentioned by this author in the last paragraph of his paper) in his equation, to the warranted degree of approximation, in the usual way. It is only necessary to subtract a term $\Sigma_n \geqslant_1 m_n b_n$ from the volume V in his Eq. (10), writing it as

$$P(V - \Sigma_n \geqslant_1 m_n b_n) = RT[1 - K_2 P + (3K_2^2 - 2K_3)P^2 + \cdots], \tag{10*}$$

m_n is the number of moles of the cluster composed of n single molecules and b_n is the average effective excluded volume of this cluster. From his Eq. (4) it is seen that $m_n = PX_n/P$ and $PX_n = K_n(P_X)^n$ from his Eq. (3). Eq. (10*) then becomes

$$PV - \Sigma (P_X)^n K_n b_n = RT[1 - K_2 P + (3K_2^2 - 2K_3)P^2 + \cdots]$$

where P_X is given by Woolley's Eq. (9) as an infinite series of powers of P. Substituting from (9) and comparison with (11) as in his procedure then yields

$$PV = RT[1 + B_v/V + C_v/V^2 + D_v/V^3 + \cdots],$$

where

$$\begin{aligned} B_v &= b_1 - K_2 RT, \\ C_v &= b_1^2 + K_2 RT(b_2 - 3b_1) + 4(K_2 RT)^2 - 2K_3 (RT)^2, \\ D_v &= b_1^3 + 3K_2 RT(b_2 b_1 - b_1^2) + (K_2 RT)^2 (17b_1 - 5b_2) \\ &\quad + K_3 (RT)^2 (b_3 - 7b_1) + [-20K_2^3 + 18K_2 K_3 - 3K_4](RT)^3. \end{aligned} \tag{3}$$

The correspondence between the terms of C_v in Eq. (2) and Eq. (3) is clear; however the terms in the more rigorous expression, Eq. (2), would only approach those in Eq. (1) if the trimer were treated as a chain and not as three equivalent molecules. In other words, the derivation of Eq. (3) assumes essentially that a single molecule "sees" the dimer as another single molecule.

If an intermolecular potential function is selected then in principle the virial coefficients may be determined completely, but in general for any very realistic function the result cannot be written out in simple form. Although not very realistic, the "square well" potential does not suffer from this disadvantage. This function was used by Hirschfelder *et al.*[4] in the calculation of the second virial and is sufficiently simple that the third virial coefficient may also be explicitly determined, as has been done by Kihara.[8] This allows a comparison of the volume terms and equilibrium constants in the two third-virial coefficients expressed in Eq. (2) and Eq. (3). The results for the "square well" of width $r_a - r_0$ and depth $-D$ ergs/molecule are:

$$\begin{aligned} B_v &= 4v_0 x^3 - 4v_0 (x^3 - 1) e^{D/kT}, \\ C_v &= 10 v_0^2 x^6 - v_0 e^{D/kT}[30x^6 - 64x^3 + 36x^2 - 2] \\ &\quad + v_0^2 e^{2D/kT}[32x^6 - 36x^4 - 64x^3 + 72x^2 - 4] \\ &\quad - v_0^2 e^{3D/kT}[12x^6 - 36x^4 + 36x^2 - 12], \end{aligned}$$

where $v_0 = 4N\pi(r_0/2)^3/3$ and $x = r_a/r_0$. From estimates of v_0 and x for spherical nonpolar gases obeying the Lennard-Jones potential[4] the excluded volume terms are found to be important in B_v but only in C_v for D/kT less than about 0.5. The assumption that $K_2' = K_2$ which occurs in Eq. (3) can however cause serious error since the $(K_2')^2$ term and the K_2 term are of comparable importance for Lennard-Jones gases at moderate temperatures. From the "square well" virial it is found that $K_2' \cong 0.6 K_2$ for a Lennard-Jones gas.

For a value of D/kT of 4 or greater the last term in C_v [and in D_v of Eq. (3)] becomes dominant because of the presence of the exponential term. Then one can infer that for hydrogen bonding substances, where D/kT is of this magnitude, only the term involving K_3 in C_v and K_4 in D_v in Eq. (3) need be retained. The

necessity for inclusion of higher polymers in the methanol equation of state[1] and also in that of water[9] has been demonstrated and such may also be the case in some nonhydrogen-bonded polar vapors.[2]

[1] W. Weltner, Jr. and K. S. Pitzer, J. Am. Chem. Soc. **73**, 2606 (1951).
[2] Lambert, Roberts, Rowlinson, and Wilkinson, Proc. Roy. Soc. (London) **A196**, 113 (1949).
[3] J. S. Rowlinson, Trans. Faraday Soc. **45**, 974 (1949).
[4] Hirschfelder, McClure, and Weeks, J. Chem. Phys. **10**, 201 (1942).
[5] R. Fowler and E. A. Guggenheim, *Statistical Thermodynamics* (Cambridge University Press, Cambridge, 1949), p. 267.
[6] J. A. Beattie and W. H. Stockmayer, *Treatise on Physical Chemistry*, edited by H. S. Taylor and S. Glasstone (D. Van Nostrand Company, Inc., New York, 1951), Vol. II, Chap. II, p. 339.
[7] H. W. Woolley, J. Chem. Phys. **21**, 236 (1953).
[8] T. Kihara, Nippon Suugaku-Buturigakkwai **17**, 11 (1943).
[9] McCullough, Pennington, and Waddington, J. Am. Chem. Soc. **74**, 4439 (1952).

Specific Heats of Simple Solids and Moments of Elastic Frequency Spectra

JENN-LIN HWANG
Department of Physics, Tiawan University, Taipei, Formosa, China
(Received October 20, 1953)

IF the specific heat data of a solid fitted in the form

$$C(T)=1+\sum_{n=1}^{\infty}(-)^n C_n X^{2n}, \tag{1}$$

where $x=h\nu_0/kT$ and ν_0 is an arbitrary parameter, are compared with the well-known expansion[1]

$$C(T)=1+\sum_{n=1}^{\infty}(-)\frac{n(2n-1)B_n}{(2n)!}\mu_{2n}x^{2n}, \quad \frac{h\nu_m}{kT}>2\pi, \tag{2}$$

the even moments of the frequency spectrum

$$\mu_{2n}=\frac{1}{\nu_0^{2n}}\int_0^{\nu_m}\rho(\nu)\nu^{2n}d\nu$$

may be easily derived.[2] And, as was demonstrated by Montroll[3] and Katz,[2] with the use of these moments one can determine a substitute spectrum from which the high-temperature part of the experimental specific-heat curve may be exactly reproduced. However, because the data are less precise, only the first several moments are obtainable,[2] and so any improvement of this kind of approximation has not yet been obtained, especially beyond the temperature limit $h\nu_m/kT>2\pi$, where the series expansion (2) is valid. A scheme to overcome this difficulty will be shown in the following.

Consider the equation of specific heat

$$C(x)=\int_0^{\gamma}E(xz)f(z)dz, \tag{3}$$

where $z=\nu/\nu_0$, $f(D/\nu_0)/\nu_0=\rho(\nu)$, and $\gamma=\nu_m/\nu_0$. As will be seen later, γ and, therefore, the maximum frequency ν_m can be approximately determined beforehand. Multiplying both sides of Eq. (3) by x^{n-1} and integrating from 0 to ∞, we get

$$\lambda_{n-1}\int_0^{\infty}C(x)x^{n-1}dx=\int_0^{\gamma}f(z)z^{-n}dz, \tag{4}$$

where $0<n<3$ and $\lambda_m=1/\zeta(m+2)\Gamma(m+3)$. When $n=0$, it is apparent from the normalization condition

$$\lim_{n\to 0}\lambda_{n-1}\int_0^{\infty}C(x)x^{n-1}dx=1. \tag{5}$$

This condition would hold for any consistent observed specific heats due to harmonic lattice vibrations. The upper limit $n=3$ may be removed as follows: as was pointed out formerly,[2,4] the extreme lower-frequency part of $f(z)$ can be accurately determined. If we cut off from both sides of Eq. (3) this part, as well as its contribution to the specific heats, and represent the residual part of each quantity by adding a bar, then Eq. (4) becomes

$$\lambda_{n-1}\int_0^{\infty}\bar{C}(x)x^{n-1}dx=\int_0^{\gamma}\bar{f}(z)z^{-n}dz \tag{6}$$

for any real positive value of n, i.e., for $0\leq n<\infty$. We will call the quantity of Eq. (5) or Eq. (6) "the nth inverse moment of $f(z)$ or $\bar{f}(z)$" and abbreviate μ_{-n} or $\bar{\mu}_{-n}$, respectively. Since μ_{-n} (or $\bar{\mu}_{-n}$) corresponds to the $(n-1)$st moment of $C(x)$ [or $\bar{C}(x)$], combining them with the ordinary moments μ_{2n} (or $\bar{\mu}_{2n}$) given by Eq. (2), one would obtain a rapid and fair reproduction of the experimental specific-heat curve through the whole temperature range.

By virtue of the inverse moments μ_{-n}, the determination of the maximum frequency ν_m becomes possible.[4] As an illustration, we take only μ_{-2} and the first $n\mu_2 n$'s and write $z^2g(z)$, M_0, M_1, $M_2\cdots M_n$ instead of $f(z)$, μ_{-2}, μ_0, $\mu_2\cdots\mu_{2n-2}$, respectively. Suppose $g(z)$ may be approximated by

$$g(z)=\sum_{j=0}^{n-1}a_j z^{2j}. \tag{7}$$

Then, using the first nM's, $\{M_0, M_1\cdots M_{n-1}\}$, we may get from a least squares consideration[1] a set of linear equations for determining a_j's

$$M_p=\sum_{j=0}^{n-1}\gamma^{2(p+j)+1}a_j/(2p+2j+1), \tag{8}$$
$$p=0, 1, 2, \cdots, (n-1).$$

Solving for a_0 by the usual Krammer method yields

$$a_0=\frac{1}{\Delta}\sum_{s=0}^{n-1}(-)^s\delta_s M_s\tau^{s+1}, \tag{9}$$

where Δ is the determinant of the coefficients $1/(2p+2j+1)$, δ_s the co-factor of M_s, and $\tau=1/\gamma=\nu_0/\nu_m$. Similarly, using the last nM's, $\{M_1, M_2\cdots M_n\}$,

$$a_0=\frac{1}{\Delta'}\sum_{s=1}^{n}(-)^{s-1}\delta_s' M_s\tau^{s+1}. \tag{10}$$

We assume that these two expressions of a_0 are identical; equating them and dividing throughout by $\delta_n' M_m\tau/\Delta'$, we get for determining γ an algebraic equation of the form

$$\tau^n-b_{n-1}\tau^{n-1}+b_{n-2}\tau^{n-2}-\cdots+(-)^n b_0=0. \tag{11}$$

The possible value of τ should be chosen from the n roots of Eq. (11) in such a manner that it can make the value of a_0, according to Eq. (9) or (10), equal to $(15/4\pi^4)[C(x')/x'^3]_{x'=0}$, since, by Eq. (7) and the last equation of my earlier letter,[4]

$$a_0=g(0)=(15/4\pi^4)[C(x')/x'^3]_{x'=0}, \quad \text{where} \quad x'=1/x=kT/h\nu_0.$$

In connection with the derivable moments μ_{-n} and μ_n (or $\bar{\mu}_{-n}$ and $\bar{\mu}_n$), we should consider the problem of finding $f(z)$ [or $\bar{f}(z)$] from them. In principle, the other a_j's can also be evaluated in such a form of a linear combination of M's as Eqs. (9) and (10), and an approximate expression of $f(z)$ may be obtained. However, it is well known that results obtained by solving a linear system are full of uncertainties unless the constants and coefficients are highly accurate. Since the significant figures of our moments M's are only several, the a_j's thus derived would be ambiguous when n is large.[5] This means that many different types of frequency spectra might exist, each of which would give the same specific heat curve within the experimental accuracy attainable at present. This state of affairs could be seen more clearly when using orthogonal polynomials. Another kind of treatment for moment problem is the so-called "Gauss mechanical quadrature method."[3,6] A modification of this method is possible: if we designate some equally spaced values for the location parameter[6] β_i, the tedious procedure for determining the self-adjoint polynomial and that for finding its zeros may be omitted. Then, if the approximating function is chosen to be a sum of the δ-functions, the weighting factor[6] n_i will tend, as the number of moments increases, to a value from which the numerical value of $f(\beta_i)$ may

be estimated. But, unfortunately, in either the original or the modified method the same difficulties as in the case of polynomial treatment still arise; and the derived $f(z)$ may be far different from the exact one. At any rate, we can conclude as follows: if the specific heat data are given with infinite accuracy, the frequency spectrum is uniquely determined; however, if the data have only the present experimental accuracy, various kinds of equivalent spectra exist, all of them being able to reproduce the same observed specific heat curve.

[1] E. W. Montroll, J. Chem. Phys. **11**, 481 (1943).
[2] E. Katz, J. Chem. Phys. **19**, 488 (1951).
[3] E. W. Montroll, Quart. Appl. Math. **5**, 223 (1947).
[4] J. L. Hwang, J. Chem. Phys. **21**, 168 (1953).
[5] In Eq. (11) this situation is not so serious because we have divided throughout by $\delta_n' M_n/\Delta'$. Nevertheless, a large number of moments should be avoided: six or so seem most appropriate to a practical purpose.
[6] L. V. Spencer, Phys. Rev. **88**, 793 (1952).

Fluorescence Spectrum of Triphenylmethyl at 4°K†

S. I. Weissman
Departments of Chemistry, Washington University, St. Louis, Missouri, and Brookhaven National Laboratory, Upton, Long Island, New York
(Received November 9, 1953)

THE fluorescence spectrum of solutions of triphenylmethyl in rigid glasses at the temperature of liquid nitrogen reveals a well-resolved structure. Lewis, Lipkin, and Magel[1] observed nine distinct peaks in an interval of 2500 cm^{-1}. Their observations have since been repeated.[2]

In the course of a study of the anisotropy of the hyperfine structure in the paramagnetic resonance of triphenylmethyl, I have prepared dilute solid solutions of triphenylmethyl in crystalline triphenylamine. These crystals luminesce brightly even at room temperature under excitation by the 3650A mercury line. At liquid nitrogen temperature the spectrum of the crystalline solid is better resolved than that of the glassy solution. Nineteen peaks are observed; their frequencies and relative intensities correspond well to a further resolution of the spectrum of the glass. At liquid helium temperature a remarkable sharpening of the spectrum of the crystals occurs. One hundred and four lines, some less than four cm^{-1} wide are observed in an interval of 1900 cm^{-1}.[3] The exposure time was not sufficient to bring out the lines corresponding to the two weak peaks of the glass at 17 200 and 16 900 cm^{-1}. A reproduction of the spectra of the crystals at 77°K and at 4°K is given in Fig. 1.

In all likelihood the fluorescence spectrum arises from transitions between a vibrationless excited electronic state and the various vibrational levels of the normal state. It is possible that the spectrum will yield a fairly complete vibrational assignment for triphenyl methyl. Studies of the polarizations and anisotropes in the fluorescence and absorption spectra of single crystals and of isotope shifts at 4°K are being undertaken in order to complete the task.

I am indebted to Jacob Bigeleisen and Morris Slavin for their assistance in the spectroscopic work.

† Assisted by the joint program of the U. S. Office of Naval Research, U. S. Atomic Energy Commission.
[1] Lewis, Lipkin, and Magel, J. Am. Chem. Soc. **66**, 1579 (1944).
[2] T. L. Chu and S. I. Weissman, J. Chem. Phys. (to be published).
[3] The spectrum was photographed in the first order of a 21-foot grating spectrograph. The dispersion was 5.2 angstroms per millimeter, the resolving power greater than 50 000.

Assignment of Torsional Frequencies in Some Halogenated Ethanes

Norbert W. Luft
Cheadle Hulme, Cheshire, England
(Received November 3, 1953)

RECENTLY the infrared and Raman spectra of halogen derivatives of ethane have been investigated by a number of authors.[1–5] As a result of their measurements, complete vibrational assignments and calculated thermodynamic functions are now available for most of the compounds in question. In several of these papers, however, the tentative nature of the low-frequency assignments has been admitted, and the possibility of errors in the identification of the torsional mode, in particular, has been pointed out repeatedly.

Although the group frequencies of a series of related molecules were sometimes compared in the usual wave-number diagram, it was never attempted to correlate the torsional frequencies δ_t by way of their threefold internal potential barriers V_0 and thus to establish their consistency. This may be achieved by means of dividing the over-all barriers into contributions from individual bonds and applying to them the additivity rule.[6,7] Naturally, this method is only an approximate one, since in molecules X_3C-CY_2Z the azimuthal angles ϕ between successive bonds are expected to differ from 120°, *viz.*, $\phi(YZ)=120+\epsilon$ and $\phi(YY)=120-2\epsilon$, say. This causes the actual barrier of X_3C-CY_2Z to be

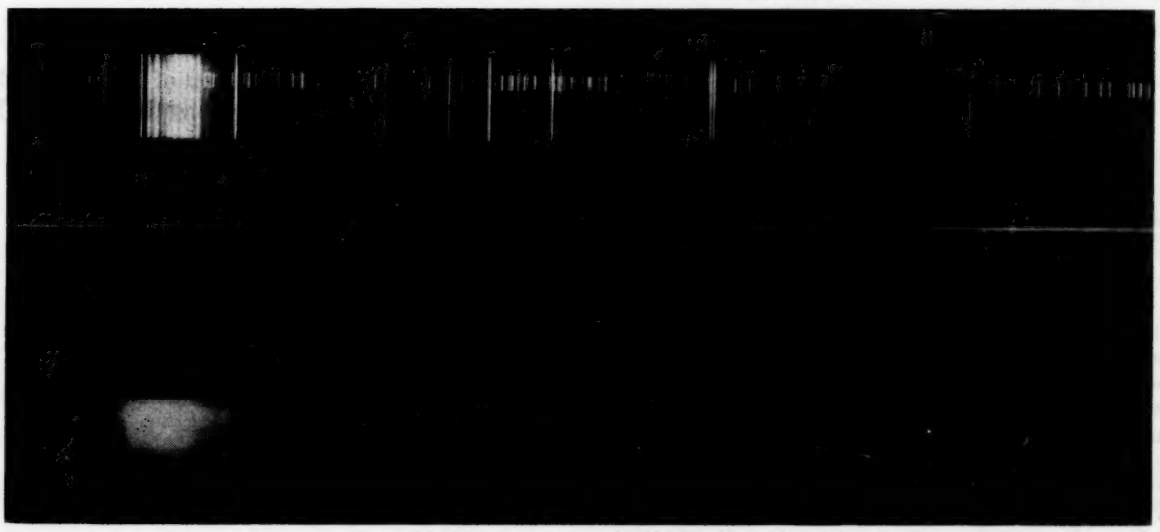

Fig. 1. Fluorescence spectra of triphenylmethyl in crystalline triphenylamine at 4°K and 77°K.

lower by $\Delta V=(\frac{2}{3})(1-\cos 3\epsilon)V_1$ than the value $V=(\frac{2}{3})V_1+(\frac{1}{3})V_2$, according to the additivity rule (V_1=internal barrier of X_3C-CY_3, V_2=internal barrier of X_3C-CZ_3). Since $\Delta V/V \lesssim 0.01$ for $\epsilon<3°$, this difference is unlikely to affect the values of internal potential barriers appreciably. Moreover, the accuracy of experimental barriers would seem to be such that this angular deviation can be safely ignored.

In many instances, recently assigned torsional barriers are found to agree with the additivity rule to within 20 percent or better, although there exist hitherto unexplained irregularities with some low substituted halogen derivatives of ethane which seem to call for a revision of torsional frequencies. The barrier height $V_0=22.3$ kcal/mole quoted[4] for $F_3C-CHCl_2$, however, is excessive. This high figure was obtained by interpreting the Raman shift at 141 cm^{-1} as the torsional mode $\delta_t(a'')$ and the shift 185R, w as the lowest a' fundamental, and by discarding 105R, liq. as spurious. Since with the assumption $141R=2\delta_t$ the resulting barrier, *viz.*, 5.7 kcal/mole, is too low, the following assignment may be proposed for these Raman shifts: $105\sim\delta_t$, $141=\omega(a')$, $185=2\delta_t$. The value $\delta_t=93$ cm^{-1}, which results in $V_0=10.1$ kcal/mole, and $\omega(a')=141$ cm^{-1} (instead of the previous value of 185 cm^{-1}) were used to recalculate the thermodynamic functions of $F_3C-CHCl_2$ (Table I).

TABLE I. Calculated thermodynamic functions for F_3C-$CHCl_2$.

T°K	S°	$-(F°-H_0°)/T$	$-(H°-H_0°)/T$	C_p°
200	75.48	62.18	13.31	19.42
298.16	84.10	67.95	16.14	24.39
400	92.09	73.24	18.85	28.58
500	98.61	77.52	21.09	31.68
600	104.78	81.75	23.03	34.21
700	110.06	85.31	24.75	35.96
800	115.17	88.88	26.29	37.34

If similar considerations are applied to the molecules F_3C-CF_2Cl and F_3C-CCl_3, the higher values of the two alternatives, *viz.*, $\delta_t=168$ or 91 and 173 or 96 cm^{-1}, respectively, proposed[3] tentatively from combination bands, can be ruled out unambiguously, since they would lead to impossibly high barriers (30.4 and 38.7 kcal/mole, respectively). The lower values, especially if considered as upper limits, yield barriers of 9.1 and 11.9 kcal/mole, which are in reasonable agreement with the additivity rule. The thermodynamic functions of F_3C-CCl_3 (Table II) were calculated for a harmonic oscillator model and a total pressure of 1 atmos, using the vibrational assignment by Nielsen *et al.*[3] and $\delta_t=90$ cm^{-1} and the calculated moments of inertia $I=638.8$, 773.3, 788.1×10^{-40} g cm^2. Since the barrier is high, the torsional mode was treated as an ordinary harmonic vibration.

TABLE II. Calculated thermodynamic functions for F_3C-CCl_3.

T°K	S°	$-(F°-H_0°)/T$	$-(H°-H_0°)/T$	C_p°
200	76.32	61.95	14.37	22.33
298.16	86.37	68.38	17.99	28.07
400	95.24	74.12	21.13	32.30
500	102.78	79.11	23.67	35.18
600	109.39	83.63	25.76	37.08
700	115.22	87.72	27.50	38.61
800	120.42	91.46	28.95	39.63

[1] Nielsen, Claasen, and Smith, J. Chem. Phys. **18**, 1471 (1950).
[2] Smith, Saunders, Nielsen, and Ferguson, J. Chem. Phys. **20**, 847 (1952).
[3] Nielsen, Liang, and Smith, J. Chem. Phys. **21**, 383 (1953).
[4] Nielsen, Liang, and Smith, J. Chem. Phys. **21**, 1060 (1953).
[5] Nielsen, Liang, Smith, and Alpert, J. Chem. Phys. **21**, 1070 (1953).
[6] N. W. Luft, Discussions Faraday Soc. **10**, 117 (1951).
[7] N. W. Luft, J. Chem. Phys. **21**, 179 (1953).

Critical Temperature and Boiling Point of Normal Paraffins

SHASHANKA SHEKHAR MITRA
Department of Physics, Allahabad Univeristy, Allahabad, India
(Received November 3, 1953)

IN a recent communication[1] the author has given an additive function connecting the critical temperature and pressure. In the present note a simple relationship between the critical temperature and boiling point of a normal paraffin will be given. If T_c and T_b are the critical temperature and boiling point, respectively, in °K, it is seen that the function $S=n(T_c-T_b)/10$ is additive for the homologous series, n being the number of carbon atoms in the paraffin. The observed data are well represented by the formula $S=18.01n-8.81$. The observed and calculated values of S are given in Table I. The agreement is fairly good (in most of the cases, error is less than 1 percent) except for the first few members, which is usually the case with the normal hydrocarbons. The mean value of S for the addition of a (CH_2) group has been found to be 18.01. The experimental data have been taken from standard sources.[2]

TABLE I.

n	Paraffins	T_c in °K	T_b in °K	S obs	S calc
1	Methane	190.7	111.5	7.92	9.20
2	Ethane	305.3	184.7	24.12	27.21
3	Propane	368.8	230.9	41.37	45.22
4	Butane	426.2	272.6	61.44	63.23
5	Pentane	470.4	309.1	80.65	80.24
6	Hexane	508.0	342.0	99.60	99.25
7	Heptane	540.0	371.5	117.95	117.26
8	Octane	569.4	397.6	137.44	135.27
9	Nonane	595.4	423.6	154.62	153.28
10	Decane	619.3	447.0	172.30	171.29
11	Undecane	642.6	470.0	189.86	189.30
12	Dodecane	663.8	489.0	209.76	207.31
13	Tridecane	683.2	507.0	227.06	225.32
14	Tetradecane	701.0	525.5	245.70	243.33
15	Pentadecane	717.6	543.5	261.15	261.34
16	Hexadecane	734.3	560.5	278.08	279.35
17	Heptadecane	749.3	576.0	294.61	297.36
18	Octadecane	763.2	590.0	311.76	315.37
19	Nonadecane	776.0	603.0	328.70	333.38

The author is very grateful to Dr. K. Majumdar and Mr. Y. P. Varshni for their interest in the investigation.

[1] S. S. Mitra, J. Chem. Phys. (to be published).
[2] Hodgman, *Handbook of Chemistry and Physics*, International Critical Tables, Landolt-Börnstein Tabellen.

Calculation of the Distribution of Relaxation Times for a Single-Axis Rotator Using the Random-Jump Hypothesis

JOHN D. HOFFMAN
General Electric Research Laboratory, The Knolls, Schenectady, New York
(Received September 2, 1953)

ELSEWHERE in this issue,[1] the distribution of dielectric relaxation times associated with a single-axis polar rotator capable of occupying various orientational sites differing in local free energy is calculated using the approximation that the only important elementary process is a single jump to an adjacent site (*single-jump hypothesis; S-J*). It is shown that a definite distribution of relaxation times develops naturally when one site is more stable than the others provided three or more sites are involved. Fluctuations of barrier height were ignored in these calculations.

Although the single-jump approximation seems physically reasonable, other hypotheses regarding the nature of the elementary reorientation process in crystals are conceivable. Kauzmann,[2] in discussing the case of essentially equivalent sites, has

proposed that a dipole may become completely disengaged from the lattice and then settle down in a new equilibrium orientation more or less at random. We shall call Kauzmann's picture of the elementary process of dipole reorientation the *random-jump hypothesis* (*R-J*). It is the object of this note to calculate the distribution of dielectric relaxation times associated with the same site model discussed previously (i.e., a single-axis rotator with one unique site designated "1" and $\Omega-1$ sites of higher and equivalent local free energy) but using the *R-J* hypothesis of Kauzmann rather than the *S-J* hypothesis. The same general method of attack will be employed, and fluctuations of barrier height will be ignored.

Using the *R-J* hypothesis, the net rate of transfer of dipoles in each of the Ω sites may be written

$$\begin{aligned} dN_1/dt &= -2kN_1+\frac{2k'}{\Omega-1}(N_2+N_3+\cdots N_\Omega),\\ dN_2/dt &= -2k'N_2+\frac{2kN_1}{\Omega-1}+\frac{2k'}{\Omega-1}(N_3+N_4\cdots N_\Omega) \qquad (1)\\ &\cdot\\ &\cdot\\ &\cdot\\ dN_\Omega/dt &= -2k'N_\Omega+\frac{2kN_1}{\Omega-1}+\frac{2k'}{\Omega-1}(N_2+N_3+\cdots N_{\Omega-1}). \end{aligned}$$

In the above equations, Ω is the number of sites, k is the probability that a dipole will leave site 1 (unique) by surmounting a local free energy barrier $W+V$, and k' the probability a dipole will leave any of the $\Omega-1$ equivalent sites by surmounting a barrier of magnitude W. N_1, N_2, $\cdots N_\Omega$ are the numbers of dipoles in sites 1, 2, $\cdots i\cdots\Omega$ at any given time; the only restriction on N_i is $\Sigma N_i=N$.

The characteristic determinant of Eq. (1) is generally

$$\begin{vmatrix} \mathbf{A} & \beta & \beta & \beta & \cdots \\ \alpha & \mathbf{B} & \beta & \beta & \cdots \\ \alpha & \beta & \mathbf{B} & \beta & \cdots \\ \alpha & \beta & \beta & \mathbf{B} & \cdots \\ \cdot & \cdot & \cdot & \cdot & \cdot \\ \cdot & \cdot & \cdot & & \end{vmatrix} =0, \qquad (2)$$

where $\mathbf{A}=(\mathbf{D}+2k)$, $\mathbf{B}=(\mathbf{D}+2k')$, $\alpha=2k/(\Omega-1)$, $\beta=2k'/(\Omega-1)$, and $\mathbf{D}$ is the operator d/dt. Solving Eq. (2), the eigenvalues of the operator $\mathbf{D}$, $f_\beta(k)$, are found to be

$$\begin{aligned} f_1(k) &= 0,\\ f_2(k) &= -2[(\Omega-1)k+k']/(\Omega-1),\\ f_3(k) &= f_4(k)=\cdots f_\Omega(k)=-2k'\Omega/(\Omega-1). \end{aligned}$$

The subscript β refers to the mode of decay. The corresponding Ω distinct solutions of Eq. (1) are therefore of the form

$$N_i=C_{i1}+C_{i2}\exp[-f_2(k)t]+\sum_{\beta\geq 3}^{\Omega} t^{\Omega-3}C_{i\beta}\exp[-f_3(k)t]. \qquad (3)$$

It may be shown by substitution of the terms in Eq. (3) into Eq. (1) that C_{i1} (the time-independent equilibrium mode), C_{i2}, and C_{i3} have nonzero values; by a rather involved procedure it may also be shown that the $C_{i\beta}$ for $\beta\geq 4$ are all zero.[3] It follows that only modes 2 and 3 will lead to active dielectric relaxation times. The relaxation times, which are given by $\tau_\beta=-1/f(k)$, are therefore

$$\begin{aligned} \tau_2 &= (\Omega-1)/2[(\Omega-1)k+k'],\\ \tau_3 &= (\Omega-1)/2k'\Omega \end{aligned}$$

for the *R-J* hypothesis.

It is interesting to compare the results obtained using the *R-J* and *S-J* hypotheses. The results for the three-position model are the same, since the differential equations are identical. When $\Omega\geq 4$ and $k'\gg k$ (one site stable) the *R-J* hypothesis yields just two relaxation times where $\tau_2/\tau_3\cong\Omega$, while the *S-J* hypothesis leads to a larger number of active relaxation times where $\tau_{\max}/\tau_{\min}>\Omega$. Both hypotheses lead to the idea that the distribution of relaxation times should become narrower as the temperature is increased (since k' will tend to approach k, particularly in cooperative systems), and yield only a single relaxation time when $k'=k$ (all sites equivalent).

The author wishes to thank Dr. J. K. Bragg for his assistance with this problem.

[1] J. D. Hoffman and H. G. Pfeiffer, J. Chem. Phys. **21** (1953).
[2] W. Kauzmann, Revs. Modern Phys. **14**, 12 (1942).
[3] In evaluating the $C_{i\beta}$ in equation 3 for $k'\neq k$ when $\beta\geq 3$, it should be noted that the sum of the solutions for $\beta\geq 3$ must be substituted *simultaneously* in Eq. 1. A general proof that the C values associated with the terms involving the pre-exponential factor t are always zero may be obtained. Similar considerations show that only one relaxation time appears when $k=k'$.

Critical Temperature and Pressure of *n*-Paraffins

L. GRUNBERG
Mechanical Engineering Research Laboratory, D.S.I.R., Thorntonhall, Glasgow, Scotland
(Received October 30, 1953)

In a recent publication Varshni[1] attempted to establish a relationship between the critical temperature T_c and the critical pressure P_c for the *n*-paraffins. Combining the equations for the viscosity at the critical point proposed by Trautz[2] and by Grunberg and Nissan[3] by means of the relationship

$$P_cV_c/RT_c=P_cM/R\rho_cT_c=\text{constant}, \qquad (1)$$

and utilizing the observation by Grunberg and Nissan that the viscosity and the density ρ_c at the critical point is the same for all the *n*-paraffins, Varshni concluded that the ratio T_c/P_c should be constant for these compounds. That a definite relationship between T_c and P_c exists for the *n*-paraffins can be deduced directly from Eq. (1) and from the fact that ρ_c is approximately constant, without involving the aforementioned viscosity equations. The relationship is, of course,

$$T_c/MP_c=\text{constant},$$

and not

$$T_c/P_c=\text{constant},$$

as suggested by Varshni. If the values of T_c/MP_c are calculated for the *n*-paraffins C_2-C_{19}, one obtains (with T_c in degrees K and P_c in atmos, values which rise slowly from 0.205 to 0.215, a variation which is well within the applicability of Eq. (1).

Varshni further discussed the additivity of T_c[2] established by Grunberg and Nissan[3] and investigated in great detail in another publication.[4] It is interesting to note that, because of the approximate constancy of T_c/MP_c and the additivity of T_c[3], the function $(MP_c)^3$ is approximately additive. Partial values of $(MP_c)^3$ for $-CH_2$ and $-CH_3$ are 2.41×10^6 and 3.40×10^6, respectively. Values of P_c calculated from additivity agree approximately within 2 percent with the observed data for the *n*-paraffins from C_5-C_{19}.

[1] Varshni, J. Chem. Phys. **21**, 1400 (1953).
[2] Trautz, Ann. phys. **11**, 190 (1931).
[3] Grunberg and Nissan, Nature **161**, 170 (1948).
[4] Grunberg and Nissan, Trans. Faraday Soc. **44**, 1013 (1948).

Photobleaching and Photorecovery of Dyes

GERALD OSTER AND NEIL WOTHERSPOON
Department of Chemistry, Polytechnic Institute of Brooklyn, Brooklyn, New York
(Received November 2, 1953)

Weiss[1] found that solutions of methylene blue or of thionine in the presence of acidified 1*M* ferrous sulphate are rapidly photoreduced by visible light, and that the color of the dye is restored rapidly in the dark even in the absence of oxygen. We have found that rapid photobleaching of these dyes (at concentration of 10^{-5}M) takes place when 10^{-3}M ascorbic acid or phenylhydrazine are used as the reducing agents, the visible light being supplied by a 100-watt tungsten lamp or by a single flash

of about 1 millisecond duration from a photographic flash bulb. In the complete absence of oxygen the color is not restored. In fact, the photobleached solution serves as a sensitive oxygen meter; bubbling through commercial nitrogen will gradually restore the color but prepurified nitrogen which had been further purified by passing over hot copper will not restore the color. A further difference between our results and those of Weiss is that in our systems the reducing agents do not quench the red fluorescence of methylene blue and of thionine. The strong fluorescence quenching which Weiss observed may be due merely to the fact that he used large concentrations of ferrous sulphate and hence the fluorescence quenching may not be intrinsic to the mechanism of photobleaching as he supposed. We also found that several substances, particularly cupric ion and hydroquinone, will inhibit the photobleaching of our systems (compare reference 2).

Acidified stannous chloride is also an effective reducing agent for the photobleaching of methylene blue or of thionine. Below *p*H 1.5, however, the reducing agent will reduce the dyes in the dark. Above this *p*H the dyes are rapidly photobleached with visible light whether the solvent is water, methanol, ethanol, glycerol, methyl cellosolve, or acetone. It was found by the use of a red transmitting interference filter ($\lambda_{max}=659m\mu$) in conjunction with a tungsten lamp that the quantum yield of photobleaching of methylene blue (10^{-5}M) with stannous chloride (10^{-4}M at *p*H 2.0) is 0.33. Still higher values (close to unity) are achieved if acetone or ethanol are the solvents. If excess stannous chloride is present the color of the dye is not restored even in the presence of air.

Both methylene blue and thionine in acetone with acidified stannous chloride are rapidly photobleached at −78.5°C. The photobleaching takes place more slowly in other solvents, the velocity of the reaction decreasing in the order: acetone, methanol, ethanol, methyl cellosolve, and glycerol. That is, the photobleaching is slower the higher the viscosity of the medium. Apparently at this temperature the reaction becomes diffusion-controlled, and the rate is determined by the chance that an excited dye molecule will collide with an electron donor. It was further found that dye-reducing agent solutions in methyl cellosolve or in glycerol which had been irradiated at low temperature and then warmed to room temperature in the dark do not show further bleaching (compare reference 3).

Photobleached products even in the absence of oxygen are restored to the original dye by irradiation with near ultraviolet light. Apparently the reduced dye does not react with the oxidized reducing agent (e.g., stannic ion) in the dark but is easily oxidizable when in the excited state. The quantum yield for the photorecovery on irradiation of photobleached methylene blue or of photobleached thionine in ethanol with the 365 mμ line of mercury was found to be close to unity. The recovered dye solution can then be photobleached with visible light, recovered with near ultraviolet, and the process can be repeated several times. The restoration of color by irradiating the leuco form of methylene blue with ultraviolet light has been reported by Clark *et al.*[4] They found that the action spectra for photorecovery has a maximum in the neighborhood of 380 mμ. We found, however, that the absorption maximum of the leuco form is in the neighborhood of 250 mμ and that the absorption at 380 mμ is very low. We further found that irradiation of the photoreduced dye with the 254 mμ line of mercury results in a rapid recovery of the dye followed by an irreversible destruction of the dye. That is, at this wavelength not only are electrons removed from the leuco form but there is also eventual photolysis of the dye. For these reasons the action spectra shows a maximum at much longer wavelengths than does the absorption spectra.

Photorecovery of the photobleached dye on irradiation with near ultraviolet also takes place at −78.5°C. Here again the reaction is slower the greater the viscosity of the medium and no dark reaction takes place when solutions of the ultraviolet-irradiated samples in methyl cellosolve or in glycerol are then warmed to room temperature. The photobleached dyes at −78.5° in these two media (glasses at this temperature) exhibit an intense yellow phosphorescence with a duration of the order of seconds. The original dyes do not exhibit a phosphorescence under these conditions. The long-lived species of the leuco dyes probably do not play an important role in the photorecovery in low-viscosity media since the quantum yield is of the order of unity (compare reference 5).

This work was supported in part under a project from the Photographic Branch of the U. S. Army Signal Corps.

[1] J. Weiss, Trans. Faraday Soc. **32**, 1331 (1936); **35**, 48 (1939); **42**, 133 (1946). See also E. Rabinowitch, *Photosynthesis* (Interscience Publishers, Inc., New York, 1945), Vol. I, p. 76.
[2] G. Oster, Photo. Eng. **4**, No. 3 (1953).
[3] E. E. Broda and C. F. Goodeve, Proc. Roy. Soc. (London) **B130**, 217 (1941–1942); Wald, Durell, and St. George, Science **111**, 179 (1950); H. Linshitz and J. Renner, Nature **169**, 193 (1952).
[4] Clark, Cohen, and Gibbs, U. S. Public Health Reports, Reprint No. 1017 (1925).
[5] J. D. Knight and R. Livingston, J. Phys. Colloid Chem. **54**, 703 (1950).